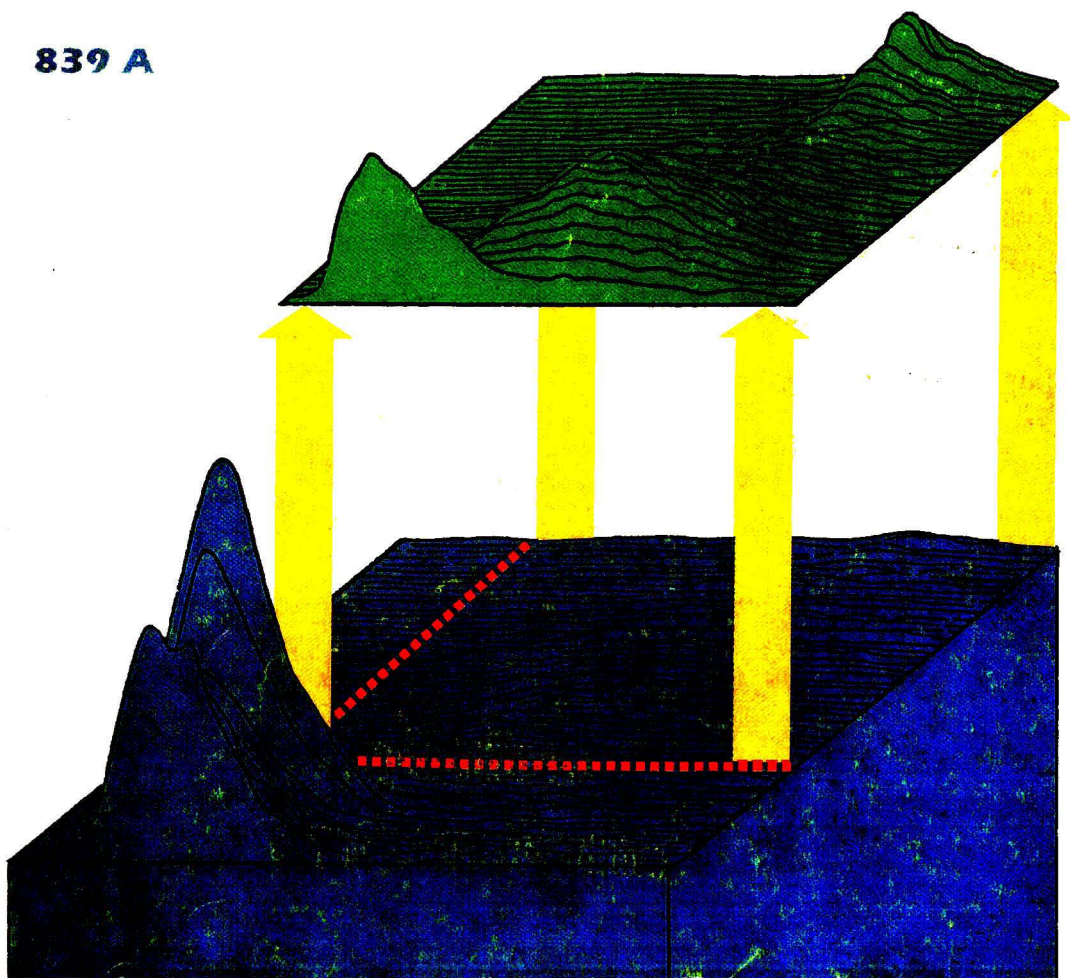


FLUORESCENCE - L - I - F - E - T - I - M - E - FILTERING

839 A



LISTEN TO THE QUIET

and have your very own gnome.

Vacuum pumps in general are a noisy sort of lab hardware. Especially during the roughing stage. But at working pressure you want quiet.

At Precision we do something about noise.

We put a unique flutter valve in our pump to help reduce irritating clatter. Less noise means less fatigue on you.

The flutter valve is just one step in our effort to remove problems. Problems with noise, vibration level, internal leakage, improper gas flow, wear on parts, and oil breakdown.

Things that reduce performance.

Because that's our business. We worry about building the pump so you can concentrate on getting good results. Accurate results. Scientific results.

So don't worry. Be precise. Pump with Precision.

The gnome is to remind you of the features of our pump—small, fast, hard working, quiet as the night.

Send for the Precision belt drive bulletin. You'll receive your very own gnome when you return the warranty registration card that comes with the purchase of a



Precision pump. Write Precision Scientific, P.O. Box 10066, Rochester, NY 14610. Or call 800-621-8820.

MEMBER
SAMA
SCIENTIFIC APPARATUS
MAKERS' ASSOCIATION

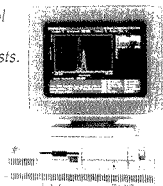
*Your Performance Demands
Precision®*

Precision Scientific

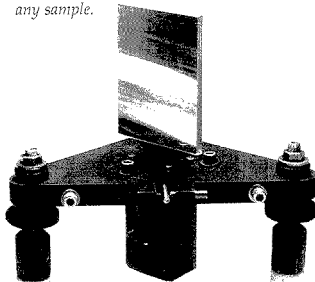
CIRCLE 127 ON READER SERVICE CARD



Easy-to-use data system. The entire spectrometer is operated from one IBM Personal System/2 Model 50 with color graphics. Our ThermoSPEC™ software offers multi-level operation including menu-driven control for novices and occasional users, and command mode control for expert spectroscopists.



Flexibility of a sequential ICP. Correct wavelengths may be identified and conditions optimized for any element in any sample.

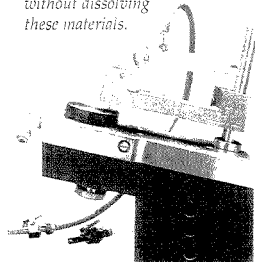


Economy from selectable low argon flow. High flow provides extra sensitivity for low concentrations or difficult samples, but low flow saves argon on routine samples.

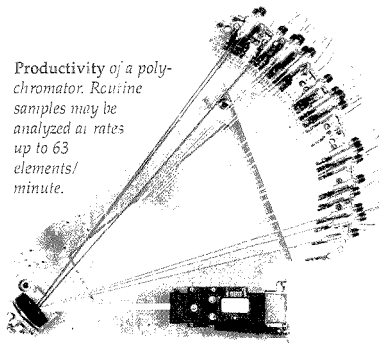


Vacuum option for P and S detection. Both the mono- and the polychromator can be outfitted for vacuum UV determinations.

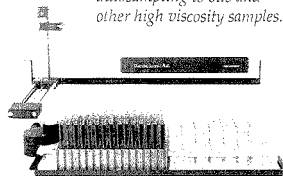
No metal prep with an optional solid sampling accessory. Spark ablation of metals and briquetted powders into the argon stream makes it possible to do "direct reading" measurements without dissolving these materials.



Productivity of a polychromator. Routine samples may be analyzed at rates up to 63 elements/minute.



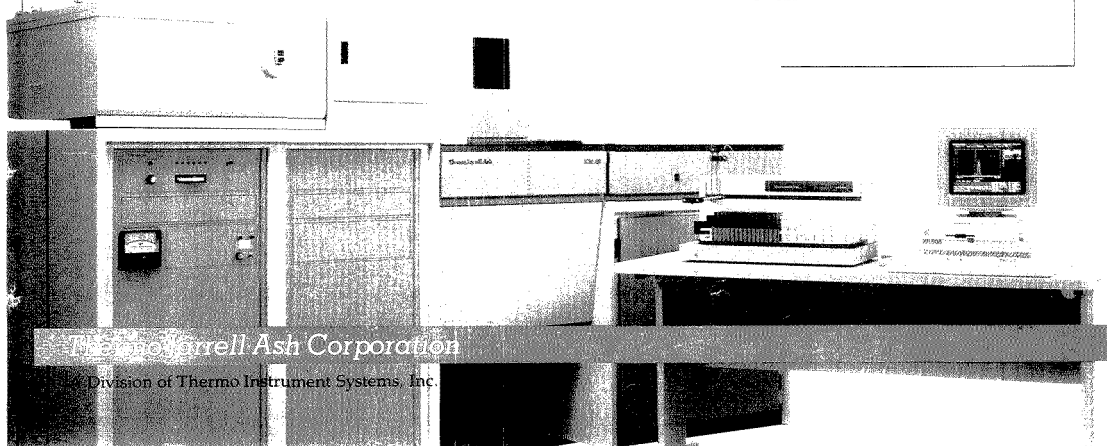
Unattended operation. With the microprocessor controlled TJA-300™ Autosampler, the PolyScan can do automatic profiling, automatic standardization, limit and other quality control checks on all samples in full compliance with CLP requirements. An optional autodilutor extends autosampling to oils and other high viscosity samples.



These Critical Details Make the PolyScan 61E The World's Most Advanced ICP.

For literature or a demonstration, call (508) 520-1880. Or write Thermo Jarrell Ash, Inc., 8 East Forge Parkway, Franklin, MA 02038-9101.

CIRCLE 158 ON READER SERVICE CARD



The Thermo Jarrell Ash Corporation

Division of Thermo Instrument Systems, Inc.

You said you needed positive and negative ions, EI/CI, DCI, FAB, Thermospray ionization, a color data system, 4,000 dalton mass range, variable resolution up to 6,000, and you wanted all that in a quadrupole mass spectrometer?



We responded.

Now you don't have to play the "assemble a mass-spec" game when you need a new ionization technique in a hurry.

The Resolver allows you to use any method by simply plugging in the appropriate source.

But more importantly, The Resolver offers the ability to obtain spectra in which the reported isotopic ratio is meaningful, while detecting even smaller quantities of the analyte.

Finally, with the power of our Spectral 30 color data system you obtain a reduced entry fee into the high performance club. . .

...at a quadrupole price.

THE RESOLVER™



Delsi Inc., 15701 West Hardy Road, Houston, Texas 77060. FAX (713) 591-2132 Tel (713) 847-0811
NERMAG 49 Quai du Halage 92500 RUEIL-MALMAISON France Tel.: (1) 47 32.92.05 Telex: Ribmag 204 029 F

 NERMAG

CIRCLE 32 ON READER SERVICE CARD



ANCHAM
 61(14) 819A-870A/1473-1600 (1989)
 ISSN 0003-2700

Registered in U.S. Patent and Trademark Office;
 Copyright 1989 by the American Chemical Society

ANALYTICAL CHEMISTRY (ISSN 0003-2700) is published semimonthly by the American Chemical Society at 1155 16th St., N.W., Washington, DC 20036. Editorial offices are located at the same ACS address (202-872-4600; TDD 202-872-8733). Second-class postage paid at Washington, DC, and additional mailing offices. Postmaster: Send address changes to ANALYTICAL CHEMISTRY Member & Subscriber Services, P.O. Box 3337, Columbus, OH 43210.

Claims for missing numbers will not be allowed if loss was due to failure of notice of change of address to be received in the time specified; if claim is dated (a) North America: more than 90 days beyond issue date, (b) all other foreign: more than one year beyond issue date, or if the reason given is "missing from files."

Copyright Permission: An individual may make a single reprographic copy of an article in this publication for personal use. Reprographic copying beyond that permitted by Section 107 or 108 of the U.S. Copyright Law is allowed, provided that the appropriate per-copy fee is paid through the Copyright Clearance Center, Inc., 27 Congress St., Salem, MA 01970. For reprint permission, write Copyright Administrator, Publications Division, ACS, 1155 16th St., N.W., Washington, DC 20036.

Registered names and trademarks, etc., used in this publication, even without specific indication thereof, are not to be considered unprotected by law.

Advertising Management: Centcom, Ltd., 500 Post Rd. East, Westport, CT 06880 (203-226-7131)

1989 subscription rates include air delivery outside the U.S., Canada, and Mexico

	1 yr	2 yr
Members		
Domestic	\$ 27	\$ 45
Canada and Mexico	56	103
Europe	83	157
All Other Countries	120	231
Nonmembers		
Domestic	49	83
Canada and Mexico	78	141
Europe	155	280
All Other Countries	192	354

Three-year and other rates contact: Member & Subscriber Services, ACS, P.O. Box 3337, Columbus, OH 43210 (614-447-3776 or 800-333-9511).

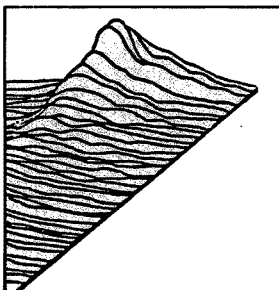
Subscription orders by phone may be charged to Visa, MasterCard, Barclay card, Access, or American Express. Call toll free at (800-ACS-5558) from anywhere in the continental United States; from Washington, DC, call 872-8065. Mail orders for new and renewal subscriptions should be sent with payment to the Business Management Division, ACS, P.O. Box 57136, West End Station, Washington, DC 20037.

Subscription service inquiries and changes of address (include both old and new addresses with ZIP code and recent mailing label) should be directed to the ACS Columbus address noted above. Please allow six weeks for change of address to become effective.

ACS membership information: Lorraine Bowlin (202-872-4567)

Single issues, current year, \$7.00 except review issue and LabGuide, \$12.00; back issues and volumes and microform editions available by single volume or back issue collection. For information or to order, call (800-ACS-5558) or write the Microform & Back Issues Office at the Washington address.

Nonmembers rates in Japan: Rates above do not apply to nonmember subscribers in Japan, who must enter subscription orders with Maruzen Company Ltd., 3-10 Nihonbashi 2-chome, Chuo-ku, Tokyo 103, Japan. Tel: (03) 272-7211.



REPORT

839 A

On the cover. Fluorescence lifetime filtering can be used to selectively view fluorescence signals within a given lifetime range. Linda B. McGown of Duke University explores filtering in both time and frequency domains and describes some applications of these filters for chemical analysis



MEETINGS

849 A

The 28th Eastern Analytical Symposium will be held at the New York Hilton Hotel in New York City, Sept. 24-29. Thirty-eight oral and three poster sessions, along with an exposition of scientific instruments and supplies, an employment service, and 17 short courses, will be held

BRIEFS

822 A

NEWS

833 A

Nine graduate students receive Division of Analytical Chemistry fellowships. ▶ Genes of a different color. ▶ Sunlight cleans polluted waters. ▶ A speedy computer chip for finding DNA patterns

BOOKS

856 A

Critical reviews. Recently released books on computer experimentation, microcomputers, computer-enhanced spectroscopy, microbeam analysis, spectroelectrochemistry, and kinetics are reviewed

FOCUS

861 A

The great fruit scares of 1989. First it was a pesticide in apples, then cyanide in grapes, that triggered near panic over hidden dangers on U.S. grocery shelves. Were the dangers overstated, or did Americans react to unacceptable risks?

NEW PRODUCTS & MANUFACTURERS' LITERATURE

864 A

AUTHOR INDEX

1473

Articles

Analysis of Siderophores and Synthetic Hydroxamic Acids by High-Performance Liquid Chromatography with Amperometric Detection 1474

By carefully selecting the applied potential and the mobile-phase composition, it is possible to sensitively and selectively determine siderophores and hydroxamic acids on a metal-free HPLC system and avoid the problems associated with on-column metal sequestration.

Jeremy D. Glennon*, Michael R. Woulfe, Andrew T. Senior, and Nuala NiCholeain, Department of Chemistry, University College Cork, Cork, Ireland

Zone Gas Chromatography 1478

A slowly scanning, narrow heat pulse provides an efficient means for stopping the gas chromatographic process and creates the possibility for new types of separation.

Endre Fuggerth, Research Institute for Ferrous Metallurgy, Environmental Department, Fehervari ut 130, Budapest, Hungary

Determination of Nitrite in Drinking Water and Environmental Samples by Ion Exclusion Chromatography with Electrochemical Detection 1485

A detection limit of 0.1 ppb nitrite is obtained without sample preconcentration and without interference from inorganic and organic contaminants. Recovery results are in good agreement with those obtained by the standard photometric method.

Hie-Joon Kim*, Kim & Associates, 33 Pleasant Street, Wayland, MA 01778 and Young-Kyung Kim, Department of Chemistry and Food Science, Framingham State College, Framingham, MA 01701

Fluidic and Syringe Injection Study by Peak Shape Analysis 1489

Fluidic and syringe injections with different splitting conditions are compared using the Edgeworth-Cramér peak shape analysis. A numerical procedure for column efficiency measurements in HPLC is demonstrated.

Maurizio Remelli, Gabriella Blo, and Francesco Dondi*, Dipartimento di Chimica, Università di Ferrara, via Luigi Borsari 46, I-44100 Ferrara, Italy, Marie Claire Vidal-Madjar, Laboratoire de Physico-Chimie des Biopolymères, CNRS, Université Paris XII, Thiais, France, and Georges Guiochon, Department of Chemistry, University of Tennessee, Knoxville, TN 37996-1600

* Corresponding author

Exchange Reactions with Zinc Bis[(di-2-hydroxyethyl)dithiocarbamate] for Automated Monitoring of Metal Ions in Industrial Effluents by Liquid Chromatography with Electrochemical Detection 1494

The highly stable and water-soluble zinc bis[(di-2-hydroxyethyl)dithiocarbamate] forms a complex with metals (e.g., Co, Cu, Ni, and Cd) that allows for the long-term monitoring of the metal ions.

A. M. Bond* and T. P. Majewski, Division of Chemical and Physical Sciences, Deakin University, Geelong, 3217 Victoria, Australia

Electrochemical Probes of Oxidation State, Product Distribution, and Redox Activity for Ba₂YCu₃O_{7-x} in Halide Solutions 1497

Rotating ring-disk electrode measurements with dissolving Ba₂YCu₃O_{7-x} disks in halide solutions allow the determination of *x*, and also possibly reactive intermediates, through the ring-detected product ratios using semiconductor to superconductor compositions.

J. M. Rosamilia and B. Miller*, AT&T Bell Laboratories, Murray Hill, NJ 07974

Determination of Conjugated Dienes in Gasoline by Differential Pulse Polarography 1502

The electrochemical reduction of conjugated dienes at a dropping-mercury electrode is the basis for a method with a 15-min analysis time and an RSD of 5.3%.

Stephen J. Swarin*, Analytical Chemistry Department, General Motors Research Laboratories, Warren, MI 48090-9055 and Kevin L. Perry, Fuels and Lubricants Department, General Motors Research Laboratories, Warren, MI 48090-9055

Uranine Sensitized Chemiluminescence for Alternative Determinations of Copper(II) and Free Cyanide by the Flow Injection Method 1505

Weak light from a chemiluminescence system, consisting of Cu(II), CN⁻, and dissolved O₂, is effectively enhanced using uranine in aqueous 2-propanol solution as the sensitizer. The reaction mechanism involving singlet oxygen is discussed.

Xing-Zheng Wu, Masaaki Yamada*, Toshiyuki Hobo, and Shigetaka Suzuki, Department of Industrial Chemistry, Faculty of Technology, Tokyo Metropolitan University, Setagaya, Tokyo 158, Japan

Multicomponent Fluorometric Analysis Using a Fiber-Optic Probe 1510

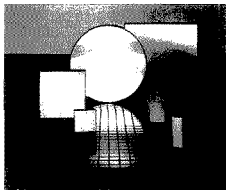
Phase-resolved fluorometric measurements are performed using a bifurcated fiber-optic probe. Multicomponent analysis of ternary and quaternary synthetic mixtures and stray light rejection are demonstrated with correlation coefficients better than 0.98.

Frank V. Bright* and Kevin S. Litwiler, Department of Chemistry, State University of New York at Buffalo, Buffalo, NY 14214

Ruled and Holographic Diffraction Gratings

Instruments SA provides a wide variety of high performance diffraction gratings. Among the many standard types available are aberration corrected blazed and ion etched concave monochromator gratings, flat field gratings for use with diode array detectors, toroidal gratings for use in the VUV and classically ruled as well as holographic plane gratings. Applications range from upper atmosphere ozone monitoring by satellite to bio testing and emission spectrometers. For further information contact Jobin Yvon, Instruments SA (201) 494-8660.

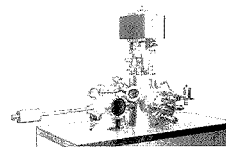
CIRCLE 72



Nanoscan 50 The Field Emission Auger Microprobe

Low energy, high brightness field emission source guarantees high signal and excellent spatial resolution in SEM and SAM. Other features include video-rate SEM/SAM image accumulation, full automation, and high constant energy resolution. For further information, contact the Riber Division of Instruments SA, Inc. at (201) 494-8660.

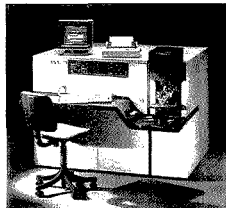
CIRCLE 73



Glow Discharge Spectroanalyzer

The GDL Excitation Source for direct solid sample analysis, uses the principle of cathodic sputtering. The conducting sample forms the cathode which is bombarded with positive argon ions to excite the sample atoms. The GDL is used for both elemental and surface analysis of metals including ferrous and non-ferrous alloys, noble metals and ceramics. For further information contact Jobin Yvon, Instruments SA (201) 494-8660.

CIRCLE 74



Compact Sequential ICP Spectrometer

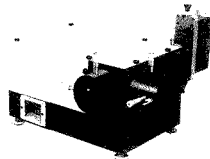
The JY 24 has the advantages of a full featured ICP spectrometer in a single, compact, space-saving unit. By using a large surface area and high groove density holographic grating, the resolution and light gathering power of the JY 24 are unequalled for its size. For further information contact Jobin Yvon, Instruments SA (201) 494-8660.

CIRCLE 75

Spectrometers

With a line of single and double spectrometers which spans from 100 to 1500 mm in focal length, Instruments SA/Jobin Yvon can furnish the ideal spectrometer for any UV, Visible or IR application. This broad range of instruments significantly reduces the need for compromise in coverage, stray light rejection or resolution when specifying a system. Each spectrometer can be automated for integration into a spectroanalytical system. For further information contact Instruments SA/Jobin Yvon (201) 494-8660.

CIRCLE 76



Simultaneous and Sequential ICP Spectrometers

The JY 70 Plus consists of an integrated direct reading double polychromator — sequential spectrometer. This ICP system combines the speed of simultaneous, multi-element analysis with the versatility and flexibility of the sequential system. For further information on the JY 70 Plus or JY 38 Plus contact Jobin Yvon, Instruments SA (201) 494-8660.

CIRCLE 77

INTRODUCING THE NEW JY 50 POLYSCAN FROM A WORLD LEADER IN ICP SYSTEMS

The JY 50 PolyScan not only provides all the advantages inherent in a simultaneous multi-element Spectroanalyzer but also offers spectral line selection flexibility which previously was found only in sequential ICP systems. Jobin Yvon has developed a new scanning entrance slit which furnishes 2.2 nm wavelength displacement from any of the preselected fixed analytical channels.

For more information on the JY 50 PolyScan and the complete spectrum of JY instruments, use the reader service card, or write or call today.

CIRCLE 78 ON READER SERVICE CARD

JOBIN YVON

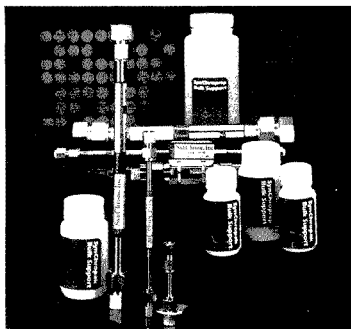


**J-Y DIVISION
Instruments SA, Inc.**

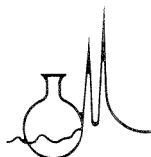
6 Olsen Avenue, Edison, NJ 08820-2419
Tel. (201) 494-8660, Telex 844516
FAX (201) 494-8796

In Europe: Jobin Yvon, 16-18 Rue du Canal 91163 Longjumeau, France
Tel. (33) 1.69.09.34.93
Telex JOBYVON 692882F
FAX 011-331-6909-0721





Full line of columns and bulk supports
Superior technical support
Competitive prices and fast delivery



802 Columbia St.
Corporate Offices • P.O. Box 310
Lafayette, Indiana 47902-0310

CIRCLE 152 ON READER SERVICE CARD

The Basics of Technical Communicat^{ing}

Communications skills—they're a must for successful scientists. Now you can increase your effectiveness and improve your communication skills with this new, easy-to-use reference book. With 18 chapters, this handy guide starts with the basics, such as eliminating wordiness and jargon in technical communications, using correct punctuation, and selecting appropriate verbs. From there, you'll learn how to assemble your papers and gather data for both written and oral reports. You'll learn correct documenting procedures, including footnoting and writing a bibliography. You'll cover the use of visual aids and graphics, abstract preparation, the use of computers and proofreading. A wide variety of practical applications is covered in this volume, including laboratory and business reports, journal publications, grants and proposals, business correspondence, resumés, and memos. *The Basics of Technical Communicat^{ing}* is a convenient, essential reference—one that you'll use time and time again! It complements *The ACS Style Guide* and *Writing the Laboratory Notebook* to give scientists a complete package for professional development in technical communication skills.

by B. Edward Cain, Rochester Institute of Technology

200 pages (1988)

ISBN 0-8412-1452-2 LC 88-3325

Paperbound:

US & Canada \$19.95, Export \$23.95

ISBN 0-8412-1451-4 LC 88-3325

Clothbound:

US & Canada \$29.95 Export \$35.95

Order from: American Chemical Society, Distribution Office Dept. 90
1155 Sixteenth St. NW, Washington, D.C. 20036

or CALL TOLL FREE **800-227-5558** and use your credit card!

BRIEFS

Binning Spectral Images in a Charge-Coupled Device 1513

Binning, the on-device combination of charge from several detector elements, in a two-dimensional CCD increases the sensitivity and dynamic range of spectroscopic measurements. Spectral line orientation, blooming, and readout speed are discussed.

Patrick M. Epperson and M. Bonner Denton*, Department of Chemistry, University of Arizona, Tucson, AZ 85721

Competitive Binding of Protons and Metal Ions in Humic Substances by Lanthanide Ion Probe Spectroscopy 1519

The inclusion of pH dependence into the Gaussian model allows prediction of metal binding constants that are more representative of true thermodynamic constants regardless of pH.

J. C. Dobbs, W. Susetyo, and L. A. Carreira*, Department of Chemistry, University of Georgia, Athens, GA 30602 and L. V. Azarraga, Environmental Research Laboratory, U.S. Environmental Protection Agency, Athens, GA 30613

Limitations of All Empirical Single-Parameter Solvent Strength Scales in Reversed-Phase Liquid Chromatography 1524

Single-parameter empirical scales of solvent strength are examined as predictors of the retention of *n*-alkylbenzenes. Both the E_T and π^* scales are shown to be only locally valid measures of solvent strength in reversed-phase LC.

Won Jo Cheong and Peter W. Carr*, Department of Chemistry, Smith and Koltzoff Halls, University of Minnesota, 207 Pleasant Street, Minneapolis, MN 55455

Supersonic Jet Spectrometry of Chemical Species Laser Ablated from Organic Polymers 1530

A styrene monomer ablated from a polymer surface is measured by supersonic jet spectrometry with fluorescence detection. Detection limits are in the subnanogram range. Selective and sensitive analysis is achieved by rotational and translational cooling.

Totaro Imasaka, Kouji Tashiro, and Nobuhiko Ishibashi*, Faculty of Engineering, Kyushu University, Hakozaki, Fukuoka 812, Japan

Infrared and Thermal Studies of *N*-(*p*-Cyanobenzylidene)-*p*-octyloxyaniline Coated on Derivatized Silica 1534

The interaction of the liquid crystal *N*-(*p*-cyanobenzylidene)-*p*-octyloxyaniline with silicas modified with mono-reactive silanes varying in chain length and blocking ability is studied by FT-IR, DSC, and TGA. Differences in the orientation of CBOA are observed as a function of derivatization.

C. J. Hann and R. K. Gilpin*, Department of Chemistry, Kent State University, Kent, OH 44242

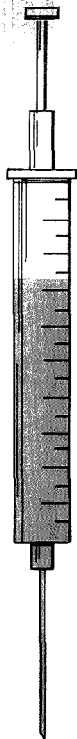
NITROGEN AND SULFUR

ONE INJECTION TWO RESULTS

Need Nitrogen and Sulfur on the same sample? Now you can do it! Couple the Antek Pyro-fluorescent™ Sulfur Detector with our Antek Pyro-chemiluminescent™ Nitrogen System.

Autosamplers and data acquisition/control systems are available for automated operation.

Chromatography detectors available:
Nitrogen Specific
Sulfur Specific



Features

- common pyroreactor for sample combustion and oxidation
- analyze gases, liquids or solids
- ppb to % range
- analysis time 30 seconds for gases and liquids. Up to 10 minutes for solids

Reduces the amount of sample prep required, the analysis time, and sample introduction by half. And, cut your instrument costs at the same time. Systems available for laboratory or process/online.

Applications

- petroleum liquids
- greases or residuals
- polymers
- biomedical samples
- high purity gases (for semi-conductors, etc.)
- LPG or other hydrocarbon gases
- atmospheric gases
- coal
- foods
- engine exhaust
- water/waste water

Typical Results

28.1ppm ±0.3	Water	148ppm±1
0.50ppm ±0.01	Naphtha	0.30ppm ±0.01
346ppm ±1.0	Diesel	48ppm±0.5
1.0ppm ±0.1	Butane	3.0ppm ±0.1
3.1ppm ±0.1	Propylene	1.8ppm ±0.1
0.9ppm ±0.1	Polyethylene	1.6ppm ±0.4
872ppm ±14	Coke	846ppm ±4
1.8ppm ±0.01	Fish Oil	4.1ppm ±0.4

For more information on your application or for a price quote, contact us in Houston or Dusseldorf.
In the USA, call toll free, (800) 365-2143

Patent Pending



ANTEK[®] INSTRUMENTS, INC.

Antek Instruments, Inc.
6005 North Freeway
Houston, Texas 77076-3998
Tel: 713/691-2265

TWX: 910-881-1792
Toll Free: 800/365-2143
FAX: 713-691-5606

Antek Instruments, GmbH
Wacholderstrasse 7
4000 Dusseldorf Angermund 31
Federal Republic of Germany

Tel: (0203) 74325/6
TLX: 8551136 ANDU D
FAX: (0203) 741545

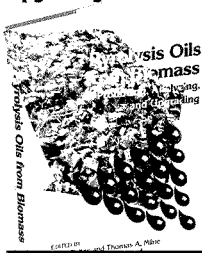
CIRCLE 1 ON READER SERVICE CARD

ANALYTICAL CHEMISTRY, VOL. 61, NO. 14, JULY 15, 1989 • 825 A

Pyrolysis Oils from Biomass

Producing, Analyzing, and Upgrading

Provides a timely and necessary update on the latest research—from feedstock to upgraded liquid fuels suitable as replacements for petroleum-derived fuels. Looks at the state of the science in the complete fuel cycle. Discusses biomass pyrolysis and its place in a renewable fuel economy. Presents the technology of pyrolysis oil production. Also offers analysis of the oils. With 27 chapters, coverage includes topics on • characterization • kinetics • chromatographic techniques and more. Concludes with seven chapters on upgrading pyrolysis oils to liquid fuels.



Serves as a collaborative effort to combat the long-term rise in CO₂ levels resulting from deforestation and the burning of fossil fuels. Specialists from five countries contributed the results of their research. A must for anyone interested in the progress in pyrolysis oil production as a long-term solution to the need for a renewable source of liquid transportation fuels.

Ed J. Soltes, *Editor*, Texas A&M University

Thomas A. Milne, *Editor*, Solar Energy Research Institute
Developed from a symposium sponsored by the Cellulose, Paper, and Textile Division and the Division of Fuel Chemistry of the American Chemical Society

ACS Symposium Series No. 376 353 pages (1988) Clothbound
ISBN 0-8412-1536-7 LC 88-24172 US & Canada \$74.95 Export \$89.95

Order from: American Chemical Society, Distribution Office, Dept. 03
1155 Sixteenth St., N.W., Washington, DC 20036

or CALL TOLL FREE **800-227-5558**
(in Washington, D.C. 872-4363) and use your credit card!

BRIEFS

Polymeric Activated Ester Reagents for Off-Line and On-Line Derivatizations of Amine Nucleophiles in High-Performance Liquid Chromatography with Ultraviolet and Fluorescence Detection 1538

A polymeric activated ester reagent is developed that improves detectability and chromatographic performance for primary and secondary amines or amine analogues. Percent derivatizations approach 90% and 70% for primary and secondary amines, respectively.

Chun-Xin Gao, Tzun-Yu Chou, and Ira S. Krull*, Department of Chemistry and The Barnett Institute, 341 Mugar Building, Northeastern University, 360 Huntington Avenue, Boston, MA 02115

Chiral Polymeric Reagents for Off-Line and On-Line Derivatizations of Enantiomers in High-Performance Liquid Chromatography with Ultraviolet and Fluorescence Detection: An Enantiomer Recognition Approach 1548

Polymeric chiral reagents are synthesized, characterized, and applied to enantiomeric recognition of primary and secondary amines and amino alcohols. The ultraviolet and fluorescence responses for known mixtures of enantiomers are compared to demonstrate the validity of the method.

Tzun-Yu Chou, Chun-Xin Gao, Nelu Grinberg, and Ira S. Krull*, Department of Chemistry and The Barnett Institute, 341 Mugar Building, Northeastern University, 360 Huntington Avenue, Boston, MA 02115

Detection of Ambient Hydrogen Chloride with a Zinc-Coated Piezoelectric Crystal Resonator Operating in a Frequency-Time Differential Mode 1559

The sensor's sensitivity is based on the formation of the hygroscopic ZnCl₂ salt and its high affinity for water. Rates of mass accumulation on the surface of the crystal are used to discriminate against common ambient interferences.

Glen G. Neuburger, Bell Communications Research, Red Bank, NJ 07701

Dimethyl Disulfide Derivatives of Long Chain Alkenes, Alkadienes, and Alkatrienes for Gas Chromatography/Mass Spectrometry 1564

Natural and synthetic unsaturated hydrocarbons are derivatized with DMDS, and their structures determined using GC/EI-MS, despite low volatility. The technique is applied to compounds found in two-winged insects, including African honeybees and fruit flies.

David A. Carlson*, USDA, ARS, Insects Affecting Man and Animals Research Laboratory, P.O. Box 14565, Gainesville, FL 32604, Chin-Shyan Roan and Richard A. Yost, Chemistry Department, University of Florida, Gainesville, FL 32611, and Julio Hector, USDA, ARS, Insects Affecting Man and Animals Research Laboratory, P.O. Box 14565, Gainesville, FL 32604

Utilization of Spectrometric Information in Linked Gas Chromatography-Fourier Transform Infrared Spectroscopy-Mass Spectrometry 1571

Results of a combined IR-mass spectral library search algorithm are evaluated for complex mixture analysis. Concurrent use of both types of spectral information increases the reliability of library search-based identifications.

John R. Cooper and Charles L. Wilkins*, Department of Chemistry, University of California, Riverside, Riverside, CA 92521

Luminescence Applications in Biological, Chemical, Environmental, and Hydrological Sciences

New techniques have made luminescence spectroscopy indispensable and crucial for fundamental investigations of the dynamics of chemical processes. This fact-filled book brings you up to date on new and original research on the uses of luminescence techniques.

You'll get a better understanding of the applications that allow research scientists to measure the interactive distance between molecules and the size and shape of molecules. Examine methods to determine electronic transition states and molecular life times. Find out how to make use of the high sensitivity available for detection of fluorescing materials. Looks at natural environments as related to earth materials both in solid and liquid form, and gives information on reactions of these materials in both solid and water systems.

This multidisciplinary volume has 14 chapters and presents the important contributions in the fields of molecular biology, environmental science, methods of standardization, and molecular structure. It offers a unique look at research results and offers suggestions and examples of luminescence methodologies.

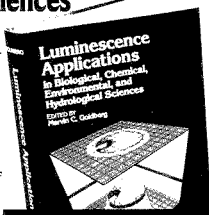
Marvin C. Goldberg, *Editor*, U.S. Geological Survey

Developed from a symposium sponsored by the Division of Environmental Chemistry of the American Chemical Society

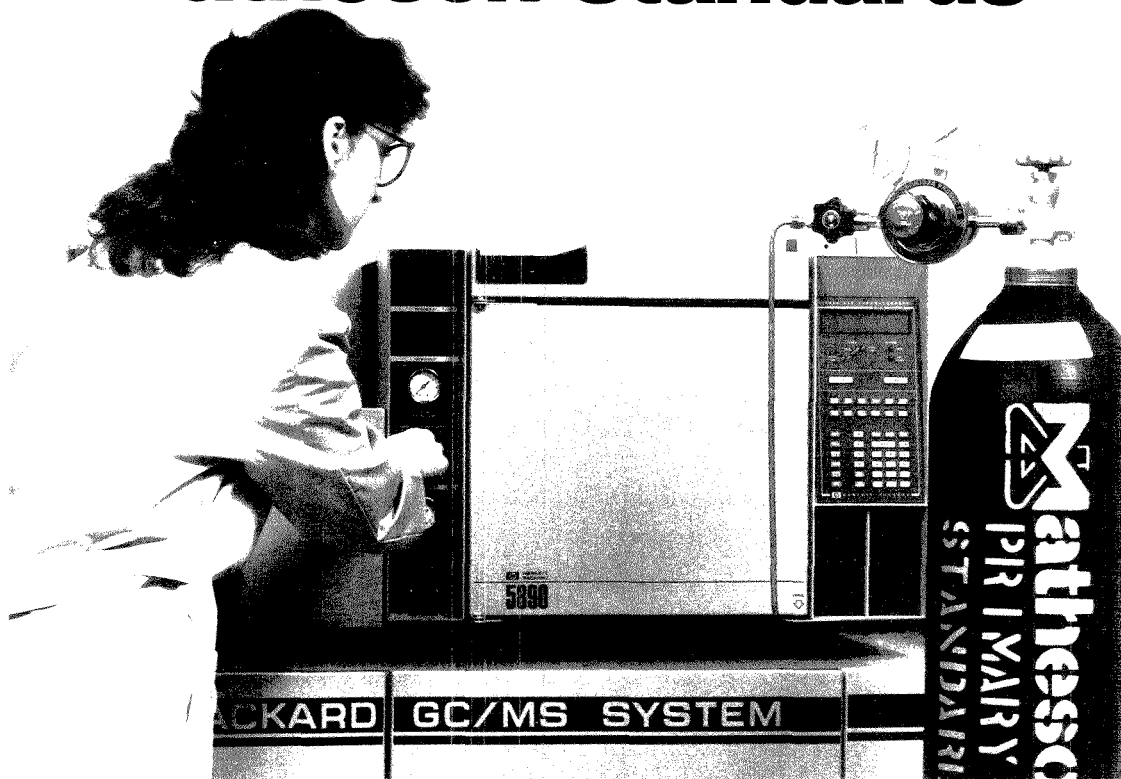
ACS Symposium Series No. 383 252 pages (1988) Clothbound
ISBN 0-8412-1560-X LC 88-39131 US & Canada \$59.95 Export \$71.95

Order from: American Chemical Society, Distribution Office, Dept. 09
1155 Sixteenth St., N.W., Washington, DC 20036

or CALL TOLL FREE **800-227-5558**
(in Washington, D.C. 872-4363) and use your credit card!



Move Up to Matheson Standards



Accurate gas chromatography is dependent upon your technique, your equipment, and your gases. A skilled gas chromatographer can enhance the accuracy of his results by using Matheson products exclusively. Three special products are of utmost importance.

Primary Standard Calibration Mixtures

The heart of your work centers around your calibration standards. Consider Matheson's Primary Standards to improve your results. The accuracy of these mixtures usually exceeds that of most analytical instruments. Matheson Primary Standards are prepared on high load, high sensitivity analytical balances. Each gas component is carefully quality controlled before being weighed into the

cylinder. Only weights traceable to the National Bureau of Standards are used. These mixtures give the highest degree of accuracy, precision and confidence. Move up today! Insist on Matheson Primary Standards.

Carrier Gases

The same exacting quality you get in Matheson Primary Standard Calibration Mixtures is also available in Matheson's carrier gases. No slipping in quality control here. Each Matheson UHP, Zero Gas, Ultra Zero Gas, and, of course, Matheson Purity Gas is guaranteed to be exactly what the label says. Nothing more, nothing less. Improve your GC operation today with the right carrier gas from Matheson.

Gas Handling Systems

Don't jeopardize the integrity of your gases with gas handling equipment of inferior quality. Matheson has

the right piece of equipment for every job. From regulators that don't outgas impurities, to filters for protecting delicate valves, to flowmeters that measure precisely, Matheson equipment is the standard.

When your work requires the best, don't settle for less than Matheson Standards.

From pharmaceuticals to petroleum, from laser technology to aerospace, when only the best will do, do what so many experienced scientists do. Move up to Matheson Standards.

For more information, contact Matheson, at (201) 867-4100, or circle the Reader Service Number below.

Matheson[®]
Gas Products
World Leader in Specialty Gases & Equipment
30 Scaview Drive, Secaucus, NJ 07094

Electrochemistry, Past and Present

The growing debate over nuclear fusion in a test tube has resulted in a renewed interest in electrochemistry. The development of the battery, pH meter, and pollution control devices, has been the result of electrochemistry. This new title highlights key advances in this exciting field—past, present and future.

Thirty-eight chapters capture major events and technologies of classical and fundamental electrochemistry, electrosynthesis, electroanalytical chemistry, industrial electrochemistry, electrode systems and pH measurement. General headings include: • foundations of electrochemistry • organic and biochemical electrochemistry • electroanalytical chemistry • industrial electrochemistry. This volume presents recent advances in novel electrochemical techniques. Applications in the large-scale production of organic compounds, the elucidation of the biogenesis of natural products by reactions at electrode surfaces, and electrochemical behavior of biological systems are reviewed. Also covered are future possibilities of portable electricity, systems for metal recovery and pollution control, and electrochemical machining.

Rich in an array of topics, this title contains many historical photographs and biographical chapters on some of the noted electro-chemists.

John T. Stock, *Editor*, University of Connecticut

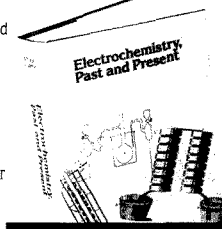
Mary Virginia Orna, *Editor*, National Institute of Environmental Health Sciences

Developed from a symposium sponsored by the Division of the History of Chemistry and the Division of Analytical Chemistry of the American Chemical Society

ACS Symposium Series No. 390 613 pages (1989) Clothbound
ISBN 0-8412-1572-3 LC 89-15 US & Canada \$69.95 Export \$107.95

Order from: American Chemical Society, Distribution Office, Dept. 21
1155 Sixteenth St., N.W., Washington, DC 20036

or CALL TOLL FREE **800-227-5558**
(in Washington, D.C. 872-4363) and use your credit card!



BRIEFS

Optimization of a Coaxial Continuous Flow Fast Atom Bombardment Interface between Capillary Liquid Chromatography and Magnetic Sector Mass Spectrometry for the Analysis of Biomolecules 1577

Mass spectra are obtained from low-picomole amounts of compounds from a variety of analyte classes, including peptides, steroids, phospholipids, and carbohydrates. A detection limit of 500 attomoles is obtained for a tripeptide.

M. Arthur Moseley, Leesa J. Deterding, J.S.M. de Wit, and Kenneth B. Tomer*, Laboratory of Molecular Biophysics, National Institute of Environmental Health Sciences, Research Triangle Park, NC 27709 and Robert T. Kennedy, Nancy Bragg, and James W. Jorgenson*, Department of Chemistry, University of North Carolina at Chapel Hill, Chapel Hill, NC 27514

Quantitation Capability of a Directly Linked Gas Chromatography/Fourier Transform Infrared/Mass Spectrometry System 1584

Regression analysis is used to evaluate GC/FT-IR/MS for on-line confirmed quantitative environmental analysis. The degree of scatter in the regression plots increases in the order total ion chromatogram ~ single ion chromatogram < maximum absorbance < integrated absorbance < Gram-Schmidt.

Donald F. Gurka*, Irene Farnham, Billy B. Potter, and Steven Pyle, United States Environmental Protection Agency, Environmental Monitoring Systems Laboratory, Las Vegas, NV 89193-3478, Richard Titus, Chemistry Department, University of Nevada, Las Vegas, NV 89154, and Wayne Duncan, Hewlett-Packard Corporation, Scientific Instruments Division, Palo Alto, CA 94304

Correspondence

Capillary Zone Electrophoresis with Analyte Velocity Modulation. Application to Refractive Index Detection 1593

Chang-Yuh Chen, Tshenge Demana, Shi-Duo Huang, and Michael D. Morris*, Department of Chemistry, The University of Michigan, Ann Arbor, MI 48109

Technical Notes

Determination of Nuclear Magnetic Resonance Sample Temperatures through Measurement of the Probe Coil Ohmic Resistance 1594

Rosemary Effiong and Ronald F. Evilia*, Department of Chemistry, University of New Orleans, New Orleans, LA 70148

Capillary Gas Chromatography/Fourier Transform Infrared Spectroscopy Using an Injector/Trap and Liquid/Liquid Extraction 1596

Allen J. Fehl and Curtis Marcott*, The Procter & Gamble Company, Miami Valley Laboratories, Cincinnati, OH 45239-8707

Use of Fumed Silica To Remove Surfactant Interferences in Continuous Flow Polarographic Measurements 1598

Wladyslaw W. Kubiak* and Zygmunt Kowalski, Institute of Materials Science, Academy of Mining and Metallurgy, 30-059 Krakow, Poland

Inverse Gas Chromatography Characterization of Polymers and Other Materials

No other single reference covers this relatively new subject area so completely! As an extension of conventional gas chromatography, inverse gas chromatography (IGC) has many advantages—simplicity, speed of data collection, accuracy, and low operating costs.

This one volume offers an in-depth look into the most recent advances in theoretical and practical aspects of this approach. Twenty-two chapters provide information on: • instrumentation and methodology • characterization of vapor-polymer systems • polymer-polymer systems • surfaces and interfaces • analytical applications • application of IGC in coal characterization and food science. This valuable title discusses the application of IGC to the thermodynamic and acid-base interaction of components in polymer systems, and the technological advances in the field.

Douglas R. Lloyd, *Editor*, University of Texas

Thomas Carl Ward, *Editor*, Virginia Polytechnic Institute and State University

Henry P. Schreiber, *Editor*, Ecole Polytechnique

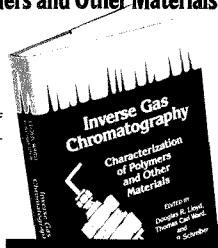
Clara C. Pizana, *Assistant Editor*

Developed from a symposium sponsored by the Division of Polymeric Materials: Science and Engineering of the American Chemical Society and the Macromolecular Science & Engineering Division of the Chemical Institute of Canada

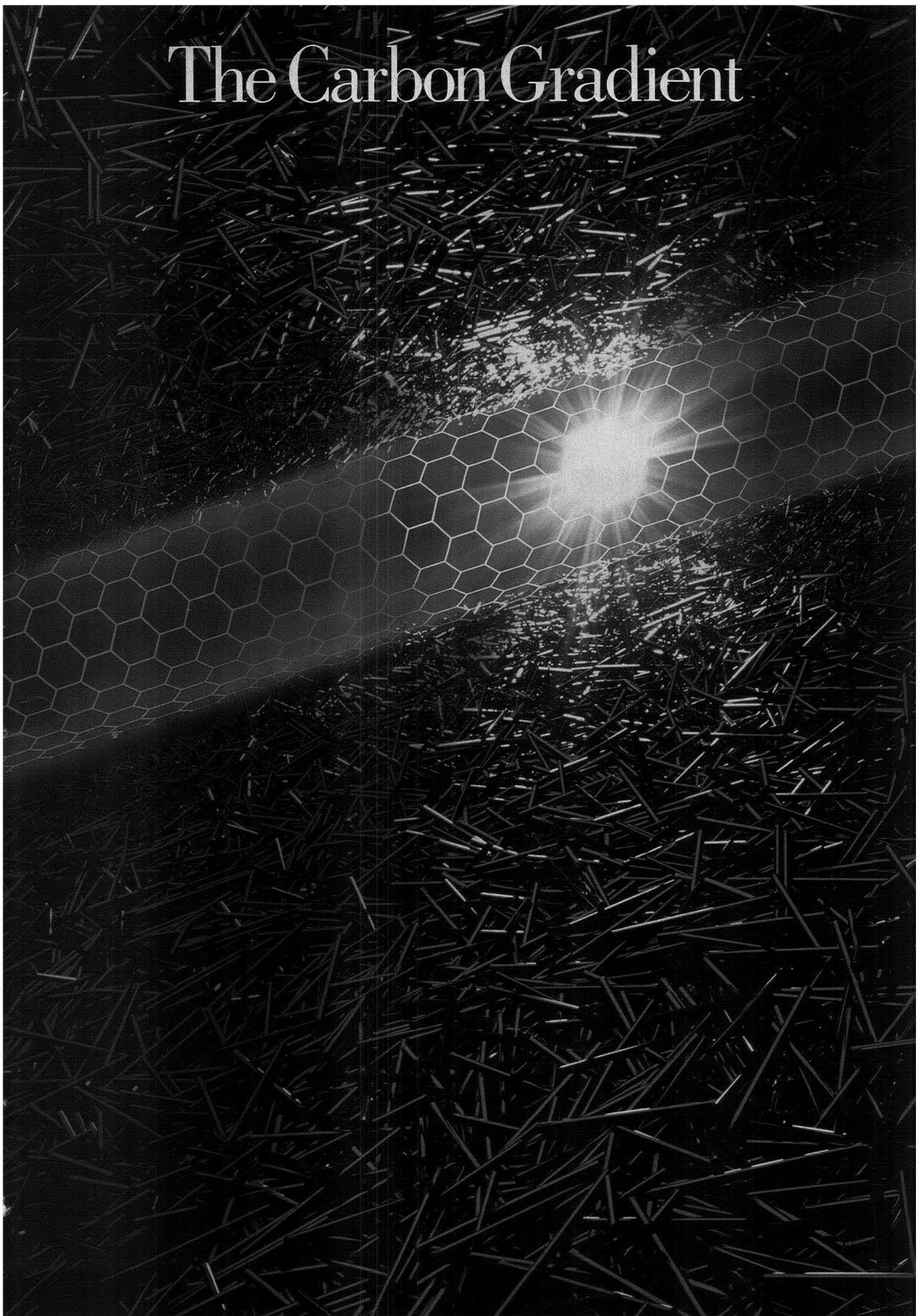
ACS Symposium Series No. 391 327 pages (1989) Clothbound
ISBN 0-8412-1610-X LC 89-6628 US & Canada \$69.95 Export \$83.95

Order from: American Chemical Society, Distribution Office, Dept. 22
1155 Sixteenth St., N.W., Washington, DC 20036

or CALL TOLL FREE **800-227-5558**
(in Washington, D.C. 872-4363) and use your credit card!



The Carbon Gradient



The Carbon Gradient

Hollow carbon filaments catalytically produced by submicron-size iron particles can be the template for larger carbon fibers used in composite structural materials. A scientist at the General Motors Research Laboratories has identified how these filaments grow and why they take their characteristic form.

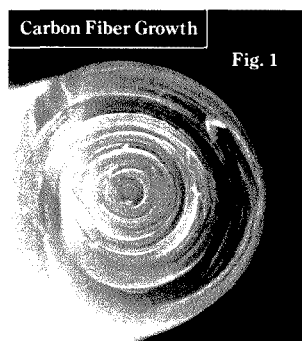


FIGURE 1: Scanning electron micrograph of a cross section of a vapor-grown carbon fiber.

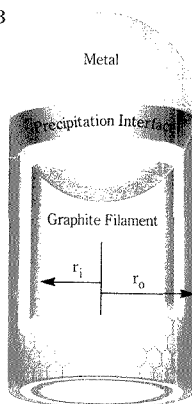
FIGURE 2: Typical carbon filament grown from natural gas by an iron catalyst particle.

FIGURE 3: Schematic model showing inner and outer radii, the precipitation interface, and the nested basal planes of the outer surface.

Fig. 2



Fig. 3



Dr. Gary Tibbetts was measuring the diffusion rate of carbon in iron when his carefully planned experiment took an unexpected turn. Dr. Tibbetts, a physicist at the General Motors Research Laboratories, had been introducing carbon to the inside surface of a hot stainless steel tube while extracting carbon from the outer surface.

At the end of one particular trial, he found the inside surface covered with a mass of black "whiskers." His initial investigations verified that the fibers were made of carbon and that they had characteristics typical of the crystal structure of graphite. But the question of how they formed was not so easily answered. The search for an answer would change the course of his investigation and dominate his research for the next ten years.

The fibers that surprised Dr. Tibbetts were made up of concentric layers primarily composed of basal (0001) plane graphite, resembling in cross section the annular rings of a tree (Figure 1). Research showed that they were formed by vapor deposition of carbon on a hollow central filament. The central filament itself was grown by catalytic action on a small metal particle (Figure 2).

These long, slender, uniform filaments had been widely observed since the availability of the electron microscope. Still, no valid explanation had been advanced to account for their hollow structure. Many scientists thought that surface diffusion of carbon-containing molecules around the catalytic particle caused the hollow core.

Instead, Gary Tibbetts proposed a model in which carbon atoms from decomposing hydrocarbons diffuse through the bulk of the catalytic particle and precipitate as graphite in the growing filament. The diffusion process is driven by the carbon gradient—the difference between carbon concentrations at the adsorbing surface of the particle and at its opposite, precipitating surface (Figure 3).

The exterior surfaces of these carbon cylinders expose the basal plane of graphite because the (0001) plane has a surface free energy at 970°C of about 77 erg cm⁻², while a typical surface perpendicular to the basal plane has a surface energy in excess of 4000 erg cm⁻². The free energy required for filament growth,

therefore, will be a minimum when the exterior surface is made up of basal planes—as observed in these filaments.

The entire filament, then, should consist of nested, rolled-up basal planes of graphite. Bending these planes into cylinders, however, requires that extra elastic energy be provided during the precipitation process. The core is left hollow because too much energy would be required to bend the planes near the axis into very small diameter tubes.

In describing the total energy necessary for filament formation, Dr. Tibbett's model takes into account the chemical potential change ($\Delta\mu_c$) when a carbon atom precipitates from the dissolved phase, as well as the energy required to form the surface, plus the energy needed to bend the basal planes into nested cylinders.

The change in chemical potential ($\Delta\mu$) driving the precipitation can be expressed as follows:

$$\Delta\mu = \Delta\mu_c - \frac{2\sigma\Omega}{r_o - r_i} - \frac{Ea^2\Omega}{12(r_o^2 - r_i^2)} \ln(r_o/r_i)$$

where σ is the energy required to form a unit area of (0001) graphite; Ω is the volume of a carbon atom in graphite; r_o and r_i are the outside and inside radii of the filament, respectively; E is the filament modulus; and a is the interplanar spacing.

A filament catalyzed by a particle of radius r_c will adjust its r_i to give the largest $\Delta\mu$ —in fact, r_i may be directly

calculated by maximizing $\Delta\mu$. Doing so yields results that compare nicely with experimental values.

Understanding the growth of the hollow core of the filaments was one key to producing them in abundance. "From there," says Gary Tibbetts, "it is a simple step to thicken the filament into a macroscopic fiber by vapor deposition of carbon on the exterior surface. The deposited carbon has a high degree of orientation parallel to the tube axis, giving the fiber exceptional stiffness.

"Fibers of this type should be excellent for making chopped-fiber composites using plastic, ceramic, metal, or cement matrices. GM's Delco Products Division is already building a pilot plant to develop a low-cost production process that would permit the use of vapor-grown fibers in high-volume applications."

General Motors



MARK OF EXCELLENCE



THE MAN BEHIND THE WORK

Dr. Gary G. Tibbetts is a Senior Staff Research Scientist in the Physics Department of the General Motors Research Laboratories.

Gary received his undergraduate degree in physics from the California Institute of Technology. He holds both an M. S. and a Ph. D. in the same discipline from the University of Illinois.

Dr. Tibbetts joined General Motors after two years of postdoctoral work as Guest Scientist at the Technical University of Munich. Since coming to the Labs in 1969, Gary has pursued interests ranging from carbon filaments, to surface physics, to chemical vapor deposition. He has published almost forty papers on the results of his research.

Gary is a member of the American Physical Society, the American Carbon Society, and the Materials Research Society. In 1988, he was a GM Campbell Award Winner. Gary lives in Birmingham, Michigan, with his wife and their three daughters.

NEW Pretested Capillary Column — Guaranteed to Work the Very First Time or Your Money Back!



If you analyze environmental samples for the semivolatile pollutants listed in US EPA Methods 625 and 1625, you can eliminate all risk by using our *PTE™-5 Fused Silica Capillary Column*.

Manufactured and tested to meet the highest analytical specifications, this column is *guaranteed* to work the first time you use it.

And every PTE-5 column must provide:

- Excellent inertness — we pretest it with highly reactive pollutants standards
- Consistently reproducible resolution — assured by monitoring film thickness and polarity
- Lowest bleed levels of any column in its class — less than 5 picoamps

If our PTE-5 capillary column should fail to perform as claimed, we'll refund your money in full or replace the column.

For more detailed information, call our Technical Service Department at 814-359-3041. To order your pretested and guaranteed PTE-5 capillary column, call us toll free:

800-247-6628
TWX: 510-670-3600
FAX: 814-359-3044



SUPELCO

SEPARATIONS TECHNOLOGIES GROUP
DIVISION OF ROHM AND HAAS

SUPELCO, INC. • Supelco Park • Bellefonte, PA 16823-0048 • Phone (814) 359-3441 and (814) 359-3446 • TWX 510 670-3600 • FAX 814-359-3044

CIRCLE 150 ON READER SERVICE CARD

1989-90 Division of Analytical Chemistry Fellowships

Nine analytical chemistry graduate students have been selected by the ACS Division of Analytical Chemistry to receive either full-year (\$9000) or summer (\$3000) fellowship awards. The fellowships are designed to encourage basic research in analytical chemistry and to recognize potential future leaders in the field.

Full-year fellowships were awarded to the following:



Kenneth Creasy of the University of Connecticut. Creasy's research, under the supervision of Brenda Shaw, focuses on the use of modified carbon composite electrodes in electroanalytical chemistry. His fellowship is sponsored by Procter and Gamble.



Randy Pell at the University of Washington in Seattle. Working with Bruce Kowalski, Pell is investigating IR emission spectroscopy for the monitoring of reactions and the subsequent data analysis using factor analysis methods. Perkin-Elmer is funding his fellowship.



James Gord from Purdue University. Gord, under the direction of Ben Freiser, is applying Fourier transform ion cyclotron resonance MS to the study of fundamental gas-phase processes. The Chemical Division of Eastman Kodak is supplying his fellowship.



Deborah Luffer of the University of Indiana. Luffer, supervised by Milos Novotny, is investigating specific solute-phase interaction in supercritical fluid chromatography. Her award is being supplied by Du Pont.

Summer fellowships were awarded to the following:



Patrick Treado from the University of Michigan. Treado, under the direction of Michael Morris, is developing Hadamard transform Raman microprobe spectroscopy. His fellowship is supplied by the Dow Chemical Corporation.



Raymond Sobocinski at the University of Arizona. Working with Jeanne Pemberton, Sobocinski is investigating Raman spectroscopic techniques to elucidate surface selectivity in studies using silver electrodes. The Pittsburgh Conference funds his fellowship.



Lyle Burton of the University of British Columbia, Vancouver. Burton's research, supervised by Michael Blades, deals with the effect of the sheath gas in inductively coupled plasma emission spectroscopy. His summer work is supported by the Pittsburgh Conference.



Kevin Litwiler from the State University of New York, Buffalo. Litwiler, under the direction of Frank Bright, is using fiber-optic probes to record excitation, emission, and phase-resolved visible and UV spectra of analytes. The Pittsburgh Conference provides his fellowship.



Steve Soper at the University of Kansas. Soper, supervised by Theodore Kuwana, is investigating spectroscopic properties of materials isolated in a supported matrix such as a TLC plate. He is also developing novel detectors for HPLC. His fellowship also comes from the Pittsburgh Conference.

In addition, honorable mentions go to Jani Cunningham Ingram of the University of Arizona, Jocelyn Dunphy of the University of Indiana, and Douglas Strong of Texas Tech University.

Color-coded Genes

Bioluminescence is emerging as a clever means to monitor genetic activity. Two years ago researchers at the University of California—San Diego introduced the gene for luciferase, the enzyme responsible for a firefly's glow, into tobacco plants. The same researchers have now taken genes for four other bioluminescent enzymes, each catalyzing a different colored luminescence, and successfully transplanted them into bacteria. Depending upon the gene, the bacteria can glow green, yellow, orange, or yellow-green.

A luminescence enzyme becomes a marker for genetic activity when its gene is coupled to another gene of interest. Expression of the latter gene also triggers the production of the enzyme. Addition of luciferin, which reacts with oxygen in the presence of ATP and luciferase-type enzymes, gener-

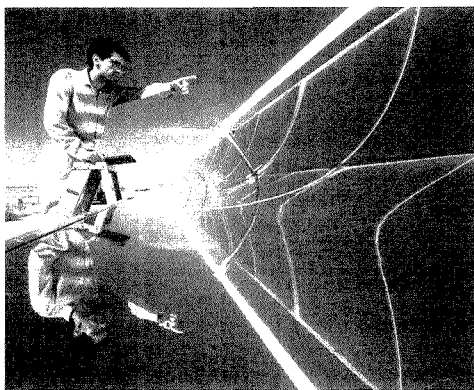
ates the chemical light. Because the new enzymes differ in their emission spectra, it would be possible to monitor several genes in this manner. Bioluminescence also can be used to track cells or genetically modified organisms.

The four marker genes were taken from the Jamaican click beetle, a firefly relative that emits light from an organ on the abdomen and a pair of organs on top of the head. Biologist William McElroy and the late biochemist Marlene Deluca began studying the beetle 30 years ago. "We measured the light with a spectrometer for the first time and found that this beetle emitted five or six different wavelengths of light," said McElroy. With the advent of the new genetic techniques, McElroy and chemists Keith Wood and Y. Amy Lam, along with biologist Howard Seliger from Johns Hopkins University, succeeded in isolating and sequencing the genes. They found the four genes to be 95%–99% homologous with each other, but, reflecting evolutionary distance, only around 50% homologous with firefly luciferase.

The Sun Shines on Pollutants

In a demonstration project, researchers from Sandia National Laboratory in Albuquerque, NM, have used sunlight to destroy salicylic acid in water. The experiment, claim the scientists, demonstrates that solar energy could be harnessed to remove organic pollutants such as PCBs or dioxins from polluted waters.

The Sandia process focuses sunlight concentrated to the equivalent of "30 to 60 suns" (about 500,000 W covering a 10-ft² surface) onto flowing water carrying TiO₂ as a photocatalyst. In less than 15 s, 30 ppm of salicylic acid was reduced to parts-per-billion levels.



Ultraviolet light initiates the process by kicking TiO₂ electrons into a conduction band and creating positively charged holes. The electrons and holes react with water, dissolved O₂, and added H₂O₂ to generate hydroxyl radicals and peroxide ions. These reactive species oxidize any dissolved organics to CO₂, water, and simple acids that can be neutralized.

In their demonstration project, the Sandia scientists pumped salicylic acid and catalyst mixture through either a long glass tube surrounded by a parabolic trough to focus the light (above), or over an 11-ft waterfall illuminated by up to 20 400-ft² heliostats (sun-tracking mirrors). The researchers also report that despite the intense solar light, flow rates of 20–70 gal/min kept temperatures below 70 °C.

Computer Chip Speeds DNA Analysis

California Institute of Technology's Center for the Development of an Integrated Protein and Nucleic Acid Biotechnology has adapted a text-searching data chip to identify patterns and similarities in DNA sequences.

Previously, "it took one day to compare a 10,000-bit gene to the preexisting data base on the Cray 2, and 10 days on a VAX," said Leroy Hood, the Center's head. "With the new technology it took 10 minutes."

Adapted by computer scientist Tim Hunkapiller at the Center, the new approach centers on TRW's Fast Data Finder chip, which is dedicated to handling only large amounts of data. The chip uses pipeline architecture, running microprocessors simultaneously to perform distinct functions at different points in the data stream. Performance in this parallel processing approach is limited by the data flow through the chip, up to 10⁶ bits of information per second. Hood's group has also written software for computer workstations, which they distribute free, to go with the chip.

For Your Information

The National Institute of Standards and Technology (NIST) and the Environmental Protection Agency have issued a **reference material kit for cotinine**, a major urinary metabolite of nicotine. Each kit contains cotinine in freeze-dried urine at blank, low, and high concentrations. NIST has also, along with the American Society for Testing and Materials, developed a **new standard for calibrating oxygen and nitrogen analyzers for the steel industry**. These gases trapped in steel contribute to the alloy's brittleness, affecting its strength and durability. The gas standard, in the form of a steel rod, and the cotinine kit can be obtained from the Office of Standard Reference Materials, NIST, B311 Chemistry Bldg., Gaithersburg, MD 20899 (301-975-6766).

Of the 389,685 chemically related journal articles, dissertations, conference papers, and reports **abstracted and indexed by Chemical Abstracts Service (CAS)** in 1988, the largest portion originated in the United States (27.4%), followed by the Soviet Union (13%), Japan (11.5%), and West Germany (6.3%). However, the Japanese patents accounted for a whopping 54% of the 80,795 patents CAS abstracted, whereas Europe contributed 10.3% and the United States a relatively small 6.9% share. These and related statistics are in the 1988 annual report, available from the CAS planning and communications department, 2540 Olentangy River Road, P.O. Box 3012, Columbus, OH 43210.

CAS has also announced an agreement with the French firm Télésystèmes, operator of the Questel online information service, and **Hampden Data Services, Ltd.**, a British developer of PC-based software, to develop chemistry-related software for search and retrieval applications. CAS and Télésystèmes will each acquire a 20% interest in Hampden Data Services.

Varian Associates, Inc. has agreed to purchase, for cash, Finnigan Corporation's technology and knowledge for the manufacture of ion trap mass detectors used in Varian gas chromatographs and to pay royalties on units manufactured under Finnigan patents. In return, Varian will serve as Finnigan's preferred supplier of certain chromatographs and related accessories that couple to mass spectrometers.

UV/VIS at its best – from the world leader. Perkin-Elmer.



Only Perkin-Elmer — the world leader in UV/VIS spectroscopy — gives you price/performance at its best. The Lambda 6 UV/VIS System blends exceptional value, performance, and flexibility into one affordable system.

PERFORMANCE AT ITS BEST

Only the Lambda 6 System delivers proven performance at such an attractive price. Double-beam design, low stray light, and low noise guarantee accurate spectroscopic results for quantitative, multiwavelength, and kinetic analyses.

SOFTWARE AT ITS BEST

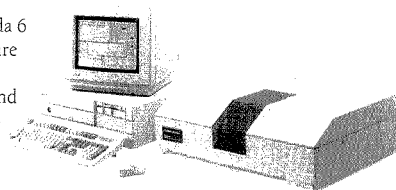
Our new UV Data Manager software is graphically oriented with pull-down menus, windows, an extensive HELP feature, and a mouse pointing device. It puts you in complete command of the instrument, accessories, and data processing routines without being a PC expert.

VERSATILITY AT ITS BEST

With the PC-controlled Lambda 6 System, data handling capabilities are never limited. Data can be quickly exported to third-party software. And with our powerful OBEY macrolanguage, you can write custom programs tailored to your lab needs.

FREE VIDEO OFFER

Send now for your free Lambda 6 System video — UV/VIS at its best. For more information and a free video, call 1-800-762-4000 or write Perkin-Elmer Corp., 761 Main Ave., Norwalk, CT 06859-0012 USA.



PERKIN ELMER

CIRCLE 129 ON READER SERVICE CARD

DIALOG INTRODUCES ANOTHER TABLE OF BASIC ELEMENTS FOR YOUR LAB.



There's no symbol for *information* in the Periodic Table. Yet nothing could be more crucial to your research than complete, accurate technical and business information.

That's why many chemists consider DIALOG[®] an essential element in the modern lab.

As the world's largest online knowledgebank, DIALOG gives you access to a whole world of critical information. Right in your own lab.

For starters, you can tap into the crucial scientific data. DIALOG has detailed information on everything from

compound identification to chemical safety data, property data, substance and substructure.

Then you can expand your focus by accessing important, related data that will enable you to look at your work in a broader context.

For example, you can investigate patents, competitive projects, new product markets, and worldwide industry trends. In fact, you can investigate any topic, anytime.

And you won't have to sacrifice depth for the sake of breadth. DIALOG is updated continuously, so the data is

always comprehensive and current. And many citations can be conveniently retrieved in full text.

Call today for more information and a free Periodic Table Reference Card. Once you've examined them, you'll see how DIALOG can become a basic element of all your research.

Call us toll free at 800-3-DIALOG, (800-334-2564). Or request information by Fax at 415-858-7069.

DIALOG INFORMATION SERVICES, INC.
A Knight-Ridder Company 

The world's largest online knowledgebank.

© 1989 Dialog Information Services, Inc., 3460 Hillview Avenue, Palo Alto, California 94304. All rights reserved. DIALOG is a service mark of Dialog Information Services, Inc. Registered U.S. Patent and Trademark Office.

CIRCLE 34 ON READER SERVICE CARD

Fluorescence Lifetime Filtering

Linda B. McGown
Department of Chemistry
P. M. Gross Chemical Laboratory
Duke University
Durham, NC 27706

State-of-the-art instrumentation has extended the frontiers of time-resolved spectroscopy to well below the nanosecond range, resulting in well-established techniques for studying the time dependence of fluorescence emission (1, 2). Although these techniques, in

REPORT

both time and frequency domains, have been widely applied in photophysical studies of chemical and biological systems, they have not often been used for chemical analysis. Recent demonstrations of convenience, accessibility, and applicability of fluorescence lifetime techniques, as well as the commercial availability of both time- and frequency-domain instruments, have generated increased activity and interest in this area (3).

Fluorescence lifetime "filtering" (4) refers to the selective viewing of fluorescence signals within a given lifetime range. By analogy with optical filtering, the filters can be described as long-pass, shortpass, or bandpass. In this REPORT, we will explore the different types of filtering used in the time and frequency domains and describe various applications of the filters for chemical analysis.

Fluorescence lifetime techniques

In the time-domain experiment, a sample is excited with a pulse of light at wavelength λ_{ex} . Assuming that the pulse is of negligible duration, the time-dependent fluorescence emission, $F(t)$, from a single component at wavelength λ_{em} , will exhibit monoexponential decay:

$$F(t) = F_0 e^{-t/\tau} \quad (1)$$

The initial intensity, F_0 , is a time-independent function of the fluorescence characteristics and concentration of the component, the intensity of the ex-

citation pulse, instrument response factors, and cell pathlength. The fluorescence lifetime, τ , is the mean excited-state lifetime, that is, the time at which the intensity equals $1/e$ of the initial intensity. For mixtures of components with different fluorescence lifetimes, excitation with an infinitely narrow pulse results in multiexponential decay curves, which can be analyzed by nonlinear least-squares methods to obtain the individual decay curves for each component.

In the frequency-domain experiment, the sample is excited with a continuous beam of monochromatic light that is modulated at a high frequency, ω . The excitation intensity, $E(t)$, consists of a time-independent (dc) component, A , and a time-dependent (ac) component, $m_{\text{ex}} \sin \omega t$:

$$E(t) = A m_{\text{ex}} \sin \omega t \quad (2)$$

The modulation depth, m_{ex} , is the ratio

of the ac amplitude to the dc intensity. Because of the finite lifetime of the excited state of the fluorescent compound, the emission signal, $F(t)$, will be phase-shifted by an angle ϕ and demodulated by a factor m relative to the exciting light:

$$F(t) = A' m_{\text{ex}} m \sin(\omega t - \phi) \quad (3)$$

The time-independent intensity, A' , is the frequency-domain analogue of F_0 in Equation 1.

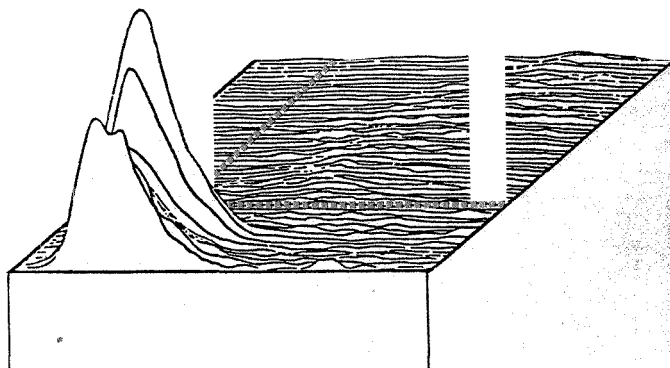
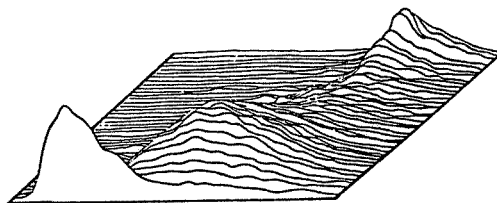
The fluorescence lifetime, τ , can be calculated independently from ϕ :

$$\tau_p = \frac{1}{\omega} \tan \phi \quad (4)$$

and from m :

$$\tau_m = \frac{1}{\omega} \left(\frac{1}{m^2} - 1 \right)^{1/2} \quad (5)$$

For mixtures of components with different fluorescence lifetimes, τ_m (ob-



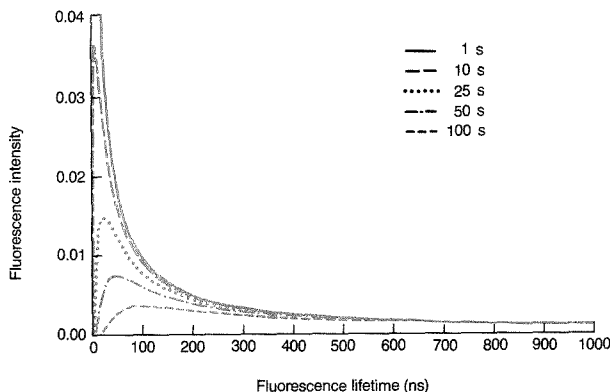


Figure 1. Time-resolved bandpass filters created at five different delay times.

served) $> \tau_p$ (observed), which is the frequency-domain equivalent of multiexponential decay. Lifetimes and intensity contributions of the individual components are obtained from heterogeneity analysis of multifrequency phase and modulation data, using either exact solutions or nonlinear least-squares analysis.

Time resolution and phase resolution

Ideally, a fluorescence lifetime technique for chemical analysis should provide a single measured quantity that is linearly dependent on concentration and linearly additive for multicomponent systems. The measured quantity should also be a function of both spectral and lifetime characteristics and of experimental variables or instrumental parameters that are directly controlled and can be continuously adjusted over an appropriately wide range of values. These requirements are satisfied in the time-domain experiment (Equation 1), in which the intensity $F(t)$ is a function of a single variable, time, which is a controlled parameter because $F(t)$ can be measured at any time following excitation. In the frequency domain (Equation 3), on the other hand, $F(t)$ is a function of both frequency, which is a controlled instrumental parameter, and time, which is a variable that cannot be directly manipulated in the experiment. However, it is possible to replace the time dependence with an adjustable phase parameter by phase-resolved fluorescence spectroscopy (PRFS).

In the PRFS experiment (1, 3), the ac component of $F(t)$ is multiplied by a periodic "on-off" function of the same frequency and integrated over time.

The resulting phase-resolved fluorescence intensity (PRFI) is given by:

$$\text{PRFI} = A' m_{\text{ex}} m \cos(\phi_D - \phi) \quad (6)$$

The detector phase angle, ϕ_D , refers to the phase of the periodic function, which is continuously adjustable from 0° to 360° . For a particular lifetime component with phase ϕ , the PRFI can range from the maximum magnitude of $A' m_{\text{ex}} m$, when ϕ_D equals 0° , to a minimum magnitude of zero when ϕ_D equals $\phi \pm 90^\circ$.

The dependence of PRFI on ω , ϕ_D , and τ is more clearly expressed by the following equation, derived by substitution of Equations 4 and 5 into Equation 6:

$$\text{PRFI} = A' m_{\text{ex}} \frac{\cos[\phi_D - \tan^{-1}(\omega\tau)]}{[(\omega\tau)^2 + 1]^{1/2}} \quad (7)$$

PRFS thus provides a total of four experimental parameters (λ_{ex} , λ_{em} , ω , and ϕ_D) in contrast to the three parameters (λ_{ex} , λ_{em} , and t) available in the time domain.

Fluorescence lifetime filters

Time and phase resolution can be compared by their fluorescence lifetime filtering capabilities—in other words, the ability to selectively view compounds as a function of their fluorescence lifetimes. In time-resolved techniques, selectivity is controlled by a single parameter, time. Time-domain techniques are, in a sense, shortpass filters (3–5), because the emission from shorter-lived components decays faster than emission from longer-lived components. However, it can be shown that the signal of the shorter-lived compo-

nent is already enhanced at $t = 0$, because F_0 (Equation 1) is proportional to $1/\tau$ (6). The result is a bandpass filter effect that passes through a maximum value at $t = \tau$. If we assume equal steady-state intensity for all components, the bandpass is described by plotting $1/\tau$ ($e^{-t/\tau}$) versus t at a given delay time, t (Figure 1). As t increases, the maximum shifts to longer τ values and the filter bandwidth increases. Integration over an appropriate t interval could also be used to enhance signals within a given τ range.

In PRFS, the two experimental parameters of detector phase angle (ϕ_D) and modulation frequency (ω) can be combined in various ways to achieve either shortpass or bandpass filtering effects. As shown in Figure 2a, the detector phase angle determines the form of the filter: A ϕ_D of 0° (in-phase with a zero lifetime component, such as scattered light) creates a shortpass effect; a ϕ_D of 90° (exactly out-of-phase with a zero lifetime component) creates an asymmetric bandpass effect; and any ϕ_D between these two extremes creates an intermediate effect. Other, less obviously useful effects can be generated when $\phi_D > 90^\circ$, limited by a shortpass effect involving negative PRFI when $\phi_D = 180^\circ$. The only effect that cannot be rigorously achieved is the longpass effect, although it can sometimes be approximated by using appropriate bandpass conditions.

Whereas ϕ_D determines the shape of the filtering effect, modulation frequency determines the lifetime range (i.e., the effective width of the filter). This is shown in Figure 2b for bandpass filters ($\phi_D = 90^\circ$), which shift to longer lifetimes and become less sharp as ω is decreased. Multifrequency phase-modulation instruments allow scanning of a particular filter type (defined by ϕ_D) over a wide range of lifetimes, thereby providing a continuous dimension of fluorescence lifetime selectivity that is readily combined with emission-excitation spectral dimensions, through measurements of PRFI (Equation 6).

The bandpass filter bandwidths at one-half peak maximum are $0.37 \tau_{\text{max}} - 4.31 \tau_{\text{max}}$, or $3.94 \tau_{\text{max}}$, for time resolution, and a slightly narrower $0.27 \tau_{\text{max}} - 3.73 \tau_{\text{max}}$, or $3.46 \tau_{\text{max}}$, for phase resolution. The phase-resolved shortpass filter extends from a maximum value at $\tau = 0$ to a value of one-half peak maximum at $\tau = 1/\omega$. For both time- and phase-resolved filters, resolution improves as fluorescence lifetime decreases (i.e., it is easier to resolve two short-lived signals with a given lifetime difference than two long-lived signals with the same lifetime difference). This

Reaching Perfection in MS and SEM.



*"A man's reach should
exceed his grasp..."*
Robert Browning

The small wonder of environmental research...

What the silicon chip did for the computer, Galileo high-performance detectors are doing for GC/MS, MS and SEM analysis. More scientific equipment manufacturers turn to Galileo for greater sensitivity, reliability, longer useful life and value.

Whether your project involves subsurface water movement from hazardous waste sites, fog water, surface water analysis, acid rain monitoring, site characterization, or general toxicology, a Galileo detector will speed sample identification while providing accurate and precise analysis.

When research projects require frequent sample analysis over a long period of time, you'll want the latest and best technology backing you up. Galileo is the innovator in analytical instrument detectors.

If you demand high performance and are concerned about instrument down time, rapid analysis, dynamic range and cost, insist on Galileo high-performance scientific detectors. You'll wonder how you ever got along without us. Galileo high-performance detectors are the heart of the instruments for Mass Spectrometry and Electron Microscopy.

Write us and ask how to ensure that your instruments have Galileo scientific detectors.

Galileo Electro-Optics Corp.
Scientific Detector Products Group
P.O. Box 550, Dept. A, Sturbridge, MA 01566
(508) 347-9191


GALILEO
Galileo Electro-Optics Corp.

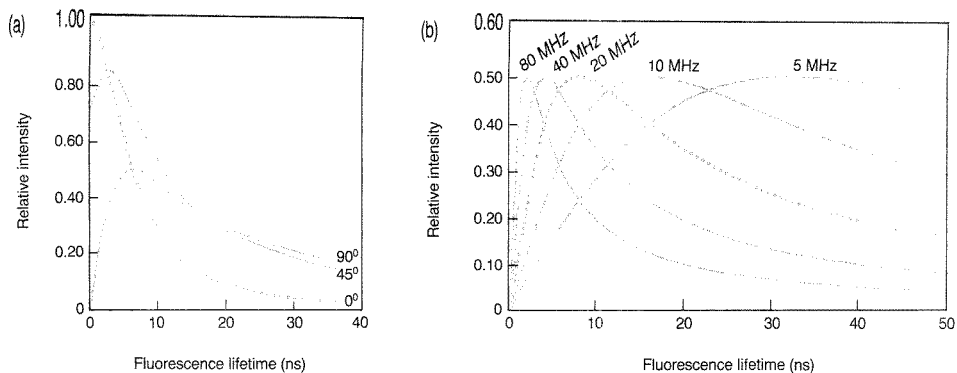


Figure 2. (a) Phase-resolved filters created at three different detector phase angles using a modulation frequency of 25 MHz. (b) Phase-resolved bandpass filters ($\phi_D = 90^\circ$) created at five different modulation frequencies. (Figure 2a adapted with permission from Reference 4.)

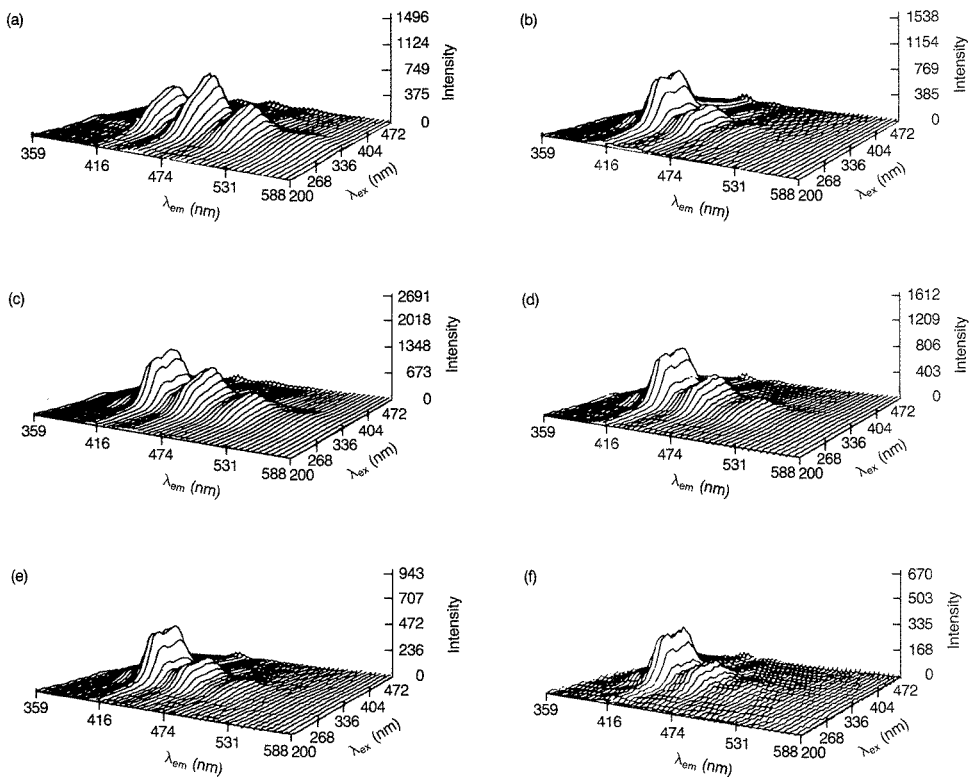


Figure 3. Phosphorescence EEMs of (a) phenanthrene and (b) triphenylene, and time-resolved phosphorescence EEMs of a mixture of the two, collected at delay times of (c) 0 s, (d) 5.5 s, (e) 12.5 s, and (f) 17.5 s. (Adapted from Reference 5.)

is reminiscent of the nonlinear dispersion provided by prisms in optical systems, which results in improved resolution at shorter wavelengths. Fluorescence lifetime filters are the basis of selectivity in any time- or frequency-domain experiment.

Applications of lifetime filtering

Excitation-emission matrices (EEMs). EEMs are matrix representations of intensity as a function of excitation wavelength on one axis and emission wavelength on the other. Fluorescence lifetime can be incorporated into the EEM in both time and frequency domains, extending the EEM data into a fourth dimension to produce three-way data arrays (intensity as a function of three independent variables: λ_{ex} , λ_{em} , and t or ω). In the time domain, each time-resolved EEM (TREEM) corresponds to a time following the excitation pulse. The intensity at a given emission-excitation wavelength point in the three-way array (Equation 1) decays through the stack of TREEMs according to the fluorescence lifetime characteristics of the sample. Time-resolved filtering in the TREEM format is shown in Figure 3 for the phosphorescence of a mixture of phenanthrene and triphenylene (7). The conventional, steady-state EEMs of the individual components show a high degree of spectral overlap. In the TREEMs, however, the long-lived triphenylene signal

is enhanced relative to the short-lived phenanthrene signal at long delay times, clearly illustrating time-domain selectivity.

The frequency-domain three-way array is composed of a stack of phase-resolved EEMs (PREEMs) collected at a series of modulation frequencies. The PRFI at each emission-excitation wavelength point in the PREEM array varies through the stack according to Equation 7. Phase-resolved filtering is demonstrated in Figure 4 for a mixture of benzo[*k*]fluoranthene (BkF, $\tau = 7$ ns) and benzo[*b*]fluoranthene (BbF, $\tau = 29$ ns) (5, 8). The PREEMs were collected with ϕ_D set to suppress scattered light, resulting in the bandpass filtering effect. The longer-lived BkF emission dominates the low-frequency (6 MHz) PREEM, and the shorter-lived BbF emission dominates the high-frequency (30 MHz) PREEM.

Factor analysis can be applied to both TREEM and PREEM arrays to extract the spectra of the individual components (8, 9). An important feature of the three-way array is the uniqueness of the extracted spectra. Factor analysis of a two-way array, which has been well described for EEMs, generates a set of eigenvectors that are ambiguously related to particular solutions in the spectral domain. Constraints such as nonnegativity of spectral intensity must be imposed to define a subset of reasonable solutions.

The addition of the independent dimension of fluorescence lifetime in a three-way array leads to a unique solution in the spectral domain, within the limitations imposed by spectral noise.

The EEM format has been applied recently to the characterization of complex samples whose spectra contain fluorescence from multiple components with complicating factors such as synergism, interferences, matrix effects, and distribution of the fluorescent molecules between different microenvironments in the sample (3). Often it is not necessary or even desirable to approach the study of such samples with the goal of identifying and quantifying every fluorescent component in the sample. Instead, we may wish to examine the intact sample as a whole that is more than the sum of its components in order to fingerprint the sample, identify patterns relating to its classification, or study the dynamic intermolecular interactions between its components. Fluorescence lifetime filtering is a powerful addition to such studies because it enables us to effectively "scan" spectral features as a function of fluorescence lifetime. For example, it can be used to enhance particular features that are good discriminators between samples but minor contributors to the total luminescence, or to characterize samples by the lifetime distribution of the spectral features. Processes such as quenching, complex-

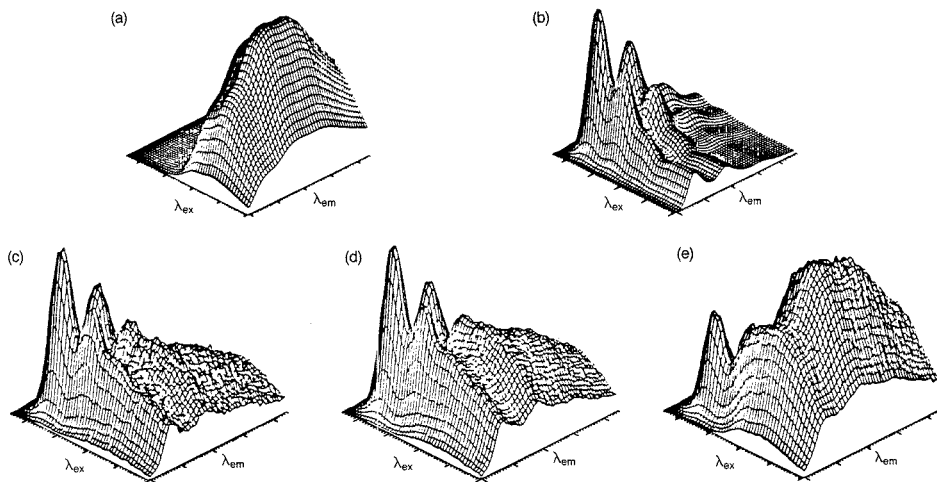


Figure 4. Fluorescence EEMs of (a) benzo[*b*]fluoranthene and (b) benzo[*k*]fluoranthene, and phase-resolved EEMs of a mixture of the two, collected at modulation frequencies of (c) 30 MHz, (d) 18 MHz, and (e) 6 MHz. (Adapted with permission from Reference 7.)

Find it FAST in the LabGuide

The *LabGuide* is where more than 140 suppliers say, "Here we are. Compare our products with those of our competitors." For example, you'll find typical product line ads in the current *LabGuide* from the following firms:

Advertisers	Pages
ACE GLASS	131
ALLTECH	62
BLUE M	181
CHEMICAL DYNAMICS	197
CONOSTAN	27-28
ELDEX	143
FLUKA CHEMICAL	205
GILMONT	111
GRAPHIC CONTROLS	147
HAMMOND DRIERITE	205
HOTPACK	99
ISCO	63
LABCONCO	145
MILTON ROY/APD	37
NEYTECH/J.M. NEY	101-175
OMEGA	IFC
PHARMACIA LKB	65
RUDOLPH RESEARCH	113
SHIMADZU	53
SWAGelok	76-77
UIC INC.	101
VALCO	141
WHEATON	99, 119

The *LabGuide* is your true one-stop buying source for scientific products.

REPORT

ation with macromolecules, and excited-state complex formation can be studied for subsets of the fluorescent components that fall within a given lifetime range.

Suppression of interfering signals. The minimization of unwanted signals is inherent to the concept of filtering. In time-resolved experiments, gated detection can be used to reduce the contribution of short-lived interfering signals to the measured intensity. In phase-resolved experiments, interfering signals that are either longer- or shorter-lived than the desired signal can be relatively suppressed in several ways: by setting the detector phase to be out-of-phase with the interfering

signal, by using a modulation frequency at which the interfering signal is greatly demodulated, or by combining detector phase and modulation frequency.

Longpass filters in the time domain are ideal for certain applications in which the desired signal is much longer-lived than the background signal. For example, scattered light interferences can be greatly reduced, improving signal-to-scattering ratios by more than twofold for short-lived ($\tau = 0.7$ ns) fluorescence and by sixfold for longer-lived fluorescence signals (10). Detection limits can also be improved for compounds with very long-lived emission, such as lanthanide chelates ($\tau =$

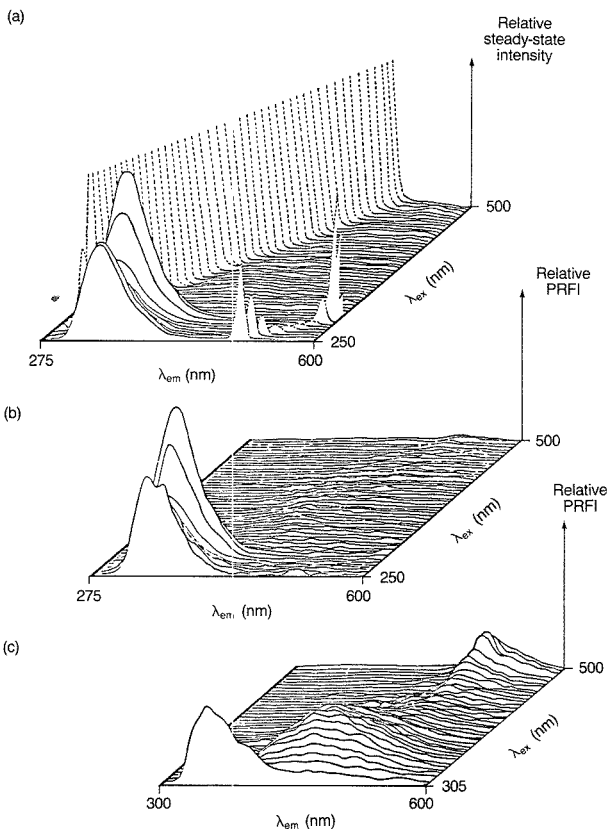


Figure 5. Fluorescence EEMs of pooled serum.

(a) Steady-state EEM of a 20-fold dilution, showing scattered light peak (extending well off-scale) at the rear and second-order scattered light in the foreground; (b) PREEM of the same solution, collected at 30 MHz, with scattered light signal suppressed; and (c) PREEM of a fivefold dilution of the serum at 30 MHz, corresponding to the right rear quadrant of the EEMs in (a) and (b).

(Adapted with permission from Reference 14.)

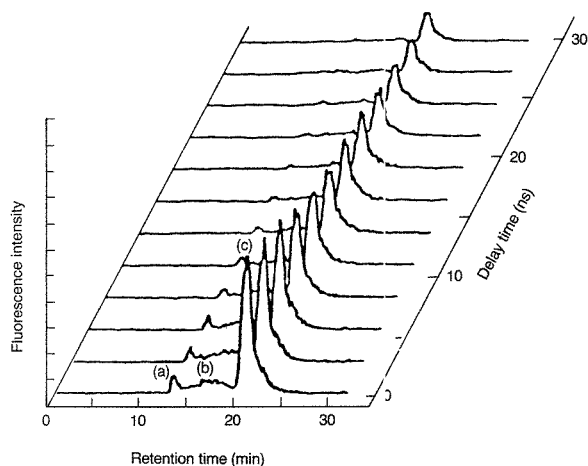


Figure 6. Time-resolved chromatograms for ANS-labeled proteins in human serum, collected at a series of delay times.

(a) α -globulin, (b) γ -globulin, (c) albumin. (Adapted with permission from Reference 16.)

10^{-6} – 10^{-3} s), by eliminating short-lived background signals. This type of application has been particularly useful for clinical immunoassays, in which gated detection is used to measure the fluorescence intensity of lanthanide-labeled antigen after the interfering background fluorescence from the biological sample has decayed (11). Another example is the use of a dye with long-lived emission for the imaging of fingerprints on surfaces such as wood, masking tape, polyethylene, or metal (12, 13).

Phase-resolved suppression of scattered light is shown in Figure 5 for the EEM of pooled human serum (14). In the steady-state EEM (Figure 5a), a broad spectral region is obscured by the large scattered light peak, reducing the spectral information and precluding the use of higher concentrations of the serum. The scattered light is essentially eliminated in the PREEM of the same solution (Figure 5b), thereby introducing the possibility of measuring higher concentrations of the serum. The PREEM shown in Figure 5c was obtained from a fivefold dilution of the same serum and corresponds to the visible region (upper right-hand quadrant) of the EEMs shown in Figures 5a and 5b. It is clear that the higher intensity from the more concentrated solution greatly enhances the ability to discern spectral features in the visible region.

Chromatographic detection. Time-resolved chromatograms can be collected (after a suitable delay time) to enhance the analyte signals relative to background signals, such as those attributable to fluorescent impurities in the solvent, Raman scattering by the solvent, scattered light from the flow cell, and the excitation pulse itself. The optimal delay time for a particular experiment will depend on the decay characteristics of both the background signal and the fluorescent analytes; a long delay maximizes the reduction of the background but also reduces the intensity of the analytes, because all of the signals decay with time. Chromatograms can also be collected at a series of delay times (15, 16), as shown in Figure 6 for the elution of proteins in human serum labeled with 1-anilino-8-naphthalene sulfonate (ANS).

Phase-resolved chromatograms can be collected with the detector phase angle set to suppress background signals that can be either longer- or shorter-lived than the analytes. Chromatograms can also be collected at a series of modulation frequencies, using the bandpass effect, to selectively enhance peaks from components with short-, medium-, and long-lived fluorescence. Phase-resolved chromatograms are shown in Figure 7 for a mixture of six fluorescent components, several of which were only partially separated (17). The relatively long-

COMPARE THE BETTER MULTI-CHANNEL MICROPIPETTE

- **Better Performance** —
Swiss precision tolerances
— accuracy and CV
guaranteed to better than
 $\pm 1\%$
- **Better Quality** —
Individually tested and
inspected — supplied with
verified calibration
certificate
- **Better Design** —
Comfortable to operate,
easy-to-read precision
setting — internal
detipping mechanism
maintains narrow profile
- **Better Value** —
Wheaton multi-channel
micropipettes provide
better performance, better
accuracy, and better price
value than any other

WHEATON

WHEATON

Manufacturers Since 1888

1501 N. Tenth Street
Milville, NJ 08332, USA
Call Toll-Free: 1-800-225-1437
Ext. 2557
TLX: 55-1295 (WHEATON US)
FAX: 1-609-825-1368

CIRCLE 174 ON READER SERVICE CARD

Expect more from FisherChemical Optima™ Acids and TraceMetal Acids ...and get less:



**Less aluminum, less cadmium,
less lead, less mercury...**

Move up to Fisher acids

Why settle for "high purity" when you can get the world's highest purity? Choose the acids that offer the most by providing the least: FisherChemical Optima Acids for the lowest metal content and highest purity available anywhere...and FisherChemical TraceMetal Acids, for exceptionally low metal content and incomparable value.

Fisher Optima Acids— The first acids good enough to be Optima

FisherChemical's new Optima Acids offer the lowest metal content of any acids available. Most metals are present in concentrations of less than one part per billion, and many are in the parts per trillion range, as indicated on the certificate of analysis supplied with each bottle. Optima Acids are the obvious choice for environmental testing, plasma analysis, electronic research...any application that demands the utmost purity and precision.

Each step in the creation of Optima Acids ensures the lowest level of metals in the acids you receive. Optima Acids are double-distilled in Teflon* or pure quartz stills at temperatures below the boiling point of the acid, then

packaged in Teflon bottles that have undergone a hot acid leaching process. And every stage of production and packaging takes place in Class 100 clean room environments.

Fisher TraceMetal Grade Acids—exceptional value FisherChemical's new TraceMetal Acids provide extraordinary purity at a lower cost and are ideal for many applications that require extremely low metal content. TraceMetal Acids are produced with low metal content in mind; the competition's so-called "metal-analyzed acids" are simply lot-selected ACS acids. TraceMetal Acids far surpass the purity of these products...and in fact are as pure as, or even purer than, many competitors' top-of-the-line acids...yet cost considerably less.

Careful sub-boiling distillation...ICP analysis... specially-treated containers designed to maintain exacting specifications...and a Certificate of Analysis with each bottle are the keys to TraceMetal Acid purity.

Select Optima or TraceMetal Acetic, Hydrochloric, Hydrofluoric, Nitric, Perchloric, Sulfuric Acids and Ammonium Hydroxide.

*Teflon is a registered trademark of E. I. du Pont de Nemours & Co., Inc.

Expect more from FisherChemical



FisherChemical

Fisher Scientific

Excellence in Serving Science...Since 1902

CIRCLE 50 ON READER SERVICE CARD

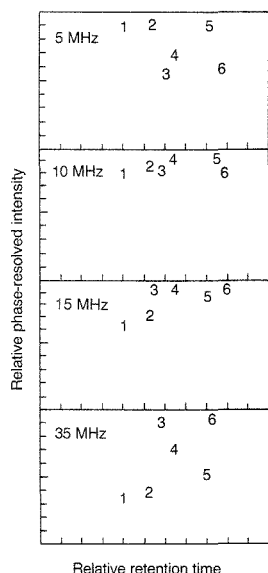


Figure 7. Phase-resolved chromatograms for a mixture of six compounds at modulation frequencies of 5, 10, 15, and 35 MHz.

lived fluorescence of peaks 1 and 2 decreases as modulation frequency increases, the intermediate lifetime fluorescence of peaks 4 and 5 is maximized around 10 MHz, and the short-lived fluorescence of peaks 3 and 6 increases with increasing frequency.

Future developments

To date, time resolution has been applied primarily in methods that use reagents with long-lived fluorescence emission to minimize background interferences from intrinsic, short-lived signals. Explorations of phase resolution, on the other hand, have focused on the systematic enhancement of both short- and long-lived signals in multi-component systems. Both techniques may greatly improve the resolution and accuracy of multicomponent analysis, chromatographic detection, spectral fingerprinting, various immunochemical and bioanalytical methods, and any other area in which luminescence analysis is limited by chromatographic or spectral resolution.

References

(1) Lakowicz, J. R. *Principles of Fluorescence Spectroscopy*; Plenum Press: New York, 1983.

(2) Demas, J. N. *Excited State Lifetime Measurements*; Academic Press: New York, 1983.
 (3) McCown, L. B. *Prog. Analyt. Spectrosc.* 1988, 11, 383.
 (4) McCown, L. B.; Millican, D. W. *Appl. Spectrosc.* 1988, 42, 1084.
 (5) Mill can, D. W.; McGown, L. B. *Anal. Chem.* 1989, 61, 580.
 (6) Love, L.J.C.; Upton, L. M. *Anal. Chem.* 1980, 52, 496.
 (7) Ho, C.-N.; Warner, I. M. *Anal. Chem.* 1982, 54, 2486.
 (8) Burdick, D. S.; Tu, X. M.; McGown, L. B.; Millican, D. W. *J. Chemom.* 1989, 3, 431.
 (9) Russell, M. D.; Gouterman, M. *Spectrochim. Acta* 1988, 44A, 857.
 (10) Russo, R. E.; Hieftje, G. M. *Anal. Chim. Acta* 1982, 134, 13.
 (11) Ekins, R. P.; Dakubu, S. *Pure Appl. Chem.* 1985, 57, 473.
 (12) Menzel, E. R. In *SPIE Proceedings, Society of Photo-Optical Instrumentation Engineers*; Bellingham, WA, 1988; Vol. 910, pp. 45-51.
 (13) Menzel, E. R. *Anal. Chem.* 1989, 61, 557 A.
 (14) Nithipatikom, K.; McGown, L. B. *Appl. Spectrosc.* 1987, 41, 1080.
 (15) Furuta, N.; Otsuki, A. *Anal. Chem.* 1983, 55, 2407.
 (16) Kavabata, Y.; Sauda, K.; Imasaka, T.; Ishibashi, N. *Anal. Chim. Acta* 1988, 208, 255.
 (17) Cobb, W. T.; McGown, L. B.; Duke University, unpublished results.



Linda B. McGown is an associate professor of chemistry at Duke University. She received her B.S. degree in chemistry from the State University of New York at Buffalo in 1975 and her Ph.D. in chemistry from the University of Washington in 1979. Her current research interests include fluorescence lifetime selectivity in chemical analysis, on-line fluorescence lifetime measurements for chromatographic detection, statistical methods of analysis for noisy data and multiway data arrays, and the characterization and analytical applications of highly organized micellar media and lyotropic liquid crystalline phases.

There are 224 reasons why...

most chemists in the U.S. belong to the American Chemical Society.

The fact is, there are more than 137,000 chemists in this vital, career-enhancing society — *the largest scientific organization in the world!* To learn those reasons, write, use coupon or CALL TOLL FREE 1-800-ACS-5558

American Chemical Society, 1155 Sixteenth St., NW, Washington, DC 20036

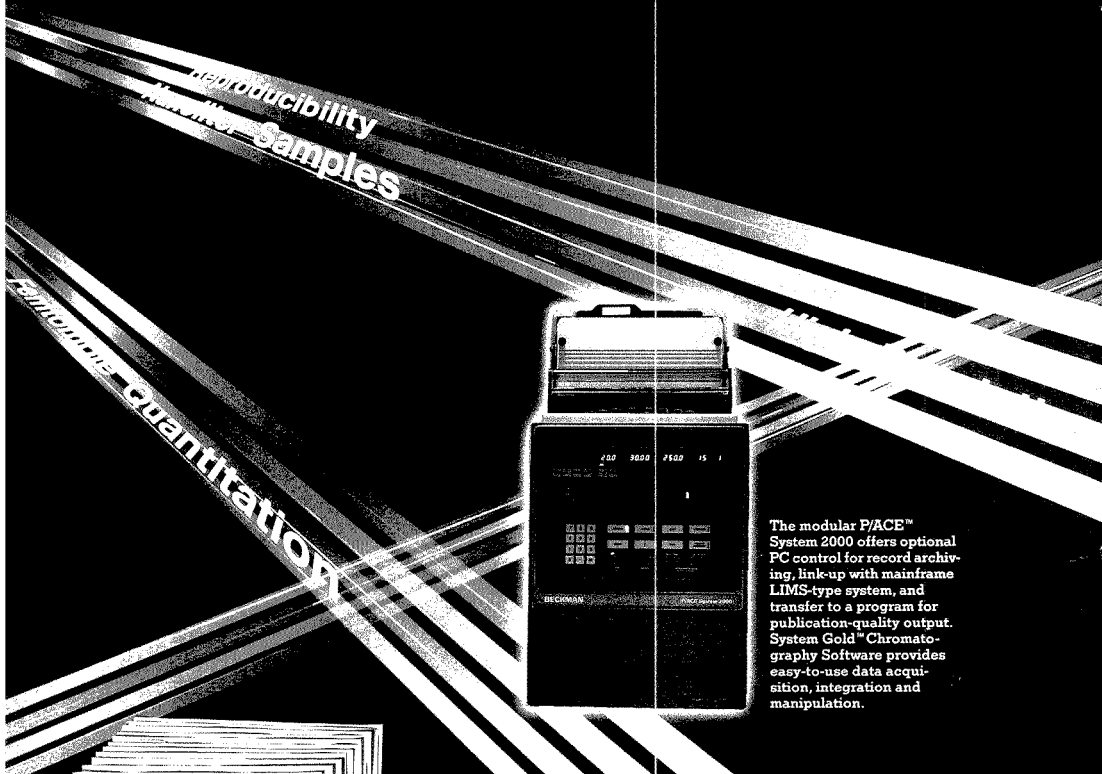
Yes! I would like to know 224 reasons to join the American Chemical Society. Please send free brochures to:

Name _____

Address _____

City, State, ZIP _____

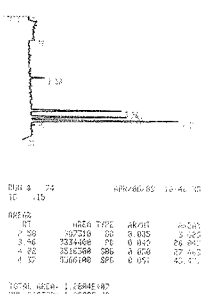
Beckman Sets the P/ACE for Automated Electrophoretic Separations...



Reproducibility
Minimal Samples

Automated Quantitation

The modular P/ACE™ System 2000 offers optional PC control for record archiving, link-up with mainframe LIMS-type system, and transfer to a program for publication-quality output. System Gold™ Chromatography Software provides easy-to-use data acquisition, integration and manipulation.



Shows 11 injections in 90 min from a total sample of 5 μ L, accomplished with P/ACE™ Migration time CV less than .25%.

The P/ACE™ System 2000 from Beckman is designed for today and tomorrow. A modular system, P/ACE leads the evolution of capillary electrophoresis.

A removable detector allows multiple future detection options. Interchangeable cartridges let you change capillaries in minutes. Temperature control provides unmatched reproducibility. And sealed vials minimize sample evaporation. All unique to P/ACE. Unique too—the surprisingly affordable price.

Keep P/ACE with the latest in electrophoretic separation techniques! And achieve rapid success separating proteins, peptides, synthetic oligonucleotides, DNA fragments, and more. Call 800/742-2345, or write to Beckman Instruments, Inc., Spinco Division, Customer Service Department, 1050 Page Mill Rd., Palo Alto, CA 94304. Offices in major cities worldwide.

BECKMAN
A SMITHKLINE BECKMAN COMPANY

Eastern Analytical Symposium

The 28th Eastern Analytical Symposium (EAS) will be held at the New York Hilton Hotel in New York City, Sept. 24-29. The meeting is sponsored by the New York and North Jersey sections of the American Chemical Society; the American Microchemical Society; the Delaware Valley, New England, and New York sections of the Society for Applied Spectroscopy; and the New York Microscopical Society.

Thirty-eight oral and three poster sessions will be held Monday, Sept. 25 through Thursday, Sept. 28. Session topics include the following:

- advances in instrumental TLC
- analytical characterization of proteins, peptides, and nucleotides
- advances in near-IR and vibrational spectroscopy
- expert systems
- environmental MS
- laboratory information management systems
- DNA fingerprinting
- biomedical analysis
- forensic science
- chemometrics and automation in the analytical laboratory
- drugs—trace analysis in athletes
- supercritical fluid extraction
- experimental NMR methods
- biochemical applications of capillary electrophoresis
- molecular spectroscopy
- microscopy—applications, techniques, and instrumentation
- pharmaceutical analysis

Five symposia will honor this year's award recipients. David Hercules will receive the EAS Award for Outstanding Achievements in the Fields of Analytical Chemistry on Thursday, Sept. 28. The EAS Award in Chromatography will be presented to Harold McNair at a symposium on Monday, Sept. 25. On Wednesday, Sept. 27, the New York Society for Applied Spec-

troscopy Medal will be presented to James Winefordner. This year's American Microchemical Society's Benedetti-Pichler Award will be presented to K. L. Cheng on Thursday, Sept. 28. The EAS Award for Achievements in Near-Infrared Spectroscopy will be presented for the first time this year. Karl Norris will receive this award at a symposium on Tuesday, Sept. 26.

An exposition of scientific instruments and supplies will also take place in the New York Hilton. In addition, 10 workshops sponsored by exhibitors will be offered on the following topics: HPLC detection, FT-IR, preparative LC of proteins and peptides, elements of chiral chromatography, capillary GC, SFC, laboratory robotics, chromatography automation, modern TLC, and strategic planning for employment. Those interested in preregistering should use the form on p. 851 A. For further information on the workshops, contact Vincent Venturella, Anaquest/BOC Group, 100 Mountain Ave., Murray Hill, NJ 07974 (201-771-6392).

The American Chemical Society will sponsor six short courses in conjunction with the meeting: Environmental Laboratory QA/QC Data Validation, Quality Assurance of Chemical Measurements, Analytical Laboratory Operations—Analysis of Water and Waste Samples, Laboratory Applications of Lotus 1-2-3 and Other Software—Beyond the Basics, Experimental Design for Productivity and Quality in R&D, and Laboratory Information Systems—from Problem Definition to System Evaluation. Additional information on these courses is on p. 855 A of this issue.

Eleven EAS-sponsored short courses will also be offered: Analytical Capillary Electrophoresis, Bioanalytical Chemistry, Solid-State NMR Spectroscopy, Application of Mass Spec-

trometry to the Analysis of Biopolymers, Applications in Supercritical Fluid Extraction, Advanced HPLC for the Practicing Chromatographer, Methods and Principles of 2D NMR, Automated Instrumentation for Supercritical Fluid Technology, Role of Modern X-ray Diffraction Techniques in Chemical and Structural Analysis, Near-IR Analysis: In the Plant and in the Laboratory, and Professional Analytical Chemists in Industry—What Does an Analytical Chemist Do? (free course for undergraduate chemistry majors). Additional information about the first 10 courses can be obtained from James Russell, E.I. du Pont de Nemours & Co., Central Research & Development Dept., Glenolden Laboratory, 500 S. Ridgeway Ave., Glenolden, PA 19036 (215-237-7859). For details about the professional analytical chemists course, contact Alan Ullman, Procter & Gamble, Winton Hill Technical Center, 6250 Hill Road, Cincinnati, OH 45224-1796.

An employment service will be available during the meeting. For details, contact Jennifer Feldman, Bausch and Lomb, 1400 N. Goodman St., P.O. Box 450, Rochester, NY 14692 (716-338-6424).

The EAS has reserved a block of rooms for conferees at the New York Hilton. To obtain special conference rates, rooms must be reserved through the EAS. Reservation forms can be obtained from Kenneth Fleischer, RD #3, Box 730, Valatie, NY 12184 (518-758-6431).

To preregister, send the completed form on p. 851 A to EAS Registration, P.O. Box 633, Montchanin, DE 19710. Preregistration forms must be postmarked by Sept. 8. For further information about the meeting, contact the EAS at the address above or call 302-453-0785.

Symposium Officers

General Chairman: Richard Saferstein, NJ State Police
Chairman-Elect: James McDivitt, Ethicon
Past Chairman: Harvey S. Gold, Du Pont Polymer Products
Secretary: Julia Vasta-Russell, Du Pont Medical Products
Treasurer: Stephen Scypinski, Berlex Laboratories
Archives Chairman: Marty Hackman, Anaquest/BOC Group
Arrangements Chairman: Neil Jespersen, St. John's University
At-Large: Evelyn Sarnoff, U.S. FDA; Hal Ferrari
Awards Chairman: Karl Bratin, Pfizer
Direct Mail Chairman: Edward R. Davis, Du Pont Polymer Products
Employment Chairman: Jennifer Feldman, Bausch and Lomb
Exposition Director: Robert W. Baudoux, RWB Convention Management
Exposition Chairman: Concetta Paralusz, Permacel, A Nitto Denko Co.
Housing Chairman: Genevieve Bonini
Legal Chairman: J. P. Luongo, AT&T Bell Laboratories
Long-Range Planning Chairman: James McDivitt, Ethicon
Message Center Chairman: William Taraszewski, Pfizer
Parliamentarian: Kenneth D. Fleischer
Printing Chairman: David Nash, AT&T Bell Laboratories
Program Chairman: Haleem J. Issaq, Program Resources
Publicity Chairman: Al Bober, Maryland Dept. of Health
Registration Chairman: Irene Nurkiewicz
Short Courses Chairman: Jim Russell, Du Pont Central Research
Special Functions Chairman: Arthur Coates, Polaroid
Technical Films Chairman: Robert Weinberger, ABI/Ramsey Analytical
Workshops Chairman: Vincent Venturella, Anaquest/BOC Group

Program

MONDAY MORNING

Advances in Instrumental TLC

Chairman: C. F. Poole, Wayne State U

- 8:45 Stationary Phases in Modern Planar LC—Characteristics and Fields of Application. **W. Fischer**, H. E. Hauck, and M. Mack, E. Merck & Co.
- 9:15 Clinical and Pharmaceutical Applications of Instrumental High-Performance TLC. **H. J. Issaq**, Program Resources
- 9:45 TLC from an Academic Perspective. **C. F. Poole** and S. K. Poole, Wayne State U
- 11:00 Increased Resolution in Planar Chromatography at Subambient Temperatures. **J. C. Touchstone**, S. U. Sheikh, J. G. Alvarez, X. Fang, and S. S. Levin, U of Pennsylvania
- 11:30 Application of High-Performance TLC Techniques To Evaluate the Flavor Quality of Orange Juice. **K. Y. Lee** and R. L. Wade, Procter & Gamble

Frontiers of Molecular Spectroscopy

Chairman: H. S. Gold, E. I. du Pont de Nemours & Co.

- 8:45 Hadamard Transform Spectrometry. **W. G. Fateley**, A. P. Bohlke, J. D. Tate, J. White, R. M. Hammaker, and B. Streusand, Kansas State U

- 9:25 Surface Raman Spectroscopy in the Study of Electrochemistry. **J. E. Pemberton**, R. L. Sobocinski, D. A. Carter, and M. A. Bryant, U of Arizona
- 10:40 Molecular Fluorescence HPLC Detection of Liquid Crystals. **L. B. McGown**, Duke U
- 11:20 Time-Resolved Molecular Fluorescence and Raman Spectroscopy. **M. J. Wirth**, J. Burbadge, and S-H. Chou, U of Delaware

High-Resolution Chromatographic Techniques—EAS Chromatography Award Symposium

Chairman: S. Cram, Hewlett-Packard

- 8:45 Presentation of the EAS Award for Achievements in the Field of Chromatography to Harold M. McNair by R. Saferstein.
- 8:50 Award Address. Milestones in High-Resolution GC. **H. M. McNair**, Virginia Tech
- 9:20 Applications Using Hyphenated SFC Techniques. **M. L. Lee**, Q. L. Xi, I. J. Koski, C.H.J. Sin, Z. Juvance, W. P. Vorkink, C. A. Rouse, and K. E. Markides, Brigham Young U
- 9:50 Advances in Multidimensional Chromatography. **J. V. Hinshavh**, Perkin-Elmer
- 11:00 Extending High-Resolution GC. **R. D. Dandeneau** and K. Klein, Hewlett-Packard
- 11:30 High-Speed Narrow-Bore Capillary GC with Heat Conductivity, Photoionization, and Mass Spectrometric Detection. **C. Cramers**, A. van Es, J. Rijks, and P. Leclercq, Eindhoven U of Technology

Analytical Characterization of Proteins, Peptides, and Nucleotides

Chairman: W. Taraszewski, Pfizer

- 8:45 Preliminary Evaluation of a Microwave-Assisted Acid Hydrolysis Technique for Peptides on Thin-Layer Plates. **Y. Du**, M. Brassard, C. Ajello, and D. C. Shelly, Stevens Institute of Technology
- 9:05 High-Speed Liquid Chromatographic Determination of Cardiac Adenine Nucleotides and Their Metabolites. **K.-J. Yu**, D. DeWitt, and D. C. Shelly, Stevens Institute of Technology
- 9:25 Flow-Injection Analysis of Proteins Using Enhanced Peroxyoxalate Chemiluminescence. **M. L. Grayeski** and R. M. de Lavalley, Seton Hall U
- 9:45 FT-IR Studies of Electropolymerized Films Containing Immobilized Proteins. **T. Chou**, T. Rush, III, and D. C. Shelly, Stevens Institute of Technology
- 10:40 Multidimensional Analysis of Peptides and Proteins Using Column-Planar Separations and Chemistries. **M. Brassard**, Y. Du, and D. C. Shelly, Stevens Institute of Technology
- 11:00 Microcolumn Liquid Chromatographic Analysis of Oligonucleotides. **J. J. Ruslik**, J. C. Bigelow, and J. J. McCormack, U of Vermont
- 11:20 Rapid HPLC of Nucleic Acids on Micropellicular Octadecyl Silica. **D. Corradini**, L. Cellai, and M. Cirelli, Institute of Chromatography
- 11:40 Factors Influencing the Performance of Tryptic Mapping by Reversed-Phase LC. **M. W. Dong** and A. D. Tran, Perkin-Elmer

MONDAY AFTERNOON

Advances in Near-IR and Vibrational Spectroscopy

Chairman: A. J. Montana, M&T Chemical

- 1:30 Molecular Reorganizations in Biological Membranes—FT and Dispersive Raman Spectroscopic Studies. **I. W. Levin**, National Institutes of Health
- 2:10 Diamond Cells and High-Resolution Gas-Phase Spectroscopy: Analytical Applications of Old Tools. **D. G. Cameron**, R. G. Kollar, and R. L. Barbour, BP Research
- 3:30 Comparison of Different Hadamard Transform Near-IR Instruments. **W. G. Fateley**, J. D. Tate, A. P. Bohlke, J. White, and R. M. Hammaker, Kansas State U
- 4:10 Fiber-Optic Near-IR Spectroscopy. **D. E. Hongis**, NIRSystems

Expert Systems—Tools for the Analytical Chemist

Chairman: F. A. Settle, Jr., Virginia Military Institute

- 1:30 Expert System Tools for the Analytical Chemist. **F. A. Settle, Jr.**, and M. A. Pleva, Virginia Military Institute
- 2:10 Expert Systems and Analytical Chemistry. **S. N. Deming**, U of Houston
- 3:30 Expert Systems and Instrumental Interfacing. **V. Kersher**, E. I. du Pont de Nemours & Co.
- 4:10 Knowledge-Based Systems and Interpretation of Analytical Data. **S. A. Tomellini**, B. J. Wythoff, and F. F. Qi, U of New Hampshire

Preregistration
Eastern Analytical Symposium
Sept. 24-29, 1989

Environmental MS

Chairman: D.C.K. Lin, Texas Gulf Research Center

- 1:30 Current Status of HPLC/MS in U.S. EPA Programs. **P. Madsen**, U.S. EPA
- 2:00 Questions You Should Ask Before You Purchase a Mass Spectrometer for Environmental Measurements. **R. G. Melton**, York Laboratories/CT
- 2:30 Efficient Collection and Transfer of Instrumental Data into an Environmental Database. **A. Dexter**, Automated Compliance Systems
- 3:40 Analysis of Environmental Samples with Thermal Chromatography/MS: No More Sample Preparation. **J. Gall**, David Sarnoff Research Center
- 4:10 Nonroutine Sorption and Capillary Techniques for Low-Level Soil Volatiles. **F. Genicola**, NJ Dept. of Environmental Protection

Istvan Halasz Memorial Symposium

Chairman: C. Horvath, Yale U

- 1:30 Early Development in Capillary GC: The Contributions of Istvan Halasz. **L. S. Ettre**, Perkin-Elmer
- 2:00 Reaction Detectors: Flow-Injection Analysis with Open-Tubular Columns. **H. Engelhardt**, U des Saarlandes
- 2:30 Experimental and Theoretical Investigation of Band Interactions in Nonlinear Chromatography. **G. Guiochon**, U of Tennessee
- 3:40 Use of Intrinsic Fluorescence To Follow Protein Conformational Changes on Chromatographic Surfaces. **B. L. Karger**, Northeastern U
- 4:10 Chromatography with Pellicular Stationary Phases. **C. Horvath**, Yale U

Innovations in GC

Chairman: H. A. Issaq, Program Resources

- 1:30 Extraction/Determination of Nitroglycerine in Nitrocellulose-Based Propellants Using a Rapid Two-Step Extraction Followed by a GC Capillary FID Analysis. **D. E. Moore**, Hercules/Radford Army Ammunition Plant
- 1:50 Comparison of Alternate Solid-Phase Extraction Approaches to Chlorophenoxy Acid Herbicide Isolation and Recovery from Water. **P. R. Loconto** and **A. K. Gaid**, NANO Laboratories
- 2:10 GC/MS Studies on the Precursors of Natural Steroids and Alkaloids in Botanicals of Economic Importance: Sesame, Poppy, and Fenugreek Seeds. **S. R. Srinivas**, ANADAMS Consulting Services
- 2:30 Analysis of Semiconductor Process Gases by GC/MS. **R. T. Talasek**, Texas Instruments
- 3:30 New Sulfur-Selective Detector for GC. **N. Johansen** and **M. Legier**, Sievers Research
- 3:50 Specific Determination of Oxygenated Compounds in GC with O FID. **U. K. Goekeler**, ES Industries
- 4:10 GC in Industrial Quality Control: Utilization of a Septum-Equipped Temperature-Programmable Injector (SPI) with a Nitrogen Detector. **Z. Penton**, Varian Instrument Group
- 4:30 Quantitative GC of Low-Volume Samples Using a New Low-Loss Autosampler with a Programmable Injector. **J. R. Berg** and **C. K. Huston**, Varian Instrument Group

Make checks payable to "Treasurer, EAS" and mail this form to EAS Registration, P.O. Box 633, Montchanin, DE 19710.

Deadline for preregistration is Sept. 8, 1989

Preregistrations postmarked after Sept. 8 will be charged the full at-meeting rates.

Fees:	Preregistration	At-Meeting
Regular	\$ 45	\$ 70
Student	10	15
Exhibit only	*	15
Workshop **	25	45
1-day EAS Short Course ***	275	325
2-day EAS Short Course ***	375	425

* Advance registration not available. ** Fee for workshops is in addition to the registration fee. *** Fee for short courses includes registration fee.

Name _____
Last First Initial

Address _____

City _____ State _____ Zip Code _____

Business Phone _____

Check applicable: This is my first EAS.
 Note change of address; former zip code _____

Check one: Mailing address is Home Business

Registration Regular Student \$ _____

Workshops

- HPLC Detection (Sept. 25, 1:30 P.M.) \$ _____
- Preparative LC of Proteins and Peptides (Sept. 25, 1:30 P.M.) \$ _____
- Supercritical Fluid Chromatography (Sept. 26, 9:00 A.M.) \$ _____
- Laboratory Robotics (Sept. 26, 9:00 A.M.) \$ _____
- FT-IR (Sept. 26, 1:30 P.M.) \$ _____
- Elements of Chiral Chromatography (Sept. 26, 1:30 P.M.) \$ _____
- Chromatography Automation (Sept. 26, 1:30 P.M.) \$ _____
- Modern TLC (Sept. 27, 9:00 A.M.) \$ _____
- Capillary GC (Sept. 27, 9:00 A.M.) \$ _____
- Don't Experiment with Your Career: Strategic Planning for Employment (Sept. 27, 1:30 P.M.)
 (This workshop is free. Please check if planning to attend) \$ _____

EAS Short Courses

- Applications in Supercritical Fluid Extraction (Sept. 25) \$ _____
- Methods and Principles of 2D NMR (Sept. 25-26) \$ _____
- Solid-State NMR Spectroscopy (Sept. 27) \$ _____
- Advanced HPLC for the Practicing Chromatographer (Sept. 27-28) \$ _____
- Bioanalytical Chemistry (Sept. 28) \$ _____
- Role of Modern X-ray Diffraction Techniques in Chemical and Structural Analysis (Sept. 28-29) \$ _____
- Near-IR Analysis: In the Plant and in the Laboratory (Sept. 28-29) \$ _____
- Application of MS to the Analysis of Biopolymers (Sept. 29) \$ _____
- Analytical Capillary Electrophoresis (Sept. 29) \$ _____
- Automated Instrumentation for Supercritical Fluid Technology (Sept. 29) . \$ _____
- Professional Analytical Chemists in Industry: What Does an Analytical Chemist Do? (Sept. 27)
 (This course is free for undergraduate chemistry majors. Please check if planning to attend) \$ _____

Total Payment Enclosed \$ _____

Payment must accompany preregistration form. Credit cards not accepted for preregistration or at the meeting.

TUESDAY MORNING

Laboratory Information Management Systems

Chairman: E. J. Subak, Jr., Pfizer

- 8:45 Electronic Communications Considerations for LIMS. **A. J. Schermaier** and E. J. Subak, Jr., PPG Industries
- 9:25 Report from the ASTM E-31.40 Committee on a Guide for LIMS. **P. G. Berthrong**, Beckman Instruments
- 10:40 Prototyping LIMS During a Detailed Vendor Product Review. **E. J. Subak, Jr.**, L. A. Broad, and T. A. Maloney, Pfizer
- 11:20 Strategy for Planning a Successful LIMS Implementation. **R. T. Earls** and G. W. Liesegang, Perkin-Elmer Nelson

Separations in the Next Decade

Chairman: R. Hartwick, Rutgers U

- 8:45 Multimodal HPLC, GC, and TLC Separations. **H. A. Issaq**, Program Resources
- 9:25 Capillary Electrophoresis. **R. Hartwick**, Rutgers U
- 10:40 Analytical Separations in the Pharmaceutical Industry. **S. D. Fazio**, Sandoz Pharmaceuticals
- 11:20 New Approaches for Preparative-Scale Separation of Isomers. **D. W. Armstrong**, U of Missouri—Rolla

New Advances in Atomic Spectroscopy

Chairman: T. C. Rains, National Institute of Standards and Technology

- 8:45 Practical Solids Analysis with Laser Sampling ICP/MS. **E. R. Denoyer**, Perkin-Elmer
- 9:15 ICP/MS—A New Dimension in Trace Elemental Analysis. **H. E. Taylor**, U.S. Geological Survey
- 9:45 Performance Characteristics of a New Ultrasonic Nebulizer for ICP-AES. **W. J. Kinsey**, Applied Research Laboratories
- 11:00 Alternate Sources for the ICP with AES and MS Detection. **J. A. Caruso**, U of Cincinnati
- 11:30 Graphite Furnace AAS. **T. C. Rains**, National Institute of Standards and Technology

Near-IR Spectroscopy: Sensing the Future—I. EAS Award for Achievements in Near-IR Spectroscopy Symposium

Chairman: F. A. DeThomas, NIRSystems

- 8:45 Presentation of the EAS Award for Achievements in Near-IR Spectroscopy to Karl Norris by R. Saferstein
- 8:50 Award Address. Moving Near-IR Spectroscopy into Medical Applications. **K. Norris**
- 9:25 Near-IR Spectroscopy of Pharmaceuticals: It's Not Just for Powders Anymore. **P. Brimmer**, NIRSystems
- 10:40 Time-Resolved Spectroscopy of Hemoglobin and Myoglobin in Exercising Limbs. **B. Chance** and M. Maris, U of Pennsylvania
- 11:20 Near-IR—A QC Tool for the Pharmaceutical Industry. **R. Torlini**, Sandoz Pharmaceuticals

DNA Fingerprinting

Chairman: L. Kobelinsky, John Jay College

- 8:45 DNA Technology: Half a Century of Progress. **J. Witkowski**, Barbur Center
- 9:10 Current Procedures of DNA Analysis for the Purpose of Blood Individualization. **R. Gaensslen**, U of New Haven
- 9:35 Alternative Methods for the Analysis of PCR Products. **R. Shaler**, Lifeccdes
- 10:40 Use of DNA Probe Technology for Identification Purposes in the Forensic Sciences. **D. D. Garner**, Cellmark Diagnostics
- 11:05 Application of the Polymerase Chain Reaction in the Analysis of Forensic Evidence. **G. Sensabaugh**, U of California
- 11:30 Validation Criteria and Data for DNA Typing for Forensic Application. **F. S. Baechtel**, FBI Academy

Poster Session

Advances in NMR

TUESDAY AFTERNOON

Advances in Biomedical Analysis

Chairman: S.H.-Y. Wong, U of Connecticut

- 1:30 Biomedical Applications of Electronic Interaction Chromatography on Porous Graphite Carbon. **C. K. Lim**, Clirical Research Centre

- 2:00 Current Assessment of Biomedical Testing in the Physician's Office. **H. Free**, Miles Laboratories
- 2:30 Cyclosporine Monitoring for Transplantation—Clinical and Methodological Update. **T. Annesley**, U of Michigan School of Medicine
- 3:40 Assessment of SFC for Clinical Drug Analysis. **S.H.-Y. Wong**, U of Connecticut
- 4:10 Optimization Strategy for HPLC Analysis of Anti-AIDS Nucleotide Drugs. **P. Brown**, U of Rhode Island

Recent Advances in Forensic Science Technology

Chairman: L. Kobelinsky, John Jay College

- 1:30 Study in Scarlet—A Historical Review of the Development of Methods for the Detection of Blood from 1875 to the Present. **S. Gerber**
- 1:50 Advances in Automated DNA Sequencing. **E. Chait**, E. I. du Pont de Nemours & Co.
- 2:10 Development of DNA Probes for Paternity Testing in Forensic Analysis. **S. D. Rose**, Collaborative Research
- 2:30 Mapping Human Genes Using Chromosome Blots. **M. Lewis**, BIOS Corp.
- 3:30 Robert Chambers Case. **P. DeForest**
- 3:50 Legal Applications of DNA in the Criminal Justice System. **J. Starrs**, George Washington U
- 4:10 Advances in Huntington's Disease Research. **N. Wexler**, Columbia U

3D Structures of Biomacromolecules by Multidimensional NMR and Computational Methods

Chairman: R. A. Byrd, U.S. FDA

- 1:30 Structure of a Retroviral Zinc Finger: 2D NMR Spectroscopy and Distance Geometry Calculations on a Synthetic Finger from the HIV-1 GAG Protein. **M. F. Summers**, D. Hare, T. L. South, and B. Kim, U of Maryland
- 2:10 Structural Elucidation of Drug-DNA Complexes Using Multinuclear 2D NMR and Distance Geometry Methods. **R. A. Byrd**, U.S. FDA
- 3:30 Isotope Edited Multidimensional NMR Approaches to Structure Determination of Larger Proteins: Staphylococcal Nuclease. **D. Torchia** and S. Sparks, National Institutes of Health
- 4:10 Studies of the 3D Structure of Complement Protein C5A and C5A Mutants by 2D and 3D NMR. **E. Zuilderweg**, Abbott Laboratories

Near-IR Spectroscopy: Sensing the Future—II. EAS Award for Achievements in Near-IR Spectroscopy Symposium

Chairman: P. Brimmer, NIRSystems

- 1:30 Construction and Application of a Near-IR Flow Cell Utilizing a Commercial Near-IR Spectrophotometer and Fiber Optics. **E. Clurczak**, College of St. Elizabeth
- 2:00 Foliage Analysis Using Near-IR Spectroscopy. **T. McLellen**, U of New Hampshire
- 2:30 Determination of Saponification Value by Near-IR Spectroscopy in a Quality Control Laboratory. **S. H. Nicholson**, WITCO Corp.



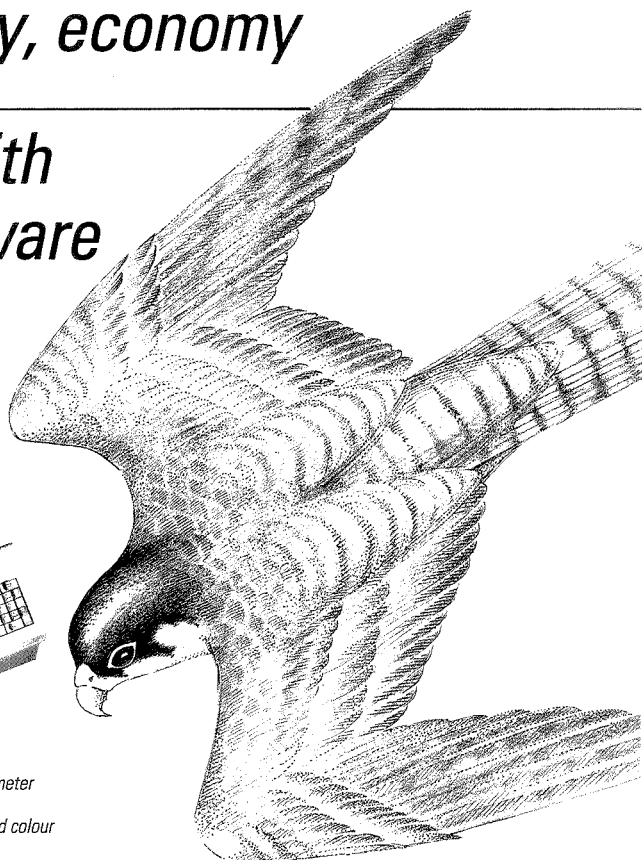
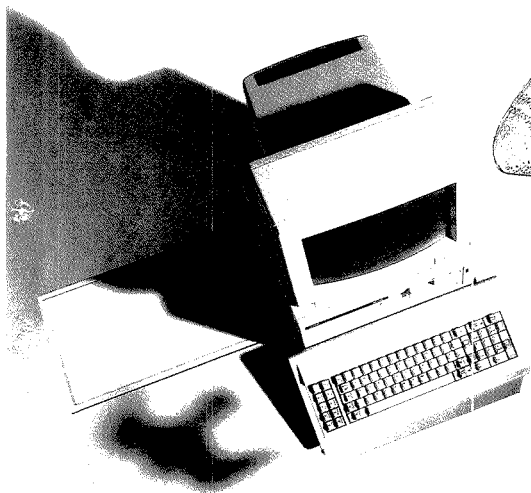


PHILIPS

Speed, accuracy, economy

Philips Analytical

New UV/VIS with Falcon PC software



*PU8710 scanning spectrophotometer
with Falcon software.
Available with or without PC and colour
plotter as required.*

Philips has introduced a new development in UV/VIS. PU8710 – a scanning spectrophotometer at a really low price.

And it's so easy to use thanks to the specially designed Falcon PC software. Now you can perform both simple and complex data handling and method storage with total confidence.

Falcon-Scan, Falcon-Quant and Falcon-Rate provide you

with an effortless step to sophistication in UV/VIS. The colour plotter ensures accurate records, too.

PU8710 is the latest addition to the very successful PU8700 range which offers the best in easy-to-use scanning UV/VIS instrumentation plus total customer support.

Swoop down on the best in UV/VIS. Contact us today and we'll wing you full details.



PHILIPS ANALYTICAL - BIGGER IDEAS FOR BETTER ANALYSIS

For more information about the Philips Analytical UV/VIS spectrophotometry range, contact:

Philips Scientific Analytical Division York Street, Cambridge Great Britain CB1 2PX Tel: 0223 358866 Telex: 817331 Fax: 0223 312764

or **Austria:** (0222) 60101 - 1792 **Belgium:** (02) 325 62 75 **Denmark:** (01) 57 22 22 **Finland:** (90) 502 63 56 **France:** (1) 49 42 81 62

Germany: (0561) 501 384 **Italy:** (02) 64 49 12 **Netherlands:** (040) 783 901 **Norway:** (02) 88 02 00 **Spain:** (1) 404 22 00 **Sweden:** (08) 782 1591
Switzerland: (01) 488 22 11

CIRCLE 125 ON READER SERVICE CARD

UV26



**Me? Enroll
in the ACS
Employment
Service?
I'm head of
a major
research
department!**

Even for the successful chemist or scientist in an allied field, sometimes the best way to get ahead is to make a change.

The ACS Employment Service offers the opportunity to investigate the possibilities discreetly—and at very low cost.

Our Employment Service is free to all ACS members. If you request confidentiality from current employers or other designated organizations there is a nominal charge.

For more information write, use coupon, or CALL TOLL FREE 800-227-5558

Employment Services Office,
American Chemical Society
1155 Sixteenth Street, NW,
Washington, DC 20036

Yes. I am a member of ACS and I would like to learn how the ACS Employment Service can help me advance my career.

Name (please print) _____

Membership # _____

Address _____

City _____

State _____

ZIP _____

- 3:40** Calibration of Near-IR Analyzers with Continuously Moving Samples. **G. J. Kemery**, Bran + Luebbe Analyzing Technologies
- 4:10** Off-Line, At-Line, and On-Line Analyses Using Near-IR Spectroscopy. **F. A. DeThomas**, NIRSystems

Condensed-Phase Separations

Chairman: K. Bratin, Pfizer

- 1:30** Cross-Fractionation HPLC of Cellulosic Polymers. **T. R. Floyd**, S. A. Wilson, and P. L. Lambdin, Eastman Kodak
- 1:50** Theoretical and Practical Considerations in Capillary Zone Electrophoresis. **R. A. Hartwick** and R. I. Robinson, Rutgers U
- 2:10** Factors Affecting Reproducibility in HPLC Analyses. **S. Schachterle** and C. Kellogg, Varian Associates
- 2:30** Determination of Carbamate Pesticides in Water with an Automated HPLC System. **J. J. Sullivan** and J. Tschida, Varian Associates
- 3:20** Applications of Automated On-Line Precolumn Derivatizations Using an HPLC Autosampler. **M. E. Swartz**, Waters Chromatography Division of Millipore
- 3:50** GPC Analysis of Polymers with an On-Line Viscometer Detector. **J. L. Ekmanis**, R. A. Skinner, and N. F. Waldhauer, Waters Chromatography Division of Millipore
- 4:10** Applicability of Chromatographic Retention Data in Quantitative Structure-Activity Relationship Investigations. **K. Valko**, Hungarian Academy of Sciences
- 4:30** Analysis of Particle Filtration Kinetics in Microcolumn HPLC Slurry Packing. **D. C. Shelly**, Stevens Institute of Technology

WEDNESDAY MORNING

Chemometrics and Automation in the Analytical Laboratory

Chairman: F. Tobin, SmithKline Beckman

- 8:45** Computer Simulations of Reversed-Phase Gradient Elution Separations. An Experimental Study of Predictive Accuracy of Bandwidths for OPA-Derivatized Amino Acids. **D. D. Lisi**, J. D. Stuart, and L. R. Snyder, U of Connecticut
- 9:05** Separation of Unresolved HPLC Peaks by Factor Analysis. **K. J. Schostack** and E. R. Malinowski, Stevens Institute of Technology
- 9:25** Restoration of Noisy Overlapped Chromatographic Peaks Using Iterative Deconvolution. **P. B. Crilly**, Hewlett-Packard
- 9:45** Recent Advances in Liquid-Borne Particle Inspection Using Digital Signal Processing. **J. Feld** and J. Cammarata, Monitek Technologies
- 10:40** New Source of Computer-Readable Analytical Data of Organic Chemicals—Beilstein Online. **R. C. Badger** and C. Jochum, Springer-Verlag
- 11:00** LIMS—Unequivocal Identification of Organic Compounds by an Interactive Search and Retrieval of Spectro-Chromatic (GC, GC/MS, NMR, and UV-Vis) Database. **S. R. Srinivas**, ANADAMS Consulting Services

- 11:20** Delineation of Polytypical Mass Spectra into Spectra of Organic Compounds. **S. R. Srinivas**, ANADAMS Consulting Services
- 11:40** Recycling A/D Converters from Minicomputers to PC-Based Automation Systems. **M. McGinnis**, Sievers Research

High-Resolution Microcolumn Chromatography for Pharmaceutical and Biochemical Applications

Chairman: J. G. Feldman, Bausch and Lomb

- 8:45** Bioanalytical Separations Using Capillary Electrokinetic Techniques. **M. J. Sepaniak**, D. F. Swaile, A. Craig, and R. O. Cole, U of Tennessee
- 9:25** Determination of Fatty Acids and Prostaglandins by Capillary LC with Laser Fluorescence Detection. **V. L. McGuffin** and J.-S. Yoo, Michigan State U
- 10:40** Microbore LC/MS and CZE/MS: Applications to Biological Samples. **R. M. Caprioli**, U of Texas Medical School
- 11:20** Multidimensional Chromatography Using On-Line Microcolumn LC and Capillary GC in Industry. **H. J. Cortes** and C. D. Pfeiffer, Dow Chemical Co.

Recent Advances in Analytical Spectroscopy

Chairman: C. Paralusz, Permacel, A Nitto Denko Company

- 8:45** Hyperthermal Surface Ionization—A Novel Ion Source with Analytical Applications. **A. Amirav** and A. Danon, Tel Aviv U
- 9:05** Analytical Application of a Near-IR Laser Diode Intracavity Spectrometer. **C. Patonay**, Georgia State U
- 9:25** NMR Method for Determining Stabilizer Concentrations in Polyolefins. **F. C. Schilling** and V. J. Kuck, AT&T Bell Laboratories
- 9:45** FT-IR Studies of Electropolymerized Copolymer Films. **T. Rush**, III, T. Chou, and D. C. Shelly, Stevens Institute of Technology
- 10:40** Comparison of Ion Mobility Spectrometry (IMS) with Conventional Chemical Detectors in Environmental Monitoring Applications. **J. E. Roehl**, Environmental Technologies Group
- 11:00** Surface Characterization of Graphite-Like Carbons and Silicon Carbide Ceramics Using Surface-Enhanced Raman Spectroscopy. **M. A. Tadayoni** and N. R. Dando, Long Island U
- 11:20** Recent Advances and Results Obtained with an FT-Raman Module Coupled to an FT-IR Spectrometer. **R. Rubino** and A. Simon, Bruker Instruments

Technological Advances in Separations

Chairman: W. Caldwell, ES Industries

- 8:45** Limits of LC Peak Purity Assessment by PDA Absorbance Detectors—Computer-Simulated Estimations. **M. E. Adaskaveg**, T. L. Sheehan, and J. L. Excoffier, Varian Instrument Group
- 9:05** Multidimensional Chromatographic Materials for Protein Purification. **S. A. Berkowitz**, J. T. Baker, Inc.
- 9:25** Selectivity of Substituted Phenyl HPLC Stationary Phases. **W. B. Caldwell**, ES Industries

- 9:45** Calibration of a Computerized Laser-Induced Fluorescence Micro LC Detector. **T. Edkins**, D. C. Shelly, and V. Antonucci, Stevens Institute of Technology
- 10:40** Ultrasensitive UV Detection in Micro Separations. **J. P. Chervet**, M. Uferm, and J. P. Salzmann, LC Packings
- 11:00** New Enzyme Immobilized Phases for HPLC and HPLC-Affinity Chromatographic Analyses. **A. L. Khurana**, E. T. Butts, and C.-T. Ho, Whatman
- 11:20** Very Basic Compounds and Drugs by Silica-Based Reversed-Phase HPLC—Development of Highly Deactivated Column Material. **T. L. Ascah** and B. Feibus, Supelco
- 11:40** Sulfur-Selective Detection for SFC. **M. Legier** and N. Johansen, Sievers Research

Drugs—Trace Analysis in Athletes

Chairman: P. Straus, Hewlett-Packard

- 8:45** Analysis of Controlled Substances Using Mass Selective Detection. **M. Clifford**, NY State Police Crime Lab
- 9:25** Stanazolol, Furazabol, or ? **C. Kammerer**, Schering Plough
- 10:40** Mandrolone Metabolite: Is It Real or Is It a Birth Control Pill? **B. Sample**, Indiana U School of Medicine

Poster Session Advances in NMR

WEDNESDAY AFTERNOON

Supercritical Fluid Extraction

Chairman: M. E. McNally, E. I. du Pont de Nemours & Co.

- 1:30** Theoretical Considerations Required in Cryotrapping for SFE. **M. Anderson**, J. Swanson, and B. E. Richter, Lee Scientific
- 2:10** Rapid Sample Preparation Using SFE. **D. C. Locke**, J. Cai, K.R.R. Mahanama, A. K. Sharma, M. A. Schneiderman, and E. Wolfe, Queens College, CUNY
- 3:30** Extractions from Aqueous Media by SFE. **L. Taylor**, Virginia Tech
- 4:10** Thermophysical Properties Studies for the Supercritical Extraction of β -Carotene. **T. J. Bruno**, W. D. Seider, and M. Cyganowicz, National Institute of Standards and Technology

Atomic Spectroscopy at the Cutting Edge—New York SAS Award Symposium

Chairman: S. Scypinski, Berlex Laboratories

- 1:30** Opening Remarks: The Future of Atomic Spectroscopy. **S. Scypinski**, Berlex Laboratories
- 1:35** Role of Solvents in ICP-AES and ICP/MS: New Tricks for Old Techniques. **R. F. Browner**, Georgia Institute of Technology
- 2:15** Nonstationary Noise in Laser Spectrometry. **E. G. Voigtmann**, U of Massachusetts
- 3:30** Laser-Excited Atomic Fluorescence and Ionization in Graphite Furnaces—Ferrogram Sensitivity and Practical Analyses. **R. G. Michel**, G.-T. Wei, R. Irwin, and D. Butcher, U of Connecticut

MEETINGS

- 4:10 Presentation of the NY SAS Award Medal to James D. Winefordner by M. L. Grayeski
- 4:15 Award Address. Atomic Spectroscopy at the Sub-Parts-per-Trillion Level. **J. D. Winefordner**, U of Florida

Experimental NMR Methods

Chairman: D. Cowburn, Rockefeller U

- 1:30 Isotope Edited Proton NMR of Larger Proteins: Site-Directed NMR of ras P21 Oncogen Products. **A. G. Redfield**, Brandeis U
- 2:10 NMR Methods for the Study of Cell Surface Carbohydrates. **J. H. Prestegard**, Yale U
- 3:30 New 3D and Isotope Edited NMR Techniques for Structure Determination of Proteins. **A. Bax**, National Institutes of Health
- 4:10 NMR Structure of Transforming Growth Factor- α . **L. Mueller**, SmithKline Beckman

Practical Applications of Pharmaceutical Analysis

Chairman: J. McDivitt, Ethicon

- 1:30 Analytical- and Preparative-Scale Separations of Pharmaceutical Compounds Using Deactivated Stationary Phases. **C. M. Conroy** and **P. Jedzrewski**, Virginia Polytechnic Institute and State U
- 1:50 Rapid HPLC Assay for Malondialdehyde and Related Diobarbituric Acid-Reactive Substances. **H. Haas**, West Virginia State College
- 2:10 Separation of the Four Optical Isomers of a Dihydropyridine Calcium Channel Antagonist. **K. D. Ward** and **L. V. Manes**, Syntex
- 2:30 Expert System for Prediction of Metabolites and of their HPLC Retention Properties of Newly Synthesized Drug Molecules. **K. Valko** and **F. Darvas**, Hungarian Academy of Sciences
- 3:30 Combination of Automated Dissolution Testing and Content Uniformity Determinations by HPLC. **M. E. Swartz**, Waters Chromatography Division of Millipore
- 3:50 Separation of the Isomers of Drugs Derived from Proline by HPLC Using Ion Chromatography. **J. Noroski**, **D. Mayo**, **A. Cosey**, **W. Merkl**, and **J. Kirschbaum**, Squibb Institute for Medical Research
- 4:10 Novel Preparative-Scale Chiral Separations on Pirkle-Type Columns Using Displacement Chromatography. **G. Y. Vigh**, **P. Camacho**, **G. Quintero**, **E. Geiger**, **G. Y. Farkas**, and **A. Bartha**, Texas A&M U
- 4:30 Practical Selection of Eluent Parameters for the Optimization of Reversed-Phase Ion Pair Chromatographic Separations. **A. Bartha** and **G. Y. Vigh**, Texas A&M U

Trace Metal Analysis

Chairman: G. Celikiz, Philadelphia College of Textiles

- 1:30 Lead Determination in Whole Blood by Graphite Furnace AAS with L'vov Platform, Oxygen Ashing, and Matrix Modification. **R. A. Romero** and **V. A. Granadillo**, Universidad del Zulia
- 1:50 Multielement AAS Analysis of Solid and Liquid Samples. **H. L. Kahn** and **A. E. Bernhard**, MARS Co.

- 2:10 Improvement of Detection Sensitivity in Ion Chromatographic Separations. **I. T. Urasa** and **S. H. Marr**, Hampton U
- 2:30 Determination of Organolead and Organotin Compounds Using GC/AAS. **D. S. Forsyth**, Health & Welfare Canada
- 3:30 Determination of Country of Origin of Agricultural Products Using Trace Element Profiles and Multivariate Data Analysis. **R. S. Schwartz** and **L. Hecking**, U.S. Customs Service
- 3:50 Use of Argon-Based Ions as Internal Standards in ICP/MS. **S. A. Fricmann**, IBM
- 4:10 Multielement Helium After-Glow Discharge Detector as a Part of a GC/FT-IR/MS/AE Detector System. **J. W. Diehl** and **E. S. Olson**, U of North Dakota
- 4:30 Novel Field-Portable Microprocessor-Controlled Bichromat Instrument for Measurement of Lead in Drinking Water and Wastewater. **N. Spokes** and **D. J. Lohr**, CHEMetrics

THURSDAY MORNING

Biochemical Applications of Capillary Electrophoresis

Chairman: A. Ewing, Pennsylvania State U

- 8:45 Application of Capillary Zone Electrophoresis with Tandem MS for the Characterization of Enzymatic Digests. **J. Henion**, Cornell U
- 9:25 Probing Single-Cell Neurochemistry with Capillary Electrophoresis. **A. Ewing**, Pennsylvania State U
- 10:40 Use of High-Performance Capillary Electrophoresis in Biomolecular Studies. **A. Cohen** and **B. L. Karger**, Northeastern U
- 11:20 Title not available. **H. Schwartz**, Microphoretic Systems

Microscopy: Applications, Techniques, and Instrumentation

Chairman: W. C. McCrone, McCrone Research Institute

- 8:45 What's with Microscopy? **W. C. McCrone**, McCrone Research Institute
- 9:25 Restoration Enhancement of Microscopical Images. **J. G. Dodd** and **L. K. DeNoyer**, Spectrum Associates

- 10:40 Applications of Modulation Contrast in Analytical Optical Microscopy. **R. Hoffman**, Modulation Optics
- 11:20 Optical Characterization of Crystals by the Spindle Stage Method. **J. Hirsch**

Concepts of Current Good Manufacturing Practices in Bulk Pharmaceutical Analysis

Chairman: J. P. Gilbert, Merck & Co.

- 8:45 Current GMP in the Research and Development of Bulk Drugs. **J. P. Gilbert**, Merck & Co.
- 9:25 Current GMP Impact on Investigational Drug Synthesis. **J. W. Scott**, Hoffman-La Roche
- 10:40 Scale-Up and Validation of Bulk Pharmaceuticals. **H. Avallone**, U.S. FDA
- 11:20 Application of GMP Concepts in Bulk Pharmaceutical Chemical Research: Regulation vs. Sound Scientific Research Practices. **J. C. LoCiero, Jr.**

Chemistry in Many Dimensions. EAS Analytical Chemistry Award Symposium

Chairman: D. Leyden, Philip Morris USA

- 8:45 Multidimensional Analysis. **H. N. Blount, III**, National Science Foundation
- 9:10 Remote Optical Detection of Nitro-Organics. **W. R. Seitz**, **Y. Zhang**, **C. Jian**, and **D. C. Sundberg**, U of New Hampshire
- 9:35 Can the Counterfeit Bill Be Detected? **L. N. Klatt** and **J. M. Dale**, Oak Ridge National Laboratory
- 10:40 Solvatochromic Studies of Mobile and Stationary Phases in Reversed-Phase LC. **P. W. Carr**, **A. Dallas**, and **W. J. Cheong**, U of Minnesota
- 11:05 Surface Investigations Using FT-IR, Solid-State NMR, and Photoacoustic Spectroscopy. **D. E. Leyden**, Philip Morris USA
- 11:30 Presentation of the EAS Award for Outstanding Achievements in the Fields of Analytical Chemistry to D. M. Hercules by R. Saferstein
- 11:35 Award Address. Surface Analysis—A New Dimension. **D. M. Hercules**, U of Pittsburgh



Computers in Magnetic Resonance

Chairman: G. N. McGregor, National Cancer Institute/FCRF

- 8:45 3D Angiography. **C. Dumoulin**, GE Research and Development
9:25 Applications Software for NMR Analysis. **J. Hoch**, Roland Institute
10:40 Data Format Standardization. **R. Moore**, Eastman Kodak
11:20 NMR Software System Design Features and Criteria. **T. E. Raidy**, GE NMR Systems Division

Poster Session

At the Forefront of Analytical Chemistry

THURSDAY AFTERNOON

American Microchemical Society
Benedetti-Pichler Award Symposium

Chairman: M. Myers

- 1:30 Presentation of the Benedetti-Pichler Award to K. L. Cheng by R. Saferstein
1:35 Award Address. Double-Capacitor Theory for Nonfaradaic Potentiometry. **K. L. Cheng**, U of Missouri—Kansas City
2:25 Raman Spectroscopy of Electrode Surfaces. **T. M. Cotton**, U of Nebraska
3:30 Donor-Acceptor Properties of Solid Surfaces: Proton and Electron Transfer. **M. Labib**, David Sarnoff Research Center
4:00 Surface Characterization of Lead Ion Selective Electrode Membranes. **V. Y. Young**, U of Florida
4:30 Positron Annihilation Spectroscopy for Chemical Analysis. **J.Y.C. Jean**, U of Missouri—Kansas City

Current Frontiers in Bioanalytical Techniques

Chairman: A. Fell, U of Bradford

- 1:30 Coupled-Column Separations Using Chiral-Achiral Phases for Clinical Applications. **I. W. Wainer**, St. Jude's Children's Hospital
2:10 Rational Design of Fluorogenic Amine Derivatization Reagents for Use in LC. **J. F. Stobaugh**, U of Kansas
3:30 Advances in Therapeutic Drug Monitoring of Antidepressants by Reversed-Phase HPLC. **S.H.-Y. Wong**, U of Connecticut
4:10 Chemometrics and Photodiode Array Detection in HPLC for the Bioanalysis of Drugs and Metabolites. **A. Fell**, U of Bradford

Solids in NMR

Chairman: P. Mirau, AT&T Bell Laboratories

- 1:30 ¹³C and ²H NMR Studies of *trans*-1,4-Polybutadiene in Inclusion Compounds. **F. A. Bovey**, AT&T Bell Laboratories
2:10 Molecular Dynamics of Nylon 6,6 Crystals. **A. D. English**, E. I. du Pont de Nemours & Co.
3:30 Solid-State NMR Studies of Poly(ethylene terephthalate). **M. Henrichs**, Eastman Kodak
4:10 Solid-State 2D NMR Studies of Oriented DNA Polymers. **G. Harbison**, SUNY, Stony Brook

Influence of Solute/Solvent Properties on Retention and Diffusivity in LC

Chairman: D. Martire, Georgetown U

- 1:30 Isocratic Elution Behavior of Polystyrene Polymers in Bonded-Phase LC. **C. H. Lochmüller** and M. B. McGranahan, Duke U
2:10 Determination of Polymer Diffusivity and Molecular Weight by LC. **E. D. Katz**, C. F. Simpson, and R.P.W. Scott, Perkin-Elmer
3:30 Methanol-Water Association and Its Effect on Solute Retention in LC. **R.P.W. Scott**, Georgetown U
4:10 Infinite Dilution Activity Coefficients in Exploring the Mechanism of Reversed-Phase LC. **P. W. Carr**, W. J. Chong, and A. Hussam, U of Minnesota

ACS Courses

- **Mass Spectrometry: Principles and Practice.** East Lansing, MI. Sept. 11-15 and Dec. 11-15. **J. T. Watson**
■ **Thermal Analysis in Materials Characterization.** San Diego, CA. Sept. 23-24. **Edith Turi**, Patrick Gallagher, and **James Seferis**

The following courses are offered in conjunction with the Eastern Analytical Symposium in New York City.

- **Environmental Laboratory QA/QC Data Validation.** Sept. 25-26. **Henry Nowicki** and **William Purves**
■ **Quality Assurance of Chemical Measurements.** Sept. 25-26. **John K. Taylor**
■ **Analytical Laboratory Operations: Analysis of Water and Waste Samples.** Sept. 25-26. **Marcus Cooke**
■ **Laboratory Applications of Lotus 1-2-3 and Other Software: Beyond the Basics.** Sept. 25-26. **Glenn Ouchi**
■ **Experimental Design for Productivity and Quality in R & D.** Sept. 25-27. **Stanley Deming** and **Stephen Morgan**
■ **Laboratory Information Management Systems: From Problem Definition to System Evaluation.** Sept. 27-28. **Gerst Gibbon**

For information on these and other ACS courses, contact the Dept. of Continuing Education, American Chemical Society, 1155 16th St., N.W., Washington, DC 20036 (202-872-4508).

Get the whole picture from
the world's most cited
chemical publication

JOURNAL OF THE AMERICAN CHEMICAL SOCIETY

Editor: **Allen J. Bard**
University of Texas

Each biweekly issue of JACS gives you authoritative, original articles (plus concise communications hot off the press!) in every key arena of chemical research. What's more, JACS is the most competitively priced journal of its kind. Order your subscription today!

Call Toll Free 1-800-227-5558
Telex: 440159 ACSPUI or 892582 ACSPUB
Cable Address: JEICHEM

American Chemical Society
1155 16th Street, NW,
Washington, D.C. 20036
202-872-4363

FOR NEW CORRELATIONS AND INSIGHTS!

CHEMICAL REVIEWS

Editor: **Josef Michl**, University of Texas, Austin
Associate Editor: **John A. Gladys**, University of Utah

In eight issues a year, *Chemical Reviews* helps you critically evaluate ongoing developments in biochemistry, inorganic, organic, analytical, and physical chemistry... wherever your interests lie! It's peer-reviewed articles provide incisive data -- keeping you "up to speed" in minimal time.

1989 Rates	Member**		Nonmember 1 Year
	1 Year	2 Years	
US	\$26	\$ 46	\$161
Canada & Mexico	\$38	\$ 70	\$173
Europe*	\$59	\$112	\$194
All other countries*	\$74	\$142	\$209

*Air service included

**Member rates are for personal use only



AMERICAN CHEMICAL SOCIETY
1155 SIXTEENTH STREET, NW
WASHINGTON, DC 20036
202/872-4363

This publication is available on microfilm, microfiche, and electronically through Chemical Journals Online on STN International.

Computers, Spectroscopy, Kinetics

Introduction to Computer-Assisted Experimentation. Kenneth L. Ratzlaff. xv + 438 pp. John Wiley & Sons, 605 Third Ave., New York, NY 10158. 1987. \$50

Reviewed by Raymond E. Dessy, Chemistry Department, Virginia Polytechnic Institute and State University, Blacksburg, VA 24061

It is difficult to review a book whose information is useful for only a few years. People tend to regard such texts as outdated if even a small portion of the book contains information on "currently" popular PC models. This book, however, provides good coverage of the fundamentals of successful equipment automation.

The first quarter of the book (100 pages) discusses general PC architecture and introduces the vocabulary and philosophy of this area. Except for references to things such as the Apple Lisa and the Xerox Star system, the material is current. CPU architecture, bus design, operating systems, and languages are examined, and the basics of disk technology and numbering systems are described.

Analog interfacing and analog-to-digital converter subsystems are covered in the next 100 pages. Each common ADC type is discussed, and the trade-offs of the approaches are examined.

A short discussion on digital electronics is followed by another 100 pages on the transducers, sensors, and actuators used in interfacing. This critical area receives little, if any, coverage in most of the competing texts, and scientists who are unfamiliar with these topics can benefit from the excellent tutorial provided by this book.

A potpourri of subjects, including networking (RS 232 and IEEE 488), graphics, and some chemometrics techniques, are briefly introduced in the last 100 pages.

The text does not cover local area networks to any great extent, nor are the problems of connecting instruments to a laboratory information management system discussed. How-

ever, the purpose of the book is to examine the interfacing of a stand-alone system, and in this the author has done an excellent job. The text is suitable for university courses and might also be useful for industrial scientists coping with PC-based automation problems.

Microcomputers and Laboratory Instrumentation, 2nd edition. David J. Malcolm-Lawes. xi + 272 pp. Plenum Publishing, 233 Spring St., New York, NY 10013. 1988. \$40

Reviewed by Peter de B. Harrington, Department of Chemistry and Geochemistry, Colorado School of Mines, Golden, CO 80401

This book introduces the principles of communication between computers and laboratory apparatus. Written for scientists who do not specialize in electronics or computers, the book consists of excerpts from undergraduate, graduate, and short courses given by the author at King's College London.

It is difficult to cover the topic of computer interfacing in a pragmatic and contemporary manner while keeping pace with the rapidly advancing computer hardware and electronic technology. The author does not address some of the newer technology such as the VGA and IBM 8513 graphic adapters, the OS/2 operating system, the Micro-Channel bus architecture, the NeXT workstation, protected memory, cache memory, and wait states. However, I know of no other similar books that are as current as this text.

The book is very well written, although it does contain a couple of grammatical errors. The material is presented in a concise and germane format. The presentation of technical information along with the basic information, however, has a tendency to distract the reader from the concepts. The author occasionally uses abbreviations and acronyms without defining them. He also is inconsistent with his hexadecimal number convention, for in some cases the numbers have a trailing H. Some bus addresses given on p. 119

are in an undefined numbering system.

The first part of the book (Chapters 1-6) provides a somewhat pithy background on electronics and computers. Operational amplifiers and basic digital circuits, computer software and hardware, a general discussion of various microcomputers, and details about the IBM PC are provided in these chapters. However, basic dc and ac electronics, passive circuits, nonlinear electronics, and basic electronic transducers are not included. The omission of such topics can hinder novices in the field of electronics who might not understand the circuits and material (e.g., impedance matching).

The second portion of the book (Chapters 7-10), which presents the computer interfaces, is the essence of the book. Representative types of in-

“... a useful reference for those experienced in this field; it presents an abundance of practical and relatively current information.”

terfaces are covered, including direct bus communications with 8086, Z80, 6502, and 6800 computers; ADC and DAC cards; the 8255 Programmable Peripheral Interface; the Centronics Standard Interface; the General-Purpose Interface Bus or IEEE 488 standard interface; and the RS 232 interface.

This book may be a useful reference for those experienced in this field; it presents an abundance of practical and relatively current information. However, a substantial background in electronics is required if the reader intends to build his or her own boards. I cannot recommend it as a textbook because it contains no questions or problems, provides an inadequate background in electronics, and has a limited number of examples.

Spectroelectrochemistry: Theory and Practice. Robert James Gales, Ed. xv + 450 pp. Plenum Publishing, 233 Spring St., New York, NY 10013. 1988. \$85

Reviewed by Therese M. Cotton, Department of Chemistry, University of Nebraska—Lincoln, Lincoln, NE 68588-0304

The goal of the editor of this monograph was to examine the important practical and theoretical aspects of several spectroelectrochemistry techniques that can be used for the in situ study of electrode processes. Seven different techniques (X-ray, photoemission, UV-vis reflectance, IR reflection, surface-enhanced Raman, electron spin resonance, and Mössbauer spectroscopy) are included. Surface-enhanced Raman scattering is a relatively recent technique whereas others have a much longer history.

A brief introductory chapter provides an overview of the range of spectroelectrochemical techniques available for studying electrochemical processes and discusses computer-based data processing. Each chapter that follows has been written by an expert in the field and contains a brief historical introduction, a discussion of the theory, experimental procedures, and examples of applications of the particular technique to the study of electrode processes.

The stated objective was to introduce these topics at the graduate level. For the most part the editor and authors have achieved their goal. However, coverage of the techniques is uneven. Chapter lengths range from 30 pages (X-ray methods) to nearly 100 pages (UV-vis reflectance). In addition, coverage of the major divisions (theory, experimental aspects, and applications) varies considerably between chapters. For example, in the chapter on photoemission measurements 30 pages are devoted to theory whereas applications to physical mechanistic studies and solvated electron chemistry are covered in just three pages. A reader unfamiliar with this field might question whether such uneven treatment is attributable to the limited applicability of the technique to electrode studies or to the complexity of the process and current limitations of the theory. The chapter discussing Mössbauer spectroscopy has only six pages devoted to theory. More coverage certainly should have been warranted, because a typical graduate student may not have any previous background in this technique.

A second criticism might be made

regarding the choice of topics covered. In the preface, the editor states that the book is supposed to cover those techniques that are likely to become "routine aids to electrochemical research and analysis." In some cases the methods may not be routine simply because of the experimental difficulty (X-ray techniques), whereas in other cases (Mössbauer spectroscopy) usage may be limited because of the type of information obtained from the technique. This criticism is not meant to detract from these two techniques. Certainly X-ray techniques are emerging as an exciting new approach for the study of electrode surfaces. But the volume would have been more focused if the editor had limited the coverage to techniques involving radiation from the UV to the IR and provided more detail about each. A chapter on the optical properties of metals—a subject with which many chemists are unfamiliar—could have been included and would have minimized repetition of this area in several of the chapters. The topic is covered very well in the chapter by Kolb on UV-vis reflectance and is also mentioned in the chapters on IR reflectance and surface-enhanced Raman spectroscopy.

This book provides a good overview of the selected topics. The criticisms in this review should not discourage electrochemists from purchasing it, for it will be a valuable resource to those interested in applying spectroscopic methods for the analysis of electrodes. Most of the chapters provide a comprehensive overview of the theoretical and practical aspects of the fields. The chapter on surface-enhanced Raman scattering does a particularly exemplary job of pulling together several difficult theoretical treatments of the enhancement phenomenon and illustrating the experimental relationships to the various theories.

Kinetic Aspects of Analytical Chemistry. Horacio Mottola. xvi + 285 pp. John Wiley & Sons, 605 Third Ave., New York, NY 10158. 1988. \$70

Reviewed by F. James Holler, Department of Chemistry, University of Kentucky, Lexington, KY 40506

Despite the importance of kinetics in analytical chemistry, precious few monographs on the subject have appeared and no authoritative text on kinetics in analytical chemistry has been published since the late 1960s. In response to this need, Horacio A. Mottola has written *Kinetic Aspects of Analytical Chemistry*. This text evolved

from his lectures in a one-semester core course in equilibrium and kinetics in analytical chemistry for beginning graduate students. The book is most useful as a text, and it is also an excellent reference book for anyone interested in analytical applications of kinetics.

The quality of the book reflects the author's participation in writing the fundamental reviews on kinetic aspects of analytical chemistry and a chapter on this subject for a popular instrumental analysis textbook. Mottola's style is clear and straightforward. The book is a nice mix of clearly stated principles, a review of the important literature, and a historical perspective. The depth of the presentation promotes understanding but does not overwhelm the reader. Tables of important methods and developments in the field provide a useful springboard for detailed study of the field, and ample references to the literature are cited.

The inclusion of sections on flow-injection analysis, mixing techniques, and rate measurement methods is most welcome. Many illustrations are provided, mostly from the original literature. Unfortunately, in a few cases in which figures were redrawn, the artist idealized the curves and the central ideas that the figures illustrated were lost (e.g., Figures 10.2 and 10.3). Happily, few such errors are in evidence.

This timely book is a welcome addition to the literature of analytical chemistry. The author has achieved his goals and provided a useful text and reference book.

Computer-Enhanced Analytical Spectroscopy. H.L.C. Meuzelaar and T. L. Isenhour, Eds. xvi + 272 pp. Plenum Publishing, 233 Spring St., New York, NY 10013. 1987. \$53

Reviewed by Chris W. Brown, Department of Chemistry, University of Rhode Island, Kingston, RI 02881

This book resulted from a 1986 meeting held in Snowbird, UT. The book is divided into two parts, each of which contains six chapters. The first part, on optimization and exploratory data analysis, covers training, enhancing signals, and separating multicomponent systems into spectra and concentrations. The second part, on spectral interpretation and library searches, emphasizes the methodology for searching large databases and for interpreting spectra by reference to previously obtained data. The book also covers instrumental methods of MS, IR, and NMR. The purpose is to cut across

the three spectroscopies in all areas of major algorithm development so that methods predominately used in one area can be brought to the attention of investigators in other areas.

An interesting discussion and application of artificial intelligence are presented in Chapter 1. Wong and Brand developed a computer model to reproduce the intelligent behavior of a human expert trying to tune a tandem quadrupole mass spectrometer. The authors discuss all of the information they need to extract from an expert to construct the model. At this point, three versions of the expert system have been written. The development of each version and improvements in subsequent versions are described.

The second chapter, by Peter Griffiths and co-workers, presents an excellent compilation of methods for enhancing the information obtainable from spectra of complex mixtures. They discuss the methods and the pros and cons of reducing bandwidths using derivatives and Fourier self-deconvolution. They conclude that the latter method produces optimal results, but even after deconvolution, it is rare to find the spectral features completely resolved. They follow the deconvolution by curve fitting with bands having Gaussian, Lorentzian, or combination profiles. The standard deviation is used as a goodness of fit between the actual and synthetic spectra. The procedural method and criteria for fitting the spectra are presented and applied to complex spectra of coal.

Any discussion on optimizing spectral data would be incomplete without a discussion of factor analysis, especially one by Ed Malinowski. Chapter 3 covers the most recent advances in evolutionary factor analysis (EFA), a method for extracting spectra of unidentified components from spectra of mixtures containing an unknown number of unknown amounts of unknown components. The analysis does not require spectra of suspected components or unique wavelength points for each component. Three different methods of EFA are described, and the advantages and disadvantages of each are considered. The methodology is in its infancy, but it will solve a major stumbling block in analytical spectroscopy and shows a lot of promise for the future.

Discussions and applications of factor analysis continue in Chapter 4. Windig and Meuzelaar apply factor analysis to multivariate data analysis. Using geometrical models and an in-depth mathematical discussion, they demonstrate the methodology and then apply it to mass spectral data. The

discussion is a little long, but the geometrical figures and models greatly help the reader to understand the rather complex calculations involved.

The development of mathematics for multivariate analysis continues in Chapters 5 and 6. Chapter 5 concerns data obtained from hyphenated techniques such as GC/MS and GC/IR, which provide three-dimensional data. The methodology is developed for treating these with principal component analysis. MacFie compares the decomposition of three-dimensional data into principal components with the decomposition of two-dimensional data sets, presents the algorithms for performing the analyses, and applies them to real data sets. Chapter 6, by Naes and Martens, addresses some of the requirements for performing a calibration on multivariate data, pointing out possible interferences and their effects on the final results. The chapter concludes with a discussion on the models for fitting multivariate data with applications to near-IR diffuse reflection spectra.

The first chapter in the second part of the book, by Clerc, presents a basic discussion of the philosophy for spectral interpretation and searching. This is not an exhaustive review and does not cover the mathematics involved, but it provides an excellent stepping stone to the succeeding chapters in this part of the book.

The methodology for simulating spectra (in this case ^{13}C NMR) to assist in interpretation is discussed in Chapter 8. The general details for molecular model building, structural descriptors, and chemical shifts are described. These are applied to two complex molecules in which the simulated spectra are compared with observed spectra; the results are impressive.

Chapter 9 by A. Savitzky and Chapter 10 by H. Woodruff discuss approaches for identification of a compound by interpreting IR spectra. The discussions overlap somewhat but differ in their approaches to "teaching" the methodology and presenting the demonstrations. Savitzky addresses the problem of extracting appropriate information from experts on the subject whereas Woodruff emphasizes the role of computers in the interpretation process.

IR library databases, storage methods including the computer requirements, and searching methods are covered by Heller and Lowry in Chapter 11. In this chapter, which follows nicely from the general introduction in Chapter 7, the authors outline the available searching methods based on individual peaks and on entire spectra; these are

applied to real problems. A short section on the important problem of spectral information management systems also is included.

The final chapter describes the algorithms for performing spectral identification with data from multiple analytical methods including IR, ^{13}C NMR, and MS. The combination of GC/IR/MS, MS/IR, and MS/NMR techniques is considered; flow charts are presented for the processing algorithms; and the methods are applied to real examples.

This book is an excellent review of the current status of applying pattern recognition techniques to analytical spectroscopy. Considering the close similarity of the topics covered, the editors should be complimented for their organization and for the minimum amount of overlap in the 12 chapters. Dividing the book into two parts was a good way to enhance its readability. The authors have demonstrated the differences in the thought processes required to master the two problems of mixtures and pure unknowns.

Problem Solving with Microbeam Analysis. K. Kiss. 410 pp. Elsevier Science Publishing Co., P.O. Box 882, Madison Square Station, New York, NY 10159. 1988. \$129

Reviewed by David M. Hercules, Department of Chemistry, University of Pittsburgh, Pittsburgh, PA 15260

This is a book on microbeam analysis (broadly defined) that has been written for the nonexpert. The primary purpose is to provide a broad overview of techniques that are applicable to microbeam analysis and to present examples of their application to a diverse collection of technologies. Information about principles, instrumentation, and applications of microbeam analytical techniques is conveyed to help plant managers or engineers understand capabilities and limitations and to help them communicate with the microprobe analyst.

Part I briefly discusses the techniques and selected instrumentation and attempts to provide a critical comparison of their advantages and limitations. Such comparisons are particularly helpful in meeting the stated goal of the volume. Part II contains examples drawn from a wide array of literature.

The techniques discussed in Part I are optical microscopy, electron microscopy (SEM, TEM, AEM), electron spectroscopy (ESCA, Auger), ion beam methods (RBS, ISS, SIMS), and laser

microprobes (Raman, MS). Coverage of these methods is quite broad and thus the discussion of each is limited. A brief chapter is also provided on fitting techniques to specific problems and includes numerous comparisons of techniques according to criteria that are useful in the selection process. My only criticism of Part I is that insufficient emphasis is placed on certain areas. I find it difficult to rationalize devoting only one page to a discussion of Rutherford backscattering (RBS) whereas 18 pages are devoted to laser-based microprobes (MOLE, LAMMA). The historical use of these techniques in practical problem solving would dictate otherwise. The level of presentation of principles is below that appropriate for a textbook, but entirely appropriate for the intended audience.

Part II is really a gem. It is a collection of case histories covering polymers, microelectronics, metallurgy, corrosion, ceramics, catalysts, fibers, food products, cosmetics, and environmental problems, along with a miscellaneous collection of other applications. Parts I and II are of about equal size, which is appropriate for such a volume. The case histories in Part II are discussed briefly, often with a rationale about why a particular technique was (or was not) used to solve the problem. The sources of the examples are all referenced, although many are from manufacturers' literature that may not be readily available to the reader. If I had to criticize something, I would say that perhaps some of the examples could have been discussed in greater detail. Generally, however, I believe this is a fine volume that fits its intended purpose, and I recommend it.

Books Received

Basic Solid State Chemistry. Anthony R. West. x + 415 pp. John Wiley & Sons, 605 Third Ave., New York, NY 10158. 1988. \$33

Topics include crystal structures, bonding, crystallography, other techniques, crystal defects, and electrical properties. The book also contains four appendices, a list of questions, and an index.

Spectroscopic Analysis of Coal Liquids. John R. Kershaw, Ed. xiv + 395 pp. Elsevier Science Publishing Co., P.O. Box 882, Madison Square Station, New York, NY 10159. 1989. \$153

This is volume 12 in the *Coal Science and Technology* series. Topics include

chromatography, pyrolysis, MS, IR, UV, and NMR. The 11 contributors are from the United States, Australia, and England. References (1970s to the mid-1980s), an appendix of structures, and a subject index are provided.

Ion Chromatography in Water Analysis. O. A. Shpigun and Y. A. Zolotov. 188 pp. John Wiley & Sons, 605 Third Ave., New York, NY 10158. 1988. \$60

This book, translated from Russian, is part of the *Ellis Horwood Series in Analytical Chemistry*. The 13 chapters cover fundamentals, instrumentation, classes of compounds, samples, and other topics. References span the 1970s through 1987. An index is included.

Analytical Artifacts. GC, MS, HPLC, TLC AND PC. Brian S. Middleditch. xxiii + 1033 pp. Elsevier Science Publishing Co., P.O. Box 882, Madison Square Station, New York, NY 10159. 1989. \$242

This is volume 44 in the *Journal of Chromatography Library* series. This book presents more than 1100 monographs on interferences that pose problems in the analytical laboratory. Each monograph gives the common name, the mass spectrum, GC data, the CAS name and registry number, synonyms, and a short discussion. Molecular ion, base peak, second peak, third peak, molecular formula, and author and subject indexes are included as well as references (1970s to the mid-1980s).

Electrochemistry: Theoretical Foundations. Quantum and Statistical Mechanics, Thermodynamics, the Solid State. Jerry Goodisman. ix + 374 pp. John Wiley & Sons, 605 Third Ave., New York, NY 10158. 1987. \$58

Chapters are entitled Electrochemistry, Thermodynamics and Electrostatics, Statistical Mechanics, Structure of Surfaces, Interfaces, Further Developments, Diffusion, Electrode Kinetics, Quantum Theory of Electron Transfer, and Quantum Kinetics. Each chapter generally contains an average of six to eight topics, although Electrochemistry contains 17 topics. References (1970s to the mid-1980s) and an index are included.

Advanced Scientific Computing in BASIC with Applications in Chemistry, Biology, and Pharmacology. P. Valko and S. Vajda. xvii + 321 pp. Elsevier Science Publishing Co., P.O. Box 882, Madison Square Station, New York, NY 10159. 1989. \$93

This is volume 4 in the series *Data Handling in Science and Technology*.

The chapters are entitled Computational Linear Algebra, Nonlinear Equations and Extremum Problems, Parameter Estimation, Signal Processing, and Dynamical Models. A table on pages xii and xiii lists the available program modules suitable for MS-DOS computers. The front of the book contains an order form. References (1960s to the mid-1980s) and a subject index are included.

Introduction to Inductively Coupled Plasma Atomic Emission Spectrometry. G. L. Moore. xi + 340 pp. Elsevier Science Publishing Co., P.O. Box 882, Madison Square Station, New York, NY 10159. 1989. \$93

The 15 chapters cover topics such as principles and history, instrumentation, sample analysis, and hybrid techniques. The references are from the 1970s through the mid-1980s. An index is included.

Evaluation of Analytical Methods in Biological Systems. Determination of Beta-Blockers in Biological Material. V. Marko, Ed. xiv + 334 pp. Elsevier Science Publishing Co., P.O. Box 882, Madison Square Station, New York, NY 10159. 1989. \$153

This is part of the *Techniques and Instrumentation in Analytical Chemistry* series. The contributing authors are from Sweden, the United States, Czechoslovakia, Japan, the Federal Republic of Germany, and the German Democratic Republic. The topics covered are pharmacokinetics, sample preparation, optical methods, GC, HPLC, TLC, immunological methods, radioreceptor assays, and isomers. The supplements contain retention indexes and structures of beta-blockers. A subject index and references (1970s to the mid-1980s) are included.

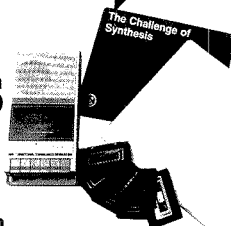
Nonlinear Regression Analysis and Its Applications. Douglas M. Bates and Donald G. Watts. xiv + 365 pp. John Wiley & Sons, 605 Third Ave., New York, NY 10158. 1988. \$40

The chapters are entitled Review of Linear Regression, Nonlinear Regression, Iterative Estimation and Linear Approximations, Practical Considerations in Nonlinear Regression, Multiresponse Parameter Estimation, Models Defined by Systems of Differential Equations, Graphical Summaries of Nonlinear Inference Regions, and Curvature Measures of Nonlinearity. Also included are seven appendices, references (1970s to the present), a bibliography, and author and subject indexes.

The Challenge of Synthesis: Techniques and Strategies

An Audio Course produced by the American Chemical Society

NEW!



Now you can get a complete and comprehensive understanding of synthetic strategies and reaction mechanisms with this unique new audiocassette course.

Learn new skills and applications as you become familiar with new reagents, reactions, and catalysis, especially transition metal catalysis, as they relate to synthesis design.

WHAT YOU'LL LEARN

IF YOU ARE A CHEMIST who works in basic research, process research, or with developing new routes to known materials, you'll especially benefit from this in-depth look into synthetic reactions. Specifically, you'll gain insight to:

- chemo- and regioselectivity of reactions
- asymmetric synthesis
- carbocyclic and heterocyclic chemistry
- retrosynthetic analysis
- stereocontrol of organic reactions
- reaction mechanisms
- correlation between new synthetic reactions and synthetic strategy

and much more! Plus this challenging course includes self exercises, an extensive bibliography, primary literature references, and examples illustrating concepts.

HOW YOU'LL BENEFIT

Designed to improve your awareness of synthetically useful reactions, you'll enhance your chemical efficiency, learn new experimental techniques, improve your analytical ability in synthesis design, and develop an understanding of the correlation between new synthetic reactions and synthetic strategy.

ABOUT THE COURSE AUTHORS

Dr. Barry M. Trost is Professor of Chemistry at Stanford University. He is the recipient of the ACS Awards for Pure Chemistry and Creative Work in Synthetic Organic Chemistry. Dr. Edwin Vedejs is Professor of Chemistry at the University of Wisconsin, and is active in the synthesis of complex molecules.

PACKAGE (Catalog No. 99)

The course comes complete with six cassettes (7 hours playing time) and a 200-page manual for \$485.00 (U.S. and Canada), \$582.00 (export). Additional manuals may be purchased at \$32.00 each (U.S. and Canada), \$39.00 (export).

**BACKED BY THE ACS
GUARANTEE**

ACS guarantees you'll benefit from this course! If you're not completely satisfied with your audio course, simply return it within ten days of receipt for a full refund, charge credit, or cancellation of invoice.

CALL TOLL FREE **1-800-227-5558!**

O · R · D · E · R · F · O · R · M

Send this Order Form with your payment or purchase order to:
**American Chemical Society, Distribution Office, Dept. 04
PO Box 57136, West End Station, Washington, DC 20037**

Qty.	US & Can Price	Export Price	Total Amount
The Challenge of Synthesis (Cat. No. 99)	\$485.00	\$582.00	\$ _____
Additional Manuals	\$ 32.00	\$ 39.00	\$ _____
Total enclosed:			\$ _____

Ship to:

Name _____
Organization _____
Address _____
City, State, Zip _____
Phone _____

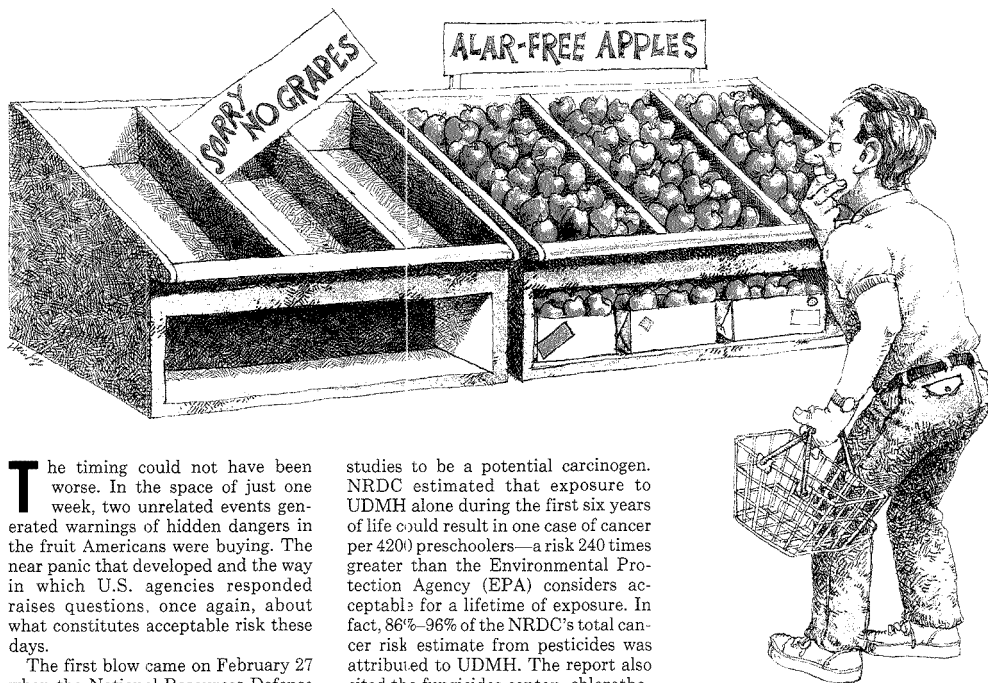
Bill to:

Name _____
Organization _____
Address _____
City, State, Zip _____
Phone _____

- Payment enclosed (make checks payable to ACS); Purchase order enclosed. PO # _____
 Charge my MasterCard VISA American Express Barclaycard ACCESS
 Diners Club/Carte Blanche

Account # _____
Expires _____ Interbank # _____ (ACCESS & MC Only)
Name of Cardholder _____
Signature _____

The Great Fruit Scares of 1989



The timing could not have been worse. In the space of just one week, two unrelated events generated warnings of hidden dangers in the fruit Americans were buying. The near panic that developed and the way in which U.S. agencies responded raises questions, once again, about what constitutes acceptable risk these days.

The first blow came on February 27 when the National Resources Defense Council (NRDC), a nonprofit environmental group, released a report charging that "little is being done by the [U.S.] government to protect children from the intolerable risk to their health posed by pesticide residues in food." All told, the NRDC calculated that pesticide residues in fruits and vegetables might contribute between 5500 and 6200 additional cases of cancer in the current population of American preschoolers (1).

Most of the NRDC's concern about intolerable risk centered on the suspected carcinogen daminozide [succinic acid mono(2,2-dimethylhydrazide), $(\text{CH}_3)_2\text{NNHCOCH}_2\text{CH}_2\text{CO}_2\text{H}$, trade name Alar], a plant growth regulator found at levels of parts per million or less in apples and apple products, and its hydrolysis product unsymmetrical dimethylhydrazine (UDMH, 1,1-dimethylhydrazine), shown by animal

studies to be a potential carcinogen. NRDC estimated that exposure to UDMH alone during the first six years of life could result in one case of cancer per 4200 preschoolers—a risk 240 times greater than the Environmental Protection Agency (EPA) considers acceptable for a lifetime of exposure. In fact, 86%–96% of the NRDC's total cancer risk estimate from pesticides was attributed to UDMH. The report also cited the fungicides captan, chlorothalonil, folpet, and mancozeb (because of its metabolite ethylenethiourea) as posing unacceptable risks (1).

Just as Americans were digesting that scary news, on March 2 the U.S. embassy in Santiago, Chile, received the first of two anonymous calls warning that fruit being shipped from that country was poisoned. Ten days later, Food and Drug Administration (FDA) inspectors found two cyanide-laced grapes in a shipment of 400,000 crates of Chilean fruit unloaded at Philadelphia's port. The FDA, already battle-hardened by the Tylenol-tampering scare, immediately adopted a safer-than-sorry policy and banned importation of all fruit from Chile. Canada and Japan followed suit (2).

Grocery store owners responded to the twin scares by clearing their shelves of Chilean grapes and posting signs that claimed apples were Alar-free.

FOCUS

New York, Los Angeles, and Chicago temporarily pulled apples from their school cafeterias. All across the United States sales of grapes and apples plummeted.

For FDA's part, chemists at several regional laboratories were pressed into action devising and testing new methods for determining cyanide in fruit. (At one point FDA had 150 inspectors sifting through the Philadelphia fruit shipment—more than 15% of the agency's field staff.) Although FDA officials are reluctant to provide too many details of their testing program for fear of tipping their hand to future poisoners,

basically the agency relies on its field inspectors to spot suspicious markings or discolorations that could indicate cyanide applied to or injected into the fruit.

Both suspect and randomly selected fruits were brought to the lab and rapidly screened with commercially available Cyantesmo paper, which turns from white to blue in the presence of cyanide. The amount of cyanide present, says Stephen Capar, head of FDA's Elemental Research Section in Washington, DC, can be determined directly on homogenized fruit using a colorimetric test that requires a pyri-

quately, and overlooks testing of "inert" materials in pesticide formulations. NRDC also demanded that FDA improve analytical methods for detecting pesticides in food and accelerate its testing program. "In the vast majority of cases," claimed the report, "FDA currently fails to take action to prevent illegal food from reaching the market and being sold" (1).

When the NRDC report was released, EPA's acting director, John Moore, called it misleading, saying that its risk estimates are too high and are based on poor data and inappropriate techniques. "Many of their conclu-

sive screens. Yet since 1981 FDA has searched for daminozide residues in selected samples every year except 1983 and 1984. Each time, agency chemists found the pesticide, usually in approximately half of the apples and always below the 20-ppm limit.

To detect the pesticide, FDA has relied on a colorimetric procedure with a detection limit of 1-2 ppm. Test samples are boiled in 50% NaOH, a process that converts daminozide to UDMH, and mixed with $\text{Na}_3[\text{Fe}(\text{CN})_5\text{NH}_3]$ at pH 5.0 to produce a red color (3). A newer procedure using GC/MS with selected ion monitoring of the fragmentation pattern further lowers the detection limit to 0.1 ppm (4).

UDMH in fruit can be detected down to 10 ppb. Samples are treated with L-ascorbic acid, derivatized to a hydrazone, and eluted on a gas chromatograph equipped with an electron capture detector (5).

Uniroyal uses isotope dilution GC/MS to determine UDMH, claiming a 1.0-ppb detection limit (6).

Ironically, it was the EPA-mandated testing for Alar and UDMH by Uniroyal, using the more sensitive methods, that provided the NRDC with data on daminozide contamination. Uniroyal's three-phase market basket survey, completed in the fall of 1986, found daminozide residues in 87% of the samples. Average Alar levels on apples steadily declined in each phase of the study, measuring 1.02 ppm overall. Uniroyal also reported detecting UDMH in 71% of its market basket sample, with a steady average of ~3.0 ppb in contaminated apples (6).

FDA chemists, now using the more sensitive techniques, do not dispute these values. However, federal agencies and the NRDC part company over how to translate these findings into estimates of cancer risk. NRDC used a "time-dependent multistage model" that estimates a greater risk from carcinogen exposure at early ages than later. EPA's time-independent model, on the other hand, assumes the same risk for persons of all ages, yielding much lower cancer estimates. In fact, EPA had used some of the same data as the NRDC—the estimate of cancer cases per given dose—when it tried to ban daminozide in 1985, only to have the Scientific Advisory Panel reject the values as flawed. The NRDC, in turn, asserts that EPA's approach underestimates lifetime cancer risk.

The NRDC and EPA also differ over how much fruit children eat. The activist group uses data indicating that fruit amounts to 34% of a preschooler's diet, compared with 20% for adults. Given a child's body weight, this represents six

“NRDC charged that EPA underestimates cancer risks for children and fails to regulate and test pesticides adequately.”

dine-barbituric acid solution and chloramine T. Alternatively, the cyanide can be volatilized as HCN, collected in a NaOH trap, and then measured by square wave voltammetry or the pyridine-barbituric acid test. Volatilizing the cyanide provides a cleaner solution, but direct testing on homogenized fruit is faster. Capar and other FDA scientists have tested their methods on fruit ranging from apples and pears to kiwi and raspberries.

After convincing itself that it can effectively screen for cyanide, FDA is once again allowing Chilean fruit—without the exception of melons—into the United States. To date, the only tainted fruit discovered remains the two grapes.

Was it worth carrying out this work to find two contaminated grapes? "We never know what the next tampering incident will be," says Capar. "We will be prepared for the next incident." The American people also seem to have accepted the costs and inconveniences as the price of fighting terrorism.

The reaction, however, was quite different in Chile, where more than 200,000 jobs were affected in an industry estimated to be worth \$600 million annually. Citizens fought back with protests, fruit give-aways, and bumper stickers proclaiming "My family eats Chilean fruit." Even Chile's controversial president, Augusto Pinochet, took time to savor a few grapes in public (2).

Although the cyanide scare seems to have passed, the pesticide question continues to engender debate. The NRDC's report charged that EPA underestimates cancer risks for children, fails to regulate and test pesticides ade-

quately, says Louis Carson, scientific coordinator in FDA's Division of Field Science, "play fast and loose with the law."

To understand the controversy surrounding the NRDC's charges it is important to examine the regulatory history of the group's main target, daminozide. This pesticide has been used since 1963 to control flowering, reduce fruit drop, and prevent spoilage in storage. Trace amounts of the chemical can be found in peanuts, processed sour cherries, and, of course, apples and apple products.

In the 1970s animal studies indicated daminozide's carcinogenic potential. By 1984 the metabolite UDMH was recognized from animal experiments to be a potential carcinogen, and in August 1985 EPA decided to ban the pesticide. However, the agency's Scientific Advisory Panel called for additional data to justify a ban, requesting that Uniroyal, daminozide's manufacturer, conduct additional toxicological and exposure studies. Meanwhile, growers were ordered to reduce application rates and EPA lowered its residue tolerance for daminozide on apples from 30 to 20 ppm. Sales of Alar have been dropping ever since.

Ensuring that daminozide residues stay below 20 ppm presents some problems. FDA, which routinely checks foods for contaminants, can pick up 40% of the pesticides likely to leave residues by using analytical methods sensitive to a broad class of chemicals such as organophosphates or carbamates. However, the agency must specifically request analyses for daminozide and other pesticides that slip past the rou-

times more fruit and associated pesticide residues than the average adult woman ingests.

Critics attack the NRDC's numbers as too high, yet they also point out that the group's estimate of 6200 additional cancers from pesticides pales in comparison to 5.5 million cancers predicted for America's 22 million preschoolers during their lifetimes. However, the NRDC believes that the cancer risk from pesticides may actually be higher, because it examined only 23 out of the 320 pesticides allowed on foods and just eight of the 66 that EPA labels potentially carcinogenic.

Despite the controversy, both sides have raised legitimate concerns about carcinogens and children. Cancer risk assessment is still a young field. Researchers do not understand what contribution "natural" carcinogens such as psoralen, celery's own pesticide, makes to these rates, or how exposure to different pesticides may combine synergistically to promote cancer. Considering EPA's original desire to ban Alar, the NRDC could have been an ally.

What disturbs many scientists is how the NRDC marketed its report. The group unveiled it on a segment of the popular TV show "60 Minutes" and then enlisted actress Meryl Streep to sell its findings to the public and Congress. This high-profile offensive triggered the near panic over apples. Industry officials, who had known about the impending report for about a year, underestimated its emotional appeal and the NRDC's slick campaign.

On the other hand, EPA's counter-offensive stalled when it admitted to an error in its original assertion that only 5% of the 1988 apple crop had been treated with Alar and upped its estimate to 15%. Public confidence was further shaken when different analyses for daminozide sponsored by Consumers Union, the *Los Angeles Times*, and CBS News reported finding the residues in approximately 30%-55% of apples or apple products—suggesting even higher rates of Alar application. However, given the long-term storage of apples and especially apple products, these numbers may not represent just last year's crop.

NRDC spokesperson Janet Hathaway, looking at the same numbers, charged that "EPA does not know exactly how much of the chemical has been used in the U.S. in the past year. This uncertainty should not be an excuse for regulatory inaction." Hathaway called on EPA to issue an immediate, total ban on Alar.

EPA, too, would like to get Alar out its hair but prefers to work through the normal regulatory process, which re-

quires conducting a study to weigh health risks against the added costs of banning the chemical. This review could take 18 months or longer to complete, during which time Alar will be sold. EPA says such a delay poses no undue risk to the public.

However, the agency is being left in the dust on Alar. Congress has moved to ban the pesticide and change EPA's regulatory procedure to a "health-based" approach, which will bypass the economic concerns. In May the International Apple Institute, representing 90% of U.S. growers, advised its members to abandon daminozide. Although it still declares the pesticide safe, the Institute said that by September of this year "[T]he use of Alar will be reduced to virtually zero." And in June Uniroyal announced it would no longer sell Alar to U.S. growers.

Like the FDA in March, much of the public has adopted a safe-rather-than-sorry attitude toward Alar. Apple sales have dived 20%, costing the industry approximately \$50 million. Another \$50 mill on loss is predicted by year's end. Apple Institute members find themselves in nearly the same bind as the Chileans.

In the end, the marketplace is deciding the Alar issue just as it effectively enforced the boycott of Chilean fruit. For critics of U.S. behavior, this falls into a pattern of Americans demanding zero risk for dangers outside their personal control.

The media attention given to pesticides, terrorism, or airline safety seems out of proportion when more than 40,000 Americans lose their lives each year in automobile accidents. Yet it could also be argued that the world is still ignorant of the effects of most of its pesticide arsenal, and the United States must do all it can to protect its citizens and environment. One possible outcome of these events is that greater regulatory powers will be granted to EPA and FDA. Whether that will prevent yet another great fruit scare remains an unsettling question.

Alan R. Newman

References

- (1) "Intolerable Risk: Pesticides in Our Children's Food"; Natural Resources Defense Council, Feb. 27, 1989.
- (2) *Time*, March 27, 1989, 24-27.
- (3) *Pesticide Analytical Manual*; Pesticide Reg. Sec. 180.246; 1975, Vol. II.
- (4) Condit, M. K.; Baumgardner, J. R.; Hellman, L. M. *J. Assoc. Off. Anal. Chem.* 1988, **71**, 735-39.
- (5) Wright, D., Jr. *J. Assoc. Off. Anal. Chem.* 1987, **70**, 718-20.
- (6) EPA, Office of Pesticides and Toxic Substances. *Memorandum—Daminozide Special Review*. Phase III 1986, Uniroyal Market Basket Survey. May 18, 1987.



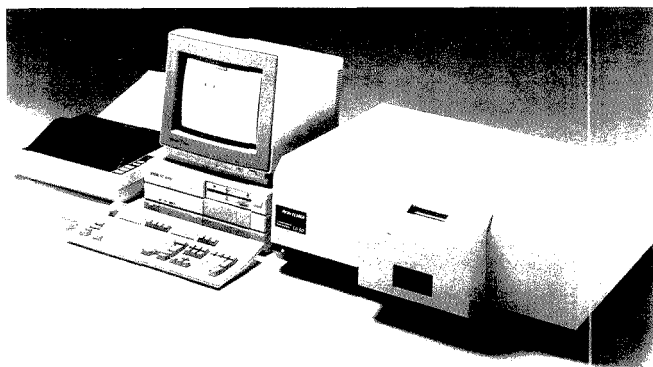
Find it FAST in the LabGuide

The *LabGuide* is where more than 140 suppliers say, "Here we are. Compare our products with those of our competitors." For example, you'll find typical product line ads in the current *LabGuide* from the following firms:

Advertisers	Pages
A&D ENGINEERING	IBC
ALCONOX	195
ANDERSON LABS	201
CERAC	186
CHEMTRONICS	125
EASTERN CHEMICAL	193
FISCHER AMERICA	151
GILFORD/CIBA CORNING	133
GILSON	147
GLAS-COL	105
HELLMA CELLS	173
INSTRUMENTS SA	165
J&L INSTRUMENTS	169
MILLIPORE	29-32, 106
NETZSCH	143
O.I. CORP	111
PARR	91
POLYSCIENCE	42
ST. CHARLES	103
SO. N.E. ULTRAVIOLET	116
TOSO HAAS	92-93
UNIMETRICS	59
WESCAN	64

The *LabGuide* is your true one-stop buying source for scientific products.

NEW PRODUCTS



Model LS-50 fluorescence spectrometer features software that provides instrument control, data-handling routines, dedicated application programs, and high-resolution graphics. Perkin-Elmer **401**

Sample preparation. Model 3000 analytical supercritical fluid extractor/accumulator can be directly coupled to gas, liquid, or supercritical fluid chromatographs. After operating parameters are entered, the microprocessor-based system initiates and runs the specified extraction, accumulation, and analysis cycle. Computer Chemical Systems **404**

Flow cytometry. ACR-1000 flow cytometer consists of an analytical measuring unit, a high-speed multichannel acquisition unit, and a PC/AT-compatible data-processing computer. Applications include lymphocyte classification and numeration, platelet measurement, and DNA analysis. Bruker Instruments **405**

Ion chromatography. ActIon analyzer is a low-dispersion, inert ion chromatograph that features a flow range of 0.01–10 mL/min, flow precision to 1%, and a 4000-psi operating limit. The conductivity detector incorporates a five-electrode cell design and auto temperature control. Waters Chromatography Division of Millipore **406**

Wafer inspection. SEM 555 features an automatic loader that uses industry-standard cassettes, a wafer aligner, an SEM with air-damped suspension, and software for linewidth measurement and system control. Inspection and

critical dimension measurement can be completed on more than 10 wafers per hour for five sites per wafer. Philips **407**

Ashing. MAS-300 microwave ashing system can fully ash a variety of materials at temperatures up to 1200 °C in 5–10 min. A sample carrier made of quartz fiber material cools rapidly, allowing the sample to be reweighed 30 s after removal from the furnace. CEM Corp. **408**

Circular dichroism. CD6 circular dichroism system includes a spectropolarimeter that covers the range of 175–700 nm and a 386 PC/AT-compatible computer. Accessories include linear dichroism and magnetic circular dichroism attachments. Spex **409**

SFE. Model SFE/10 MicroExtraction System provides detection levels as low as 1 ppm with over 90% recovery. Extraction times are reduced up to 80% compared with conventional Soxhlet extraction, and lower temperature operation permits extraction of thermally labile compounds. Suprex **412**

Air analysis. VOC air analyzer is designed for analysis of air or other gaseous samples containing low levels of volatile organic compounds. Samples collected on adsorbent tubes are reconcentrated on a liquid-nitrogen-cooled

fused-silica trap and introduced into a capillary gas chromatograph for analysis. Chrompack **413**

Prep LC. NovaPrep 5000 accommodates 10–50-mm i.d. columns and features a 140-mL/min maximum flow rate; 5000-psi pressure capability; 2-, 5-, and 10-mL interchangeable injection loops; and automated sample injection, gradient formation, and fraction collection. SepTech **410**

GC. Portable gas chromatograph, designed for use in the semiconductor industry, continuously monitors air for H₂, SiH₄, PH₃, AsH₃, GeH₄, and Si₂H₆. The system uses a controlled potentiostatic electrolysis detector and can operate with purified air or nitrogen as a carrier gas. Sensidyne **411**

Software

Statistics. Solo version 2.0 is a statistics and graphics software package that features descriptive statistics; cross tabulation; nonparametrics; multiple regression; discriminant, cluster, and factor analysis; and 3D graphics that can be rotated on screen. BMDP **415**

LIMS. Telecation Associates's Smartlab identifies and tracks samples from the time they are logged in through analysis, automatic reporting, invoicing, and archiving of results. The software is designed for MS-DOS-compatible computers. U.S. Analytical Instruments **416**

Manufacturers' Literature

LC detector. Brochure highlights the 115 UV detector, which monitors column effluent at wavelengths between 190 and 380 nm. The detector can be adapted for either analytical or preparative HPLC. 4 pp. Gilson Medical Electronics **418**

For more information on listed items, circle the appropriate numbers on one of our Readers' Service Cards



Reproducibility, time and time again

You need reproducible results from your HPLC. That's one reason your HPLC solvent delivery system is so important. That's also why you should be using our Model 9600.

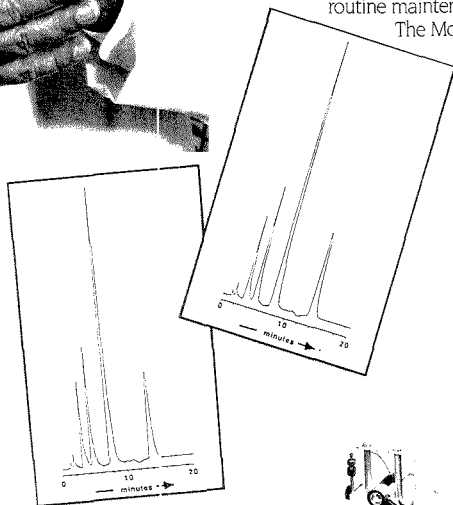
The Model 9600 has gradient and flow rate reproducibility that matches even the most expensive HPLC. It includes everything you need for a reproducible HPLC solvent delivery system; it's also easy to get at everything for routine maintenance. The Model

9600 is fully programmable, and works with any other manufacturer's equipment.

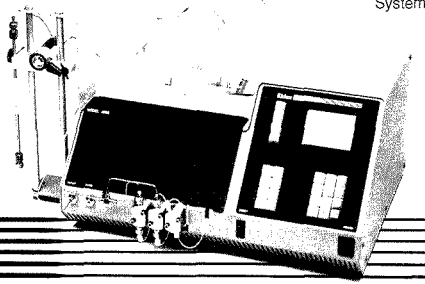
Best of all, the Model 9600 sells for thousands of dollars less than what you're used to paying.

Call or write today for a free brochure or to arrange a demonstration.

Eldex
831 Bransten Road
San Carlos, CA 94070
(415) 592-9270



Model 9600
Programmable
Solvent
Delivery
System

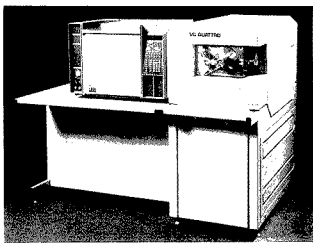


Eldex

Precision Equipment for Chromatography

CIRCLE 40 ON READER SERVICE CARD

ANALYTICAL CHEMISTRY, VOL. 61, NO. 14, JULY 15, 1989 • 865 A



Quattro, a triple quadrupole mass spectrometer, incorporates 32-bit supercomputer array technology that provides intelligent instrument control, automation, and ultra-high-speed data processing. VG Instruments 402

Chromatography newsletter. *Bio-text*, Vol. II, No. 1, discusses a narrow-bore HPLC column for glycoprotein monosaccharide analyses and determination of carbamazepine in blood plasma. 12 pp. Supelco 419

Peptide synthesis. Wall chart includes protection groups for amino acid chemistries and an amino acid selection table. Also listed are standard

abbreviations, chemical structures, and molecular weights. MilliGen/Bio-search 420

Polymeric materials. Brochure highlights the RDA II, which measures the viscoelastic properties of polymeric materials. Instrument features, test modes, principles of operation, and applications are discussed. Rheometrics 421

Newsletter. *XRF News* includes articles on sample screening in environmental analysis, elimination of liquid nitrogen, advances in X-ray diffraction, and XRF basics. 8 pp. KeveX 422

Catalogs

Scientific products. Catalog features Teflon products for research and industrial applications. Labware, tubing, fittings, valves, and vessels are included. 64 pp. Berghof/America 426

Chromatography. Catalog features GC and LC columns and supplies for GC, HPLC, UV-vis, FT-IR, C/C/MS, and LC/MS instruments. Included are

appendices of chromatographic equations and miscibility and conversion tables. 256 pp. Hewlett-Packard 424

Chromatography/solvents. Catalog includes LC columns; products for pesticide residue analysis, environmental analysis, and pilot plant applications; and high-purity solvents. 40 pp. Burdick & Jackson 425

Molecular biology. Catalog lists biochemicals for molecular biology applications. Included are nucleic acids, restriction endonucleases, and nucleic acid modifying enzymes. 116 pp. Sigma Chemical Co. 427

Instrumentation. Catalog features digital oscilloscopes, real-time FFT spectrum analyzers, digital signal-processing systems, waveform recorders, data loggers, and logic analyzers. 68 pp. Rapid Systems 428

IR. Catalog lists sampling devices for IR analysis. Included are products for liquid analysis, ATR techniques, process monitoring, polymer and solid sampling, specular reflectance, and gas analysis. ARIES/QEI 429

LABORATORY SERVICE CENTER

Alizarin Complexone • 4-Aminoantipyrine • tert-Butyl Chloride
Butyl Ethyl Ketone • p-Chloranil • Dihydroxyacetone • Dimethylurea
Diethyl-, Dimethyl-, Ethyl-, Methyl- & Trimethylamine Hydrochlorides
3,5-Dinitrobenzoic Acid • Diphenylcarbazide • Dithizone • Dulcitol
Esculin • Glutaric Acid & Anhydride • Histamine Acid Diphosphate
pH Indicators • Methyl Acetamide • Methyl Acetate • Phenolindophenol
Phenolphthalein • Sodium Diethyldithiocarbamate • Sodium Succinate
Triphenylphosphine • Triphenyltetrazolium Chloride • Veratrole

Write for our Products List of over 3,000 chemicals

Tel: 516-273-0900 • TOLL FREE: 800-645-5566

Telefax: 516-273-0858 • Telex: 497 4275

EASTERN CHEMICAL
A Division of UNITED-GUARDIAN, INC.

P.O. Box 2500
DEPT. AC
SMITHTOWN, N.Y. 11787

Laboratory Service Center (Equipment, Materials, Services, Instruments for Leasing), Maximum space — 4 inches per advertisement. Column width, 2-3/16"; two column width, 4-9/16". Artwork accepted. No combination of directory rates with ROP advertising. Rates based on number of inches used within 12 months from first date of first insertion. Per inch: 1" — \$155; 12" — \$153; 24" — \$150; 36" — \$145; 48" — \$140.

CALL OR WRITE JANE GATENBY

ANALYTICAL CHEMISTRY

500 Post Road East

P.O. Box 231

Westport, CT 06880

203-226-7131/FAX: 203-454-9939

NMR ANALYSIS

MULTINUCLEAR LIQUID or
MULTIFIELD SOLID STATE
SPECTRAL DATA SERVICES, INC.
818 Pioneer
Champaign, IL 61820
(217) 352-7084

HELP WANTED ADS

ROP display at ROP rates. Rate based on number of insertions within contract year. Cannot be combined for frequency.

Unit	1-Ti	6-Ti	12-Ti
1" (25 mm)	\$180	\$160	\$150
	24-Ti	48-Ti	72-Ti
	\$140	\$130	\$125

CALL OR WRITE JANE GATENBY

ANALYTICAL CHEMISTRY

500 Post Road East

P.O. Box 231

Westport, CT 06880

203-226-7131

FAX: 203-454-9939

INDEX TO ADVERTISERS IN THIS ISSUE

CIRCLE INQUIRY NO.	ADVERTISERS	PAGE NO.
1	Antek Instruments, Inc.	825A
18	Beckman Instruments, Inc.	848A
32	Delsi, Inc./Nermag Division	820A
34	*Dialog Information Services, Inc. Humpal, Leftwich & Sinn, Inc.	838A
40	*Eidex	865A
50	Fisher Scientific Hawbaker Communications, Inc.	846A
60	Galileo Electro-Optics Corp. Legasse Associates Advertising Inc.	841A
-	General Motors NW Ayer Incorporated	829A-831A
63	*Hewlett-Packard Company Brooks Communications	OBC
72-78	*Instruments SA, Inc./J-Y Division Kathy Wyatt & Associates, Inc.	823A
94	*Matheson Gas Products Kenyon Hoag Associates	827A
129	Perkin-Elmer Corporation Graystone	837A
125	**Philips Scientific/Analytical Division Connors Publicity Ltd.	852B
127	*Precision Scientific Winterkorn Lillis Inc.	IFC
150	Supelco, Inc.	832A
152	SynChrom	824A
156	Thermo Jarrell Ash, Inc. Noon, Inc.	819A
174	*Wheaton The Wheaton Agency	845A

Directory section, see page 866A.

* See ad in ACS Laboratory Guide.

** Company so marked has advertisement in Foreign Regional edition only.

Advertising Management for the American Chemical Society Publications

CENTCOM, LTD

President

Thomas N. J. Koerwer

Executive Vice President Senior Vice President

James A. Byrne Benjamin W. Jones

Clay S. Holden, Vice President

Robert L. Voepel, Vice President

Joseph P. Stenza, Production Director

500 Post Road East
P.O. Box 231
Westport, Connecticut 06880
(Area Code 203) 226-7131
Telex No. 643310
FAX No. 203-454-9939

ADVERTISING SALES MANAGER

Bruce E. Poorman

ADVERTISING PRODUCTION MANAGER

Jane F. Gatenby

SALES REPRESENTATIVES

Philadelphia, PA . . . Patricia O'Donnell, CENTCOM, LTD., GSB Building, Suite 405, 1 Belmont Avenue, Bala Cynwyd, Pa. 19004. Telephone: 215-667-9666, FAX: 215-667-9353

New York, NY . . . John F. Raftery, CENTCOM, LTD., 60 East 42nd St., New York, N.Y. 10165. Telephone: 212-972-9660

Westport, CT . . . Edward M. Black, CENTCOM, LTD., 500 Post Road East, P.O. Box 231, Westport, Ct. 06880. Telephone: 203-226-7131, Telex 643310, FAX: 203-454-9939

Cleveland, OH . . . Bruce E. Poorman, John C. Guyot, CENTCOM, LTD., 325 Front St., Suite 2, Berea, Ohio 44017. Telephone: 216-234-1333, FAX: 216-234-3425

Chicago, IL . . . Michael J. Pak, CENTCOM, LTD., 540 Frontage Rd., Northfield, Ill. 60093. Telephone: 312-441-6383, FAX: 312-441-6382

Houston, TX . . . Michael J. Pak, CENTCOM, LTD., Telephone: 312-441-6383

San Francisco, CA . . . Paul M. Butts, CENTCOM, LTD., Suite 1070, 2672 Bayshore Frontage Road, Mountain View, CA 94043. Telephone: 415-969-4604

Los Angeles, CA . . . Clay S. Holden, CENTCOM, LTD., Newton Pacific Center, 3142 Pacific Coast Highway, Suite 200, Torrance, CA 90505. Telephone: 213-325-1903

Boston, MA . . . Edward M. Black, CENTCOM, LTD., Telephone: 203-226-7131

Atlanta, GA . . . John F. Raftery, CENTCOM, LTD., Telephone: 212-972-9660

Denver, CO . . . Paul M. Butts, CENTCOM, LTD., Telephone: 415-969-4604

United Kingdom
Reading, England . . . Malcolm Thiele, Technomedia Ltd., Wood Cottage, Shurlock Row, Reading RG10 0QE, Berkshire, England. Telephone: 073-434-3302, Telex #848800, FAX: 073-434-3848

Lancashire, England . . . Technomedia Ltd., c/o Meconomics Ltd., Meconomics House, 31 Old Street, Ashton Under Lyne, Lancashire, England. Telephone: 061-308-3025

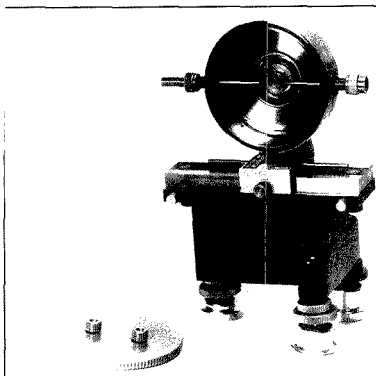
Continental Europe . . . Andre Jamar, International Communications, Inc., Rue Mallar 1, 4800 Verviers, Belgium. Telephone: (087) 22-53-85, Telex #48263, FAX: (087) 23-03-29

Tokyo, Japan . . . Sumio Oka, International Media Representatives Ltd., 2-29 Toranomon, 1-Chome Minato-ku Tokyo 105 Japan. Telephone: 502-0656, Telex #22633, FAX: 591-2530

Master the basics of this powerful analytical tool

X-RAY POWDER DIFFRACTION

**Place Your
Order Today!**



An Audio Course produced by the American Chemical Society

From geology to solid state chemistry, here is an easy-to-use audiocassette course that not only addresses basic principles, but also details techniques and procedures used in X-ray powder diffraction. Beginning with a general overview and ending with a discussion on the use of PDF for qualitative phase analysis, this course covers information on all the key subject areas of this analytical method.

WHAT YOU'LL LEARN

In just a few short hours, you'll gain an understanding of new theories, applications, and techniques. Learn how to set up, align, and run the instrument; how to set up and run diffraction experiments; and how to prepare samples for analysis. Gain a better understanding of how to perform qualitative phase analysis and how to interpret X-ray diffraction data. Plus, these topics will add to your overall understanding:

- principles of X-ray powder diffraction
- instrument selection and parameters
- sample preparation for X-ray diffractometry
- data evaluation
- qualitative methods

HOW YOU'LL BENEFIT

Because this course teaches you the basic principles involved, you'll improve your on-the-job effectiveness . . . get better data from your X-ray equipment . . . perform analyses faster and more accurately . . . learn special techniques for qualitative phase identification . . . and more!

ABOUT THE COURSE AUTHOR

Ron Jenkins, JCPDS-ICDO, Swarthmore, Pennsylvania, was formerly Principal Scientist, Philips Electronic Instruments. He has been actively involved in the application of X-ray spectrographic and diffraction techniques and has published six books and more than 100 papers on these methods.

UNIT (Catalog No. A5)

This audio course comes with four audiocassette tapes (that's 3.7 hours listening time) and a 153-page manual—packaged in a convenient reference-shelf case.

US & Canada: \$440.00; export: \$528.00.
Additional manuals: \$35.00 each, US & Canada; \$42.00 each, export.

**BACKED BY THE ACS
GUARANTEE**

ACS guarantees you'll benefit from this course! If you're not completely satisfied with your audio course, simply return it within ten days of receipt for a full refund, charge credit, or cancellation of invoice.

CALL TOLL FREE 1-800-227-5558!
In Washington DC area call (202) 872-4363!

O · R · D · E · R · F · O · R · M

Send this Order Form with your payment or purchase order to:
American Chemical Society, Distribution Office, Dept. 06
PO Box 57136, West End Station, Washington, DC 20037

	Qty.	US & Can Price	Export Price	Total Amount
X-ray Powder Diffraction (Cat. No. A5)	_____	\$440.00	\$528.00	\$ _____
Additional Manuals	_____	\$ 35.00	\$ 42.00	\$ _____
Total enclosed:				\$ _____

Ship to: Name _____
Organization _____
Address _____
City, State, Zip _____
Phone _____

Bill to: Name _____
Organization _____
Address _____
City, State, Zip _____
Phone _____

Methods of Payment:
 Payment enclosed (make checks payable to ACS). Purchase order enclosed. PO # _____
 Charge my MasterCard/VISA American Express Diners Club/Carte Blanche
 Account # _____
 Expires _____ Interbank # _____
 Name of Cardholder _____
 Signature _____
 Phone _____

Orders from individuals must be prepaid. Please allow 2-3 weeks for UPS delivery. Foreign payment must be made in US currency by international money order, UNESCO coupons, or US bank draft.

EDITOR: **GEORGE H. MORRISON**ASSOCIATE EDITORS: **Klaus Biemann,
Georges Guiochon, Walter C. Herlihy,
Robert A. Oosteryoung, Edward S. Yeung****Editorial Headquarters**1155 Sixteenth St., N.W.
Washington, DC 20036
Phone: 202-872-4570
Telefax: 202-872-6325Managing Editor: **Sharon G. Boots**Associate Editors: **Louise Voress,
Mary Warner**Assistant Editors: **Grace K. Lee,
Alan R. Newman**Editorial Assistant: **Felicia Wach**Director, Operational Support: **C. Michael
Phillippe**Production Manager: **Leroy L. Corcoran**Art Director: **Alan Kahan**Designer: **Amy Meyer Phifer**Production Editor: **Elizabeth E. Wood**Circulation: **Claud Robinson**Editorial Assistant, LabGuide: **Joanne Mullican****Journals Dept., Columbus, Ohio**Associate Head: **Marianne Brogan**Journals Editing Manager: **Joseph E. Yurvati**Associate Editor: **Rodney L. Temos**Staff Editor: **Sharon K. Hatfield**Advisory Board: **Bernard J. Bulkin, Michael S.
Epstein, Renaat Gijbels, Peter R. Griffiths,
Thomas L. Isenhour, Nobuhiko Ishibashi,
James W. Jorgenson, Peter C. Jurs, Mary A.
Kaiser, David L. Nelson, Lawrence A. Pachia,
Ralph E. Sturgeon, George S. Wilson, Mary J.
Wirth, Andrew T. Zander, Richard N. Zare**
Ex Officio: **Sam P. Perone**Instrumentation Advisory Panel: **James B.
Callis, Bruce Chase, R. Graham Cooks, L. J.
Cline Love, Sanford P. Markey, Ronald E. Ma-
jors, Linda B. McGown, Gary W. Small, R. Mark
Wightman***Published by the*
AMERICAN CHEMICAL SOCIETY
1155 16th Street, N.W.
Washington, DC 20036**Publications Division**Director: **Robert H. Marks**Journals: **Charles R. Bertsch**Special Publications: **Randall E. Wedin**Manuscript requirements are published in the
January 1, 1989 issue, page 91. Manuscripts
for publication (4 copies) should be submitted
to ANALYTICAL CHEMISTRY at the ACS Washing-
ton address.The American Chemical Society and its editors
assume no responsibility for the statements
and opinions advanced by contributors. Views
expressed in the editorials are those of the
editors and do not necessarily represent the
official position of the American Chemical
Society.

- Azarraga, L. V., 1519
- Blo, G., 1489
Bond, A. M., 1494
Bragg, N., 1577
Bright, F. V., 1510
- Carlson, D. A., 1564
Carr, P. W., 1524
Carreira, L. A., 1519
Chen, C.-Y., 1590
Cheong, W. J., 1524
Chou, T.-Y., 1538, 1548
Cooper, J. R., 1571
- Demana, T., 1590
Denton, M. B., 1513
Deterding, L. J., 1577
de Wit, J. S. M., 1577
Dobbs, J. C., 1519
Dondi, F., 1489
Duncan, W., 1584
- Effiong, R., 1594
Epperson, P. M., 1513
Evilia, R. F., 1594
- Farnham, I., 1584
Fehl, A. J., 1596
Fuggert, E., 1478
- Gao, C.-X., 1538, 1548
Gilpin, R. K., 1534
Glennon, J. D., 1474
Grinberg, N., 1548
Guiochon, G., 1489
Gurka, D. F., 1584
- Hann, C. J., 1534
Hector, J., 1564
Hobo, T., 1505
Huang, S.-D., 1590
- Imasaka, T., 1530
Ishibashi, N., 1530
- Jorgenson, J. W., 1577
- Kennedy, R. T., 1577
Kim, H.-J., 1485
Kim, Y.-K., 1485
Kowalski, Z., 1598
Krull, I. S., 1538, 1548
Kubiak, W. W., 1598
- Litwiler, K. S., 1510
- Majewski, T. P., 1494
Marcott, C., 1596
Miller, B., 1497
Morris, M. D., 1590
Moseley, M. A., 1577
- Neuburger, G. G., 1559
NiChoileain, N., 1474
- Perry, K. L., 1502
Potter, B. B., 1584
Pyle, S., 1584
- Remelli, M., 1489
Roan, C.-S., 1564
Rosamilia, J. M., 1497
- Senior, A. T., 1474
Susetyo, W., 1519
Suzuki, S., 1505
Swarin, S. J., 1502
- Tashiro, K., 1530
Titus, R., 1584
Tomer, K. B., 1577
- Vidal-Madjar, M. C., 1489
- Wilkins, C. L., 1571
Wouffe, M. R., 1474
Wu, X.-Z., 1505
- Yamada, M., 1505
Yost, R. A., 1564

Analysis of Siderophores and Synthetic Hydroxamic Acids by High-Performance Liquid Chromatography with Amperometric Detection

Jeremy D. Glennon,* Michael R. Woulfe, Andrew T. Senior, and Nuala NiCholleain

Department of Chemistry, University College Cork, Cork, Ireland

Microbial siderophores are an important class of secreted metal sequestering agent with applications ranging from chelation therapy to precious metal recovery. The analysis of siderophores and of synthetic models of siderophores by high-performance liquid chromatography (HPLC) is hampered by metal sequestering problems during the chromatography. The biocompatibility of HPLC systems is examined here by comparison of the reversed-phase chromatographic behavior of a series of synthetic dihydroxamic acids, $\text{HONH-CO-(CH}_2\text{)}_n\text{-CO-NHOH}$ ($n = 3-7$) on metal-free and stainless-steel HPLC systems. Problems associated with chelate formation on column are not encountered on the metal-free system. An applied voltage of +1.0 V (vs Ag/AgCl) is optimum for amperometric detection and is used in conjunction with detection at 220 nm. For pimelic dihydroxamic acid ($n = 5$), under the given chromatographic conditions, the limit of detection is 5.8×10^{-8} M using amperometric detection. The greater sensitivity and selectivity achievable with amperometric detection and illustrated in this work on dihydroxamic acids can be exploited in the analysis of medically and industrially important hydroxamic acids. Desferoxamine, the commercially available chelation therapy drug, and its Fe(III) complex can be simultaneously analyzed by using amperometric detection with limits of detection down to 4.1×10^{-8} and 8.4×10^{-7} M, respectively. The selective monitoring of siderophores produced in liquid culture by genetically engineered strains of *Pseudomonas fluorescens* is performed by direct injection of filtered supernatant samples.

Microbial metal mining is a term recently applied to the use of microorganisms for metal extraction and recovery (1). This development in biotechnology is boosted by the availability of genetically engineered bacterial strains with enhanced metal sequestering abilities. Both the secreted agents and the biomass itself have found applications in extractive metallurgy and waste treatment. Microbial siderophores are an important class of secreted metal sequestering agent with applications in clinical medicine, biotechnology, industry, and analytical chemistry. Functional groups particularly responsible for the high selectivity of these agents for Fe(III) include the hydroxamate and catecholate groups. The trihydroxamic acid, desferoxamine, is a commercially available siderophore used for the treatment of iron overload and aluminum intoxication (2). The immobilization of siderophores onto solid supports provides resins for the recovery of trace metals from aqueous solution (3). In particular, a polyhydroxamic acid resin was used in the recovery of uranium from seawater (4). Hydroxamic acids have received considerable attention also as reagents in analytical chemistry for gravimetric analysis (5) and for the solvent extraction and spectrophotometric determination of metals (6). The reagents have also been shown to be useful in the analysis of trace metals by flow injection analysis (7) and high-performance liquid chromatography.

Complexes of Zr(IV), Hf(IV), Fe(III), Nb(V), Al(III), and Sb(III) with *N*-methylfurohydroxamic acid have been separated on ϵ polymeric column with high chromatographic efficiency (8).

The demand for sensitive and selective methods of analysis for these hydroxamic acid ligands has increased as a result of their wide applications. Methods that have been used include hydrolysis and derivatization techniques (9), paper electrophoresis (10), spectrophotometry (11), and thin-layer (12) and gas chromatographic analysis (13). A number of HPLC methods have been reported for a select group of clinically important hydroxamic acids, in particular for aromatic hydroxamic acids believed to be activated metabolites of carcinogenic arylamides. These include the analysis of aromatic hydroxamic acids in complex mixtures (14), *N*-hydroxy derivatives of phenacetin, acetaminophen, and other hydroxamic acids as their Fe(III) complexes (15) and, more recently, desferoxamine with its Fe(III) and Al(III) chelates (16, 17). It is clear that there is an increasing need for efficient methods of analysis of these agents, whether they are products of biotechnology, chemical synthesis, the environment, or metabolism. The method of choice requires the added attribute of biocompatibility because of the strong metal binding properties of these compounds.

The hydroxamic acids under investigation here are shown in Figure 1. Research in this laboratory has led to a convenient synthesis of a series of strongly chelating dihydroxamic acids, $\text{HONH-CO-(CH}_2\text{)}_n\text{-CO-NHOH}$ ($n = 3-14$), which were previously not readily available (18). These compounds are simple models for the naturally occurring siderophore, rhodotorulic acid (19). The reagents have a particularly strong affinity for Fe(III) and are being investigated with respect to their biological activity, coordination chemistry (20), and analytical applications. In this work the chromatographic behavior of the water-soluble acids on stainless steel and inert HPLC systems is investigated. Chromatographic conditions are optimized on a metal-free system and an improvement in sensitivity is demonstrated by the use of amperometric detection. The combination of amperometric detection with chromatography on an inert system offers considerable advantages in the general area of hydroxamic acid analysis. The method is applied to the detection of the important chelation drug desferoxamine (DFA) and to its Fe(III) complex ferrioxamine (FA). The monitoring of siderophore production by *Pseudomonas fluorescens* can be carried out by direct injection of filtered supernatant samples.

EXPERIMENTAL SECTION

Instrumentation. Two HPLC systems were employed in this work. The first chromatographic analyses were carried out on a stainless steel chromatograph consisting of a Pye-Unicam LC3-XP pump, a Rheodyne Model 7125 sample injector (20 μL), and an LC3-UV detector. Separator columns used include a Chrompack Nucleosil C18 (25 cm \times 4.0 mm i.d.) and a Waters μ Bondapak C18 column (25 cm \times 4.6 mm i.d.). The inert HPLC system consisted of a Dionex analytical pump, an inert high-pressure injection valve (10 μL), and a Dionex RPLC C18 10- μm

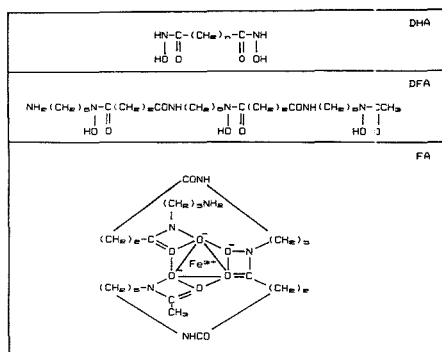


Figure 1. Structures of di- and trihydroxamic acids.

Table I. Relative Standard Deviations and Limits of Detection for Hydroxamic Acids, HOHN-CO-(CH₂)_n-CO-NHOH and Siderophores^a

n	product	UV		EC	
		mean % RSD	LOD, M × 10 ⁺⁶	mean % RSD	LOD, M × 10 ⁺⁶
3	glutaric	1.1	6.1	1.7	3.2
4	adipic	0.8	7.4	2.4	4.9
5	pimelic	0.9	8.4	2.3	5.8
6	suberic	1.4	15.6	3.2	1.2
	DFA	2.7	1.8	3.6	0.04
	FA	3.4	0.6	3.8	0.8

^a Concentration ranges studied: DHA, 6.0×10^{-6} to 2.5×10^{-4} M; DFA, 1.0×10^{-5} to 1.0×10^{-4} M; FA, 5.0×10^{-6} to 4.0×10^{-5} M.

analytical column (25 cm × 6 mm i.d.). Dual detection was carried out by using UV detection at 220 nm in conjunction with an LC-17 amperometric detection system from Bioanalytical Systems Inc. dc amperometric detection was carried out with a Metrohm 626 Polarecord. An applied potential of +1.0 V (vs Ag/AgCl) was found to be optimum. A flow rate of 1.5 mL/min was used, unless otherwise stated. For stationary cell work a mini glassy carbon electrode, obtained from Metrohm (Herisau, Switzerland), was used in conjunction with a platinum wire auxiliary electrode and a Ag/AgCl (3 M KCl) reference. A Princeton Applied Research Model 364 polarographic analyzer was also employed. Infrared spectra were recorded as 1% KBr disks on a Perkin-Elmer Model 682 spectrophotometer. Proton NMR spectra were recorded in Me₂SO-*d*₆ on JEOL GX270, JOEL PS100, and Perkin-Elmer R12 60-MHz instruments.

Synthesis and Characterization of Reagents. The two-step derivatization reaction of aliphatic dicarboxylic acids using *N,N'*-carbonyldiimidazole as previously reported from our laboratory was employed to produce the series of water-soluble reagents shown in Table I (18). Important practical advantages of this method are the mild conditions used, the stability of the diimidazole intermediates, and the direct precipitation of the desired product from the reaction mixture. The products were characterized by infrared and proton NMR spectroscopy. The proton NMR spectrum obtained for pimelidihydroxamic acid (*n* = 5) reveals the important characteristic resonances for the N-OH and N-H protons at 10.35 and 8.69 ppm (18).

Bacterial Culture Supernatant Samples. A selected strain of *Pseudomonas fluorescens* was maintained on minimal asparagine agar consisting of sucrose (20 g), L-asparagine (2 g), K₂HPO₄ (1 g), MgSO₄·7H₂O (0.5 g), and agar (15 g) in a liter of triply distilled water. Liquid medium contains all of the above constituents except agar. Colonies from agar plates were transferred to liquid media and the liquid cultures were grown overnight at 30 °C, with aeration by vigorous shaking. Overnight cultures were then used to inoculate (1% inoculum) 100-mL volumes of sterile media in 500-mL Erlenmeyer flasks. After 12 h, bacteria were removed from the cultures by centrifugation at 10 000 rpm for

10 min. The supernatants were collected and filtered prior to injection on the HPLC system.

Reagents and Standard Solutions. All reagents were of analytical grade purity unless otherwise stated. Desferoxamine (DFA) was obtained from Ciba Geigy, as the commercially available drug "desferal mesylate". *N,N'*-Carbonyldiimidazole was obtained from Sigma Chemical Co. The chemicals used for mobile phase preparation were obtained from BDH Chemicals (sodium chloride, sodium nitrate, acetic acid, citric acid, ethylenediaminetetraacetic acid, and sodium hydroxide). HPLC grade methanol was obtained from Rathburn Chemicals (Walkerburn, UK).

AnalaR ferric nitrate was used to prepare a 0.1 M Fe(III) stock solution in 1% HNO₃. Stock solutions (0.1 M) of the dihydroxamic acids listed in Table I were prepared by using the relevant mobile phase as sample solvent. Standard solutions were subsequently prepared from the stock in the concentration range 2.5×10^{-4} to 1.0×10^{-5} M. A reduction in the solubility of the longer chained dihydroxamic acids (*n* = 6, 7) was observed for sample solvents with low methanol concentrations (i.e. <2%). Standard solutions of desferoxamine were prepared in the concentration range 1×10^{-3} to 1×10^{-8} M. The solutions were spiked with Fe(III) to produce mixtures of desferoxamine and ferroxamine.

A series of mobile phases were prepared to optimize the detection and chromatographic resolution of the hydroxamic acids, by examining the effects of percentage organic modifier, pH, EDTA concentration, and the background electrolyte. Stock solutions of acetic acid (1.05 M) and sodium hydroxide (1.00 M) were used to prepare a 15 mM acetate buffer. The organic modifier, methanol was incorporated to provide a range of study from 0.5 to 10%, while pH was varied from 3.6 to 5.6 by adjustment with sodium hydroxide. The concentration of EDTA in the mobile phase was varied from 0.0 to 2.5×10^{-2} M at a 5% methanol level. In the analysis of DFA and FA, 5 mM citric acid was incorporated into a mobile phase of 33/67 methanol-water containing 15 mM acetate buffer. Siderophore supernatant samples were injected into a mobile phase of 8/92 methanol-water containing 15 mM acetate buffer (pH = 5.0).

Amperometric Detection. Stationary cell voltammetry of the dihydroxamic acids showed that the acids are oxidized at potentials greater than +0.5 V (vs Ag/AgCl) and the oxidation wave reaches a maximum at 1.3 V. An applied potential of +1.0 V was chosen for amperometric detection of the synthetic dihydroxamic acids following chromatographic separation to remain within the glassy carbon working range (27). In the simultaneous analysis of DFA and FA an applied potential of +1.1 V was used to enhance the response of FA relative to DFA, at a flow rate of 1.3 mL/min while +0.5 V was chosen for optimum siderophore detection in supernatant samples. A polishing procedure for the glassy carbon working electrode was carried out at set intervals (22).

The effect of background electrolyte concentration on the detector responses was studied by using sodium nitrate in the 10–200 mM range at +1.0 V and a flow rate of 1.5 mL/min. The electrochemical response was largest in the 100–200 mM electrolyte range and a level of 100 mM was chosen for incorporation into the mobile phase composition. Sodium nitrate was later replaced by sodium chloride for dual chromatographic detection at 220 nm and 1.0 V as the nitrate absorbs strongly in the 190–250 nm wavelength range.

RESULTS AND DISCUSSION

The question of the biocompatibility of HPLC systems for the analysis and isolation of biologically viable products is of major concern in biotechnology. The strong chelating ability of hydroxamic acids and siderophores in particular for Fe(III) and Al(III) has resulted in their use in chelation therapy and metal sequestration. This useful attribute is a troublesome feature in the analysis of these compounds by HPLC, as evidenced by a number of workers. Attempts to chromatograph mononuclear aromatic hydroxamic acids resulted in serious chemisorption in both the adsorption and partition modes (14). This chemisorption and pronounced tailing of the chromatographic peaks were attributed to strong chelate

formation with trace metals predominantly Fe(III) present as impurities in the silica matrix. Incorporation of a chelating agent such as DFA itself into the mobile phase suppressed the chemisorption effects between the stationary phase and the sample hydroxamic acids. Similar effects in the HPLC analysis of *N*-hydroxy derivatives of phenacetin, acetaminophen, and 2-acetylaminofluorene were overcome by the incorporation of ferric chloride into the mobile phase, resulting in a method of detection as ferric chelates (15). Poor chromatographic behavior of naphtho- and anthranilohydroxamic acids in aqueous methanol eluents disappeared when phosphate buffer was added.

A HPLC method for the determination of the important drug desferoxamine and its Fe(III) chelate involves purging the system with desferoxamine or the incorporation of EDTA into the mobile phase (16). The problem of sample contamination on the HPLC system is particularly acute when as in the above case it is required to quantify both the strongly chelating hydroxamic acid and its Fe(III) complex (23). The series of hydroxamic acids under study here represents a timely and useful opportunity to obtain some basic information on the chromatographic behavior and detection of this class of compound.

Analysis on Stainless Steel HPLC System. Initially, aqueous solutions of each dihydroxamic acid were injected onto the stainless steel system in a mobile phase of 20/80 acetonitrile-water with detection at 218 nm. Each chromatogram showed a series of broad and overlapping peaks with retention times up to 1 h in some cases. The behavior is a further example of interference by iron present in the chromatographic system resulting in the appearance of extra peaks, severe tailing, and long retention times (16). Single peaks were obtained when pH control was introduced by using an acetate buffer, with retention increasing with chain length. However, severe tailing was still evident and for suberic dihydroxamic acid only a broad disturbance of the base line was observed. The effects of adding trimethylamine (TMA), triethylamine (TEA), and EDTA into the mobile phase were examined. The addition of 4 mM TMA resulted in a significant sharpening of all peaks and a decrease in retention times. Further improvements were obtained with TEA and EDTA in terms of peak shape and width. The results show that improved chromatography is achievable by masking active silanol groups or by removing metallic impurities in the chromatographic system. EDTA would appear to be a convenient and effective choice for a mobile phase additive to overcome iron interference. However the shorter chain dihydroxamic acids ($n = 3-5$) had low retention times and were difficult to resolve despite the use of 3 mM EDTA in the mobile phase. Linear calibration graphs were constructed over the concentration range 1.0×10^{-3} to 1.0×10^{-2} M for pimelic, suberic, and azelaic dihydroxamic acids but sensitivity was never high in a background of EDTA at 218 nm.

Metal-Free HPLC System. Problems associated with chelate formation on the column by the dihydroxamic acids were not encountered on the metal-free system. The order of elution was in accordance with molecular weight and good chromatographic behavior was obtained with or without EDTA in the mobile phase. Figure 2 shows a plot of k' values against percent methanol in the mobile phase. As expected capacity factors decrease with increasing methanol concentration for the series of hydroxamic acids. A mobile phase containing 0.5% methanol was found to be optimum for the separation. A typical chromatogram obtained with detection at 220 nm is shown in Figure 3. Under these conditions, azelaic dihydroxamic acid is retained much longer and is not shown. The front-running peak is imidazole, a byproduct of the synthetic reaction, which absorbs strongly at 220 nm.

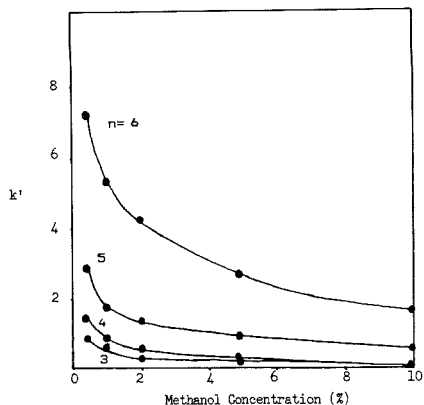


Figure 2. Plot of capacity factors as a function of percentage methanol for the series of dihydroxamic acids.

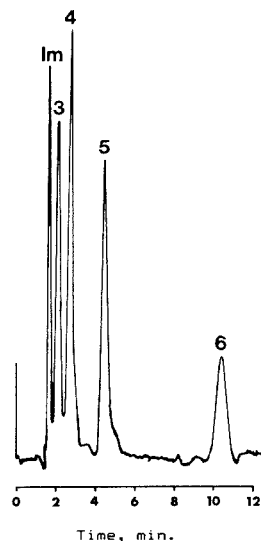
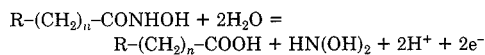


Figure 3. Chromatogram obtained for a mixture of dihydroxamic acids ($n = 3-6$) with UV detection at 220 nm: sample concentrations, 2.0×10^{-4} each; column, Dionex Ion pac, RPIC-C₁₈ 10 μ m; injection volume, 10 μ L into a mobile phase of 0.5/99.5 methanol-water containing 15 mM acetate buffer (pH 4.7) and 100 mM NaCl; flow rate, 1.5 mL/min.

Amperometric Detection. Monohydroxamic acids undergo an irreversible electrochemical oxidation process at positive potentials according to the equation



The intermediate product, $\text{HN}(\text{OH})_2$, slowly converts to hyponitrous acid (24). A recent detailed voltammetric study of the dihydroxamic acids has shown that none of the acids could be reduced (at a DME) but confirms that all the electrode processes are irreversible (25). The electrochemical reduction of hydroxamate and siderophore complexes of ferric ion has been studied by cyclic voltammetry and shown to be reversible or quasi-reversible under suitable conditions (26). However, despite the interest in the voltammetry of these acids in

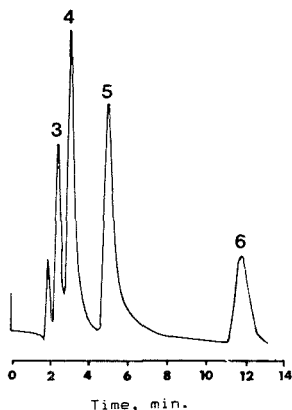


Figure 4. Corresponding chromatogram obtained for a mixture of dihydroxamic acids with amperometric detection at +1.0 V.

stationary cells, no reports have appeared on the amperometric detection of hydroxamic acids in flowing systems.

Initial amperometric results obtained on single injections of suberic dihydroxamic acid showed a varying response with time at the glassy carbon electrode. On further investigations, it was discovered that following an initial sharp drop in response after polishing the electrode, the response then remained constant. This useful working period generally allowed in the order of 70 injections (depending on sample concentration) before giving way to a gradual decline in response. The optimization of the amperometric response involved studies of the effects of flow rate, pH, and background electrolyte. These studies led to the selection of a mobile phase of 0.5/99.5 methanol-water containing 15 mM acetate and 100 mM NaCl. Figure 4 shows the corresponding chromatogram obtained by using amperometric detection. The most obvious difference between the chromatograms obtained by UV and amperometric detection is the absence of an imidazole peak in the latter, highlighting the selectivity advantage of this mode of detection.

Calibration graphs obtained by using dual detection displayed good linearity for each of the dihydroxamic acids. Correlation coefficients for UV detection varied from 0.9991 to 0.9808 as compared to 0.9986 to 0.9791 for amperometric detection. The mean percent relative standard deviations ($n = 5$) obtained together with the limits of detection are shown in Table I. UV detection is seen to have a slight advantage in terms of linearity and reproducibility. However, the disadvantages associated with amperometric detection such as electrode contamination, degree of complexity (relative to UV), and dependence on chromatographic parameters can be significantly outweighed by the advantages of increased selectivity and lower limits of detection.

Detection of Siderophores. The feasibility of directly and simultaneously determining DFA and FA using amperometric detection was investigated. The results indicate that even on a metal-free HPLC system, the presence of a chelating agent is necessary to prevent sample contamination of DFA with Fe(III). With detection at 255 nm evidence for on-column complex formation was obtained for injections of DFA, even after system purging with 20 mM aqueous DFA solution. The incorporation of EDTA suppresses this complex formation. Its use is not, however, compatible with the amperometric detection of DFA or FA due to the background oxidation of EDTA at 1.1 V (27). Figure 5 shows a typical chromatogram obtained for a mixture of DFA and FA using amperometric

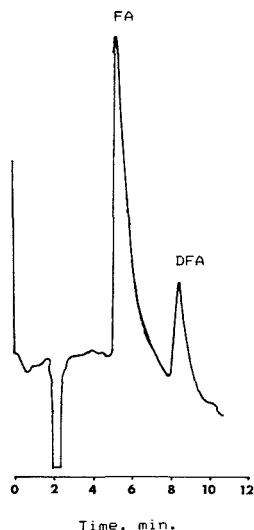


Figure 5. Simultaneous chromatographic analysis of DFA (1×10^{-4} M) and FA (2×10^{-3} M) by amperometric detection on a metal-free HPLC system: mobile phase, 67/33 water-methanol containing 15 mM acetate buffer and 5 mM citric acid (pH = 4.7); flow rate, 1.3 mL/min; 10 μ L injection volume; detection at +1.1 V.

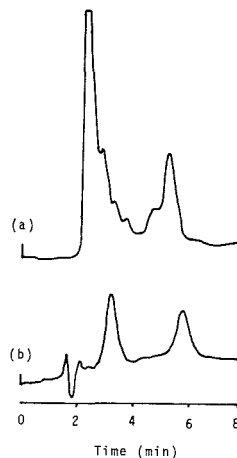


Figure 6. Detection of siderophores in supernatant samples of *Pseudomonas fluorescens* using (a) UV, 254 nm; (b) amperometric detection, +0.5 V. Mobile phase was 92/8 water-methanol containing 15 mM acetate buffer (pH = 5.0); flow rate was 1.5 mL/min.

detection, achieved by substitution of citric acid for EDTA in the mobile phase. No evidence for sample contamination of DFA was observed under these conditions. Amperometric detection yields the lower limit of detection for DFA (Table I).

A further illustration of the selectivity of the method is obtained when analyzing supernatant samples from growing cultures of *Pseudomonas* species (28, 29). Despite the complexity of the sample matrix as revealed by detection at 254 nm, only bands for the secreted siderophores appear in the chromatogram with amperometric detection at +0.5 V (Figure 6). To monitor siderophore production in biotechnology,

amperometric detection on a metal-free HPLC system is a convenient method that is selective, sensitive, and biocompatible.

ACKNOWLEDGMENT

Thanks are due to our colleagues in the laboratories of Dr. F. O'Gara (Biotechnology Centre, UCC), Professor D. A. Brown (Department of Chemistry, UCD), and Professor G. Svehla (Department of Chemistry, UCC).

LITERATURE CITED

- (1) Monroe, D. *International Biotechnology Laboratory*, 1985 (June), 19-29.
- (2) Rawls, R. L. *Chem. Eng. News* 1977, 55, 24.
- (3) DeVoe, I. W.; Holbein, B. E. *Trace Metal Removal from Aqueous Solution*; Special Publication No. 61, Thompson, R., Ed.; Royal Society of Chemistry: London, 1986.
- (4) Vernon, F.; Eccles, H. *Anal. Chim. Acta* 1977, 94, 317.
- (5) Agrawal, Y. K.; Roshania, R. D. *Bull. Soc. Chim. Belg.* 1980, 89(3), 159-174.
- (6) Agrawal, Y. K.; Patel, S. A. *Rev. Anal. Chem.* 1980, 4(4), 237-278.
- (7) Glennon, J. D.; Senior, A. T. *Anal. Chim. Acta* 1967, 196, 333-336.
- (8) Palmieri, M. D.; Fritz, T. S. *Anal. Chem.* 1987, 59, 2226-2231.
- (9) Gillam, A. H.; Lewis, A. G.; Anderson, R. J. *Anal. Chem.* 1981, 53, 841-844.
- (10) Fekete, F. A.; Spence, J. T.; Emery, T. F. *Anal. Biochem.* 1983, 131, 516-519.
- (11) Emery, T. F.; Neilands, J. B. *J. Org. Chem.* 1962, 27, 1075-1076.
- (12) Lepri, L.; Desideri, P. G.; Heimler, D. *J. Chromatogr.* 1983, 268, 495-501.
- (13) Razzoek, C.; Lhoest, G.; Roberfroid, M.; Mercier, M. *Anal. Biochem.* 1977, 83, 194-203.
- (14) Corbett, M. D.; Chipko, B. R. *Anal. Biochem.* 1979, 98, 169.
- (15) Hinson, J. A.; Pohl, L. R.; Gillette, J. F. *Anal. Biochem.* 1980, 101, 462.
- (16) Cramér, S. M.; Nathanael, B.; Horvath, C. *J. Chromatogr.* 1984, 295, 405-411.
- (17) Van der Horst, A.; DeGoede, P. N.; Willems, H. J. J.; VanLoenen, A. C. *J. Chromatogr. Biomed. Appl.* 1986, 381, 185-191.
- (18) Brown, D. A.; Geraty, R. A.; Glennon, J. D.; Ni Choileain, N. *Synth. Commun.* 1985, 15(13), 1159-1164.
- (19) Barclay, S. J.; Huynh, B. H.; Raymond, K. N. *Inorg. Chem.* 1984, 23, 2011-2018.
- (20) Brown, D. A.; Geraty, R. A.; Glennon, J. D.; Ni, Choileain, N. *Inorg. Chem.* 1986, 25, 3792-3796.
- (21) Rucki, R. J. *Talanta* 1980, 27, 147-156.
- (22) Panzur, R. E.; Elving, P. J. *J. Electrochem. Soc.* 1972, 119, 864.
- (23) Kruch, T. P. A.; Kalow, W.; Crapper-McLachlan, D. R. *J. Chromatogr.* 1985, 347, 123-130.
- (24) Ramsbottom, J. V.; Waters, N. A. *J. Chem. Soc. B* 1967, 180.
- (25) Amberson, J. A.; Svehla, G. *Anal. Proc.* 1966, 23, 443-446.
- (26) Abu-Dari, K.; Cooper, S. R.; Raymond, K. N. *Inorg. Chem.* 1978, 17(12), 3394-3397.
- (27) Dai, J.; Helz, R. *Anal. Chem.* 1988, 60, 301-305.
- (28) Stranier, R. Y.; Palleroni, N. J.; Doudoroff, M. *J. Gen. Microbiol.* 1966, 43, 159-271.
- (29) Teintze, M.; et al. *Biochemistry* 1981, 20, 6446-6457.

RECEIVED for review July 7, 1988. Resubmitted December 8, 1988. Accepted April 11, 1989. The support in-kind of the Dionex Corporation C.A. is gratefully acknowledged.

Zone Gas Chromatography

Endre Fuggerth¹

Research Institute for Ferrous Metallurgy, Environmental Department, Fehervari ut 130, Budapest, Hungary

A new gas chromatographic arrangement is outlined in which a narrow heat pulse scans slowly down a relatively short column. The above scan effects unusual separations and simultaneously creates favorable boundary conditions for cold storing of the uneluted component. This cold-storing feature offers a new approach to any stopped-flow gas chromatographic application; multidimensional gas chromatography stands to benefit if this new arrangement replaces the usual precolumn.

INTRODUCTION

Decades ago, Zhukhovitskii (1) investigated the application of moving thermal gradients to gas-solid chromatography. His method was later reinvestigated, extended to gas-liquid chromatography (2), and theoretized (3), and the whole topic was recently reviewed (4). In his technique, called chromatothermography, a mild thermal gradient while traveling down the column desorbs and keeps each component moving at a characteristic temperature, thus effecting a separation that travels with the velocity of the gradient. As a result, samples ranging widely in polarity can be rapidly analyzed and special peak compression occurs. The method claims particular effectiveness in trace enrichment. The whole separation, however, is confined to the length of the applied gradient, which therefore should be reasonably long enough

to suit any practical purpose. (In fact, furnaces longer than 30 cm were applied (alongside columns 30-56 cm in length), with longitudinal temperature gradients of 2 °C/cm (2) and of an adjustable 1.0-8.5 °C/cm (3).) The ultimate separation efficiency, at the same time, obviously decreases with the steepness of the applied thermal gradient, and it is always less than that of the isotherm method (3).

With this review in mind, here we would like to call attention to a seemingly similar arrangement of moving but a narrow (and preferably square) heat pulse alongside a (short) column: An entirely dissimilar—and new—separation mechanism, chromatographic domain, and application area emerge.

THEORY

Consider a heat pulse traveling slowly downward alongside a column that otherwise is in the elution mode (i.e., swept by a carrier gas, with analytes already present), as shown in Figure 1.

Analytes experiencing the low thermal field are traveling at a rather insignificant speed. When they encounter the high thermal field, the analytes are mobilized at once (according to their respective volatility at the sensed higher temperature over the applied stationary phase) and begin to travel with markedly higher speed: They maintain this higher speed as long as they are within the high thermal field window. Any analyte whose speed becomes higher than the velocity of the heat pulse will run into the low thermal field ahead, whereupon its speed decreases to a marginal value again; thus, no analyte can move faster than the heat pulse itself. Other

¹ Current address: Hotel Grüner Baum, Grazerstr. 39, 4820 Bad Ischl, Austria.

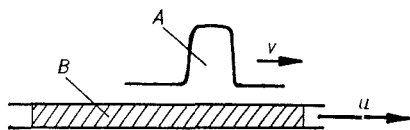


Figure 1. Essence of zone gas chromatography: a (narrow) heat pulse (A) (serving as the high thermal field) of v velocity moves down the column (B) through which carrier gas flows with u velocity ($v < u$).

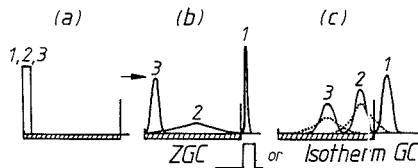


Figure 2. ZGC vs IGC: the case of injection.

analytes, whose gained speed is lower than the velocity of the heat pulse, will—sooner or later—lag behind, where the low thermal field turns them into slow-moving species anew: They are practically bound to the place, or “frozen”.

As soon as the heat pulse has completed a scan over the packed section, the column can safely be bypassed, without any further action needed to ensure that the separation inside the column remains intact. This is because the analytes locked inside now experience the low thermal field throughout the entire column length, and therefore they remain “frozen” (owing to the greatly reduced diffusion at the sensed low temperature), thus storing the separation during the ensuing stopped-flow condition. Naturally, the column that stores the “frozen” separation can be subjected to repeated scans—with long pauses in between (which enable the swept-off (i.e. eluted) portions to be further resolved chromatographically or to be dealt with according to any particular conception)—as many times as wanted. In this way one can obtain many contiguous preprepared fractions, without any loss, all from a single sampling. With this technique delicate applications that require not merely stopping the flow in GC, but rather stopping the GC process itself, will become feasible.

The characteristics of this type of separation will become more elucidated as the following modifications are implemented: (a) applied heat pulses of decreasing width, (b) sensed heat pulses that become increasingly square-like, and (c) a lower thermal field that allows even less movement of the analytes therein.

Decreasing the width of the heat pulse, at the same time, means that the whole column, except a tiny length, experiences the low thermal field throughout the scanning time. This reduces the overall unwanted diffusion even further, rendering the method very attractive for any GC application where stopped flow is a must. This type of chromatography, which uses a narrow heat pulse to scan slowly down a gas chromatographic column, is henceforth referred to as “zone gas chromatography” (ZGC).

Figures 2 and 3 illustrate the effect of ZGC on two basic cases (of narrow and wide starting input profiles, respectively), in comparison with that of isotherm gas chromatography (IGC).

Figure 2a illustrates the distribution of three overlapping components introduced to the column as a narrow input (i.e. injected). The length of the column and its elution side are indicated on the abscissa by hatching and a vertical mark, respectively. Figure 2b sketches the result after the first ZGC scan (position of the heat pulse is as indicated): A sufficiently volatilized component (1) travels along with (and within) the heat pulse and is eluted completely. An insufficiently vola-

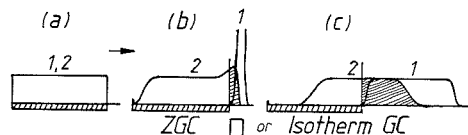


Figure 3. ZGC vs IGC: the case of wide initial input.

tilized component (2) slowly phases out, and thus considerably spreads throughout the column, with only traces of it eluting. A component of still lower volatility (3) experiences even less of the heat pulse while it is overhead, and therefore, its travel and distortion are both marginal. When elution is conducted to the same extent but now isothermally (Figure 2c), separation surely cannot be worse. However, with the flow stopped for a longer period, considerable deterioration of the locked isotherm separation will inevitably occur (see the dotted line in Figure 2c) due to the prevailing higher temperature, while the already frozen ZGC prepreparation faces no such effect (because of ZGC's inherent, low thermal field conception). Thus, advantages of ZGC over isotherm stopped-flow GC may be beginning with the second scan.

A more drastic difference between the capabilities of ZGC and IGC can be foreseen when the components to be separated are already spread over the entire length of the column; yet, a certain degree of separation would have to be effected (see Figure 3). Clearly, ZGC is by far superior, in this case in the absolute separation efficiency (and now on the grounds of ZGC's delicate separation mechanism). Since elongated/spread component profiles are commonly produced from the narrow input case by ZGC also (see 2 in Figure 2b), Figure 3 is also quite suggestive as to why ZGC is expected to retain much of its separation efficiency throughout the ensuing scans. Otherwise, wide initial input profiles are commonly found in cases of environmental sampling tubes, which points to another application area where ZGC seems to hold promise as a classic tool.

EXPERIMENTAL SECTION

Equipment. The complex ZGC arrangement was a home-fabricated unit. The effluent from the ZGC column was monitored and analyzed by a directly coupled packed column housed in a Fractovap 2450 GC Model (Carlo Erba) chromatograph working in the programmed temperature mode. The temperature measurements inside the ZGC columns were carried out with the aid of a long, 0.02 in. o.d. sheathed NiCr/Ni thermocouple, with its linearized read-out meter (Ahlborn) connected to a Linseis recorder. Processing, storing, and retrieving of ZGC experimental data, as well as all chromatographic modeling, were done on a HP-85A (Hewlett-Packard) desktop computer (32K RAM plus one driving cassette).

Columns. The ZGC columns were made of Pyrex glass tubes of 6/3, 4/2.4, and 2/1 mm o.d./i.d. and were filled over sections varying from 45 to 100 mm. The analyzer was a 150-cm packed column made of 4/2.4 mm o.d./i.d. Pyrex glass tubing. The packing material was 100/120 mesh Supelcoport coated with 10% GE SE 30 for both types of columns. (ZGC columns of 5 and 25% loading were also packed and examined.)

Materials. Stock mixtures prepared from *n*-alkanes of different commercial sources and stored refrigerated in Teflon-capped Wheaton vials were used throughout the study.

Procedure. After a ZGC setup was assembled and fixed, sample was injected to the top of the ZGC column, which was then subjected to a number of scans with predetermined scan parameters (i.e. furnace temperature (T_f), scanning velocity (v), total time of flush (Zt), carrier gas flow (u), start and end positions of the furnace). After each completed scan, the ZGC column was bypassed to stimulate stopped-flow conditions. This period—lasting for about 25 min—was taken to determine the composition of the eluted portion that arrived from the just-completed ZGC scan by the help of the analyzer column, in order to examine ZGC's

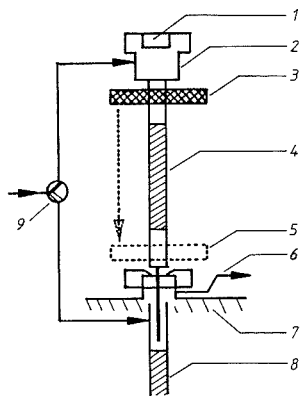


Figure 4. Experimental arrangement for ZGC in this study: 1, septa; 2, tee; 3, narrow furnace (start position); 4, ZGC column; 5, furnace at the end of a normal ZGC scan; 6, septum purge; 7, GC oven boundary; 8, analyzer column; 9, selecto valve.

performance. ZGC flushes (i.e. Σt) ranged from 1 to 4 min, so cycles from one scan to the next took about 30 min. The ZGC column was made clear and ready for the next experiment (injection plus a predetermined set of scans) via sweeping it with a ZGC scan of low velocity and high (290 °C) temperature.

RESULTS AND DISCUSSION

The basic prerequisite of ZGC can be satisfied by a great diversity of contrivances of different levels of sophistication. In our rudimentary model (see Figure 4) the heat pulse was generated by a heat-regulated furnace (3) (serving as the high thermal field) moving down alongside the ZGC column (4), which otherwise experienced the ambient (serving as the low thermal field). Furnaces were constructed to fit the corresponding ZGC tubes into their central bore with minimal clearance to ensure good heat transfer. They were built to be as narrow as 8 mm; 5 mm was a uniformly heated brass body and the remaining 3 mm was insulation at the top and bottom. The ZGC effect was thought to become practically observable for traveling distances at least several times longer than the width of the heat pulse applied. In accordance, ZGC

columns having packed sections in the range of 45–100 mm were used in our investigations. Each furnace maintained reliable temperature controllability over the combined range of 60–280 °C furnace temperature and of 0–2 mm/s scan velocity, which covered and surpassed the range intended to be used.

ZGC has many variables affecting the separation: four setup parameters (i.e., heat dynamics of the ZGC tube, length of its filled section (L), loading %, and type of stationary phase applied) and six scan parameters. The effect of all these variables (except the type of stationary phase) was studied and data were collected from 218 ZGC experiments carried out systematically. Preparations of different types and degrees were achieved over the n -alkane range of C_9 – C_{18} with near and consistent 100% recoveries observed in each experiment. (Corresponding normalized area counts were compared with results from direct GC analysis of the same mixtures.) To elute a component from a column by ZGC always requires a somewhat higher furnace temperature than a GC oven temperature to do the same task isothermally, because the heat pulse in ZGC assists (at it) only at a fraction of the column at a time. This restriction, however, is not a hampering limitation to ZGC, because it can be largely counterbalanced by, say, lowering the scan velocity.

Figure 5 presents the traces of two experiments: approximately 1–1.5 μ L of C_9 – C_{13} stock solution was injected, which was subjected to successive ZGC scans (indicated by arabic numbers encircled). Each portion so eluted was analyzed by programmed temperature gas chromatography (PTGC) (with integrator report stuck overhead). The numbers above the peaks denote carbon numbers (i.e., 9 stands for nonane, etc.). Detection sensitivity was kept adjusted to have 0.3% of the n -alkane components still area-reported. (To compress the whole picture to a manageable size, early parts of the PTGC traces were omitted in the cases of late ZGC scans. They were obviously free of peaks, according to the integrator reports.) The setup for Figure 5a was as follows: ZGC tube of 6/3 mm o.d./i.d. having $L = 50$ mm; packed section filled with 10% GE SE 30 on Supelport 100/120. For Figure 5b the setup was the same except $L = 100$ mm. The scan parameters were common for both: $v = 0.85$ mm/s, Σt in accordance with L (to which small, standardized distances were added at both the top and bottom of the ZGC column (as is suggested in

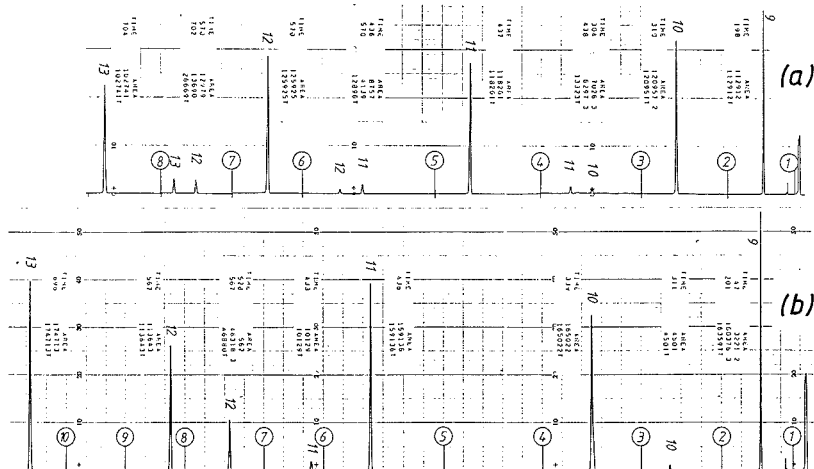


Figure 5. Traces of two ZGC experiments, analytically resolved. T_r was programmed upward from scan to scan; L , 50 (a) and 100 mm (b). Other parameters are given in the text.

Table I. Preseparation by ZGC (Elution Percentages), Compressed Report^a

scans	<i>n</i> -alkane components				
	C-9	C-10	C-11	C-12	C-13
Section A					
1	all				
2		94.5			
3		5.5	4.7		
4			88.7		
5			6.6		
6				2.9	
7				88.0	
8				9.1	8.5
					63.9
Section B					
1	all				
2		2.7			
3		97.3			
4					
5			94.0		
6			6.0		
7				29.0	
8				71.0	
9					
10					94.0

^a*L* = 50 (A) and 100 mm (B). See both text and Figure 5.

Figure 4) to facilitate certain pre- and postflushes, respectively). T_r was 80 °C during the first scan, 90 °C during the second scan and so on; it was 10°C higher during each following scan. Carrier gas velocity was kept identical, calculated to be about 20–23 mm/s throughout the ZGC tube. These traces together with the integrator reports demonstrate that even our rudimentary model produces results free of artifacts, and as such, it is suitable to study ZGC.

Table I contains the processed results of the two ZGC experiments shown in Figure 5. The compositions of successive scans are in rows. The values in a column mean the eluted percentages of the compound designated at the top of that column. From the rows one can see that significant preseparation was effected by ZGC on a column as short as 5 cm and that an added 5 cm offered tremendous further improvement. To describe efficiency in ZGC quantitatively the term "cut width" seems useful. It refers to a window range on the index scale of the stationary phase in the ZGC column and is measured in index units (IU), from which range components were eluted by the actual ZGC scan and represent themselves, say, above their 1%. In this terminology, the cut width proves to be close to but higher than 100 for $L = 50$ mm in Table I, Section A (see third, fifth, and seventh scans), and it is clearly less than 100 for the $L = 100$ mm case there (since no two *n*-alkanes are present in any row, moreover, there are two rows apparently empty). Quantitative values of cut

width, however, cannot be extracted from these reports (at least not until more is known about ZGC itself). Fortunately, another experiment described later allows for its direct determination.

Doubling the column length caused the same *n*-alkanes to be swept off the ZGC column by later scans, except for nonane. Quite obviously, if a component keeps moving with the heat pulse, then the length it has to travel does not matter: It is completely eluted by the scan (as C₉ did here). If, however, the component phases out, no matter how slowly, (like C₁₀, of which 5.5% was left uneluted after the second scan) then any further length it has to travel will retard an additional amount. (In this case, the second scan eluted only 2.7% of the C₁₀ from the column of double length as compared with 94.5%. This is a rather puzzling difference, but the far-from-ideal profile of our experimentally generated heat pulse (in conjunction with the necessarily longer postflush applied) may provide an explanation.)

The fact that both C₁₁ and C₁₂ were eluted within two scans from the longer column as compared with three scans from the shorter one is also noteworthy: Since the successive scans were carried out at higher and higher T_r , this meant more effective compression for C₁₁ during the fifth and sixth scans than during the third, fourth, and fifth scans, despite the fact that it was spread considerably more over the longer column at comparable stages. So, besides cut width, another useful term inherent to ZGC seems to be "slicing". By definition it means the number of scans in which a given component is present (again, above 1% of its total amount in the sample).

The lowest attainable cut width of a given ZGC column is certainly well defined, and it is advisable to work close to it to exploit maximal preseparation. The slicing, on the contrary, is more or less a question of designing the set of scans to be performed, and it is worth taking advantage of the variations it can offer. High slicing value is especially rewarding in such cases when reanalysis is needed for any reason but the sample is available only once. High slicing no only lessens the risk of wasting a precious or unique sample through incidental mishandling and offers all conceivable advantages that can be gained via repeated analyses, but also facilitates data reduction in peak pairing for multidimensional GC (see below).

One of the easiest ways to effect and study slicing is to repeat identical ZGC scans over and again. The smaller the phasing out of a given component under a ZGC scan of fixed parameters, the lower the slicing value for that component. Extensive phasing out of a component, on the other hand, will adversely delay its appearance in the ZGC cuts. The experiments reported in Table II illustrate these points. The setup was as follows: ZGC tube of 2/1 mm o.d./i.d. having $L = 100$ mm; packed section filled with 10% GE SE 30 on Supelcoport 100/120. The scan parameters were $T_r = 100$ °C, $v = 1.7$ mm/s, $\Sigma t = 85$ s (including pre- and postflush), and u constant

Table II. Slicing by ZGC^a

	a			b			c			d			
	C-13	C-14	C-15	C-12	C-13	C-14	C-11	C-12	C-13	C-10	C-11	C-12	C-13
1	98.8			1	all	28.3	1	all	63.5	1	all	0.5	
2	1.2			2		60.1	2		35.9	2		33.9	
3		2.6		3		11.6	3		0.6	3		60.6	
4		32.0		4			4			4		5.1	
5		43.0		5			5			5			
6		14.8		6			6			6			
				7			7			7			1.1
						1.5	8			8			28.2
						20.0	9			9			50.7
										10			18.7
										11			1.3

^aCarrier gas velocity (u) was decreased stepwise from experiment to experiment (from left to right).

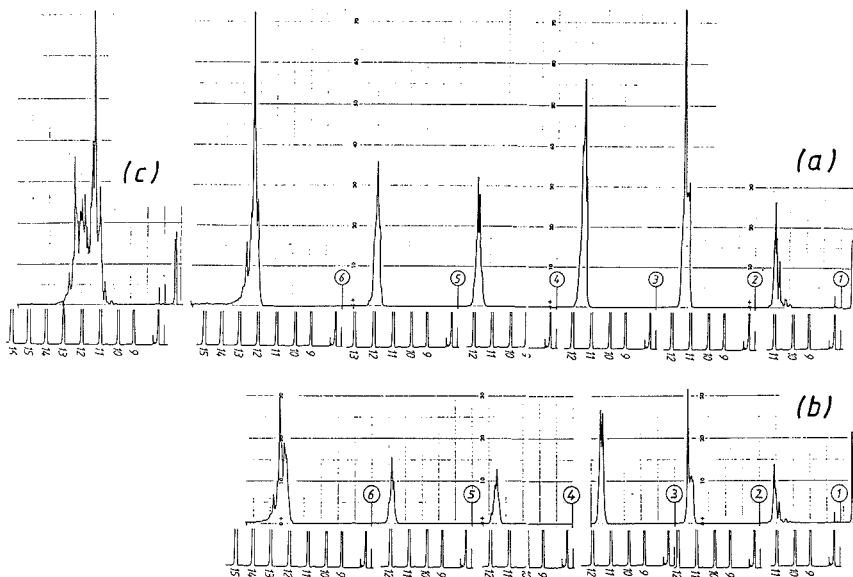


Figure 6. Direct determination of ZGC cut width. (See text.)

throughout each experiment; such scans were repeated the number of times indicated. Between the experiments u was varied. A special flow arrangement placed before the ZGC column allowed (via a combination of adjustable metric valves and shutoff valves) resettable (though unmeasured) proportions of the carrier gas to be flushed through the ZGC column, leaving the total (i.e. combined) amount of carrier gas that flowed through the analyzer column unaltered. The effective linear carrier gas velocity was about 9 times higher for the experiment in Table IIa than for those reported in Table I because, during all these experiments, the total amount of carrier gas was switched to flush the ZGC columns but the respective inner diameters were 1 versus 3 mm. This alone may account for the great decrease in overall efficiency seen in Table IIa on the grounds that u was certainly far beyond the optimal height equivalent of a theoretical plate (HETP) range. However, as soon as u was decreased (see b, c, and d in Table II), efficiency returned. Even the superiority of the 2/1 mm o.d./i.d. ZGC tube over the 6/3 one (L was 100 mm for both), in terms of "successive scans containing no or only traces of n -alkanes" (loosely related to cut width), began to show: The obviously faster heat response of the much narrower tube surely enabled clearer ZGC effects to be operative. It is also clearly seen that slicing and cut width are practically independent; the former is an option available to ZGC and can be varied at will without causing deterioration to the latter.

An obvious area where ZGC may find promising application is multidimensional gas chromatography (MDGC). Replacing the usual precolumn by a ZGC arrangement will hold the prepreparation while resolution on the second column proceeds. Prospects for ZGC, however, very much depend on whether its efficiency will ever become high enough to produce sufficiently narrow cuts. We believe that cut widths of approximately 10 IU will certainly satisfy most requirements. When such a cut is resolved on an analyzer column of highly different polarity, its components have a range of at least several hundred IU on the analyzer column's stationary phase available to repopulate, with the resolution power of the analyzer column applied. ZGC cut widths much narrower than 10 IU, however, would only excessively lengthen the total

MDGC analysis time for those samples that really cry out for MDGC.

At present, a 6/3 mm o.d./i.d. and $L = 100$ mm long ZGC column offered a ~ 60 -IU cut width (see Figure 6a), and another ZGC tube of the same filled length but with better heat dynamics (4/2.4 mm o.d./i.d.) gave cut-width values smaller than 50 IU (see Figure 6b). These readings can be taken directly from Figure 6: Instead of injections from stock mixtures of n -alkanes, a heavy fraction of reformed benzene (courtesy of Dr. Tibor Tóth, ELTE, Budapest) was injected. This sample was so abundant in components over a range of at least 150 IU that to our analyzer it appeared as if it were practically contiguous (see its total chromatogram in Figure 6c). Now, if the ZGC column and the analyzer use identical GC stationary phases, then any "resolved", non-empty ZGC scan leaves a trace of fused peaks whose width at the base gives the wanted cut-width value after masking it against the n -alkane scale (recorded under similar conditions). (For greater accuracy the direct reading should be down-corrected with a value of one peak width, right available from the n -alkane traces). Figure 6a,b shows exactly such experiments: Five identical scans were repeated, and a final sixth at high T_r brought down the residue. If we recall by comparison the fact from Table I, Section A, that a 50 mm long ZGC column gave a cut width definitely higher than 100 IU, then reaching the 10-IU goal does not seem to be a far-away target.

To realize that goal, three principal factors are the most beneficial: the length of the ZGC column, the narrowness of the heat-pulse-generating device, and better (i.e., delayless and distortion-free) transmission of the primary heat pulse. All results in our present study were achieved in spite of a serious lack of such transmission, due to the rudimentary model.

To gain an insight into the real shape of the transmitted heat pulse (i.e., which is in fact sensed by the analytes inside the ZGC column), each furnace was tested as follows. After assembly of the usual setup (see Figure 4), a thin (0.02-in. o.d.) thermocouple sensor was centrally introduced through the septa deep into the filled section of the ZGC column. T_r was set, and the signal from the sensor was recorded, superimposed

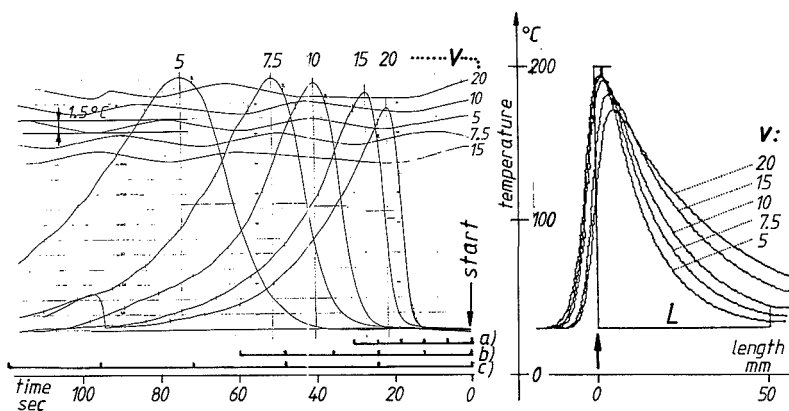


Figure 7. Shape of the transmitted heat pulse: experimental (left side) and computer-reconstructed (right side). Active furnace width was 5 mm; ZGC tube was 2/1 mm o.d./i.d.

from five scans of different v . This was carried out at five furnace temperatures (60, 100, 150, 200, and 280 °C). The resultant picture for $T_f = 200$ °C and for the furnace that accommodated a 2/1 mm o.d./i.d. ZGC column is shown on the left side of Figure 7. Controllability of furnace heating was also recorded simultaneously (at increased amplification, of course). The corresponding traces are labeled by experimental v values; to convert them to mm/s, multiply by 0.085. The experimental data gathered this way enabled us to generate heat distributions over the ZGC column length by computer from input parameters of T_f , v , and L for each experimental setup in good agreement. The reconstructed curves are placed opposite, on the right side of Figure 7. The middle of the furnace (on the move from right to left) is indicated by an arrow. (To ease comparison, distances marked as a, b, and c each equivalent to a furnace movement of 50 mm, were set against the abscissa on the left side for the cases of $v = 20$, 10, and 5, respectively.)

It is surprising to see how strongly the effective traveling heat profiles (Figure 7, right side) deviated from the aimed heat pulse (Figure 1), yet ZGC was found definitively to be operative throughout the experiments. True, the temperature dropped rather gently (and increasingly so for ZGC tubes of greater heat inertia), but migration capabilities were affected in a more direct way by corresponding capacity factors, which decreased more steeply. Lower scan velocities afforded more effective cooldown and thus purer ZGC effects. Parallel with increasing v values, the drop in the maximum values of sensed temperature as well as the increasing delay in their positions underscored other weak points of our technical implementation. These together made direct comparisons between ZGC experiments often cumbersome. The most important future task to increase the ZGC character of the method is, however, beyond dispute: Rendering the effective (i.e. transmitted) heat pulse significantly narrower and more square like is expected to greatly enhance the already-found advantages.

To use ZGC with MDGC, refocusing the components arrived by the scan is a must (in order to meet the stringent input conditions for any capillary column coupled as analyzer). The refocusing can be accomplished either by applying the PTGC technique to the analyzer or, allowing for more flexible manipulations, via inserting a small cold trap. Splitting the components held in a cold trap between two different-polarity capillary columns in parallel is quite feasible today. When this trap is fed by ZGC, the incidental coelution of components within a cut width of ~ 10 IU decreases further significantly

while "dimensionality" advances smoothly.

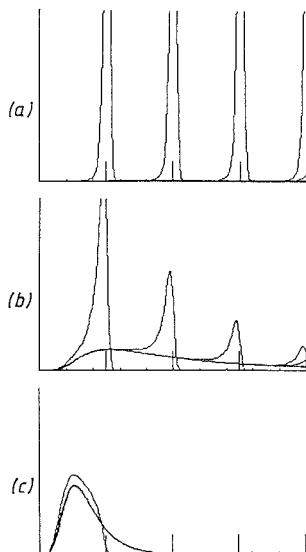
An added benefit to MDGC comes from the slicing effect: When two different-polarity capillary column analyzers in parallel are fed by ZGC, the task of peak pairing on the chromatograms from the different columns is as easy as looking for slicing patterns of a perfect match. Information from comparative peak intensities—which is the only chromatographic clue for data reduction in the absence of slicing—comes as supplementary aid to confirm the pairing, except in rare cases where several identical slicing patterns are manifested, when cross reference has to rely on matching intensities alone. But, how often are several identical slicing patterns to be encountered? Table II_d seems to be informative: The slicing patterns of C_{11} and C_{12} components exactly 100 IU apart, are so immensely different (throughout the 1–11 scans) that a difference of 1 IU is almost sure to cause a recognizable shift in the percent values that constitute the slicing pattern. Obviously, a decrease in cut width means that the same shift in slicing patterns will be observed, but for compounds even less apart. So, if the cut width in Table II_d is estimated at 50 IU, then a cut width as narrow as 10 IU might sufficiently differentiate between the slicing patterns of two components eluting from the ZGC column as close to each other as 0.2 IU.

Another uncommon potential can be realized by breaking the tacit rules so far adhered to that a scan should always start from a position well above the top of the filled section and that it should necessarily last until the furnace moves well below the bottom of the packed section. For, on the one hand, components can be accumulated on any discretionary section of the ZGC column, supposing that scans are conducted only up to that point (followed by rapid removal of the furnace to its next starting position). On the other hand, when a partial scan begins from a certain mid-position (to which point the furnace has to be moved in split seconds again), component distributions ahead can be ZGC-affected at will (up to the extremes of sweeping off all components present, either to gain information on their amounts or to prepare a clear section for the benefit of the scans that follow) while component distributions behind are left only marginally disturbed. Predictable exploitation of such scans, of course, would require substantial knowledge of component distributions along the ZGC column.

The exotic and rather complex separation mechanism in conjunction with the great diversity in the scan parameters that can be selected makes the outcome of a ZGC experiment,

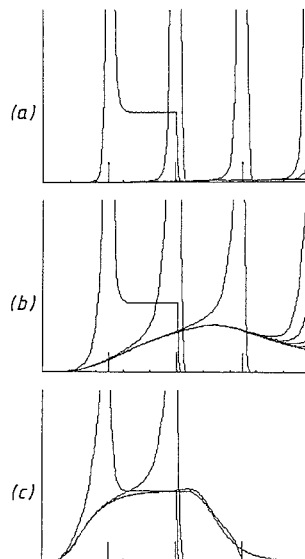
Table III. Monitoring of Elution Percentage Values via Computer Simulation of the First ZGC Scan for Two Different Initial Input Widths (W)^a

monitoring	scan time, s	elution, %						
		$W = 1$ mm			$W = 50$ mm			
		C-12.5	C-13	C-13.5	C-12.5	C-13	C-13.5	
at quarters of the filled section	1/4	30	0.00	0.00	0.00	0.00	0.00	0.00
	1/2	60	0.00	0.00	0.00	0.00	0.00	0.00
	3/4	89	0.00	0.00	0.00	0.00	0.00	0.00
	1	119	0.00	0.73	38.50	0.00	1.62	39.15
over the postflush period	124	0.00	7.22	93.61	0.03	15.92	95.15	
	129	0.00	9.06	95.06	0.05	20.23	96.63	
	133	0.00	9.60	95.27	0.06	21.45	96.84	
	138	0.00	9.83	95.34	0.07	21.93	96.91	
	143	0.00	9.95	95.37	0.07	22.16	96.95	
at end of scan	144	0.00	9.97	95.38	0.07	22.20	96.96	

^a $L = 100$ mm. See text and Figures 8 and 9.**Figure 8.** Computer-simulated ZGC transformation: monitored distributions for cases of $W = 1$ mm (i.e., injection).

at present, quite difficult to predict. However, because of ZGC's numerous conceivable future applications, a deeper understanding of the roles and effects of each parameter in detail would be advantageous. Therefore, computer software was developed to run on the HP-85 to simulate the ZGC process. Special features of the software included declaring still nonexisting ZGC setups at will, visualizing the component's distributions over the filled section of the ZGC column at any optional predetermined stage, and offering IGC modeling as well. The software had been thoroughly tested, and an acceptable match was found with the ZGC experiments over a diverging parameter field.

With the aid of this software the progress of the ZGC process can be monitored. Figure 8 and Figure 9 illustrate component distributions. The abscissa refers to the filled section of the ZGC column, with its open, right end denoting the elution side. The ordinate signifies the relative intensity of the component present, in arbitrary units. The compounds examined are hypothetical n -alkanes of 12.5 (a), 13 (b), and 13.5 (c) effective carbon number, with initial input widths of

**Figure 9.** Computer-simulated ZGC transformation: monitored distributions for $W = L/2$.

$W = 1$ mm (Figure 8) and $W = 50$ mm (Figure 9) on filled sections of $L = 100$ mm. Otherwise, both the setup and the scan parameters were identical as follows: $T_r = 120$ °C, $v = 0.85$ mm/s, $u = 22$ mm/s, and $\Sigma t = 144$ s. To examine the clearest ZGC effect already available but without losing the ground of reality, characteristics of the fastest heat response ZGC tube (i.e., the one with 2/1 mm o.d./i.d.) were chosen to govern the computation. Monitoring took place at stages when the furnace reached quarters of the filled length (where longer ticks on the abscissa mark out the corresponding furnace positions), more frequently during the postflush period, and finally, at the end of the scan. Though it is only the first ZGC scan that is examined in Figure 8 and Figure 9, the proceeding "peak" transformations seen on them entirely support all statements on the mechanism that were merely foreshadowed in the theory section. Table III is a collection of elution data from these simulated experiments, with the monitoring points stated. The "elugrams" indicate an important but not awaited feature in common: No matter what overall degree of elution takes place and what kind of

Table IV. Computer-Simulated Elution Percentage Values for ZGC vs IGC^c

	W = 1 mm (L/100)	W = 50 mm (L/2)	W = 100 mm (L)
ZGC^b			
C-12.5	95.4	97	98.2
C-13	10	22.2	49.5
C-13.5	0	0.1	17.4
	T 115 °C t ₀ 23.10	T 115 °C t ₀ 20.02	T 104 °C t ₀ 32.56
			T 104 °C t ₀ 31.46
IGC^c			
C-12.5	98.6	95.1	96.1
C-13	4.9	51.6	51.4
C-13.5	0	14.1	11.6
			53.4

^a L = 100 mm; for other conditions, see text. ^b T_i = 120 °C, T_{eff} = 115 °C, t₀ = 31.68. ^c t₀ values indicate elution volumes in void volume units.

input it comes from, the bulk amount always arrives within the same, and quite narrow, time window. In other words, anything that moves during ZGC moves with (and within) the heat pulse. These same "elugrams" seem to support the view that postflush as a variable will have limited importance if improved ZGC technology produces more definite edges for the effective heat pulse.

Preliminary results of comparing ZGC versus IGC comprise Table IV. Again, computer modeling was used. Column parameters and carrier gas flow were identical. For ZGC,

conditions were the same as for Figure 8 and Figure 9. (In fact, the corresponding total elution percent values were taken out of Table III!) To ensure comparability between ZGC and IGC, each elution was conducted roughly to the same extent, until the most volatile component (here n-C_{12.5}) eluted 95-98%. To accomplish this by IGC, either the temperature or the elution volume (measured in void volume units (t₀)) was adjusted for direct comparison. While the comparative elution values for W = 1 mm verify our introductory statement that ZGC can never be better than (uninterrupted) IGC in term of resolution, data from the longer initial input experiments confirm the view, also, that ZGC is a clear winner there.

Finally, here are a few brief, closing remarks: (1) ZGC would seem to be easily adaptable for chromatographic on-line sample pretreatment and also for small-scale preparative separations, especially in the case of a low or unforeseen duty cycle. (2) Serially coupled ZGC columns add stopped-flow potential to cross separation. (3) ZGC's stopped flow also translates into a certain storability and as such, provides the opportunity for detaching, transporting, and reassembling ZGC columns of a certain prehistory.

LITERATURE CITED

- (1) Zhukhovitskii, A. A.; Zolotareva, O. V.; Sokolov, V. A.; Turkel'taub, N. M. *Dokl. Akad. Nauk SSSR* 1951, 77, 435.
- (2) Nerheim, Glenn A. *Anal. Chem.* 1960, 32, 436-437.
- (3) Ohline, Wayne, R.; DeFord, Donald D. *Anal. Chem.* 1963, 35, 227-234.
- (4) Berezkin, V. G.; Chernysheva, T. Yu.; Buzajev, V. V.; Koshevnik, M. A. *J. Chromatogr.* 1986, 373, 21-44.

RECEIVED for review December 14, 1988. Accepted April 3, 1989.

Determination of Nitrite in Drinking Water and Environmental Samples by Ion Exclusion Chromatography with Electrochemical Detection

Hie-Joon Kim*

Kim & Associates, 33 Pleasant Street, Wayland, Massachusetts 01778

Young-Kyung Kim

Department of Chemistry and Food Science, Framingham State College, Framingham, Massachusetts 01701

An extremely sensitive determination of nitrite in drinking water (tap water and underground water) and environmental samples (rain, lake water, and soil) was achieved by ion exclusion chromatography (IEC) with electrochemical (EC) detection. Potential interferences in the determination of nitrite by the standard spectrophotometric method or by the ion exchange chromatographic method with either conductivity detection or UV detection were eliminated. The detection limit was 0.1 ppb without preconcentration. No nitrite was observed from tap water or underground drinking water. The recoveries of nitrite added to tap water at 0.02, 0.1, and 1 ppm levels were between 96 and 104.5%. The average coefficient of variation was 4.7%. The recovery results were in good agreement with those obtained by the standard spectrophotometric method. Nitrite concentrations between 0.068 and 0.19 ppm were observed in rain within a week period. A greater variation, between 0.015 and 0.26 ppm, was observed in lake water. Amounts of 19.1 ppm and 0.50 ppm nitrite were observed from fertilized and unfertilized soil, respectively.

Nitrite in the environment is derived from biological denitrification, acid rain, and industrial waste. Nitrite can induce methaemoglobinemia and react with secondary and tertiary amines forming carcinogenic nitrosamines (1). Such nitrosation reactions can take place in vivo. Even though saliva is the primary source of human exposure to nitrite (1), it is desirable to monitor the nitrite level in the environment, particularly in drinking water.

The current standard method for nitrite analysis in water is based upon spectrophotometric determination of an azo dye formed by coupling diazotized sulfanilamide with N-(1-naphthyl)ethylenediamine dihydrochloride (Griess reaction) (2). It takes about 30 min; however, a parallel determination of multiple samples is possible. The detection limit is about 10 ppb as NO₂⁻ if a 1-cm light path is used. The problem of this chemical method is that it is subject to interference by some reducing compounds (3) and metal ions or color (2).

Recently, ion chromatography has become popular for analysis of various ionic species. Ion exchange chromatography with conductivity detection developed by Small et al. (4)

utilized a suppressor column to eliminate the background conductivity of the eluant. It is a versatile technique for inorganic ions and was approved jointly by the American Public Health Association, American Water Works Association, and Water Pollution Control Federation for analysis of anions in water (2). The detection limit for nitrite by this method was 0.1 ppm.

In single column ion chromatography developed several years later by Gjerde et al. (5), anions were analyzed without the suppressor column using a low capacity anion exchange column and a dilute eluant. In either case, such common anions as chloride, nitrate, and phosphate are eluted close to nitrite in the ion exchange chromatographic separation and can interfere with nitrite in the conductivity detection if they are present in large excess.

The potential interference by most common anions in the conductometric determination of nitrite can be eliminated by UV detection. Jackson et al. (6) demonstrated that nitrite in several food samples could be determined with a detection limit of about 2 ng using anion exchange chromatographic separation and UV detection at 214 nm. Even though interference by most inorganic anions is eliminated by UV detection, nitrate could still interfere if present in large excess. The UV detection might also introduce interference by some organic contaminants.

Several new ion chromatographic methods were published recently that greatly increased the sensitivity of nitrite analysis. Okada (7) used a high capacity ion exchange column to concentrate nitrite from a large volume (10–50 ml) of sample solution and could detect 0.1 ppb nitrite with UV detection. Kordorouba and Pelletier (8) reported a significant increase in sensitivity (1 ppb nitrite) without concentration using ion exchange chromatography with electrochemical detection.

In anion exchange chromatography, the eluant pH is above the pK of nitrous acid, 3.37. As a result, nitrous acid is fully ionized and the weak acid nature of nitrous acid is not utilized for separation of nitrite from strong acid anions. In anion exclusion chromatography, strong acid anions are excluded from the column and eluted in the void volume, whereas weak acids are eluted in the order of increasing pK values (9). Therefore, ion exclusion chromatography is ideal for separation of nitrite from other weak acids as well as from strong acid anions. The high selectivity of ion exclusion chromatography is due to the fact that (a) the separation is achieved by a combination of several mechanisms such as Donnan exclusion, partitioning, and van der Waals interaction (9) and (b) the pK values of weak acids are different from each other.

Electrochemical detection offers additional selectivity due to the fact that the standard reduction potential varies among different analytes. The combination of these two selective processes yields an extremely high overall specificity. The IEC-EC method has been successfully applied by the authors to the analysis of such weak acids as sulfite (10, 11) and vitamin C (12, 13) in foods.

Nitrite can be oxidized to nitrate at the normal oxidizing potential of an electrochemical (amperometric) detector. Moreover, most common anions are not oxidized at the same potential. We demonstrated that the ion exclusion chromatographic separation-electrochemical detection (IEC-EC) system could be used for determination of nitrite in cured meat, saliva, beer, and lettuce (14). It is the purpose of this paper to show that the IEC-EC system is ideal for separation and detection of nitrite from a complex mixture containing excess amounts of other common anions. We also demonstrate that it is useful for a sensitive determination of nitrite in drinking water and environmental samples.

EXPERIMENTAL SECTION

IEC-EC Method. A Wescan Model 361 Sulfite Analyzer

(Deerfield, IL) equipped with an anion exclusion Ion Guard cartridge, anion exclusion/HS column (4.6 × 100 mm), Rheodyne injector with a 50- μ L sample loop, Model 271 electrochemical detector with a Pt working electrode, and computing integrator (Spectra Physics 4290, San Jose, CA) was used. The eluant was a 5 mM sulfuric acid solution and the flow rate was 0.6 mL/min. An oxidative potential of 1.0 V vs Ag/AgCl reference electrode was used except for obtaining the hydrodynamic voltammogram. The detector sensitivity was set at 100 nA full scale range.

Hydrodynamic Voltammogram. To determine the optimal oxidative potential, a standard solution containing 0.2 ppm NO_2^- (diluted with deionized water from 1000 ppm stock solution made with sodium nitrite) was injected after the detector was equilibrated between 0.6 and 1.2 V at 0.1-V increments. The peak current was determined from the detector readout as the maximum increase in the detector current from the background level. In order to verify the hydrodynamic voltammogram, standard solutions containing 0.25, 0.50, 0.75, and 1.0 ppm NO_2^- were injected at 0.8, 1.0, and 1.2 V.

Separation of Common Anions. To demonstrate the selectivity of the ion exclusion chromatographic separation and the electrochemical detection for nitrite, the following four solutions were analyzed by the IEC-EC method. Solution (A) contained 1 ppm nitrite as NO_2^- . Solution (B) contained 100 ppm each of chloride, nitrate, sulfate, phosphate, carbonate, and fluoride. Solution (C) contained 100 ppm bromide. Solution (D) contained all of these anions at the stated concentrations. The detector voltage was set at 1.0 V for all solutions.

Analysis of Drinking Water and Environmental Samples. Tap water collected in Wayland, MA, and underground drinking water collected in Dover, MA, were injected directly into the chromatograph. Rain water collected (approximately 20-mL aliquots) in Wayland, MA, and lake water collected (50-mL aliquots) from Lake Cochituate in Wayland, MA, were injected after filtration through a 0.45- μ m membrane filter (Nylon 66, Alltech, Deerfield, IL) prewashed with deionized water. Soil samples were collected from approximately 1 in. under the surface of both fertilized (about a month before analysis) and unfertilized ground in Wayland, MA. A 0.5-g aliquot of the soil samples was mixed with 5 mL of deionized water in a test tube, and nitrite was extracted for 2 min by shaking vigorously with a vortex mixer. The extract was filtered through a 0.45- μ m membrane filter and injected.

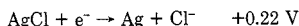
Recovery of Added Nitrite from Tap Water. Tap water was spiked with 0.020, 0.10, and 1.0 ppm NO_2^- by mixing 29.7 mL of tap water with a 0.30-mL aliquot of 2.0, 10, and 100 ppm NO_2^- standard solutions, respectively. The amount of nitrite in the spiked water samples was determined by comparing the signal intensity obtained from these samples by the IEC-EC method with that of 0.020, 0.10, and 1.0 ppm standard NO_2^- solutions prepared in deionized water also obtained by the IEC-EC method. The recovery was determined as the difference between the observed amount of nitrite in the spiked and unspiked water. The recovery was also determined by the standard spectrophotometric method (2) using the same spiked tap water samples and the standard NO_2^- solutions. Five replicate determinations were made by both the IEC-EC method and the spectrophotometric method at all three spiking levels.

Spectrophotometric Method. The standard spectrophotometric method utilizing diazotization-coupling reactions (2) was scaled down. 0.06 mL sulfanilamide solution was added to 3-mL aliquots of the tap water, spiked tap water, and the standard NO_2^- solutions. After 5 min, 0.06 mL of *N*-(1-naphthyl)ethylenediamine dihydrochloride solution was added. Absorbance at 543 nm was measured after 15 min. Deionized water treated similarly was used to zero the spectrophotometer. Absorbance of the reaction mixture containing sample solution was compared with that of the corresponding standard solution.

RESULTS AND DISCUSSION

Hydrodynamic Voltammogram. The standard reduction potentials for the nitrate-nitrite half-reaction and for the reference electrode reaction are (15)



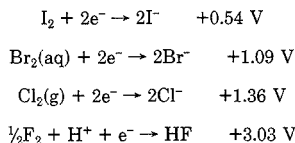


The standard reduction potential for nitrate–nitrite reaction is 0.72 V higher than that of the Ag/AgCl reference electrode reaction. Therefore, a positive oxidizing potential vs the reference electrode is needed to cause oxidation of nitrite at the working electrode. Figure 1 shows the dependence of the detector peak current on the applied voltage (hydrodynamic voltammogram). As expected, the detector output increased significantly between 0.6 and 1.0 V. Nevertheless, it showed a decrease after 1.0 V. A similar behavior was reported in the amperometric detection of iodide with a silver working electrode (16). The calibration curve was linear up to 1.0 ppm at 0.8, 1.0, and 1.2 V with a linear correlation coefficient of 0.998, 0.999, and 0.998, respectively, when the peak height was used. The result was similar when the peak area was used. The slope of the calibration curve was approximately proportional to the peak current at the respective potential in Figure 1. Moreover, this behavior was observed on three separate electrochemical detectors manufactured by Wescan. No explanation was found in the literature. We feel that the reduced signal at high potential might be due to the formation of oxide layers at the surface of the electrode which would decrease the effective potential that the analyte experience. If interference at a higher voltage is suspected, 0.8 V could be used for nitrite even though the sensitivity is somewhat sacrificed. We have not observed any interference for nitrite in many food, water, and environmental samples tested so far. The same results were obtained whether 0.8 or 1.0 V was used. Therefore, 1.0 V is routinely used for maximum sensitivity.

Separation of Common Anions. The elution behavior of many strong and weak acids on the ion exclusion column is well documented (17, 18). Of all the common anions we tested, chloride, nitrate, sulfate, and bromide are anions of strong acids. Therefore, they are eluted in the void volume of the anion exclusion column. The pK_1 of phosphoric acid is 2.12; therefore, phosphate is expected to be eluted after the void volume but ahead of nitrite ($pK = 3.37$) at pH 2 of the eluant. Fluoride ($pK = 3.45$) might show a retention time close to that of nitrite. Carbonate ($pK_1 = 6.37$) will be eluted much later than nitrite.

Figure 2A shows a signal from 1 ppm NO_2^- . The retention time was about 5.2 min when the flow rate was 0.3 mL/min. Figure 2B shows that such anions as nitrate, sulfate, phosphate, and carbonate are not detected by electrochemical detection at 1 V as expected.

The standard reduction potentials involving halide ions are (15)



The standard reduction potential for bromide is 0.15 V higher than that for nitrite. Therefore, bromide was expected to be detected at 1.0 V even though the sensitivity would be less than that for nitrite. However, since HBr is a strong acid, bromide is eluted before nitrite and would not interfere. When a solution containing 100 ppm bromide was injected, a large peak was observed in the void volume as shown in Figure 2C. The standard reduction potentials for chloride and fluoride are much higher than that for nitrite, and these anions were not detected at 1.0 V as shown in Figure 2B.

When a solution containing all these anions at 100 ppm and nitrite at 1 ppm concentration was injected, only bromide and nitrite were observed as shown in Figure 2D. The standard

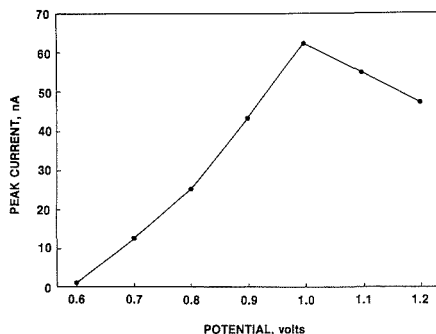


Figure 1. Hydrodynamic voltammogram for nitrite obtained by injecting a 0.2 ppm solution into the IEC–EC system equilibrated at various detector voltages.

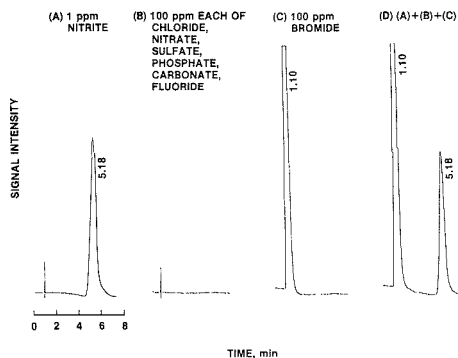


Figure 2. Chromatograms obtained by the IEC–EC method from a solution containing (A) 1 ppm nitrite, (B) 100 ppm each of six common anions not detected by electrochemical detection, (C) 100 ppm bromide, and (D) mixture of all of these anions at the stated concentrations.

reduction potential for iodide is smaller than that for nitrite; therefore iodide would be detected by electrochemical detection at 1.0 V. Since HI is a strong acid, an iodide peak was expected near the void volume. When a solution containing 10 ppm iodide was injected, a large peak immediately after the void volume was observed (chromatogram not shown). Sulfite is eluted between the void volume and nitrite (retention time 2 min at a flow rate of 0.6 mL/min) (14) and does not interfere. These results demonstrate that none of the common anions interfere with nitrite by the IEC–EC method.

Nitrite in Drinking Water. Nitrate and nitrite are the two contaminants of primary importance in drinking water (19). The most sensitive detection for nitrite in drinking water reported to date is 0.1 ppb obtained by concentrating nitrite on a high capacity anion exchanger and detecting the eluted nitrite by UV absorbance at 210 nm (7). Three parts per billion nitrite in tap water was observed by this method.

A similar detection limit can be achieved by the IEC–EC method without concentration. With a Pt working electrode operating at 1.0 V, a signal with a signal-to-noise ratio of 2 was observed under optimal conditions when a 50- μL solution containing 0.1 ppb NO_2^- was injected. This observed sensitivity is 10 times higher than that achieved by ion exchange chromatography with electrochemical detection (1 ppb detection limit) (8).

Figure 3 shows chromatograms obtained from underground drinking water and tap water as well as tap water spiked with 2 ppb NO_2^- . Clearly, both underground water and tap water

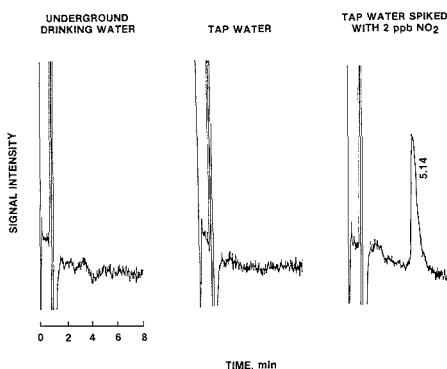


Figure 3. Chromatograms obtained by the IEC-EC method from direct injection of underground drinking water and tap water as well as tap water spiked with 2 ppb NO_2^- .

Table I. Recovery of Added Nitrite from Tap Water Determined by the IEC-EC Method and the Spectrophotometric Method

sample	nitrite, ^a ppm	
	IEC-EC method	spectrophotometric method
tap water	0 ^b	0
tap water, 0.02 ppm spike	0.0209 (± 0.0008)	0.0202 (± 0.0014)
tap water, 0.10 ppm spike	0.096 (± 0.007)	0.095 (± 0.004)
tap water, 1.0 ppm spike	1.02 (± 0.03)	0.98 (± 0.01)

^a Average of five determinations. Standard deviations in parentheses. ^b Less than 0.1 ppb.

examined contain less than 0.1 ppb NO_2^- . It is also clear from the chromatograms that such anions as chloride and nitrate, which are commonly present in drinking water (6, 20), do not interfere with nitrite.

Recovery of Added Nitrite from Drinking Water. The recovery of nitrite added to tap water at 0.020, 0.10, and 1.0 ppm spiking levels was determined by both the IEC-EC method and the standard spectrophotometric method (diazotization-coupling). The 0.02 ppm spiking level is near the detection limit of the spectrophotometric method. Absorbance of 0.013 at 543 nm was observed with a 1-cm light path using a standard solution containing 0.02 ppm NO_2^- .

The recovery of added nitrite varied from 96 to 104.5% by the IEC-EC method (average 101%) and from 95 to 101% by the spectrophotometric method (average 98%) (Table I). The coefficient of variation for five replicate determinations varied from 2.9 to 7.3% by the IEC-EC method (average 4.7%) and from 1.0 to 6.9% by the spectrophotometric method (average 4.0%). The quantitative recovery and the good agreement with the standard method suggest that an accurate determination of nitrite is achieved by the IEC-EC method.

Nitrite in Environmental Samples. The IEC-EC method was applied to the analysis of nitrite in rain, lake water, and fertilized and unfertilized soil samples. Figure 4 shows typical chromatograms obtained by injection of rain and lake water samples after filtration. Nitrite concentration in three rain samples collected on 18, 19, and 24 October, 1988, in Wayland, MA, was 0.11, 0.068, and 0.19 ppm, respectively. These concentrations are significantly higher than the 0.028–0.060 ppm NO_2^- observed in rain at Allegheny Mountain and Laurel Hill in 1983 (21). Nitrite concentration in six lake water

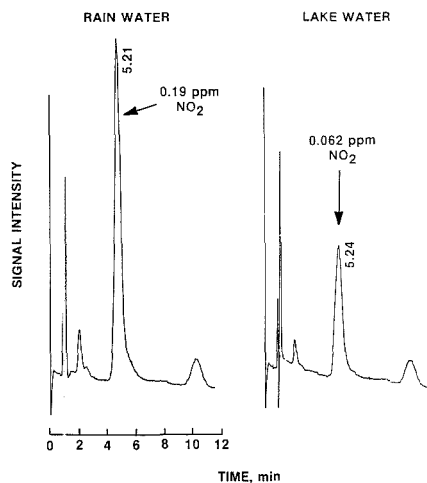


Figure 4. Chromatograms showing nitrite in rain and lake water obtained by the IEC-EC method.

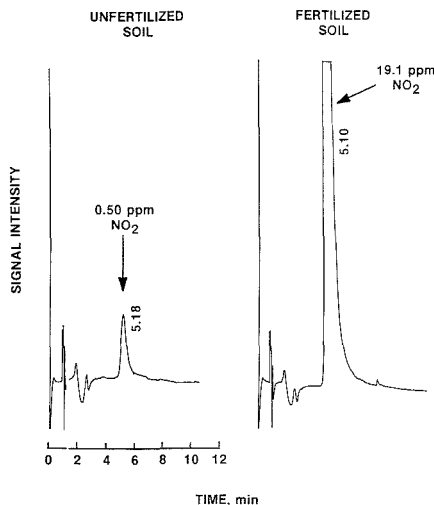


Figure 5. Chromatograms showing nitrite in unfertilized and fertilized soil diluted 10-fold during extraction obtained by the IEC-EC method.

samples collected from three different locations of Lake Cochituate on five different dates during a month period in October 1988 varied widely from 0.015 to 0.26 ppm with an average of 0.14 ppm. Clearly, nitrite is the primary component in both rain and lake water detected by the IEC-EC method. Sulfite is much more readily oxidized than nitrite in water. Sulfite also forms a stable complex with formaldehyde which is the predominant aldehyde in the atmosphere. This adduct, hydroxymethylsulfonate, is not detected by the IEC-EC method. We observed the release of sulfite, upon addition of alkali, from the adduct in rain samples. Further investigation is in progress. The identity of the peaks observed at about 2 and 10 min was not determined. It is interesting that almost identical chromatograms were obtained from rain and lake water in spite of the fact that lake water should contain more organic and inorganic contaminants. This observation

further demonstrates the specificity of the IEC-EC method.

The chromatograms in Figure 5 indicate that the IEC-EC method can be used for determination of nitrite in soil, which is another complex sample matrix. Nitrite concentrations of 0.50 ppm and 19.1 ppm were observed from unfertilized and fertilized soil, respectively. After 10-fold dilution during the extraction, nitrite concentration in the extract was approximately within the linear range of detection (0-1.5 ppm NO₂⁻). Nitrite in unfertilized soil might be derived from the rain and microbial reduction of nitrate in the soil. Nitrite in fertilized soil present at a much higher concentration is believed to be due to microbial reduction of nitrate in the fertilizer. In either case, no interference was observed from other components of the soil. Total analysis time for nitrite in soil was about 10 min including extraction, filtration, and chromatography. Less analysis time is needed for water samples.

LITERATURE CITED

- (1) Green, L. C.; Ralt, D.; Tannenbaum, S. R. In *Human Nutrition*; Neuberger, A., Jukes, T. H., Eds.; Jack K. Burgess: Englewood, NJ, 1982; p 87.
- (2) *Standard Methods for the Examination of Water and Waste water*; 16th ed.; American Public Health Association: Washington, DC, 1985.
- (3) Usher, C. D.; Telling, G. M. *J. Sci. Food Agric.* **1975**, *2*, 1793.
- (4) Small, H.; Stevens, T. S.; Bauman, W. C. *Anal. Chem.* **1975**, *47*, 1801.
- (5) Gjerde, D. T.; Fritz, J. S.; Schmuckler, G. J. *Chromatogr.* **1979**, *186*, 509.
- (6) Jackson, P. E.; Haddad, P. R.; Dilli, S. J. *Chromatogr.* **1984**, *295*, 471.
- (7) Okada, T. *Bunseki Kagaku* **1987**, *36*, 702.
- (8) Kordorouba, V.; Pelletier, M. *Mitt. Geb. Lebensmittelunters. Hyg.* **1988**, *79*, 90.
- (9) Gjerde, D. T.; Fritz, J. S. *Ion Chromatography*; 2nd ed.; Huthig: Heidelberg, 1987; p 235.
- (10) Kim, H.-J.; Kim, Y.-K. *J. Food Sci.* **1986**, *51*, 1360.
- (11) Kim, H.-J.; Park, G. Y.; Kim, Y.-K. *Food Technol.* **1987**, *41*(1), 85.
- (12) Kim, H.-J.; Kim, Y.-K. *J. Food Sci.* **1988**, *53*, 1525.
- (13) Kim, H.-J. *J. Assoc. Off. Anal. Chem.*, in press.
- (14) Kim, H.-J.; Kim, Y.-K. In *Advances in Ion Chromatography*; Jandik, P., Cassidy, R. M., Eds.; Century International: Franklin, MA, 1989; Vol. 1, p 391.
- (15) *Handbook of Chemistry and Physics*; 61st ed.; Weast, R. C., Ed.; CRC Press: Boca Raton, FL, 1980; p D-155.
- (16) Yang, X.-H.; Zhang, H. J. *Chromatogr.* **1988**, *436*, 107.
- (17) Harlow, G. A.; Morman, D. H. *Anal. Chem.* **1964**, *36*, 2438.
- (18) Tanaka, K.; Ishizuka, T.; Sunahara, H. *J. Chromatogr.* **1979**, *174*, 153.
- (19) Pfaff, J. "Ion Chromatography-Needed Analytical Techniques". Presented at the International Ion Chromatography Forum, Sep 27, Boston, MA.
- (20) Iskandarani, Z.; Pietrzyk, D. J. *Anal. Chem.* **1982**, *54*, 2601.
- (21) Pierson, W. R.; Brachaczek, W. W.; Gorse, R. A., Jr.; Japar, S. M.; Norbeck, J. M.; Keeler, G. J. *Environ. Sci. Technol.* **1987**, *21*, 679.

RECEIVED for review December 15, 1988. Accepted April 21, 1989.

Fluidic and Syringe Injection Study by Peak Shape Analysis

Maurizio Remelli, Gabriella Blo, and Francesco Dondi*

Dipartimento di Chimica, Università di Ferrara, via Luigi Borsari 46, I-44100 Ferrara, Italy

Marie Claire Vidal-Madjar

Laboratoire de Physico-Chimie des Biopolymères, CNRS, Université Paris XII, Thiais, France

Georges Guiochon

Department of Chemistry, University of Tennessee, Knoxville, Tennessee 37996-1600

Fluidic and syringe injections with different splitting conditions are compared by using the Edgeworth-Cramér peak shape analysis. Nonretained component peaks on capillary and packed columns were considered. Skewness values as low as 0.02, with precision and repeatability of ± 0.005 , were obtained when using the capillary column with fluidic injection. Extracolumn contributions coming from the injection system were evaluated by using peak skewness under the hypothesis of exponential decay extracolumn factor. The corrected column efficiency values are in good agreement with the theoretically expected van Deemter equation data. A syringe injection system with high split rate can produce, for unretained samples, peak fidelity values greater than 0.8, which are comparable with those observed with the fluidic injection system. Applications in column performance studies are discussed.

INTRODUCTION

Most chromatographic theories characterize the shape of elution peaks or derive exact expressions of statistical quantities (moments or cumulants) as a function of structural and working conditions of the column and of physicochemical

properties of the solute and the stationary phase (1-3). When these models are considered for column efficiency studies or for physicochemical measurements, their complexity must be verified through accurate measurement of that part of the band broadening which depends on the column alone and thus the various extracolumn band distortion effects arising from injection, tubing, and electronics must be kept under control (4-7).

In this work the fast fluidic injection (8), which is known to be the most efficient method for introducing sharp solute pulses into the column, is compared with conventional syringe injection with a split system. A certain amount of experimental work has been done in characterizing extracolumn band broadening contributions of electronics and fluidic injection in high-speed gas chromatography (9). The basic principles followed were first to measure peak parameters and then extract from these the band extracolumn contribution on the basis of hypotheses regarding either the column or the band-broadening contribution. The numerical procedure employed here to determine the peak parameters—the Edgeworth-Cramér (EC) series fitting method—not only more powerful because it is able to give peak parameters with definite precision but, in addition, is also a self-validating method, able to give accurate peak parameter values under definite conditions (10-14). The purpose of this study is to

characterize the above mentioned injection systems in order to assess the most suitable experimental procedures to use in column efficiency measurements.

THEORY

A chromatographic peak, $f(x)$, with mean m and standard deviation σ , normalized to a unit area and expressed as a function of the standardized time variable $x = (t - m)/\sigma$, is approximated by the EC series (15), developed up to the k_{th} order, as follows:

$$f(x) = Z(x) + \sum Q_v(-Z) + R_k(x) \quad (1)$$

where $Q_v(-Z)$ is a linear aggregate of the derivatives of the normal frequency function $Z(x)$, of a maximum order $3v$, and contains cumulant coefficients of a given frequency function $f(x)$ of maximum order v . $R_k(x)$ is the remainder. The detailed expressions of the $Q_v(-Z)$ and $Z(x)$ terms are reported elsewhere (10, 15).

If an experimental chromatographic peak is subjected to nonlinear least-squares fitting, fundamental statistical peak parameters m , σ , S (the peak skewness), E (the peak excess), and higher cumulant coefficients are obtained together with their precision (10). The peak parameter accuracy proves to hold whenever, in the fitting procedure, the following attributes are observed: (1) the maximum series expansion order degree, k_{mak} , necessary to attain the most significant approximation fitting degree under given skewness and signal to noise (S/N) ratios, must achieve expected values; (2) the fitting degree must be of the same order of magnitude as the S/N ratio; (3) the correlation among different parameters must be low (10-12). If this overall fitting pattern is followed, peak parameter accuracy is about equal to that peak parameter precision obtained from fitting by assuming a 3-fold increase in the mean approximation error (12).

From peak skewness and excess, different extracolumn band broadening models (e.g. exponential dilution) can be checked and their characteristic parameters evaluated (6, 9, 13, 16, 17). In fact, the extracolumn effect variances are independent and additive (5, 18, 19)

$$\sigma_{tot}^2 = \sigma_{col}^2 + \sigma_{det}^2 + \sigma_{el}^2 + \sigma_{cnn}^2 + \sigma_{in}^2 \quad (2)$$

where the σ^2 values are various peak variance contributions, that is, respectively, total value and column, detector, electronics, connections, and injection contributions. Similar additivity also holds for higher cumulants of all orders, v , (13)

$$K_{tot}^{(v)} = K_{col}^{(v)} + K_{det}^{(v)} + K_{el}^{(v)} + K_{cnn}^{(v)} + K_{in}^{(v)} \quad (3)$$

Among various extracolumn contributions the most important is the exponential decay factor (5), which usually arises from electronics and from void volumes, such as in the injection system, which behave as an exponential dilution flask. In this last case

$$\sigma_{ex}^2 = \tau_{ex}^2 \quad (4)$$

$$K_{ex}^{(3)} = 2\tau_{ex}^3 \quad (5)$$

where τ_{ex} is the time constant. For the exponential dilution flask

$$\tau_{ex} = V_{ex}/F \quad (6)$$

where V_{ex} and F are respectively the flask volume and the flow rate. When only one exponential factor acts on a perfectly Gaussian peak shape, having standard deviation σ_{col} , it is possible to determine σ_{col}^2 once the peak skewness and the total standard deviation σ_{tot} have been measured. In fact in this case $K_{col}^{(3)}$ is zero and thus

$$S = K_{tot}^{(3)}/\sigma_{tot}^3 = 2\tau_{ex}^3/\sigma_{tot}^3 \quad (7)$$

and

$$\tau_{ex} = \sigma_{tot}(S/2)^{1/3} \quad (8)$$

Finally, by use of eq 2

$$\sigma_{col}^2 = \sigma_{tot}^2 - \tau_{ex}^2 \quad (9)$$

With a similar procedure σ_{col}^2 can be obtained by using E instead of S (13).

There are several possibilities for measuring an extracolumn effect. For example, one consists of individual evaluations of τ_{ex} from S and/or E ; another consists of independent evaluations of σ_{col}^2 from different experimental extracolumn arrangements: (a) with and without the considered extracolumn effect; (b) with experimental conditions where the same extracolumn factor has different weights; or (c) with different extracolumn effects (9). Syringe injection is known to give an exponential band broadening contribution, according to eq 6. This contribution can be made to give low σ_{in}^2 by using a high flow rate split system. In fact, assuming the mixing chamber model; the time constant is inversely proportional to the total flow rate and the overall effect of V_{ex} is thus substantially reduced.

From τ_{tot}^2 an apparent value of column efficiency can be computed

$$H_a = \frac{\sigma_{tot}^2 L}{m^2} \quad (10)$$

From σ_{col}^2 the column efficiency can be computed

$$H_c = \frac{\sigma_{col}^2 L}{m_c^2} \quad (11)$$

where m_c is the retention time (corrected for extracolumn factors) and L is the column length.

The peak fidelity, introduced by Sternberg (5) can therefore be computed. It is defined as

$$\phi = \sigma_{col}/\sigma_{tot} \quad (12)$$

In this paper only nonretained methane samples are considered and the column efficiency is, in this case, expressed for capillary and packed column respectively as (20)

$$H_c \approx \frac{2D_{go}}{u_o} G(P_i, P_o) \quad (13)$$

$$H_c \approx \left(2\lambda d_p + \frac{2\gamma D_{go}}{u_o} \right) G(P_i, P_o) \quad (14)$$

where u_o is the outlet gas velocity, D_{go} is the gas diffusion constant at the column outlet pressure, d_p is the particle diameter, and λ and γ are constants. $G(P_i, P_o)$ is defined as

$$G(P_i, P_o) = \frac{9[P^4 - 1][P^2 - 1]}{8[P^8 - 1]^2} \quad (15)$$

where P is the ratio between the inlet and the outlet pressure, respectively, P_i and P_o (9, 20).

The fluidic injection system proved to allow a fast sample introduction as a rectangular pulse. If the pulse duration is τ_{in} , the second moment contribution from the injection is (9)

$$\sigma_{in}^2 = \tau_{in}^2/12 \quad (16)$$

which is usually a very low extracolumn contribution.

EXPERIMENTAL SECTION AND CALCULATIONS

The gas chromatographic instrument was equipped with a Model 191445/191453 monostable OR/NOR fluidic logic gate (Corning Glass Works, NY) to control the injection of methane as nonretained sample. Detailed description of this injection apparatus can be found elsewhere (9, 21). With this type of

Table I. Parameter Values and Precisions of Repeated Peaks Obtained with Fluidic Injection^a

<i>m</i>	σ^2_{tot}	<i>S</i>	<i>E</i>	<i>K</i> _{max}	<i>S/N</i>	CV%
127.63 (1)	0.2174 (4)	0.025 (2)	-0.019 (6)	2	1335	0.084
127.68 (1)	0.2172 (2)	0.021 (1)	-0.015 (4)	2	1537	0.052
127.67 (1)	0.2167 (3)	0.025 (1)	-0.017 (5)	2	1277	0.072

^a Methane on capillary column; 3σ in parentheses; column temperature 80 °C.

equipment, injection bandwidths of a few milliseconds can be obtained. The signal from the flame ionization detector (FID) was amplified by a Model 427 fast current amplifier (Keithley Instruments, Cleveland, OH) with a selectable time constant. The time constant used in this work was 10 ms. The amplified signal was then digitized and stored on a Model 21 M 30 minicomputer system (Hewlett-Packard, Palo Alto, CA), which was also used to command the injection valve and then to select the injection bandwidth. The sampling rate was regulated by an external clock and it was changed in function of the final peak width, in order to collect about 200 equally spaced (in respect to the time axis) points in the range of $\pm 5\sigma$ (10). An impulse ranging from 30 to 50 ms was used for the injection valve, thus, owing to the suggested solenoid inertia of about 25 ms, obtaining an injection bandwidth of $\tau_{in} = 5-25$ ms. The second moment contribution can be computed according to eq 16 and thus the extracolumn contribution coming from injection and electronics can be evaluated (9) as $25^2/12 + 10^2 = 152 \text{ ms}^2$; the additional contribution coming from the FID is almost negligible ($\approx 0.48 \text{ ms}^2$) (9). Alternative measurements were made by substituting the fluidic injection system with a classical syringe injection apparatus having an adjustable split system. Two split rates were employed: 20 and 75(1) cm^3/min .

Two chromatographic columns were employed. The first (2 m \times 2.1 mm i.d., stainless steel) was packed with porous glass beads (125-160 μm , DMCS, Corning) coated with squalane (about 0.5% (w/w) on the beads, corresponding to a total stationary phase amount of 53 mg) (9). The second was a Pyrex glass capillary column (40 m \times 0.25 mm i.d.) coated with OV73. Only methane peaks with a helium as carrier gas were studied on such a column.

All calculations were run on a CDC Cyber 76 computer (CIN-ECA, Casalecchio, Bologna, Italy). The minimization procedure was performed by using the CERN library utilities and the plots were obtained by using Calcomp software, as previously described (10).

RESULTS AND DISCUSSION

In this work the fluidic injection system was studied first with a 40 m long capillary column and the results of this study were compared with those previously obtained with a very short (1 m long) capillary column (9). The fluidic system thus characterized was then compared to syringe injection with a split system over the same packed column. The peak parameter repeatability of fluidic injection over capillary column is reported in Table I. An example of fitting graphics is reported in Figure 1. The three most characteristic findings of these data are (1) peak parameters are highly repeatable (2) very low *S* and *E* values are detected, and (3) precision and repeatability are nearly equal. *S* and *E* accuracy can be checked against the simulation study results reported elsewhere (12). For such symmetric peaks ($S \approx 0.03$) with $S/N > 1000$, a K_{max} value of 1-2 and a fitting degree (CV%) lower than 0.1% could be obtained, as is the experimental case observed here. In these cases the *S* determination is mean-

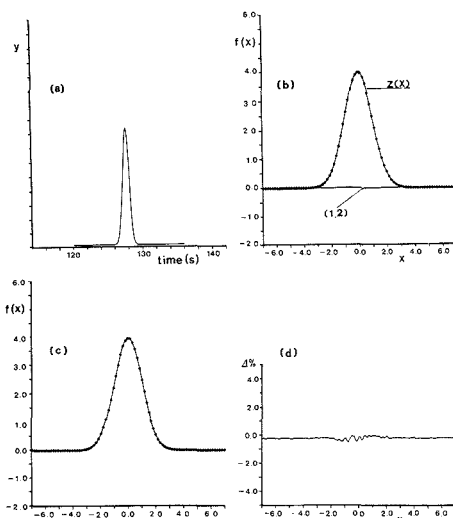


Figure 1. EC fitting example on a methane peak obtained with fluidic injection over capillary column: (a) experimental peak; (b) normalized peak (\diamond) and terms of the EC series expansion: $1 = Q_1(-Z)$, $2 = Q_2(-Z)$, $Z(x) = \text{Gaussian}$; (c) comparison between the normalized (\diamond) and fitted peak (—); (d) differences between the original and the fitted peak.

ingful and it has an accuracy value of about 5-10%. The accuracy on *E* is poorer (>40%), strongly dependent on base-line location, and the quoted values must be considered as practically equal to zero; thus this parameter will not be considered hereafter. These points prove how good experimental precision combined with the EC series numerical method makes it possible to determine *m*, σ^2 , and *S* values with good precision and accuracy even over very symmetric peaks. Indeed the reported example is, to our knowledge, the only example of peak parameter determination on highly symmetric peaks with verified precision, accuracy, and repeatability.

Table II reports the peak parameter data obtained with the same system at different flow rates. The observed peak skewness value can be used to compute an exponential extracolumn band distortion effect (τ_{ex}) according to eq 8 and to evaluate H_c according to eq 9 and 11, assuming that only one τ_{ex} has an effect (see Table II). The peak fidelity ϕ (≈ 0.9) obtained is greater than that previously found by using the same injection system (9). In the present work, in fact, the band distortion coming from electronics, detection, and injection has less weight because a longer column (40 m instead of 1 m) was employed here, thus producing a 40-fold σ^2_{col} . Nonetheless, the τ_{ex} values detected are greater than those expected from the above mentioned extracolumn effects. In addition they are dependent on the flow rate. If V_{ex} and D_{go} are evaluated by using respectively eq 6 and 13 (see Table II), not only are constant values obtained but the agreement of D_{go} values with theoretical data (22) is on about the same order

Table II. Peak Parameters, Computation of Extracolumn Factors, Corrected Column Efficiency, and Peak Fidelity^a

<i>P</i>	<i>m</i>	σ^2_{tot}	<i>S</i>	γ_{ex} , s	V_{ex} , mL	H_c	ϕ	D_{go}
1.801	157.02	0.432	0.030	0.162	2.71	0.063	0.969	1.063
2.001	127.68	0.217	0.021	0.111	2.51	0.048	0.971	1.071
2.201	107.72	0.124	0.028	0.085	2.46	0.038	0.970	1.087

^a Capillary column, fluidic injection; column temperature 80 °C.

Table III. Peak Parameters, Computation of Extracolumn Factors, Corrected Column Efficiency, and Peak Fidelity^a

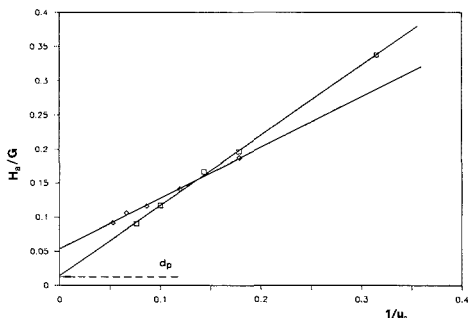
<i>P</i>	<i>m</i>	σ_{tot}^2	<i>S</i>	γ_{ext} , s	V_{ext} , mL	H_c	ϕ
1.301	72.840	8.990	0.154	1.277	42.1	0.287	0.905
1.502	45.320	2.040	0.096	0.520	30.2	0.176	0.931
1.603	37.940	1.220	0.073	0.367	26.6	0.154	0.943
1.804	28.820	0.499	0.085	0.247	25.6	0.107	0.937
2.005	23.720	0.263	0.088	0.181	24.7	0.083	0.935

^a Packed column, fluidic injection; column temperature 50 °C.Table IV. Peak Parameters, Computation of Extracolumn Factors, Corrected Column Efficiency, and Peak Fidelity^a

<i>P</i>	<i>m</i>	σ_{tot}^2	<i>S</i>	γ_{ext} , s	V_{ext} , mL	H_c	ϕ
1.500	45.390	1.953	0.169	0.614	35.6	0.157	0.898
1.700	32.940	0.783	0.204	0.414	36.0	0.116	0.884
1.900	25.840	0.399	0.240	0.312	37.5	0.093	0.870
2.100	21.426	0.253	0.293	0.265	41.5	0.081	0.850
2.300	18.280	0.160	0.336	0.221	43.5	0.068	0.834

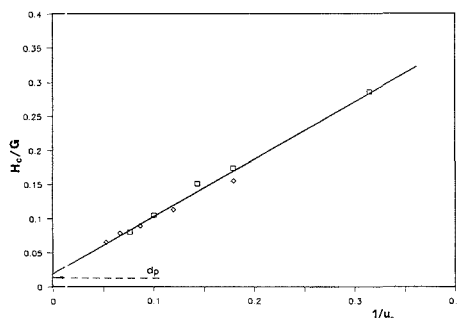
^a Packed column, syringe injection with high split rate, 750 cm³/min; column temperature 50 °C.Table V. Peak Parameters, Computation of Extracolumn Factors, Corrected Column Efficiency, and Peak Fidelity^a

<i>P</i>	<i>m</i>	σ_{tot}^2	<i>S</i>	γ_{ext} , s	V_{ext} , mL	H_c	ϕ
1.300	72.880	10.643	0.564	2.140	70.5	0.242	0.755
1.500	44.940	2.599	0.606	1.083	63.4	0.148	0.741
1.700	33.630	1.676	0.834	0.967	82.4	0.139	0.664
1.800	28.840	1.085	0.821	0.774	80.2	0.123	0.669
1.900	26.000	0.757	0.824	0.648	77.4	0.105	0.668
2.000	22.800	0.435	0.807	0.488	69.1	0.079	0.674
2.100	20.890	0.327	0.625	0.388	62.3	0.084	0.734
2.200	19.500	0.399	0.790	0.464	82.7	0.102	0.679
2.300	18.330	0.326	0.825	0.425	83.6	0.091	0.667

^a Packed column, syringe injection with low split rate, 20 cm³/min; column temperature 50 °C.Figure 2. $H_a/G(P_r, P_c)$ vs $1/u_0$ plots: experimental data for fluidic (\square) and high split rate syringe (\diamond) injections and corresponding fitted straight lines.

($\approx 80\%$) as that already found in a previous work (9). These findings substantiate the band distortion likely coming from an exponential mixing chamber within the column itself where flow rate disturbances may be responsible for the detected exponential tailing. It can be noticed that this effect is only about 0.1% of the total column void volume ($\approx 2000 \mu\text{L}$). As this effect is proportional to column length (9), it would have been extremely low, and therefore undetectable, in the previously investigated experimental arrangement where the total column volume was much smaller. If the reported V_{ext} value had instead been an extracolumn mixing chamber contribution, it would have been observed even with the shorter columns, but this was never the case (9, 21).

Tables III, IV, and V, respectively, report the results obtained with the packed column and with fluidic and syringe

Figure 3. $H_c/G(P_r, P_c)$ vs $1/u_0$ plots: experimental data for fluidic (\square) and high split rate syringe (\diamond) injections and corresponding fitted straight line.

injection (high and low split rate conditions). In these tables the same computation procedure was followed in evaluating τ_{ext} , V_{ext} , γ , and H_c . In this case the H_a and H_c values are to be checked by using eq 14 valid for nonretained samples in packed columns. Figures 2 and 3 report respectively the H_a/G and H_c/G vs $1/u_0$ plots (eq 14 and 15). It can be seen that the H_a/G values for fluidic and syringe injections with a high split rate system fall over different lines but when the extracolumn correction is applied they converge over the same line. In addition, both the slope ($\approx 2\gamma D_{g0}$) and intercept ($2\lambda d_p$) have meaningful values. The slope is 0.84 vs a value of 0.74 theoretically computed by assuming $\gamma = 0.5$ and $D_{g0} = 0.74$; the intercept is $190 \mu\text{m}$ vs a value of $150 \mu\text{m}$ which is computed by assuming a λ value of 0.5 (23). A similar procedure was suggested and followed by Giddings (6) with the aim of dis-

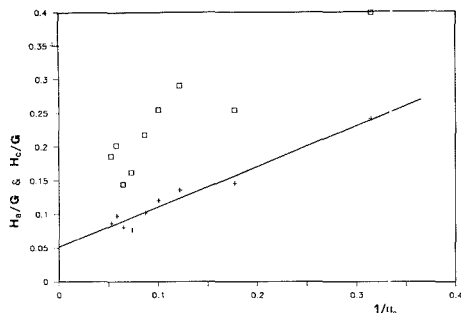


Figure 4. $H_e/G(P_r, P_o)$ (\square) and $H_c/G(P_r, P_o)$ ($+$) vs $1/u_0$ plots for low split rate syringe injection and corresponding fitted straight line (H_c case).

criminating between classical eddy diffusion and coupling eddy diffusion: a zero instead of $2\gamma d_p$ intercept would argue for the coupling theory rather than the classical eddy theory. The results here obtained agree with the second hypothesis; however they are too limited to settle this controversy; a longer column and carefully constant particle size dimensions should be employed (6). What is more interesting for the purposes of the present work is that both syringe and fluidic injection fall over the same meaningful line (see Figure 2) and thus the extracolumn contributions determined by the present method can be compared. In addition, it can be seen that the increase in v_{ex} in high split rate syringe conditions is about 40% in respect to the fluidic system, in the great majority of cases (Tables III and IV). Most likely, the observed values come from different parts of the apparatus: injection and connections which act differently in the different flow rate conditions (Table IV). The peak fidelity, which is about 0.93 for fluidic injection, lowers only to 0.85 when these syringe injection conditions are employed; indeed a satisfactory result for such a system.

Finally it can be observed that peak skewness values under low split rate syringe injection conditions are very high (0.6–0.8) (see Table V). The increase in computed V_{ex} on passing from high to low split rate syringe injection is about 150% (see Tables IV and V) and peak fidelity values are low (≈ 0.7). On the other hand, the H_e/G vs $1/u_0$ plot has scattered points and it does not substantiate any acceptable physical meaning (see Figure 4) of the computed V_{ex} , H_c , and ϕ parameters. Most likely, the extracolumn band broadening model, based on only one exponential dilution flask, is unable

to describe the overall observed band broadening in this last experimental arrangement.

CONCLUSIONS

By use of EC series peak parameter determination and extracolumn band broadening evaluation from S measured values, meaningful H_c estimations for nonretained solutes are obtained, both with fluidic injection over capillary columns and with fluidic and high split rate syringe injection systems over packed columns. It is likely that these estimated values are also very accurate, with a maximum error of about 20% (estimated from theoretically computed D_{90}). This maximum error would be even lower with retained samples (9). Both of these injection systems can be employed for column efficiency studies and physicochemical measurements by chromatographic techniques even with slightly retained compounds. Finally the high precision which can be attained with fluidic injection, and this peak shape analysis, allows for very accurate column efficiency measurements for high-speed chromatographic system developments.

LITERATURE CITED

- (1) Giddings, J. C. *Dynamics of Chromatography. Part I: Principles and Theory*; Marcel Dekker: New York, 1965.
- (2) Grubner, O. *Anal. Chem.* **1971**, *43*, 1934.
- (3) Grushka, E. J. *Phys. Chem.* **1972**, *76*, 2586.
- (4) Guiochon, G. *J. Gas Chromatogr.* **1964**, (May), 139.
- (5) Sternberg, J. C. *Advan. Chromatogr.* **1966**, *2*, 205.
- (6) Giddings, J. C.; Robison, R. A. *Anal. Chem.* **1962**, *34*, 865.
- (7) Maynard, V.; Grushka, E. *Anal. Chem.* **1972**, *44*, 1427.
- (8) Gaspar, G.; Arpino, P.; Guiochon, G. *J. Chromatogr. Sci.* **1977**, *15*, 256.
- (9) Gaspar, G.; Annino, R.; Vidal-Madjar, M. C.; Guiochon, G. *Anal. Chem.* **1978**, *50*, 1512.
- (10) Dondi, F.; Betti, A.; Blo, G.; Bighi, C. *Anal. Chem.* **1981**, *53*, 496.
- (11) Dondi, F. *Anal. Chem.* **1982**, *54*, 473.
- (12) Dondi, F.; Pulidori, F. *J. Chromatogr.* **1984**, *284*, 293.
- (13) Dondi, F.; Remelli, M. *J. Chromatogr.* **1984**, *315*, 67.
- (14) Dondi, F.; Remelli, M. *J. Phys. Chem.* **1986**, *90*, 1885.
- (15) Cramér, H. *Mathematical Methods of Statistics*, 7th ed.; Princeton University Press: Princeton, NJ, 1957; Chapter 17.
- (16) Cram, S. P.; Glenn, T. H. *J. Chromatogr.* **1975**, *112*, 329.
- (17) Cram, S. P.; Glenn, T. H. *J. Chromatogr.* **1976**, *119*, 55.
- (18) Conder, J. R. *HRC CC, J. High Resolut. Chromatogr. Chromatogr. Commun.* **1982**, *5*, 341.
- (19) Conder, J. R. *HRC CC, J. High Resolut. Chromatogr. Chromatogr. Commun.* **1982**, *5*, 397.
- (20) Littlewood, A. B. *Gas Chromatography*, 2nd ed.; Academic Press: New York and London, 1970; p 222.
- (21) Schuitjes, C. P. M.; Cramers, C. A.; Vidal-Madjar, M. C.; Guiochon, G. *J. Chromatogr.* **1983**, *279*, 269.
- (22) Fuller, E. N.; Schettler, P. D.; Giddings, J. C. *Ind. Eng. Chem.* **1966**, *58*, 19.
- (23) Purnell, H. *Gas Chromatography*; John Wiley and Sons, Inc.: New York, 1967; p 192.

RECEIVED for review January 3, 1989. Accepted March 29, 1989.

Exchange Reactions with Zinc Bis[(2-hydroxyethyl)dithiocarbamate] for Automated Monitoring of Metal Ions in Industrial Effluents by Liquid Chromatography with Electrochemical Detection

A. M. Bond* and T. P. Majewski¹

Division of Chemical and Physical Sciences, Deakin University, Geelong, 3217 Victoria, Australia

On-line mixing of industrial effluents with a buffered aqueous solution of the water-soluble zinc bis[(2-hydroxyethyl)dithiocarbamate] complex (or mixtures of zinc nitrate and ammonium bis[(2-hydroxyethyl)dithiocarbamate]) leads to the automated formation of dithiocarbamate complexes of metals such as copper, cobalt, nickel, and cadmium. Automated injection of the complexes formed in this way into a slowly flowing (<0.8 mL min⁻¹) 40/60 methanol-water (buffer) solvent mixture followed by oxidative electrochemical detection at +0.9 V vs Ag/AgCl of the dithiocarbamate complexes separated on a C₁₈ chromatographic column completes the development of a highly efficient microprocessor-controlled system for trace metal determination in industrial effluents. The high stability of the zinc complex, the absence of any electroactive ligand, the ability to use water-soluble complexes, and the requirement of only small amounts of non-aqueous solvent allow considerable improvements to be made in long-term (7 day) monitoring of metals in industrial effluents relative to existing approaches.

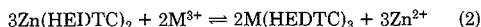
INTRODUCTION

The determination of low concentrations of metal ions by formation of metal complexes with a suitable ligand, chromatographic separation of the mixtures of complexes, and detection of the separated complexes by spectrophotometric, electrochemical, or atomic absorption methods, etc., has become increasingly popular (1).

In the case of electrochemical detection, complete automation of the HPLC/EC (high-performance liquid chromatography with electrochemical detection) method has been achieved and continuous monitoring of metal ions in industrial effluents has been attempted for 7-day periods without operator intervention (2). In the previously described study (2), diethyldithiocarbamate or pyrrolidinedicarbodithioate complexes of metal ions were prepared automatically in a reactor coil by using a low-pressure pumping system that mixed the industrial effluent and an acetonitrile solution containing the dithiocarbamate ligand. The acetonitrile-water solvent mixture formed in the complex preparation stage was then used as the solvent medium for the chromatographic separation of the metal dithiocarbamate complexes via the use of a high-pressure pump. Electrochemical detection at a glassy carbon electrode was achieved by oxidation of the metal complex or ligand attached to the metal. After extensive experience with this automated system, it has been recognized that deficiencies in the completely automated procedure arise from the slow decomposition of the dithiocarbamate ligand over the 7-day operation period, the necessary presence of

excess electroactive dithiocarbamate ligand which has to be removed prior to electrochemical detection by an anion exchange column, and the use of the relatively expensive and toxic acetonitrile solvent required for the preparation of the water-insoluble dithiocarbamate complexes.

In the present communication we describe the use of the water-soluble, complexing agent zinc bis[(2-hydroxyethyl)dithiocarbamate], Zn(HEDTC)₂, as an alternative to salts of diethyldithiocarbamate or pyrrolidinedicarbodithioate. Zn(HEDTC)₂ has a low stability constant relative to other metals of interest and participates in exchange reactions with many divalent (M²⁺) and trivalent (M³⁺) metals



The Zn(HEDTC)₂ complex is water soluble and unlike the previously used dithiocarbamate salts can be stored in aqueous media for several weeks without decomposition. Additionally, the Zn(HEDTC)₂ complex is more difficult to oxidize than the free ligand and does not need to be removed from the solution by ion chromatography prior to electrochemical detection of most M(HEDTC)₂ or M(HEDTC)₃ complexes. Finally, M(HEDTC)₂ and M(HEDTC)₃ complexes formed via the exchange reaction prior to chromatographic separation are also water soluble so that a relatively high percentage of water with a correspondingly smaller quantity of solvents such as methanol can be used instead of the more expensive and more toxic water-acetonitrile mixtures used previously.

The alteration to the methodology as described in this paper therefore achieves simplification to the experiment, a decrease in operational costs, improved performance, and fewer problems with potentially hazardous and toxic organic solvents in the automated continuous 7-day operation of the HPLC/EC method for the on-line fully automated method for the continual determination of metals in industrial effluents. The HEDTC ligand has been used previously for postcolumn complex formation (3), the separation of metal complexes following precolumn derivatization (4) and in situ ligand exchange chromatography (5). Details on the stability of zinc complex and the free ligand under a range of conditions are available from these studies.

EXPERIMENTAL SECTION

Instrumentation. The instrumentation used in the present study is closely related to that described elsewhere (2). A reservoir of zinc bis[(di-2-hydroxyethyl)dithiocarbamate] reagent is automatically mixed with the industrial effluent in a reactor coil. A bubble chamber removes any air bubbles formed during the mixing stage and the sample is then automatically injected onto the HPLC/EC part of the system. The flow rate of the eluting chromatographic solvent can be carefully controlled in the 0.1-0.8 mL min⁻¹ range. The glassy carbon working electrode, Ag/AgCl reference electrode, the potentiostat, chromatographic columns as well as other aspects of the instrumentation are the same as those described previously (2). Spectrophotometric detection was

¹ On leave from Institute of General Chemistry, Technical University, 90-924 Lodz, Poland.

achieved with a Waters Model 450 variable-wavelength detector.

Reagents. All chemicals and solvents were of analytical or chromatographic grade purity.

Ammonium bis(2-hydroxyethyl)dithiocarbamate was prepared as follows: 10.5 g (0.10 mol) of diethanolamine was dissolved in 50 mL of methanol. A 150-mL portion of tetrahydrofuran and 10 mL (0.15 mol) of concentrated ammonium hydroxide were then added, and the resultant solution was cooled to below 10 °C in an ice bath. To the cooled solution, 5.0 mL (0.11 mol) of carbon disulfide was added dropwise with stirring. After the required product crystallized out from solution over a period of several hours, it was filtered, washed with tetrahydrofuran, and dried under vacuum at ambient temperature. The method is closely related to that described in ref 4.

The metal complexes, Zn(HEDTC)₂, Ni(HEDTC)₂, Co(HEDTC)₂, Cu(HEDTC)₂, and Cd(HEDTC)₂ were prepared by mixing aqueous solutions of concentrated ammonium bis(2-hydroxyethyl)dithiocarbamate salt, [NH₄][HEDTC], and zinc(II) nitrate, nickel(II) nitrate, cobalt(II) nitrate, copper(II) nitrate, and cadmium(II) nitrate salts or their acetate salts respectively. The resultant precipitates were filtered, washed with water, dried under vacuum, and recrystallized from an ethanol/water mixture.

The chromatographic solvent was prepared by mixing an aqueous buffer (pH 6.5) solution made from conductivity grade water having extremely low metal ion contamination and HPLC grade methanol in the ratio 60:40. Methanol concentrations up to 80% can be used, but these decrease the retention times and increase the problem of organic solvent cost and toxicity. A stock solution of triethylammonium acetate buffer was prepared by dissolving 25.3 g of triethylamine in 300 mL of water and neutralizing to pH 6.5 with acetic acid. The finally recommended chromatographic solvent contains 0.025 M triethylammonium acetate buffer and was degassed with helium sparging during the course of all experiments.

RESULTS AND DISCUSSION

The stability of Zn(HEDTC)₂ was examined over a range of conditions. At a concentration of 1×10^{-4} M and in the presence of 0.025 M triethylammonium acetate buffer, no detectable change in Zn(HEDTC)₂ concentration was observed over a 2-week period. These zinc complex concentration and buffer conditions were therefore considered to be suitable for the HPLC/EC method which requires a 1-week continuous operation period without replacement of reagents or operator intervention. As an alternative, a mixture of 1×10^{-4} M Zn(NO₃)₂ and 1×10^{-4} [NH₄][HEDTC] can be used in the buffered solution. This has the advantage of ensuring that only a minimal amount of uncomplexed and readily oxidized free ligand [HEDTC]⁻ is present because the equilibrium



is shifted further to the right-hand side by the presence of excess zinc ions. The 10^{-4} M Zn(HEDTC)₂ complex in aqueous buffered media is stored in the HPLC/EC instrument related to that described in detail in ref 2 and is available for mixing when required with the industrial effluent or other aqueous sample via the use of a low-pressure pump (2). The exchange reactions given in eq 1 and 2 enable M(HEDTC)₂ and M(HEDTC)₂ complexes to be formed after zinc reagent and industrial effluent or other water sample are mixed. It is assumed that the metal ions of interest rapidly form the M(HEDTC)₂ and M(HEDTC)₂ complexes in the reaction chamber described in ref 2. In the industrial effluents examined in this work the metal ions are present at a concentration below 10^{-4} M so there is a significant excess of Zn(HEDTC)₂ present to ensure that the equilibrium positions in eq 1 and 2 lie well to the right.

The complexes of the metals of interest formed by the exchange reaction, along with excess Zn(HEDTC)₂, are automatically injected into the flowing chromatographic solvent. A potential of +0.9 V vs Ag/AgCl gives a very sensitive response for oxidation of nickel, copper, cobalt (metal based

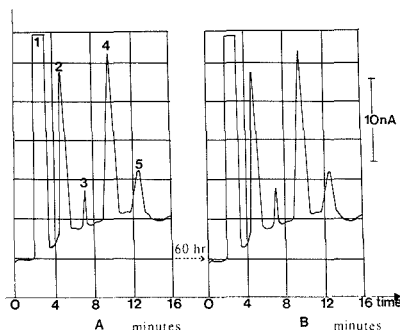


Figure 1. Chromatogram of 20- μ L injection of a solution containing 500 ppb of Cu, Ni, and Co and 1000 ppb of Cd. A is the response observed initially and B the response after 60 h of continual operation of the automated HPLC/EC system. Responses are due to (1) excess of Zn(HEDTC)₂, (2) Co(HEDTC)₂, (3) Cd(HEDTC)₂, (4) Ni(HEDTC)₂, and (5) Cu(HEDTC)₂. Experimental parameters and conditions were as follows: complexing reagents 10^{-4} M Zn(HEDTC)₂; Altex C₁₈ Spherisorb column; chromatographic solvent, 40:60 methanol-water (buffer); flow rate, 0.8 mL min⁻¹; electrode detection potential, +0.9 V vs Ag/AgCl; temperature, 18 °C.

oxidation), and cadmium (ligand based oxidation) complexes and an insensitive response for Zn(HEDTC)₂ (ligand based oxidation) so that this potential is very suitable for multi-element determinations. Measurement of the Zn(HEDTC)₂ response is a useful marker to ensure that an excess of the reagent was actually present and the decrease in peak height of this response relative to a control experiment provides information on how much [HEDTC]⁻ has been complexed by other metals present. If the Zn(HEDTC)₂ response is not observed, then an insufficient concentration of this reagent is present and calculated values of metal ions in the industrial effluents represent lower limits, rather than correct values.

In the absence of the triethylammonium acetate buffer in the chromatographic solvent, peak heights were nonreproducible. The buffer presumably blocks residual silanol groups on the C₁₈ column which would otherwise be available for metal complexation (4). The presence of this buffer in the zinc reagent also ensures that reproducible conditions are available for metal complex formation in the reaction chamber.

Figure 1A shows a chromatogram of the observed response for a mixture of Cu, Co, Cd, and Ni metal ions in a standard solution of known composition. A low flow rate of 0.8 mL min⁻¹ or less can be used because of the high resolution obtained with the column and conditions used. In the experiment described in Figure 1 a new injection of the same solution was undertaken every 20 min. The response in Figure 1B, which was observed after 60 h of running time, is virtually identical with the initially observed response.

After a 1-week continual operating period with a sample injected every 20 min, less than 5% variation in peak height was found in data obtained via the automated HPLC/EC method and the use of the exchange reaction with Zn(HEDTC)₂, provided the glassy electrode was cleaned every 10 h (or approximately every 60 injections) by application of a potential of -1.2 V vs Ag/AgCl for 30 s. In the absence of this cleaning pulse, a gradual deterioration in response is observed (peak diminishes in height). The application of the pulsed potential restores the response to the initial value. Data in Table I illustrate the gradual decay of the response and the restoration achieved by application of the pulse.

While the calibration curves are linear for each element, the sensitivity (peak current per unit concentration) is metal dependent (Figure 1). The limits of detection for each element are given in Table II.

Table I. Variation of the Measured Current Peak Height for Copper, Nickel, Cobalt, and Cadmium as a Function of Time of Continuous Operation of the Automated HPLC/EC System^a

time, h	% decrease in peak height with respect to the initial peak height			
	Cu	Ni	Co	Cd
2	0.5	0.5	0.4	0.3
4	1.3	1.2	1.2	1.0
6	3.4	3.0	3.2	2.8
8	4.2	4.3	4.0	4.2
10	5.4	5.2	5.3	5.0
10 ^b	0.1	0.0	0.1	0.0

^a Experimental conditions are given in caption to Figure 1.^b Data obtained after a cleaning potential of -1.2 V vs Ag/AgCl has been applied for 30 s.**Table II.** Limits of Detection for Determination of Copper, Nickel, Cobalt, and Cadmium by the Fully Automated HPLC/EC Method^a

metal	detection limit, ^b ppb
copper	20
nickel	10
cobalt	10
cadmium	100

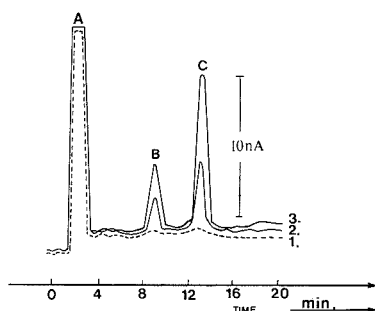
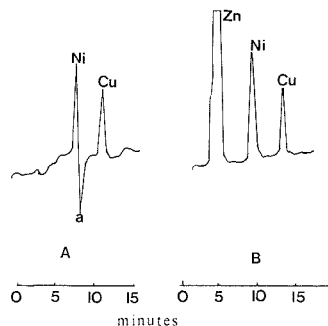
^a Complex forming reagent, aqueous, buffered 1×10^{-4} M Zn(NO₂)₂/ 1×10^{-4} M [NH₄][HEDTC]; chromatographic solvent, 40/60 methanol/water (buffer); flow rate, 0.8 mL min⁻¹; detection potential +0.9 V vs Ag/AgCl; Altex C₁₈ Spherisorb column; temperature, 18 °C. ^b Calculated as a signal to noise ratio of 3:1.**Figure 2.** Determination of copper and nickel by HPLC/EC in (1) distilled water, (2) river water, and (3) drinking water: (A) excess Zn(HEDTC)₂; (B) Ni(HEDTC)₂; (C) Cu(HEDTC)₂. Experimental parameters and conditions are given in Figure 1.

Figure 2 shows the chromatogram observed on drinking water which passes through copper pipes and from river water. Both these samples were obtained from sources on the Deakin University campus in Geelong, Victoria, Australia. In these two examples, nickel and copper levels may be determined but cobalt and cadmium levels are too low to be detected. Table III and Figure 3 provide a comparison of data obtained by electrochemical and spectrophotometric detection for nickel and copper. Excellent agreement is obtained for both methods of detection and the performance appears to be superior to that reported in ref 5. The "dip" in the chromatogram with spectrophotometric detection is caused by depletion of Zn(HEDTC)₂ (5). This elution dip is not observed under the

Table III. Determination of Copper and Nickel in Water Samples by HPLC with Automated Electrochemical and Spectrophotometric Detection^a

sample	metal	concn found, ^b ppm	
		electrochemical	spectrophotometric
drinking water	Cu	0.395 ± 0.012	0.420 ± 0.015
	Ni	0.120 ± 0.005	0.135 ± 0.010
river water	Cu	0.140 ± 0.015	0.160 ± 0.010
	Ni	0.090 ± 0.008	0.095 ± 0.010

^a Experimental details are given in caption to Figure 1.^b Average of five experiments obtained by using the fully automated sample preparation and injection system with direct calibration.**Figure 3.** Determination of copper and nickel in drinking water by HPLC with electrochemical and spectrophotometric detection: (A) spectrophotometric detection at a wavelength of 300 nm; (B) electrochemical detection at +0.8 V vs Ag/AgCl. Other experimental parameters and conditions are given in Figure 1.

conditions of the present study with electrochemical detection at +0.8 V vs Ag/AgCl.

Industrial liquors and effluents from electroplating or electrorefining industries often have considerably elevated cobalt and cadmium levels that can be routinely monitored by the method described in this work for 1-week periods, without operator intervention or maintenance. The concept of using an exchange reaction with Zn(HEDTC)₂ instead of in situ complex formation with an excess of dithiocarbamate ligand (6) or ex situ complex formation in the reaction chamber (2) offers a considerable improvement in reproducibility, stability, cost of reagents, and safety and has enabled objectives of the kind outlined in ref 2 for long-term monitoring of metal ion concentrations by the HPLC/EC method to be achieved more efficiently and effectively.

Registry No. Zn(HEDTC)₂, 94023-61-7; Cu, 7440-50-8; Ni, 7440-02-6; Co, 7440-48-4; Cd, 7440-43-9; water, 7732-18-5.

LITERATURE CITED

- (1) Timerbaev, A. R.; Petrukhin, O. M.; Zolotov, Yu A. *Fresenius' Z. Anal. Chem.* **1987**, *327*, 87, and references cited therein.
- (2) Bondi, A. M.; Garrard, W. N. C.; Heritage, I. D.; Majewski, T. P.; Wallace, G. G.; McBurney, M. J. P.; Crosher, E. T.; McLachlan, L. S. *Anal. Chem.* **1988**, *60*, 1357, and references cited therein.
- (3) Fu, C.; Zuo, B. *Fenxi Huaxue* **1981**, *9*, 635.
- (4) King, J. N.; Fritz, J. S. *Anal. Chem.* **1987**, *59*, 703.
- (5) Ge, H.; Wallace, G. G. *Anal. Chem.* **1988**, *60*, 830.
- (6) Bondi, A. M.; Wallace, G. G. *Anal. Chem.* **1983**, *55*, 718.

RECEIVED for review December 27, 1988. Accepted March 14, 1989.

Electrochemical Probes of Oxidation State, Product Distribution, and Redox Activity for $\text{Ba}_2\text{YCu}_3\text{O}_{7-x}$ in Halide Solutions

J. M. Rosamilia and B. Miller*

AT&T Bell Laboratories, Murray Hill, New Jersey 07974

Measurements at a carbon or platinum ring electrode of a rotating $\text{Ba}_2\text{YCu}_3\text{O}_{7-x}$ disk-ring electrode configuration in acidified aqueous halide solutions allow several schemes for the real-time analysis of x . These methods, based on analyzing the flux of soluble material from the disk into chloride, bromide, and iodide solutions, can be applied over the range from semiconductor ($\text{O}_6\text{-O}_{6.5}$) to superconductive phases ($\text{O}_{6.5}\text{-O}_7$). Since the analytical methods depend on measuring either $\text{Cu}^{2+}:\text{Cu}^{1+}$ ratios (for semiconductor phases) or the ratios (for superconducting phases) of oxidized products to copper species (Br_2 to Cu^{2+} , I_3^- to CuI_2^- , in the respective halides), they are independent of such factors as sample size and dissolution rate, as long as the latter process is nonselective. Results for O_7 and $\text{O}_{6.2}$ content specimens have been confirmed against standard procedures. No Cu^{3+} or readily reducible species surviving beyond the tens of milliseconds transit time from the disk to the ring are detectable in the chloride experiments. Model experiments with CuO and Cu_2O disks established the identification of species and the quantitative basis of the methods.

INTRODUCTION

The stoichiometry of $\text{Ba}_2\text{YCu}_3\text{O}_{7-x}$ is continuously variable over the range $0 \leq x \leq 1$, with increasing oxygen content progressively yielding the $\text{O}_6\text{-O}_{6.5}$ semiconductor, a tetragonal-orthorhombic phase transition at $x \sim 0.5$, and the $\text{O}_{6.5}\text{-O}_7$ superconductor phases, with T_c of 93 K near the O_7 composition (1-6). Oxidation state changes produced by the oxide content can be formally assigned to copper when barium and yttrium are assumed always to have +2 and +3 states, respectively. Conversely, determining the average oxidation state of copper by chemical (7, 8) or thermal (1, 7) analysis allows calculation of x . This redox analysis can be accomplished chemically by classical iodometry (9, 10) wherein all Cu^{2+} or Cu^{3+} is reacted to the +1 state with generation of equivalent iodine (as triiodide). In principle, for $x < 0.5$, the Cu^{3+} content in the various cuprate-based superconductors can be obtained without complication of the Cu^{2+} state reaction by using other reducing agents that will reduce only the nominal Cu^{3+} quantitatively back to +2 (11). In all these instances, location of the excess positive charge in an O^- species, rather than in Cu^{3+} , in the solid will make no difference in calculating electron equivalents for the determination of x as long as the same net oxidation of halides proceeds as will be written here for Cu^{3+} .

In this work we have allowed the superconductor ($x \sim 0$) and the semiconductor (x near 1), as the respective disk electrodes of rotating ring-disk electrode configurations, to react in halide (chloride, bromide, and iodide) environments as initiated by proton attack on the cuprate compound. We have then made real-time measurements at the coplanar, surrounding ring electrode of the product flux resulting from the overall disk reaction (12, 13). In the given halide system and for different ranges of the x parameter, we are able to monitor selectively several possible products and draw con-

clusions on original composition and the fate of intermediates from the cuprate disk. We note that since all these measurements are made under conditions of simultaneous proton attack (14), rapid rearrangements of charge may occur in concert with the redox reactions such that the species of fragments accepting electrons may not be the same as oxidized centers in the original solid superconductor.

The experiments we shall describe include measuring the ratios of limiting currents of the products of iodide reaction, which are well separated in their reduction reactions at the ring electrode and allow real-time determination of the value of x . The degree of oxidation of bromide can be defined by similar experiments without complication of Cu^{2+} oxidation reactions of such media. The absence of detectable electrolyte oxidation, or of species reducible at more positive potentials than Cu^{2+} in chloride solution, enables us to place limits on reaction and stability of intermediates for the superconductor. When the oxygen composition of the $\text{Ba}_2\text{YCu}_3\text{O}_{7-x}$ is between O_6 and $\text{O}_{6.5}$, the dissolution in chloride or bromide provides direct analysis for the value of x through copper collection voltammetry at the ring.

The results of these experiments will be related to the determination of x , the lifetime and redox behavior of oxidizing species, and time-dependent surface activity of $\text{Ba}_2\text{YCu}_3\text{O}_{7-x}$ under reaction conditions. In all halide media copper(II) oxide disks have been used as model compounds to identify product electrochemistry when reacted under parallel conditions. In addition these experiments have been performed with copper(I) oxide disks to make appropriate comparisons to the behavior of the $\text{O}_{6-6.5}$ content semiconductor disks, which have nominal Cu^{1+} content.

EXPERIMENTAL SECTION

Sintered pellets approaching the $\text{Ba}_2\text{YCu}_3\text{O}_7$ composition were prepared from high-purity BaCO_3 , Y_2O_3 , and CuO by using standard powder ceramic procedures. Processing steps include reaction at 950 °C with intermediate grindings, pressing into pellets, and a final anneal at 500 °C in an O_2 atmosphere. Samples were characterized by powder X-ray diffraction and measurements of temperature dependence of the resistivity and ac susceptibility. We are grateful to L. F. Schneemeyer and J. V. Waszczak for these specimens and their characterization. Thermal gravimetric analysis (TGA) for the $\text{Ba}_2\text{YCu}_3\text{O}_7$ specimen was kindly provided by P. K. Gallagher.

The $\text{Ba}_2\text{YCu}_3\text{O}_{6.2}$ and CuO pellets were supplied by H. M. O'Bryan, Jr. The $\text{Ba}_2\text{YCu}_3\text{O}_{6.2}$ pellet was prepared initially as for $\text{Ba}_2\text{YCu}_3\text{O}_7$, but after being heated above 900 °C, the pellet was allowed to cool to room temperature under a controlled atmosphere of mainly nitrogen to limit oxidation of the ceramic. The oxygen content was confirmed with X-ray lattice measurements.

High-purity CuO powder was pressed into a pellet by using a standard metallurgical die and sintered under oxygen below 1000 °C. In the case of Cu_2O , instead of construction with a pressed pellet, the powder was mixed with epoxy (30 wt % polymer) and the mixture pressed into the disk portion of a completed rotating ring-disk electrode that had the disk region drilled out below the plane of the ring. The electrode was cured at 70 °C.

$\text{Ba}_2\text{YCu}_3\text{O}_{7-x}$ and CuO pellets were used to fabricate the disk portion of the rotating ring-disk electrodes (RRDE). Electrical contact to the disks was made by coating the backside of the pellet

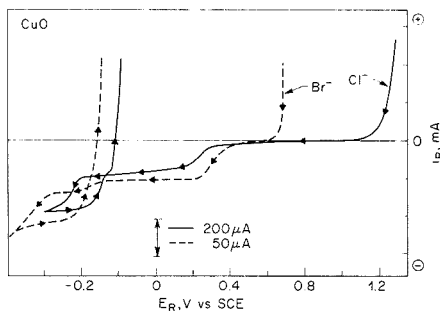


Figure 1. i_R vs E_R for a carbon ring electrode in 1.0 M NaCl/0.6 M HCl (solid line) and 1.0 M NaBr/0.45 M HBr (dashed line) with CuO disk at open circuit; rotation speed (ω) is 900 rpm and scan rate (sr) is 10 mV/s.

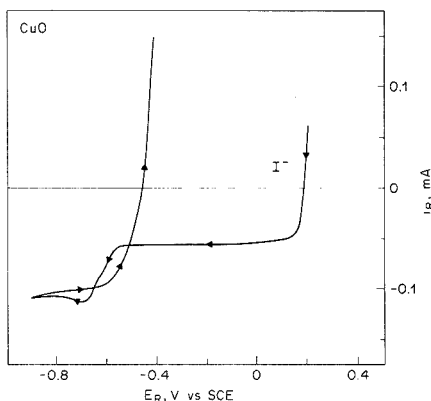


Figure 2. i_R vs E_R for a carbon ring electrode in 1.0 M NaI/48 mM HClO₄ with CuO disk at open circuit; ω is 900 rpm and sr is 5 mV/s.

with a thin layer of indium metal and then attaching a stainless steel rod with silver epoxy. In these experiments, however, the disks were always used under open circuit conditions. The rod was then coupled to a tube supplied with a Pt ring and potted with epoxy to form the RRDE. Construction details of the RRDE have been described elsewhere (15). Typical dimensions for disk and ring radii are 0.238, 0.262, and 0.318 cm. Prior to use, all electrodes were polished with 5- μ m Al₂O₃ paper (Ultralap). The conditions of the experiments themselves continuously generated a freshly etched disk surface.

All electrolyte solutions were prepared from commercially available reagent grade chemicals and 18-M Ω water. Electrochemical measurements were made by using a Pine Instrument Model RDE3 bipotentiostat. However, since the superconductor material disk need not be connected (is left open circuit), the single working electrode potentiostat configuration was used for the ring electrode (ring connected to the usual Pine K1 disk input, K2 left open). Experiments employed a three-electrode cell arrangement with carbon rod counter and saturated calomel reference electrodes (SCE). Nitrogen was purged through the electrolyte prior to and during the potential scan. All electrochemical measurements were made at room temperature.

RESULTS AND DISCUSSION

CuO and Cu₂O. The CuO and Cu₂O disk dissolution reactions in acidified solutions of each of the three halides, Cl⁻, Br⁻, and I⁻, have been examined by the ring-disk electrode method in Figures 1–3. We will use these subsequently for reference to the copper oxidation states seen in the Ba₂YCu₃O_{7-x} cases and to lend credence to the reaction ratio

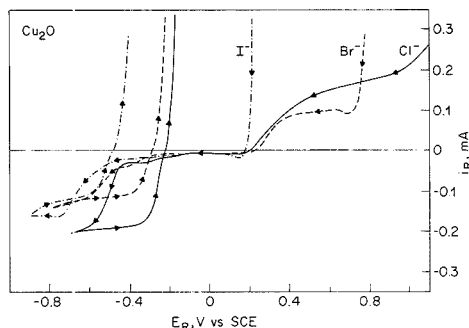
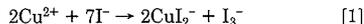


Figure 3. i_R vs E_R for a carbon ring electrode with Cu₂O disk at open circuit in 1.0 M NaCl (solid line), 1.0 M NaBr (dashed line), and 1.0 M NaI (dashed dotted line), each containing 18 mM H⁺; ω is 900 rpm and sr is 10 mV/s.

methods we will use to determine x and to examine the disk to ring flux for intermediates.

In Figure 1 are shown the ring current-potential traces for the CuO disk dissolving in HX–NaX, X = Br⁻ and Cl⁻, and in Figure 2 those for X = I⁻. In Br⁻ and Cl⁻ media the stabilization of the Cu(I) state by CuX₂⁻ complexation makes the reduction of Cu(II) occur in well-defined successive one-electron steps. (The even larger stabilization by I⁻ shifts the Cu(II)/Cu(I) potential much more positive than that of I₃⁻/I⁻). In the Br⁻ and Cl⁻ cases, with carbon ring monitoring of the “downstream” flow from the disk dissolution reaction, these two 1-e⁻ reductions, Cu(II) + e⁻ → Cu(I) and Cu(I) + e⁻ → Cu(0), are within 0.1 V of each other for the respective steps in the different halides. There is a ~0.4-V separation of the corresponding halide → halogen oxidation steps for the two solutions. The limiting currents of the two copper steps are equal when the return (positive) potential scan is used to measure the metal (I + e⁻ → 0) deposition wave to eliminate the uncertainties caused by nucleation overpotentials leading into H⁺ reduction interference on the forward (negative) potential scan. No comparison is to be made here of the relative total heights for solubilized copper between Cl⁻ and Br⁻ since these reactions of CuO are far from mass transport control and are surface and time dependent. Note that the H⁺ concentration required to obtain these ring current levels is much higher than those used for the Ba₂YCu₃O_{7-x} composition below.

For the iodide case in Figure 2, the products are different, reflecting the well-known quantitative reaction between Cu²⁺ and I⁻ (9, 10)

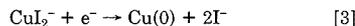


When bulk solutions of I⁻ and Cu²⁺ are mixed, a CuI precipitate is usually visible, except when sufficiently high I⁻ concentrations are used (10). In the ring-disk measurements we have noted no effects of phase separation and have thus written (1) in terms of soluble products CuI₂⁻ and I₃⁻. All experiments were done with a large excess of I⁻ present (also ensuring I₃⁻ dominance over I₂); only stoichiometry contributing to product ratios is of importance here.

In the ring current-potential trace of Figure 2, at more positive potentials, is thus seen the composite step of



from the disk product stream and the reverse oxidation of bulk I⁻ at +0.2 V vs SCE. The second cathodic step



occurs at ~-0.5 V, with its reverse reaction of metal stripping

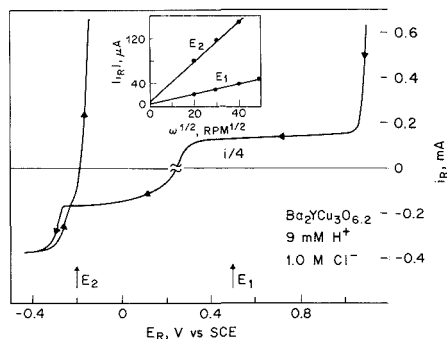
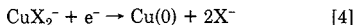


Figure 4. i_R vs E_R for a platinum ring electrode with $\text{Ba}_2\text{YCu}_3\text{O}_{6.2}$ disk at open circuit in 9.0 mM $\text{HCl}/1.0\text{ M NaCl}$; ω is 900 rpm and sr is 10 mV/s. Insert is i_R vs $\omega^{1/2}$ for 6 mM $\text{H}^+/1.0\text{ M NaCl}$, with anodic current for the $\text{Cu(I)} \rightarrow \text{Cu(II)}$ step measured at +0.5 V (E_1) and cathodic current for the $\text{Cu(II)} \rightarrow \text{Cu(I)}$ step measured at -0.2 V (E_2). i/m means the scale markers for that part of the trace should be divided by m .

proceeding on positive potential scan. As expected for the stoichiometries of (1)–(3), the cathodic steps are of equal height when careful steady-state measurements are made on the wave plateaus. This care is necessary to eliminate slow overall reaction rate changes at the CuO disk that may occur within a single ring potential scan at 5 mV/s, as the flux generated from the initial $\text{Cu}^{2+}\text{-I}^-$ surface reaction varies with disk surface activity that takes time to stabilize. The step heights typically agree to within $\pm 5\%$. If the chemistry in transit from disk to ring follows (1), it is likely to be complete in less than the transit time, which is of the order of tens of milliseconds (16) at our usual speeds.

In the case of Cu_2O in Figure 3, where all the halide results are collected together, the Br^- and Cl^- traces are similar with cathodic and anodic ring electrode steps that are respectively



and



The steps in each halide solution are thus of equal height, but of opposite sign, since they are oxidation or reduction of the same limiting CuX_2^- flux. The anodic current for I^- results from (2) to the left since (5) is shifted to sufficiently positive potentials by the strong $\text{Cu}^+\text{-I}^-$ interaction that it is not reached. The stability of the CuI_2^- complex is also seen in the more negative potential corresponding to (4) than that for the respective Cl^- or Br^- complexes.

$\text{Ba}_2\text{YCu}_3\text{O}_{6.2}$. Figure 4 shows the ring current-potential results when $\text{Ba}_2\text{YCu}_3\text{O}_{6.2}$ is reacted as the disk in 9 mM $\text{HCl}/1\text{ M NaCl}$ and the ring is Pt. The negative ring scan from +1.1 V vs SCE shows an anodic/cathodic composite wave and a second cathodic step. On positive potential reverse scan, a stripping peak of copper is clearly indicated. The ring traces follow from a combination of the behavior of CuO and Cu_2O in this medium (Figures 1 and 3). In contrast, however, the reactivity of the quaternary material to H^+ is much higher than that of the pure copper oxides, as shown in the inserts, which monitor the ring currents at +0.5 and -0.2 V as a function of square root of rotation speed $\omega^{1/2}$. The linearity of these plots suggests mass-transfer-controlled proton dissolution rates, as we earlier showed for the superconductive O_7 compositions (14).

The reactions monitored for the linear $i_R\text{-}\omega^{1/2}$ plots are the anodic and cathodic directions of eq 5 at 0.5 and -0.2 V,

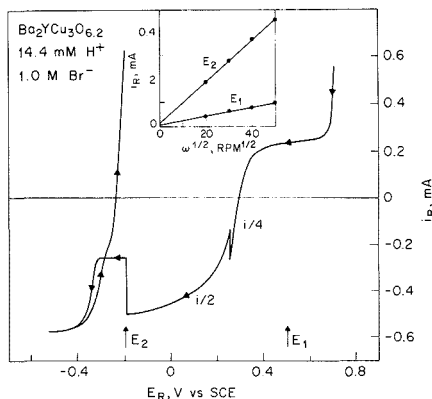


Figure 5. i_R vs E_R for a platinum ring electrode with $\text{Ba}_2\text{YCu}_3\text{O}_{6.2}$ disk at open circuit in 14.4 mM $\text{H}^+/1.0\text{ M NaBr}$; ω is 900 rpm and sr is 5 mV/s. Insert is i_R vs $\omega^{1/2}$ in the above solution, with current measured at +0.5 (E_1) and -0.2 V (E_2) for the anodic ($\text{Cu(I)} \rightarrow \text{Cu(II)}$) and first cathodic ($\text{Cu(II)} \rightarrow \text{Cu(I)}$) waves, respectively. i/m as for Figure 4.

respectively. The ratio of the slopes of these plots (or of the two limiting currents obtained in a single scan, $i_{R,0.5}$ and $i_{R,-0.2}$) can be related to oxygen content of the disk cuprate as follows. For $6 \leq (7-x) \leq 6.5$

$$n_1 + n_2 = 3 \quad [6]$$

where n_1 and n_2 are the numbers of Cu^+ and Cu^{2+} in the molecular formula, respectively, and thus

$$x = (7 - n_1 - 2n_2)/2 \quad [7]$$

From the experiment of Figure 4

$$\frac{i_{R,0.5}}{i_{R,-0.2}} = \frac{n_1}{n_2} \quad [8]$$

The average value of $i_{R,0.5}/i_{R,-0.2}$ for a number of experiments of this type has been 0.248 ± 0.004 for the electrode of Figure 4. This yields $n_2 = 2.40$ and $n_1 = 0.60$; thus $x = 0.80$ or $\text{Ba}_2\text{YCu}_3\text{O}_{6.20}$, in agreement with the estimate from X-ray lattice measurements.

This analysis does not depend on a mass-transport-limited rate of dissolution, but only on the ring current ratio from a given experiment, as long as the dissolution reaction is non-selective for oxidation state. Selectivity would be highly unlikely at any reasonable dissolution rate, especially the mass-transport-limited value indicated in this case, since the exposed surface composition and product distribution would rapidly change. Mass transport dependence allows the slope of the $i_R\text{-}\omega^{1/2}$ plots to be used, as well as individual pairs of $i_{R,0.5}$ and $i_{R,-0.2}$ values, in calculations from (8).

Figure 5 shows this experiment with $\text{Ba}_2\text{YCu}_3\text{O}_{6.2}$ conducted in bromide media. Since the comparable CuO experiment shows no indication of any Br_2 generation, the Br^- and Cl^- experiments with $\text{O}_{6.2}$ compound should give parallel results and be subject to the same analysis. The rate of dissolution, as monitored at +0.5 and -0.2 V, is also mass-transport-controlled, from the linear plots of the Figure 5 insert. The ratio $i_{R,0.5}/i_{R,-0.2} = 0.240$, yielding $n_1 = 0.58$ and $n_2 = 2.42$. The value corresponds to $x = 0.79$, or $\text{Ba}_2\text{YCu}_3\text{O}_{6.21}$. Either Cl^- or Br^- media would thus be suitable to this method of analysis.

In the case of reaction with I^- , the Cu^{2+} content of the $0.5 \leq x \leq 1$ composition ought to follow the redox pathway of (1), whereas the Cu^+ content will simply dissolve as the iodide complex. In the $0 \leq x \leq 0.5$ superconductor region, where Cu^{3+} states may be present, it is assumed that the reaction

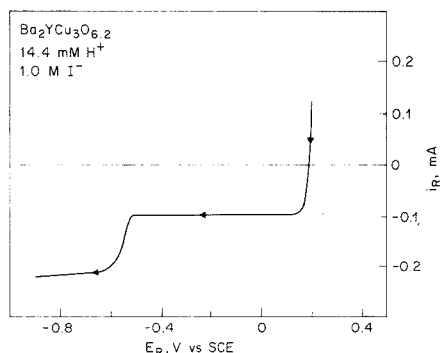
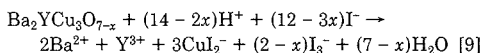


Figure 6. i_R vs E_R for a platinum ring electrode with $\text{Ba}_2\text{YCu}_3\text{O}_{6.2}$ disk at open circuit in 14.4 mM H^+ /1.0 M NaI; ω is 900 rpm and sr is 5 mV/s.

with I^- to yield I_3^- will also consume the equivalents of this copper species prior to the occurrence of (1). Thus the products will still only be CuI_2^- and I_3^- , but in ratios that will vary with x . The general equation for the full range of x between 0 and 1 is



The ratio of the limiting currents detected at the ring for a disk reacting according to (9) will involve both the coefficients of (9) and the electrons transferred in the ring reactions (2) and (3). For the experiment shown in Figure 6, where the reduction waves for I_3^- and CuI_2^- are excellently defined, the ratio Q of the two individual limiting currents, i_{L,I_3^-} and i_{L,CuI_2^-} , is then given in terms of x from (9), (2), and (3) by

$$Q = \frac{i_{L,\text{I}_3^-}}{i_{L,\text{CuI}_2^-}} = \frac{2(2 - x)}{3} \quad [10]$$

Rearranging gives

$$x = 2 - \frac{3}{2} \frac{i_{L,\text{I}_3^-}}{i_{L,\text{CuI}_2^-}} = 2 - \frac{3}{2}Q \quad [11]$$

For $x = 0$ and $x = 1$ limits, this corresponds to a range of Q from $4/3$ to $2/3$.

For the Figure 6 experiment the ratio is 0.773 for $x = 0.84$ and thus gives $\text{Ba}_2\text{YCu}_3\text{O}_{6.16}$, consistent with the results of the different method used for Cl^- and Br^- solution. The standard deviation of x for five experiments is ± 0.02 .

$\text{Ba}_2\text{YCu}_3\text{O}_{6.99}$. When the fully oxidized superconductor disk material is reacted in 6 mM HCl-1.0 M NaCl, we obtain the ring scans shown in Figure 7. In the insert are plotted $i_R - \omega^{1/2}$ data taken with 7.2 mM H^+ at the potentials E_1 and E_2 indicated on the main figure. There are two notable aspects to this experiment: One, there is no reducible species detected in the potential window between the response for Cl^- oxidation (>1 V vs SCE) and that of Cu^{2+} reduction (<0.3 V vs SCE); and two, the two steps for copper species reduction are equal, as is found for a CuO disk. (This latter conclusion is supported in the insert of Figure 7 by the exact 2:1 ratio of the $i_R - \omega^{1/2}$ slopes of the total waves). Both of these facts are consistent with no Cu^{3+} or other easily reducible (strongly oxidizing) species reaching the ring; the only copper species detected is $+2$. If so, then the original oxidizing power for $(7 - x) > 6.5$ must end up as O_2 in the electrolyte transiting from the disk to the ring. In the presence of copper, the reduction of O_2 at the ring in the region of the first (more positive) copper wave is completely suppressed (17). While this phenomenon

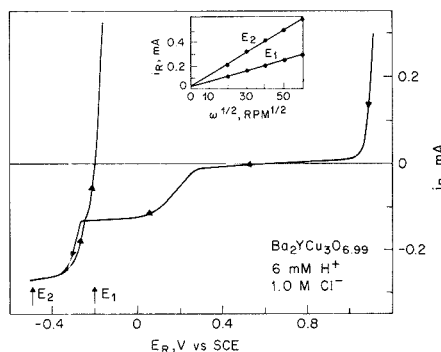


Figure 7. i_R vs E_R for a platinum ring electrode with $\text{Ba}_2\text{YCu}_3\text{O}_{6.99}$ disk at open circuit in 6 mM H^+ /1.0 M NaCl; ω is 900 rpm and sr is 10 mV/s. Insert is plot of i_R vs $\omega^{1/2}$ with 7.2 mM H^+ /1.0 M NaCl; i_R for $\text{Cu(II)} \rightarrow \text{Cu(I)}$ and overall $\text{Cu(II)} \rightarrow \text{Cu(0)}$ limiting currents was measured at -0.2 (E_1) and -0.5 V (E_2), respectively.

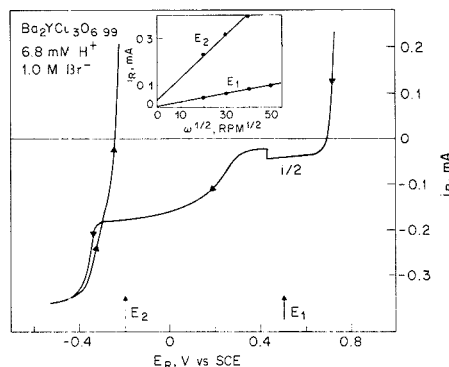
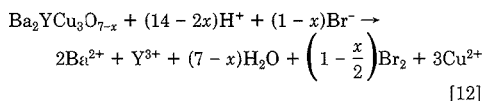


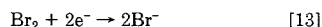
Figure 8. i_R vs E_R for a platinum ring electrode with $\text{Ba}_2\text{YCu}_3\text{O}_{6.99}$ disk at open circuit in 6.8 mM H^+ /1.0 M NaBr. Anodic and cathodic scales are given by i and $i/2$, respectively; ω is 900 rpm and sr is 10 mV/s. Insert is i_R vs $\omega^{1/2}$ for 14.4 mM H^+ ; current was measured at $+0.5$ V (E_1) for the $\text{Br}_2 \rightarrow \text{Br}^-$ and -0.2 V (E_2) for the $\text{Cu}^{2+} \rightarrow \text{Cu}^+$ plus $\text{Br}_2 \rightarrow \text{Br}^-$ waves. i/m as for Figure 4.

might also affect the reduction of peroxidic species, it ought not have any influence on the detectability of Cu^{3+} . The latter current is absent to the experimental limit of being indistinguishable from the residual level at the Pt ring without a reacting disk.

When the superconductor composition disk is reacted in bromide medium, three reduction waves can be distinguished in the ring scan, as seen in Figure 8 where the most positive reduction wave is amplified by a factor of 2 for clarity. These waves can result from the stoichiometry



From positive to negative potentials the ring waves are successively from the reactions



and then (5) to the left, followed by (4), the latter pair being the two one-electron steps of Cu(II) . The limiting currents at $+0.5$ (from (13)) and -0.2 V (from (13) plus (5)) are plotted

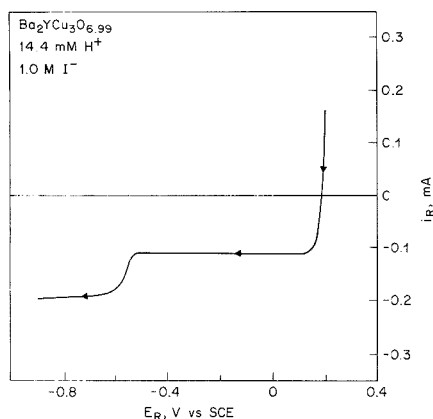


Figure 9. i_R vs E_R for a platinum ring electrode with $\text{Ba}_2\text{YCu}_3\text{O}_{6.99}$ disk at open circuit in 14.4 mM H^+ /1.0 M NaI; ω is 900 rpm and s_r is 5 mV/s.

vs $\omega^{1/2}$ in the insert. The linearity of both is indicative of both mass transfer control and complete reaction according to (12). The current for reaction of Br_2 (13) is the same as the current that would have passed if Cu^{3+} (or other species carrying the oxidizing power) had been stable and reached the ring for collection.

For the superconductor region where $0 \leq x \leq 0.5$, n_3 is the number of Cu^{3+} in the molecular formula, and thus

$$n_2 + n_3 = 3 \quad [14]$$

The $i_R \sim \omega^{1/2}$ slope at +0.5 V is proportional to n_3 and that at -0.2 V to $n_2 + 2n_3$. This follows from $n_2\text{Cu}^{3+}$ and $n_2\text{Cl}^{2+}$ giving a $\text{Cu(II)} + e^- \rightarrow \text{Cu(I)}$ ring wave proportional to $n_3 + n_2$. (The last total wave at -0.5 V adds $n_2 + n_3$ to be proportional to $2n_2 + 3n_3$). The experimental value of the ratio of -0.2- and +0.5-V $i_R \sim \omega^{1/2}$ slopes is

$$(n_2 + 2n_3)/n_3 = 4.45 \quad [15]$$

Combining this with (14) yields $n_3 = 0.87$ and $n_2 = 2.13$, which corresponds to $\text{Ba}_2\text{YCu}_3\text{O}_{6.94}$.

The comparable experiment of this disk with iodide produces the two-cathodic-wave pattern at the ring (Figure 9) with composite transition to iodide oxidation at ~ 0.2 V vs SCE, the latter as expected from the CuO or $\text{Ba}_2\text{YCu}_3\text{O}_{6.2}$ experiments (Figures 2 and 6). However, in this instance the $\text{I}_3^- + 2e^- \rightarrow 3\text{I}^-$ wave is larger than the CuL_2^- second step. The experimental value of Q for (11) is, from Figure 9 type results, 1.28 ± 0.05 , yielding $\text{Ba}_2\text{YCu}_3\text{O}_{6.92}$. The iodide and bromide results are in excellent mutual agreement and close to the TGA value of 6.99. The latter gravimetry has not been corrected for any traces of occluded water in the pellet. If this factor were 0.14% of the sample weight, difficult to see in the constant heat rate method, the TGA result would be $\text{O}_{6.92}$. Thus we expect the rotating ring-disk electrode method, which is independent of such parameters as sample size, to be capable of accuracy equal to that of the present standard methods of thermal analysis or iodometric titrimetry.

SUMMARY AND CONCLUSIONS

The reactions of $\text{Ba}_2\text{YCu}_3\text{O}_{7-x}$ in acidified halide solutions, as monitored through the rotating ring-disk electrode configuration, allow both the identification of products, by comparison to copper electrochemistry established with CuO and Cu_2O disks, and the setting of limits on the absence of product species. For example, in the presence of chloride, which is

itself stable to the cuprate solid disk even at $x = 0$, no Cu^{3+} or other readily reducible product is found by the ring electrode after proton attack. From the transit time (t_0) from disk to ring of these electrodes, for approximate convective parameters applying to these solutions, the lifetimes of such species, if they exist at all, must be less than a few tens of milliseconds.

Quantitative procedures for the determination of the oxygen stoichiometry, through iodide and bromide reactions at the cuprate disk and resulting halogen:copper ion ratios at the ring, have been developed and corroborated against other methods. For the compositions in the semiconductive region of cuprate composition, $(1-x) < 0.5$, it is only necessary to make measurements in chloride media and obtain the $\text{Cu}^{2+}:\text{Cu}^{1+}$ product ratios to make the analysis.

Since these methods depend purely on ring current ratios, they are independent of sample size and the rate at which the initial disk decomposition reaction occurs. They do depend, where iodide or bromide oxidation is involved, on complete reaction of the Cu^{3+} content, when Cu^{3+} formally represents the excess oxidizing power beyond Cu^{2+} in the molecular composition. The absence of complete reaction, however, could be detected by the rotation speed dependence of the x determination in the case of either halide.

The absence of a soluble highly oxidizing species reaching the ring in the chloride experiments is consistent with the results of oxygen isotopically labeled mass spectrometric experiments, which show that all the oxygen evolved on aqueous decomposition of the O_7 compound comes from the solid phase (18). Thus there is no reaction of a diffusing intermediate oxidizing water in a manner incorporating aqueous oxygen into the gaseous product and thus no possibility of its reaching a ring electrode through a trajectory in the aqueous phase. Such a detection would imply that oxygen would be subsequently generated through a water reaction/exchange in the solution. Since both the mass spectrometric and rotating ring-disk electrode experiments involve a decomposition of the solid, definitive assignment of the oxidizing power to a location in the original material is not feasible since charges can rearrange at an early stage. The fact that the oxidation reaction, either oxygen evolution or halide \rightarrow halogen conversion, occurs at a very early stage of aqueous decomposition is clear from both experimental viewpoints.

ACKNOWLEDGMENT

We are grateful to H. M. O'Bryan, Jr., and L. F. Schneemeyer for providing us with materials and characterization as well as for many helpful discussions. We also thank P. K. Gallagher for the TGA measurement.

LITERATURE CITED

- Gallagher, P. K.; O'Bryan, H. M., Jr.; Sunshine, S. A.; Murphy, D. W. *Mater. Res. Bull.* **1987**, *22*, 995.
- Beyers, R.; Lim, G.; Engler, E. M.; Savoy, R. J.; Shaw, T. M.; Dinger, T. R.; Gallagher, W. T.; Sandstrom, R. L. *Appl. Phys. Lett.* **1987**, *50*, 1918.
- Jorgensen, J. D.; Veal, B. W.; Kwok, W. K.; Crabtree, G. W.; Umezawa, A.; Nowicki, L. J.; Paulikas, A. P. *Phys. Rev.* **1987**, *B36*, 5731.
- Cava, R. J.; Battlogg, B.; Chen, C. H.; Rietman, E. A.; Zahurak, S. M.; Werder, D. *Phys. Rev.* **1987**, *B36*, 5719.
- Santoro, A.; Miraglia, S.; Beech, F.; Sunshine, S. A.; Murphy, D. W.; Schneemeyer, L. F.; Waszczak, J. V. *Mater. Res. Bull.* **1987**, *22*, 1007.
- Schuller, I. K.; Hinks, D. G.; Beno, M. A.; Capone, D. W., III; Soudnerholm, L.; Locoquet, J. P.; Bruynseraede, Y.; Segre, C. U.; Zhang, K. *Solid State Commun.* **1987**, *66*, 365.
- Harris, D. C.; Hewston, T. A. *J. Solid State Chem.* **1987**, *69*, 182.
- Appelman, E. V.; Morss, L. R.; Kini, A. M.; Geiser, U.; Umezawa, A.; Crabtree, G. W.; Carlson, K. D. *Inorg. Chem.* **1987**, *26*, 3237.
- Koltoff, I. M.; Belcher, R. *Volumetric Analysis Vol. III*; Interscience: New York, 1957; pp 347-365.
- Laitinen, H. A.; Harris, W. E. *Chemical Analysis*, 2nd ed.; McGraw-Hill: New York, 1975; pp 358-360.
- Shafer, M. W.; Penney, T.; Olson, B. L. *Phys. Rev.* **1987**, *B36*, 4047.
- Albery, W. J.; Hitchman, M. L. *Ring-Disk Electrodes*; Clarendon Press: Oxford, UK, 1971.

- (13) Bruckenstein, S.; Miller, B. *Acc. Chem. Res.* **1977**, *10*, 54.
 (14) Rosamilia, J. M.; Miller, B.; Schneemeyer, L. F.; Waszczak, J. V.; O'-Bryan, H. M., Jr. *J. Electrochem. Soc.* **1987**, *134*, 1863.
 (15) Miller, B. *J. Electrochem. Soc.* **1969**, *116*, 1117.
 (16) Bruckenstein, S.; Feldman, G. A. *J. Electrochem. Soc.* **1965**, *9*, 395.
 (17) Tindall, G. W.; Cadle, S. H.; Bruckenstein, S. *J. Am. Chem. Soc.*

- 1969**, *91*, 2119.
 (18) Shaier, M. W.; de Grott, R. A.; Plechaty, M. M.; Scilla, G. J. *Physica C* **1980**, *153-155*, 836.

RECEIVED for review January 6, 1989. Accepted April 5, 1989.

Determination of Conjugated Dienes in Gasoline by Differential Pulse Polarography

Stephen J. Swarin*

Analytical Chemistry Department, General Motors Research Laboratories, Warren, Michigan 48090-9055

Kevin L. Perry

Fuels and Lubricants Department, General Motors Research Laboratories, Warren, Michigan 48090-9055

A rapid, repeatable technique for the determination of conjugated dienes in gasoline has been developed. The method, which is based on the reduction of conjugated dienes at a dropping-mercury electrode, is faster (15 min vs 160 min) and more precise (5.3% vs 10% relative standard deviation) than the maleic anhydride method currently used. It is applicable to fuels containing alcohols, which cannot be analyzed by the current method. Application of this method to 25 model compounds and 37 gasolines of varying conjugated diene contents demonstrates that it is the method of choice for this determination.

INTRODUCTION

During the past several years, some cars with multiport fuel injection systems have had driveability problems caused by deposits that form at the tip of the fuel injector. These deposits were found to be fuel dependent, and extensive use was made of a wide variety of analytical techniques for the characterization of "deposit-forming" and "non-deposit-forming" fuels (1, 2). One fuel characteristic that showed correlation with the deposit-forming tendency of base fuels (without detergent additives) was the total conjugated diene content (3), but further investigations were hampered by the poor repeatability and long analysis time of the analytical method used to obtain the conjugated diene content—the maleic anhydride (MA) method (4). High-resolution capillary column gas chromatography was considered for this analysis (5) but, at the current state of development, analysis times are long and resolution is insufficient for the unambiguous analysis of all the possible conjugated diene isomers. Therefore, a method that quickly determined the total conjugated diene content of gasoline was still needed.

In a recent publication, Polak et al. (6) described a polarographic method to determine the conjugated diene content of "pyrolyzed" gasoline and distillation and hydrogenation refinery fractions. Although the samples analyzed in that report were not numerous (four), not commercial gasolines, and of high conjugated diene content, it was decided to try to extend this technique, which is based on the well-known electrochemical reduction of conjugated dienes (7), to commercial gasolines.

Table I. Experimental Parameters for Determination of Conjugated Dienes in Gasoline

	Mode: Differential Pulse Polarography	
initial E	-1.500 V	replications: 1
final E	-2.800 V	standard curve
		blank subtraction: yes
drop time	0.5 s	tangent fit: no
scan increment	2 mV	peak location: yes
pulse height	0.050 V	derivative: no

EXPERIMENTAL SECTION

Chemicals. Diene compounds used in this work were the best available grades from Pfaltz and Bauer (Stamford, CT) or Chem Service, Inc. (West Chester, PA). Gasoline samples were obtained from retail service stations throughout the United States and were stored at 0 °C. Dimethylformamide (DMF) was Baker Phrotex grade (Phillipsburg, NJ) or Aldrich HPLC grade (Milwaukee, WI), used as received. All other chemicals were ACS reagent grade. The supporting electrolyte was 0.02 M tetrabutylammonium iodide in DMF.

Apparatus. An EG&G Princeton Applied Research (Princeton, NJ) Model 384 polarographic analyzer, Model 303A mercury drop electrode, and Model RE 0082 digital plotter were used. The experimental parameters used in this method are shown in Table I. Measurements were performed with a dropping mercury electrode (0.08 mm i.d.), a platinum counter electrode, and a nonaqueous reference electrode (silver wire) filled with 20% LiCl/saturated AgCl in methanol.

Procedure. Ten milliliters of supporting electrolyte was pipetted into the Model 303A cell and the system was purged with argon for 300 s. A blank run was performed by using the experimental parameters in Table I. This run was stored in the memory of the Model 384 polarographic analyzer. Then a gasoline sample (100 μ L) or standard solution (50–200 μ L) was injected into the supporting electrolyte with stirring. The solution was purged for 10 s, and a sample run was performed using the experimental parameters in Table I. The data were then printed on the digital plotter with the blank run subtracted from the sample run.

Reference Method. The diene values of the gasoline samples were determined by the maleic anhydride (MA) method (4). The diene value is defined by the MA method as the number of grams of iodine equivalent to the amount of maleic anhydride that reacts with 100 g of sample.

RESULTS AND DISCUSSION

Electrochemical Reduction of Conjugated Dienes. Conjugated dienes undergo a two-electron reduction at a

Table II. Peak Currents for Dienes at -2.7 V^a

conjugated dienes	current, ^b nA/ μ g	isolated dienes	current, nA/ μ g
1,3-butadiene, 2,3-dimethyl-	2.04	1,4-pentadiene	0.09
1,3-butadiene, 2-methyl-	3.52	1,4-pentadiene, 2-methyl-	0.31
1,2-butadiene, 3-methyl- ^c	2.84	1,4-pentadiene, 3-methyl-	0.37
1,3-pentadiene	1.60	1,4-hexadiene	0.20
1,3-pentadiene, 3-methyl-	3.60	1,5-hexadiene	0.05
1,3-pentadiene, 2,4-dimethyl-	3.81	1,5-hexadiene, 2-methyl-	0.24
1,3-hexadiene	1.86	1,5-hexadiene, 3-methyl-	0.38
2,4-hexadiene	3.11	1,5-hexadiene, 2,5-dimethyl-	0.42
2,4-hexadiene, 2,5-dimethyl-	0.40	1,5-heptadiene	0.29
1,3-octadiene	3.17	1,6-heptadiene	0.34
1,3,7-octatriene	1.10	1,4-octadiene	0.34
		1,7-octadiene	0.16
		1,6-octadiene, 5,7-dimethyl-	0.24
		1,9-decadiene	0.30
average	2.66	average	0.27

^a Vs nonaqueous Ag electrode. 250- μ g sample in 10 mL of electrolyte. ^b nA/ μ g = nanoamperes per microgram. ^c 1,2-Butadiene, 3-methyl, is a cumulated diene—the two double bonds are on the same central carbon atom.

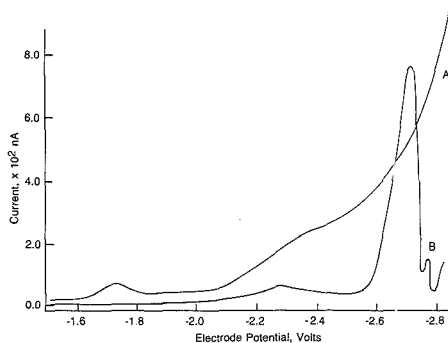
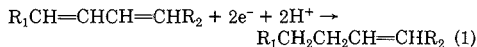


Figure 1. DPP curves for (A) supporting electrolyte and (E) 250 μ g of 2,4-hexadiene in supporting electrolyte. Curve B has been blank corrected.

dropping mercury electrode in the presence of a proton donor according to eq 1. Isolated double bonds, such as those in monoolefins (i.e., RCH=CHR) and nonconjugated dienes (i.e., RCH=CHCH₂CH₂CH=CHR) do not react electrochemically.



R₁ and R₂ may be the same and may be H

For analytical purposes, the current generated at the electrode by this electron transfer and measured by the polarographic analyzer is directly related to the conjugated diene content of a sample. Figure 1 is a differential pulse polarography (DPP) curve for a typical conjugated diene, 2,4-hexadiene. Also shown is the DPP curve for the blank (supporting electrolyte), which has been subtracted from the curve for 2,4-hexadiene. The DPP peak which occurs at approximately -2.7 V (vs the nonaqueous silver reference electrode) is due to the reduction of 2,4-hexadiene as shown in eq 1. The area or height of this peak is a measure of the amount of 2,4-hexadiene in the supporting electrolyte solution.

Table II contains the DPP data for 25 dienes, 11 containing conjugated double bonds and 14 containing isolated double bonds. Allowing for the variable purity of the samples obtained, the conjugated dienes exhibit, on average, about 10 times the peak current of the isolated dienes at -2.7 V. One exception to this trend is 2,5-dimethyl-2,4-hexadiene, which

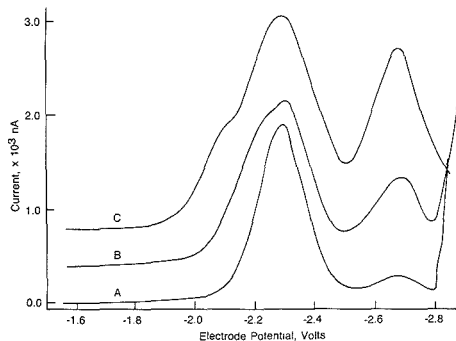


Figure 2. DPP curves for 100 μ L of (A) fuel no. 4 (diene value = 0.2), (B) fuel no. 17 (diene value = 0.57), and (C) fuel no. 33 (diene value = 1.5) in supporting electrolyte. Curves B and C are shifted on the vertical axis for clarity.

has been shown to exhibit steric hindrance in other reactions (8).

Aromatic compounds with two or more rings, such as naphthalene, and aromatics conjugated with the side chain, such as styrene, exhibit a large DPP peak, but this reduction occurs at approximately -2.3 V, so these types of compounds have not been included in Table II. Olefins containing only one double bond exhibit currents that are indistinguishable from the blank. Other chemical species that are electrochemically reducible, such as aldehydes, ketones, halogens, and peroxides, were found to give DPP peaks at less reducing potentials. Although it is difficult to assess all interferences, our results indicate that the DPP peak at -2.7 V is a selective and sensitive measure of conjugated dienes.

Application to Gasoline Analysis. Figure 2 shows the DPP curves for three gasoline samples that exhibited different diene values as measured by the MA method and different degrees of deposit formation as measured by visual comparison. The gasolines exhibit two DPP peaks—one at -2.3 V and the other at -2.7 V. The set of peaks at -2.3 V may be due to aromatic compounds with two or more rings or conjugated with side chains. However, the peaks are approximately equal in height for all three gasolines and thus do not correlate with the diene value or deposit-forming tendency of the samples. The DPP peaks at -2.7 V, which appear to be due to aliphatic conjugated dienes such as those in Table II, do vary in height according to the diene value of the sample.

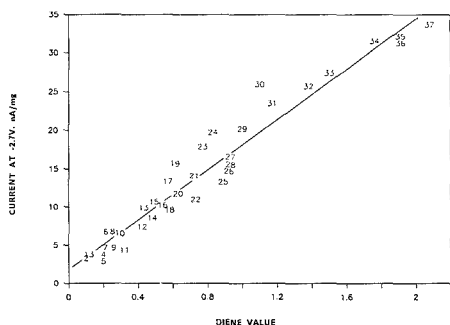


Figure 3. Correlation between diene value, measured by the MA method, and the peak current at -2.7 V, measured by DPP.

Table III. Repeatability of Peak Current Measurement

sample	peak current ^a	SD ^b	RSD ^c
no. 4	3.99	0.20	5.4
no. 19	15.72	0.97	6.2
no. 29	20.19	0.38	1.9
no. 33	27.41	2.06	7.5

Average Relative Standard Deviation = 5.3%

^aAverage of six determinations of peak current at -2.7 V, nA/mg. ^bSD, standard deviation. ^cRSD, relative standard deviation, percent.

Therefore this DPP peak was further investigated.

Figure 3 shows the diene values and DPP peak currents (at -2.7 V) for 37 gasolines which exhibited increasing fuel injector plugging tendencies with increasing sample number. The data correlate with a coefficient of determination (R^2) of 0.947. Thus it appears that both techniques are measuring the conjugated diene content of the sample.

A key factor in the DPP technique is the capability of the microprocessor-based analyzer to subtract the current due to the blank (supporting electrolyte) from that due to the fuel sample (Figure 1). This capability is reflected in the repeatability of the measurement of DPP current at -2.7 V which was evaluated by performing six determinations on each of four gasoline samples (Table III). The average repeatability was 5.3% (relative standard deviation) which is certainly acceptable for this type of measurement, and which is better than the reported repeatability of the MA method, which is the larger of 10% or 0.1 unit.

Since it appears that the DPP current at -2.7 V is a selective and sensitive measure of conjugated dienes in gasoline, it is possible to calculate the actual conjugated diene content of gasolines by using the average current value for known conjugated dienes from Table II and the DPP currents for 37 gasolines analyzed by DPP. The conjugated diene content calculated in this way ranges from 0.12 to 1.2% which is in agreement with approximate values determined by high-

Table IV. Effect of Oxygenates on Conjugated Diene Measurements

sample description	diene value	DPP currents, ^a nA/mg
no. 30	1.1	26.0
no. 30 + 10% methanol	>3.0	26.8
no. 30 + 10% ethanol	>3.0	26.2
no. 30 + 10% methyl <i>tert</i> -butyl ether	1.0	26.2

^aAverage of at least three determinations of peak current at -2.7 V. Currents are corrected for 10% dilution by oxygenates.

resolution capillary column gas chromatography. The gas chromatography values are approximate because not all conjugated dienes are identified and quantified by this technique.

A serious shortcoming of the MA method that the authors have noted is the dramatically high diene values obtained for fuel samples containing methanol or ethanol. This is caused by the esterification reaction between maleic anhydride and primary alcohols. However, the DPP method should not be affected by oxygenates in gasoline since they are not electrochemically active. Indeed, our results on fuels containing conjugated dienes that were spiked with methanol, ethanol, or methyl *tert*-butyl ether showed that the oxygenates had no effect on the DPP currents within the repeatability of the method (Table IV).

Finally, the analysis time for a set of three samples using the MA method is about 8 h, of which about 4 h require direct operator involvement for adding reagents, extracting, and titrating. In contrast, the DPP method would require about 40 min (all operator time) to run a set of three samples.

CONCLUSIONS

The electrochemical reduction of conjugated dienes in gasoline can be measured by DPP, and the currents obtained correlate with the diene value of the fuel as measured by the MA method. The DPP method is faster and more repeatable than the MA method, and it can provide reliable results on fuels containing primary alcohols which cannot be analyzed by the MA method.

LITERATURE CITED

- Beison, J. D.; Yaccarino, P. A. *Soc. Automat. Eng. Tech. Pap. Ser.* No. 861533.
- Taniguchi, B.; Pryla, R.; Parsons, G.; Hockman, S.; Voss, D. *Soc. Automat. Eng. Tech. Pap. Ser.* No. 861534.
- Hillien, D. L. *Soc. Automat. Eng. Tech. Pap. Ser.* No. 881642.
- Diene Value by Maleic Acid Anhydride Addition Reaction, UOP Method 323-62*; Universal Oil Products: Des Plaines, IL, 1982.
- Johansen, N. G.; Ettre, L. S.; Miller, R. R. *J. Chromatogr.* **1983**, *256*, 393-417.
- Poak, J.; Janacek, L.; Volke, J. *Analyst* **1986**, *111*, 1207-1211.
- Zuman, P.; Kolthoff, I. M. *Progress in Polarography*; Interscience: New York, 1962; Vol. II, Chapter XXXII.
- Yung, D. C.; Vouras, P.; Decosta, B.; Holick, M. F. *Anal. Chem.* **1987**, *59*, 1954-1957.

RECEIVED for review February 21, 1989. Accepted April 18, 1989.

Uranine Sensitized Chemiluminescence for Alternative Determinations of Copper(II) and Free Cyanide by the Flow Injection Method

Xing-Zheng Wu,¹ Masaaki Yamada,* Toshiyuki Hobo, and Shigetaka Suzuki

Department of Industrial Chemistry, Faculty of Technology, Tokyo Metropolitan University, Setagaya, Tokyo 158, Japan

A novel chemiluminescence system Cu(II)/CN⁻/uranine is described for the determinations of copper(II) and free cyanide by the flow injection method with a single flow system. The weak light emission arising from excited oxygen molecules (singlet oxygen) produced by the system Cu(II)/CN⁻ in the presence of dissolved O₂ is effectively sensitized by uranine in aqueous 2-propanol solution. Under the conditions of 4 × 10⁻⁴ M uranine, 5 × 10⁻⁵ M CN⁻ for the copper mode (1 × 10⁻⁵ M Cu(II) for the cyanide mode), 80% 2-propanol, and a flow rate of 4 mL min⁻¹, the calibration graphs provide the determination limits of 6 pg (20-μL injection of 5 × 10⁻⁹ M) for Cu(II) and 5 pg (20-μL injection of 1 × 10⁻⁸ M) for CN⁻ and the linear dynamic range of 10³. This CL system is very selective; only permanganate gives comparatively intense light emission in both modes, 1 × 10⁻³ M permanganate providing signals 150% and 210% of those for 1 × 10⁻⁶ M Cu(II) and 5 × 10⁻⁶ M CN⁻, respectively. Species complexing Cu(II) and/or CN⁻, precipitating Cu(II), and reducing Cu(II) interfere. The method is successfully applied to real samples. The mechanistic study of the present chemiluminescent reaction is also undertaken in detail.

Flow chemiluminescence (CL) analysis in solution is becoming increasingly important in various fields because of high sensitivity, wide linear dynamic range, reproducibility, simplicity, and rapidity (1-6). Especially, the combination of the flow injection method with CL detection has received considerable attention, since its simple instrumentation makes many applications feasible (5, 6). To date, a fair number of investigations have been conducted for the CL determination of organic and inorganic analytes. Most of them, however, are based on the use of established CL reagents like luminol, lucigenin, lophine, and oxalate esters. It is obvious that limited CL reaction systems have caused the slow recognition of flow CL analysis, in spite of the many advantages stated above. That is to say, the reason why the flow CL method has not been potentially used seems to lie mostly in the detection itself, i.e., its often poor selectivity and the paucity of usable CL reaction systems. Accordingly, the development of new CL systems of high selectivity is essential for wider acceptance of the method.

Our effort has been devoted to seeking new CL reactions. During the works, it has been seen that most oxidative reactions are accompanied by luminescence, although the intensity is too weak to be directly applied for analytical usage, and also that such a low CL quantum yield can greatly be improved through the selection of reaction medium like organized surfactant molecular assemblies (micelle, vesicle) and/or the use of sensitizer. In that way, several CL systems have been developed and applied to flow CL analysis (7-9).

There are many analytical methods available for the determination of copper(II) or free cyanide in solution. One of the most frequently employed methods for copper(II) determination is spectrometry; furnace atomic absorption spectrometry (detection limit: picogram levels with the use of only a 5- to 20-μL sample solution) possesses sensitivity 10 to 100 times higher than those for flame atomic absorption spectrometry and inductively coupled plasma emission spectrometry, although there are some difficulties in reproducibility and interference (10). Free cyanide is most frequently determined by spectrophotometric methods based on König's reaction, which has a reasonably high sensitivity and reproducibility; the pyridine-pyrazolone method is applicable to water samples containing 0-0.5 μg mL⁻¹ of cyanide and recommended for water analysis by the American Public Health Association, despite a disadvantage of the instability of reagent (11). On the other hand, CL methods are also available for the determinations of both analytes. The most sensitive and selective methods have recently been developed on the use of organized surfactant molecular assemblies, the 1,10-phenanthroline CL method for copper(II) determination (detection limit: 0.3 pg for 20-μL sample injection) (12, 13) and the uranine-sensitized CL method for cyanide determination (detection limit: 1 pg for 20-μL sample injection) (14, 15). However, there have been no CL methods of permitting alternative determinations of both analytes.

In this paper we describe a novel CL system, Cu(II)/CN⁻/uranine/dissolved O₂/2-propanol, capable of alternatively determining copper(II) and free cyanide by the flow injection method with a single flow system. The luminescence comes basically from the reaction system consisting of copper(II), cyanide, and dissolved oxygen; uranine and 2-propanol are added to the system as sensitizer and reaction medium, respectively, in order to enhance luminescence intensity. To our knowledge, this is the first observation of light emission from the system Cu(II)/CN⁻/O₂.

EXPERIMENTAL SECTION

Apparatus. Prior to flow experiments, batch experiments were conducted as described before in order to obtain CL profiles (16). Each 0.2 mL of reagent solutions was transferred to a reaction vessel (ca. 3.5 mL) in various mixing orders at the flow rate of ca. 10 mL min⁻¹ by a peristaltic pump.

A flow system consisting of a single line is used, and materials and equipment are basically as before (9). A uranine solution containing cyanide for the copper(II) determination (copper mode) or copper(II) for the cyanide determination (cyanide mode) is delivered by a peristaltic pump. Copper(II), cyanide, and other species are injected by means of a 20-μL rotary valve injector. The peak height of the signal recorded was measured as a CL signal.

UV and visible spectra of uranine were measured by a spectrophotometer (Shimadzu UV-240) and their fluorescence spectra by a fluorescence spectrometer (Shimadzu RF-540). The determination of copper(II) in tap water was carried out with a furnace atomic absorption spectrometer (Shimadzu AA-670G). ESR spectra of superoxide anion radical were taken on a JEOL JES-FE2XG spectrometer at liquid nitrogen temperature. The

¹ Present address: Department of Applied Chemistry, Faculty of Technology, The University of Tokyo, Tokyo 113.

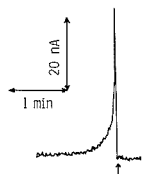


Figure 1. CL signal profile in the uranine/Cu(II)/CN⁻ system (batch method). Arrow indicates the transfer of reagent solution to a reaction vessel: mixing order, 1×10^{-4} M uranine/ 1×10^{-5} M CN⁻ + 1×10^{-4} M Cu(II).

spectra of CL from the Cu(II)/CN⁻/uranine system were measured by use of a flow cell for the UV/visible absorption measurement with the fluorescence spectrometer by closing an excitation slit. In order to determine the wavelength distribution of CL arising from the Cu(II)/CN⁻ system, the CL intensity was measured every 10 nm in the wavelength range of 450–650 nm by using a photon counter (Hamamatsu photonics C767) and 11 cutoff filters with 80% transmittance (Toshiba Glass).

Reagents. Chemicals of reagent grade were used as received. The water used was prepared by deionization of distilled water from a stainless steel apparatus. Each reagent solution was prepared daily from a 10^{-2} M stock solution. Cyanide stock solution was prepared by dissolving potassium cyanide into 10^{-3} M sodium hydroxide solution.

Analysis of Real Samples. Tomato leaves (0.5 g) were boiled with 10–20 mL of concentrated nitric acid on a hot plate until the appearance of white fumes and with concentrated sulfuric acid until the solution became colorless. After being cooled, the solution was diluted to 100 mL. A 10-mL portion of the acid-digested sample was neutralized to about pH 6–8 with 2 M sodium hydroxide and diluted to 100 mL. A 10-mL portion was added to each of several 50-mL volumetric flasks for standard addition of copper before dilution to volume, and copper was determined as described above.

Tap water from Tokyo Metropolitan University was subjected to the analysis of copper without any pretreatment, but for free cyanide determination, water samples from the Tama and Arakawa Rivers were filtered with a Millipore filter (pore size 0.45 μ m).

RESULTS AND DISCUSSION

CL Profile. To know the speed of the CL reaction and the effect of mixing reagent on CL intensity is of significant importance for the design of the flow system. In general, the mixing ways (i.e., mixing order and mixing time interval) of reagent solution play a key role in CL reaction; no or weakened light emission may often be observed with different mixing ways, and also how fast the CL reaction proceeds is a dominant factor that decides sensitivity in flow CL analysis because transient light emission is monitored.

Thus time courses of CL from the system were measured by the batch method, and one of them is depicted in Figure 1. It was found from the CL profiles that the emission intensity was almost independent of the mixing ways of reagent (Cu(II), CN⁻, and uranine) solutions. This allows the delivery of the reagent solution mixed in advance, i.e., the CN⁻/uranine solution for the copper mode and the Cu(II)/uranine solution for the cyanide mode, in the flow experiment. On the other hand, the light emission occurred with rather high speed and reached the maximum intensity within several seconds. This clearly suggests that the sample injector should be placed as close as possible to the detection flow cell because the CL reaction is considered to proceed faster in flowing solution. Hence the flow system consisting of a single flow line was assembled so that the distance between the injector and the detector flow cell became minimum.

Reaction Medium. The Cu(II)/CN⁻/uranine system did not elicit a strong light enough to meet practical use; e.g. the limit of detection for copper is only on the order of 10^{-5} M.

Table I. Effect of Reaction Media on CL Signal for Cu(II) in CN⁻/Uranine System^a

medium	concn ^b	CL signal ^c
organic solvent		
methanol	35	10
ethanol	35	15
1-propanol	35	20
2-propanol	35	30
acetonitrile	35	12
acetone	35	2
tetrahydrofuran	35	7
dimethyl sulfoxide	35	8
<i>N,N</i> -dimethylformamide	35	6
surfactant		
dodecyltrimethylammonium bromide	48 (16)	1.3
didodecyltrimethylammonium bromide	0.54 (0.18)	1.1
tetradecyltrimethylammonium bromide	11 (3.5)	5.0
hexadecyltrimethylammonium bromide	2.7 (0.9)	5.4
octadecyltrimethylammonium chloride	1.0 (0.34)	4.5
dioctadecyltrimethylammonium chloride	0.54	4.5
sodium dodecyl sulfate	24 (8)	1.3
polyoxyethylene (23) dodecanol ^d	3.0 (0.06)	1.3

^a Conditions: 1×10^{-5} M CN⁻, 1×10^{-4} M uranine, 1×10^{-5} M Cu(II), flow rate 4 mL min⁻¹. ^b % for organic solvents and 10^{-3} M for surfactants (values in parentheses show critical micelle concentration). ^c Normalized with respect to the signal (=1.0) when reaction medium is water alone. ^d Brij 35.

So far we have made it clear that in such a case the modification of reaction medium frequently brings about the increase in CL quantum yield. That is to say, as reaction medium the use of solution containing organic solvent or organized molecular assemblies leads to great acceleration of CL reaction, resulting in marked improvement of sensitivity (7).

In order to investigate whether the modification of reaction medium functions effectively for the present CL system, modifiers like organic solvents and surfactants were added to the cyanide/uranine solution and the signal for copper was compared with that in the absence of modifier. The results are summarized in Table I, indicating that of the modifiers tested, 2-propanol is the most promising modifier, giving a 30-fold enhanced signal. Other organic solvents, especially alcohols, also mediated the CL reaction more efficiently compared to surfactants. Interesting features appear in surfactant micellar media. The signal suppression is not observed for any surfactants. It had been often encountered in analogous works that anionic and/or nonionic micellar media suppressed signal, when cationic micellar media enhanced. Furthermore, with the surfactants possessing dodecyl groups in the hydrophobic moiety, the signal enhancement is less than those with surfactants possessing longer alkyl chains. Although any simple explanation for these characteristics cannot be offered at the present time, it is likely that uncharged species play an important role in the emitter formation in the hydrophobic environment. This idea is not in conflict with the results obtained in the organic solvent media, showing that the signal is enhanced by all organic solvents and the extent of enhancement approximately parallels the hydrophobicity of organic solvent, especially with alcohols. Aqueous 2-propanol solution was chosen as reaction medium for further experiments.

Optimization. Operating conditions were optimized with respect to reaction variables, the concentrations of 2-propanol, uranine, and cyanide (or copper), the apparent pH of reagent solution, and the flow rate of reagent solution.

First, the optimization was conducted for the copper mode. The dependency of the 2-propanol concentration is shown in

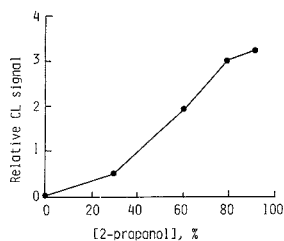


Figure 2. Effect of the 2-propanol concentration on the CL signal for 1×10^{-6} M Cu(II); 4×10^{-4} M uranine, 1×10^{-5} M CN⁻; flow rate 4 mL min^{-1} .

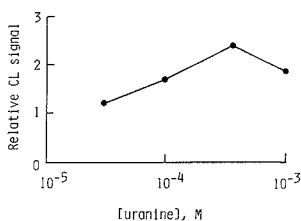


Figure 3. Effect of the uranine concentration on the CL signal for 1×10^{-6} M Cu(II); 80% 2-propanol, 5×10^{-5} M CN⁻; flow rate 4 mL min^{-1} .

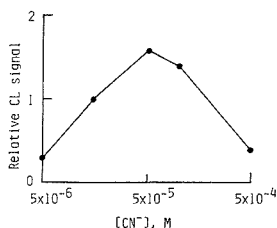


Figure 4. Effect of the cyanide concentration on the CL signal for 1×10^{-6} M Cu(II); 80% 2-propanol, 4×10^{-4} M uranine, flow rate 4 mL min^{-1} .

Figure 2, indicating that the higher the 2-propanol concentration, the higher the signal for copper. On account of undesirable effects on the silicon pump tubing and PVC flow cell, the concentration of 2-propanol was determined to be 80%, at which the signal was increased by a factor of ca. 180 compared to that in the absence of 2-propanol. The uranine and cyanide concentrations which give a maximal signal can be deduced from Figures 3 and 4, respectively. An increase in the uranine concentration above its optimal concentration (4×10^{-4} M) causes a decrease in the signal ($\lambda_{\text{max}} = 530\text{--}540$ nm, a maximum wavelength for uranine fluorescence in 80% 2-propanol solution, because uranine works as a sensitizer as described later) which is conceivably due to the concentration quenching rather than the inner-filter effect based on the intense color of uranine solution, showing the absorption maximum at ca. 490 nm. As can be seen from Figure 4, the dependency of cyanide concentration also exhibits a decrease in signal beyond the optimal concentration (5×10^{-5} M). This might be ascribable to the preferential formation of copper-cyanide complexes at higher cyanide concentrations which are no longer labile.

The experiments above mentioned were undertaken under unbuffered conditions. Most CL reactions are liable to proceed efficiently under alkaline conditions. Thus, in order to in-

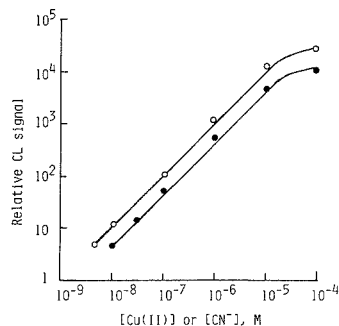


Figure 5. Calibration graphs for Cu(II) (O) and CN⁻ (●). Conditions are given in the text.

vestigate the effect of apparent pH on the signal for copper, hydrochloric acid or sodium hydroxide was added into the reagent solution. The results showed that the signal remained constant under the weakly acidic (10^{-5} M hydrochloric acid) to weakly alkaline condition (10^{-5} M sodium hydroxide). The weakly alkaline condition was chosen to allow as little evolution of hydrogen cyanide gas as possible from the reagent solution. The increasing flow rate of reagent solution gradually increased the signal and 4 mL min^{-1} was chosen as an optimal flow rate, considering the consumption of reagent solution.

As to the optimization for the cyanide mode, the copper concentration, the flow rate, and the apparent pH of reagent solution were examined in a similar manner under the conditions of 4×10^{-4} M uranine and 80% 2-propanol. The dependency of copper concentration on the signal for CN⁻ exhibited a maximum at 1×10^{-5} M and beyond its concentration the signal decreased gradually due to the same reason as for the copper(II) mode and/or due to the quenching of uranine fluorescence by copper(II) in excess. The effects of flow rate and apparent pH exhibited trends similar to those for the copper mode; the same flow rate as that for the copper mode but the unbuffered condition was chosen as optimum.

Characteristics of the System. Under the recommended conditions of 4×10^{-4} M uranine, 5×10^{-5} M CN⁻ for the copper mode (1×10^{-5} M Cu(II) for the cyanide mode), 80% 2-propanol, and a flow rate of 4 mL min^{-1} , the analytical characteristics of the system were investigated. Almost no background current and low noise current (1×10^{-12} A) were observed in both modes. In general, CL systems yielding high background and hence high noise are not usable for sensitive analysis.

Logarithmic calibration graphs for copper(II) and cyanide are illustrated in Figure 5. The signal for CN⁻ is slightly lower than that for Cu(II). This is probably due to the quenching of uranine fluorescence by copper ion present in excess in reagent solution. In both modes, linear signals with a slope of unity were obtained over 3 orders of magnitude. The limit of determination for a signal-to-noise ratio of 3 was 5×10^{-9} M (ca. 6 pg in $20 \mu\text{L}$) for copper and 1×10^{-8} M (ca. 5 pg in $20 \mu\text{L}$) for cyanide. The relative standard deviation ($n = 10$) was 3.1% and 3.3% for 3×10^{-8} M Cu(II) and CN⁻, respectively. The sampling rate can be as high as 700 h^{-1} for both modes.

A flow injection CL system consisting of a single flow line may make the circulating use of reagent stream feasible, namely, the realization of cyclic flow injection method as reported previously (17). This has the advantage of permitting long running of the flow system without additional supply of reagent solution. With the present system, the circulating reagent solution (100 mL) allowed the signal for 5×10^{-7} M Cu(II) to remain unchanged in 500 successive injections.

Table II. Selectivity of the Present CL System^a

detection mode	species ^b	CL signal ^c
copper(II)	MnO ₄ ⁻	150
	Fe(II)	40
	Ni(II)	30
	Fe(III)	20
	Co(II)	13
	Zn(II)	7
cyanide	MnO ₄ ⁻	210
	Cr(III)	14
	S ₂ O ₈ ²⁻	11
	CO ₃ ²⁻	7
	S ₂ ²⁻	4
	Fe(III)	1

^a Performed under recommended conditions shown in the text. ^b 20- μ L injection of 10^{-3} M solution. ^c Normalized with respect to the signal (=100) for 1×10^{-6} M Cu(II) and that for 5×10^{-6} M CN⁻.

Effect of Other Species. Possible CL generation by other species was investigated to evaluate the selectivity of the present CL system. The results are summarized in Table II. It can be seen from the table that the present system is highly selective for copper(II) and cyanide. In both modes, only permanganate provided signals 0.2% and 1% of those for copper and cyanide, respectively. This CL originates from the permanganate oxidation of uranine. The following species (10^{-3} M) gave rise to very weak or no light emission: Cr(III), S²⁻, S₂O₈²⁻, and CO₃²⁻ in the copper(II) mode; Cu(II), Fe(II), Co(II), Ni(II), and Zn(II) in the cyanide mode; Cr(VI), Cd(II), Mn(II), Hg(II), Pb(II), Ag(I), Al(III), Ca(II), Mg(II), NH₄⁺, F⁻, Cl⁻, Br⁻, I⁻, ClO₄⁻, BrO₃⁻, IO₃⁻, NO₃⁻, NO₂⁻, SCN⁻, HPO₄²⁻, oxalate, and acetate in both modes.

In order to check the effect of concomitant species on the signal in both modes, a 10^{-6} M Cu(II) or CN⁻ solution containing each common species was injected. The results are shown in Table III, indicating interferences by many species. Negative interferences can be mostly explained on the basis of the complex formation with cyanide, the precipitation formation with copper(II), or the reduction of copper(II). No explanation can be offered for positive interferences by Co(II), Ni(II), and Pb(II) in the copper mode, because they are no or minor light inducers per se as shown in Table II. However, most of these interferences are not so serious in practice because the complex formation, the precipitation formation, and the reduction would have already taken place in naturally occurring samples and/or because such interferents would not coexist at high concentration levels. The following species (5×10^{-3} M) were found not to interfere: NH₄Cl, KH₂PO₄, and AgNO₃ in the copper(II) mode; Na₂S₂O₃ and Pb(NO₃)₂ in the cyanide mode; NaF, NaCl, NaI, KBr, KClO₃, KBrO₃, KIO₃, KSCN, Na₂CO₃, CaCl₂, Mg(NO₃)₂, CdCl₂, ZnCl₂, K₂Cr₂O₇, and CH₃COONa in both modes.

Application to Real Samples. The applicability of the proposed method was evaluated by assaying tomato leaves (NBS standard reference material 1573) and tap water with the copper mode and river waters with the cyanide mode. Standard additions of copper to acid-digested sample and tap water indicated that the results obtained for tomato leaves (11, 11, 11 ppm) and tap water (1.0, 1.1 ppb) were within the certified value (11 \pm 1 ppm) and the value determined by flameless absorption spectroscopy (1.1, 0.9 ppb), respectively. On the other hand, no cyanide was detected in water samples from the Tama and Arakawa Rivers, and therefore recovery tests were performed by adding trace amounts of cyanide to them. The results indicated good recoveries, 97–102% for 3×10^{-8} to 3×10^{-6} M cyanide in river waters.

Mechanistic Study of the Present CL Reaction. It is well documented that light emission is frequently accompanied

Table III. Interference Study for the Present CL System^a

detection mode	species ^b	relative error, %	
		5×10^{-6} M	5×10^{-6} M
copper(II)	CoCl ₂	320	190
	NiCl ₂	180	NI ^c
	Pb(NO ₃) ₂	61	17
	FeSO ₄ (NH ₄) ₂ SO ₄	-97	-97
	MnCl ₂	-83	-52
	CrCl ₃	-80	-21
	FeCl ₃	-59	NI
	Na ₂ S	-53	NI
	KNO ₃	-35	NI
	Na ₂ C ₂ O ₄	-35	NI
	HgCl ₂	-36	NI
	Na ₂ S ₂ O ₃	-30	NI
	AlCl ₃	-30	NI
	AgNO ₃	-100	-100
	HgCl ₂	-100	-100
	NiCl ₂	-96	-96
	FeSO ₄ (NH ₄) ₂ SO ₄	-96	-40
CoCl ₂	-95	-82	
CrCl ₃	-91	-7	
MnCl ₂	-90	-40	
CuCl ₂	-81	-40	
Na ₂ C ₂ O ₄	-65	NI	
Na ₂ S	-57	-27	
NH ₄ Cl	-51	NI	
KH ₂ PO ₄	-49	NI	
FeCl ₃	-39	-25	
AlCl ₃	-23	NI	
cyanide			

^a Conditions as in Table II. ^b Added to 10^{-6} M Cu(II) or CN⁻ solution. ^c No interference.

by oxidation reactions involving large free energy changes. Most luminous oxidative reactions for analytical usage need CL reagent and oxidizing agent, e.g. luminol and hydrogen peroxide, respectively. In contrast, the present CL system has no such reagents added deliberately. This enables us to expect the participation of uranine as sensitizer and dissolved oxygen as oxidizing agent in the CL reaction.

Sensitization is an effective means to enhance light emission by an energy transfer from an excited intermediate which is a poor emitter in itself to a fluorescent compound (sensitizer) added purposely; the light observed is usually a fluorescence of the sensitizer. That uranine worked as a sensitizer was unambiguously evidenced by the following facts: light emission was observed even in the absence of uranine although its intensity was very weak, the weak light was also enhanced by not only other xanthene dyes (eosin Y, rhodamine B, pyronin B, etc.) but also non-xanthene dyes (brilliant sulfoflavine, riboflavin), and the CL spectrum was similar to the fluorescence spectra ($\lambda_{\max} = 530\text{--}540$ nm) of uranine solution before and after CL reaction.

In order to confirm that dissolved oxygen is responsible for eliciting light, the signal for cyanide was taken by using the reagent and cyanide (10^{-6} M) solutions degassed with N₂. As expected, the signal for cyanide was decreased; about two-thirds that in the presence of dissolved oxygen disappeared. The decrease in signal was not due to the concentration changes of the reagent and/or cyanide solutions through the bubbling with N₂. This was ascertained by use of the 2-propanol free reagent and cyanide (10^{-3} M) solutions prepared with degassed water. Furthermore, the requirement of dissolved oxygen for the light emission was also revealed by the fact that the decreased signal for cyanide was gradually recovered with bubbling O₂ through the above 2-propanol free reagent and 10^{-3} M cyanide solutions.

It is reasonable to consider that dissolved oxygen will take part in the CL reaction as its reactive states, so-called activated oxygen (O₂⁻, ¹O₂, OH, H₂O₂) (18–21). Of these activated ox-

Table IV. Effects of O_2^- Trappers and 1O_2 Quenchers on CL Signal

		concn, M	CL signal ^a
O_2^- trapper	NBT ^b	0	1.0
		3×10^{-6}	0.90
		3×10^{-5}	0.55
	Tiron	3×10^{-4}	0.05
		0	1.0
		3×10^{-6}	0.30
1O_2 quencher	NaN ₃	3×10^{-5}	0.10
		3×10^{-4}	0.03
		0	1.0
	α -tocopherol	1×10^{-5}	0.85
		1×10^{-4}	0.67
		1×10^{-3}	0.56
α -tocopherol	0	1.0	
	1×10^{-5}	0.80	
	1×10^{-4}	0.14	
	1×10^{-3}	0.04	

^a Obtained by batch experiments, in which 10^{-4} M uranine, 10^{-6} M Cu(II), and 10^{-5} M CN⁻ were mixed in that order, and normalized with respect to the signal in the absence of trapper or quencher. ^b Nitro Blue Tetrazolium.

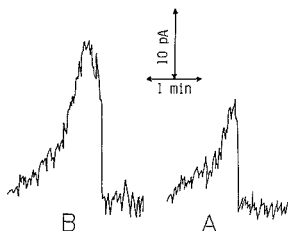
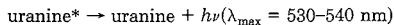
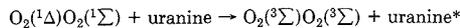


Figure 6. Effect of 2-propanol deuteration on the CL signal in the Cu(II)/CN⁻ system (batch method): (A) 2-C₃H₇OH; (B) 2-C₃D₇OD; mixing order, 80% 2-propanol + 1×10^{-4} M Cu(II) + 5×10^{-4} M CN⁻.

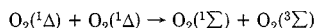
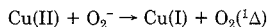
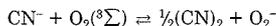
xygen species, the involvement of both superoxide ion O_2^- and singlet oxygen 1O_2 was strongly suggested by the batch experiments, in which CL signals were compared or addition of trappers or quenchers for O_2^- (20) and 1O_2 (18) to the CL system (Table IV). As noticed later, the production of 1O_2 is closely related to O_2^- . Hydroxyl radical OH may be excluded since the reaction medium, 2-propanol, is an effective OH scavenger and also the participation of hydrogen peroxide H₂O₂ was in conflict with the fact based on batch experiments that the addition of H₂O₂ brought about the decrease in signal.

Further corroboration for the production of 1O_2 is seen in the solvent deuteration effect on the lifetime of 1O_2 and in the wavelength distribution of light from the Cu(II)/CN⁻ system. The solvent deuteration leads to less solvent-induced deactivation of 1O_2 and thus to its increased lifetime (22), resulting in an enhancement of light intensity. The results are shown in Figure 6, indicating that deuterated 2-propanol clearly increases total CL intensity (peak area), an increase of a factor of 5 with 75% deuteration. It is known that there are several maximum wavelengths in the emission spectra of singlet oxygen, i.e. 1269, 762, 634, 476, and 381 nm based on the transition from the states $^1\Delta$, $^1\Sigma$, $^1\Delta^1\Delta$ (molecular pair), $^1\Delta^1\Sigma$ (molecular pair), $^1\Sigma^1\Sigma$ (molecular pair), respectively (23). The wavelength distribution of light from the Cu(II)/CN⁻ system exhibited an emission maximum in the vicinity of 480 nm. This may be assigned to the transition from the singlet oxygen molecular pair state $^1\Delta^1\Sigma$, the energy (59.8 kcal mol⁻¹) of which is high enough to excite uranine (55.5 kcal mol⁻¹). No appearance of other emission maxima in the wavelength distribution is due to the low sensitivity of the

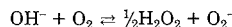
photomultiplier tube (maximum sensitivity at ca. 400 nm) at longer wavelengths and the low provability of the $^1\Sigma^1\Sigma$ state production. Thus, it can be said that the excited intermediate is singlet oxygen produced through the reaction involving Cu(II), CN⁻, and dissolved O₂ and that the light observed is sensitized CL as the result of excitation by a physical energy transfer from the singlet oxygen simultaneous transition state $^1\Delta^1\Sigma$ to uranine (23)



One possible explanation for the generation of singlet oxygen is given by the formation of O_2^- followed by its one-electron oxidation with Cu(II) (and/or a copper-cyanide complex), although there has been considerable discussion regarding the possibility of singlet oxygen generation (24–26)



Superoxide ion O_2^- originates conceivably from the reduction of dissolved oxygen by CN⁻ (and/or a copper(I)-cyanide complex). Very recently it has been reported that O_2^- exists in alkaline solution (27) although its formation is thermodynamically unfavorable, namely



Accordingly, it is reasonable to assume the existence of O_2^- in 2-propanol solution containing CN⁻ since CN⁻ ($E^\circ = -0.18$ V for CN⁻/CN⁻) is more reductive than OH⁻ ($E^\circ = 1.55$ V for OH⁻/OH⁻). This was confirmed by the ESR spectrum ($g = 2.0084$), which coincided in g value with that ($g = 2.0091$) of O_2^- prepared by decomposing potassium superoxide KO₂ (O_2^- producing agent) in 2-propanol. In any event, the equilibrium will lie far to the left since E° for O_2/O_2^- is -0.33 V and thus the concentration of O_2^- is believed to be low. The generation of 1O_2 based on the one-electron oxidation of O_2^- by Cu(II) which is thermodynamically favorable may be allowed because the total spin is conserved. In fact, the addition of Cu(II) to 2-propanol in which KO₂ was decomposed gave CL and furthermore its wavelength distribution was analogous to that for CL from the Cu(II)/CN⁻ system. Of course, it is difficult to rule out the possibility of the participation of copper-cyanide complexes in the O_2^- and/or 1O_2 generation, but at present no detailed elucidation can be offered. The lifetime of $O_2(^1\Delta)$ is long (10^{-6} – 10^{-8} s) because $^1\Delta \rightarrow ^3\Sigma$ is a forbidden transition and therefore there is much possibility of the generation of $O_2(^1\Sigma)$ and thus a molecular pair $O_2(^1\Delta)O_2(^1\Sigma)$.

ACKNOWLEDGMENT

We thank Susumu Nakamura of the National Chemical Laboratory for Industry for supplying a tomato leaf sample, Yo-ichi Ohno of Cosmo Research Institute for the ESR measurements, and Takamichi Yamagishi of this university for useful suggestions about the ESR spectrum analysis.

LITERATURE CITED

- (1) Kricka, L. J.; Thorpe, G. H. G. *Analyst (London)* **1983**, *108*, 1274–1296.
- (2) Yamada, M.; Suzuki, S. *Bunseki* **1985**, 104–110.
- (3) Schulman, S. G. *Molecular Luminescence Spectroscopy: Methods and Applications Part 1*; Wiley-Interscience: New York, 1985; pp 463–467, 754–762.
- (4) Burr, J. G. *Chemil- and Bioluminescence*; Marcel Dekker: New York, 1985.
- (5) Townshend, A. *Anal. Proc.* **1985**, *22*, 370–371.
- (6) Yamada, M. *Bunseki* **1987**, 879–882.
- (7) Yamada, M.; Hobe, T.; Suzuki, S. *Anal. Lett.* **1988**, *21*, 1887–1900.

- (8) Xue-Xin, Q.; Yue-Ying, G.; Yamada, M.; Kobayashi, E.; Suzuki, S. *Talanta* **1989**, *36*, 505-508.
- (9) Nakagama, T.; Yamada, M.; Suzuki, S. *Anal. Chim. Acta* **1989**, *217*, 371-376.
- (10) Van Loon, J. C. *Analytical Atomic Absorption Spectroscopy: Selected Methods*; Academic: New York, 1980.
- (11) Williams, W. J. *Handbook of Anion Determination*; Butterworths: Boston, MA, 1979; pp 78.
- (12) Yamada, M.; Suzuki, S. *Anal. Lett.* **1984**, *17*, 251-263.
- (13) Ishii, M.; Yamada, M.; Suzuki, S. *Bunseki Kagaku* **1986**, *35*, 373-378.
- (14) Ishii, M.; Yamada, M.; Suzuki, S. *Anal. Lett.* **1986**, *19*, 1591-1601.
- (15) Ishii, M.; Yamada, M.; Suzuki, S. *Bunseki Kagaku* **1986**, *35*, 955-960.
- (16) Yamada, M.; Kanai, H.; Suzuki, S. *Bull. Chem. Soc. Jpn.* **1985**, *58*, 1137-1142.
- (17) Yamada, M.; Suzuki, S. *Anal. Chim. Acta* **1987**, *193*, 337-341.
- (18) Wasserman, H. H.; Murray, R. W. *Singlet Oxygen*; Academic: New York, 1979.
- (19) Adam, W.; Ciento, G. *Chemical and Biological Generation of Excited States*; Academic: New York, 1982.
- (20) Ingraham, L. L.; Meyer, D. L. *Biochemistry of Dioxygen*; Plenum: New York, 1985.
- (21) Gundermann, K.-D.; McCapra, F. *Chemiluminescence in Organic Chemistry*; Springer-Verlag: Berlin, 1987.
- (22) Wasserman, H. H.; Murray, R. W. *Singlet Oxygen*; Academic: New York, 1979; pp 115.
- (23) Wasserman, H. H.; Murray, R. W. *Singlet Oxygen*; Academic: New York, 1979; pp 24.
- (24) Nanni, E. J., Jr.; Birge, R. R.; Hubbard, L. M.; Morrison, M. M.; Sawyer, M. M. *Inorg. Chem.* **1981**, *20*, 737-741.
- (25) Kanofsky, J. R. *J. Am. Chem. Soc.* **1986**, *108*, 2977-2979.
- (26) Mulazzani, Q. G.; Ciano, M.; D'Angelantonio, M.; Venturi, M.; Rodgers, M. A. J. *J. Am. Chem. Soc.* **1988**, *110*, 2451-2457.
- (27) Ohya-Nishiguchi, H. *Kagaku to Seibutsu* **1986**, *24*, 638-644.

RECEIVED for review December 27, 1988. Accepted April 4, 1989.

Multicomponent Fluorometric Analysis Using a Fiber-Optic Probe

Frank V. Bright* and Kevin S. Litwiler

Department of Chemistry, State University of New York at Buffalo, Buffalo, New York 14214

Single-frequency phase-resolved fluorometry through single and bifurcated fiber-optic probes is used to quantify mixtures of spectrally similar fluorophores. Correlation coefficients from correlation plots are greater than 0.98, and standard errors of estimate are less than 0.13 μM for 80 binary mixtures. Quantification of fluorophores at up to 10:1 molar ratios with lifetime separations of less than 200 ps is possible. The simultaneous quantification of the individual components of ternary and quaternary synthetic mixtures is demonstrated. Application of phase resolution to ambient light rejection is reported also. In this case, the emission spectrum of 10 nM Rhodamine 6G is easily obtained in the presence of a fluctuating, unmodulated background.

INTRODUCTION

Over the last few decades, numerous research groups have increased analytical sensitivity by using the inherent multidimensional nature of fluorescence processes (1, 2). In addition to its great selectivity, fluorescence spectroscopy has gained additional popularity because of its intrinsically high sensitivity (zero background) and relative simplicity (1, 2).

For the most part, all of these extremely powerful fluorescence-based methods of analysis have been carried out using conventional cuvettes and simple chambers. That is, the ability to perform these same types of measurements remote from the laboratory location was generally impossible. Fortunately, over the last decade, the telecommunications industry has developed high-light-transmitting optical fibers. Because optical fibers provide a convenient means of transporting light from one location to another, many spectroscopic techniques that were once laboratory bound have been implemented remotely by using fiber-optic probes. Several excellent reviews dealing with fiber-optic-based sensors in chemical analysis have been published recently (3-5).

The majority of the past fiber-optic-based fluorescence sensors have employed either excitation or emission wavelength selectivity (3-5). Other selectivity parameters such as

fluorescence lifetime, steady-state polarization, and rotational diffusion rates have received little if any attention. The acquisition of fluorescence lifetime information via optical fibers has been demonstrated previously (6). However, the time resolution and ability to resolve multiexponential decays of fluorescence were not demonstrated until recently (7-9). Our own group (7-9) has developed and described fiber-optic-based fluorescence lifetime instrumentation capable of (in favorable situations) recovering single, double, and/or triple exponential decay laws of fluorescence in remotely located samples. However, in the previous reports from this laboratory we did not demonstrate quantitative analysis of mixtures.

In this report, we use an improved version of this fiber-optic-based multifrequency phase and modulation fluorometer which is capable of making phase-resolved measurements (10). In this work we describe the use of this instrument for the simultaneous quantification of the individual components in binary, ternary, and quaternary mixtures and the minimization of stray light interference in single-component determinations.

INSTRUMENTATION

The multifrequency phase and modulation fluorometer used in these studies has been described in detail previously (9). In the present configuration, the optical-fiber sensor consists of two identical 10-m segments joined (epoxied) at the distal end within a 3-mm i.d. capillary tube. This capillary tube is in turn epoxied into an SMA adaptor (catalog no. 905-120-5003) and capped with a cable nut from an Amphenol connector. The nut opening is fitted with a 0.15 mm thick piece of quartz plate, which protects the bare, polished ends of the fiber optic. In addition, the small gap (3-4 mm) between the bare fiber optics and the solution minimize any deleterious heating effects of the sample. We have found that simply placing the bare fiber probe in contact with the sample results in a signal that exponentially decreases and approaches a steady-state intensity. By using the configuration described above, we notice very little if any signal fluctuation over the time of our experiments.

Fluorescence is collected by the second optical fiber whose output end is held rigidly via an Amphenol connector and

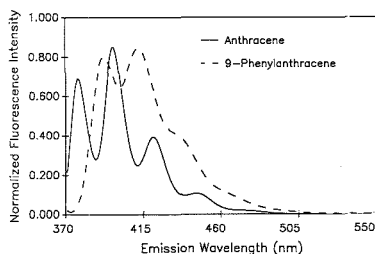


Figure 1. Normalized steady-state fluorescence spectra for anthracene and 9-phenylanthracene. Laser excitation was at 351.1 nm.

receptacle in an in-house fiber-optic mount (FOM). The light (laser scatter and sample fluorescence) from this fiber is imaged with a lens (L; Oriol, focal length 33 mm) onto the entrance slit of a monochromator (SLM-Aminco, Ir.c.) with a spectral band-pass of 4 nm. All data regressions were performed off-line with an IBM-PC/AT computer using SLM-Aminco software, a global analysis package (11), or software described elsewhere (12).

EXPERIMENTAL SECTION

Unless otherwise noted all reagents were used as received and all samples were prepared in nondegassed ethanol (Aaper Chemical Co.). Pyrene (P), benzo[a]pyrene (B[a]P), benzo[e]pyrene (B[e]P), 1,4-bis(5-phenyloxazol-2-yl)benzene (POPOP), 1,4-bis(4-methyl-5-phenyloxazol-2-yl)benzene (Me_2POPOP), Rhodamine B (RB), Rhodamine 6G (R6G), anthracene (A), and 9-phenylanthracene (9PA) were purchased from Aldrich. All samples were prepared in the appropriate solvent and sonicated for at least 15 min.

Synthetic binary, ternary, and quaternary mixtures were prepared covering a broad concentration range. Typically, this range was from 1 μM to 100 nM, although a larger range was explored for several of the mixtures. Each of these species was chosen because their emission spectra overlapped (typical spectra are shown in Figure 1) and are difficult to resolve by using simple wavelength selectivity alone. Thus, they provide us with useful mixtures to test the abilities of the fiber-optic-based phase-resolved fluorometer.

Data collection consisted of two steps. First, the phase-resolved emission spectra for each of the pure fluorophores was collected at 5-nm increments as a function of detector phase angle setting. A typical scan takes about 5 min to complete. In all cases, detector phase angle settings used are 0, 45, 90, 135, 180, 225, 270, and 315°. These spectra served as the standards from which the molar fluorescence intensities were subsequently calculated (10, 12). In the second step, the phase-resolved spectra for each mixture is collected by using the identical conditions used for acquisition of the standards. Data analysis followed the same protocols outlined elsewhere (10, 12). In all cases, we overdetermine the system by using at least 25 and sometimes up to 100 simultaneous equations.

RESULTS AND DISCUSSION

The power of phase-resolved fluorescence lies in its ability to resolve individual components in complex mixtures based on the differences of the component lifetimes. Specifically, two components can have identical emission and excitation spectra which make them unresolvable by spectral selectivity alone; however, if these components exhibit different fluorescence lifetimes, one can successfully quantify each component (10).

For this work fluorescence lifetime values range from near 1 ns to around 100 ns, which is inclusive of the lifetimes for the majority of the typical fluorescent species encountered in biochemistry and chemistry. In all cases studied, the degree of spectral overlap varies from a moderate case like Rhodamine B and Rhodamine 6G to more severe cases like an-

Table I. Recovered Slopes, Intercepts, Correlation Coefficients, and Standard Errors of Estimates for Plots of Recovered Concentration Versus Prepared Concentration for Binary Fluorophore Mixtures

mixture	slope	intercept	r^{2a}	SEE ^b
RB ^c	1.002	-0.003	0.9986	0.015
R6G ^c	0.994	0.014	0.9929	0.009
A ^d	1.021	0.008	0.9972	0.006
9PA ^d	1.008	0.017	0.9918	0.027
B[a]P ^e	0.987	0.007	0.9994	0.009
B[e]P ^e	1.045	-0.019	0.9872	0.039
$\text{Me}_2\text{POPOP}^f$	1.187	0.038	0.9968	0.128
POPOP ^f	1.086	0.008	0.9951	0.098

^a Correlation coefficient. ^b Standard error of estimate (μM). ^c 75-MHz modulation frequency; 20 samples; concentrations ranged from 10 nM to 1 μM for each component. Laser excitation was at 514.5 nm. ^d 40-MHz modulation frequency; 10 samples; concentrations ranged from 100 nM to 3 μM for each component. Laser excitation was at 351.1 nm. ^e 20-MHz modulation frequency; 30 samples; concentrations ranged from 100 nM to 4 μM for each component. Laser excitation was at 351.1 nm. ^f 150-MHz modulation frequency; 20 samples; concentrations ranged from 10 nM to 2 μM for each component. Laser excitation was at 351.1 nm.

Table II. Typical Recovered Concentrations for a Binary Mixture of Me_2POPOP and POPOP^a

actual, ^b μM	recovered, ^b μM
1.00/1.00	0.92/1.05
1.00/2.00	0.97/2.06
2.00/1.00	2.11/1.03
0.10/1.00	0.13/0.92
1.00/0.10	1.10/0.07
0.010/1.00	0.004/0.96
1.00/0.010	1.05/0.013

^a Results from 100 simultaneous equations. ^b $\text{Me}_2\text{POPOP}/\text{POPOP}$.

thracene and 9-phenylanthracene (Figure 1) and Me_2POPOP and POPOP. The benzo[a]pyrene-benzo[e]pyrene binary system illustrates an intermediate degree of spectral overlap and was included because of its biological importance (e.g., benzo[a]pyrene is a potent carcinogen, but benzo[e]pyrene is not).

Table I summarizes the results of simultaneous determinations of the individual components in each of the binary mixtures. The actual modulation frequencies employed for a given binary mixture are listed in the footnotes of Table I. The modulation frequencies were chosen by using the protocols discussed elsewhere (12, 13). These results represent a summary of 80 multicomponent analyses and are generated by plotting the recovered concentration of a given fluorescent species versus the actual concentration prepared in the synthetic mixture. For "perfect" data, the slope and intercept should be 1.00 and 0.00, respectively. Clearly, the recovered slopes and intercepts are very near the ideal values, the correlation coefficients are all good (greater than 0.98), and the standard errors of estimate are all low (less than 0.13 μM).

Table II shows a portion of the actual recovered concentrations for binary mixtures of Me_2POPOP and POPOP. Of all the binary mixtures studied, this pair is the most difficult to resolve. They are spectrally very similar and have lifetimes that differ by only 200 ps. Thus, these values represent the worst case investigated with our fiber-optic phase-resolved fluorometer. Inspection of Table II shows that reasonably accurate results are recovered at up to a 10:1 molar ratio of the two components, but above that level the accuracy is much poorer and is indicative of both the degree of spectral overlap and low temporal selectivity between Me_2POPOP and POPOP.

Table III. Recovered Slopes, Intercepts, Correlation Coefficients, and Standard Errors of Estimates for Plots of Recovered Concentration Versus Prepared Concentration for Ternary and Quaternary Fluorophore Mixtures

mixture	slope	intercept	r^2 ^a	SEE ^b
ternary				
POPOP ^c	1.096	-0.045	0.9832	0.26
A ^c	0.967	-0.067	0.9924	0.19
B[a]P ^c	1.078	0.041	0.9799	0.31
quaternary				
POPOP ^d	0.961	0.008	0.9768	0.36
A ^d	1.189	0.124	0.9821	0.42
B[a]P ^d	1.073	0.050	0.9962	0.39
P ^d	1.005	0.135	0.9633	0.45

^aCorrelation coefficient. ^bStandard error of estimate (μM). ^c45-MHz modulation frequency; 20 samples: concentrations ranged from 100 nM to 1 μM for each component. ^d30-MHz modulation frequency; 25 samples: concentrations ranged from 100 nM to 5 μM for each component.

Table III compiles the results for recovery studies of ternary and quaternary mixtures containing POPOP, anthracene, benzo[a]pyrene, and pyrene. For this compilation, the fractional contributions of each component is varied over at least a 10-fold range. The ternary results are quite good and it appears that we can accurately recover the concentrations of the three fluorophores (POPOP, A, and B[a]P) when all of the components contribute at least 10% or more to the total signal. However, when we attempt to recover quantitative information for samples in which the fractional contribution of one of the components is less than 10% of the total signal, much poorer results were obtained. Compared to the simpler binary systems studied, all the analytical figures of merit (SEE, slope, intercept, and r^2) are poorer. The major cause of this is again attributed to the samples containing 10% or less of either of the fluorophores. In fact, when we do not include samples in which the components contribute 10% or less, we find that our analytical figures of merit improve by about 10–15%. For synthetic quaternary samples we find that we are able to recover accurate concentrations for moderately heterogeneous mixtures (e.g., 2 μM P, 0.25 μM A, 0.8 μM B[a]P, and 0.15 μM POPOP). But, overall the analytical figures of merit are poorer than the ternary case and in effect we cannot recover accurate concentration information when any one or more of the components contribute less than 15% to the total signal. This was not a totally unexpected result; however, we point out that these results were obtained at only a single modulation frequency. We expect that significant accuracy improvements can be realized for the recovered concentrations in complex mixtures if multiple frequencies are used (14).

A major interferent, when using fiber-optic probes, is the presence of ambient room or outdoor light which is collected by the fiber and subsequently sent on to the detection electronics. The result is a tremendous and often unstable background signal that buries the fluorescence. Fortunately, because ambient light is not modulated at the modulation frequency of the excitation source, it can be eliminated by using phase-resolved fluorescence. Figure 2 depicts the steady-state emission spectra for a 10 nM Rhodamine 6G solution with (curve B) and without (curve A) room lights. The room-light signal totally overwhelms the much weaker fluorescence signal. In addition, because the signal varies with time (personnel walking by the fiber probe, etc.), we have found that simple blank subtraction fails. However, using phase-resolution one can null the ambient light signal and acquire an emission spectrum devoid of any ambient light interferences or fluctuations. Curve C in Figure 2 is the phase-resolved emission spectrum for the 10 nM Rhodamine

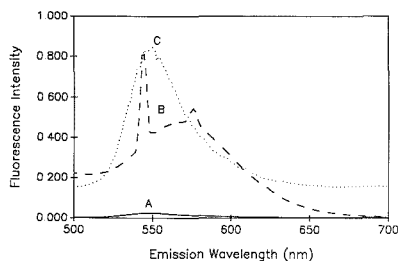


Figure 2. Steady-state fluorescence spectra for 10 nM Rhodamine 6G with (B) and without (A) room lights. Curve C is the phase-resolved emission spectrum collected with the room lights on. Laser excitation was at 483.0 nm. Modulation frequency for curve C is 50 MHz.

6G sample collected with the laboratory lights on, but the ambient light signal nulled. We have successfully recovered the same spectrum by pseudorandomly turning the room lights off and on throughout the scan also. Thus, it appears that the fluctuations in light levels encountered in this experiment do not affect the phase-resolved results.

CONCLUSIONS

Phase-resolved fluorescence measurements are demonstrated by using a simple bifurcated fiber-optic probe. Results show that simultaneous multicomponent analysis can be performed with this fiber probe on remotely located samples. Earlier work in this laboratory (9) has demonstrated measurements with fiber optics up to 175 m in length. We feel nothing prevents one from performing phase-resolved measurements using even longer lengths of fiber. In fact, still longer single-mode fiber optics could be used with much less loss than encountered with the present multimode fibers. In this present study, we are limited by the fiber available to us. Of course, detection limits would suffer because of the attenuation of the longer fiber lengths. However, with the present configuration, detection limits ($S/N = 3$) are quite respectable, typically at the high picomolar level with the monochromator (4 nm band-pass). With a long pass filter we have achieved a detection limit of about 25 pM for Rhodamine 6G with 300 mW of 514.5-nm radiation launched into the fiber.

Ambient light signals that often plague fluorescence-based measurements can be minimized significantly by using the phase-resolved approach. This allows remote analysis of complex samples in just about any environment having moderate background light levels (e.g., clinical settings). Although we did not explore the effects here, we anticipate that by using the true multifrequency character of our fluorometer, we can more accurately resolve the individual components in extremely complex samples (e.g., oil wells, in vivo). In the future, we plan to use phase resolution to enhance the selectivity for fiber-optic-based immunosensors.

ACKNOWLEDGMENT

The authors acknowledge Steve Palstra and Gary Sagermar for construction of many of the special optical mounts used in this study.

LITERATURE CITED

- Warner, I. M.; Patony, G.; Thomas, M. P. *Anal. Chem.* **1988**, *60*, 463A.
- Bright, F. V. *Anal. Chem.* **1988**, *60*, 1031A.
- Angel, S. M. *Spectroscopy* **1987**, *2*(4), 38.
- Seitz, W. R. *CRC Crit. Rev. Anal. Chem.* **1988**, *19*, 135.
- Arnold, M. A.; Myerhoff, M. E. *CRC Crit. Rev. Anal. Chem.* **1988**, *20*, 149.
- Bright, F. V.; Monnig, C. A.; Hietje, G. M. *Anal. Chem.* **1986**, *58*, 3139.
- Bright, F. V. *SPIE Conf. Proc.* **1988**, *909*, 23.
- Bright, F. V. *Appl. Spectrosc.* **1988**, *42*, 1531.
- Litwiler, K. S.; Bright, F. V. *ACS Symposium Series on Chemical Sensors and Microinstrumentation*; Murray, R. W., Dessey, R. E., Heine-

- man, W. R., Janata, J., Seitz, W. R., Eds.; American Chemical Society: Washington, DC, in press.
- (10) McGown, L. B.; Bright, F. V. *CRC Crit. Rev. Anal. Chem.* **1987**, *18*, 245.
- (11) Beecham, J. M.; Gratton, E. *SPIE Conf. Proc.* **1988**, *979*, 70.
- (12) Bright, F. V. Ph.D. Thesis, Oklahoma State University, Stillwater, OK, 1985.
- (13) Jameson, D. M.; Gratton, E.; Hall, R. D. *Appl. Spectrosc. Rev.* **1984**, *20*, 55.
- (14) Keating-Nakamoto, S. M.; Cherek, H.; Lakowicz, J. R. *Anal. Chem.* **1987**, *57*, 271.

RECEIVED for review January 17, 1989. Accepted March 30,

1989. This work was supported by BRSO S07 RR 07066 awarded by the Biomedical Research Support Grant Program, Division of Resources, National Institutes of Health, by the donors of the Petroleum Research Fund, administered by the American Chemical Society, the Health Care Instruments and Devices Institute at SUNY—Buffalo, by a Non-Tenured Faculty Grant from 3M, Inc., by a New Faculty Development Award from the New York State/United University Professions, by the Center for Advanced Technology (SUNY—Buffalo), and by the National Institute of Mental Health.

Binning Spectral Images in a Charge-Coupled Device

Patrick M. Epperson¹ and M. Bonner Denton*

Department of Chemistry, University of Arizona, Tucson, Arizona 85721

A charge-coupled device (CCD) can selectively combine photogenerated charge from several detector elements into a single charge packet via a special charge readout mode called binning. This article focuses on the use of charge binning in a two-dimensional CCD for increasing the sensitivity and dynamic range of spectroscopic measurements. Binning allows the effective detector element size to be matched to the size of the slit image. Equations describing the signal-to-noise ratio and dynamic range of the binned readout of spectral lines are developed. Results of binning to increase the sensitivity of atomic emission and molecular fluorescence measurements are presented. An intraspectral dynamic range of 500 000 is achieved by mixing binned and normal readout modes of a Hg atomic emission spectrum. Practical factors related to binning spectral images including spectral line orientation, readout speed, and blooming are discussed.

Charge-coupled devices (CCDs) are the most sensitive array detectors available for low-light-level scientific imaging applications. The factors responsible for the sensitivity of CCDs include high quantum efficiency, the ability to integrate charge for hours, negligible dark current, and most importantly, an extremely low detector read noise (1-3). Although they are primarily used for imaging, there is a great deal of interest in the use of CCDs for spectroscopy in the near-infrared to X-ray region (4-6). Unfortunately, the spatial format of two-dimensional CCDs is designed primarily for imaging applications and not for spectroscopy. The height to width aspect ratio of a single detector element is poorly matched to the images of a slit normally encountered in spectroscopy. Most CCD detector elements range in size from 7×7 to $30 \times 30 \mu\text{m}$ (6), whereas the size of spectrograph slits ranges from 10 to 500 μm wide and 1 to 10 mm tall. A spectral line focused onto a two-dimensional CCD typically covers 100 or more detector elements. The measurement of a single wavelength requires that photogenerated charge packets from the detector elements illuminated by the slit image be summed together.

The manner of summing photogenerated charge from several detector elements directly affects the single-to-noise ratio (S/N) and dynamic range of the measurement of spectral

line intensities. The method of summation can be either digital or analog. Digital summation is accomplished by individually reading out and digitizing each charge packet, followed by storing and summing the digitized intensities in a computer. Analog summation is performed by physically combining the photogenerated charge packets into a single charge packet in a process called *binning*. Compared to digital summation, binning reduces the number of analog to digital operations needed to quantitate the amount of charge associated with a group of charge packets and thereby reduces the total detector noise and increases the readout speed. In spectroscopic applications, binning is used to gather and noiselessly collect the photogenerated charge packets from a spectral line illuminating many detector elements of a CCD.

The utility of binning for spectral imaging was first recognized by astronomers (7, 8), and the process has since become used in other areas of low-light-level spectroscopy (9, 10). Although the technique of binning in scientific CCD applications is now fairly widespread, an analysis of the theoretical and practical aspects of binning does not exist. This paper presents a detailed description of binning and its significance in spectroscopic applications.

Serial, Parallel, and Two-Dimensional Binning. A description of the three binned readout modes of a two-dimensional CCD is presented to provide a framework for the discussion of binned spectral images. Charge is binned by combining charge packets contained in two or more adjacent potential wells into a single potential well during charge readout. Adjacent charge packets in both the serial and parallel directions as defined in Figure 1 can be combined.

Charge is binned serially in the output node during the transfer of charge in the serial register. Two-fold serial binning is illustrated in Figure 2. The digital image from a 2-fold binned readout has half the serial resolution of an unbinned image. Each point of the digitized image represents the sum of two adjacent charge packets. Serial binning of charge from any number of adjacent detector elements is possible, including binning all of the charge packets in the serial register into a single charge packet. Binned and nonbinned readout of groups of charge packets in the serial register can be mixed in any combination. The only limitation to serial binning is that the combined charge packet does not exceed the charge holding capacity of the output node or the on-chip amplifier. Exceeding the charge capacity of any potential well in a CCD can cause the excess charge to spill into adjacent potential wells, a condition known as blooming. Blooming can be

¹Current address: Chemistry and Materials Science Department, L-499, Lawrence Livermore National Laboratory, Livermore, CA 94550.

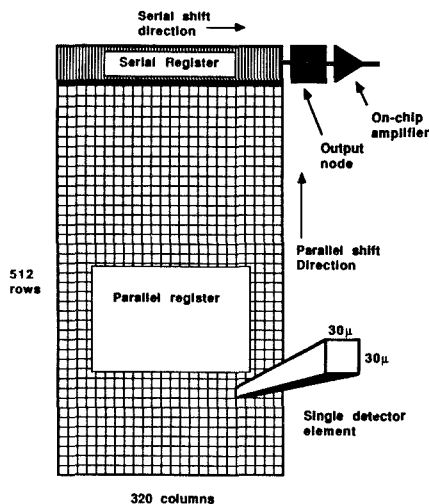


Figure 1. Diagram of the RCA-SID501EX CCD showing the method of charge transfer in a two-dimensional CCD. Photogenerated charge from an image is integrated in the parallel register. During charge readout, rows of charge packets are shifted in parallel by the parallel register electrodes. The top row of charge in the parallel register is transferred into the serial register. The serial register then transfers a single row of charge to the output node of the on-chip amplifier. The parallel and serial shifting of charge is repeated until every row is transferred to the serial register and read out.

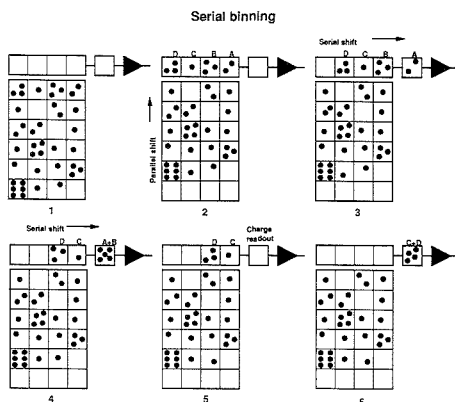


Figure 2. Simplified diagram of 2-fold serial binning of charge in the output node of a 4×6 element CCD. (1) Photogenerated electrons are integrated in parallel register. (2) Charge in the parallel register is shifted upward by one row, causing charge from the top row of the parallel register to transfer into the serial register. (3) Charge packet A is transferred into the output node potential well. (4) Charge packet B is transferred to the output node and combined with charge packet A. (5) The combined charge packets are sensed by the on-chip amplifier, and the output node potential is reset. (6) Steps 3 and 4 are repeated to bin charge packets C and D.

disastrous when charge from a strong spectral line spills into the charge packets from a weak spectral line and must be avoided when one is making quantitative spectral measurements (4).

Parallel binning is similar to serial binning except that rows of charge packets are combined instead of single charge packets. Three-fold parallel binning is illustrated in Figure 3. Parallel binning any number of rows of charge packets

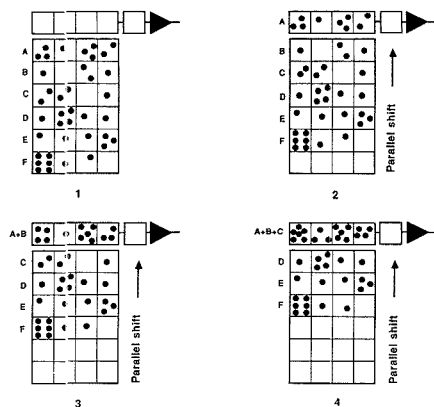


Figure 3. Simplified diagram of 3-fold parallel binning of charge in the serial register of a 4×6 element CCD. (1) Shown are photogenerated charge packets corresponding to the 4×6 image. (2) Charge in the parallel register is shifted upward by one row, causing charge from the top row of the parallel register to transfer into the serial register. (3) Charge is parallel shifted again, transferring charge from row B into the serial register and combining it with charge from row A. (4) The parallel register is clocked a third time, and charge from row C is added to charge from rows A and B in the serial register. The binned charge packets in the serial register are shifted to the output node and read out in a normal fashion.

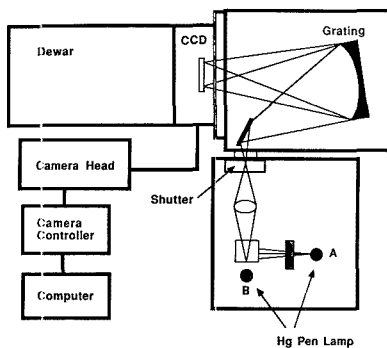


Figure 4. Block diagram of CCD spectrograph. The Hg pen lamp is placed at A when used as a molecular fluorescence excitation source and at B when used as an atomic emission source.

into a single row is possible, including binning charge from every row of the parallel register into a single row. Binned and nonbinned readout of rows can be mixed in any combination; the number of rows that can be parallel binned is limited only by the charge capacity of the serial register.

Binning of charge in two dimensions is possible from any rectangular group of detector elements. Binning in both dimensions is accomplished by combining serial and parallel binning. For example, a 4-fold serial and 4-fold parallel binning of a 512×320 array results in a 128×80 element image as listed in Table I. Each element of the image represents the charge from a 4×4 rectangle of CCD detector elements. As in the case of serial and parallel binning, the only limitation to the number of charge packets that can be binned is the finite charge capacities of the serial register, the output node, and the on-chip amplifier.

EXPERIMENTAL SECTION

The CCD-based spectrograph constructed in our laboratories is shown in Figure 4. The fluorescence excitation source is a Hg

Table I. Image Format Size, Effective Detector Element Area, Number of Data Points per Image, and Read Time for a 512 Row \times 320 Column CCD Readout with Various Bin Factors^a

mode	binning ($B_p \times B_s$)	image format ($R_{\text{image}} \times C_{\text{image}}$)	$A_{\text{image}}, \text{mm}^2$	Z	read time, ms	notes
1	1 \times 1	512 \times 320	0.0009	163840	3612	normal readout
2	4 \times 4	128 \times 80	0.0144	10240	294	4 \times 4 mode
3	1 \times 64	512 \times 5	0.0576	2560	387	64-fold serial bin
4	1 \times 320	512 \times 1	0.2880	512	346	linear array mode
5	64 \times 1	8 \times 320	0.0576	2560	64.0	64-fold parallel bin
6	256 \times 1	2 \times 320	0.2304	640	21.8	double-beam mode
7	512 \times 1	1 \times 320	0.4608	320	14.7	linear array mode
8	512 \times 320	1 \times 1	147.5000	1	8.3	single-detector mode

^aTerms are defined in the text.

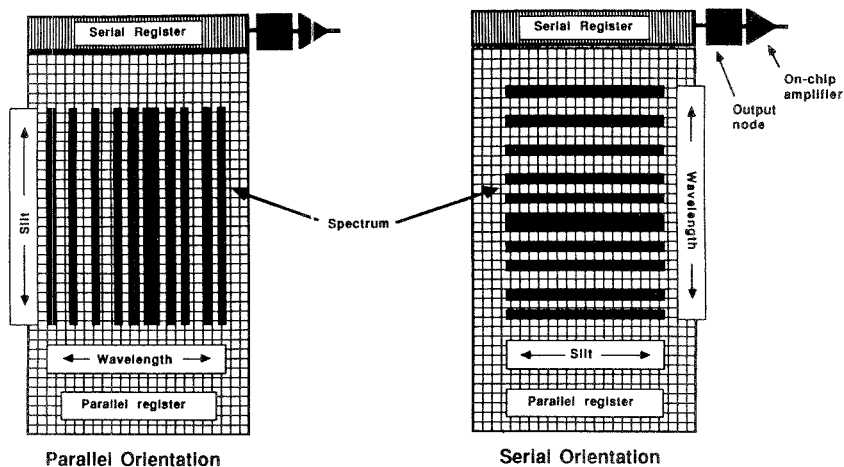


Figure 5. Parallel and serial orientations of a linear spectrum dispersed across a two-dimensional CCD.

pen lamp (Ultra-violet Products, Inc.) filtered with a 250-nm bandpass interference filter and focused onto a quartz cuvette. The fluorescence emission is collected at right angles to the excitation and focused onto the entrance slit of the 200 mm focal length $f/3$ spectrograph (Instruments SA, Model UFS 200). The 200 groove/mm grating disperses light across the CCD at 23 nm/mm (0.7 nm/detector element). A computer controlled shutter controls the exposure time and blocks the light during readout of the CCD. The Hg emission spectrum from the pen lamp is measured by directly focusing the light from the pen lamp onto the slits of the spectrograph.

The CCD device is a 320 \times 512 element RCA-SID501EX backside-illuminated CCD with 30 \times 30 μm detector elements as shown in Figure 1. The on-chip amplifier noise associated with measuring a single charge packet is 50 e (electrons) at the 50-kHz data rate used in these studies. The CCD is housed in a liquid nitrogen cryostat and cooled to 123 K to reduce dark current to negligible levels. The associated CCD electronics (Model CH181, Photometrics Ltd., Tucson, AZ) allows independent control of serial and parallel binning factors. Charge packets are measured by using the correlated double sampling technique (11) and digitized to 14 bits. The gain of the CCD electronics is 35 e/digital number. A more detailed description of the instrument is given in ref 12.

RESULTS AND DISCUSSION

Sensitivity and S/N Ratio. The effect of binning on the S/N ratio of a measurement of a spectral line intensity was evaluated by measuring the 404.7-nm Hg emission line from the pen lamp. The atomic emission spectrum was dispersed in the parallel orientation described in Figure 5. A 100 μm

wide \times 3 mm tall slit produced an emission spectrum that covered approximately 100 of the 512 rows of the CCD. The S/N ratio of the 404.7-nm line was measured by using normal and 100-fold parallel binned readout modes. The integration time varied from 0.1 to 300 s, and the line was measured five times for each integration time. A dark exposure of equal integration time was subtracted from each measurement.

The S/N ratio for the measurement of a spectral line that illuminates several detector elements depends on the method by which the charge packets from the detector elements are summed. A spectral line may be measured by reading out each charge packet independently followed by summing the digitized intensities in the computer, or by binning all of the charge from a spectral line into a single charge packet and then subjecting this binned charge packet to a single digitization. The total charge and the photon shot noise are identical in both cases; however, the detector noise is smaller in the binned readout mode.

The S/N ratio for a spectral line measured by reading out charge packets individually and then summing the digitized intensities in computer memory is

$$S/N_{\text{normal}} = KS / (KS + KN_e^2)^{1/2} \quad (1)$$

where S is the average photogenerated signal integrated in a single detector element, K is the number of detector elements illuminated by the spectral line, and N_e is the detector electronic noise associated with digitizing a charge packet. The photon signal is assumed to be noiseless except for shot noise, and the energy of the photons is assumed to be low enough

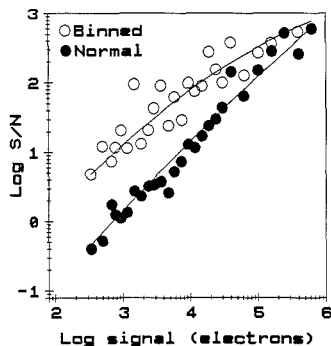


Figure 6. log signal to noise (S/N) versus log signal (S) for 404.7-nm Hg emission line illuminating 100 detector elements. Open circles are from a 100-fold binned readout, and closed circles are from a normal readout. Bottom and top lines are the S/N behavior predicted from 1 and 2, respectively.

that only one electron is created per absorbed photon. The read noise of a CCD is largely determined by the noise of the on-chip amplifier and is independent of the signal (3).

The S/N ratio for the same spectral line measured by binning K charge packets followed by a single digitization is

$$S/N_{\text{binned}} = KS / (KS + N_r^2)^{1/2} \quad (2)$$

Equations 1 and 2 differ only in that summing in computer memory subjects the photogenerated charge to the detector noise from K reads, but binning subjects the same charge information to the detector noise of only a single read. It is important to note that the output amplifier sensitivity and noise depend only on the amount of charge transferred onto the output node and are independent of the area of silicon involved in collecting and transferring the photogenerated charge. For a bright spectral line where $S \gg KN_r^2$, the dominant noise is the photon shot noise and both equations predict the same approximate S/N ratio. However, for a weak spectral line where $KN_r^2 \gg S$, the measurement is detector noise limited and binning results in a S/N advantage of $K^{1/2}$. When a CCD is used to detect extremely weak spectral lines that cover several detector elements, the highest possible S/N ratio is realized by binning all of the photogenerated charge from the line into a single charge packet. Equations 1 and 2 assume that the detector noise is independent of integration time, signal level, and binning conditions, a condition that is generally true for most scientific grade CCDs under typical operating conditions. For spectral measurements using long integration times or high serial binning factors, the read noise may become dominated by secondary noise sources (13) and binning may not achieve as large a S/N enhancement as predicted.

The predicted and experimental results for the normal and 100-fold binned readout modes for the Hg emission line are shown in Figure 6. The curved lines are the theoretically predicted S/N ratio based on a read noise of $50 \cdot 2^{1/2}$ (the $2^{1/2}$ arises from the two read noises in each measurement of signal minus dark background). Note that at low signal levels, binning improves the S/N ratio by a factor equal to the square root of the number of detector elements binned; however, at high signal levels, the S/N ratio for the normal readout mode approaches the binned S/N . The agreement between the predicted and experimental S/N ratios indicates that the read noise in these measurements is independent of binning.

The effect of binning in improving the S/N ratio was also investigated by qualitatively measuring the molecular fluorescence spectrum of anthracene. The fluorescence

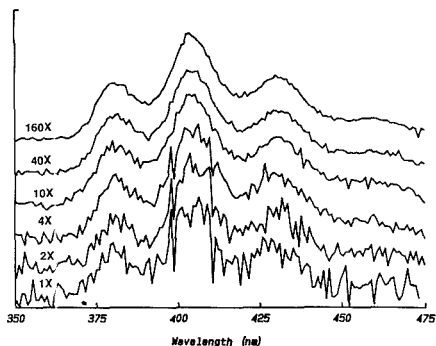


Figure 7. Fluorescence emission spectra of 10^{-6} M anthracene for a 1-s exposure with different parallel binning parameters. Spectra are offset for clarity. Charge was binned in the slit dimension of the spectral image. Each spectrum is the result of digital and analog (binning) summing of charge information from 160 rows of the CCD. Key: 1X digital summation of 160 digitized rows; 2X, digital summation of 80, 2-fold binned rows; 4X digital summation of 40, 4-fold binned rows, 10X digital summation of 16, 10-fold binned rows; 40X, digital summation of 4, 40-fold binned rows; 160X, single 160-fold binned row. The intensity at 400 nm is approximately 8000 photogenerated electrons, or 50 e/CCD detector element.

emission from a 10^{-6} molar solution of anthracene in ethanol was dispersed across the CCD in the parallel orientation of Figure 5 for a 1-s integration. The $250 \mu\text{m} \times 5 \text{ mm}$ slit produced a spectral image covering approximately 160 of the 512 rows of the CCD. The 320 elements/row provided a wavelength coverage of approximately 220 nm and 0.7 nm/detector element and a spectral resolution of 5 nm. The result of parallel binning along the slit dimension to increase the S/N ratio of the anthracene spectrum is shown in Figure 7. The six spectra are the result of different combinations of binning and digital summing the charge intensities from the 160 illuminated rows using parallel binning factors of 1X, 2X, 4X, 10X, 40X, and 160X (a binning factor of 1X is a normal readout). For example, in the case of 4X binning, the 160 rows of charge were binned 4-fold into 40 rows and read out, followed by the summation of the 40 digitized rows in computer memory. Each spectrum represents the detection of the same amount of photogenerated charge. The increased S/N ratio achieved by charge binning is realized at the expense of spatial resolution in the slit dimension, a loss that is insignificant in this example.

The result of binning in the direction of wavelength dispersion on the anthracene spectrum under the same conditions as above is shown in Figure 8. In this case, binning increases the S/N ratio, but at the expense of spectral resolution. However, due to the relatively broad spectral features a certain amount of binning is tolerated without loss of spectral information. The ability to bin in both directions allows the effective detector element size to be conveniently adjusted to match the requirements of wavelength resolution and sensitivity.

It must be emphasized that binning is simply a means of increasing the already excellent sensitivity of a CCD and should be employed whenever advantageous. However, even without binning, CCDs are still quite sensitive spectroscopic detectors compared to other array detectors. For example, the read noise associated with sensing charge from 100 detector elements from the RCA-SID501EX is 50 e with binning and 500 e without binning. The 500 e is still less than half the detector noise found in a single element of a photodiode array especially made for spectroscopy with a comparable imaging area (14).

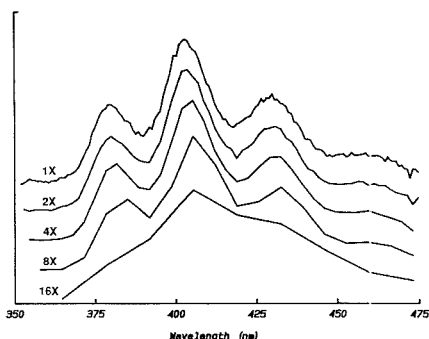


Figure 8. Fluorescence emission spectra of 10^{-6} M anthracene for a 1-s exposure with 1–16-fold binning in the direction of wavelength dispersion (serial). The spectra are also binned 160-fold in the slit (parallel) dimension. The intensities of the 2–16X spectra are normalized to the 1X spectrum (normal readout) by dividing by the serial binning factor. Note the slight increase in S/N ratio at the expense of wavelength resolution.

Dynamic Range. The simple dynamic range (SDR) of a solid-state detector is the ratio of the largest to smallest measurable charge packet of a single detector element from a single exposure. The largest measurable charge packet is limited by the maximum amount of charge containable in a detector element well before charge blooms, Q_{well} . The smallest measurable charge packet at a S/N ratio of 2 is approximately equal to twice the detector read noise:

$$\text{SDR} = Q_{\text{well}}/2N_r \quad (3)$$

The intraspectral dynamic range (ISDR) of an array detector, as defined by Talmi (14), is the ratio of the brightest to weakest spectral line that can be simultaneously measured from a single exposure. The ISDR of a CCD used for spectroscopic measurements depends on the SDR, the number of detector elements illuminated by the spectral line, and whether normal or binned readout modes are used. For a binned readout, the intensity in electrons of the weakest measurable spectral line focused onto K detector elements is approximately twice the read noise. The intensity of the brightest measurable spectral line uniformly illuminating K detector elements depends on the maximum amount of charge that can be binned in the serial register potential wells and the output node before blooming occurs. The ISDR for a binned readout measurement is

$$\text{ISDR}_{\text{binning}} = Q_{\text{limiting}}/2N_r \quad (4)$$

where Q_{limiting} is the limiting full well capacity of either the serial register or output node. The serial register and output node well capacities are usually 2–10 times as large as the parallel register well capacities; thus, $\text{ISDR}_{\text{binning}}$ is greater than the SDR by an equivalent factor. This dynamic range is realized only if the associated CCD electronics is capable of measuring such a large dynamic range. The ISDRs of certain ultralow-noise CCDs with large full well capacities are beyond the limits of 16-bit analog to digital converters (15).

For a normal readout, the intensity in photogenerated electrons of the weakest measurable line at a S/N ratio of 2 focused onto K detector elements is approximately $2N_r K^{1/2}$. The intensity of the brightest measurable line is KQ_{well} giving an ISDR of

$$\text{ISDR}_{\text{normal}} = KQ_{\text{well}}/(2N_r K^{1/2}) = \text{SDR} \cdot K^{1/2} \quad (5)$$

Binned and normal readout modes can be mixed to increase the ISDR beyond that of either the $\text{ISDR}_{\text{binned}}$ or $\text{ISDR}_{\text{normal}}$.

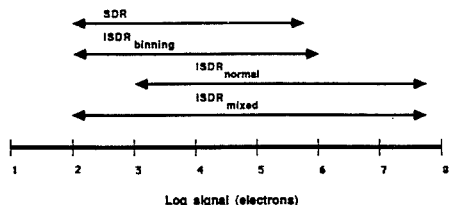


Figure 9. SDR and ISDR of the RCA-SID501EX CCD for a spectral line illuminating 100 detector elements, based on eq 3–6 and a parallel register full well capacity of 500 000 e, serial register full well capacity of 1 000 000 e, and a read noise of 50 e.

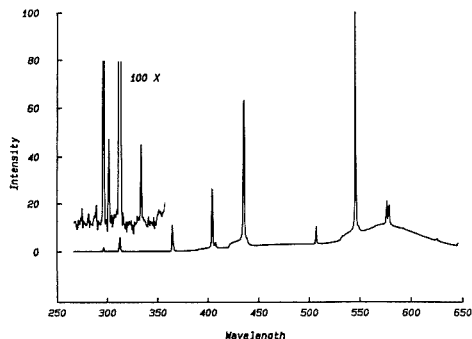


Figure 10. Hg spectrum obtained by using a mixed readout mode. Inset is the spectral region from 270 to 360 nm expanded 100-fold. Charge from selected weak spectral lines was binned 80×2 -fold into a single charge packet. Charge from intense spectral lines was read out normally. The minimum detectable emission line at 275.3 nm was 150 e; the maximum at 546.1 nm was over 80 million e. The dynamic range was 530 000 for a single exposure of the CCD to an atomic emission spectrum.

In a mixed readout mode, charge from weak spectral lines is selectively binned in the serial register, whereas charge from strong spectral lines is read out normally. The ISDR obtained with a mixed readout mode is

$$\text{ISDR}_{\text{mixed}} = KQ_{\text{well}}/2N_r = K \cdot \text{SDR} \quad (6)$$

Two restrictions apply to the use of a mixed readout mode. First, because of the nature of charge transfer in a two-dimensional CCD, a mixed readout is possible only when the spectral lines are oriented in the serial orientation of Figure 5. Second, binning must be limited to spectral lines of low intensity to avoid overflowing the output node. The second restriction requires that the approximate intensity of each spectral line be known before it is completely read out. One method of determining the approximate intensity is to shift the charge from a spectral line into the serial register and then read out the first few charge packets. If the average signal from the first few charge packets is below a certain threshold, the remaining charge packets are binned into a single charge packet; however, if the signal is above a certain threshold, the remainder of the charge packets are read out normally.

The SDR and ISDR of the RCA-SID501EX CCD for a slit image that illuminates 100 detector elements are illustrated in Figure 9. Note that the low end of $\text{ISDR}_{\text{mixed}}$ is set by $\text{ISDR}_{\text{binned}}$ and the high end is determined by $\text{ISDR}_{\text{normal}}$.

The use of selective binning to increase the ISDR of a measurement of the Hg emission spectrum is shown in Figure 10. Light from the lamp was focused onto the $100 \mu\text{m} \times 3$ mm slits and dispersed across the CCD in the serial orientation of Figure 5. The spectrum illuminated approximately 80

columns of the CCD. Strong emission lines were read out without binning and summed in computer memory. Charge from weak spectral lines covering 160 detector elements was read by 80-fold serial binning and 2-fold parallel binning. The weakest feature measured was the 275.3-nm Hg line at an intensity of 150 photogenerated electrons or approximately 1 e/detector element. The most intense spectral feature was the 546.1-nm Hg line with an intensity of approximately 80 million photogenerated electrons or 500 000 e/detector element. The dynamic range of spectral intensities from this single exposure of the CCD using the mixed readout mode was 530 000.

Spectral Line Orientation. A linear spectrum can be dispersed across a two-dimensional CCD with the spectral lines parallel or perpendicular to the serial register as shown in Figure 5. Each orientation has certain advantages and disadvantages depending upon the properties of the CCD and the demands of the spectral measurement. The serial orientation allows the mixing of binned and normal readout modes in a single exposure as discussed in the previous section. Parallel orientation results in a faster readout than does the serial orientation because it reduces the number of serial transfers. The parallel orientation is also more resistant to crosstalk between adjacent spectral lines due to blooming. When a detector element in a particular column is filled past saturation, charge in most CCDs spills into adjacent detector elements in the same column until the column is saturated and then into the serial register. Charge from one column does not usually spill across the channel stop diffusions into adjacent columns in the parallel register. The parallel register ensures that charge from an intense spectral line that blooms will not spill into adjacent weaker spectral lines.

CCD and Binned Image Formats. When binned readout modes are employed, there is no longer a one-to-one relationship between a CCD detector element and an element of the digitized image. The relationship between the CCD format and the image format as a function of binning parameters is defined in the following sections. Table I illustrates the CCD-to-image relationship by listing several parameters of an image acquired with seven different readout modes of a 512 × 320 element CCD.

The area of the CCD corresponding to one element of the image, A_{image} , increases with binning according to

$$A_{\text{image}} = A_{\text{ccd}} B_s B_p \quad (7)$$

where A_{ccd} is the area of a single detector element of the CCD, B_p is the binning factor in the parallel direction, and B_s is the binning factor in the serial direction. A_{image} increases 160 000-fold in going from a normal to a completely binned readout mode, as noted by comparing modes 1 and 7 of Table I.

The image format is reduced by binning according to

$$C_{\text{image}} \times R_{\text{image}} = (C_{\text{ccd}}/B_s) \times (R_{\text{ccd}}/B_p) \quad (8)$$

where C_{image} and R_{image} are the number of columns and rows of the digitized image and C_{ccd} and R_{ccd} are the number of columns and rows of the CCD. Binning reduces the total amount of information transferred to and stored by the computer for each image according to

$$Z_{\text{image}} = Z_{\text{ccd}}/B_s B_p \quad (9)$$

where Z_{image} is the number of elements in the digital image and Z_{ccd} is the number of detector elements in the CCD.

Readout Rates of Binned and Normal Images. Binning decreases the time required to read out an image compared to that for a normal readout. The time required for digitizing an image with a given serial and parallel binning is

$$\text{readout time} = R_{\text{ccd}} T_p + Z_{\text{ccd}} T_s / B_p + Z_{\text{ccd}} T_d / B_s B_p \quad (10)$$

where T_p and T_s are the times required for one transfer of charge in the parallel and serial directions and T_d is the time required to perform a double correlated sampling and digitization of a charge packet. For the CCD detector system employed in these studies using relatively slow clock rates to ensure optimal charge-transfer efficiencies, T_s is 2 ms, T_p is 15 ms, and T_d is 20 ms. Because the majority of the readout time for an unbinned image is devoted to digitizing charge packets to 14 bits, binning significantly decreases the time required to read the charge from the CCD. Parallel binning decreases the number of serial transfers in addition to the number of digitizations and results in a shorter read time than equivalent serial binning. A comparison of the readout times of modes 3 and 5 of Table I shows that the 64-fold parallel binned readout is more than twice as fast as the 64-fold serial binned readout. The faster readout obtained with parallel binning may be important when the CCD is used as a pseudolinear detector for temporally resolved spectroscopy (i.e. as a detector for high-performance liquid chromatography).

CONCLUSIONS

The above examples of binning applied to spectral measurements demonstrate the added flexibility that binning imparts to the CCD. The names assigned to several of the readout modes in Table I point to several promising uses of binned readout modes in spectroscopic measurements, which will be briefly described. The "single-element" mode bins charge from the entire CCD into a single charge packet. This reduces the 320 × 512 element CCD to a single-channel detector with an active area of 147 mm². Modes 4 and 7 are both termed the "linear array mode" because complete parallel or serial binning effectively turns the two-dimensional array into a linear array of detector elements having a high height-to-width aspect ratio. Mode 6 effectively changes the 320 × 512 CCD into two 320-element linear arrays, one stacked on top of the other. With proper optics, this CCD binning mode can acquire a sample and blank spectrum simultaneously with a high degree of detector and mechanical stability. In this true multichannel "double-beam" mode, both spectra are acquired during one integration period, totally eliminating problems caused by source drift. The sample and blank spectra would be recorded with the same CCD electronics within 16 ms, thereby greatly minimizing any detector electronic drift errors.

Registry No. Hg, 7439-97-6; anthracene, 120-12-7.

LITERATURE CITED

- Kristian, J.; Blouke, M. *Sci. Am.* **1982**, *247*, 78-74.
- Dereniak, E. L.; Crowe, D. G. *Optical Radiation Detectors*; John Wiley and Sons: New York, 1984; Chapter 4.
- Janesick, J. R.; Elliot, T.; Collins, S.; Blouke, M.; Freeman, J. *Opt. Eng.* **1987**, *26*, 692-714.
- Denton, M. B.; Lewis, H. A.; Sims, G. R. Charge-Injection and Charge-Coupled Devices in Practical Chemical Analysis. In *Multichannel Image Detectors*; Talmi, Y., Ed.; ACS Symposium Series 236, American Chemical Society: Washington, DC, 1983; Vol. 2, pp 133-154.
- Epperson, P. M.; Sweedler, J. V.; Bilhorn, R. B.; Sims, G. R.; Denton, M. B. *Anal. Chem.* **1988**, *60*, 327A.
- Bilhorn, R. B.; Epperson, P. M.; Sweedler, J. V.; Denton, M. B. *Appl. Spectrosc.* **1987**, *41*, 1125-1136.
- York, D. G.; Jenkins, E. B.; Zucchini, P.; Lowrance, J. L.; Long, D.; Songella, A. Echelle Spectroscopy with a Charge-Coupled Device (CCD). In *Solid State Imagers for Astronomy*; Geary, J. C.; Latham, D. W., Eds.; Proceedings of SPIE 290, Bellingham, WA, 1981; pp 202-207.
- Roesler, F. L.; Scherb, F.; Oliversen, K.; Jaehnnig, K.; Williams, T.; York, D. G.; Jenkins, E. B. Observations of the Plasma Torus of Jupiter with a Fabry-Perot/Charge-Coupled Device (CCD) Imaging Spectrometer. In *Solid State Imagers for Astronomy*; Geary, J. C., Latham, D. W., Eds.; Proceedings of SPIE 290, Bellingham, WA, 1981; pp 180-185.
- Strauss, M. G.; Naday, I.; Sherman, I. S.; Zaluzec, N. J. *Ultramicroscopy* **1987**, *22*, 117-124.
- Murray, C. A.; Dierker, S. B. *J. Opt. Soc. Am. A* **1986**, *3*, 2151-2159.

- (11) White, M. H.; Lampe, D. R.; Blaha, F. C.; Mack, I. A. *IEEE J. Solid-State Circuits* 1974, *SC-9*(1), 1-13.
- (12) Epperson, P. M.; Jalkian, R. D.; Denton, M. B. Molecular Fluorescence Measurements with a Charge-Coupled Device Detector. *Anal. Chem.* 1989, *61*, 282.
- (13) Sims, G. R. Principles and Applications of Charge Binning in Slow Scan CCD Readout. *Paper Summaries 26th Fall Symposium, Society of Photographic Scientists and Engineers*; October 13-17, 1986, Arlington, VA; pp 52-60.
- (14) Talmi, Y.; Simpson, R. W. *Appl. Opt.* 1980, *19*, 1401-1414.
- (15) Epperson, P. M.; Sweedler, J. V.; Denton, M. B.; Sims, G. R.; McCurnin, T. W.; Aikens, R. S. *Opt. Eng.* 1987, *26*, 715-724.

RECEIVED for review December 9, 1987. Revised March 17, 1989. Accepted April 3, 1989.

Competitive Binding of Protons and Metal Ions in Humic Substances by Lanthanide Ion Probe Spectroscopy

J. C. Dobbs, W. Susetyo, and L. A. Carreira*

Department of Chemistry, University of Georgia, Athens, Georgia 30602

L. V. Azarraga

Environmental Research Laboratory, U.S. Environmental Protection Agency, Athens, Georgia 30613

A pH-dependent, continuous, multiligand model is described. It is based on the Gaussian distribution model, which has been used to describe both proton binding by humic substances as well as metal binding by humic substances. However, the Gaussian distribution model has never been used to describe the competitive binding of the metalated and protonated ligand species. The inclusion of pH dependence should allow one to predict metal binding constants that are more representative of the true thermodynamic binding constants rather than curve-fitting parameters with no chemical significance.

INTRODUCTION

An understanding of metal-humic interactions is important from an environmental viewpoint, and research advances have been the subject of several recent review articles (1-4). A more thorough understanding of the interactions between metals and humic substances is necessary in order to predict the environmental fate of these metals and their complexes. This requires the development of both analytical methodology and mathematical models to facilitate the necessary distinction between complexed and free metal ions.

In a recent paper (5), we reported on the development of a spectroscopic technique designed to probe metal binding sites of humic substances. This spectroscopic technique was based on the unique fluorescence properties of the trivalent europium ion, Eu^{3+} . We demonstrated that the fluorescence spectrum of the probe metal ion was sensitive to the ligation of the metal ion with humic material. The sensitive nature of the fluorescence measurements permitted the detection of metal-humic complexation at humic material concentrations found in the environment.

In this paper, we utilized the Gaussian distribution complexation model to describe the speciation reactions between Eu^{3+} and Suwannee River fulvic acids. This continuous multiligand model was based on the assumption that complex humic substances contain a large number of nonidentical ligand sites that are normally distributed about an average or mean $\log K_{M_i}$ value, where K_{M_i} is the complex formation constant. The Gaussian distribution model was initially developed by other researchers (6-9) to describe proton binding

by humic materials. In other cases where this model has been used to describe metal binding by humic acids (8, 9), including our recent application (5), the inherent competition between protons and the metal ions for the same set of ligand sites was ignored. As a result of the neglect of competitive binding, this model predicts conditional binding constants of the metal of interest. Since conditional binding constants are only constant at constant pH, different sets of experimental data measured at a different pH value cannot be fitted with same set of parameters.

In this paper, we report the effect of pH on metal-humic complexation from a true competitive reaction point of view. The inclusion of the pH dependence into the previously described Gaussian distribution model allowed us to predict the average binding constant (μ_M) of the fluorescent probe metal ion and the standard deviation of this average $\log K_{M_i}$ value (σ) which is representative of the width of the ligand distribution. These predicted values of μ_M and σ are more representative of true thermodynamic constants, regardless of pH. This model is more realistic continuous-multiligand model that better describes metal-humic interactions. It should also be emphasized that the method is an equilibrium method and not a kinetic method for determining trace-metal binding constants.

EXPERIMENTAL SECTION

Instrumentation. The instrumentation, optical configuration, and the preparation of the Suwannee River fulvic acid (10) samples have been described elsewhere (5). In these metal-humic titrations, the europium concentrations typically ranged from 1×10^{-2} to 1×10^{-6} M and the fulvic acid concentrations were held constant at 10 ppm. The relative concentrations of the titrant and the fulvic acid assured a wide range of coverage of the metal binding sites with Eu^{3+} ions.

THEORY

The theory and principles regarding the implementation of the lanthanide ion probe have been discussed previously (5); therefore, only a brief review will be given. As was previously mentioned, the fluorescence spectrum of the probe metal ion is sensitive to ligation of the metal ion with humic substances. The sensitive nature of these spectra is due to the existence of a hypersensitive transition that is common to lanthanide ions. Hypersensitive transitions are emissive transitions of the lanthanide ion that are sensitive to ligation.

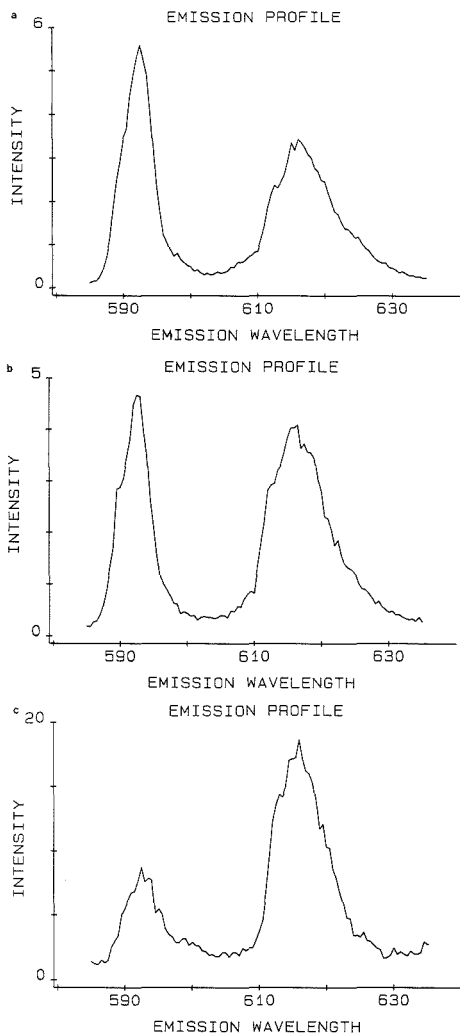


Figure 1. (a) Emission spectrum of 5×10^{-2} M Eu^{3+} and 100 ppm Suwannee River fulvic acid. The excitation wavelength was 394.3 nm and the pH of the solution was 3.5. (b) Emission spectrum of 2.5×10^{-3} M Eu^{3+} and 100 ppm Suwannee River fulvic acid. The excitation wavelength was 394.3 nm and the pH of the solution was 3.5. (c) Emission spectrum of 5×10^{-5} M Eu^{3+} and 100 ppm Suwannee River fulvic acid. The excitation wavelength was 394.3 nm and the pH of the solution was 3.5.

The hypersensitive transition of the Eu^{3+} ion occurs at 616 nm (11). The effect of the hypersensitive transition is illustrated in Figure 1. Three different emission profiles of the Eu^{3+} are shown. For each, the concentration of metal ion was varied, but the humic concentration remained constant. At very large values of C_M/C_L (where C_M is the total concentration of metal and C_L is the total concentration of ligand), the majority of the metal is free (aquo) ion and the corresponding fluorescence spectrum is representative of the free metal ion. For the case of the free metal ion, the intensity of the hypersensitive transition is not enhanced. If μ_M is large enough, at very small values of C_M/C_L , the majority of the

metal M is bound and the intensity of the hypersensitive transition in the corresponding spectrum is enhanced relative to the nonhypersensitive band. This effect is a continuous function of the metal ligation and is assumed constant for all acidic sites of the humic substance. Theories and mechanisms of the hypersensitive transitions have been discussed by Mason et al. (12).

The ratio of the integrated peak intensity of these bands is

$$R = I_{592}/I_{616} \quad (1)$$

Plotting R as a function of logarithm of the total metal, $\log C_M$, yields a sigmoidal shaped curve. This plot, can be viewed as a spectral titration curve. We have shown in our previous report (5) that the intensity ratio R was mathematically related to the concentrations of the bound and free metal species.

This mathematical relationship was derived previously and $[M]$, the concentration of the free metal ion, is given as

$$[M] = \frac{C_M^*(X_b - R^*X_b/X_s)}{R^*(1 - X_b/X_s)} \quad (2)$$

where X , is the observed value of R in the absence of any humic material and X_s is the observed value of R at the minimum limiting condition where all Eu^{3+} ions are bound to the humic sites. The values of X_b and X_s were experimentally measured. Because the expression for $[M]$ is related to $\Sigma[\text{ML}_i]$ through the mass balance equation of C_M , the total bound metal can be expressed as

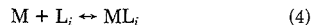
$$\Sigma[\text{ML}_i] = C_M - [M] \quad (3)$$

This mathematical analysis of the experimental data provided the means to determine quantitatively the concentrations of the bound and free metal species at any point during the titration process.

CONTINUOUS MULTILIGAND pH DEPENDENT MODEL

To facilitate the incorporation of the effects of ionization of the humic substance into the previous single-species, pH-independent model, it was assumed that two distinct distributions for the competitive species, protons and metal ions, exist for a single population of humic ligands. Both distributions are Gaussian in nature and differ only by a constant displacement of the $\log K_i$ values. The widths of these distributions (σ) remained constant for both species. This assumption implies that the ratio of K_{Mi}/K_{Hi} is constant, where K_{Hi} is the proton binding constant at sites of type i and K_{Mi} is the binding constant for the metal at sites of type i .

With this assumption in mind, the objective of the following derivation was to develop an expression for $[\text{ML}_i]$ in terms of all previously known variables, including $[\text{H}]$ and K_{Hi} . In our previous application of the Gaussian distribution model, the complexation reaction for single metal-humic interaction, where a 1:1 stoichiometric concentration of metal (M) and ligand (L) was assumed, was written as



The formation constant K_{Mi} was written as

$$K_{Mi} = \frac{[\text{ML}_i]}{[M][L_i]} \quad (5)$$

In its final form, the generalized chemical equilibrium equation, that was representative of the single-species, pH-independent model was expressed as

$$[\text{ML}_i] = \frac{K_{Mi}^*[M]^*C_i}{1 + K_{Mi}^*[M]} \quad (6)$$

where C_i is the concentration of the binding site of type i .

Similar to eq 4, the protonation reaction for sites of the type i can be written as



The formation constant $K_{\text{H}i}$ is

$$K_{\text{H}i} = \frac{[\text{HL}_i]}{[\text{H}][\text{L}_i]} \quad (8)$$

where $[\text{HL}_i]$ is the concentration of the protonated sites of type i and $[\text{H}]$ is the concentration of the proton. The ratio of the two formation constants ($K_{\text{M}i}$ and $K_{\text{H}i}$) can be expressed as

$$\frac{K_{\text{M}i}}{K_{\text{H}i}} = \frac{[\text{ML}_i][\text{H}]}{[\text{M}][\text{HL}_i]} \quad (9)$$

The protonated ligand, $[\text{HL}_i]$, is difficult to measure; therefore, it should be expressed in other terms. From the mass balance equation of the binding sites of type i , $[\text{HL}_i]$ can be written as

$$[\text{HL}_i] = C_i - [\text{ML}_i] - [\text{L}_i] \quad (10)$$

and from eq 5 $[\text{L}_i]$ can be expressed as

$$[\text{L}_i] = \frac{[\text{ML}_i]}{K_{\text{M}i}[\text{M}]} \quad (11)$$

Following the successive substitutions of the above expression of $[\text{L}_i]$ into eq 10 and the expression of $[\text{HL}_i]$ into eq 9, followed by simplification and final rearrangement, an expression for $[\text{ML}_i]$ is written as

$$[\text{ML}_i] = \frac{K_{\text{M}i}[\text{M}]C_i}{1 + K_{\text{M}i}[\text{M}] + K_{\text{H}i}[\text{H}]} \quad (12)$$

The only difference between the final expression of $[\text{ML}_i]$ shown above and the expression for $[\text{ML}_i]$ for the single metal-pH independent model (eq 6) is the additional term ($K_{\text{H}i}[\text{H}]$), found in the denominator. The inclusion of this term accounts for the inherent competition of the protons and the probe metal ions. This generalized expression can be made more specific as needed. In the continuation of our metal-humic complexation studies, we have applied this general competitive species (protons and metal ions) chemical equilibrium model to the Gaussian distribution complexation model.

The Gaussian distribution model yields the following expression for the ligand distribution (8, 9):

$$C_i = \frac{C_L}{\sigma(2\pi)^{1/2}} \exp \left[-\frac{1}{2} \left[\frac{\mu - \log K_i}{\sigma} \right]^2 \right] d \log K \quad (13)$$

where C_i is the concentration of the ligand of type i , C_L is the total concentration of carboxylic ligands of the humic substance, μ is the mean $\log K_i$ value of the sites of type i , and σ is one standard deviation of the mean binding constant. Note that eq 13 is written in a general form, i.e. without using subscript M or H.

This expression for C_i was substituted into eq 12. Solutions to this equation yield the concentrations of the bound metal at a single binding site i ($[\text{ML}_i]$). The objective in this modeling exercise is to compare the calculated values of the bound metal concentrations with the experimental values of the total bound metal concentrations obtained from the analysis of europium emission spectra. In order to facilitate the comparison of the calculated values, $[\text{ML}_i]$, and the observed values, $\sum[\text{ML}_i]$, these two expressions must parallel each other. Therefore, it is necessary to sum eq 12 over all i values to obtain an expression for the total bound metal, $\sum[\text{ML}_i]$. This summation is expressed as the following integral:

$$\sum_i [\text{ML}_i] = \frac{C_L}{\sigma(2\pi)^{1/2}} \int_{-\infty}^{+\infty} \frac{K_{\text{M}i}[\text{M}]}{1 + K_{\text{M}i}[\text{M}] + K_{\text{H}i}[\text{H}]} \times \left[-\frac{1}{2} \left[\frac{\mu_{\text{M}} - \log K_{\text{M}i}}{\sigma} \right]^2 \right] d \log K_{\text{M}} \quad (14)$$

The solutions to this integral provided expressions for the total bound metal according to the pH-dependent Gaussian model. It is similar to the final expression derived for the pH-independent model, where the modeling parameters μ_{M} and σ are characteristics of the humic materials and represent the mean binding constant of Eu^{3+} and the breadth of the distribution of the binding sites, respectively. The additional $K_{\text{H}i}[\text{H}]$ term in the denominator, however, denotes the humic acid ionization and the competition of protons and metal ions for the available binding sites. Initial guesses for the modeling parameters μ_{M} and σ are provided. The integral limits are set to $\pm 4\sigma$, and this expression is numerically evaluated. For each individual calculated $K_{\text{M}i}$ value, the corresponding $K_{\text{H}i}$ value is known through the initial assumption that $K_{\text{M}i}/K_{\text{H}i}$ remains constant over all i values. The value of this constant was taken to be the ratio of $10^{\mu_{\text{M}}}/10^{\mu_{\text{H}}}$ where μ_{M} was taken to be the mean binding constant of europium ion and μ_{H} was the mean binding constant for proton. The value of μ_{H} was taken to be 4.0. The value of $[\text{H}]$ was estimated from the measured pH. The modeling parameters μ_{M} and σ were fitted by means of the previously described least-squares fitting routine (5).

Prior to the discussion of the experimental results in this study, we have chosen to illustrate the effects of competitive binding of the hydrogen ion and the probe metal ion according to this pH-dependent model with aid of a computer-simulated speciation study. The relative distributions of the various ligand species are shown in Figure 2 as a function of pH. The outer curve in each figure is representative of the entire C_i ligand distribution; therefore, by definition, the three individual ligand species (protonated ligands, metalated ligands, and free ligands) are subspecies of this distribution. The distributions of these various species have been plotted as concentration of C_i vs site number. The relative distributions of the individual ligand species are of course dependent on the values of C_L , C_{M} , pH, μ_{M} , and μ_{H} . In each figure, all values were held constant with the exception of pH. The result of varying the pH illustrates the competitive binding nature of the hydrogen ion. In figure 2, the total metal concentration is held constant at 1×10^{-4} M. The different proton concentrations 1×10^{-2} , 1×10^{-3} , 1×10^{-4} , and 1×10^{-6} M result in a significantly altered distribution of the various ligand species. The protonated ligand species dominate the distribution at a pH of 2.0. The protons are preferentially bound to the stronger sites, indicated by the skewed Gaussian curve. The metalated ligand species are also present but at smaller concentrations. Even though free binding sites are still available, the metal ions are also preferentially bound to the same stronger ligand sites. The remaining free ligand sites, represented by the L_i distribution curve, are recognized as weaker binding sites of the C_i distribution, i.e. located at the left-hand side in the C_i distribution. As the proton concentration is decreased (pH is increased from 2.0 to 3.0), the concentration of the protonated ligand species decreases and the concentration of the metalated ligand species increases. The metalated ligand species dominate the distribution at pH 5.0. These distribution curves illustrate that protons and metal ions are truly competitive species that compete for the same set of binding sites.

RESULTS AND DISCUSSION

The conclusions drawn from the previous simulation study via the ligand distribution curves indicated that as the concentration of hydrogen ion was increased, a smaller percentage

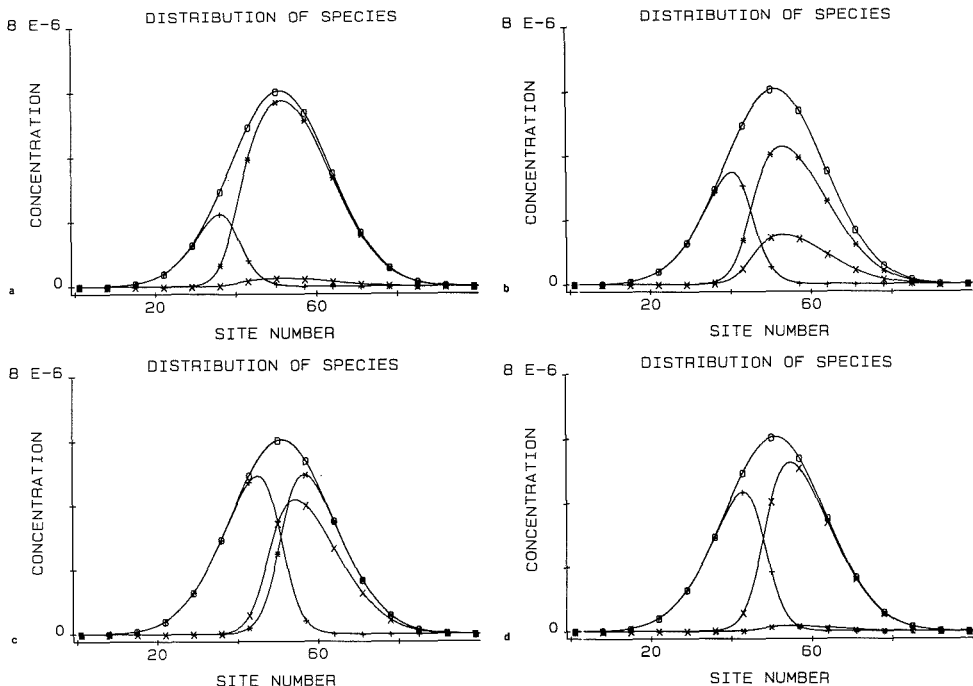


Figure 2. Distribution curves of various ligand species to illustrate the competitive binding nature of the proton and the metal ion. The pH was varied from 2.0 to 5.0 and the concentration of Eu^{3+} ion was held constant at 1×10^{-4} M: (a) pH = 2.0, (b) pH = 3.0, (c) pH = 4.0, (d) pH = 5.0; (O) total ligand distribution, (*) protonated ligand distribution, (X) Eu^{3+} metalated ligand species, (+) free ligand species.

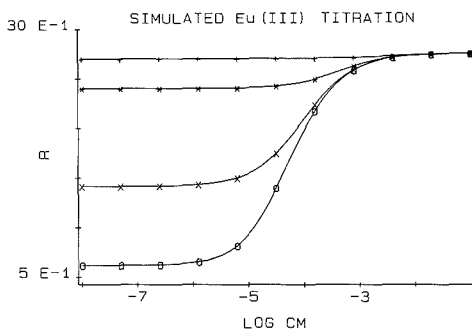


Figure 3. Computer-simulated fulvic acid and Eu^{3+} titration curves at various pH values: (O) pH = 5.0, (X) pH = 4.0, (*) pH = 3.0, (+) pH = 2.0.

of the total metal was bound. In parallel with this simulation study, displacement of the probe metal ion should be readily observable in a Eu^{3+} -humic titration experiment. We were able to predict the results of the titration curves, R versus $\log C_M$, via another simulation study according to the pH-dependent model. The results of this pH simulation study are illustrated in the Figure 3. As the pH is decreased from 5.0 to 2.0, a larger percentage of the Eu^{3+} is displaced due to the larger concentration of the competing hydrogen ion. Therefore, for a given C_M value, the intensity ratio values R (I_{592}/I_{616}) increase, indicating that less of the total Eu^{3+} ion is bound.

The Eu^{3+} metal titrations of the Suwannee River fulvic acids were performed at pH 2.5, 3.0, and 3.5. The experimentally

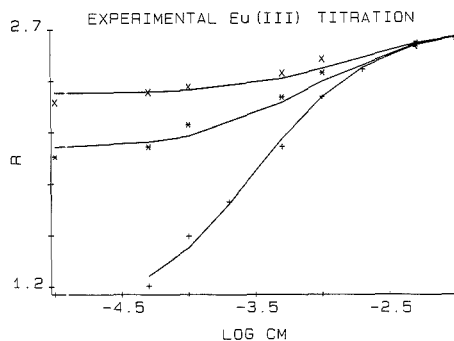


Figure 4. Experimental and calculated Eu^{3+} and Suwannee River fulvic acid titration curves, R vs $\log C_M$, as predicted by the pH-dependent continuous multiligand model: (X) pH = 2.5, (*) pH = 3.0, and (+) pH = 3.5; 10 ppm FA.

observed and calculated titration curves, R versus $\log C_M$, are shown in Figure 4. The calculated curves were fitted to the experimental results with a best fitted μ_M value of 4.4 and a σ value of 2.17. The measure of the binding constant of the most probable site in the ligand distribution (μ_M) and the width of the distribution (σ) were constant for each titration.

The pH-dependent model predicted larger values for both fitting parameters, μ_M and σ , than the previous pH-independent model (5), 4.5 vs 3.5 and 2.17 vs 1.1, respectively. The interaction between the protons and the binding sites changes both the effective complex formation strengths of the binding sites and the effective width of the binding sites distribution.

The higher the proton concentration, the weaker the effective complex formation strengths, and the narrower the effective width of the Gaussian distribution representing the humic materials. This can be explained as follows: at low pH, before titration even begins, a significant portion of the binding sites are already occupied by the protons. The Eu^{3+} ions need to compete with the protons in order to form each and every ML_i complex molecule. Relative to the case where the existence of protons can be neglected, it is obvious that in order to occupy all of the binding sites, more metal ions are needed. This implies that if the existence of protons is neglected, while in reality they exist independent of the model being used, then the metal ions Eu^{3+} appear to be more weakly bound or μ_M appears to have a smaller value than it should be. Similar rationalization can be used to explain why the presence of competing protons makes the distribution of the binding sites appear narrower. During the titration some of the binding sites, preferentially the stronger sites, are occupied by the protons and are less available to Eu^{3+} and therefore make the effective width of the binding site distribution appear to be narrower.

Consequently, when this mathematical model was applied to the experimental results of identical humic substance materials, the predicted values for both modeling parameters, μ_M and σ , were greater than previous predictions obtained from the pH-independent model (5). The predicted values of the modeling parameters obtained from the pH-dependent model were constant, whereas the modeling parameters predicted by the pH-independent model were conditional and related directly to pH.

Because the initial pH-independent model predictive lower values for μ_M and σ , we proposed a simple test which verified that the results obtained from that study were correctly biased in the direction of lower μ_M and σ values. This test consisted of creating a set of computer-generated R values (where $R = I_{592}/I_{616}$), via a computer program based on the pH-dependent, Gaussian distribution model discussed in this paper. These data were generated at constant pH and at predetermined values of the curve fitting parameters μ_M , σ , and C_L . These plotted data represented the titration curve of a noiseless data set. The absence of any noise in the data of course allowed the fitting programs to fit the modeling parameters μ_M and σ exactly. The initial value of μ_M and σ that were used to generate the data were 4.5 and 2.17. These values were used since they corresponded to the best fitted results of the actual experimental data. This set of computer-generated data was then submitted to the original pH-independent model and the modeling parameters, μ_M and σ , were fitted. The result of fitting the same data to the pH-independent modeling program lowered these values of μ_M and σ to 3.5 and 0.55. After several attempts, the pH-independent modeling technique consistently lowered both parameters. Both experimental and simulated data resulted in lower values for μ_M and σ when subjected to the initial pH-independent modeling routine.

A number of models have been used to model the proton or metal titration characteristics of humic substances. Cabaniss and Shuman (13) measured and modeled cupric ion binding in Suwannee fulvic acids as a function of pH and other chemical parameters. A discrete multisite model (3, 14) of binding sites was used. The presence of five types of binding sites was used to fit the experimental data. Five pairs of C_i and K_{M_i} values were produced. The C_i values were not constant among titrations at the same C_L but different pH. Consequently, data from different pH values could not be fit with one set of parameters, indicating that the parameters were conditional and not thermodynamic constants. While the Gaussian model assumes an infinite number of types of sites, these sites are described by only three parameters: the

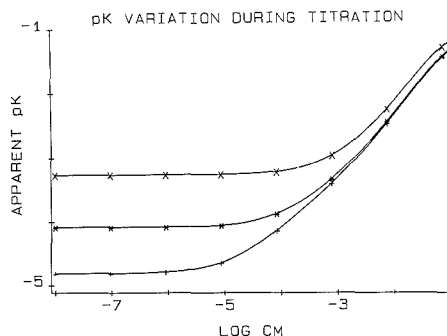


Figure 5. Variation of apparent pK during titration at different pH values: (X) pH = 2.5, (*) pH = 3.5, and (+) pH = 4.5.

center of the distribution, μ_X (where X denotes proton or any metal ions that bound to the humic sites), the width of the distribution, σ , and the total binding capacity for all sites C_L .

Other workers, Marinsky et al. (15-17), modeled Cu^{2+} and Eu^{3+} binding by fulvic acids using an electrostatic polymer model. The model is based on the assumption that the chemistry of humic substances is similar to that of polymers and attempts to include Donnan potential effects on proton binding equilibria. Protonation behavior of fulvic acids was found to be always directly related to its polyelectrolyte nature and its functional group heterogeneity. A large change in apparent pK_H of the humic substances was observed with degree of neutralization (α) during titration with base, indicating that the various acidic sites that comprise the humic substances were sufficiently different in acid strength. This observation was also confirmed by our experiments. Figure 5 illustrates the change of apparent pK_M with $\log C_M$ at different pH. We used the following definition of apparent pK_M :

$$K_M^{\text{app}} = \frac{\sum [\text{ML}_i]}{[\text{M}][\sum [\text{L}_i]]} \quad (15)$$

Marinsky et al. used the displacement of plots of apparent pK_H versus α as a function of ionic strength for electrostatic correction. The capability to estimate the nonideality contributions to the apparent pK_H has permitted the assignment of four pairs of abundance and intrinsic pK_H values related to four types of binding sites. These intrinsic pK_H values were constant, in the absence of metal ions, for different ionic strength.

CONCLUSIONS

The pH-dependent model represents a more chemically realistic model than the previous pH-independent model. This model should more accurately predict metal-humic complexation reactions that occur in the environment. It should be pointed out that the binding of Eu^{3+} itself to humic substances is not of primary interest. The Eu^{3+} ion is used only as a sensitive probe for measuring the binding of other cations to the humic substances. The single most important conclusion drawn from this study was that this model could be used to predict the thermodynamic binding constant of a single metal species in the complexed humic substance and not conditional binding constants that are usually predicted.

In theory, this model should hold for all pH conditions. At higher pH, however, the formation of metal hydroxides will interfere with the ability to differentiate between bound metal-humic complexes and metal-hydroxide complexes. At very low pH conditions very little metal is bound and it becomes extremely difficult to make accurate ratio measure-

ments over the range of metal concentrations. A compromise of intermediate pH conditions must be made.

LITERATURE CITED

- (1) Fish, W.; Dzombak, D. A.; Morel, F. M. M. *Environ. Sci. Technol.* **1986**, *20*, 676-683.
- (2) Sposito, G. *CRC Crit. Rev. Environ. Control* **1986**, *16*, 193-229.
- (3) Turner, D. R.; Varney, M. S.; Whittfield, M.; Mantoura, R. F. C.; Riley, J. P. *Geochim. Cosmochim. Acta* **1986**, *50*, 289-297.
- (4) Cabaniss, S. E.; Shuman, M. S.; Collins, B. J. *Complexation of Trace Metals in Natural Waters*; Kramer, C. J. M., Duinker, J. C., Ed.; Junk Publishers: The Hague, 1984; pp 239-273.
- (5) Dobbs, J. C.; Susetyo, W.; Knight, F. E.; Castles, M. A.; Carreira, L. A.; Azarraga, L. V. *Anal. Chem.* **1989**, *61*, 483-488.
- (6) Posner, A. M. *8th Int. Congress Soil Sci.* **1964**, 161.
- (7) Posner, A. M. *J. Soil Sci.* **1966**, *17*, 65-78.
- (8) Perdue, E. M.; Lytle, C. R. *Environ. Sci. Technol.*, **1983**, *17*, 654.
- (9) Perdue, E. M.; Reuter, J. H.; Parrish, R. S. *Geochim. Cosmochim. Acta* **1984**, *48*, 1257-1263.
- (10) Leenreer, J. A.; Wilson, M. A.; Malcolm, R. L. *Org. Geochem.* **1987**, *11*(No. 4), 273-280.
- (11) Horrocks, W. DeW.; Ailbin, M. *Progress in Inorganic Chemistry*; Wiley: New York, 1984; Vol. 31.
- (12) Mascn, S. F.; Peacock, R. D.; Stewart, B. *Chem. Phys. Lett.* **1974**, *29*, 149.
- (13) Cabaniss, S. E.; Shuman, M. S. *Geochim. Cosmochim. Acta* **1987**, *52*, 185-193.
- (14) Dzombak, D. A.; Fish, W.; Morel, F. M. M. *Environ. Sci. Technol.* **1986**, *20*, 669-675.
- (15) Marinsky, J. A.; Ephraim, J. *Environ. Sci. Technol.* **1986**, *20*, 349-353.
- (16) Ephraim, J.; Alegret, S.; Mathuthu, A.; Bicking, M.; Malcolm, R. L.; Marinsky, J. A. *Environ. Sci. Technol.* **1986**, *20*, 354-366.
- (17) Ephraim, J.; Marinsky, J. A. *Environ. Sci. Technol.* **1986**, *20*, 367-376.

RECEIVED for review February 2, 1989. Accepted April 17, 1989.

Limitations of All Empirical Single-Parameter Solvent Strength Scales in Reversed-Phase Liquid Chromatography

Won Jo Cheong and Peter W. Carr*

Department of Chemistry, Smith and Koltzoff Halls, University of Minnesota, 207 Pleasant Street, Minneapolis, Minnesota 55455

The relationships between the solute capacity factor and Reichardt's E_T or the Kamlet-Taft π^* scale in hydroorganic mixtures have been studied for a series of alkylbenzenes. It has been shown that, for such simple nonpolar solutes, linearity in plots of $\ln k'$ against a single solvent polarity parameter is observed only over a limited range in composition. At least two solvent parameters are needed in order to account for the cavity formation and solute-solvent interaction processes that control retention in reversed-phase liquid chromatography.

The "polarity" of the mobile phase is a major factor that influences solute retention in reversed-phase liquid chromatography (RPLC). Except in rare instances, retention in this mode of liquid chromatography increases as the "polarity" of the mobile phase is increased by the addition of water. Many empirical scales of overall solvent strength have been proposed, including the so-called Y (1-3), X (4), Ω (5), Z (6, 7), R and S (8), and E_T values (9, 10). Typically, such solvent polarity scales are based on either the effect of solvent on the rate of a chemical reaction or its influence on some spectroscopic property of an indicator. All of the above have been proposed as single-parameter overall scales of solvent strength. In contrast, the Kamlet-Taft multiparameter solvent scales (11-13) are based on the differential evaluation of solvent dipolarity/polarizability (π^*), solvent hydrogen bond donating acidity (α), and solvent hydrogen bond accepting basicity (β).

Recently, both the E_T scale (14, 15) and a linear solvation energy relationship (LSER) based on the Kamlet-Taft multiparameter scales (16) were used to study retention in RPLC. As will be discussed, these two approaches are fundamentally quite different.

Dorsey (15) has conclusively shown that plots of $\ln k'$ vs the mobile phases' E_T solvatochromic parameter are very often

more linear than are plots of $\ln k'$ vs volume fraction of organic modifier (ϕ). These results were obtained with a large number of solutes, but did not encompass the entire range in solvent composition. In contrast, the solvatochromic LSER approach of Kamlet and Taft seeks to relate retention in fixed mobile phase-stationary phase systems to variations in solute properties. Although these two approaches are superficially unrelated, a detailed examination indicates that they are conceptually at odds with one another. For example, according to the Kamlet-Taft formalism, it is only possible for a global single-parameter solvent strength scale to exist when the solvent and solute are incapable of forming hydrogen bonds and, in addition, the energy of cavity formation either is negligible compared to the strength of the solute-solvent interactions or is strictly proportional to the strength of such interactions. In RPLC, cavity formation in the mobile phase is usually considered to be one of the most important factors, and consequently, if valid, the Kamlet-Taft formalism would preclude the existence of a single-parameter universal solvent strength scale in RPLC.

We will adopt the LSER formalism to make our point in detail because the essential input parameters such as solvatochromic measures of solvent strength are available. Other models of retention in liquid chromatography, particularly those based on the separation of cohesive energy density (for example, the multicomponent solubility parameter model of Karger ('6)), lead to the same qualitative conclusion.

In order to explore the difficulty outlined above, we briefly restate below the basis of the LSER formalism when applied to phase-transfer processes. A general solute property (SP), such as a logarithmic capacity factor, can be correlated via the use of three types of terms as shown below (17):

$$SP = SP_0 + \text{cavity term} + \text{dipolar term} + \text{hydrogen bond term(s)} \quad (1)$$

The cavity term is usually taken as the product of the solute molar volume and the square of the Hildebrand solubility

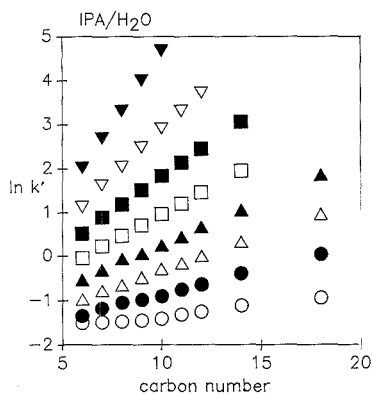


Figure 1. In k' vs solute carbon number for the 2-propanol (IPA)/water system: (O) $\phi = 1.0$, (●) $\phi = 0.9$, (Δ) $\phi = 0.8$, (\blacktriangle) $\phi = 0.7$, (\square) $\phi = 0.6$, (\blacksquare) $\phi = 0.5$, (∇) $\phi = 0.4$, (\blacktriangledown) $\phi = 0.3$.

parameter (δ_H) of the solvent. The dipolar term is the product of the solute, π^* , and the solvent, π^* . π^* is a measure of the dipolarity/polarizability of the species in question. The hydrogen bonding terms are written as a cross product of the solute α (an empirical measure of hydrogen bond donating acidity) and the solvent β (a similar scale of hydrogen bond acceptor basicity) and the product of the solute ξ and the solvent α . In the case of chromatographic retention, SP in the equation below denotes a logarithmic capacity factor and the subscript 2 designates a solute property. The subscripts s and m denote the stationary and mobile phases, respectively (19).

$$SP = SP_0 + m(\delta_s^2 - \delta_m^2)\bar{V}_2/100 + s(\pi_s^* - \pi_m^*)\tau^* + \alpha(\beta_s - \beta_m)\alpha_2 + b(\alpha_s - \alpha_m)\beta_2 \quad (2)$$

The coefficients m , s , a , and b are fitting parameters. They are independent of the solutes, and if the model were rigorously correct, they should be independent of the phases. Equation 2 constitutes the basis of the LSER formalism. It indicates that it is the differences in the properties of the two phases that influence retention. Equation 2 has not been tested in general, although specific subclasses have been tested. For example, the gas-liquid partition coefficients of a series of solutes have been correlated against solvent properties to demonstrate the validity of the solvent dependencies. Similarly, the solute dependencies for fixed phases have been validated.

When a system with a fixed pair of mobile and stationary phases is considered, eq 2 reduces to

$$SP = SP_0 + m\bar{V}_2/100 + s\pi^* + a\alpha_2 + b\beta_2 \quad (3)$$

This equation has been verified for RPLC to the extent that it successfully correlates the retention of a large number of solutes on a variety of bonded phase columns, at a variety of temperatures with several different mobile phase modifiers at a number of values of ϕ (17, 19, 20).

Inspection of eq 2 indicates that unless one assumes that all of the mobile phase parameters (δ_m , π_m^* , α_m , and β_m) vary collinearly as ϕ is varied, a single global solvent strength parameter for RPLC cannot, in general, exist. In order to see under what specific conditions, namely for what types of solutes, a single-parameter solvent scale might exist, we will attempt to simplify eq 2 by making some assumptions. It will become apparent that the assumptions that one has to make are quite severe. It is well-known that as the mobile phase composition is varied in RPLC, the stationary phase is

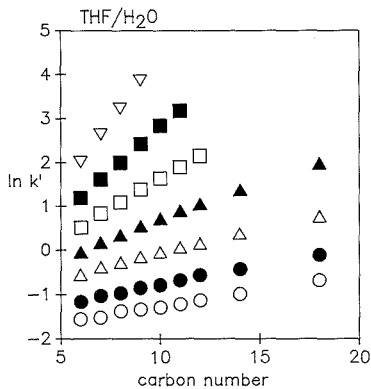


Figure 2. In k' vs solute carbon number for the tetrahydrofuran/water system: (O) $\phi = 0.9$, (●) $\phi = 0.8$, (Δ) $\phi = 0.7$, (\blacktriangle) $\phi = 0.6$, (\square) $\phi = 0.5$, (\blacksquare) $\phi = 0.4$, (∇) $\phi = 0.3$.

modified. This means that δ_s will vary with ϕ . In order to obtain a single-parameter scale of mobile phase strength, one must assume that the stationary phase is independent of ϕ . Examination of the Karger model (16) shows that a similar assumption must be made in that approach to reach the same point.

Under this condition, eq 2 produces the following relationship between the capacity factor and the properties of the mobile phase:

$$SP = SP_0 + m\delta_m^2 + s'\pi_m^* + a\beta_m + b'\alpha_m \quad (4)$$

Clearly, eq 4 indicates that solute retention will be a complex function of the mobile phase properties. As yet, there have not been any reported correlations based on eq 4.

It has been shown that retention in RPLC does not depend strongly on solute hydrogen bonding acidity; thus to simplify eq 4, we neglect the contribution of the β_m term (18). Under this condition, it reduces to

$$SP = SP_0 + m\delta_m^2 + s'\pi_m^* + b'\alpha_m \quad (5)$$

In any case, for non hydrogen bond donor solutes, that is, when alcohols, phenols, carboxylic acids, etc., are excluded from consideration, it is certainly valid to discount the dependence on solvent basicity. This is the case in this work since we have restricted our attention to the alkylbenzenes.

Equation 5 could be reduced to a two-parameter dependence on the mobile phase by further assuming that the solutes are not hydrogen bond bases. This assumption would be true for saturated alkanes, but the alkylbenzenes are definitely slightly basic (for example, β (benzene) = 0.13 compared to β (nitrobenzene) = 0.30). Based on the above, it appears that at least two solvent-dependent factors would be needed to correlate retention in RPLC for non hydrogen bond donor weak acceptors such as the alkylbenzenes, while three mobile phase parameters would be needed for polar compounds, since such compounds invariably have significant basicities. This issue will be discussed more extensively below.

The major alternative to the use of empirical scales of solvent strength for correlating retention in RPLC is the use of the mobile phase composition, that is, the volume fraction of organic modifier in the mobile phase (ϕ), per se. Snyder and co-workers noted a linear relationship between $\ln k'$ and ϕ (21), whereas Schoenmakers (22), on the basis of solubility parameter theory, and Martire (23) and Dill (24), using lattice models, advocate quadratic dependencies on ϕ . This work will focus on the relative merits of the empirical scales.

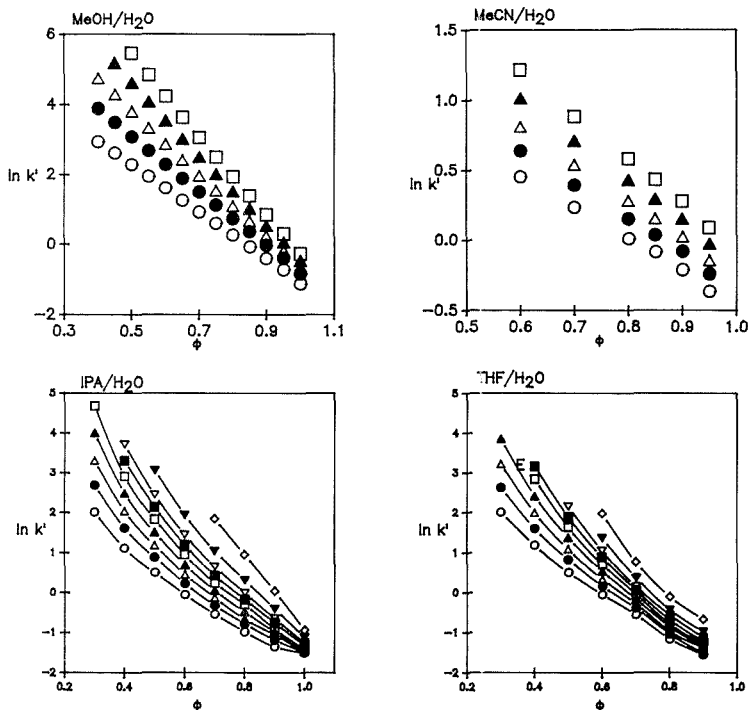


Figure 3. $\ln k'$ vs volume fraction of organic modifier for the methanol/water system (Marire's data (24)), acetonitrile/water system, 2-propanol/water system, and tetrahydrofuran/water system: (O) benzene, (●) toluene, (Δ) ethylbenzene, (\blacktriangle) propylbenzene, (\square) butylbenzene, (\blacksquare) pentylbenzene, (∇) hexylbenzene, (\blacktriangledown) octylbenzene, (\diamond) dodecylbenzene.

EXPERIMENTAL SECTION

Retention data for the methanol/water system (22, 25) and the acetonitrile/water system (26) were taken from the literature. The data for the 2-propanol/water and tetrahydrofuran/water systems were measured in this laboratory. A Hypersil ODS column (100×4.6 mm, $5 \mu\text{m}$, Hewlett-Packard, Avondale, PA) was used throughout this study. The column was placed in a water jacket, and the temperature was controlled at 25 ± 0.2 °C. An Altex pump with a pulse dampener (Model 110AQ, Altex Scientific, Inc., Berkeley, CA) was used to deliver the mobile phase. Samples were injected via a homemade autoinjector using a Valco air-actuated injector (Model AC6W, Valco Instruments Co., Inc., Houston, TX) equipped with a $10\text{-}\mu\text{L}$ loop. A Hitachi variable wavelength UV-vis detector (Model 100-10, NSI/Hitachi Scientific Instruments, Mountain View, CA) set to a wavelength of 265 nm was used to generate the solute elution profiles. All retention times were based on the peak maximum position. The eluent flow rate was varied from 0.2 to 1.0 mL/min depending on the mobile phase composition. Water was used as the void volume marker (27, 28), and the void volume was determined at each mobile phase composition throughout the course of the series of measurements. We also used uracil as the dead volume marker; although the dead volumes were systematically different, the trends in the resultant k' values were so similar that our conclusions were not altered.

RESULTS AND DISCUSSION

The retention data for benzene through hexylbenzene, octylbenzene, and dodecylbenzene for the 2-propanol/water and tetrahydrofuran/water systems were plotted with respect to solute carbon number (see Figures 1 and 2). As expected, good linear relationships were obtained. These plots are presented only to validate the measurements. The accuracy

of the high k' data is better than the low k' data since the retention data at low water content are subject to high errors due to the very low retention and difficulties in defining the column void volume.

Among the many solvent polarity scales, E_T values (29) and π^* values (as well as approximate α values) (30) have been reported for mixtures of water and a number of organic solvents. Only these data will be discussed below.

It is important to understand the interrelationship between E_T , the Kamlet-Taft scales, and the solubility parameter. Kamlet has shown that there is a linear relationship between E_T and the π^* and α scales for a large number of pure polar (both aprotic and protic) and nonpolar solvents (12).

$$E_T = 31.00 + 13.43\pi^* + 15.06\alpha$$

$$n = 40, r = 0.984, \text{std dev} = 1.65 \quad (6)$$

An approximate linear relationship between π^* and the solubility parameter has also been reported (31) for the select solvents (nonaromatic, nonhalogenated, aprotic species), but it is certainly not nearly so general, or as accurate, as that between E_T , π^* , and α . We report here a slightly modified correlation.

$$\delta_H^2 = 44.1 + 95.6\pi^*$$

$$n = 17, r = 0.858, \text{std dev} = 19.7 \quad (7)$$

As we will show below, if these relationships also hold for aqueous mixtures, then eq 5 can be reduced to a single-parameter correlation. Only if all of the above conditions are true will Dorsey's assertion that the E_T scale (or any other

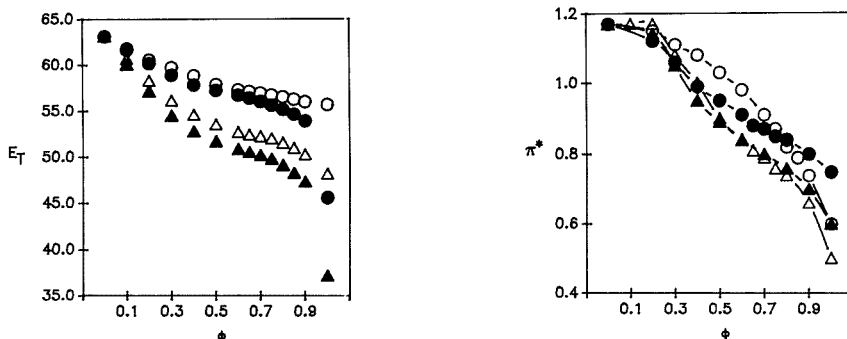


Figure 4. Comparison of E_T and π^* with respect to volume fraction of organic modifier: (O) methanol/water system, (●) acetonitrile/water system, (Δ) 2-propanol/water system, (\blacktriangle) tetrahydrofuran/water system.

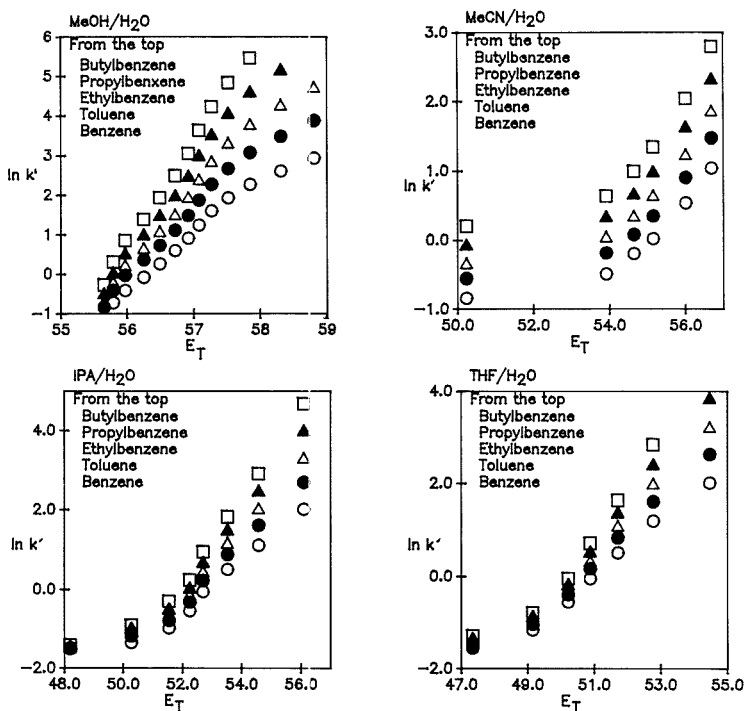


Figure 5. $\ln k'$ vs E_T for the methanol/water system (Martire's data), acetonitrile/water system, 2-propanol/water system, and tetrahydrofuran/water system: (O) benzene, (●) toluene, (Δ) ethylbenzene, (\blacktriangle) propylbenzene, (\square) butylbenzene.

single parameter) is an accurate descriptor of strength in RPLC be in agreement with the LSER methodology.

As mentioned above, the hydrogen bonding terms can be neglected when one is considering the retention of nonpolar solutes; consequently eq 5 reduces to

$$SP = SP_0 + m\delta_m^2 + s'\pi_m^* \quad (8)$$

Clearly, over a sufficiently narrow range in arguments, any two monotonic functions will appear to be collinear. Thus over a narrow range in solvent composition, it is likely that E_T will be linearly correlated with δ_m^2 . Under this condition,

eq 8 reduces to

$$SP = SP_0 + eE_T \quad (9)$$

For the same reason, it can be assumed that for some data sets π^* will be linearly correlated with δ_m^2 , and eq 8 can be reduced to

$$SP = SP_0 + s'\pi_m^* \quad (10)$$

In order to examine the validity of eq 9 and 10, $\ln k'$ (SP), π^* , and E_T were plotted against ϕ (see Figures 3 and 4). Plots of E_T vs ϕ and π^* vs ϕ are shown in Figure 4. We see that

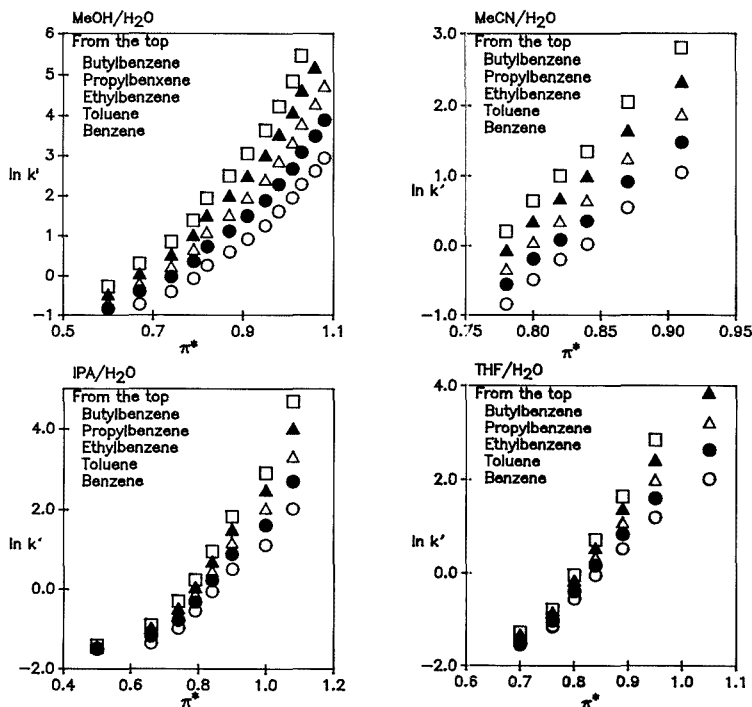


Figure 6. In k' vs π^* for the methanol/water system (Marire's data), acetonitrile/water system, 2-propanol/water system, and tetrahydrofuran/water system: (O) benzene, (●) toluene, (Δ) ethylbenzene, (\blacktriangle) propylbenzene, (\square) butylbenzene.

the variations in $\ln k'$, E_T , and π^* with respect to the volume fraction of the organic modifier are very different. Plots of $\ln k'$ vs E_T , and of $\ln k'$ vs π^* , are shown in Figures 5 and 6, respectively. A linear relationship between $\ln k'$ and E_T is observed only in a limited range of solvent composition. Not surprisingly, the same is true of the correlation of $\ln k'$ against π^* . It is clear that neither E_T nor π^* is generally linearly correlated with $\ln k'$, and one is not necessarily better than the other. Indeed, the superiority of one type of single-parameter scale is not the issue we are raising.

Indeed, we believe that the general failure of linear correlations of $\ln k'$ with E_T and π^* is due to the extremely crude series of approximations that must be made to obtain either eq 9 or 10 from eq 2. Any other single-parameter solvent polarity scale will give the same result. When the plots of $\ln k'$ vs E_T or π^* (Figures 5 and 6) are compared with Figure 3, $\ln k'$ is sometimes more linear with ϕ than with either E_T or π^* . We observe a linear relationship for the methanol/water system (ϕ : 0.4–1.0) and the acetonitrile/water system (ϕ : 0.6–0.95), but very considerable curvature is evident at high water content for the 2-propanol/water (ϕ : 0.3–1.0) and tetrahydrofuran/water (ϕ : 0.3–0.9) systems. Note that this curvature is not an artifact due to an error in the void volume since the retention is quite high when the water content is high.

As shown in Figures 5 and 6, the amount of curvature in the correlations depends systematically on the solute. Such systematic failure is clearly unacceptable in view of the chemical simplicity of the test solutes. We believe that this observation, along with the severity of the assumptions needed to reduce eq 2 to a single-parameter model, obviates the generality of any single-parameter solvent strength scale in

RPLC, be it the E_T or π^* scale.

Finally, in view of the complexity of the retention process in bonded phase RPLC, we will consider the effect of solvent composition on a solute property that is solely dependent on the mobile phase, namely, the infinite dilution activity coefficient (γ^∞) (32). Plots of γ^∞ for two alkylbenzenes vs E_T are shown in Figure 7. If E_T were a universal measure of the strength of the mobile phase and its interactions with the solute, a single curve would result. That is, plots of $\ln \gamma^\infty$ vs E_T should all fall on a common curve for all mobile phase modifiers. These solvents are clearly systematically different for both toluene and *n*-butylbenzene as test solutes. It does appear that over a limited range in composition methanol and acetonitrile form a similar pair, as do 2-propanol and tetrahydrofuran, but the two pairs are quite dissimilar. It should be noted that when plots are made vs π^* a similar tendency is observed.

As shown here, it is entirely possible that a single-parameter solvent scale may provide a set of plotting coordinates that linearizes the data for some solutes over some range in composition better than does a plot vs ϕ , and as such, it would be useful for data interpolation and other practical concerns, but one should avoid theoretical interpretation of the meaning of the regression coefficients.

Based on the Kamlet-Taft formalism, the systematic failure of any single-parameter scale to serve as a universal correlator of retention in RPLC lies in the complexity of the overall process. That is, the solution process has two distinct components that are globally unrelated, viz. cavity formation and solute-solvent interaction. Over a narrow range in composition, these processes may covary and a single parameter might be locally valid. Over a wide range in compositions,

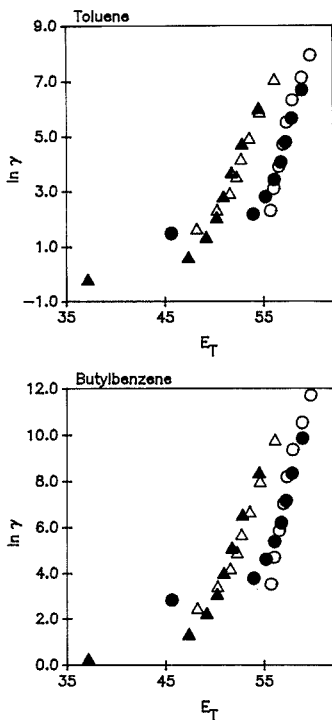


Figure 7. Logarithmic infinite dilution activity coefficient of toluene and *n*-butylbenzene vs E_T : (O) methanol/water system, (●) acetonitrile/water system, (Δ) 2-propanol/water system, (▲) tetrahydrofuran/water system.

the cavity term (solvent-solvent interaction) and the solute-solvent interaction cannot be collapsed into a single solvent parameter.

CONCLUSIONS

We have shown that the linear relationship between $\ln k'$ and E_T or π^* in RPLC is, in general, only valid for a limited range in solvent composition. It is not universally true that E_T or any other single-parameter scale, such as π^* , is necessarily a better correlator of retention for all solutes than is the volume fraction of organic modifier in the mobile phase. We believe that it may be possible to develop a universal

solvent strength function if it were possible to predict both the cavity formation energy and the solute-solvent interaction energy.

ACKNOWLEDGMENT

We acknowledge fruitful discussions with Prof. Sarah C. Rutan during the course of this work.

LITERATURE CITED

- (1) Grundwald, E.; Winstein, S. *J. Am. Chem. Soc.* **1948**, *70*, 846.
- (2) Winstein, S.; Grundwald, E.; Jones, H. W. *J. Am. Chem. Soc.* **1951**, *73*, 2700.
- (3) Finberg, A. H.; Winstein, S. *J. Am. Chem. Soc.* **1956**, *78*, 2770.
- (4) Gielen, M.; Nasielski, J. *J. Organomet. Chem.* **1964**, *1*, 173.
- (5) Benson, A.; Hamlet, Z.; Mueller, W. A. *J. Am. Chem. Soc.* **1962**, *84*, 297.
- (6) Kosower, E. M. *J. Am. Chem. Soc.* **1958**, *80*, 3253.
- (7) Kosower, E. M. *Molecular Biochemistry*; McGraw-Hill: London, 1962; p 180.
- (8) Brownstein, S. *Can. J. Chem.* **1960**, *38*, 1590.
- (9) Dimroth, K.; Reichardt, C.; Slepmann, T.; Bohlmann, F. *Liebigs Ann. Chem.* **1963**, *661*, 1.
- (10) Dimroth, K.; Reichardt, C.; Schweig, A. *Liebigs Ann. Chem.* **1963**, *669*, 95.
- (11) Kamlet, M. J.; Abboud, J. L. M.; Taft, R. W. *J. Am. Chem. Soc.* **1977**, *99*, 6027.
- (12) Kamlet, M. J.; Abboud, J. L. M.; Taft, R. W. *Prog. Phys. Org. Chem.* **1983**, *13*, 485.
- (13) Kamlet, M. J.; Abboud, J. L. M.; Abraham, M. H.; Taft, R. W. *J. Org. Chem.* **1983**, *48*, 2877.
- (14) Johnson, B. P.; Khaledi, M. G.; Dorsey, J. G. *J. Chromatogr.* **1987**, *384*, 221.
- (15) Johnson, B. P.; Khaledi, M. G.; Dorsey, J. G. *Anal. Chem.* **1986**, *58*, 2354.
- (16) Karger, B. L.; Snyder, L. R.; Eon, C. *Anal. Chem.* **1978**, *50*, 2126.
- (17) Kamlet, M. J.; Doherty, R. M.; Abboud, J. M.; Abraham, M. H.; Taft, R. W. *J. Pharm. Sci.* **1986**, *75*, 338.
- (18) Sadek, P. C.; Carr, P. W.; Doherty, R. M.; Kamlet, M. J.; Taft, R. M.; Abraham, M. H. *Anal. Chem.* **1985**, *57*, 2971.
- (19) Carr, P. W.; Doherty, R. M.; Kamlet, M. J.; Taft, R. W.; Melander, W.; Horvath, C. *Anal. Chem.* **1986**, *58*, 2674.
- (20) Park, J. H.; Carr, P. W.; Abraham, M. H.; Taft, R. W.; Doherty, R. M.; Kamlet, M. J. *Chromatographia* **1988**, *25*, 373.
- (21) Snyder, L. R.; Dolan, J. W.; Gant, J. R. *J. Chromatogr.* **1979**, *165*, 3.
- (22) Schoenmakers, P. J.; Bilet, H. A. H.; Galan, L. *J. Chromatogr.* **1983**, *282*, 107.
- (23) Martire, D. E. *J. Liq. Chromatogr.* **1987**, *10*, 1569.
- (24) Dill, K. A. *J. Phys. Chem.* **1987**, *91*, 1980.
- (25) Barman, B. N. Ph.D. Thesis, Georgetown University, Washington, DC, 1985.
- (26) Hanai, T.; Hubert, J. *J. Chromatogr.* **1984**, *290*, 197.
- (27) Djerki, R. A.; Laub, R. J. *J. Liq. Chromatogr.* **1987**, *10*, 1749.
- (28) Colin, H.; Ward, N.; Guichon, G. *J. Chromatogr.* **1978**, *149*, 169.
- (29) Krygowski, T. M.; Wirona, P. K.; Zielkowska, U.; Reichardt, C. *Tetrahedron* **1985**, *41*, 4519.
- (30) Cheong, W. J.; Carr, P. W. *Anal. Chem.* **1988**, *60*, 820.
- (31) Kamlet, M. J.; Carr, P. W.; Taft, R. W.; Abraham, M. H. *J. Am. Chem. Soc.* **1981**, *103*, 6062.
- (32) Cheong, W. J.; Carr, P. W., unpublished results.

RECEIVED for review September 13, 1988. Revised March 9, 1989. Accepted March 29, 1989. This work was supported by a grant from the National Science Foundation and by donors of the Petroleum Research Fund, administered by the American Chemical Society.

Supersonic Jet Spectrometry of Chemical Species Laser Ablated from Organic Polymers

Totaro Imasaka, Kouji Tashiro, and Nobuhiko Ishibashi*

Faculty of Engineering, Kyushu University, Hakozaki, Fukuoka 812, Japan

Laser ablation/supersonic jet spectrometry is applied to several organic polymers. For sample ablation, a first dye laser beam (337.5 nm) is focused onto the polymer surface. A second synchronized tunable dye laser excites ablated chemical species in a supersonic jet. A sharp spectral feature (7.3 cm^{-1}) is observed in the excitation spectrum for the polystyrene sample, which is assigned to originate from a styrene monomer. The signal is much weaker for acrylonitrile/butadiene/styrene copolymer (ABS resin), and no peak is observed for polycarbonate containing no styrene segments. The ablated chemical species is localized to 2.4 mm ($4 \mu\text{s}$) in the jet pulse. Sufficient rotational and translational coolings provide good selectivity and sensitivity, by spectral narrowing and sample focusing in the jet pulse.

Various methods have been developed for analysis of nonvolatile macromolecules such as organic polymers. Recently laser microprobe mass analysis (LAMMA or LA/MS) gained its importance because of its capability for microanalysis of the polymer surface (1, 2). Performance has further been improved by using a Fourier transform technique; it allows direct determination of the chemical formula for ejected ions, because of its ultrahigh mass resolution (3-5). However, this method still has some difficulties in the analysis of samples containing many chemical species with similar structures, such as isomers.

Laser ablation (desorption) supersonic jet (LA-SSJ) spectrometry has recently been developed for analysis of nonvolatile or thermally labile molecules. This method is applied to spectroscopic studies of metal clusters such as Cu_2 (6), Mo_2 (7), Al_3 (8), etc., inorganic molecules such as Ga_2As_3 (9), SiC_2 (10), etc., and organic molecules such as naphthalene (11). Furthermore, it is also used for determination of biological molecules such as amino acids, peptides, and tryptophan analogues (12-17). The observed line width is so narrow that even rotational isomers can be resolved. Some other molecules such as insulin have been measured by supersonic jet spectrometry, but no advantage of spectral selectivity has been demonstrated (18-27).

In this study we first apply laser ablation supersonic jet spectrometry to organic polymers. The present approach provides a great advantage for analysis of constituents in a polymer material, because of its good selectivity, given by a narrow line width due to rotational cooling, and high sensitivity, given by sample focusing in the jet pulse due to translational cooling. The process of monomer ablation from a polymer surface is also discussed in this study.

EXPERIMENTAL SECTION

Apparatus. A block diagram of the experimental apparatus is shown in Figure 1. A structure of the nozzle is essentially identical with the one reported (6) (whose structure is schematically illustrated in Figure 5). A rotating polymer rod sample

is located 6.5 mm away from an orifice of the pulsed nozzle (0.8 mm i.d.). After an argon gas is injected into a nozzle throat (1.5 mm i.d.), a first dye laser for sample ablation (Lambda Physik, EMG102MSC, FL2002, *p*-terphenyl, 2 mJ) is fired and focused by a lens (30 cm focal length) onto the polymer surface through a hole (2.5 mm i.d.). The ablated chemical species is entrained into a stream of argon and is successively expanded into a vacuum from the nozzle throat. The distance between the sample and the outlet of the nozzle throat is 6.5 mm. The molecule in the supersonic jet is excited by a second dye laser (Quantel, YG581C, TDL50, rhodamine 6G, UVX-2, DCC-3, 3 mJ). The laser beam is focused by a lens (30 cm focal length) at 15 mm away from the point of sample ablation. Fluorescence from the molecule in the jet is collected by a lens (10 cm focal length) and measured by a monochromator (Jasco, CT-100) equipped with a photomultiplier (Hamamatsu, R928). The signal is measured by a boxcar integrator (NF Circuit Design Block, BX-530A) and is displayed by a strip chart recorder. The vacuum system used is described in detail elsewhere (28).

Sample. Polystyrene beads supplied from Wako Pure Chemical Industries ($n = 1600-1800$) were melted in the test tube (10 mm i.d.), and a brass or aluminum rod (8 mm diameter) was inserted coaxially to fix as a holder. After polystyrene was cooled, the test tube was removed. The polystyrene rod was re-formed by sandpaper to a rod diameter of 10 mm. Other polymers such as acrylonitrile/butadiene/styrene copolymer (ABS resin) and polycarbonate were purchased as 10-mm rods from Sanko Plastic Co. The sample rod was rotated and translated through a hole (10 mm i.d.) located just below the nozzle throat to expose a new surface by using a screw combined with a speed control motor (Oriental Motor, 2JJ 3RGA-A₂). The rotating speed was changed from 0.03 to 6 rpm by using two speed-reduction gears (Oriental Motor, 2GA 10XL, 10 times; 2GA 60K, 30 times). At this speed range the sample lasted from 13 min to 40 h, depending on the rotating speed used.

The reagent of styrene monomer was obtained from Wako Pure Chemical Industries, which was used without further purification.

RESULTS AND DISCUSSION

Wavelength of Ablation Laser. For recording an absorption spectrum of polystyrene, polymer beads were melted on a microscope cover glass to form a thin film (thickness, ~ 1 mm). Absorbance of the polystyrene sample increased with decreasing the wavelength, gradually from 400 nm and more rapidly from 300 nm. This is due to light absorption by benzene rings in polystyrene. In the present study the wavelength of the dye laser for ablation is adjusted to 337.5 nm, which is the shortest wavelength available for the excimer-laser-pumped dye laser. Threshold for ablation depends on the wavelength of the exciting laser. It is reported that the signal intensity increases by a factor of 50 by changing the wavelength from 355 nm to 266 nm for tryptophan, which has a strong absorption band at 266 nm (29). Probably, more efficient sample ablation might be achieved by using the fourth harmonic of a Nd:YAG laser (266 nm) or a CO_2 laser (10.6 μm), but the present wavelength (337.5 nm) is used because of its convenience in this study.

Polystyrene. A supersonic jet excitation spectrum measured for a sample of polystyrene is shown in Figure 2A. The sharp spectral feature is similar to that observed for a styrene monomer, as shown in Figure 2B, measured by conventional

* Author to whom correspondence should be addressed.

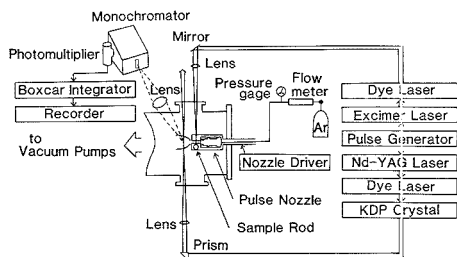


Figure 1. Block diagram of experimental apparatus.

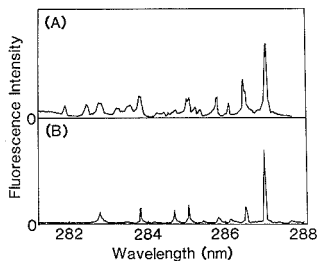


Figure 2. Supersonic jet excitation spectrum: (A) chemical species ejected from polystyrene surface by laser vaporization; (B) styrene monomer introduced by conventional pulsed supersonic jet nozzle. The fluorescence wavelength is adjusted to 295.9 nm (slit width, 2.4 nm).

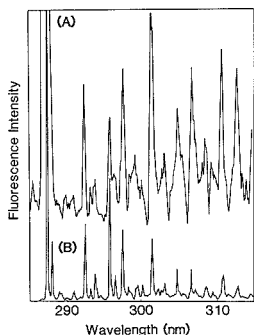


Figure 3. Supersonic jet fluorescence spectrum: (A) polystyrene; (B) styrene monomer. The excitation wavelength is adjusted to the largest peak in Figure 2.

supersonic jet spectrometry. The present result clearly shows that styrene monomers are ablated from the surface of polystyrene. This is consistent with reported efficient ablation of the styrene monomer from polystyrene by ArF laser (193 nm) and KrF laser (248 nm) excitations (30, 31). This assignment is further confirmed by measuring the fluorescence spectrum, as shown in Figure 3. Peak-to-peak correspondence between the spectra for styrene ablated from polystyrene and styrene monomer is excellent. It is reported that other chemical species such as C_6H_6 and C_4H_2 are also ejected from the polystyrene surface by ArF laser and KrF laser excitations (30, 31). The fragments might be detected by charging the wavelengths for excitation and fluorescence detection, though such experimental works have not been performed in this study because of limited tunability of the laser.

Other Polymers. Fluorescence excitation spectra for three polymers, including polystyrene, are shown in Figure 4. Polystyrene consists of styrene segments, so that it gives the

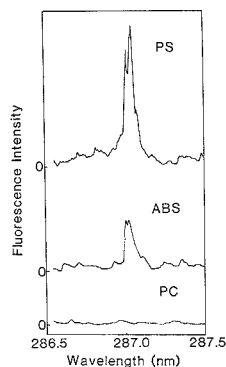


Figure 4. Supersonic jet excitation spectrum for polystyrene (PS), acrylonitrile/butadiene/styrene copolymer (ABS), and polycarbonate (PC).

largest signal. The ABS resin, partly consisting of styrene segments, gives a smaller signal. On the other hand no signal peak is observed at all for polycarbonate, containing no styrene segments. Thus present spectrometric technique is useful to discuss chemical constituents of the polymer material without any pretreatment.

Sensitivity. The signal intensity was recorded by stopping sample rotation for polystyrene. The signal intensity decreased to zero in 50 s, and the depth of the hole reached 1 mm. The repetition rate of the ablation laser is 20 Hz, so that a 1- μ m sample is ablated every shot on the average. The sample ablated by a single laser shot was calculated to 1 ng, assuming a beam diameter of 50 μ m at the polymer surface. The signal-to-noise ratio is about 5 in the excitation spectrum, then the detection limit is estimated to a subnanogram range. This is similar to the values (0.056–1 ng) reported for carbobenzoxy-derivatized peptides measured by laser ablation supersonic jet/multiphoton ionization mass spectrometry (LA-SSJ/MPI-MS); this work is performed under incomplete rovibronic cooling and a wavelength-fixed laser (266 nm) with a large pulse energy (~ 10 mJ) is used for multiphoton ionization (32). The present detection limit is poorer than picogram and femtogram detection limits obtained for phenylthiohydantoin and protoporphyrin IX dimethyl ester by nonjet LA-MPI-MS (33–35). Needless to say, the present method has a distinct advantage over nonjet LA-MPI-MS with respect to spectral selectivity, given by efficient rotational cooling as shown in the following section.

Rotational Cooling. The signal peak for 0–0 transition of styrene was more carefully measured for the sample of polystyrene. The spectral line was slightly split to two peaks and an overall line width was 7.3 cm^{-1} , which was contrast to a line width of 3.6 cm^{-1} observed for the styrene monomer measured by using a conventional supersonic jet nozzle. Because of a rather poor signal-to-noise ratio, quantitative discussion is difficult, but a slightly broader line width observed for polystyrene might be due to inefficient rotational cooling caused by the structure of the nozzle throat or by the elevated temperature with laser heating. However, it should be emphasized that the spectrum for polystyrene is completely resolved and rovibronic cooling is sufficient for demonstration of spectral selectivity in supersonic jet spectrometry.

Translational Cooling. In laser ablation, the sample is immediately heated (10^8 K s^{-1}) in the nanosecond range (35, 36). Then, it may be possible to prepare the sample molecule to a well-localized region in a jet pulse. If so, it is quite useful to focus chemical species to a limited region to enhance the signal intensity. Figure 5 shows dependence of the time be-

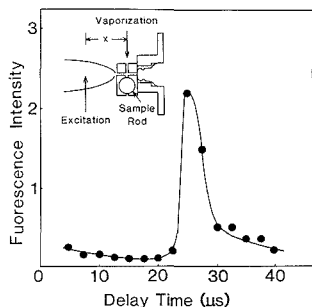


Figure 5. Dependence of time between vaporization and excitation lasers on fluorescence intensity. The separation (x) between the vaporization and excitation lasers is 15 mm.

tween ablation and excitation laser pulses on the fluorescence intensity. The signal increases rapidly after 25 μs from the ablation laser pulse, and it gradually decreases in 4 μs . The average velocity of the jet is calculated to 600 m/s (15 mm/25 μs), corresponding to a pulse width of 2.4 mm (600 m/s \times 4 μs) in the jet.

The mach number, M , in supersonic jet expansion is calculated by

$$M = A(X/D)^{2/3} \quad (1)$$

where A (≈ 3.26) is constant, X is the distance between the nozzle and the sample detection position, and D is the nozzle diameter (37). The ratio of the molecular velocity in the jet, u , and the most probable velocity, v_{mp} , in a Maxwell-Boltzmann's distribution corresponding to $M = 0$ is given by

$$u/v_{\text{mp}} = M[\gamma/(3 + (3/2)(\gamma - 1)M^2)]^{1/2} \quad (2)$$

$$v_{\text{mp}} = (3kT_0/m)^{1/2} \quad (3)$$

where γ is the ratio of the specific heats at constant pressure and temperature ($\gamma = C_p/C_v = 5/3$). Assuming $T_0 = 300$ K and $X = 15$ mm, the mach number is calculated to $M = 18$. The final velocity of the molecule at the sample detection position under present experimental conditions ($M = 18$) is calculated to 800 m/s. The velocity of the molecule immediately after jet expansion is much lower, so that the average velocity is estimated to be slightly less than 800 m/s. This value is consistent with the average velocity of 600 m/s observed.

The translational temperature is simply estimated by the following equation in this study, instead of a more complicated one (eq 6 in ref 37)

$$f(v) = (m/2\pi kT)^{1/2} \exp(-mv^2/2kT) \quad (4)$$

where m is the mass of the molecule, k is the Boltzmann constant, and T is the temperature. From the observed curve in Figure 5, the translational temperature was well-fitted to 25 K. On the other hand, the theoretical translational temperature, T_s , calculated from the nozzle parameter etc. is given by (37)

$$T_s/T_0 = [1 + (\gamma - 1)M^2/2]^{-1} \quad (5)$$

The estimated value from present experimental conditions is 3 K, which is obtained by assuming $M = 18$ and $T_0 = 300$ K. It is difficult to discuss discrepancy quantitatively due to rather poor accuracy in the experimental data. However, it is possible to ascribe it to sample spread immediately after laser ablation, which is considered to be 1–2 mm (1.7–3.3 μs in the time domain) and is not negligible in comparison with 4 μs . Temperature rise in the nozzle throat by laser heating may also increase T_0 , increasing T_s . However, if one explains

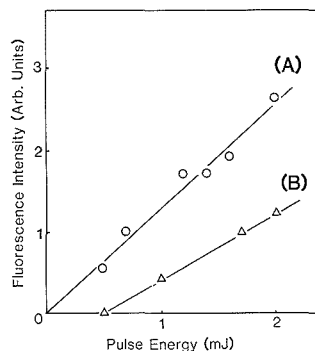


Figure 6. Dependence of pulse energy for sample vaporization on fluorescence intensity: (A) tightly focused; (B) poorly focused. Two independent results, circle and triangle, are presented in the same graph.

this discrepancy only with this temperature rise, the temperature in the nozzle throat (T_0) should exceed 3000 K. This is not reasonable, since heated chemical species by laser radiation (6000 K (31), 350–450 K (36)) is rapidly cooled by collision with Ar. This rather high translational temperature may be also attributed to an imperfect nozzle structure. Nonsymmetric distribution of the styrene molecule, shown in Figure 5, may support this discussion; the tail after 27 μs implies presence of the dead volume in the nozzle throat.

Signal Enhancement. In conventional pulsed supersonic jet spectrometry, the typical pulse width is 1 ms (38). The sample molecule can be more efficiently detected by localizing it in spatial and time domains. Sheath flow gas dynamic focusing to a central core in the jet has been demonstrated, and a signal enhancement factor of 30 is achieved (39). As shown in Figure 5, the sample molecule is focused into 4 μs ; then an enhancement factor of 250 is achieved in the present study. The laser ablation technique has a distinct advantage over a gas-flowing pulsed supersonic jet technique with respect to sensitivity, when the sample amount is limited. Present results are consistent to a reported value of ~ 5 μs obtained by LA-SSJ placing the sample outside the nozzle for jet expansion (40).

It is noted that the unused sample remains on the rod surface. Therefore, very toxic chemicals doped in a polymer are quite safely measured and easily recovered. This is a practical but important advantage, when supersonic jet spectrometry is applied to hazardous substances such as dioxines and polychlorinated biphenyls.

Threshold Energy for Vaporization. Figure 6 shows dependence of the pulse energy on the signal intensity. Two experiments are performed by changing the beam focusing condition. When the ablation laser is tightly focused onto the polymer surface, threshold for signal appearance decreases to almost zero. In this case the observed signal was stronger, and the spectrum could be measured in a better signal-to-noise ratio. When the laser beam is poorly focused, the signal appears from 0.5 mJ. In this case the signal intensity was weak. These results imply that a threshold energy is necessary for sample ablation. This fact is consistent with the result obtained by nonjet LA-MPI-MS (30).

Beam Diameter at Sample Surface. In our preliminary study the sample rod was rotated fast enough to irradiate a new polymer surface. However, it is noticed in later works that the signal intensity increases with decreasing the rotating speed. Figure 7 shows dependence of the beam separation between successive laser shots. The signal intensity increases with decreasing the separation gradually from 140 μm and

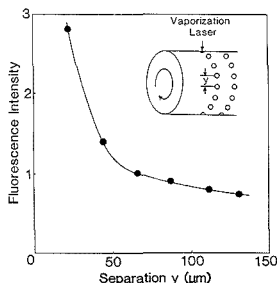


Figure 7. Dependence of separation (y) between successive laser shots on fluorescence intensity.

more rapidly from 50 μm . In this experiment the laser with a beam diameter of 6 mm is focused onto the polymer surface by the lens with a focal length of 30 cm. Then, the diameter at a beam waist is calculated to 20 μm , by assuming a Gaussian beam. Apparently, the actual beam diameter for a non-Gaussian beam, inevitable for the excimer-laser-pumped dye laser, is much larger than the above value by a factor of 2 or 3. Then, the beam diameter of the ablation laser at the polymer surface is estimated to be 40–60 μm , which coincides with the separation, at which the signal rapidly increases. This fact implies that sample ablation becomes more efficient by superposition of successive laser shots. Thus the signal increase may be attributed to temperature rise and acceleration of the vaporization rate by laser heating with previous laser shots. The fluence of the ablation laser is calculated to 100 J/cm^2 at present experimental conditions (2 mJ, 50 μm diameter). This fluence is much larger than a value of 20 mJ/cm^2 used for ablation of polystyrene by KrF laser excitation (31). It might be ascribed to difference in molar absorptivities at 337.5 nm and 248 nm.

Process of Sample Ablation. Under strong laser radiation chemical species are ablated from the polymer surface through two possible mechanisms: (1) a thermal process due to surface temperature rise and (2) a photochemical process through multiphoton excitation. The experimental result shown in Figure 7 may be discussed by separating it to two parts: regions (1) above and (2) below 50 μm . Region 1 is characterized by rapid signal increase with decreasing beam separation. By the previous laser shot the temperature of the polymer surface increases. Generated heat cannot be dissipated in 50 ms (20 Hz), and the polymer surface is kept partially melted or softened until the next laser shot. It is reported that a local pressure of 10^7 Pa (100 atm) is generated immediately after laser pulse at the solid surface (41). Thus efficient evaporation or microexplosion may occur from the partially melted polymer surface to form monomers. Therefore, this is ascribed to the thermal process. In region 2, the signal intensity decreases with increasing the separation but does not reach zero. In this case (>140 μm) ejection of the styrene monomer is achieved by a single laser shot. Two possibilities might be still considered; one possibility is generation of monomers through a thermal effect by a single laser shot and another possibility is photochemical decomposition by multiphoton excitation. It is, unfortunately, difficult to specify one of these possibilities from the present data. However, the rotating speed of the sample rod is adjusted low enough to enhance the signal intensity (<50 μm), and the major process concerned

in this study is the thermal process rather than the photochemical one.

Photofragment spectroscopy of polymer material has been studied by nonjet LA-MPI-MS (30, 31). Because of the poor spectral selectivity, it is difficult to determine the chemical structure of the product molecule since so many isomers are possible. Because of this reason, a photochemical process in laser ablation has not been clarified in detail. The present LA-SSJ technique may allow assignment of the chemical structure and provide information about ablation and fragmentation mechanisms.

LITERATURE CITED

- Hong, R. E.; Woolston, J. R. *Appl. Phys. Lett.* **1963**, *2*, 138.
- Hercules, D. M.; Day, R. J.; Balasannmagan, K.; Dang, T. A.; Li, C. P. *Anal. Chem.* **1982**, *54*, 260A.
- McCreey, D. A.; Ledford, E. B., Jr.; Gross, M. L. *Anal. Chem.* **1982**, *54*, 1435.
- Wilkins, C. L.; Weil, D. A.; Yang, C. L. C.; James, C. F. *Anal. Chem.* **1985**, *57*, 520.
- Brown, R. S.; Wilkins, C. L. *Anal. Chem.* **1986**, *58*, 3196.
- Powers, D. E.; Hansen, S. G.; Geusic, M. E.; Puiu, A. C.; Hopkins, J. B.; Dietz, T. G.; Duncan, M. A.; Langridge-Smith, P. R. R.; Smalley, R. E. *J. Phys. Chem.* **1982**, *86*, 2556.
- Hopkins, J. B.; Langridge-Smith, P. R. R.; Morse, M. D.; Smalley, R. E. *J. Chem. Phys.* **1983**, *78*, 1627.
- Fu, Z.; Lemire, G. W.; Hamrick, Y. M.; Taylor, S.; Shui, J. C.; Morse, M. D. *J. Chem. Phys.* **1988**, *89*, 3524.
- O'Brien, S. C.; Liu, Y.; Zhang, Q.; Heath, J. R.; Tittle, F. K. Cur, R. F.; Smalley, R. E. *J. Chem. Phys.* **1986**, *84*, 4074.
- Michalopoulos, D. L.; Geusic, M. E.; Langridge-Smith, P. R. R.; Smalley, R. E. *J. Chem. Phys.* **1984**, *80*, 3556.
- Syage, J. A.; Wessel, J. E. *J. Chem. Phys.* **1988**, *89*, 5962.
- Tembreull, R.; Lubman, D. M. *Appl. Spectrosc.* **1987**, *41*, 431.
- Li, L.; Lubman, D. M. *Rev. Sci. Instrum.* **1988**, *59*, 557.
- Li, L.; Lubman, D. M. *Appl. Spectrosc.* **1988**, *42*, 418.
- Cable, J. R.; Tubergen, M. J.; Levy, D. H. *J. Am. Chem. Soc.* **1987**, *109*, 6188.
- Phillips, L. A.; Levy, D. H. *J. Chem. Phys.* **1988**, *89*, 85.
- Cable, J. R.; Tubergen, M. J.; Levy, D. H. *J. Am. Chem. Soc.* **1988**, *110*, 7349.
- Tembreull, R.; Lubman, D. M. *Anal. Chem.* **1986**, *58*, 1299.
- Tembreull, R.; Lubman, D. M. *Anal. Chem.* **1987**, *59*, 1003.
- Tembreull, R.; Lubman, D. M. *Anal. Chem.* **1987**, *59*, 1082.
- Lubman, D. M.; Tembreull, R. *Anal. Instrum.* **1987**, *16*, 117.
- Li, L.; Lubman, D. M. *Anal. Chem.* **1988**, *60*, 1409.
- Li, L.; Lubman, D. M. *Appl. Spectrosc.* **1988**, *42*, 411.
- Grottemeyer, J.; Walter, K.; Boest, U.; Schlag, E. W. *Int. J. Mass Spectrom.* **1987**, *78*, 69.
- Boest, U.; Grottemeyer, J.; Walter, K.; Schlag, E. W. *Anal. Instrum.* **1987**, *16*, 151.
- Grottemeyer, J.; Schlag, E. W. *Org. Mass Spectrom.* **1987**, *22*, 758.
- Grottemeyer, J.; Schlag, E. W. *Org. Mass Spectrom.* **1988**, *23*, 388.
- Imasaka, T.; Fukuoka, H.; Hayashi, T.; Ishibashi, N. *Nal. Chim. Acta* **1984**, *156*, 111.
- Karas, M.; Bachmann, D.; Hillenkamp, F. *Anal. Chem.* **1985**, *57*, 2935.
- Feldmann, D.; Kutzner, J.; Laukemper, J.; MacRobert, S.; Welge, K. H. *Appl. Phys. B* **1987**, *44*, 81.
- Larciprete, R.; Stuke, M. *Appl. Phys. B* **1987**, *42*, 181.
- Li, L.; Lubman, D. M. *Appl. Spectrosc.* **1988**, *42*, 411.
- Engelke, F.; Hahn, J. H.; Henke, W.; Zare, R. N. *Anal. Chem.* **1987**, *59*, 909.
- Hahn, J. H.; Zenobi, R.; Zare, R. N. *J. Am. Chem. Soc.* **1987**, *109*, 2842.
- Zare, R. N.; Hahn, J. H.; Zenobi, R. *Bull. Chem. Soc. Jpn.* **1988**, *61*, 87.
- Meyer, J.; Kutzner, J.; Feldmann, D.; Welge, K. H. *Appl. Phys. B* **1988**, *45*, 7.
- Mikami, N. *Oyo Buturi* **1980**, *49*, 802.
- Imasaka, T.; Okamura, T.; Ishibashi, N. *Anal. Chem.* **1986**, *58*, 2152.
- Stiller, S. W.; Johnston, M. *Anal. Chem.* **1987**, *59*, 567.
- Arrowsmith, P.; de Vries, M. S.; Hunziker, H. E.; Wendt, H. R. *Appl. Phys. B* **1988**, *46*, 165.
- Dyer, P. E.; Srinivasan, R. *Appl. Phys. Lett.* **1986**, *48*, 445.

RECEIVED for review August 30, 1988. Revised April 6, 1989. Accepted April 14, 1989. This research is supported by Grant-in-Aid for Scientific Research from the Ministry of Education of Japan and by Nissan and Kurata Foundations.

Infrared and Thermal Studies of *N*-(*p*-Cyanobenzylidene)-*p*-octyloxyaniline Coated on Derivatized Silica

C. J. Hann¹ and R. K. Gilpin*

Department of Chemistry, Kent State University, Kent, Ohio 44242

The interaction of *N*-(*p*-cyanobenzylidene)-*p*-octyloxyaniline (CBOA) with silicas modified with monoreactive silanes varying in chain length and blocking ability has been studied by Fourier transform infrared spectroscopy, differential scanning calorimetry (DSC), and thermogravimetric analysis (TGA). The derivative TGA curves for the various coated silicas contain two peaks indicating the presence of a two-step desorption process. The complex shapes of the infrared nitrile stretch bands suggest three different interactions. Populations with cyano-cyano interactions, isolated nitrile groups, and hydrogen-bonded nitrile groups are feasible orientations. DSC data support the idea of three populations of liquid crystals with different interactions. Differences in the nitrile stretching frequencies for the octyldimethyl- and decyldimethylsilicas can be explained in terms of a dynamic surface model where the bonded chains in contact with the coating reorient at a characteristic temperature and perturb the CBOA.

INTRODUCTION

Although boundary ordering mechanisms of liquid crystals are not fully understood, unquestionably it is the interfacial orientation that controls many of their display properties (1). Likewise, display failures often result from degradation of the orientation at the interface (2). In an effort to minimize this problem, more stable interfaces have been produced by modification of the substrate with reactive silanes (2).

The purpose of the current work has been to develop surface modification procedures to control the orientation of liquid crystalline molecules as well as to examine the mesogen-substrate interface. Techniques developed for related systems (i.e., silica immobilized ligands) have been used to probe the microstructure of liquid crystals in contact with several alkylchlorosilane modified silicas. Porous silica was chosen because of its high surface area which facilitates characterization and because its surface chemistry is similar (i.e., silanol groups) to glass which is commonly used in display construction.

Previously (3) the interaction of the liquid crystal *N*-(*p*-cyanobenzylidene)-*p*-octyloxyaniline (CBOA) with underivatized and trimethylsilyl-derivatized silica was studied as a function of coating level. For most samples broad asymmetrical absorption bands for the nitrile stretch suggested the presence of at least two populations of cyano groups. Subsequently, a two-site adsorption mechanism was proposed in which the nitrile groups of CBOA either formed hydrogen bonds with surface silanols or were sterically hindered from this type of interaction. Although the ratio of molecules which did not hydrogen-bond with the surface to those that did increased as the amount of the physically sorbed liquid crystal

increased for both the modified and unmodified surfaces, at any given coating level, the ratio was higher for the trimethylsilyl-derivatized silica than for the underivatized silica.

As a follow up to this earlier work (3), the interaction of CBOA with silicas modified with monoreactive silanes varying in chain length and blocking ability has been studied by Fourier transform infrared (FT-IR) spectroscopy, differential scanning calorimetry (DSC), and thermogravimetric analysis (TGA). The derivative TGA curves for the various coated silicas contain two peaks indicating the presence of a multistep desorption process. Additionally, the complex shapes of the infrared nitrile stretch bands and the changes in the DSC thermograms support the idea of three populations of liquid crystals with different interactions.

EXPERIMENTAL SECTION

Materials. The bonded phases were synthesized by refluxing Silica Gel 60 (particle size 0.040-0.063 mm, surface area 550 m²/g [E. Merck]) overnight in a toluene solution of a given monochlorosilane (Petrarch Systems, Inc.). During the reaction dry nitrogen was bubbled through the solution. The resulting silica was washed 4 times with toluene, 2 times with methanol, and 2 times with ether and then dried overnight at 110 °C in a vacuum oven (4). The amounts of bound carbon (measured by a combustion process using a Leco 244 Carbon-Sulfur Determinator) and normalized carbon (amount of bound carbon divided by the number of carbons in the silane) for the various silicas are reported in Table I. Subsequently, modified silicas were physically coated with between 20 and 100 wt % CBOA. This was done by first dissolving a known amount of CBOA in ether and then adding the desired amount of silica adjusted to compensate for the weight of the immobilized silane. The mixture was allowed to equilibrate for approximately 15 min and the solvent slowly removed under vacuum at 38-40 °C with a rotary evaporator. The coated silica was dried in a vacuum oven for 48 h at 40 °C and stored in a brown bottle.

Spectrometry. Each undiluted sample was loaded into a 1-cm diameter diffuse reflectance cup, gently tapped to facilitate settling, and positioned in a Barnes diffuse reflectance accessory. FT-IR spectra were collected at a resolution of 4 cm⁻¹ with an IBM Instruments Model IR/32 spectrometer equipped with a DTGS detector. The number of sample scans needed for an adequate signal to noise ratio (i.e., 1000 to 20000) vs 1000 background scans was used. Base-line corrections and full scale normalizations were performed by using the instrument's software.

Thermal Analysis. All thermal analysis experiments were performed in a helium atmosphere by using a Du Pont 9900 system for control, data collection, and data manipulation. Thermogravimetric analysis (TGA) was carried out with a Du Pont 951 TGA. Samples (8-10 mg) were conditioned at 120 °C for 20 min to remove adsorbed water and then analyzed at a heating rate of 5 °C/min. The differential scanning calorimetry (DSC) studies were made on 8-10 mg of the coated silica or 14-15 mg of the uncoated silica with a Du Pont 910 DSC. Coating weights determined by TGA were used to calculate the weight of CBOA for the coated specimens. Heating rates were 1 °C/min for the coated and 10 °C/min for the uncoated samples.

RESULTS AND DISCUSSION

Surfaces were reacted with alkylmonochlorosilanes differing in chain length and blocking ability and then physically

* Author to whom correspondence should be addressed.
¹ Current address: Loral Defense Systems—Akron, Akron, OH 44315.

Table I. Enthalpies (J/g) of the Solid to Mesophase Transition for Silica Derivatized with Different Silyl Ligands and Coated with Varying Amounts of CBOA

wt % CBOA	DSC scan no.	underivatized (0-0) ^a	butyldi- methyl (5.3-0.88)	octyldi- methyl (9.0-0.90)	decyldi- methyl (10.8-0.90)	tributyl (10.8-0.90)
100	1	14.7	24.5	18.8	17.2	35.5
	2	3.6	23.4	17.5	16.3	32.6
	3	3.4	23.2	17.3	16.2	32.6
80	1	6.3	2.5	5.4	15.9	34.3
	2	- ^b	-	-	13.8	32.2
	3	-	-	-	13.4	32.2
60	1	2.1	1.6	0.8	4.1	4.6
	2	-	-	-	-	-
	3	-	-	-	-	-

^aPercent carbon-normalized carbon. ^bNo transition detected.

modified with from 20 to 100 wt % CBOA. Approximately 20% CBOA has been found to correspond to a monolayer of coverage on the unmodified silica (3). This estimate will vary depending on pore geometry of the matrix (i.e., molecular exclusion effects which increase as the surface area increases), size and shape of the mesogen, and molecular alignment (5).

Infrared Studies. Diffuse reflectance spectra were collected at room temperature. Shown in Figure 1 are expanded spectra from the nitrile stretching region for the various coated silicas chemically derivatized to a similar degree. Since the normalized carbon value was nearly the same for each material (i.e., 0.9 ± 0.05) the relative number of unreacted surface silanols was approximately identical. In most cases broad, asymmetrical bands were observed.

The infrared spectra reflect differences in the steric accessibility of the surface silanols depending on the immobilized group. The nitrile band was severely skewed to high frequency for butyldimethyl (Figure 1A, bands 1 and 2 for 20% and 60% CBOA, respectively) and octyldimethyl (Figure 1B, bands 1 and 2 for 20% and 60% CBOA, respectively) surfaces indicating a relatively large population of groups which hydrogen-bond with surface silanols. For the same coating levels on the decyldimethylsilica (Figure 1C, bands 1 and 2 for 20% and 60% CBOA, respectively) the ratio of hydrogen-bonded to non-hydrogen-bonded nitrile groups decreased. This ratio was even lower for the more sterically hindered tributyl surface (Figure 1D, bands 1 and 2 for 20% and 60% CBOA, respectively).

The nitrile band appears to be composed of at least three spectral components. The higher frequency component has been assigned previously to cyano-silanol interactions (3). The remaining two bands are especially apparent for the decyldimethyl surface. The 20% and 60% levels are shown respectively as bands 1 and 2 in Figure 2C. As an aid in assigning these bands, infrared spectra were collected from CBOA dissolved in hexane, the crystalline form of CBOA, and CBOA coated on silica highly derivatized with cyanopropyl dimethyl groups (9.4% bound, 1.6 normalized carbon value). For CBOA levels of 20% and 60% on the butyldimethyl (Figure 1A, respectively bands 1 and 2) and octyldimethyl (Figure 1B, respectively bands 1 and 2) silicas, the band maxima, were at approximately the same frequency as CBOA dissolved in hexane (2233 cm^{-1}). The frequencies for the 20% coating on the decyldimethyl (Figure 1C, band 1) and tributyl (Figure 1D, band 1) substrates were shifted toward the cyano-cyano frequency with the decyldimethyl band shifted more than the tributyl band.

The nitrile stretch bands for 60% CBOA coated on silica with different levels of decyldimethyl derivatization (i.e., 0.8 and 0.9 normalized carbon) are shown in Figure 2. The ratio of hydrogen-bonded to non-hydrogen-bonded groups was largest on the underivatized silica (Figure 2A) and successively

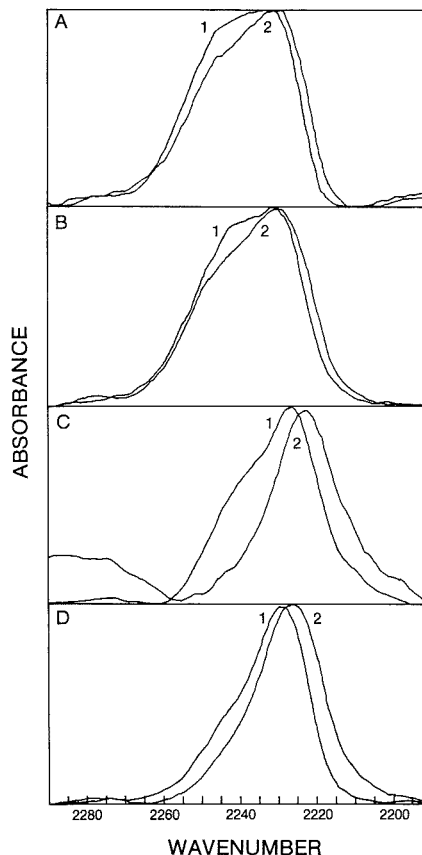


Figure 1. Comparison of the nitrile stretch region for (1) 20% and 60% CBOA: normalized carbon = 0.9; (A) *n*-butyl dimethyl-, (B) octyldimethyl-, (C) decyldimethyl-, (D) tributylsilicas.

decreased for increasing derivatization (Figure 2, parts B and C, respectively).

A sample of 60% CBOA on each modified silica was heated to 120°C (i.e., above the clearing point of the liquid crystal), maintained at this temperature for 10 min, and then allowed to cool to room temperature. Representative spectra from the nitrile stretching region for thermally conditioned samples

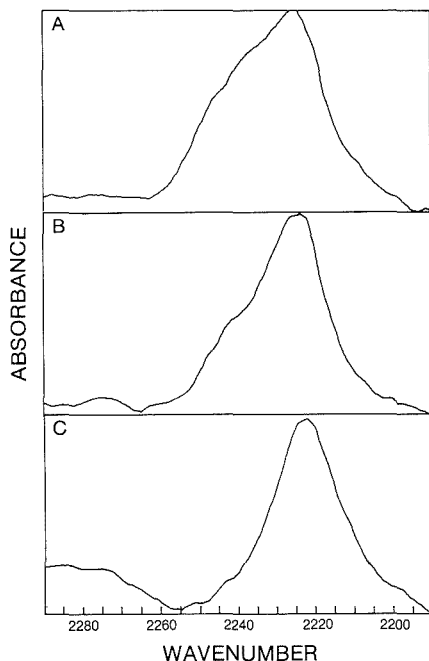


Figure 2. Comparison of the nitrile stretch region for 60% CBOA: (A) underivatized, (B) decyldimethyl-, 0.8 normalized carbon; (C) decyldimethylsilicas, 0.9 normalized carbon.

and equivalent unheated samples are shown in Figure 3. For the underivatized surface (Figure 3A) the spectra before and after heating were nearly identical (i.e., bands 1 and 2). This was true also for the tributyl (Figure 3D) derivatized silica. Although the nitrile bands are at the same frequency for the octyldimethyl and decyldimethyl surfaces following heat treatment, this corresponds respectively to a shift to a higher and to a lower frequency for the two surface types. The nitrile frequency of the band after heat treatment was approximately the same for all four silicas. Differences between these bands can be attributed to differences in the ratio of molecules that hydrogen-bond to those that do not. This ratio was highest for the underivatized silica, the surface with the largest number of silanol groups, and lowest for the tributylsilica, the bulkiest surface with the least sterically accessible silanols.

Thermal Studies. The phase transitions for CBOA are the crystal to smectic A (73 °C, 19 cal/g), the smectic A to nematic (83 °C, 0.06 cal/g (6)), and the nematic to isotropic (107 °C, 0.5 cal/g). The smectic A to nematic transition has been reported to be detectable by DSC only after successive recrystallizations (6, 7).

DSC thermograms were collected on each surface for a series of three heating and cooling cycles. The smectic to nematic transition was not detected in any of these scans. The crystal to smectic and nematic to isotropic transitions were readily observed for coating levels of 60%, 80%, and 100% CBOA. These observations are consistent with our initial studies and are likely due to very thin coverages on the high surface area materials used (3). The enthalpies for these changes (Table I) correlate with the infrared data. These results reflect reasonable differences in hydrogen-bonding between the different coatings. Since the hydrogen-bonded CBOA molecules should not contribute to the transition enthalpies (5), a correlation should be possible between the transition en-

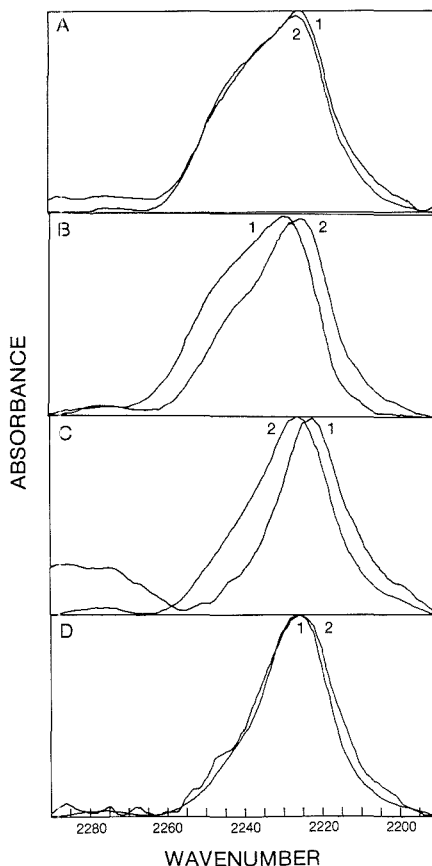


Figure 3. Comparison of the nitrile stretch region (1) before and (2) after heating to 120 °C for 60% CBOA: (A) underivatized, (B) octyldimethyl-, (C) decyldimethyl-, (D) tributylsilicas.

thalpies and the relative population of hydrogen-bonded cyano groups for each coated silica. Enthalpy values for coated tributyl silica were the highest. Anomalously high values on the first scan for the underivatized substrate are likely due to uneven coating of CBOA during the rotary evaporation deposition process. This is supported by the observation that at the 60% level, no endothermic changes (i.e., no liquid crystalline activity) were observed for the second and third scans. After the initial scan the CBOA is believed to spread out on the surface which results in a loss of liquid crystalline properties. At the 80% coating level, liquid crystalline behavior was noted only for the decyldimethyl- and tributylsilicas after a heating and cooling cycle. However at the 100% coating level, endothermic changes were observed for each silica for all scans. After a heating and cooling cycle, approximately one extra monolayer (i.e., 20%) of CBOA was required for liquid crystalline activity for the surfaces with a larger degree of hydrogen-bonding. These results support the idea of puddling during the sorption process.

Besides using DSC to investigate the thermal transitions of the coated materials, TGA also was used to study the desorption of CBOA. In several cases a two-step desorption was observed. Derivative TGA thermograms for these systems can be correlated with the second and third scan transition

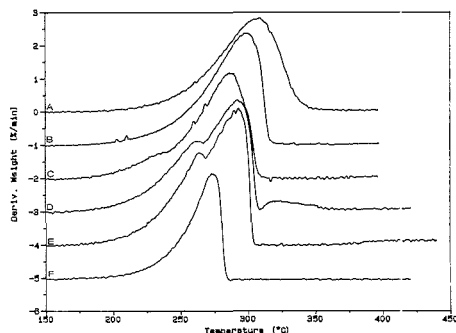


Figure 4. Derivative TGA thermograms for 80% CBOA: (A) underivatized, (B) butyldimethyl, (C) octyldimethyl-, (D) decyldimethyl-, (E) tributylsilicas, (F) pure CBOA, peak factor 0.2.

data measured by DSC. The single derivative peak of the TGA curve for the pure liquid crystals is shown as curve F in Figure 4. At the 100% coating level, derivative curves for the various coated silicas exhibited higher and lower temperature peaks indicating the presence of two types of desorption corresponding respectively to loss of liquid crystals from the surface at their volatilization temperature and loss at a higher temperature (i.e., a population with some interaction hindering desorption). At the 80% coating level, only the thermograms from the coated decyldimethyl- and tributylsilicas (Figure 4, bands D and E) exhibited the lower temperature desorption peak. This peak was not observed at the 60% coating level. The ratio of CBOA molecules that desorb at the liquid crystal vaporization temperature to those that interact with the surface should increase with coating weight and surface derivatization and should mimic FT-IR and DSC trends. The temperature that all of the CBOA was desorbed from each surface (i.e., the temperature the derivative curve returned to the flat base line) is related to the degree of surface derivatization. This temperature was highest for underivatized silica and equal within experimental error for the different silicas with the same level of derivatization. Sinha and Mukherjee (8) and Harrison and Guest (9) have demonstrated differences in desorption temperature for physisorbed and hydrogen-bonded water molecules using similar TGA methods.

The differences in infrared band frequencies (Figure 3) and the lower transition enthalpies (Table I) following a heating and cooling cycle suggest that the CBOA molecules undergo orientational changes following heating above their clearing point. A plausible explanation for these changes is that the molecules puddle or clump on the surface during the physical coating process and spread out upon heating. Hydrogen bonding trends can be accounted for by differences in the steric accessibility of the silanols for the different derivatized silicas. However, this "puddling-spreading out" mechanism does not explain the non-hydrogen-bonded infrared band frequencies for the octyl and decyl surfaces or the frequency shifts for the heat-treated samples (Figure 3).

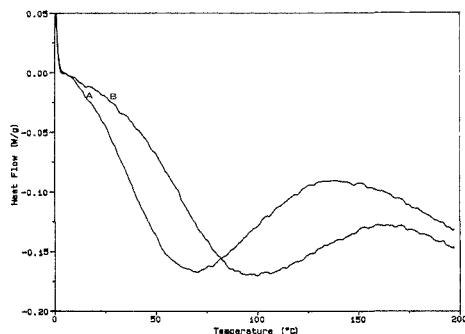


Figure 5. DSC thermograms for uncoated (A) octyldimethyl- and (B) decyldimethylsilicas.

Both cross polarization magic angle spinning nuclear magnetic resonance spectrometry and gas chromatography have been used to suggest a dynamic surface model where orientation and motion of the immobilized ligands are chain length dependent. The surfaces modified with long chains behaved more like liquids while shorter chains behaved more like solids. For intermediate chains their behavior (i.e., liquid vs solid) is temperature dependent. Thus, a possible explanation for the difference in band frequency for the CBOA coated on the octyldimethyl- and decyldimethylsilicas may be related to orientational changes of the immobilized ligand which occur upon heating. To judge the feasibility of this mechanism, DSC thermograms (shown in Figure 5) were collected from the uncoated octyldimethyl and decyldimethyl derivatized surfaces. For the octyldimethylsilica an endothermic transition occurred approximately 20 °C lower than was observed for the decyldimethylsilica. The drying temperature of the coated silicas (40 °C) is respectively above and below the endothermic transition temperatures of the octyl and decyl surfaces.

The above data demonstrate that there are differences in the orientation and interaction of CBOA with alkyl-modified silicas and that these differences can be correlated to size, shape, and blocking ability of the immobilized groups.

LITERATURE CITED

- (1) Miyano, K. *Jpn. J. Appl. Phys.* **1985**, *24*, 1379.
- (2) Kahn, F. J. *J. Appl. Phys. Lett.* **1973**, *22*, 386.
- (3) Hann, C. J.; Gilpin, R. K. *Anal. Chem.* **1987**, *59*, 2460.
- (4) Gilpin, R. K.; Gangoda, M. E. *J. Chromatogr. Sci.* **1983**, *21*, 352.
- (5) Marciniak, W.; Wikiewicz, Z. *J. Chromatogr.* **1985**, *324*, 299.
- (6) Cladis, P. E. *Phys. Rev. Lett.* **1973**, *31*(19), 1200.
- (7) McMillan, W. L. *Phys. Rev. A* **1973**, *7*(9), 1419.
- (8) Sinha, A.; Mukherjee, P. K. *Technology* **1971**, *7*(4), 314.
- (9) Harrison, P. G.; Guest, A. J. *Chem. Soc., Faraday Trans. 1* **1987**, *83*(11), 3383.
- (10) Sindorf, D. W.; Maciel, G. E. *J. Am. Chem. Soc.* **1983**, *105*, 1848.
- (11) Sindorf, D. W.; Maciel, G. E. *J. Am. Chem. Soc.* **1983**, *105*, 3767.
- (12) Gilpin, R. K. Dissertation, University of Arizona, (1973).

RECEIVED for review August 16, 1988. Accepted April 7, 1989. Support from DARPA-ONR Contract N0014-86-K-0772 is acknowledged.

Polymeric Activated Ester Reagents for Off-Line and On-Line Derivatizations of Amine Nucleophiles in High-Performance Liquid Chromatography with Ultraviolet and Fluorescence Detection

Chun-Xin Gao, Tzun-Yu Chou, and Ira S. Krull*

Department of Chemistry and The Barnett Institute, 341 Mugar Building, Northeastern University, 360 Huntington Avenue, Boston, Massachusetts 02115

A novel polymeric activated ester reagent has been developed that improves final detectability and chromatographic performance in high-performance liquid chromatography (HPLC) for virtually all primary and secondary amines or amine analogues. This has involved the synthesis, characterization of final reagent, optimization of derivatization and separation conditions, and determination of analytical figures of merit. The polymeric reagent contained an activated ester linkage to the 9-fluorenyl group, which imparted ultraviolet (UV) and fluorescence (FL) detector properties to the final derivatives. Kinetic studies of these solid-phase (heterogeneous) reactions have been conducted, and specific rate constants were compared with those of the analogous solution reaction for the same substrates. Percent derivatizations have reached 90% and 70% for primary and secondary amines, respectively, under optimized conditions. High reaction reproducibility has been obtained by using the on-line approach, for more than 50 separate injections of the same amine substrate with a single solid-phase reactor. These solid-phase derivatizations have led to detection limits for typical amines in the low-parts-per-billion range. The final, overall methods can provide rapid, automatable, accurate, and precise detection and quantitation of primary/secondary amines and amine-like compounds in real-world sample matrices. As an illustrative example, amphetamine spiked in urine has been derivatized off-line and on-line, with minimum sample preparation, and detected via HPLC-UV/FL with acceptable accuracy and precision.

INTRODUCTION

Perhaps a major obstacle remaining for the greater implementation of high-performance liquid chromatography (HPLC) in many areas is the detectabilities of substrates at trace levels. There is, for example, a limited sensitivity of most naturally occurring bioorganics and amine-like drugs via most current detection approaches (ultraviolet, fluorescence, electrochemical). In addition, most primary and secondary amines exhibit poor chromatographic performance via direct HPLC approaches, making trace analysis more difficult (1, 2). Solution chemical derivatization has long been accepted as an effective modification technique in HPLC, improving the overall specificity, chromatographic performance, and sensitivity for the original trace analyte (3-7).

There are a number of significant advantages that accrue in using heterogeneous reactions, that is, those that utilize solid-supported or solid-attached (ionically/covalently)

reagents in comparison to homogeneous derivatizations performed in a one-phase solution (8-10). Just within the past decade, solid-phase approaches have significantly increased in popularity and usage. A number of reports have appeared describing such approaches in HPLC (8-13). However, relatively few approaches today routinely incorporate any on-line, precolumn, solid-phase derivatizations for any class of substrates. Therefore, we have been developing new generations of solid-phase reagents and approaches for future HPLC applications.

Following our earlier results that used a polymeric *o*-acetylsalicyl activated anhydride for improved UV and electrochemical (EC) detection of primary and secondary amines (11), we have recently described a derivatization scheme for these same nucleophiles that used a polymeric benzotriazole activated ester reagent (12). An application of such polymeric reagent was successful in the determination of polyamines in human urine (13).

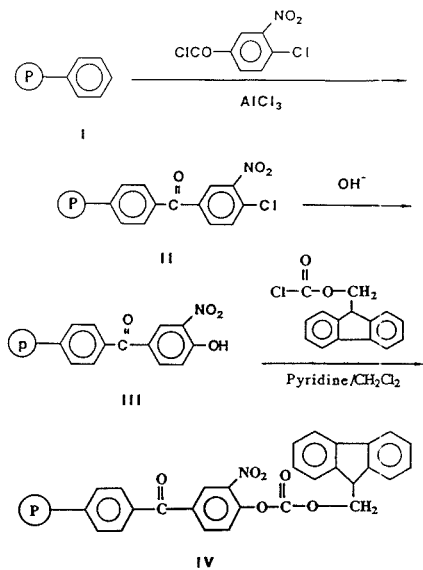
Though studies with the polymeric benzotriazole reagents were successful off-line, it was apparent that such materials could not be easily used on-line, at least in the precolumn, reversed-phase mode. The polymeric benzotriazole reagents were too sensitive to moisture and elevated temperatures, perhaps because of the unstable triazole ring. Continued use of these in a precolumn, on-line manner led to the gradual degradation of the materials and loss of all tagging properties (12). Success would reside in the utilization of a different leashing approach, which retained lability of the tagging group but exhibited greater stability of the overall reagent for on-line reaction and separation conditions.

An earlier report, by Patchornik's group in Israel, provided polymer structures for peptide synthesis, totally unrelated to HPLC derivatizations (14). The *o*-nitrobenzophenone moiety was highly reactive toward nucleophilic attack. In addition, this particular polymeric reagent was shown to be more stable to moisture at both room and elevated temperatures, because of its more stable leashing arrangement.

It appeared at the outset of these studies that such features would certainly make the reagents suitable for off-line applications, but more than likely also for on-line needs in HPLC. We have prepared one example of these improved polymeric reagents, a fluorenyl-attached polymeric *o*-nitrobenzophenone reagent (Scheme I), again for nucleophiles. Additional useful reagents for HPLC could readily be prepared by modifying the nature of the tagging reagent added in the last step of this synthesis. These might include *o*-acetylsalicyl, anthryl, naphthyl, 3,5-dinitrophenyl, and 9-fluorenylmethyl chloroformate-L-proline for chiral separation, dependent on what type of detection properties would be desired in the final amine derivatives.

Primary and secondary amines have again been chosen as substrates for the evaluation and application of the polymeric

* Author to whom reprint requests and correspondence should be addressed.

Scheme I. Synthesis of the Polymeric Reagent^a

^aKey: I, polystyrene-divinylbenzene copolymer; II, polymeric 3-nitro-4-chlorobenzophenone; III, polymeric 3-nitro-4-hydroxybenzophenone; IV, polymeric 3-nitro-4-[[9-fluorenylmethoxy]carbonyloxy]benzophenone.

reagent in view of their good nucleophilicity and their importance as drugs, biologically active materials, and biopolymers, as well as their prevalence as environmental pollutants. Chemical derivatizations remain the preferred approach, together with GC/HPLC, as opposed to any direct determinations, though this is now possible with certain deactivated GC supports or capillary columns. A large number of solution reactions (15–18) and solid-phase off-line derivatizations (11–13) have been reported for the detection of amines in HPLC. However, an on-line solid-phase derivatization approach for amines in connection with HPLC detection has apparently never been described.

The final polymeric reagent, synthesized by conventional reactions, has been characterized with regard to percent loading and percent derivatizations of standard amines. Such derivatization efficiencies were determined by authentic, external standards prepared and characterized by their physical properties. The heterogeneous reactions were further understood by kinetic studies. Detection limits, calibration plots and linearities, efficiencies of derivatizations as a function of amine concentrations, and other analytical figures of merit have been determined. Studies have demonstrated the experimental reproducibility, within-day or from day-to-day in some cases.

As one application, amphetamine in urine was derivatized/quantitated, off-line and on-line. Amphetamine is an important substance in toxicology, clinical, and forensic laboratories (19). However, it has low UV absorptivity and relatively poor detection limits by current GC-FID (flame ionization detection) approaches (20, 21). The current screening method using HPLC on bare silica suffers from a relatively poor selectivity and separation of amphetamine from the sample matrix (22). Another approach involving off-line extraction/HPLC has a detection limit of about 0.1 ppm for amphetamine in urine. However, the entire procedure was

quite cumbersome and time-consuming (23).

In this paper, the on-line, precolumn solid-phase derivatization method for amphetamine in urine involves the least sample workup and direct simultaneous UV/FL (fluorescence) detection. The detection limit is comparable to that in the literature (23), and the overall approach is simple, fast, accurate and precise, reproducible, and fully automatable.

EXPERIMENTAL SECTION

Chemicals, Reagents, and Solvents. The polymeric support was a macroporous polystyrene-divinylbenzene copolymer (particle size 60–90 μm) obtained from Fluka Chemical Co. Ronkonkoma, NY). Chemicals were obtained from Aldrich Chemical Co. Milwaukee, WI) J. T. Baker Chemical Co. (Phillipsburg, NJ), Alfa Products, Division Morton Thiokol Corp. (Danvers, MA), and Sigma Chemical Co. (St. Louis, MO). Amphetamine sulfate was obtained from Research Biochemicals, Inc. (Natick, MA). These chemicals were all of the highest purity available and were used without further purification. HPLC solvents were obtained from EM Science, Inc. (Cherry Hill, NJ), as their Omnisolv HPLC grade.

Apparatus. The HPLC system consisted of a Waters Model 6000A solvent delivery system (Waters Chromatography Division, Millipore Corp., Milford, MA), a Waters Model U6K syringe loading injection valve, an EM Science LiChrospher C₁₈ column, 250 \times 4.6 mm i.d., 5 μm , a Model SE 120 dual pen recorder (Brown, Boveri and Co., Metrawatt/Goerz Division, Vienna, Austria), and an EM Science Model D-2000 ChromatoIntegrator. The detectors included a Waters Model 480 variable wavelength UV-vis detector, a Schoeffel Model FS-970 fluorescence spectrophotometer (Westwood, NJ), and a HP Model 1040A linear diode array UV-vis spectrophotometric detector (Hewlett-Packard Corp., Palo Alto, CA). The instrumentation used to characterize the synthesized, isolated standards was described in our earlier publication (12).

Synthesis of the Polymeric Reagent. To the polymer (5 g) (polymer I, Scheme I) and 4-chloro-3-nitrobenzoyl chloride (10 g) was added 3 g of aluminum trichloride (AlCl_3) in dry nitrobenzene (100 mL). The mixture was stirred at 60 $^\circ\text{C}$ for 5 h and poured into a mixture of 75 mL of *N,N'*-dimethylformamide (DMF), 50 mL of concentrated hydrochloric acid (HCl), and 50 g of ice. The product, II, was filtered and washed with DMF-water (3:1) (3 \times 50 mL), then with warm (60 $^\circ\text{C}$) DMF (30 mL), and finally with methylene chloride (CH_2Cl_2)-methanol (MeOH) (2:1) (5 \times 50 mL). The product, III, was obtained via base hydrolysis. This was carried out with a mixture of 15 mL of 40% benzyltrimethylammonium hydroxide in water, 15 mL of water, and 30 mL of dioxane, for 8 h at 90 $^\circ\text{C}$. The polymeric product was filtered and then washed with warm (60 $^\circ\text{C}$) dioxane (4 \times 50 mL). Acetic acid (30 mL) was added with stirring for 15 min. The polymer was then washed with dioxane (3 \times 50 mL), until the washings were neutral, followed by washing with 4 \times 50 mL of CH_2Cl_2 -MeOH (2:1). This product, III, (yellow, 1.0 g) was stirred in a mixture of CH_2Cl_2 (10 mL), pyridine (0.5 mL), and the labeling moiety, 9-fluorenylmethyl chloroformate (FMOC-Cl) (1.24 g, 4.8 mmol), for 30 min at room temperature. The reaction mixture was filtered and washed with DMF (3 \times 20 mL), CH_2Cl_2 (3 \times 20 mL), dry ethyl ether (3 \times 20 mL), and finally dried under vacuum. The product, IV, polymer-bound *o*-nitrobenzophenone FMOC reagent, was obtained (yellow, 1.08 g). Alternative labeling reagents, such as *o*-acetylsalicyl chloride, could be substituted in this last synthetic step.

Characterization of the Final Polymeric Reagent. All elemental analyses were performed at Galbraith Laboratories, Inc. (Knoxville, TN). The numbers in parentheses represent the theoretical values. For the polymeric fluorenyl reagent: C, 75.13 (75.23); H, 4.85 (4.86); N, 2.71 (2.52); O, 12.53 (17.30). The theoretical data were calculated from the assumed loading of 1.1 mequiv/g, as determined by the hydrolysis of the polymeric *o*-acetylsalicyl reagent, and the experimentally determined elemental composition of the starting polystyrene-divinylbenzene copolymer (C, 91.76; H, 7.75; N, <0.1; O, 0.37).

Preparation of the External Standards. FMOC-Cl (0.2 mol) was added separately into two round-bottom flasks (250 mL) containing *n*-propylamine (0.1 mol) or diethylamine (0.1 mol),

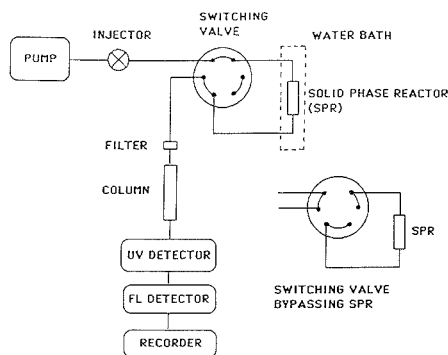


Figure 1. Instrumentation used for on-line, precolumn solid-phase derivatizations in HPLC.

in chloroform (20 mL) and pyridine (1 mL). The reaction was at room temperature for 30 min with stirring. The pure product was obtained after recrystallization from MeOH/H₂O.

On-Line Derivatizations. The reaction columns (27 mm × 3.0 mm i.d.) were made in this laboratory. Hardware was obtained from Alltech Associates, Inc. (Deerfield, IL). The reaction column was positioned before the analytical column and immersed into a constant-temperature water bath (30–90 °C). The substrates were directly injected into the HPLC; the reaction, separation, and detection were all achieved in real time. For trace (ppb) levels of substrate, a switching valve was used, with varying delay times. The analyte was held in the reaction column at the correct time from injection, calculated from analysis of the flow rate and holdup volume in the connecting tubing/valves/fittings. The derivatization was held in the reaction column for 3–5 min, at elevated temperature, and the valve was then switched back to flush the derivative(s) from the reaction column into the separation column (Figure 1). The detailed procedures for off-line derivatizations were described in our earlier publication (12).

Kinetic Study for Solid-Phase Reaction. Twelve reaction cartridges (three for each data point) were prepared, each containing 30 mg of polymeric fluorenyl reagent. A mixture of propyl- and diethylamine was prepared (200 ppm) as a mixture, and 20 μL of this solution (4 μg of each amine) was injected into each cartridge. The reactions were stopped by adding 20 μL of 1 M acetic acid at reaction times of 20, 40, 80, and 160 s, exactly. The polymer bed was then washed with 500 μL of acetonitrile (ACN). The eluted solution was accurately measured with a gastight syringe. Each time point was repeated in triplicate plus one blank. Each individual derivatization solution was injected (20 μL) in triplicate ($n = 9$) together with an accurately known external standard to quantitate the mole concentration of carbamate (product) formed. This was then converted to the mole concentration of amine initially consumed.

Kinetic Study for Solution Reactions. Individual Reaction Vials were prepared to contain 20 μL of the amine mixture (propyl- and diethylamine, 0.06 μmol in each amine) in 20 μL of the borate buffer (pH = 8). To this was added 180 μL of an FMOC-Cl solution (0.32 μmol), and timing was immediately started. The reactions were stopped by adding 30 μL of 1 M acetic acid solution at each time interval (20, 40, 80, and 160 s). Each solution study was also repeated in triplicate for each time point. Each derivatization solution was injected (20 μL) in triplicate along with one blank and external standards of the expected derivatives.

Off-Line and On-Line Derivatizations of Amphetamine Standard. Amphetamine sulfate was dissolved in water, neutralized with 0.1 N NaOH to a pH = 10, and then diluted with 50/50 ACN/H₂O to different concentrations (1, 10, and 100 ppm). For the off-line approach, the standard solution (20 μL, 10 and 100 ppm) was added into reaction cartridges containing 30 mg of polymeric reagent at 60 °C for 5 min and eluted into a final volume of 500 μL of ACN. This mixture was injected (20 μL) into the HPLC. For the on-line approach, the standard solution (20 μL, 1 ppm) was injected directly into the on-line derivatization

system and held up with a switching valve for 5 min at 60 °C. For both off-line and on-line approaches, each sample was injected in triplicate with one blank. HPLC conditions were as follows: flow rate 1.5 mL/min; 50/50, 80/20 ACN/H₂O isocratically; UV at 254 nm and FL at 265/320 nm.

Spiking Amphetamine in Human Urine and Standard Addition Analysis. This study was performed in a "single blind" manner. Fresh urine was spiked at two different concentrations and neutralized with 0.1 M NaOH to pH = 10. Spiked urine was then simply filtered to remove particles and precipitates. Each spiked urine sample was spiked with two additional concentration levels of amphetamine, and one spiked sample without standard addition was used as a blank. These three samples represented only one original urine sample. Each sample was directly injected (10 μL) into an on-line derivatization HPLC in triplicate at 60 °C for 5 min, with the switching valve. Three point calibration plots were constructed for the quantitation of amphetamine in individual urine samples.

RESULTS AND DISCUSSION

Loading Determinations via Hydrolysis and Elemental Analysis. We have used two approaches to determine final loading of the tagging species, solution hydrolysis and quantitation of the hydrolysis product, as well as elemental analysis. We have assumed that the loading by the hydrolysis measurement should give a theoretical elemental percentage that could then be confirmed experimentally. The procedure for the hydrolysis was described in our earlier publication (12). After the hydrolysis of the polymeric fluorenyl reagent, a intermediate fluorenylmethanol was formed, which quickly dehydrated into dibenzofulvene (24). There was no stable dibenzofulvene substance available. However, hydrolysis of another polymeric reagent containing the *o*-acetylsalicyl tag was done instead of using the polymeric fluorenyl reagent. Since the method of synthesis for both reagents and the key intermediate (Scheme I, compound III) was identical, it was apparently valid to assume a similar loading for both polymeric reagents. Other hydrolysis studies for analogous polymeric reagents, starting with the same intermediate (Scheme I, compound III) have shown loadings from 0.3 to 1.8 mequiv/g (25). The loading calculated by using the calibration plot method was 1.1 mequiv/g, which indicated that for 1 g of the final polymeric reagent, there was 1.1 mequiv of *o*-acetylsalicyl (or fluorenylmethyl) tag attached.

Far fewer reports exist in the literature using elemental analysis methods for loading, but together with hydrolysis data, as here, this can be a confirmatory technique. The numbers obtained from elemental analyses agreed with theoretical calculations (Experimental Section). All available information from the loading determination and elemental analyses indicated that the correct synthetic route was followed and that the desired polymeric reagents were obtained.

Characterization of Synthesized External Standards. The standards were characterized by UV, IR, NMR, MS, and melting point determinations. A linear diode array UV-vis spectrophotometric detector was also used to confirm the purity of standard derivatives and to obtain the UV spectra for confirmation of the derivatives formed via polymeric reagent reactions. All of the analytical and structural data were fully consistent with the expected structures. These were demonstrated in our earlier publication (12). The characterized compounds were then used as external standards to determine percent reactions under varying conditions.

Solvent, Temperature, and Time Optimization. The general reaction for an amine with the polymeric *o*-nitrobenzophenone fluorenyl reagent (Scheme I, compound IV) is given in Scheme II. To optimize derivatization conditions, we used a univariate system optimization approach. This involved holding all conditions but one constant and varying that systematically while the percent derivatizations were measured.

Scheme II. Derivatization of Typical Amines with the Polymeric Reagent

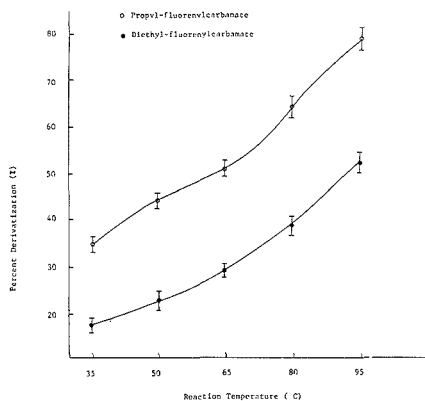
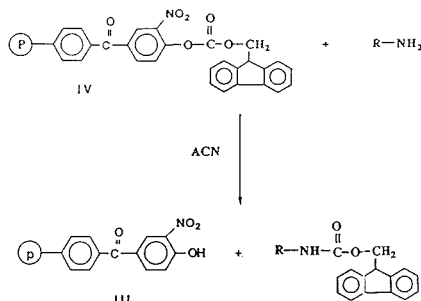


Figure 2. Optimization of temperature for off-line solid-phase derivatizations of amines. A mixture of propylamine and diethylamine in ACN (each amine at 20 ppm) was added to 30 mg of polymeric reagent IV. Conditions: 35–95 °C; 3 min; 25- μ L injections of 1 mL of washing solvent (ACN); 70/30 (v/v) ACN/H₂O; 1.5 mL/min flow rate.

By adoption of an arbitrary, initial setting for temperature and time, a variety of solvents have been evaluated for optimum derivatization yield, including hexane, dioxane, methanol, and acetonitrile. Of these, acetonitrile, due to its good swelling property and solvability, consistently provided the highest percent derivatizations for all amine substrates. With ACN as the solvent, a mixture of propylamine and diethylamine was used to optimize off-line temperature/time conditions. The temperature was varied from 35 to 95 °C, while the reaction times were held constant at 3 min (Figure 2). The percent derivatization was proportional to the temperature, as expected for a heterogeneous reaction, where the rate of molecular collision is increased with temperature, leading to an increase in molecular diffusion and overall reaction rates.

With the temperature held constant at 90 °C, the reaction time was then varied from 1 to 30 min. The results (Figure 3) showed that the highest conversions of 94% for propylamine and 78% for diethylamine were obtained from 5 to 10 min at 90 °C. Percent derivatizations dropped about 10% beyond 15 min, probably due to a concomitant decomposition of the final derivatives at high temperature for a relatively long reaction time. The relatively lower percent conversion for the secondary amine may be caused by its steric hindrance and by the protonation from the medium. The percent conversion for the secondary amines can be improved by (1) increasing the reaction time at a relatively lower temperature and (2)

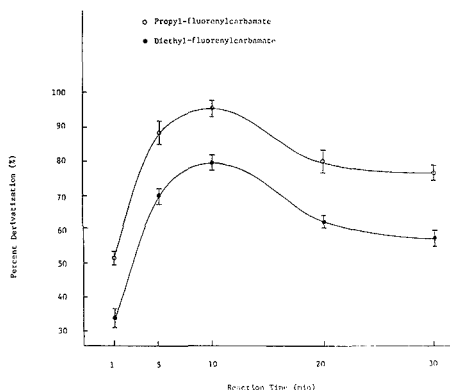


Figure 3. Optimization of reaction time for off-line solid-phase derivatizations of amines: reaction temperature, 90 °C; times, 1–30 min; all other conditions are as in Figure 2.

adding a competitive base (e.g. a small amount of triethylamine) into samples to catalyze the reaction. The final, ideal, practical derivatization conditions were acetonitrile solvent, at 60 °C, with a 5-min reaction time.

Percent Derivatization vs Amine Concentration. Most analysts assume that percent derivatizations are totally independent of concentration of the substrate and whether the amine substrates are derivatized together or separately. For solid-phase reagents, it has been shown that, at least for one particular silica-adsorbed reagent, percent derivatizations can change drastically with changes in substrate concentration (26). For other reagents, as here, such drastic differences were not observed. Off-line derivatizations have been performed with a mixture of propylamine and diethylamine in ACN, at 60 °C for 5 min. The percent derivatizations were constant, within experimental error, from 200 ppb (parts per billion) to 20 ppbth (parts per thousand) (67 fmol to 6.7 μ mol). This constancy must have been due to the relatively high concentration of tagging species per gram of polymer vs the absolute amounts of amines reacted. At an amine concentration of 20 ppth in each substrate, percent derivatizations dropped by about 20% from the original values. This may have been due to a localized depletion of the concentration of active reagent by the high concentrations of the amine substrates, thereby decreasing the overall reaction efficiency.

Calibration Plots for Amine Derivatives and Their Detection Limits. Calibration plots of 9-fluorenylmethyl carbamates (standard derivatives of amines) were constructed by using UV and FL detection in series. The concentration range was from 2 ppb to 20 ppm for both primary and secondary derivatized amines. Linear calibration plots were obtained within the given concentration ranges with a line correlation coefficient of 0.999. These calibration plots could then be used as the external standard method for the quantitation of amines. The detection limits of the 9-fluorenylmethyl carbamates obtained with FL at 265/320 nm (maximum excitation/emission wavelengths) and UV at 254 nm were 1.8 and 11 ppb, respectively. These detection limits were calculated by using a signal-to-noise ratio of 2/1.

Calibration Plots for Amines and Their Smallest Detectable Amounts. Calibration curves for on-line derivatizations of amines were also constructed to understand the concentration range of the amine over which the UV/FL detector responses would be linear. Amine concentrations (primary and secondary together) were prepared from 0.2 to 20 000 ppm, and derivatizations were carried out on-line in real time at 60 °C. The final calibration curves for each amine

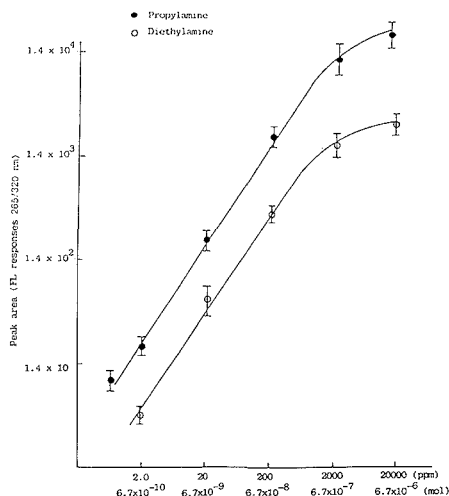


Figure 4. Calibration curve for on-line, precolumn derivatizations of typical amines: temperature, 60 °C, real time; amine mixtures of 0.2–20000 ppm; HPLC conditions, 60/40 ACN/H₂O; other conditions are as in Figure 2.

were constructed (Figure 4). The linear ranges for these curves were about 4 orders of magnitude of amine concentrations. The calibration plots of amine concentrations greater than 2000 ppm became nonlinear due to (1) localized depletion of the concentration of active reagent by the higher amine concentration and (2) highly dense amine coating the surface of the polymer bead and blocking further diffusion of analyte molecules into the polymer network. The upper limit could be improved by using a higher temperature and slower flow rate or by using a stop-flow technique.

Under optimized conditions, the minimum amounts of amines that could be both derivatized and chromatographically detected on-line, precolumn were found to be 34 ppb for propylamine and 60 ppb for diethylamine with the signal-to-noise ratio 3/1. Most analysts report the detection limits of the derivatives, rather than reporting the minimum detectable amounts of amine. However, it is more practical and meaningful to report the detectable amount of amine because the original analyte, amines in the sample, is of interest, not their derivatives. The sensitivity of the method is comparable with that in the literature (15–18).

Kinetic Study of Solid-Phase Reactions. Most analytical studies with new reagents for chromatography have not involved detailed kinetic studies for various substrates. One outstanding exception to this general rule was that by Barends et al. (27). We were interested in confirming relative percent derivatizations by certain traditional kinetic studies, as usually performed in physical-organic chemistry. Very little information is available regarding kinetic studies with heterogeneous derivatizations (14).

Solution amine FMOC-Cl (9-fluorenylmethyl chloroformate) derivatization reactions are second-order, because the reaction rate has been found to be proportional to both amine and FMOC reagent concentrations (28, 29). This fits the rate law principle (30). In our solid-phase situation, the amount of FMOC tag was very concentrated on the polymeric support. Using normal derivatization conditions and amounts of substrate (ca. 0.2 μmol), we found that the mole ratio of FMOC tag to amine was about 100–300:1, depending on the specific loading of reagent. We have made the normal assumption that the FMOC concentration changed little with

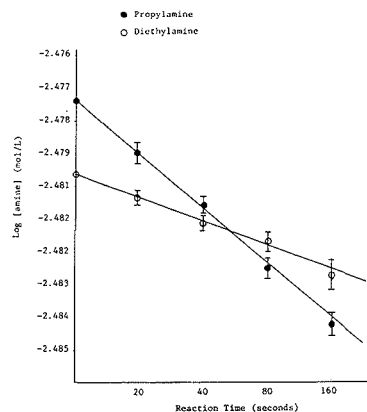


Figure 5. Kinetic study for off-line solid-phase derivatizations of amines: room temperature for 20, 40, 80, and 160 s; HPLC conditions are as in Figure 2.

low amine concentrations, and the rate of the overall reaction would then only depend on the amine concentration change. Under such conditions, the definition for a pseudo-first-order reaction would apply (31). Therefore, the general rate law expression could be written as

$$-d[\text{amine}]/dt = k[\text{FMOC}][\text{amine}]$$

for a second-order reaction in solution where k is a specific rate constant.

$$-d[\text{amine}]/dt = k_{\text{obs}}[\text{amine}]$$

for a heterogeneous, pseudo-first-order reaction where $k_{\text{obs}} = k[\text{FMOC}]$. After mathematical treatment of the above, we obtain

$$\log [\text{amine}]_t = (-k_{\text{obs}}/2.303)t + \log [\text{amine}]_0$$

$$Y = mX + b$$

$$-k_{\text{obs}}/2.303 = m = \text{slope}, \quad k_{\text{obs}} = -\text{slope} \times 2.303$$

A second assumption made was that 1 mol of an amine reacted or consumed 1 mol of the FMOC tag to form 1 mol of derivative. Therefore, the change or decrease in the mole concentration of amine, [amine], could be determined by following [carbamate] product formed. This was done by performing off-line kinetic studies followed by HPLC–UV/FL determination of the carbamate formed vs an external standard. If these assumptions were correct, a straight line would be obtained upon plotting the disappearance of [amine] or formation of [carbamate] vs time. The rate constant was then calculated according to the pseudo-first-order kinetic treatment, as above.

Another assumption made was that a mixture of primary and secondary amines would not influence each other's specific rate constants when compared with rate constants determined for each amine alone. Because these reactions appear subject to general base catalysis, e.g., with triethylamine (25), this initial assumption may not be entirely valid. In order to demonstrate this, we have physically measured the percent derivatizations for individual propylamine and diethylamine, alone and as a mixture. At the concentration levels usually used, within the linear range and within experimental error, differences of percent derivatizations between the individual amine and the amine mixture were insignificant. At much higher concentrations, differences in percent derivatizations

Table I. Specific Rate Constant Comparison for Reactions of Amines with FMOC-Cl in Solution, Polymeric Benzotriazole FMOC Reagent, and Polymeric *o*-Nitrobenzophenone FMOC Reagent^a

derivatizing reagent	specific rate constant, ^b s ⁻¹	
	<i>n</i> -propylamine	diethylamine
FMOC-Cl in solution	$(6.4 \pm 2.3) \times 10^{-2}$	$(2.8 \pm 1.6) \times 10^{-2}$
polymeric benzotriazole FMOC	$(6.2 \pm 2.0) \times 10^{-3}$	$(1.5 \pm 0.6) \times 10^{-3}$
polymeric <i>o</i> -nitrobenzophenone FMOC	$(5.2 \pm 1.8) \times 10^{-4}$	$(1.4 \pm 0.5) \times 10^{-4}$

^a Reaction conditions: room temperature (26 °C) for 20, 40, 80, and 160 s. See text for additional details. ^b The numbers are average \pm the standard deviation for $n = 9$. HPLC conditions: 60% ACN/H₂O, 1.5 mL/min, UV 254 nm, FL 265/320 nm.

with an analogous polymeric reagent have recently been observed (25). However, for very short reaction times, as here, and for low concentrations of amines vs the polymeric reagent concentration, differences in rate constants for the mixture of amines vs individual amines may be slight.

The final data (Figure 5) showed a slope that was used to calculate the specific rate constants. Different starting amine concentrations were used for these kinetic studies, and under identical reaction conditions, the same rate constant was always obtained. These initial studies were conducted with the polymer *o*-nitrobenzophenone fluorenyl reagent, IV. In order to compare the specific rate constants for different polymeric reagents having different linkages, we also performed this kinetic study with a polymeric benzotriazole fluorenyl reagent reported earlier (12). Basically, the tags on these two polymeric reagents were identical, but for the linkage arrangement and degree of reactivity toward amines. The final specific rate constants at room temperature are indicated in Table I.

The polymeric benzotriazole reagent had a rate constant that was more than an order of magnitude greater than that for the *o*-nitrobenzophenone reagent. It was also true that percent derivatizations for the same amines when the polymeric benzotriazole reagent was used were always at least twice that for the *o*-nitrobenzophenone. The data is internally self-consistent. It is possible that the benzotriazole ring has a greater electron-withdrawing inductive effect that makes the acyl carbon of the activated ester more susceptible to nucleophilic attack by amines. Patchornik et al. have discussed relative reactivities of these reagents in some depth, and they have come to the very same conclusions (14).

Kinetic Study for the Solution Reaction. Since this was apparently the first attempt to utilize any polymeric fluorenyl reagent for off-line or on-line derivatizations of nucleophiles, it was of interest to compare reactivities vs the analogous solution reactions (28, 29). We compared the polymeric benzotriazole reagent with the analogous solution reaction, using optimized solid-phase conditions for both reactions, but not optimized for solution reactions (12). Under those conditions, percent derivatizations for the solid-phase reaction were considerably higher. Here we have compared the literature optimized conditions for the solution reaction with our now optimized solid-phase conditions. The kinetic studies for both solution and heterogeneous cases were performed under the same solvent, time scale, and HPLC analytical conditions. Table I summarizes the specific rate constants for the solution reaction. It is apparent that the solution reaction was faster by about 1 order of magnitude than the polymeric benzotriazole reagent, and about 2 orders of magnitude faster than the polymeric *o*-nitrobenzophenone one. This may have been due to (1) the faster molecular diffusion of the reagents in solution, whereas in the heterogeneous

Table II. Regeneration of Exhausted Polymeric *o*-Nitrobenzophenone FMOC Reagent^a

reagent status	substrate	%
		derivatization ^b
fresh, newly synthesized	<i>n</i> -propylamine	55.2 \pm 3.2
	diethylamine	20.4 \pm 2.5
exhausted	<i>n</i> -propylamine	7.5 \pm 0.8
	diethylamine	3.3 \pm 0.4
regenerated	<i>n</i> -propylamine	51.3 \pm 2.8
	diethylamine	18.6 \pm 1.9

^a Reaction conditions: room temperature (27 °C) for 5 min, each amine at 20 ppm added to 30 mg of polymeric reagent, off-line, precolumn. Twenty-five microliters out of final 500 μ L injections. ^b The numbers are average \pm the standard deviation ($n = 9$). HPLC conditions were identical with those in Table I.

reactions, only the substrate can diffuse; (2) the solution reactions having been done in a basic medium, which catalyzed the reaction (28, 29). The solid-phase reactions were only done under neutral conditions in this study. However, about 1 order of magnitude increase in reaction rate was obtained when triethylamine was used as a catalyst for an analogous solid-phase reaction (25).

However, it should be noted that there are still many advantages in pursuing solid-phase reagents for derivatizations in HPLC in spite of their slower reactions than solution reactions. First, the reaction conditions for solid-phase reagents require shorter times and less solvent dilutions. Second, the final chromatograms for the solid-phase case are almost always similar, cleaner, and without any excess reagent peaks evident (Figure 6). Third, as indicated below, solid-phase reagents can be very easily and simply used on-line, precolumn, in a continuous manner at any practical temperature under reversed- or normal-phase conditions in real or delayed time.

Regeneration of the Spent Polymeric Reagent. All remaining studies were performed with the polymeric *o*-nitrobenzophenone fluorenyl reagent. As with any solid-phase reagent, prolonged, continuous usage for a given amount of material resulted in a gradual decrease in reactivity. Since only the activated ester linkage was consumed in reaction with amines, this left the activated phenolic site remaining on the polymeric support (Scheme I), compound III. It was possible to regenerate the spent polymeric reagent by using the last synthetic step employed to prepare reagent IV in Scheme I. To demonstrate this, we intentionally reacted a small amount of the polymeric reagent with high concentrations of amines (20 ppt) several times. The percent derivatization with this batch before intentional consumption of tag and that afterwards was measured under normal reaction and detection conditions. Table II indicates that the percent derivatization after expenditure of the tag was considerably lower than for the fresh reagent. Regeneration was then performed off-line (Experimental Section), and the newly regenerated reagent was immediately used for another derivatization reaction of the same amine substrate. The final reactivity, as evidenced by percent derivatization, was almost equal to that of the fresh reagent.

Shelf-Life Determination. Solution derivatizations usually involve a fresh preparation of the reagent at a known level each time it is to be employed. However, for polymeric reagents that might be allowed to sit on the shelf or in the freezer for prolonged periods of time in-between usage, it was of interest to demonstrate shelf-life stability. Percent derivatizations were determined immediately after synthesis of a fresh batch of the polymeric reagent and after it had been stored at room temperature on the laboratory shelf for various periods of time (Table III). The overall results suggested that there was no change in reactivity or percent derivatizations

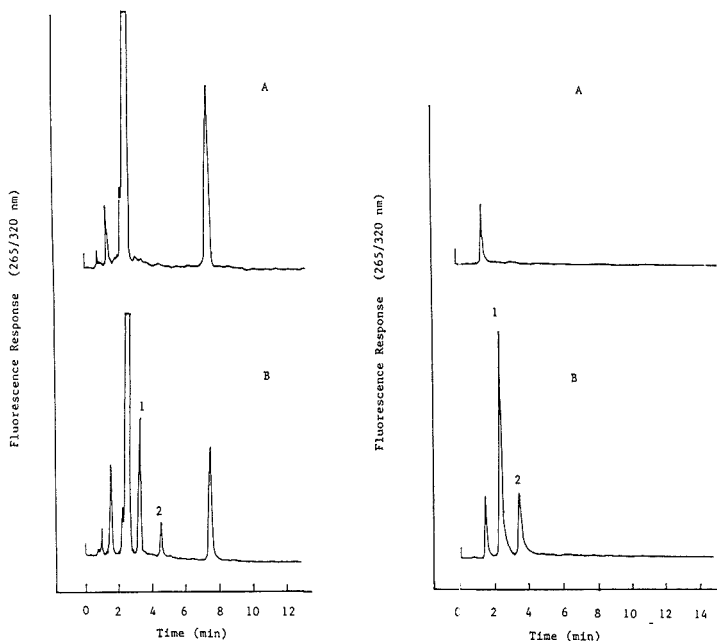


Figure 6. Comparison of chromatograms for solution (left panel) vs solid-phase (right) on-line, precolumn derivatizations of amines: A, blank injections; B, sample of amines; 1, propylamine FMOc derivative; 2, diethylamine FMOc derivative. Other conditions are as in Figure 2.

Table III. Determination of Shelf-Life Stability for Polymeric *o*-Nitrobenzophenone FMOc Reagent^a

storage status	substrate	% derivatization ^b
fresh, newly synthesized	<i>n</i> -propylamine	50.5 ± 2.6
	diethylamine	16.7 ± 2.1
2 months storage	<i>n</i> -propylamine	48.4 ± 2.8
	diethylamine	17.6 ± 1.9
4 months storage	<i>n</i> -propylamine	51.8 ± 3.2
	diethylamine	17.4 ± 2.0

^a Reaction conditions: room temperature (26 °C) for 5 min; other conditions were the same as those in Table II. ^b The numbers are average ± the standard deviation (*n* = 9). HPLC conditions were identical with those in Table I.

after at least 4 months of such storage. We have done another experiment in which the reactivity of the polymeric reagent was determined after it was stored in a freezer (-5 °C) for more than 1 year. There was very little change in its reactivity for the same substrate. Again, it shows one of the advantages in using solid-phase reagents over solution ones. Once the polymeric reagent is synthesized, there is no need to prepare fresh derivatizing reagent again for a long period of time, leading to savings in analysis time and expense.

pH Tolerance Range for the Polymeric Reagent. Any basic moiety in the mobile phase would be expected to cleave the tag, lead to elevated UV/FL base lines, and severely reduce the overall lifetime and usability of the reagents. We determined the usable pH range of a typical 70% ACN/H₂O mobile phase by adjusting the pH from 2.5 to 8.0 with borate buffer. Mobile phase was then pumped at 0.5-pH increments through the reagent precolumn, on-line in HPLC at 70 °C overnight. Changes in the base line were taken as an indication of reagent destruction, and the base lines were flat from pH 2.5 to 7.5. At a pH of 8.0 and above, there was a gradual

elevation in the base line until it went and remained off-scale.

Derivatization Recovery. All percent derivatizations should take into account percent recovery of the once-formed derivative from either the solution- or solid-phase reagent. The adsorption of the derivative by the solid beads would be a major concern. We have demonstrated this by purposely spiking several reaction cartridges containing the normal amount of polymeric reagent (30 mg) with amounts of standard derivatives (2 μmol) normally formed. The standard derivatives of both primary and secondary amines could be recovered from 90 to 100% when elution volumes of ACN from 100 to 1000 μL were used. This covered the usual elution volumes used for all off-line derivatizations, and the adsorption of the derivative by the reaction bed was slight. At lower levels of standard derivatives, perhaps in the range of real-world sample applications, we would expect quantitative recoveries, since it is easier to elute all of a smaller amount of derivative from the polymer bed.

Thermal Stability of the Polymeric Reagent. Because an elevated temperature was used in on-line derivatizations, we first demonstrated the relative stability of the polymeric reagent under prolonged, elevated temperature conditions in reversed-phase HPLC. A typical reaction column containing 120 mg of the polymeric reagent was kept in a water bath at 85 °C. A mobile phase of ACN/H₂O (70/30), pH 6.5, was pumped through the reaction column overnight. Percent derivatizations, on-line, were determined and compared with the analogous data before overnight treatment. Percent derivatizations for propylamine and band broadening were both the same, within experimental error. This was encouraging, in that it suggested that the reagent would be stable to repeated on-line derivatizations at elevated temperatures.

Band Broadening and Percent Derivatizations vs Temperature and Flow Rate. The reaction band broadening and percent derivatization vs temperature were determined on-line. A standard derivative of propylamine was

Table IV. Reaction Band Broadening and Percent Derivatizations for On-Line Polymeric *o*-Nitrobenzophenone Reagent as a Function of Temperature^a

temp, °C	substrate	% derivatization ^b	RBB ^c
25	<i>n</i> -propylamine	0.8 ± 0.3	135 ± 24
	diethylamine	0.2 ± 0.1	180 ± 23
45	<i>n</i> -propylamine	1.6 ± 0.6	104 ± 13
	diethylamine	0.4 ± 0.1	155 ± 17
65	<i>n</i> -propylamine	9.6 ± 1.1	84 ± 11
	diethylamine	1.8 ± 1.2	101 ± 13
85	<i>n</i> -propylamine	13.7 ± 1.5	65 ± 8.0
	diethylamine	3.4 ± 1.8	87 ± 10
95	<i>n</i> -propylamine	23.8 ± 2.3	29 ± 6.7
	diethylamine	8.3 ± 3.0	47 ± 5.8

^a Reaction-detection conditions: 10- μ L injection of the amine mixture 2 μ g of each amine; real-time detection. ^b The numbers are the average \pm standard deviation ($n = 3$). HPLC conditions were the same as those in Table I. ^c RBB is reaction band broadening in seconds squared.

injected with the solid-phase reactor precolumn and analytical column on-line, in order to determine the system band broadening (chromatographic vs reaction variance). The reaction band broadening was determined by subtracting the on-line formed derivative band broadening (variance) from just the system or chromatographic band broadening. System variance, in seconds squared, was calculated from the chromatographic peaks obtained according to the formula by Foley and Dorsey (32). The final data for percent derivatization and variance are indicated in Table IV.

Percent derivatizations were favored by higher temperatures, which increased the rate of bimolecular collisions between the solid-phase reagent and the analyte in solution. Mass-transfer increases eventually increased the rate constants, as above, and final percent derivatizations, on-line. According to the reaction band broadening (RBE) formula presented by Frei et al., the RBB was inversely proportional to the rate constant (33). Therefore, RBB decreases with increasing temperature, or increased rate constant, which was exactly the case here. It is possible that in our situation, RBB was partially caused by hydrogen bonding between the final derivative and the resultant phenolic groups formed on the polymeric reagent III in Scheme II. Increases in the temperature would then decrease the hydrogen bonding effect and lead to a decreased RBB.

It was apparent that a slower mobile-phase flow rate would increase residence times and increase overall rates and percent derivatizations. We have measured actual residence times within the precolumn reactor as a function of flow rates, using a flow injection approach. In this scheme, the reaction column was directly connected to the UV detector at room temperature, propylamine was injected, and its elution time was checked. The results indicated that by going from 0.5 to 2.5 mL/min flow rates, the residence times could change by 10 times (from 30 to 3 s); percent derivatizations (from 18.5 to 1.2%) and RBB (from 90 to 64 s²) both decreased with decreased residence times or increased flow rates. This was because, at lower flow rates, a longer residence time led to increased reactant collisions and greater conversion to product. Higher flow rates condensed elution of the final derivatives, once formed, and reduced diffusion of these within the reaction and separation columns, thus leading to decreased RBB. Although slow flow rates would be desirable from a percent reaction viewpoint, they are less desirable for RBB and analysis time requirements. Therefore, a compromise was made with a flow rate of 1.5 mL/min for the rest of these on-line, real-time derivatization studies. If the analyte is held in the reaction column at higher temperature for a longer time, improved percent

conversion and peak symmetry could be obtained.

Reproducibility of Amine Derivatizations On-Line via Repeat Injections. In order to demonstrate the reproducibility of derivatizations of amines, we have injected propylamine (0.2 μ g) into the same reaction column at 60 °C for 50 times. The percent derivatizations were $15.3 \pm 1.3\%$ ($n = 50$). Reaction band broadening was 74 s² for the first injection and 79 s² for the 50th. This was significant, because it proved that the reaction column could be safely used for trace level determinations over many repeat injections, leading to excellent precision and reproducibility of the derivatizations. Because we had a large reservoir of active labeling reagent present relative to the much smaller amounts of amines injected, percent derivatizations did not show any significant decrease. Using a theoretical calculation derived from the amount of polymeric reagent available, loading of the tagging species, and amount of tag consumed per injection of a given level of amine, we have estimated that typical columns could last for over 300 analyses. This means that a single column could be placed on-line, and as a function of the sample matrix and levels of nucleophiles present, it should be usable for hundreds of determinations without changing columns or conditions. That clearly lends the entire procedure of on-line precolumn and postcolumn solid-phase derivatizations, with at least these polymeric reagents, to automation of sample introduction, derivatization, separation, detection, and data accumulation.

Separation of a Mixture of Amine Derivatives. We were next interested in demonstrating that a variety of typical amines could be simultaneously derivatized by a single cartridge or precolumn of the polymeric reagent. In this study, four different amines (propyl, butyl, diethyl, and morpholine) were all reacted as a mixture, off-line and on-line, in real-time under optimized conditions, and derivatives were detected by HPLC-UV/FL. Typical chromatograms for the final derivative mixture are given in Figures 7 and 8. All four amines could be simultaneously derivatized and separated within 15 min in either approach. Base-line resolutions were possible with capacity factors between 3.3 and 7.5.

It is noticed that tailing peaks are realized from the chromatogram of on-line, real-time derivatization. In general, any on-line, real-time approach possessed both reaction and chromatographic/system band broadening, which was difficult to avoid, although it could be minimized. This is because the reaction may occur anywhere on the polymeric reagent, or the analyte reacts with the reagent all the way through the bed when the analyte is carried by the mobile phase. Peak tailing (band broadening) is then caused by the speed or sluggishness of the on-line reaction (kinetics). Though elevated temperatures could be used, this would only reduce, but not eliminate, reaction variance. However, we have developed a specific way to avoid or overcome the added reaction band broadening involved in these on-line reactions in HPLC, as described below.

Derivatizations of Standard Amphetamine and Detection Limits. As an application of this polymeric fluorenyl reagent to real-world samples, we chose to determine an amine-like drug, amphetamine, in human urine. This is a commonly abused drug often found in drug overdose cases, and current methods can use immunoassays, which are less than 100% specific. Current GC or HPLC approaches require some type of sample preparation and precolumn derivatization in solution to improve both chromatography and detection properties of the drug. We have accomplished off-line derivatizations of amphetamine after first releasing the free base by pH adjustment (Experimental Section). A single peak was observed, as compared with blanks run under identical conditions (Figure 9). The peak height for the suspected

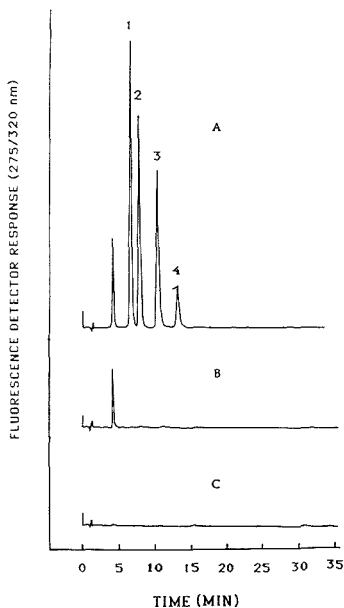


Figure 7. HPLC chromatograms for off-line solid-phase derivatization of a typical amine mixture. The amine mixture (0.02 μmol of morpholine, 0.01 μmol of other amines) was added to 30 mg of polymeric reagent at 25 $^{\circ}\text{C}$ for 3 min; 25 μL (total washing volume 1 mL of ACN) was injected. The mobile phase was 60/40 ACN/ H_2O ; other conditions are as in Figure 2. Key: A, chromatogram of amine derivatives; B, chromatogram of polymeric reagent blank (ACN as the solvent); C, chromatogram of amine solution without derivatization; 1, morpholine FMOc derivative; 2, *n*-propyl FMOc derivative; 3, *n*-butyl FMOc derivative; 4, diethyl FMOc derivative.

amphetamine derivative increased with increasing levels of amphetamine derivatized off-line. To determine small amounts of amphetamine existing in real-world samples, it was necessary to employ a delayed reaction time for the on-line mode. This involved a switching valve arrangement (Experimental Section). The minimum amount of amphetamine that could be detected by using this approach was about 0.1 ppm. This on-line approach was nevertheless quite effective, reproducible, fast and convenient; it produced symmetric peak shapes (no peak tailing) for the derivatives, together with a perfectly flat base line. This was because when the analyte was "staying" in the reaction column, higher temperatures and longer times not only favored the collisions of molecules, but also favored the diffusion of reactant(s) and product(s) in and out of the polymer network. The reaction was almost completed (85% conversion for propylamine at 60 $^{\circ}\text{C}$ for 5 min) and the product(s) was formed in that localized area in the reactor without continuous reaction through the bed. Sharp and symmetric peaks would be eluted as soon as the mobile phase flushed out the product(s) onto the separation column, as if a direct injection of the standard derivative(s) were made. Figure 9 illustrates a typical HPLC-FL chromatogram for a standard amphetamine injected under optimized conditions with on-line, precolumn derivatization.

Determination of Amphetamine in Human Urine with Standard Addition Methods. The only sample preparation was pH adjustment following filtration. A 5- μL aliquot of a urine sample was directly injected into the on-line derivatization-HPLC system. Standard addition methods were used for final quantitation because an authentic external standard of the amphetamine derivative was not readily available. Four

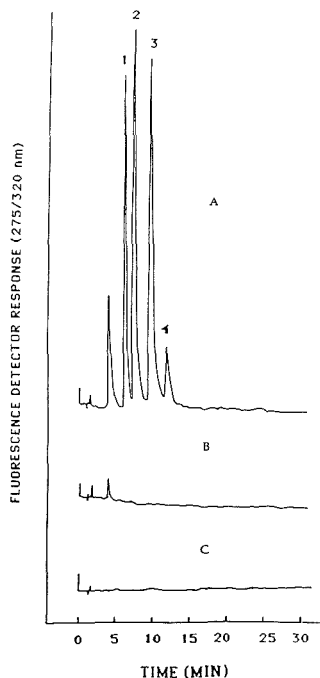


Figure 8. HPLC chromatograms for on-line, precolumn solid-phase derivatization of a typical amine mixture: amine mixture of 0.02 μmol in each, 60 $^{\circ}\text{C}$, real time; HPLC conditions as in Figure 7; A, chromatogram of amine derivatives; B, chromatogram of polymeric reagent blank; C, chromatogram of amine solution injected into dummy precolumn. The amines are numbered as in Figure 7.

Table V. Determination of Amphetamine Spiked in Urine Using Standard Addition Technique^a

spike level, ppm	found, ppm \pm SD ^b	% RSD ^c
52	48 \pm 3.2	7.6%
120	130 \pm 5.4	8.3%
137	140 \pm 6.7	2.1%
179	198 \pm 10.0	9.6%

^a Reaction-detection conditions: 60 $^{\circ}\text{C}$ for 5 min; HPLC conditions were the same as those in Table I. ^b ppm is parts per million; SD is standard deviation ($n = 3$). ^c Relative standard deviation = $(\text{SD}/X) \times 100$.

different concentration levels of amphetamine were determined. Table V summarizes the data for this application. Figure 10 illustrates a typical HPLC-FL chromatogram for a spiked urine sample with precolumn, on-line derivatization. Peak symmetry was excellent for the amphetamine in urine samples. For most of the results in Table V, the relative standard deviations (% RSD) were <10%, but these errors could be reduced with more careful sample handling, spiking, and injections of small volumes. Nevertheless, in most cases, the final values are acceptable and % RSDs are comparable to those of most other HPLC drug assays in common use today. Reproducibilities for these spiked urine samples were less than ± 10 SD units.

At present, most HPLC analyses for this drug require some type of initial analyte extraction with an organic solvent, derivatization off-line, and then injection into the HPLC system. The approach described here avoids extra sample preparation and solvent- or solid-phase extraction and allows

environmentally present amines (34).

CONCLUSIONS

We have demonstrated the synthesis and the evaluation of polystyrene-divinylbenzene-based, *o*-nitrobenzophenone-attached, labeling reagents containing *o*-acetylsalicyl or fluorenyl tags. Such reagents were designed for derivatizations of primary and secondary amines, on-line and off-line, in HPLC with UV/FL detection. Slower kinetics for these heterogeneous reactions, when compared with those of analogous solution reactions, could be offset by many other analytical figures of merit obtained by using these reagents. These particular polymeric reagents have exhibited good thermal and aqueous stability, high percent derivatizations, low detection limits for amines, fewer interferences in the final HPLC-UV/FL chromatograms compared with the analogous solution reactions, and faster quantitation of nucleophilic analytes via the on-line approach. Finally, the method has been shown practical and valid by its application to urine samples, with a minimum of sample preparation prior to direct injection into the on-line derivatization-HPLC system. Clearly, the newer approach is fully automatable, only requiring automated sample introduction instrumentation for repetitive sample determinations in the minimum time possible.

ACKNOWLEDGMENT

We acknowledge our colleagues for their technical assistance, discussions, and cooperation: C. Selavka, J. R. Yang, T. Baker, H. H. Stuting, B. D. Karcher, N. Grinberg, and S. Krzysko. Special gratitude is due A. J. Bourque, who synthesized the polymeric intermediate that was used as the starting material for these polymeric reagents.

The Model Spectronic 1201 scanning UV-vis spectrophotometer was donated by Milton Roy Corp./Analytical Products Division (formerly Division of Bausch & Lomb) through the valuable assistance of R. Jarrett and R. Flores. We acknowledge the donation to NU by Hewlett-Packard Corp. of an HP Model 1040A linear diode array spectrophotometer. A Hitachi Model D2000 ChromatoIntegrator was donated to NU by EM Science, Inc., through the gracious assistance of M. Gurkin and G. Desotelle.

LITERATURE CITED

- White, P. C. *Analyst* **1984**, *109*, 677.
- White, P. C. *Analyst* **1984**, *109*, 973.
- Krull, I. S.; Lankmayr, E. P. *Am. Lab. (Fairfield, Conn.)* **1982**, *14*, 18.
- Chemical Derivatization in Liquid Chromatography*; Lawrence, J. F., Frei, R. W., Eds.; Elsevier Scientific Publishing Co.: Amsterdam, 1976; pp 1-3.
- Cochrane, W. P.; Sternson, L. A.; Frei, R. W. In *Chemical Derivatization in Analytical Chemistry: Introduction, Volume 1*; Frei, R. W.; Lawrence, J. F., Eds.; Plenum Press, Inc.: New York, 1981; pp 1, 2.
- Krull, I. S.; Selavka, C. M.; Jacobs, W.; Duda, C. J. *Liq. Chromatogr.* **1985**, *8*(15), 2845.
- Blau, K.; King, G. *Handbook of Derivatives for Chromatography*; Heyden & Sons, Ltd.: London, 1977; pp 1-3.
- Xie, K.-H.; Colgan, S. T.; Krull, I. S. *J. Liq. Chromatogr.* **1983**, *6*(S-2), 125.
- Colgan, S. T.; Krull, I. S.; Dorschel, C.; Biddingmeyer, B. J. *Chromatogr. Sci.* **1988**, *26*, 501.
- Colgan, S. T.; Krull, I. S. In *Reaction Detection in Liquid Chromatography*; Krull, I. S., Ed.; Marcel Dekker: New York, 1988; Chapter 5.
- Chou, T.-Y.; Colgan, S. T.; Kao, D.-M.; Krull, I. S.; Dorschel, C.; Biddingmeyer, B. J. *Chromatogr.* **1986**, *367*, 335.
- Gao, C.-X.; Chou, T.-Y.; Colgan, S. T.; Krull, I. S.; Dorschel, C.; Biddingmeyer, B. J. *Chromatogr. Sci.* **1988**, *26*, 449.
- Chou, T.-Y.; Gao, C.-X.; Colgan, S. T.; Krull, I. S.; Dorschel, C.; Biddingmeyer, B. J. *Chromatogr.* **1988**, *454*, 69.
- Cohen, B. J.; Karoly-Hafeli, H.; Patchornik, A. *J. Org. Chem.* **1984**, *49*, 922.
- Abdel-Monem, M. M.; Merdink, J. L. *J. Chromatogr.* **1981**, *222*, 363.
- Skaaden, T.; Greibrokk, T. *J. Chromatogr.* **1982**, *247*, 111.
- Veening, H.; Pitt, W. W.; Jones, G. *J. Chromatogr.* **1974**, *90*, 129.
- Kai, M.; Ogata, T.; Harguchi, K.; Ohkura, Y. *J. Chromatogr.* **1979**, *163*, 151.
- Schwarz, V.; Deyl, Z.; Macek, K. *J. Chromatogr.* **1985**, *340*, 401.
- Jain, N. C.; Smeath, T. C.; Budd, R. D.; Olson, B. A. *J. Anal. Toxicol.* **1977**, *1*, 233.

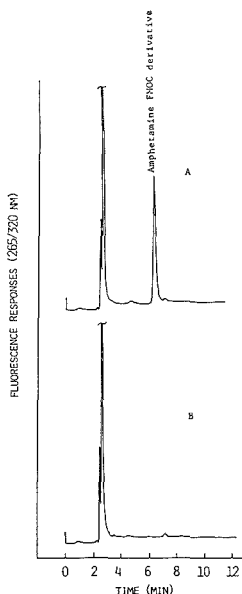


Figure 9. HPLC chromatogram of amphetamine standard: derivatized on-line, precolumn with polymeric reagent: amphetamine 100 ppm (pH = 10), 20- μ L injection, held at 60 °C for 5 min; 50/50 ACN/H₂O, 1.5 mL/min; other conditions as in Figure 2; A, sample; B, blank.

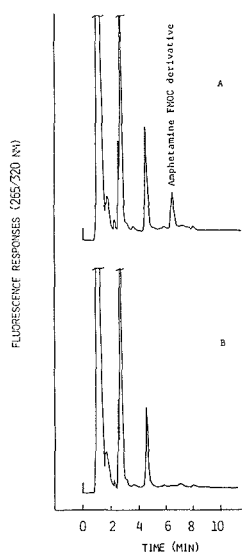


Figure 10. HPLC chromatogram of spiked amphetamine in urine, derivatized on-line, precolumn with polymeric reagent: amphetamine 52 ppm, 5- μ L injection; all other conditions as in Figure 9; A, urine sample; B, urine blank.

just filtration and direct injection. It is perhaps the *simplest* of all imaginable analytical schemes for this drug and many other drugs commonly found in biological fluids or tissues. We believe such a polymeric reagent is amenable to virtually all primary and secondary amine like drugs, as well as to

- (21) Nakahara, Y.; Sekine, H. *Chromatographia* **1984**, *19*, 131.
(22) Jane, I.; McKinnone, A.; Flannagan, R. J. *J. Chromatogr.* **1985**, *323*, 191.
(23) Slais, K.; Nielsen, M. W. F.; Brinkman, U. A. Th.; Frel, R. W. *J. Chromatogr.* **1987**, *393*, 57.
(24) Carpino, L. A.; Han, G. Y. *J. Org. Chem.* **1972**, *37*, 3404.
(25) Bourque, A. J.; Gao, C.-X.; Krull, I. S., unpublished results, Northeastern University, Boston, MA, 1987.
(26) Colgan, S. T.; Krull, I. S.; Dorschel, C.; Bidlingmeyer, B. *Anal. Chem.* **1986**, *58*, 2366.
(27) Barends, D. M.; Blauw, J. S.; Mijnsbergen, C. W.; Govers, C. J. L. R.; Hulshof, A. J. *Chromatogr.* **1985**, *322*, 321.
(28) Einarsson, S.; Solestad, S.; Josefsson, B.; Lagerkvist, S. *Anal. Chem.* **1986**, *58*, 1638.
(29) Einarsson, S.; Josefsson, B.; Moller, P.; Sanchez, D. *Anal. Chem.* **1987**, *59*, 1191.
(30) Petrucci, R. H. *General Chemistry*; 4th ed.; MacMillan: New York, 1982; pp 424-426.
(31) Lowry, T. H.; Richardson, K. S. *Mechanism and Theory in Organic Chemistry*, 2nd ed.; Harper & Row: New York, 1981; pp 180-181.
(32) Foley, J. P.; Dorsey, J. G. *Anal. Chem.* **1983**, *55*, 730.
(33) Nondek, L.; Brinkman, U. A. Th.; Frel, R. W. *Anal. Chem.* **1983**, *55*, 730.
(34) Gao, C.-X.; Krull, I. S.; Trainor, T. J. *Chromatogr.* **1989**, *463*, 192.

RECEIVED for review October 26, 1988. Accepted April 3, 1989. Financial assistance was provided by the Analytical Research Department, Pfizer Central Research, Pfizer, Inc., Groton, CT, and by an NIH Biomedical Research Support Grant to Northeastern University, No. RR07143, Department of Health and Human Services. This is contribution no. 377 from The Barnett Institute at Northeastern University.

Chiral Polymeric Reagents for Off-Line and On-Line Derivatizations of Enantiomers in High-Performance Liquid Chromatography with Ultraviolet and Fluorescence Detection: An Enantiomer Recognition Approach

Tzun-Yu Chou, Chun-Xin Gao, Nelu Grinberg,¹ and Ira S. Krull*

Department of Chemistry and The Barnett Institute, 341 Mugar Building, Northeastern University, 360 Huntington Avenue, Boston, Massachusetts 02115

Optically active and detector-sensitive polymeric reagents have been synthesized, loadings determined, derivatizations/separations/detection optimized, and applications to simple amines and amino alcohols described. Such reagents have been designed to contain different chiral centers, usually amino acids, leashed via an activated ester attachment to an insoluble, structurally rigid, organic polymer backbone. 9-Fluorenylmethyl (Fmoc) moieties chemically bonded to the amino acids were used as ultraviolet (UV) and fluorescence (FL) sensitive detector probes to the final diastereomers of enantiomer substrates. Such diastereomers can be readily separated by isocratic or gradient elution normal-phase methods. The kinetics for diastereomer formation have been determined, and final UV/FL responses for known mixtures of enantiomers have been compared to demonstrate overall validity of the method. Minimum detection limits, linearity of calibration plots, dual detector responses, and linear diode array spectra and absorbance ratios have also been demonstrated. In some cases, authentic standards have been prepared to calculate absolute percent derivatizations for specific enantiomer pairs. The overall approach permits, for the very first time, off-line or on-line precolumn derivatization for the formation of diastereomers having unique detector properties. It has been proven that the rates and rate constants for such formations are identical for at least those pairs of enantiomers studied. Separations are base-line or near-base-line, permitting accurate and precise quantitative determinations, by both UV and FL, of enantiomer/optical purity and chemical purity.

* Author to whom reprint requests and correspondence should be addressed.

¹ Current address: Analytical Research Dept., Merck Sharp & Dohme Research Laboratories, Inc., P.O. Box 2000, Rahway, NJ 07065.

INTRODUCTION

At present, there is much interest in resolving and quantitating biologically active enantiomers in the fields of pharmaceutical, biochemical, and biotechnology research and production. The importance of resolving these enantiomers is well-known in many publications (1-3). It has been shown for many years that, besides classical methods for separation of racemates, e.g., fractional crystallization of the enantiomers or diastereomeric intermediates, direct separations of enantiomers by high-performance liquid chromatography (HPLC) or thin-layer chromatography (TLC) can be a very powerful tool. At least three main approaches have been described for HPLC enantiomer resolutions: (1) an indirect method of achiral mobile phase and achiral stationary phase with diastereomers formed off-line, in precolumn derivatizations or in situ or on-line (precolumn), all via solution reactions; (2) a direct method of chiral stationary phase with achiral mobile phase for original enantiomers; and (3) a direct method of achiral stationary phase with chiral mobile phase for original enantiomers.

Commercially available chiral columns and mobile phases have been introduced, as well as solution chiral derivatization reagents (4-7). Even chiral ion-pairing reagents have been successfully used with normal- or reversed-phase type packings for enantiomer resolution, but this is actually a form of temporary diastereomer formation in the mobile phase (8). Many optically active mobile-phase additives have been introduced, often by using ligand-exchange chromatography, at times with an amino acid and copper as the metal (9, 10). Immobilized, chiral amino acids have also been used for ligand-exchange resolutions, again with a metal in the mobile phase (11-15). HPLC solution derivatizations for improved detection of chiral molecules have also been extensively reported and reviewed (16-20). Many of these chiral derivatizing reagents are commercially available, neat or in solution, and it is quite com-

monplace to perform off-line reactions prior to chromatographic analysis. Thus, virtually all chiral derivatizations leading to diastereomers of the original enantiomers prior to HPLC or TLC, are still performed off-line, using solution reagents (21-23).

Each of the above approaches in HPLC has advantages and disadvantages. None are ideal, and too often one method will work with one class of enantiomers, but not with others. There are still no clear-cut rules that can be easily applied to determine exactly which derivatization reagent, chiral mobile phase, or chiral stationary phase should work with a particular pair of enantiomers. There are no computer programs that can yet be used to predict just which HPLC separation approach will work for a given enantiomer pair.

There have been no reports of any solid-phase reagents leading to improved detection and enantiomer recognition for chiral substrates in chromatography. It would be quite useful to undertake the off-line and on-line, precolumn solid-phase derivatization of enantiomers with HPLC separations of the resultant diastereomers. In the design of the particular polymeric derivatizing reagents used, final diastereomers might be detected at trace levels by both ultraviolet (UV) and fluorescence (FL).

Some solid-phase or supported reagents have been successfully used for batch-type synthetic reactions leading to specific products, but without any HPLC derivatizations (24-28). Most recently, attempts have been made to utilize solid-phase reagents in a continuous mode, especially via immobilized enzymes for highly specific, catalytic chemical conversions (29). It is only within the past 10 years that analytical chemists have been attracted to the possible uses of solid-phase reagents for improved derivatization related to HPLC. We and others have described the significant advantages possible in using this newer approach to achiral derivatizations in analytical chemistry and HPLC (30-37).

Solid-phase chiral derivatizations, off-line or on-line, in HPLC appear to offer some significant advantages, such as (1) applicability to a wide range of substrates including amino acids, amines, polyamines, catecholamines, peptides, proteins, polypeptides, nucleosides, nucleotides, nucleic acids, etc., with a minimum of sample handling and HPLC optimization; (2) usefulness with conventional, high-efficiency normal- and reversed-phase stationary phases, avoiding the use of often expensive, low-efficiency chiral stationary phases; (3) usefulness with low-cost, high-purity, readily available achiral mobile phases having low detector noise properties; (4) improved detector properties of the diastereomers formed by the inclusion in the derivatization reagent of suitable chromophores, fluorophores, and/or electrophores; (5) potential for automation, since the on-line reagents could be made into a precolumn for the analytical-separation column; (6) reduced expense as compared with chiral columns or chiral solvents; (7) potential for disposable, off-line cartridges that could be used once or several times; (8) highly loaded on-line cartridges that could be used for many repetitive resolutions, especially at trace, analytical levels. Finally, these particular polymeric chiral reagents in HPLC could conceivably be used for all classes of strong nucleophilic substrates, chiral or achiral, and provide chemical purity, as well as enantiomeric/optical purity, where possible for enantiomeric substrates.

This work describes an entirely new experimental approach for the determination of enantiomeric purity and composition, as well as chemical purity, of virtually all "strong" nucleophiles, such as primary and secondary optically active amines and amine-like analogues. Such organics could include peptides, amino acids, catecholamines, amino alcohols, polyamines, aminoglycosides, and virtually any drug or bioorganic that contains, somewhere within its structure, either a primary or

secondary amine group. These particular reagents have not been successful for "soft" nucleophiles, such as alcohols, thiols, carboxylate anions, etc. The overall approach has utilized a polymer covalently attached to a chiral molecule, such as an amino acid, to which was covalently bonded a detector-sensitive molecule, such as the 9-fluorenylmethyl moiety (FMOC). Other tags should be just as feasible, such as: *o*-acetylsalicyl, naphthyl, fluorescein, or any other UV/FL/EC (electrochemical) sensitive probe. The chiral detector probe portions were attached to the polymeric support through an activated ester linkage, which was readily susceptible to nucleophilic attack.

Reactions with suitable amine substrates, off-line or on-line, under very mild reaction conditions of solvent, time, and temperature, have resulted in the almost quantitative formation of the expected diastereomers, which could be separated by isocratic or gradient elution, normal-phase conditions. Multidetector of the once-separated diastereomers has been accomplished by using series UV/FL detectors. The peak heights or peak areas of the final diastereomer peaks, having equal detector responses, were direct measures of the original enantiomeric composition and optical purity.

This approach represents a totally general methodology for the widespread solid-phase-reagent, indirect determination of both chemical and enantiomeric purities, with high-sensitivity detection possible. Though the method has been used thus far for chiral amine substrates, it is clear that other classes of nucleophiles will prove suitable, whether these be chiral or achiral.

EXPERIMENTAL SECTION

Chemicals, Reagents, and Solvents. The starting polymer, a copolymer of 96% styrene-4% divinylbenzene (200-400 mesh), was obtained from Fluka Chemical Co. (Buchs, Switzerland). FMOC-L-proline (98.8% optical purity) and FMOC-L-phenylalanine were purchased from Chemical Dynamics Corp. (South Plainfield, NJ). Dicyclohexylcarbodiimide (DCC), (S)-(-)/(R)-(+)-methylbenzylamine, (S)-(-)/(R)-(+)-1-naphthylethylamine, (\pm)-1-methylheptylamine, (S)-(+)/(\pm)-2-amino-1-butanol, and (R)-(-)/(\pm)-1-amino-2-propanol were obtained from Aldrich Chemical Co. (Milwaukee, WI). Other chemicals used were obtained from Aldrich, Burdick & Jackson Laboratories, Inc. (Muskegon, MI), J. T. Baker Chemical Co. (Phillipsburg, NJ), Alfa Products (Danvers, MA), and Sigma Chemical Co. (St. Louis, MO). These chemicals were of the highest purity available and were used without further purification, but were checked for purity, at times, before use. HPLC solvents were obtained from EM Science, Inc. (Cherry Hill, NJ), as their Omnisol HPLC grade.

Apparatus. The HPLC system consisted of a Waters Model 6000A solvent delivery system, a Rheodyne Model 7010 injection valve, and a Brown, Boveri & Co. Model SE 120 dual pen recorder (Metrawatt/Goerz Division, Vienna, Austria). Chromatographic columns consisted of an EM Science LiChroCART HPLC cartridge system of a LiChrospher Si-60, 250 mm \times 4 mm i.d., 5 μ m, and a semipreparative LiChrosorb Si column, 10 mm i.d. \times 25 cm, 7 μ m. The detectors included a Waters Model 480 variable wavelength UV detector and a Hitachi Model F1000 fluorescence spectrophotometer and a Hitachi Model D-2000 integrator. The instrumentation used to characterize the isolated, authentic standards was described in our publication (36).

Preparation of Polymeric FMOC-L-Proline Reagent. The preparation of the intermediate, polymer-bound 4-hydroxy-3-nitrobenzophenone was described in the preceding article in this issue (37). FMOC-L-proline (5.0 g, 14.8 mmol), compound in Figure 1, (reported melting point, 114-116 °C; measured melting point, 114-115 °C; optical rotation reported, $[\alpha]_D^{20}$ -33.9°; measured, -31 \pm 2.5°; 98.8% optical (purity) was dissolved in 25 mL of dichloromethane. The solution was cooled to 0 °C, and 14.8 mmol of DCC was added. After 30 min at 0 °C, the mixture was filtered into the boiling flask containing 2 g of polymer-bound 4-hydroxy-3-nitrobenzophenone, I. Pyridine (2 mL) was added, and the mixture was shaken for 1 h at room temperature. The

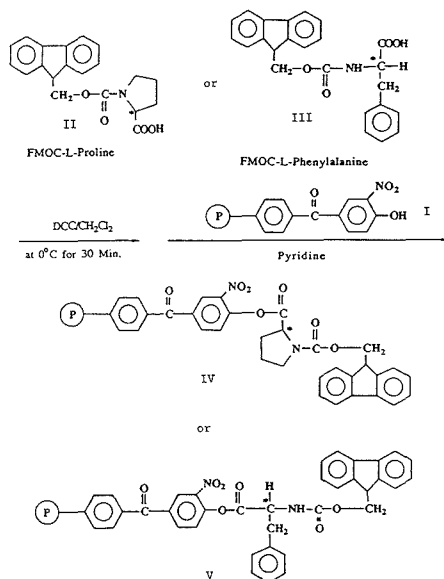


Figure 1. Synthetic scheme for preparation of polymer-bound 4-hydroxy-3-nitrobenzophenone containing FMOC-L-proline, IV, and FMOC-L-phenylalanine, V.

polymer was washed with chloroform (3 × 200 mL) and hexane (3 × 200 mL) and dried under vacuum. The polymeric FMOC-L-proline chiral reagent (2.1 g), IV, was collected. The same procedure was followed as described above for the synthesis of the polymeric FMOC-L-phenylalanine reagent, V.

Characterization of FMOC-L-Proline Chiral Reagent. 1. Hydrolysis Method. The polymeric FMOC-L-proline reagent (100 mg), IV, was suspended in a solution of 10 mL of dioxane and 10 mL of NaOH (0.1 N) and refluxed for 3–4 h. The solution was then neutralized with HCl (0.1 N), and 20 mL of this solution was injected into the HPLC. A fluorenylmethanol peak was seen when compared with the external standard. Since fluorenylmethanol was not stable to base hydrolysis conditions (35, 37), a portion of fluorenylmethanol remained in solution after the base hydrolysis reaction. This was checked by following experiments.

Fluorenylmethanol in two portions (2.5 and 5.0 mg) was base-hydrolyzed by following the same procedure as above. The percentages of fluorenylmethanol remaining after hydrolysis, calculated from an external standard of fluorenylmethanol, were 1.2% and 1.3%, respectively. By use of these conversion factors, the loading of the chiral reagent was calculated to be 0.46 and 0.43 mequiv/g. The HPLC conditions were as follows: 11% 2-propanol/hexane; 0.65 mL/min; 20- μ L injection; LiChrospher Si-60, 250 mm × 4 mm i.d. (5 μ m); FL 275/315 nm.

2. Elemental Analysis Method. The elemental analysis was performed at Galbraith Laboratories, Inc. The results were 80.61% C, 6.32% H, 2.28% N, and 6.75% O for the intermediate and 79.96% C, 6.13% H, 2.33% N, 8.73% O for the final reagent. The loading based on oxygen was calculated as follows:

$$\frac{(8.73 - 6.75) \text{ mg of O}}{100 \text{ mg of polymer}} \times \frac{\text{mmol of O}}{16 \text{ mg}} \times \frac{\text{mmol of tag}}{3 \text{ mmol of O}} \times \frac{1000 \text{ mg}}{\text{g}} = 0.41 \text{ mequiv/g}$$

This number agreed well with that obtained by the hydrolysis method.

Procedures for Off- and On-Line Derivatization Reactions. Procedures for off-line and on-line derivatization reactions were described in our previous reports, ref 36 and 37, respectively. A diagram of the instrumentation for on-line derivatization HPLC-UV/FL detection system is shown in Figure 2.

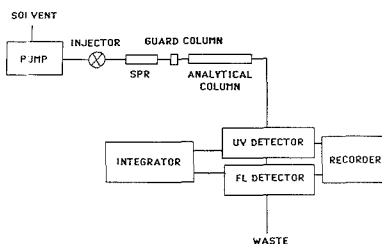


Figure 2. Schematic diagram of the instrumentation used for on-line derivatization reactions with the polymeric chiral reagents.

Table I. Physical and Spectral Properties of FMOC-L-Proline Derivatives of *l*- and *d*-Methylbenzylamines

property	<i>l</i> -diastereomer	<i>d</i> -diastereomer
mp	115–118 °C	117–120 °C
ϵ_{max} (266 nm) ^a , cm ⁻¹ M ⁻¹	1.71 × 10 ⁴	1.66 × 10 ⁴
retention time ^b	14 min 48 s	16 min 48 s
mw	440	440
mass spectra, ^c	441 (M + 1) ^{Cl}	441 (M + 1) ^{Cl}
<i>m/z</i>	337	337
	259	259
	247	247
	219	219
	207	207
	187	193
	179 (base peak)	179 (base peak)
	133	133
	115	115
	105	105
NMR spectra ^d	NA	1.9 ppm, d, 3 H
		2.4 ppm, s, 1 H
		3.3–3.6 ppm, m, 4 H
		4.1–4.6 ppm, m, 6 H
		5.1 ppm, s, 1 H
		7.1–7.8 ppm, m, 13 H

^aThe UV spectra were obtained on a Perkin-Elmer Model Lambda 2B UV-vis spectrophotometer, and the molar absorptivities at 266 nm were calculated on the basis of Beer's law. ^bHPLC conditions: LiChroCART HPLC cartridge, 250 mm × 4 mm i.d., LiChrospher Si-60 (5 μ m), 12% 2-propanol/hexane (v/v); flow rate, 0.7 mL/min. ^cChemical ionization (CI) mass spectra were obtained on a Finnigan 4000 mass spectrometer. ^dChemical shifts are in ppm (parts per million) from TMS (0 ppm): s = singlet, d = doublet, m = multiplet.

Synthesis, Isolation, and Characterization of External Standards of FMOC-L-Proline Derivatives of *d*- and *l*-Methylbenzylamines. 1. Synthesis. FMOC-L-proline (8.25 mmol, 2.78 g) was dissolved in 30 mL of dichloromethane. The solution was cooled to 0 °C, and 8.25 mmol of DCC was added. After 30 min at 0 °C, the mixture was filtered into a flask containing an equimolar mixture of *d,l*-methylbenzylamines (6.2 mmol) with pyridine (1.5 mL) added. The mixture was shaken for 1 h at room temperature.

2. Isolation. The solution containing diastereomers was injected into a semipreparative, EM Science LiChrosorb Si column under the following conditions: mobile phase, 12% 2-propanol/hexane; flow rate, 1.5 mL/min; injection volume, 200 μ L; UV at 266 nm; *d*- and *l*-diastereomers were collected separately.

3. Characterization. *d,l*-Diastereomer standards were characterized by melting point, UV, NMR, and MS. These were then used as external standards to determine the percent derivatizations of the same substrates with the polymeric chiral reagent. The physical and spectral characteristics of FMOC-L-proline standard derivatives of *d*- and *l*-methylbenzylamines are summarized in Table I. All of this data was consistent with the structures suggested, VI in Figures 3 and 4. The UV spectra of these authentic, external standards were also compared with those of

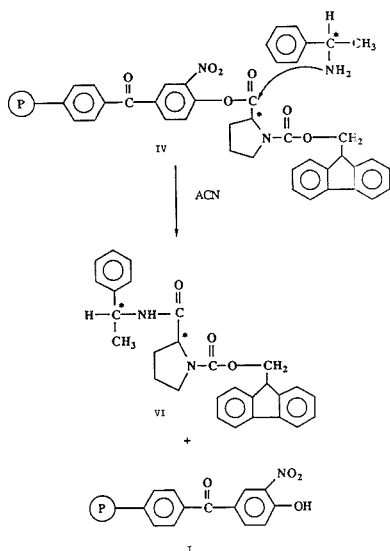


Figure 3. Derivatization reactions of *d,l*-methylbenzylamine with the polymeric FMOC-L-proline chiral reagent, IV.

the derivative peaks obtained via solid-phase derivatizations of the same *d,l*-methylbenzylamine, and identical UV spectra were realized.

Kinetic Study of *d,l*-Methylbenzylamines with FMOC-L-Proline Chiral Reagent. A mixture of *d*- and *l*-methylbenzylamine (5 ppm) was injected into a reaction pipette containing 40 mg of FMOC-L-proline chiral reagent. For each time interval (20, 40, 80, 120, and 160 s) at room temperature, the reaction products were washed into a volumetric flask with acetonitrile. The concentrations of unreacted *d,l*-methylbenzylamines at a certain time interval were calculated by using external standards of the *d*- and *l*-diastereomers. This assumed that the only reaction occurring was that of conversion of each enantiomer into its corresponding diastereomer. The same procedure was repeated three times, and all reaction products were injected three times ($n = 9$).

RESULTS AND DISCUSSION

Our work with this class of polymeric reagents followed a related work that involved polymeric benzotriazole activated esters as derivatization agents in HPLC (35, 36). Those reagents had incorporated an *o*-acetylsalicyl or 9-fluorenylmethyl tag and had been used exclusively as off-line reagents for simple amines or polyamines. No attempts were made to utilize such earlier reagents for diastereomer formation in HPLC via the inclusion of a chiral portion, though that would have been entirely feasible. Although the polymeric benzotriazole reagents had proven very reactive and effective for off-line derivatizations, all efforts to effect their use in an on-line mode, precolumn, met with failure because those reagents were too sensitive to moisture and temperature (36, 37).

We have chosen the particular polymeric backbone derived from the polymer-attached 3-nitro-4-hydroxybenzophenone, I, as the starting material for attachment of two chiral, detector-sensitive tags, FMOC-L-proline, IV, and FMOC-L-phenylalanine, V. These materials showed extreme reactivity and lability toward reactive nucleophiles because of the presence of electron-withdrawing groups (*o*-nitro, *p*-ketone) on the same ring as the activated ester function, and they were relatively stable at elevated temperatures (36, 37).

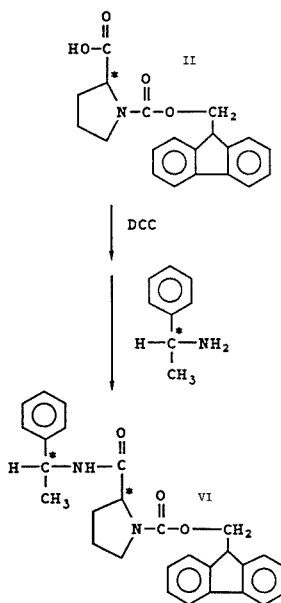


Figure 4. Synthetic preparation of the external standard diastereomers derived from *d,l*-methylbenzylamine and the FMOC-L-proline chiral reagent, IV.

We have recently completed both off-line and on-line derivatizations with achiral analogues of reagent IV, lacking a chiral center, where the 9-fluorenylmethyl group was directly attached to the hydroxy function in polymer I via its acid chloride (FMOC-Cl). That reagent has proven ideal for real- or delayed-time precolumn, on-line derivatizations of amine analogues in reversed-phase HPLC, with a successful application of on-line derivatizations of amphetamine in urine (37). That work is discussed in the preceding article in this issue. Though some of the basic synthetic steps in the preparation of intermediate I are identical, the rest of the syntheses, characterizations, derivatizations, and overall results are quite different, though still related. The reader is encouraged to read these companion articles in sequence.

Optimization of Derivatization Conditions Off-Line.

The loadings of the two polymeric chiral reagents, IV and V, have been determined by using base-catalyzed hydrolysis and quantitation of the fluorenylmethanol produced that survived reaction conditions. Elemental analyses were also obtained on the intermediate, I, as well as the final chiral reagents, IV and V. The results indicated a loading of about 0.40–0.45 mequiv of tag/g on the final polymer. This has been within the normal ranges reported for loadings on similar polymeric reagents (36, 37). The method of synthesis and formation of diastereomers of known structures, at least in the case of *d,l*-methylbenzylamine, were strong evidences of the assumed structures, IV and V.

It was important that the intermediates and final polymeric reagents were exhaustively solvent-washed (Experimental Section) so that the off-line blanks contained no potentially interfering peaks in the HPLC of the final diastereomers. Although two polymeric chiral reagents were prepared and evaluated, separations of the diastereomers derived from the L-phenylalanine-incorporated reagent, V, were less than ideal. Thus, V was eventually abandoned in favor of polymeric reagent IV, containing L-proline. The criteria for solid-phase

Table II. Percent Reaction of *d*-Methylbenzylamine as a Function of Temperature, Off-Line^a

temp, °C	% derivatizations ^b
25	72.2 (3.2)
40	78.6 (6.0)
50	70.2 (3.9)
60	62.4 (6.0)
70	38.7 (2.8)

^a *d*-Methylbenzylamine (0.413 μ mol) was reacted with 30 mg of polymeric chiral reagent IV for 10 min, at 25–70 °C. Dilution volume, 2 mL; injection volume, 20 μ L. HPLC conditions: 40% 2-propanol/hexane, 0.7 mL/min, LiChrospher Si-60, 250 mm \times 4 mm i.d. (5 μ m). ^b Numbers represent the average (\pm standard deviation) of three separate derivatizations; each reaction solution was injected three times ($n = 9$).

Table III. Percent Reaction as a Function of Reaction Time for Off-Line Derivatization of *d*-Methylbenzylamine^a

reactn time, min	% derivatization ^b
10	78.6 (6.0)
20	82.7 (4.5)
30	85.0 (5.8)
40	87.0 (4.2)

^a Reaction temperature: 40 °C; other conditions as in Table II. ^b Numbers represent the average (\pm standard deviation) of three separate derivatizations; each reaction solution was injected three times ($n = 9$).

derivatizations have involved the optimization of reaction conditions, including time, temperature, and solvent. In view of the optimization of the analogous polymeric achiral reagents and certain polymeric benzotriazole reagents, it was already apparent that ACN was an ideal solvent (36, 37).

Temperature and Time Optimization. Optimizations were performed using typical amine or amino alcohol substrates. No work has yet been undertaken with other amine analogues, such as amino acids, catecholamines, or chiral amine drugs, though these were obvious candidates. We have utilized, as elsewhere, a univariate system optimization scheme to reach optimal derivatization conditions. Because we had authentic standard diastereomers from *d,l*-methylbenzylamine, absolute percent derivatizations/reactions could be easily determined. In the case of the *d*-1-amino-2-butanol, no such authentic standard was available. We therefore used relative FL responses of the final diastereomers to indicate optimum conditions.

The reaction temperatures for off-line derivatizations of *d*-methylbenzylamine and *d*-1-amino-2-butanol were varied from room temperature to 70 °C, holding time constant at 10 min. For both compounds, the peak areas of the derivatives or percent reactions rapidly reached a maximum at 40 °C. With further increase in temperature, the peak areas or percent reactions decreased (Table II). This suggested that the reaction products may not have been stable at higher temperatures, and reactions under mild conditions were preferred. This same effect has been observed with related polymeric achiral reagents (37).

The optimum temperature of 40 °C was held constant as time varied from 10 to 40 min. The peak areas of the derivatives or percent reactions increased very little after 20 min (Table III). This suggested that the derivatizations were almost completed at that time and temperature. The final optimized conditions used for the off-line approach were 20 min at 40 °C.

Comparison of UV Spectra of Diastereomer Pairs. For this overall enantiomer recognition approach to be valid, each component of a given pair of diastereomers had to have

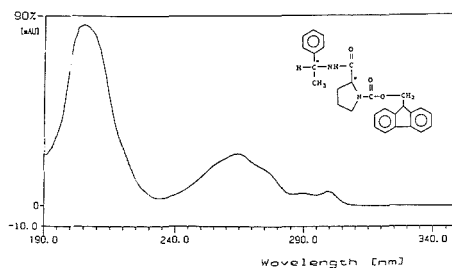


Figure 5. Linear diode array UV spectra of *d,l*-methylbenzylamine FMOC-L-proline authentic diastereomers formed in solution reactions, isolated by preparative HPLC, and characterized. Solid line represents *l*-diastereomer standard; dotted line is *d*-diastereomer standard.

identical UV and/or FL spectra, in every detail. Otherwise, authentic external standards of each pure enantiomer would be necessary to accurately determine optical purity. Only when detector responses are identical, in every regard, can relative peak heights or peak areas be taken to represent enantiomer composition. There were several methods to demonstrate if this were true or not. Known ratios of five enantiomer pairs of methylbenzylamine, naphthylethylamine, methylheptylamine, 1-amino-2-propanol, and 2-amino-1-butanol were separately derivatized off-line and chromatographically separated.

The UV spectra for each pair of diastereomers were separately obtained and superimposed by using an on-line linear diode array (LDA) UV detection system. The wavelengths of maximum absorbance, spectral shapes, and relative intensities of absorbance in the UV spectra for each diastereomer pair were similar, if not identical, which strongly suggested the UV properties for each pair of diastereomers were also similar, if not identical. However, UV spectra from one diastereomer pair to another could be quite different. All the diastereomers had maximum absorbance wavelengths at around 225 and 266 nm (Figure 5). The diastereomers of *d,l*-naphthylethylamine had an extra maximum absorbance wavelength at 225 nm. The above data strongly suggested that all of the enantiomer pairs studied to date formed diastereomers that had matching/identical UV spectra, in all respects. This was a necessary condition in order to eventually use fixed or variable wavelength UV detection for the final diastereomers formed off- or on-line. However, because we did not have exactly known ratios of enantiomers or each pure enantiomer of a given pair, except in two instances (*d,l*-methylbenzylamine and *d,l*-naphthylethylamine), further evidence for equal UV spectra and absorbance responses was desirable via authentic, external standards, in at least one typical amine case.

Molar Absorptivities of the Diastereomer Pair of Methylbenzylamine. Though the shapes of the UV spectra for the diastereomer pair of *d,l*-methylbenzylamine were indeed similar, this did not mean that the molar absorptivities were identical. The molar absorptivities for the diastereomer pair of FMOC-L-proline *d,l*-methylbenzylamine were separately measured by using a stand-alone UV spectrophotometer and authentic, external standards of each diastereomer isolated by preparative LC (Experimental Section). The molar absorptivities of the *l*- and *d*-diastereomers were 1.71×10^4 and $1.66 \times 10^4 \text{ cm}^{-1} \text{ M}^{-1}$, respectively, at 266 nm. The small difference was probably due to experimental error. Because of the difficulties involved in obtaining adequate, known amounts of each pure diastereomer via preparative LC, similar determinations with other diastereomer pairs were not performed. However, all of the above evidence, when taken collectively, strongly suggests that, at least for those enan-

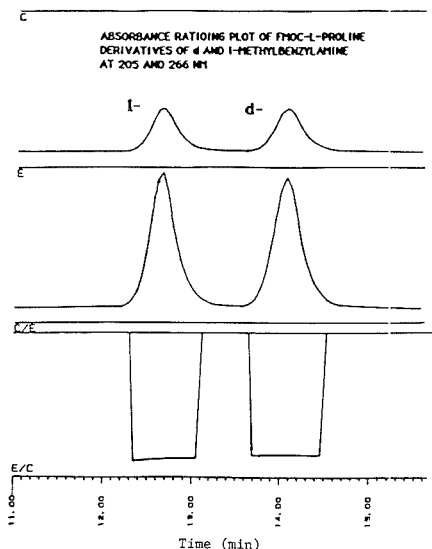


Figure 6. HPLC-linear diode array UV traces, 205 and 266 nm, monitored simultaneously for the off-line formation of FMOC-L-proline *d,l*-methylbenzylamine diastereomers; plot of dual wavelength absorbance ratios across each elution peak.

tiomer pairs studied thus far, they appear to form diastereomer pairs having identical UV spectra and extinction coefficients. It seems only fair to admit that it may very well be the case that there exist other enantiomer pairs that will form diastereomers with this particular polymeric reagent that will not have identical UV spectra and absorbance. An illustration of how and when this might happen is provided below in the case of the FL spectra for the FMOC-L-proline *d,l*-naphthylethylamine diastereomers.

Dual Wavelength Absorbance Ratioing of FMOC-L-Proline Derivatives of *d,l*-Methylbenzylamine. In order to demonstrate that chromatographically resolved diastereomers, formed off-line or on-line, were indeed chemically pure, we have used dual wavelength absorbance ratioing for a typical mixture (38, 39). The absorbances at two different maximum wavelengths, 205 and 266 nm, were monitored simultaneously. After the analysis, the ratios of these two signals were calculated and plotted (Figure 6). The ratios were constant over the entire widths of the two derivative peaks, confirming the assumed purity of each diastereomer. In every instance where this was determined for other diastereomer pairs, 100% purities were the case. Since diastereomer pairs had identical UV spectra, this approach could not be used to indicate 100% separation of such pairs. This could only be determined by chromatographic retention times or capacity factors.

Rates of Diastereomer Formations. Any determination of enantiomeric ratios using a derivatization approach may lead to false values, if the enantiomers have quite different rates in their reactions with another chiral molecule. As a result, the generation of two diastereomeric products in proportions (peak height/area ratios) different from the starting enantiomeric composition could occur (1, 7, 16). Kinetic studies of diastereomer formations with the polymeric reagent IV and *d,l*-methylbenzylamine were thus motivated by these reasons. Of course, though these rates may be identical for 100 pairs of enantiomers with this polymeric reagent, it does not mean that other pairs of enantiomers will have identical reaction rates.

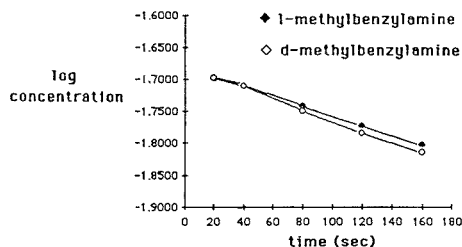


Figure 7. Kinetic plots of $\log [\text{amine}]_t$ vs time for off-line reactions of *d*- and *l*-methylbenzylamine with polymeric FMOC-L-proline chiral reagent, IV.

Table IV. Comparison of Determined and Actual Enantiomeric Compositions of *d*- and *l*-Methylbenzylamines as Synthetic Mixtures^a

<i>l</i> -methylbenzylamine, %	<i>d</i> -methylbenzylamine, %	% diff ^d
92.4 ^b (92.5) ^c	7.6 (7.5)	0.1
73.8 (73.5)	26.2 (26.5)	0.3
48.3 (49.6)	51.7 (50.4)	1.3
26.2 (25.5)	73.8 (74.5)	0.7
7.6 (6.5)	62.4 (93.5)	1.1

^a Conditions as in Figure 8. ^b Determined enantiomeric ratio. ^c Actual enantiomeric ratio. ^d % Difference = % determined composition - % actual composition.

Kinetic Studies of Diastereomer Formations via Solid-Phase Derivatizations. A design of the kinetic study of such heterogeneous reactions was illustrated in our publication (37). For the reaction of a pair of chiral amines with a chiral solid-phase reagent, the same treatment can be employed. By plotting $\log [\text{amine}]_t$ vs time and overlaying the lines for each enantiomer, we obtained the plots in Figure 7. These plots showed a slight difference between the two lines, since all the data points were simply connected by using Apple graphic software (Microsoft Chart) and no regression analysis was done. From a regression analysis using Apple statistics software (Statview), the regression line equations were obtained. The slopes of the two regression lines were identical with slight differences in their standard deviations. From the equations described in ref 37, the observed rate constants (*k*) for *l*- and *d*-methylbenzylamine were calculated to be $(2.30 \pm 0.03) \times 10^{-4}$ and $(2.30 \pm 0.05) \times 10^{-4} \text{ s}^{-1}$, respectively. Within experimental error, these data confirmed that the rates for diastereomer formations were identical. It should be emphasized, however, that though *d,l*-methylbenzylamine is perhaps a typical primary amine substrate, there may exist other enantiomeric substrate amines that will not have identical rate constants with this polymeric reagent, IV.

Comparison of Determined and Actual Enantiomeric Ratios of *d*- and *l*-Methylbenzylamine. Since the molar absorptivities (extinction coefficients) of typical *l*- and *d*-diastereomers and the rates of diastereomer formation were shown identical, the FMOC-L-proline chiral reagent, IV, was then used for final determinations of enantiomeric purity. It had apparently met most, if not all, of the suggested requirements for successful enantiomer recognition with a polymeric chiral reagent.

Mixtures of *d*- and *l*-methylbenzylamines of different compositions were derivatized off-line with FMOC-L-proline chiral reagent. A typical resultant chromatogram is indicated in Figure 8 for an approximately 50/50 ratio of the two original enantiomers. The peak areas of the two diastereomers formed were calculated with the Hitachi Model D-2000 integrator, and final enantiomeric ratios were determined. These de-

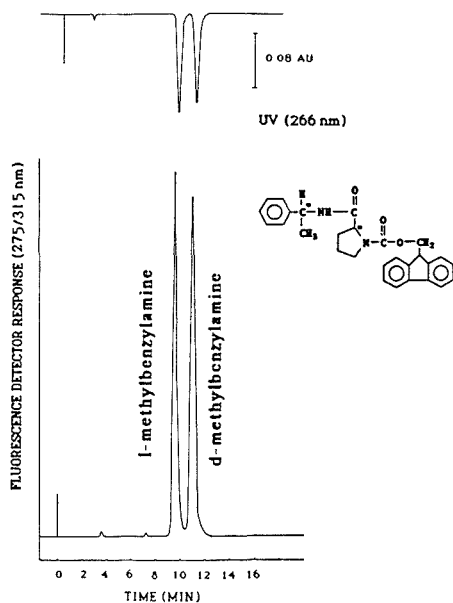


Figure 8. HPLC-UV/FL chromatograms for a typical 50/50 mixture of *d*- and *l*-methylbenzylamines derivatized off-line with FMOCC-L-proline chiral reagent, IV. Conditions: mobile phase, 10–20% 2-propanol/hexane, 20-min gradient, 0.7 mL/min; LiChrospher Si-60 column, 5 μ m, 250 mm \times 4 mm i.d.; FL 275/315 nm; UV 266 nm.

termined ratios were then compared with the actual, known enantiomeric ratios (Table IV). The differences between the determined and actual enantiomeric ratios agreed within 0.1–1.3%, which suggested that there was no racemization during reactions or racemization was small enough to be ignored. These results also confirmed the equivalences of the UV spectra and specific rate constants for these two diastereomers. That is, all of the data generated thus far was internally self-consistent.

Optimization of Reaction Temperature for On-Line Derivatizations of *l*-Methylbenzylamine. All of the results thus far have dealt with off-line polymeric derivatizations for enantiomers. As discussed elsewhere, on-line solid-phase reactions have some very important advantages for derivatizations precolumn or postcolumn in HPLC (30, 37). Of course, in the case of polymeric chiral reagents, only the on-line, precolumn mode would prove useful for enantiomer recognition. Reactions on-line, postcolumn for such reagents could only demonstrate chemical, not optical, purity.

Reaction temperature was an extremely important factor for all on-line derivatizations. Increasing the reaction temperature not only increased the percent reaction, but also reduced reaction band broadening (37). *l*-Methylbenzylamine (5 ppm) was directly injected into the on-line solid-phase derivatization HPLC system, in real time, at reaction temperatures varied from 25 to 75 °C. The percent derivatization reached the maximum (76%) at 75 °C (Table V). Although 34% conversion was realized at 40 °C, this was still chosen as a suitable condition for on-line derivatizations, because it was easier to operate at that temperature with good reproducibility.

Band Broadening (Variance) as a Function of Reaction Temperature for On-Line Derivatizations of *l*-Methylbenzylamine. The influence of the final reaction temperature on reaction band broadening was also studied

Table V. Percent Reaction as a Function of Temperature for On-Line Derivatizations of *l*-Methylbenzylamine^a

temp, °C	% derivatizations ^b
22	10.1 (1.3)
32	22.0 (1.1)
40	34.0 (4.1)
50	62.1 (8.2)
60	64.0 (5.4)
67	71.0 (3.5)
75	75.7 (4.1)

^a Conditions for on-line derivatizations: 20 μ L of *l*-methylbenzylamine solution (5 ppm) was injected directly into the HPLC, real time at 22–75 °C; 12% 2-propanol/hexane, 0.7 mL/min; LiChrospher Si-60, 250 mm \times 4 i.d. (5 μ m); reaction column dimensions, 28 mm \times 3 mm i.d. ^b Numbers represent the average (\pm standard deviation) of three separate injections ($n = 3$).

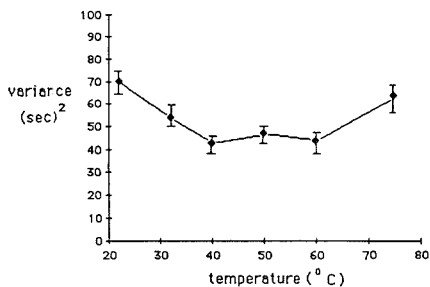


Figure 9. Plot of variance (σ^2) vs reaction temperature for the on-line derivatization of *l*-methylbenzylamine with polymeric chiral reagent IV. Conditions: 20% 2-propanol/hexane, 0.7 mL/min isocratic elution, 20- μ L injection, concentration of 5 ppm. Other conditions are as in Figure 8.

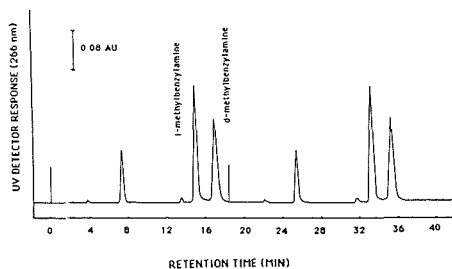


Figure 10. Repetitive, consecutive on-line derivatizations of *d,l*-methylbenzylamine enantiomers with polymeric chiral reagent IV. Conditions: 40 °C, real time, 12% 2-propanol/hexane, 0.7 mL/min, UV 266 nm. Other conditions are as in Figure 9.

by plotting variance (σ^2) vs reaction temperature (Figure 9). The variance decreased with increasing temperature from room temperature to 40 °C and remained constant from 40 to 60 °C. This suggested that the reaction band broadening was reduced to a minimum in the range of 40–60 °C, assuming system band broadening was independent of reaction temperature. The total variance increased at 75 °C, probably due to a trace impurity that overlapped in HPLC with the derivative peak.

Reproducibility Study for On-Line Derivatization of *d,l*-Methylbenzylamine. The reproducibility of on-line derivatizations was studied by consecutive injections of the same ratio of enantiomers of *d,l*-methylbenzylamine. A chromatogram for duplicate derivatizations at 40 °C of these enantiomers (0.5 μ g of each) is shown in Figure 10, with

Table VI. Reproducibility of Reaction Columns for On-Line Derivatizations of *d*- and *l*-Methylbenzylamine with the FMOC-*L*-Proline Chiral Reagent^a

reactn column	av peak height, ^b mm	
	<i>l</i> -enantiomer	<i>d</i> -enantiomer
1	60.8 (4.1)	43.6 (2.8)
2	58.8 (2.8)	40.6 (1.8)
3	60.0 (4.7)	41.8 (4.0)

^a *d,l*-Methylbenzylamine (4.1 nmol of each) reacted, on-line with the polymeric chiral reagent, VI, at 40 °C, real time; 12% 2-propanol/hexane, 0.7 mL/min; LiChroSpher Si-60, 4 mm i.d. × 25 cm (5 μm); UV at 266 nm. ^b Numbers represent the average (± standard deviation) of five separate derivatizations (*n* = 5).

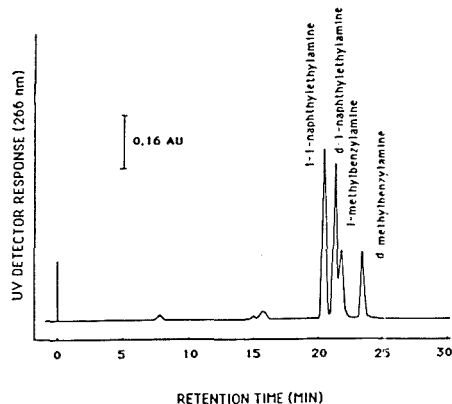


Figure 11. On-line precolumn derivatizations of *d,l*-naphthylethylamine and *d,l*-methylbenzylamine. The order of elution for each pair of enantiomers is as indicated. Conditions: mobile phase, 10–20% 2-propanol/hexane; gradient in 60 min; flow rate 0.7 mL/min; UV, 266 nm; injection amount, 12 nmol for *d,l*-naphthylethylamine and 3.3 nmol for *d,l*-methylbenzylamine, at 40 °C, real time.

conditions as indicated. Note that the derivative peaks were very symmetric (asymmetry factor = 1.14). Though only duplicate injections are illustrated, these were repeated at least five times (*n* = 5). Reproducibility figures (plus or minus standard deviations) were as in Table VI, fully acceptable for any on-line, precolumn derivatization approach in HPLC.

To validate the dry packing method we used to prepare the on-line reaction columns, three identical reaction columns were packed and on-line derivatizations were performed (Experimental Section). The reproducibility for these reaction columns was within ±3.3% (Table VI). This number was obtained as follows: (60.8 – 58.8)/59.9 × 100% = 3.3%, where 59.9 is the mean value of the peak heights.

On-Line Derivatizations of Enantiomeric Mixtures of *d,l*-Methylbenzylamine and *d,l*-1-Naphthylethylamine. A 20-μL solution of an enantiomeric mixture containing *d,l*-methylbenzylamine (0.4 μg of each enantiomer) and *d,l*-1-naphthylethylamine (2.0 μg of each enantiomer) was injected and derivatized on-line at 40 °C. The four diastereomers were separated and detected by UV (Figure 11). The *l*-diastereomer eluted earlier than the *d*-diastereomer for both *d,l*-naphthylethylamine and *d,l*-methylbenzylamine. Indeed, in all cases studied thus far, the *l*-diastereomer has always eluted first. The mechanism of diastereomer separations was probably due to the differential hydrogen-bonding interactions between the diastereomers and the stationary phase. By making space-filling molecular models, one can see that the *d*-diastereomers can sit better on the surface of silica gel. This

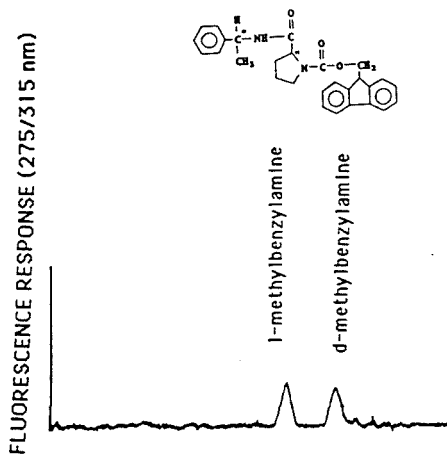


Figure 12. HPLC-FL chromatogram of a diastereomer pair derived from *d,l*-methylbenzylamine and FMOC-*L*-proline chiral reagent IV, at a concentration near the limit of detection (10 ppb each). Off-line derivatizations were performed. Conditions: derivatization volume, 50 μL; dilution volume, 2 mL; 10–20% 2-propanol/hexane gradient in 20 min; 0.7 mL/min; column, Alltech UltraSphere Si-60, 5 μm, 150 mm × 4.6 mm i.d.

would provide them with stronger hydrogen-bonding interactions than those of the *l*-diastereomers, and hence they eluted later. This order of elution can apparently be reversed by using a bonded stationary phase in place of bare silica gel, as below. The *d,l*-naphthylethylamine diastereomers eluted earlier than those from *d,l*-methylbenzylamine, since the former were more nonpolar and more soluble in the organic mobile phase.

Construction of Calibration Plots and Determination of Limits of Detection for Diastereomers of *d,l*-Methylbenzylamine. Calibration plots were constructed for authentic standards of the *d*- and *l*-methylbenzylamine diastereomers of FMOC-*L*-proline. From log concentration vs log peak height, line equations and plots were obtained with the correlation coefficient 0.999 (*r*) for both diastereomers. The concentration range for each diastereomer was 10–10000 ppb. The limits of detection determined by FL were 3.9 and 4.4 ppb, for *l*- and *d*-diastereomer, respectively, at a signal-to-noise ratio of 2/1. The chromatogram in Figure 12 shows a separation of a diastereomer pair at a concentration near the limit of detection (10 ppb each). These detection limits were comparable to those for the analogous solution derivatizations (16–23).

Separability of Diastereomer Pairs with Different Polymeric Chiral Reagents. Thus far, only derivatizations and HPLC detection of the final diastereomers, off-line or on-line formation, were performed with a single polymeric chiral reagent. That was derived from FMOC-*L*-proline (Figure 1, reagent IV), but another polymeric chiral reagent was prepared, that derived from FMOC-*L*-phenylalanine (Figure 1, reagent V). It was of interest to determine the effect of molecular rigidity at the chiral center on the separability of diastereomer pairs. To do this, the HPLC separabilities of the off-line formed diastereomers of *d,l*-methylbenzylamine using both polymeric FMOC-*L*-proline and FMOC-*L*-phenylalanine reagents were compared.

Several chromatographic conditions have been tried to separate the FMOC-*L*-phenylalanine diastereomers of *d,l*-methylbenzylamine and other amines, but most were unsuccessful. Most of these same conditions were successful, to

Table VII. Separation of Enantiomeric Amines and Amino Alcohols as Their Derivatives Formed from FMOC-L-Proline Chiral Reagent Using Isocratic HPLC Conditions

compound	k'	α	R_s	t_r
methylbenzylamine ^a	3.00/3.54	1.18	2.22	14.8/16.8
1-(α -naphthyl)ethylamine ^b	4.12/4.47	1.08	1.41	15.8/16.8
2-amino-1-butanol ^c	7.12/9.00	1.26	2.14	26.0/32.0
1-amino-2-propanol ^c	11.25/14.50	1.29	1.58	39.2/49.6
1-methylheptylamine ^d	2.00/2.36	1.18	1.11	8.4/9.4

^a Mobile phase was 12% 2-propanol/hexane, 0.7 mL/min. ^b Mobile phase was 11% 2-propanol/hexane, 0.7 mL/min. ^c Mobile phase was 18% 2-propanol/hexane, 0.7 mL/min. ^d Mobile phase was 10% 2-propanol/hexane, 0.8 mL/min. Other conditions for α - d : column, LichroCART HPLC cartridge, 250 \times 4 mm, Lichrospher Si-60, 5 μ m; UV at 266 nm. All diastereomers were formed off-line using optimum derivatization conditions of 40 °C and 20 min in ACN. Terms used: k' = capacity factor; α = alpha values = ratio of k' 's; R_s = resolution factor; t_r = retention time in minutes.

varying degrees, with the FMOC-L-proline diastereomers. It was of interest to determine why the replacement of proline by phenylalanine made the separation of its diastereomers more difficult. In all cases, we found the FMOC-L-phenylalanine derivatives were retained longer than FMOC-L-proline derivatives on a reversed-phase column; the reverse occurred on a normal-phase column. This suggested that the FMOC-L-phenylalanine derivatives were more hydrophobic than FMOC-L-proline derivatives, which agrees with their structures. The differences in separability between FMOC-L-phenylalanine and FMOC-L-proline diastereomers were possibly due to the differences in rigidity of the chiral amino acid. L-Proline has a much more rigid structure at the chiral center than L-phenylalanine. Its diastereomers exist in very different, more rigid conformations and exhibit much different interactions with the stationary phase, assuming about equal mobile-phase solubilities. Thus, the FMOC-L-proline diastereomers were more easily separated, but the FMOC-L-phenylalanine diastereomers were not. Similar arguments have been made in the literature by others involved in chromatographic resolutions of enantiomers and diastereomers (1, 16, 41).

Chromatographic Data (k' , t_r , R_s , α) for Enantiomeric Amines and Amino Alcohols. We have evaluated many different HPLC conditions for the eventual separation of the diastereomers derived from FMOC-L-proline described above. The enantiomer pairs studied here can all be resolved by using normal-phase, isocratic, or gradient conditions. Table VII summarizes the HPLC data for some typical amines and amino alcohols under isocratic conditions. The resolutions for each diastereomer pair are close to base-line resolution except for d,l -methylheptylamine. This was predictable, since this particular amine shows the least rigidity of all those studied, and its diastereomers probably interact most closely/similarly with the stationary and mobile phases. The resolution of the d,l -methylheptylamine enantiomers may be improved by further optimizing of chromatographic conditions.

Table VIII summarizes the analogous HPLC data for the same substrates under gradient normal-phase conditions. Thus, one has the option, depending on instrumentation availability, of using either isocratic or gradient elutions in normal-phase HPLC, though one might now predict more facile resolutions of these diastereomers in the isocratic elution mode. It may be that gradient conditions do not allow the subtle chromatographic differences between pairs of diastereomers to come into play sufficiently, and thus isocratic conditions seem to offer improved α values and resolutions.

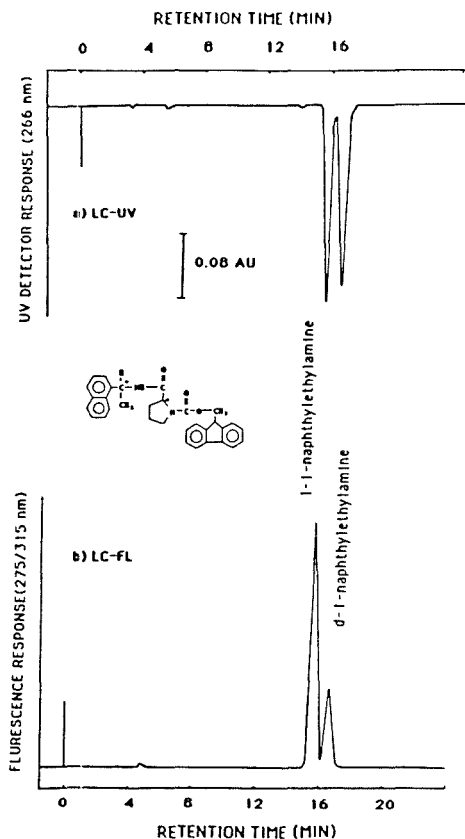


Figure 13. HPLC-UV/FL chromatograms for a 50/50 mixture of the diastereomers of d,l -naphthylethylamine, derivatized off-line with the polymeric chiral reagent IV. Conditions: 11% 2-propanol/hexane, 0.7 mL/min. 1 ppt for each enantiomer; derivatization volume, 50 μ L; dilution volume, 2 mL; injection volume, 20 μ L. Other HPLC conditions are as in Figure 9.

Comparisons of LC-UV and LC-FL Chromatograms for FMOC-L-Proline Derivatives of d,l -Methylbenzylamine and d,l -Naphthylethylamine. In all HPLC-UV studies obtained thus far with a variety of diastereomers derived from the FMOC-L-proline chiral reagent, with known ratios of enantiomers, the expected UV peak heights/areas were obtained. That is, a 50/50 ratio of enantiomers always provided a 50/50 peak height/area ratio of final diastereomers. This was expected since we have shown that the overall UV spectra of all diastereomers studied thus far were seemingly identical. This was a necessary condition in order to use the approach for enantiomer recognition and optical purity determinations, without authentic external standards of each enantiomer or diastereomer in-hand.

In UV/FL chromatograms obtained for the mixture of diastereomers described above, the same UV/FL response ratio for d - and l -diastereomers was realized. Derivatizations of d,l -methylbenzylamine with polymeric FMOC-L-proline was an example (Figure 8). However, when a 50/50 mixture of the enantiomers of d,l -naphthylethylamine was derivatized with the same reagent, though the UV peak heights/areas were again identical, the FL responses at 275/315 nm were vastly different (Figure 13). It was apparent that the l -diastereomer,

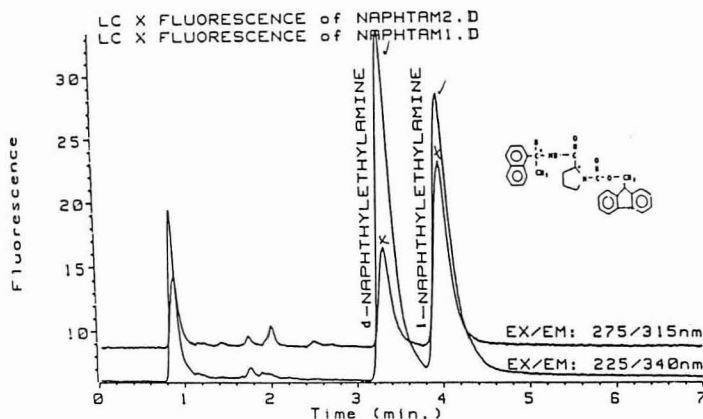


Figure 14. HPLC-FL chromatogram for a 50/50 mixture of the diastereomers of *d,l*-naphthylethylamine, derivatized off-line with the polymeric chiral reagent IV. HPLC conditions: μ -diol bonded phase column, 10 cm \times 2.1 mm i.d., 5 μ m; 3% 2-propanol/hexane, 0.7 mL/min.

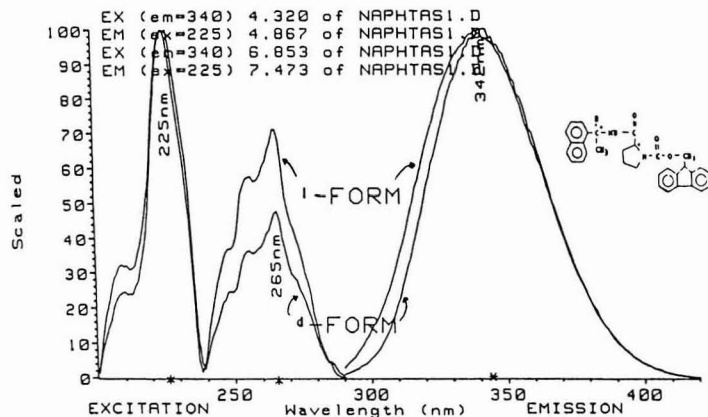


Figure 15. Excitation and emission spectra for the two diastereomers of *d,l*-naphthylethylamine with the FMOc-L-proline reagent IV. Spectra were obtained in HPLC-FL with the Hewlett-Packard scanning FL detector, Model No. 1046A. HPLC conditions: μ -diol bonded phase column, 10 cm \times 2.1 mm i.d., 5 μ m; 3% 2-propanol/hexane, 0.7 mL/min.

Table VIII. Separation of Enantiomeric Amines and Amino Alcohols as Their Derivatives Formed from FMOc-L-Proline Chiral Reagent Using Gradient HPLC Conditions

compound	k'	α	R_s	t_r
methylbenzylamine ^a	2.54/2.86	1.12	2.00	15.6/17.0
1-(α -naphthyl)ethylamine ^b	3.36/3.64	1.08	1.33	12.2/13.0
1-methylheptylamine ^b	2.08/2.22	1.07	1.25	11.4/11.9
2-amino-1-butanol ^c	6.38/7.38	1.16	1.88	23.6/26.8
1-amino-2-propanol ^c	9.25/9.62	1.04	0.60	32.8/34.0

^a Mobile phase was 10–20% 2-propanol/hexane; 20-min gradient, 0.7 mL/min. ^b Mobile phase was 10–20% 2-propanol/hexane; 30-min gradient, 0.7 mL/min. ^c Mobile phase was 15–35% 2-propanol/hexane; 40 min, 0.7 mL/min. Other conditions were as in Table VII.

that eluting first, had a larger FL response than the *d*-diastereomer. This was unusual, in that it was the only mixture of diastereomers of all those studied to show any differences in FL responses. To understand this better, a solution sample of the preformed *d,l*-naphthylethylamine diastereomers (50/50) was sent to the LC Applications Laboratory of Hewlett-Packard GmbH in Waldbronn, FRG. There, it was

possible to obtain the excitation and emission spectra for each diastereomer by using an on-line, Model 1046A scanning FL detector to capture the data after HPLC separation of the diastereomers.

The HPLC-FL chromatogram in Figure 14 shows the FL responses of the diastereomer pair at two sets of excitation and emission wavelengths (275/315 and 225/340 nm). It is important to note that the elution order of the diastereomers was changed under these HPLC conditions, with the *d*-form eluted before the *l*-form with a μ -diol column. The elution order was further confirmed by us, using a similar μ -diol column of slightly different dimensions and packing material (25 cm \times 4 mm i.d., 7 μ m), but with the same mobile phase and flow rate. Again, we too observed a reversal of the elution order, *d*- before *l*-diastereomer, opposite to what was always observed with the bare silica gel columns used before.

The FL peak areas of the diastereomers at 275/315 nm were quite different, as in Figures 13 or 14. However, the FL peak areas of the diastereomers were almost identical at 225/340 nm (Figure 14). This was understood by studying the excitation and emission spectra, also obtained by Hewlett-Packard in Germany, shown in Figure 15. The excitation and emission intensities of the *d*-diastereomer at 275/315 nm were obviously lower than those for the *l*-diastereomer and caused a lower

FL response at these HPLC-FL wavelengths for the *d*-diastereomer (Figures 13, 14). We appreciate a reviewer's suggestion that this may be caused by the quenching phenomenon involved, emanating from intramolecular arrangement of the *d*-diastereomer.

In most instances, the excitation/emission spectra, or for that matter the UV spectra, of each diastereomer formed from a given enantiomer pair are not available. It is thus difficult to predict if every single enantiomer pair that reacts with this polymeric chiral reagent IV will give identical UV or FL spectra for the diastereomers. Though every single pair of diastereomers examined thus far had identical UV spectra and FL properties, it is now clear that at least one pair of these showed different FL properties.

If HPLC-FL at the "wrong" wavelengths had been used, quantitative results would have been in error for enantiomeric composition. Our data seems to suggest that HPLC-UV may be a more reliable and overall valid approach than perhaps HPLC-FL. These results also showed that the selection of excitation and emission wavelengths can be essential in order to get meaningful results when a FL detector is used.

CONCLUSIONS

Polymeric chiral reagents were designed for performing efficient and rapid derivatizations of enantiomer amines and amino alcohols, off-line and on-line in normal-phase HPLC. The reaction products were easy to separate by isocratic or gradient conditions. The kinetics of diastereomer formations and the molar absorptivities of the diastereomers were identical. The enantiomeric ratios determined by using this approach have been valid, as confirmed by our existing experiments. Applications to the quantitation and chiral recognition of enantiomeric bioactive materials and drugs in complex matrices, using such polymeric chiral reagents off-line and on-line in conjunction with HPLC, are entirely possible (42).

The diastereomers formed via solid-phase chiral derivatizations have excellent detector properties (UV/FL). The limits of detection (LODs) of the diastereomers were in the low parts per billion or picomole range. These low LODs lead to successful trace analyte or impurity identification and diastereomer resolutions at the trace levels. Multidetector ratioing and/or subtraction of peak heights and areas can lead to improved enantiomer identification via this type of derivatization.

These polymeric chiral reagents represent but one additional type of solid-phase derivatization in HPLC. Numerous variations on what has been presented are possible, such as (1) different polymeric backbones, organic or inorganic (silica gel); (2) alterations in the nature of the attachment of the chiral detector tag to the polymeric backbone; (3) changes in the nature of the chiral portion of the tag to improve diastereomer separations possible under both normal- and reversed-phase conditions; and (4) differences in the type of detector-sensitive tags, so that future diastereomers will be detectable by UV and FL, as well as by oxidative or reductive EC. It is entirely conceivable that one single detector-sensitive tag could provide all three responses at trace levels.

ACKNOWLEDGMENT

We acknowledge the following colleagues for their assistance: C. Selavka, N. Chen, S. Krzysko, R. Mhatre, T. Baker, H. H. Stuting, and B. D. Karcher. Special gratitude is due A. J. Bourque, who synthesized the polymeric intermediate.

The Model Spectronic 1201 scanning UV-vis spectrophotometer was donated by Milton Roy Corp./Analytical Products Division. We appreciate the donation to NU by Hewlett-Packard Corp. of an HP Model 1040A linear diode array UV spectrophotometer for HPLC. A Hitachi Model D2000 ChromatoIntegrator was donated to NU by EM Science, Inc.

J. Neumeayer provided certain samples of enantiomers. We thank Hewlett-Packard GmbH in Walldbronn, FRG, especially A. Mautz and R. Schuster, for providing us with certain UV and FL spectra for the *d,l*-naphthylethylamine diastereomers.

LITERATURE CITED

- (1) Souer, R. W. *Chromatographic Separations of Stereoisomers*; CRC Press, Inc.: Boca Raton, FL, 1985; Chapter 3, p 143.
- (2) Gal, J. *J. Liq. Chromatogr.* **1986**, *9*, 673.
- (3) Goto, J.; Ito, M.; Katsuki, S.; Saito, N.; Nambara, T. *J. Liq. Chromatogr.* **1986**, *9*(2/3), 683.
- (4) Pirke, W. H.; Pochapsky, T. C. *Adv. Chromatogr.* **1987**, *27*, 73.
- (5) Pirke, W. H.; McCune, J. E. *J. Chromatogr.* **1988**, *441*, 311.
- (6) Finn, J. M. in *Chromatographic Chiral Separations*; Zief, M., Crane, L. J., Eds.; Marcel Dekker, Inc.: New York, 1988; Chapter 3.
- (7) Gal, J.; Ames, M. M. *Anal. Biochem.* **1977**, *83*, 266.
- (8) Petterson, C.; Schill, G. *J. Liq. Chrom.* **1986**, *9*, 289.
- (9) Grushka, E.; Leshe, R. *TrAC, Trends Anal. Chem. (Pers. Ed.)* **1981**, *1*, 55.
- (10) Nimura, N.; Toyama, A.; Kasahara, Y.; Kinoshita, T. *J. Chromatogr.* **1982**, *239*, 671.
- (11) Davankov, V. A. *Pure Appl. Chem.* **1982**, *54*, 2159.
- (12) Davankov, V. A.; Kurganov, A. S.; Buchkov, A. S. In *Advances in Chromatography, Vol. 22*; Giddings, J. C., Grushka, E., Cazes, J., Brown, P. R., Eds.; Marcel Dekker, Inc.: New York, 1983; p 71.
- (13) Shieh, C. H.; Karger, B. L.; Gelber, L. R.; Feibush, B. *J. Chromatogr.* **1987**, *406*, 343.
- (14) Gelber, L. R.; Karger, B. L.; Neumeayer, J. L.; Feibush, B. *J. Am. Chem. Soc.* **1984**, *106*, 7729.
- (15) Gil-av, E.; Weinstein, S. In *Handbook of HPLC for Separation of Amino Acids, Peptides, and Proteins, Vol. 1*; Hancock, W. S., Ed.; CRC Press, Inc.: Boca Raton, FL, 1982; p 429.
- (16) Gal, J. In *Drug Stereochemistry Analytical Methods and Pharmacology*; Wainer, I. W., Drayer, D. E., Eds.; Marcel Dekker, Inc.: New York, 1988; Chapter 4.
- (17) Gil-av, E. In *The Science of Chromatography*; Bruner, F., Ed.; Elsevier Science Publishers, Inc.: Amsterdam, 1985; p 111.
- (18) Einarsson, S.; Josefsson, B.; Moller, P.; Sanchez, D. *Anal. Chem.* **1987**, *59*, 1191.
- (19) Gal, J.; Brown, T. R. *J. Pharmacol. Methods* **1986**, *16*, 261.
- (20) Gal, J.; Sedman, A. J. *J. Chromatogr.* **1984**, *314*, 275.
- (21) Nimura, N.; Kinoshita, T. *J. Chromatogr.* **1986**, *352*, 169.
- (22) Lim, K. H.; Hubbard, J. W.; Midha, K. K. *J. Chromatogr.* **1986**, *378*, 108.
- (23) Gal, J.; Murphy, R. C. *J. Liq. Chromatogr.* **1984**, *7*, 2307.
- (24) Matsuur, N. K.; Narang, C. K.; Williams, R. E. *Polymers as Aids in Organic Chemistry*; Academic Press, Inc.: New York, 1980.
- (25) *Polymeric Reagents and Catalysts*; Ford, W. T., Ed.; ACS Symposium Series 308; American Chemical Society: Washington, DC, 1986.
- (26) Cohen, B. J.; Karoly-Hafeli, H.; Patchornik, A. *J. Org. Chem.* **1984**, *49*, 922.
- (27) Shai, Y.; Jacobson, K. A.; Patchornik, A. *J. Am. Chem. Soc.* **1985**, *107*, 4249.
- (28) Patchornik, A. *ChemTech* **1987**, January, 58.
- (29) Gulloualt, G. G. *Analytical Uses of Immobilized Enzymes*; Marcel Dekker Inc.: New York and Basel, 1984.
- (30) Colgan, S. T.; Krull, I. S. In *Reaction Detection in Liquid Chromatography*; Krull, I. S., Ed.; Marcel Dekker: New York, 1986; p 227.
- (31) Norddek, L.; Frei, R. W.; Brinkman, U. A. Th. *J. Chromatogr.* **1983**, *282*, 141.
- (32) Jansen, H.; Brinkman, U. A. Th.; Frei, R. W. *Chromatographia* **1985**, *20*(8), 453.
- (33) Colgan, S. T.; Krull, I. S.; Dorschel, C.; Bidlingmeyer, B. *Anal. Chem.* **1986**, *58*, 2366.
- (34) Colgan, S. T.; Krull, I. S.; Dorschel, C.; Bidlingmeyer, B. *J. Chromatogr. Sci.* **1988**, *26*, 501.
- (35) Chcu, T.-Y.; Gao, C.-X.; Colgan, S. T.; Krull, I. S.; Dorschel, C.; Bidlingmeyer, B. *J. Chromatogr.* **1988**, *454*, 169.
- (36) Gao, C.-X.; Chou, T.-Y.; Colgan, S. T.; Krull, I. S.; Dorschel, C.; Bidlingmeyer, B. *J. Chromatogr. Sci.* **1988**, *26*, 449.
- (37) Gao, C.-X.; Chou, T.-Y.; Krull, I. S. *Anal. Chem.*, preceding paper in this issue.
- (38) Drouen, A. C. J. H.; Billiet, H. A. H.; De Galan, L. *Anal. Chem.* **1984**, *56*, 971.
- (39) Schieffer, G. W. *J. Chromatogr.* **1985**, *319*, 387.
- (40) Foley, J. P.; Dorsey, J. G. *Anal. Chem.* **1983**, *55*, 730.
- (41) Feibush, B.; Grinberg, N. In *Chromatographic Chiral Separations*; Zief, M., Crane, L. J., Eds.; Marcel Dekker, Inc.: New York, 1988; Chapter 1.
- (42) Gao, C.-X.; Krull, I. S. *J. Pharm. Biomed. Anal.*, in press.

RECEIVED for review October 28, 1988. Accepted April 3, 1989. Financial assistance was provided by a grant from the Analytical Research Department, Pfizer Central Research, Pfizer, Inc., Groton, CT, and by an NIH Biomedical Research Support Grant to Northeastern University, No. RR07143, Department of Health and Human Services. This is contribution no. 378 from The Barnett Institute at Northeastern University.

Detection of Ambient Hydrogen Chloride with a Zinc-Coated Piezoelectric Crystal Resonator Operating in a Frequency-Time Differential Mode

Glen G. Neuburger

Bell Communications Research, Red Bank, New Jersey 07701

A scheme is described for the selective and highly sensitive detection of gaseous HCl utilizing a Zn-coated quartz crystal as the sensing element in a piezoelectric microbalance operating in a frequency-time differential mode. The extraordinarily high sensitivity of this sensor for HCl is based on the formation of the hygroscopic ZnCl_2 salt and its exceedingly high affinity for water. The sensitivity ratio for detection of HCl as compared to all gases tested, viz., CO, CO_2 , NO, NO_2 , O_2 , H_2S , NH_3 , SO_2 , is 100:1 or greater. For detection of 50 ppm HCl this would require that interfering gases be present at a concentration 10^3 - 10^7 times their normal indoor ambient levels. Upon exposure to an indoor laboratory environment at 50-70% relative humidity the average lifetime of the Zn-coated resonator is >2.5 years. Compensation for ubiquitous low-frequency background drifts, commonly associated with ambient temperature and humidity fluctuations as well as mild corrosion of the Zn surface, is accomplished by numerical differentiation of the oscillator response, thus making this system highly suited for chemical alarm applications where triggering is based on exceeding a specified threshold rate of mass accumulation.

INTRODUCTION

Hydrogen chloride is a noxious and highly reactive byproduct of many anthropogenic processes including combustion of fossil fuels (primarily coal) and chlorinated synthetic materials. For example, combustion of poly(vinyl chloride) (PVC), which is widely used in indoor wire insulation and floor tile, yields 580 g of HCl per kilogram of polymer (1, 2); i.e., essentially all Cl in the polymer can be accounted for in the form of HCl. As a result of the high reactivity of gaseous HCl with many metallic surfaces, even small, internally localized, building fires involving combustion of PVC and other chlorinated materials can cause widespread damage to electronic equipment. Given the large amount of PVC in many telephone central office environments, it would seem desirable to devise a chemical sensor/alarm for monitoring the concentration of ambient HCl.

Many methods have been devised for the detection of gaseous HCl. The impetus for such work has resulted from the detrimental effects of dry and wet deposition of HCl in the troposphere, and the need to monitor the effects of halocarbons on ozone depletion in the stratosphere. Techniques based on light scattering, IR absorption spectroscopy, indirect chemiluminescence, and gas trapping followed by acid-base titrimetry, coulometry, or colorimetry have been reported and discussed in a recent review (3). Of these methods, those requiring gas trapping for sampling often lack specificity and are not amenable to real-time analysis. In addition, many of the techniques presented involving spectroscopic measurements required design modifications to increase performance reliability. Continued work on an indirect chemiluminescence

scheme (4) demonstrated a limit of detection of ca. 10 ppb at the expense of poor response times, approaching several minutes for sub-part-per-million levels. However, interference from strong acids, halogens, and acid-forming gases was expected. Several optical methods based on IR absorption (excitation) have been introduced recently (5-7). Little interference from other ambient gases is expected with proper selection of excitation wavelength, and detection limits <50 ppb have been demonstrated. However, these methods are often impractical for widespread use because of their high cost.

The use of piezoelectric quartz crystal resonators as a viable means for gas detection is well established (8-10), where specificity is gained primarily through the use of selective coatings. In fact, the use of tertiary amine coatings for gaseous HCl detection has been presented (11, 12). However, these coatings suffer from interference by water vapor. Additionally, the use of low molecular weight organic coatings without specific surface binding sites will result in the loss in sensitivity with time owing to film sublimation.

The response for an oscillating quartz crystal as originally derived by Sauerbrey (13, 14) is given by

$$\Delta F = \frac{-2F^2}{\rho_q v_q} \Delta m / A \quad (1)$$

where ΔF is the change in frequency (Hz) as a result of mass loading, F is the resonant frequency of the quartz crystal (Hz), ρ_q is the density of the quartz (kg/m^3), v_q is the shear wave velocity (m/s), and $\Delta m/A$ is the change in areal density (kg/m^2). This latter quantity may be rewritten as $\rho_f t_f$ and the film thickness, t_f , can be calculated if the density, ρ_f , is known. For AT-cut quartz, $\rho_q = 2648 \text{ kg}/\text{m}^3$ and $v_q = 3340 \text{ m/s}$ (15), and eq 1 takes the form

$$\Delta F = -(2.3 \times 10^{-7}) F^2 \Delta m / A \quad (2)$$

Equation 2 has been commonly rewritten as

$$\Delta F = -(2.3 \times 10^6) F^2 \Delta m / A \quad (3)$$

where ΔF , F , and $\Delta m/A$ are expressed in units of Hz, MHz, and g/cm^2 , respectively.

Equations 1 through 3 are applicable for low mass loads only and deviation is expected for thick films where the acoustic impedance of the film, $\rho_f v_f$, is not equal to that of quartz, and when losses associated with film imperfections (insertion losses) are significant (15). For nonrigid films, i.e., those containing organic molecules or hydrated salts and characterized by a low shear modulus, deviation is expected at much lower mass loads since $\rho_f v_f \ll \rho_q v_q$. The actual film thickness required to cause deviation is also dependent upon the type and quality of crystal employed. As a result, the proportionality between ΔF and Δm in eq 1-3 becomes highly nonlinear when the acoustic impedance of the film is significantly different from that of quartz, thus causing deviation in ΔF vs gas concentration plots. Several models have been proposed (15) to compensate for these errors by taking into

account the variation of film acoustic impedance, resulting in an overall increase in the linear dynamic range.

Previous techniques utilizing quartz crystal resonators have relied on the use of a "reference oscillator" to compensate for ambient fluctuations in temperature and humidity and, to a lesser extent pressure. For such systems the frequency response is calculated as $\Delta F = F_s - F_r$, where F_s and F_r refer to the frequencies of the sensing and reference oscillators, respectively. Corrections of this type are at best empirical and rely heavily on similar reference and sensing crystal/coating characteristics, e.g., temperature coefficients, rates of water adsorption, and aging specifications. It is questionable, however, whether a reference oscillator, exposed to the gas stream, can exactly compensate for environmental fluctuations since the surface coating of the reference crystal must necessarily be different from the sensing crystal. In addition, the reference oscillator must be inert to all gases being sensed. Isolation of the reference crystal from the gas stream is not expected to compensate for any environmental changes.

Compensation for ubiquitous low-frequency background drifts and elimination of continual adjustment of zero response can be accomplished by monitoring the rate of change of oscillator response with time. Here dF/dt denotes the change in response of the sensing crystal only and can be estimated by the finite difference of adjacent measurements, i.e., $\Delta F_{i,i} = F_{i+1} - F_i$, for a fixed time interval Δt where the sampling frequency $f_s = 1/\Delta t$. For a background response with $f \gg f_s$ complete rejection is expected; for $0 < f \ll f_s$ an offset from $dF/dt = 0$ is noted. For normal measurements the latter case is applicable where $f_s = 0.1 - 1 \text{ s}^{-1}$ for precise frequency measurements and where background frequencies are on the order of 0.001–0.05 Hz. Thus, base-line drifts commonly associated with temperature and humidity fluctuations, crystal aging, as well as variations in sensor film state (e.g., oxidation/reduction, corrosion, etc. of the surface film) can be compensated, automatically eliminating the need for constant adjustment of zero response.

In this paper we describe a gaseous HCl detector based on a piezoelectric quartz crystal resonator suitable for widespread distribution, i.e., low cost, while retaining the qualities of specificity and sensitivity. The detector utilizes a Zn-coated AT-cut quartz crystal and relies on the formation of the hygroscopic ZnCl_2 salt upon reaction with gaseous HCl. A description of the detector is provided together with some preliminary results on detector response, specificity, sensitivity, and lifetime. Particular emphasis is placed on operating as a chemical alarm for gaseous HCl detection where actuation is caused by exceeding a predefined threshold rate of mass accumulation.

EXPERIMENTAL SECTION

Microbalance Design. The quartz microbalance had a resolution of 2 parts in 10^9 utilizing a 10-MHz AT-cut quartz crystal. All of the critical electronic components were mounted in a chamber (Model CU250-6; MDC Vacuum; Hayward, CA) in an effort to reduce electromagnetic interferences, and eliminate any high-frequency temperature fluctuations. The chamber also served as a means for venting any toxic gases resulting from leaks in the test cell and its associated connections. No provisions were made for direct temperature compensation.

The series resonance oscillator circuits were constructed from common components and sealed in metal cases to reduce external electromagnetic interference. External solderable contacts were made available for all oscillator inputs and outputs; external chamber contacts were made with BNC connectors. Simultaneous measurements were carried out by using two oscillators which were mounted into each of two isolated nipples extending from the chamber to minimize electrical crosstalk. The quartz crystals, mounted in HC-33 spring wire crystal holders, were inserted into a small cavity within a Teflon block and held firm with a pressure mounted stainless steel plate. The softness of Teflon facilitated

forming an airtight seal for low cell pressure drops. To minimize the effects of ground current loops, the stainless steel chamber served as a common ground.

Instrumentation. All frequencies were measured with a 1-s gate time utilizing a high precision counter (Model 5334B; Hewlett-Packard; Palo Alto, CA) with analog gate offset interpolation. Filtered outputs of an isolated dc power supply (Model 6621A; Hewlett-Packard) were used to drive each oscillator. The system was interfaced to a microcomputer (Model AT, IBM Corp., Boca Raton, FL) to enhance data acquisition capabilities and achieve the rated accuracy of the frequency counter.

Crystal Preparation. Optically smooth 10-MHz AT-cut quartz crystals (Anderson Electronics, Hollidaysburg, PA) were used for all studies. The crystal diameter was 1.4 cm and the deposited Cr/Au electrodes had a central diameter of 0.65 cm with spring wire contacts 180° apart. Prior to film deposition all crystals were chemically cleaned in a 4:1 mixture of H_2SO_4 and H_2O_2 . After being rinsed with deionized water the crystals were dried in a N_2 -purged chamber and subsequently mounted in a masking frame (Photofabrication Corp., Chicago, IL) for film deposition.

Thin film deposition was performed in two stages with two isolated, cryogenically pumped, bell jar systems (Thermionics Laboratory, Hayward, CA). Chromium and gold layers were applied sequentially by evaporation of pure metal from resistively heated tungsten boats. After Cr and Au deposition the crystals were transferred to a separate masking frame and deposition system for thermal evaporation of Zn. The metal film thicknesses for each side of the crystal were, 50 Å Cr, 500 Å Au, and ca. 500–2000 Å Zn. A quartz crystal thickness monitor (Model QM-331, Veeco Instruments, Plainville, NY) was used to follow the progression of all evaporation processes. All depositions were performed at a pressure of $<10^{-6}$ Torr.

Gas Blending. All gas mixtures were made with a multipoint gas blending system (Model 8219, Matheson Gas Products, East Rutherford, NJ) capable of simultaneously controlling the flow rate of four gas streams. Mass flow controllers for use with this blending system were constructed from either Monel for HCl or stainless steel for all other gases. The total flow rate for all studies was 400 mL min^{-1} ($\pm 2\%$); thus, with a cell volume of 1.8 mL, a high gas turnover rate was achieved, i.e., 3.7 exchanges s^{-1} .

Water vapor was added to the support stream before adding component gases with the use of a sealed gas washing bottle (VWR Scientific, Piscataway, NJ). The system was purged for ca. 1 h before use to ensure a constant rate of evaporation. The relative humidity (RH) was controlled by varying the flow rate ratio of component to support gas streams.

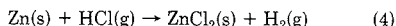
All interconnecting fittings and tubing were of Teflon construction; therefore the only metal in contact with the gas stream was the body of the mass flow controller. The internal dead volume of the mass flow controller was ca. $>10 \text{ mL}$.

Gas connections to the Teflon cell block were made with the use of knurled Teflon pressure fittings. The input gas stream was biselected by the quartz crystal to minimize pressure fluctuations at the surface of the crystal. To ensure rapid mixing within the gas flow cell, the gas inlet and outlet were located in the same face of the cell cavity.

Chemicals. Metals used in thin film preparation were purchased in either shot or wire form (Aldrich Chemical, Milwaukee, WI) with purities $>99.9\%$. Component gases were obtained as certified binary mixtures (Scott Specialty Gases, Plumsteadville, PA) in pretreated high-pressure cylinders. Nitrogen and synthetic compressed air (80% N_2 , 20% O_2) were obtained in high purity (Air Products, Allentown, PA) with a water vapor concentration $<1 \text{ ppm}$. All chemicals were used as supplied.

RESULTS AND DISCUSSION

It is well-known that rapid corrosion of a Zn surface will occur upon exposure to gaseous HCl (16). This results from the high reducing strength of Zn, causing reduction of H^+ to $\text{H}_2(\text{g})$ with the subsequent formation of the hygroscopic ZnCl_2 salt



Upon formation, ZnCl_2 readily absorbs water for $>10\%$ RH

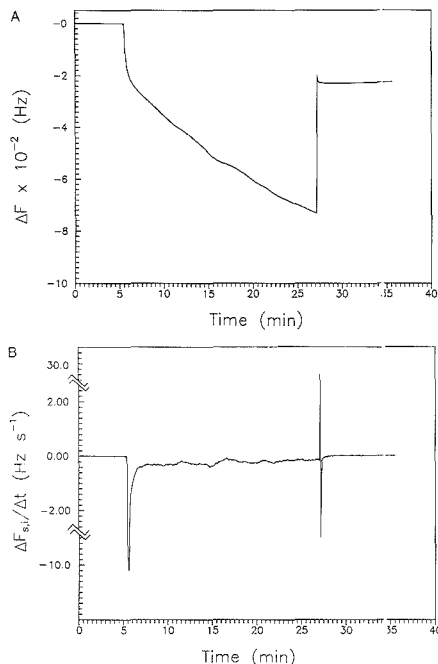
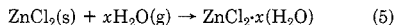
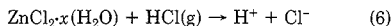


Figure 1. Comparison of the base-line response for (A) frequency difference and (B) frequency-time differential modes of operation, with a step in RH.

and thereby increases the rate of mass accumulation onto the surface of the crystal



In addition, the absorption of water vapor enhances the corrosion rate by facilitating the deposition/transport of H^+Cl^- to the Zn/ZnCl_2 interface



Whereby the presence of HCl is necessary to initiate a response, the addition of water vapor causes an additional "internal" amplification when monitoring a change in mass.

Base-Line Response. The frequency response for a Zn-coated quartz resonator associated with the RH step from 50% to 95% is shown in Figure 1A. The change in oscillator frequency as a result of a step in RH simulates the effects commonly observed for ambient temperature and humidity fluctuations as well as the gradual corrosion of the Zn surface. With a switch to 95% RH at $t = 5$ min, the change in oscillator frequency, where $\Delta F = (F_{s,i} - F_1)$, rapidly approaches ca. -0.04 Hz s^{-1} (-20 Hz h^{-1}). This continual decrease in oscillator frequency results from the slow oxidation of the Zn film. Reversal to 50% RH at $t = 28$ min causes the rapid loss of adsorbed water, noted as a sudden increase in ΔF , with a much slower rate of oxidation for $t > 28$ min.

Numerical differentiation of the oscillator response (Figure 1B), approximated by $(F_{s,i+1} - F_{s,i})/\Delta t = \Delta F_{s,i}/\Delta t$, results in automatic compensation for the low frequency drift where the rate of water vapor adsorption and corrosion on the crystal surface is noted by an offset from zero. The large peak at $t = 5$ min is a result of the rapid sorption of water onto the

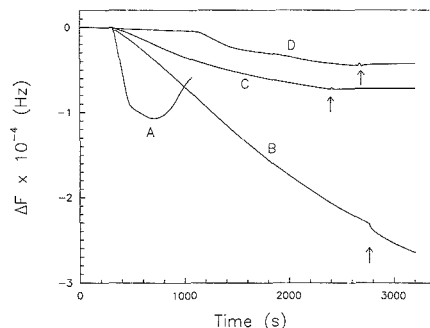


Figure 2. Frequency response of a Zn-coated quartz resonator to (A) 50 ppm HCl, (B) 5 ppm HCl, (C) 500 ppm NO_2 , and (D) 500 ppm SO_2 at a RH of (A) 20% and (B-D) 50%.

crystal surface coincident with the step in RH from 50 to 95%. The peak at $t = 28$ min is coincident with the step in RH from 95 to 50%. Daily variations in humidity and temperature will result in a low-amplitude, low-frequency oscillation of the differential base-line response about zero. The additional response from mild corrosion of the crystal surface will offset the low-amplitude background oscillation from $\Delta F_{s,i}/\Delta t = 0$ (e.g., $8 < t < 25$ min, Figure 1B). The ability to monitor a low-amplitude differential response (i.e., numerical differentiation) requires the use of a high-resolution (low noise) piezoelectric microbalance.

Response to Gaseous HCl. The frequency response for the Zn-coated quartz resonator continuously exposed to 5 and 50 ppm HCl with 50% and 20% RH, respectively, is shown in Figure 2, where $\Delta F = F_{s,i} - F_1$. For comparison, exposures to 500 ppm NO_2 and SO_2 at 50% RH are also shown. The overall response for 5 ppm HCl during a 35-min exposure is in excess of 20 kHz with an initial reaction rate corresponding to ca. -10 Hz s^{-1} . For 50 ppm HCl the mass accumulation rate is so great, i.e., ca. -60 Hz s^{-1} , that the oscillator is forced to shift to a sideband or overtone frequency at $t \sim 500$ s. This is noted in Figure 2 (curve A) by a decrease in ΔF for $t > 700$ s. The loss of oscillation is a consequence of the poor acoustic quality (lack of rigidity and increased film imperfections) of the resultant film in conjunction with the high mass loading of the quartz resonator and is not a result of mass loss from the crystal surface.

For reactions limited by the rate of diffusion of a reactant through a growing surface film, it is expected that the overall reaction rate will vary with time, decreasing as the film thickness increases. The decreasing reaction rate with increasing film thickness is noted in Figure 2 for 5 ppm HCl and 500 ppm NO_2 and SO_2 where the slope is increasing (less negative) with exposure time. It is apparent from the data of Figure 2 that reporting an average frequency response for a given exposure time can be misleading and may not be representative of the initial response rate, especially for long exposure times. Therefore, we emphasize the use of a differential rate of change and report the maximum differential response, $[-dF/dt]_{\text{max}} \sim [-\Delta F_{s,i}/\Delta t]_{\text{max}}$, for a given system. The data of Figure 2 are replotted in Figure 3 with respect to this finite differential. The maximum differential response for 5 and 50 ppm HCl is 12 and 64 Hz s^{-1} , respectively. Clearly the response for 50 ppm HCl is easily discerned from that for 5 ppm HCl and 500 ppm NO_2 and SO_2 , where the maximum rates for the latter are 5.5 and 6.9 Hz s^{-1} , respectively.

The response time, defined here as the time required to reach a predefined threshold rate of mass accumulation, $[-\Delta F/\Delta t]_{\text{th}}$, is directly correlated to the gas-Zn reaction rate and

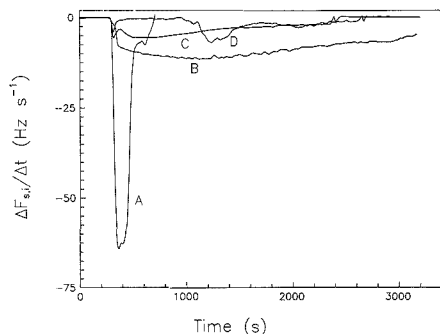


Figure 3. Differential frequency response of a Zn-coated quartz resonator exposed to (A) 50 ppm HCl, (B) 5 ppm HCl, (C) 500 ppm NO₂, and (D) 500 ppm SO₂ at a RH of (A) 20% and (B–D) 50%.

Table I. Frequency Response $(-F_{s,i} - F_1)$; Hz of a Zn-Coated Crystal for 35-min Exposures to Various Gases

gas	0% RH (<1 ppm H ₂ O)		50% RH	
	5 ppm	500 ppm	5 ppm	500 ppm
HCl	310	500 ^a	27000	>10000 ^b
CO	7	27	3	90
CO ₂	10	53	40	40
H ₂ S	18	67	200	200
NH ₃	3	133	100	70
NO	3	48	300	300
NO ₂	35	460	190	7300
O ₂		3 ^c		30 ^c
SO ₂	25	56	250	4550

^a Tested at 50 ppm HCl. ^b Tested at 50 ppm HCl, 20% RH; loss of oscillation. ^c Tested with a N₂ support gas.

the hygroscopicity of the salt formed. Note, with such a definition it is entirely possible to have an infinite response time for a reactive gas if $\Delta F_{s,i}/\Delta t < [\Delta F/\Delta t]_{th}$. For 50 ppm HCl, and with a differential rate threshold set at 10 Hz s⁻¹, the response time is <10 s. With this same threshold limit, the response time for 500 ppm NO₂ and SO₂ at 50% RH is infinity.

Specificity. The usefulness of this sensor for detection of ambient HCl is limited by the specificity of the Zn coating and the RH of the surrounding environment. Other acids or acid-forming gases such as NO₂ and SO₂ are expected to react with Zn (see Figures 2 and 3); however, specificity can ultimately be controlled by differentiating between the reaction rates of the interfering gases with the Zn surface and the hygroscopicity of the salt formed. As a result gases that readily react with the Zn surface but display a response with $F_{s,i}/\Delta t < [\Delta F/\Delta t]_{th} < [\Delta F/\Delta t]_{HCl}$ do not interfere with the detection of HCl. The presence of these gases can, however, reduce the lifetime of the Zn-coated quartz resonator. To test the possible interference from common ambient gases, freshly prepared crystals were subjected to 35-min exposures of 5 and 500 ppm levels of CO, CO₂, H₂S, NH₃, NO, NO₂, O₂, and SO₂ at 0% (<1 ppm H₂O) and 50% RH. The total frequency change and the maximum differential response, $[-\Delta F_{s,i}/\Delta t]_{max}$, for each of these gases are shown in Tables I and II, respectively. The response for 5 and 500 ppm HCl is also tabulated.

Of all the gases tested, none would interfere with the detection of HCl when present at normal ambient concentrations. Only the acid-forming gases, such as NO₂ and SO₂, would interfere if present at ca. 100 times the concentration of HCl. For detection of 50 ppm HCl, for example, this would

Table II. Maximum Frequency-Time Differential Response $([-F_{s,i+1} - F_{s,i}]/\Delta t)_{max}$; Hz s⁻¹ of a Zn-Coated Crystal to Various Gases

gas	0% RH (<1 ppm H ₂ O)		50% RH	
	5 ppm	500 ppm	5 ppm	500 ppm
HCl	1.0	5.3 ^a	12	64 ^b
CO	0.005	0.083		0.014
CO ₂		0.19		0.026
H ₂ S	0.04	0.54	0.27	1.50
NH ₃		1.2	0.095	0.037
NO		0.32	0.22	0.26
NO ₂	0.10	2.2	0.13	5.5
O ₂		0.042 ^c		
SO ₂	0.10	1.2	0.35	6.9

^a Testec. at 50 ppm HCl. ^b Tested at 50 ppm HCl, 20% RH; loss of oscillation. ^c Tested with a N₂ support gas.

require that either NO₂ or SO₂ be present at a concentration 10⁴–10⁶ greater than their normal indoor ambient levels (17). Gases that show an appreciable initial rate of reaction, i.e., 0.1–2 Hz s⁻¹ at 500 ppm (Table II), would cause no interference since this rate is sustained for a very short period (Table I).

Effects of Water Vapor. ZnCl₂ is one of the most hygroscopic salts known with a critical relative humidity (CRH) of 10% (18). For comparison, the CRH of the hydrated salts of Zn(NO₃)₂ and ZnSO₄ is 42% and 90%, respectively (19). Assuming that only these salts are formed in the presence of their respective gases and water, a higher sensitivity is expected for detection of HCl as compared to NO₂ and SO₂ for >10% RH as a result of the increased mass loading from absorption of water vapor. Having exceeded the CRH for ZnCl₂ at >20% RH, water uptake is expected to continue after exposure to HCl. As shown in Figure 2 (curve B) the frequency decreases by a further 600 Hz after exposure to 5 ppm HCl at 50% RH and with continued exposure to air at 50% RH. (The arrows in Figure 2 depict the point at which the component gas stream was switched to compressed air at 50% RH.) The initial postexposure rate of water absorption corresponds to 6.7 Hz s⁻¹, approximately half of the mass accumulation rate. In strong contrast, little weight gain is noted for postexposure to NO₂ (curve C) or SO₂ (curve D). This suggests that for continued exposure to low levels of NO₂ or SO₂, as would be expected in a normal indoor environment, the sensor will continue to operate for an extended length of time at a moderate RH. However, once exposed to a significant dose of HCl, oscillation is expected to cease in a short period of time for >10% RH.

Analytical Calibration. From Tables I and II, it is apparent that neither the total frequency change nor the maximum differential response is proportional to gas concentration. For example, in the absence of H₂O only a 70% increase in response is noted (Table I) for a 10-fold increase in HCl concentration. This nonlinearity is caused by the combined effects of (1) the high mass loading of the quartz resonator, (2) the low shear modulus (nonrigidity) of the hydrated film for >0% RH, and (3) the adsorption and diffusion controlled reaction kinetics for the formation of ZnCl₂. For high mass loads deviation from linearity is expected when the acoustic impedance of the adsorbed film ($\rho_s v_s$) differs significantly from that for quartz ($\rho_q v_q$). For RH > 0% the adsorption of water vapor and subsequent dissolution of ZnCl₂ on the crystal surface dampen the shear wave motion due to the low shear modulus of the surface film. Reaction kinetics will also adversely affect analytical calibration. Upon initial exposure to gaseous HCl the entire surface is free to react; however, at longer times HCl must effectively penetrate the surface film thereby lowering the expected overall response as the surface

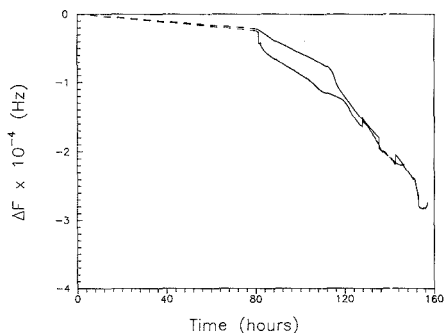


Figure 4. Exposure of two Zn-coated quartz resonators to (---) 2 ppm NO₂, followed by (—) 5 ppm NO₂, at 50% RH.

film thickness increases. For chemical alarm applications the nonlinear response is of little or no consequence since actuation is based on exceeding a specified threshold rate of mass accumulation.

Lifetime. The lifetime of the Zn-coated quartz resonator is dictated by the maximum mass loading before loss of oscillation. Secondary considerations must be given to the rate of mass loading and the rigidity of the film produced. Large mass accumulation rates produce poorer films with high insertion losses (film imperfections). Films with a low shear modulus, i.e., those containing H₂O or organics, inhibit or impede oscillation as a result of damping of the shear mode vibration.

Exposure to any acid or acid-forming gas is expected to limit the overall lifetime of the Zn-coated quartz resonator. In a normal indoor ambient environment NO₂ and SO₂ present at sub-part-per-million levels, CO₂ present at ca. 500 ppm, and H₂O are expected to cause the greatest corrosion of the Zn surface; the effects of other common ambient gases at their normal indoor ambient concentrations are considered to be insignificant (see Tables I and II). The lifetime of the resonator will also be limited by the operational RH, where for RH > CRH of the Zn salt formed, the lifetimes are expected to be less.

The lifetime of the Zn-coated quartz resonator can be calculated from the maximum mass loading of the crystal before loss of oscillation, and the background corrosion rate resulting from exposure to a common indoor environment. As shown in Figure 4, accelerated corrosion of the Zn-coated resonator, by exposure to 2 and 5 ppm NO₂ at 50% RH, yields an average maximum mass loading equivalent to 25 kHz. For crystals exposed to an indoor lab environment at 50–70% RH (Figure 5) the corrosion rate rapidly approaches ca. –20 Hz day⁻¹. With a 5-kHz allowance for response to HCl, the average lifetime of a Zn-coated resonator is >2.5 years. This value is in good agreement with the calculated 1.7-year lifetime, based on the corrosion rate of 0.26 μm year⁻¹ for rolled Zn (16) in an indoor industrial atmosphere, and with the allowance of a maximum mass loading of 20 kHz (eq 3).

CONCLUSION

The use of a Zn-coated quartz resonator is not expected to

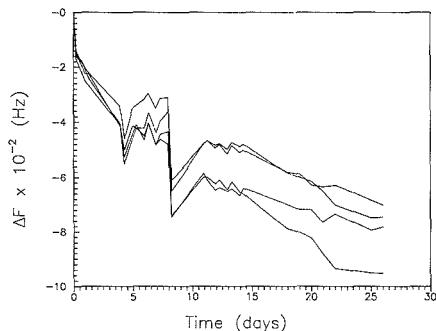


Figure 5. Exposure of four Zn-coated quartz crystals to an indoor ambient environment at 50–70% RH.

be useful for continuous monitoring of a HCl stream owing to the irreversible reaction between Zn and HCl. However, it holds great promise for applications requiring monitoring of office or laboratory environments where concentrations of gaseous HCl are normally low. Real-time differentiation of the response of a single sensing crystal provides compensation for low-frequency background variations commonly attributed to ambient temperature and RH fluctuations.

ACKNOWLEDGMENT

Discussions with B. T. Reagor and J. Jenson are gratefully acknowledged.

Registry No. HCl, 7647-01-0; quartz, 14808-60-7.

LITERATURE CITED

- Boettner, E. A.; Ball, G.; Weiss, B. J. *Appl. Polym. Sci.* **1969**, *13*, 377.
- O'Mara, M. M. *J. Polym. Sci., Part A-1* **1970**, *8*, 1887.
- Gregory, G. L. NASA TM D-8352, 1976.
- Gregory, G. L. *Rev. Sci. Instrum.* **1977**, *48*, 1464.
- Fried, A.; Berg, W. W. *Opt. Lett.* **1983**, *8*, 160.
- Fried, A.; Sams, R.; Berg, W. W. *Appl. Opt.* **1984**, *23*, 1867.
- Pokrowsky, P.; Herrmann, W. *Opt. Eng.* **1984**, *23*, 88.
- King, W. H. *Anal. Chem.* **1964**, *36*, 1735.
- King, W. H. *Res. Dev.* **1969**, *20*, 28.
- Guilbault, G. G. In *Applications of Piezoelectric Quartz Crystal Microbalances*; Lu, C., Czanderna, A. W., Eds.; Elsevier: New York, 1984; Vol. 7, Chapter 8.
- Jex, D. W.; Workman, G. L. NASA TM X-64984, 1976, 14(8).
- Hlavay, J.; Guilbault, G. G. *Anal. Chem.* **1978**, *50*, 965.
- Sauerbrey, G. *Phys. Verh.* **1957**, *8*, 113.
- Sauerbrey, G. *Z. Phys.* **1959**, *155*, 206.
- Lu, C. In *Applications of Piezoelectric Quartz Crystal Microbalances*; Lu, C., Czanderna, A. W., Eds.; Elsevier: New York, 1984; Vol. 7, Chapter 2.
- The Corrosion Handbook*; Uhlig, H. H., Ed.; John Wiley and Sons, Inc.: New York, 1948.
- Graedel, T. E.; Hawkins, D. T.; Claxton, L. D. *Atmospheric Chemical Compounds*, Academic Press: Orlando, FL, 1986; Chapter 2 and p 557.
- Nelson, G. O. *Controlled Test Atmospheres*; Ann Arbor Science Publishers: Ann Arbor, MI, 1972; p 184.
- CRG Handbook of Chemistry and Physics*; Weast, R. C., Ed.; CRC Press, Inc.: Boca Raton, FL, 1978.

RECEIVED for review November 28, 1988. Accepted April 14, 1989.

Dimethyl Disulfide Derivatives of Long Chain Alkenes, Alkadienes, and Alkatrienes for Gas Chromatography/Mass Spectrometry

David A. Carlson*

USDA, ARS, Insects Affecting Man and Animals Research Laboratory, P.O. Box 14565, Gainesville, Florida 32604

Chin-Shyan Roan and Richard A. Yost

Chemistry Department, University of Florida, Gainesville, Florida 32611

Julio Hector

USDA, ARS, Insects Affecting Man and Animals Research Laboratory, P.O. Box 14565, Gainesville, Florida 32604

Natural and synthetic long-chain alkenes, alkadienes, and alkatrienes (C_{25} – C_{37}) were readily derivatized to stable adducts with dimethyl disulfide (DMDS). This technique was extended to mixtures of unseparated alkanes, alkenes, alkadienes, and alkatrienes, but limited here to the types found in two-winged insects including African honey bees, fruit flies, and stable flies, which included several unreported compounds. Capillary column gas chromatography/electron ionization mass spectrometry (GC/EI-MS) of stable DMDS adducts allowed location of both internal and terminal unsaturated sites. Derivatization of the total hydrocarbon fraction gave excellent results after only 4 h of reaction time. Alkanes eluted first, followed by the alkene adducts, then the diadducts of dienes, with each group well separated from the others. Molecular ions of di- and triadducts were observed, together with ions showing losses of 48, 94, 141, and 188; cleavage at carbons bearing SCH_3 , then losses of 48 and 94 located both double bonds. The C_{35} and C_{37} diadducts were well separated during GC/MS or GC, with no thermal cleavage observed. Homologous C_{23} , C_{24} , and C_{25} triene diadducts and the C_{25} triene triadduct survived GC/MS and displayed characteristic cleavage patterns. Major differences were found in proportions of honey bee alkenes that differentiated European and African races, as the C_{31} , C_{33} , and C_{35} alkenes, mentioned as diagnostic for the races, were present in the diagnostic proportion when viewed as adducts. Also, a 9-isomer in the C_{31} homologue indicated the presence of African genetic material in worker bees and wax. The variety of dienes giving linear adducts was limited in that the double bonds were separated by four or more methylenes; otherwise cyclic derivatives of up to 29 carbons were observed.

INTRODUCTION

Electron impact (EI) mass spectra of positional isomers of unsaturated aliphatic compounds are usually indistinguishable, rendering gas chromatography/mass spectrometry (GC/MS) useless in determining double bond positions. This has been generally attributed to lack of cleavage between carbon-carbon double bonds or to extensive and facile hydrogen rearrangement (i.e., double bond migration) along the chain after molecular ion formation and before fragmentation (1). Remote-site fragmentation using tandem mass spectrometry for determination of double bond location via allylic cleavage has been described (2). However, this indirect method requires an instrument that is not available to most potential users

and appears difficult to apply to mixtures of isomers that are often present in natural samples.

Classical approaches to location of double bonds employ isolation followed by ozonolysis and GC but require tedious separation steps that can be difficult with trace quantities (3). Alternatively, derivatization before GC/MS includes: osmium tetroxide oxidation to the vicinal diol followed by silylation (4), epoxidation of acetates and aldehydes (5) and alkadienes (6). Methoxy derivatives cleave at the methoxy group (7–9); however the former workers could not locate double bonds in beeswax alkadienes despite excellent results with alkenes. Contributing to the difficulty of locating the second double bond is the additional cleanup needed for separation of polymethoxy derivatives before analysis. Such difficulties are worse when more than one double bond is present in more than one isomer, as in dienes (10) or trienes where multiple combinations of methoxy-substituted ethers are formed uncontrollably.

The derivatization of alkenes with dimethyl disulfide (DMDS) was described for GC (11). The capillary GC/EI-MS analysis of the DMDS adducts of monounsaturated acetates (12) was extended to monounsaturated fatty acids from four moth species (13). The results of DMDS derivatization of diunsaturated acetates and alcohols of up to 18 carbons that formed linear or cyclic polythioether adducts during 60-h reaction times were recently reported (14).

We describe the first derivatization of long chain alkenes (C_{23} to C_{37}) to form noncyclic linear adducts with DMDS reagent. Also, we describe the first DMDS derivatization of long chain alkadienes and alkatrienes and extension of the method to the elucidation of structures in mixtures of alkanes, alkenes, alkadienes, and alkatrienes. The utility and the limitations of this technique are described.

EXPERIMENTAL SECTION

Biological Materials. Male tephritid fruit flies, *Anastrepha suspensa*, and mixed sex *Drosophila melanogaster* were laboratory-reared on a standard synthetic diet and collected at 3 days of age for extraction in hexane (15, 16). Laboratory colony stable flies, *Stomoxys calcitrans* (L.), were reared on citrated bovine blood and collected at 3 days of age for extraction. African honey bee workers, *Apis mellifera scutellata*, were collected from colonies near Harare, Zimbabwe. European/Florida bees, *A. m. mellifera*, were collected from colonies in Gainesville, FL. Africanized bees were obtained from Panama and also from Panama City, FL. Extracts of all samples were obtained by soaking intact specimens in hexane for 2–10 min. The total hydrocarbon fraction was obtained by elution from a 2-cm column of silica gel with hexane only (17). Wax samples were collected from colonies at the same

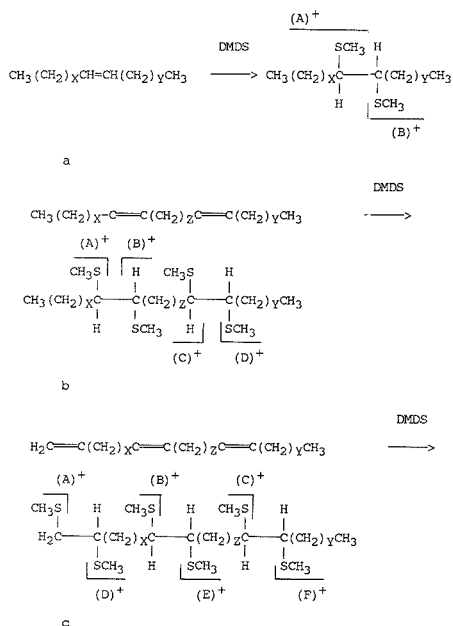


Figure 1. Fragmentation scheme for DMDS adducts of unsaturated hydrocarbons: (a) alkenes; (b) alkenes; (c) alatrienes.

locations and treated the same as the bees.

Reagents. Alkenes and alkenes were separated from synthetic and natural long-chain hydrocarbons by using silver nitrate thin-layer chromatography (TLC) with 1% ether/hexane or 20% benzene/hexane and checked against the appropriate synthetic standards. Derivatives were prepared from the following standards synthesized in our laboratory, donated, or purchased: (*Z*)-7-heptacosene, (*Z*)-7-pentacosene, (*Z*)-9-pentacosene (17), 1-tetradecene, 1-pentadecene, (*Z*)-7,11-pentacosadiene (6), and (*Z*)-9,19-heptatriacontadiene (18).

Derivatization. Samples (1–10 μg) in hexane (200 μL) were treated with 200 μL of neat DMDS (Eastman Kodak Co., Rochester, NY) and 100 μL of iodine solution (60 mg of iodine in 1 mL of diethyl ether) (13). Reaction mixtures were held for 4 h or overnight at 40 $^\circ\text{C}$, diluted with *n*-hexane, 5% sodium thiosulfate and the organic phase was dried over anhydrous Na_2SO_4 . The samples were blown dry, frozen, then redissolved in a minimum of hexane, and analyzed by capillary column GC and GC/MS.

Instrumentation. A Tracor Model 540 GC was used for GC analysis with on-column injection (OCI-3, SGE PTY, Austin, TX) using a capillary column of DB-1 (30 m \times 0.32 mm i.d., 0.25- μm film, J&W Co., Folsom, CA). The GC oven was programmed from 60 to 200 $^\circ\text{C}$ at 30 $^\circ\text{C}/\text{min}$, then to 320 $^\circ\text{C}$ at 7 $^\circ\text{C}/\text{min}$.

A Finnigan MAT (San Jose, CA) triple stage quadrupole GC/MS/MS system equipped with a Finnigan 4500 series ion source that was operated at a pressure of 0.05 Torr and an INCOS data system was used for GC/MS analyses, scanning at 1 cycle/s. The Finnigan 9610 GC was equipped with a splitless Grob capillary injector and a short capillary column (3 m \times 0.25 mm i.d., DB-1), with carrier gas (He) at ca. 1 psig. The injection and GC/MS interface temperatures were 320 and 330 $^\circ\text{C}$, respectively. The GC oven was held at 100 $^\circ\text{C}$ for 30 s, then ramped to 320 $^\circ\text{C}$ at 20 $^\circ\text{C}/\text{min}$. Sample introduction via solid probe was also used for high molecular weight derivatives. The amount of sample injected varied from 1 to 10 μg in 1 to 3 μL of hexane. Mass spectra also were obtained on a Hewlett-Packard 5985A GC/MS that was operated in the EI mode (70 eV), equipped with a HP 9000-300 Chromstation and interfaced with a HP 5890 GC operated in the splitless mode or with an on-column injector as above,

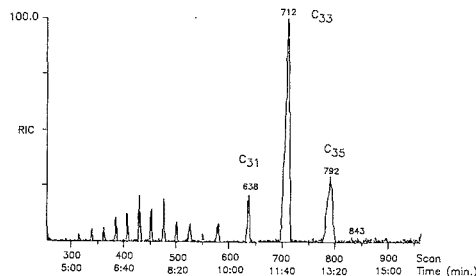


Figure 2. Reconstructed ion chromatogram of DMDS adducts of Africanized honey bee alkenes.

and fitted with a HP-1 capillary column (12 m \times 0.20 mm i.d.) operated as above, but with the injector at 320 $^\circ\text{C}$ and the interface at 320 $^\circ\text{C}$.

RESULTS AND DISCUSSION

Alkenes. Derivatives were formed by the addition of DMDS (mol wt 94) as in Figure 1a. Only one peak was detected by GC analysis of an alkene adduct. Mass spectra of the derivatives show recognizable molecular ions (M^+) under EI (70 eV) conditions. The double bond is located easily since cleavage of the carbon-carbon bond between the adjacent carbons carrying the methyl sulfide (CH_2S) substituents leads to the major fragment ions (A^+) and (B^+) as previously reported (11). One of these diagnostic fragments is often the base peak in the spectrum. The m/z values characteristic for these key fragments are identified by the series of $m/z = 61$ ($\text{CH}_2\text{SCH}_3^+$) with addition of 14 (CH_2) mass unit intervals. Pairs of (A^+) and (B^+) ions can be easily recognized because the sums of their m/z values equal (M^+). The derivative of (*Z*)-9-heptacosene gave fragment ions (A^+) = m/z 173 and (B^+) = m/z 299, showing the double bond to be between carbon 9 and 10, and (M^+) at $m/z = 472$. The EI spectra of all DMDS adducts showed a significant and diagnostic fragment ion, ($M - 47$) $^+$, due to loss of SCH_3 from the molecular ion, and another at ($M - 94$) $^+$, due to loss of DMDS to regenerate the original compound.

In methane CI spectra, derivatives of (*Z*)-7-pentacosene and (*Z*)-9-heptacosene both displayed small quasi-molecular ions at m/z 397 and m/z 425 ($M - H$) $^+$, respectively, as well as base peaks at ($M - 47$) $^+$. The diagnostic (A^+) and (B^+) ions observed by EI were missing in the CI spectra of the derivative, however.

Terminally unsaturated 1-tetradecene and 1-pentadecene were derivatized and showed prominent fragments; (A^+) = m/z 61 and (B^+) = m/z 243 for 1-pentadecene, (A^+) = m/z 61 and (B^+) = m/z 229 for 1-tetradecene, demonstrating that this method can be applied to terminal (11) as well as internal alkenes.

Derivatization was applied to alkene mixtures which may have chemotaxonomic value from three populations of honey bees. *Apis mellifera mellifera* is the commercial hybrid, now present in the USA that was derived from honey bees imported from Europe, whereas *A. mellifera scutellata* is a type of Southeast African honey bee. The term "Africanized honey bee" describes the race that has become dominant in South and Central America. DMDS derivatives were analyzed from hydrocarbons extracted from European/Florida (hereafter referred to as European), African, and Africanized worker bees as well as from extracts of comb wax produced by European or Africanized honey bees. Figure 2 displays the reconstructed ion chromatogram of alkene adducts from African honey bees. The major peaks at scan numbers 638, 712, and 792 represented the alkenes of C_{31} , C_{33} , and C_{35} chain length, respec-

Table II. Mass-to-Charge Ratio of Diagnostic Ions of DMDS Derivatives of Alkenes in European/Florida (FL) Burr Wax and Comb Wax, and Africanized Comb Wax

compound ^a <i>n</i> -C _m	<i>x</i>	<i>y</i>	<i>m/z</i> (% relative abundance, FL burr wax)				% of each isomer ^b		
			(M) ⁺	(M - 47) ⁺	(A) ⁺	(B) ⁺	FL burr	FL comb	AF comb
7-C ₂₃	5	14	416 (17)	369 (5)	145 (15)	271 (21)	17	-	-
9-C ₂₃	7	12	-	-	173 (81)	243 (100)	83	-	-
7-C ₂₅	5	16	444 (14)	397 (3)	145 (10)	299 (13)	11	-	-
9-C ₂₅	7	14	-	-	173 (85)	271 (100)	89	-	-
7-C ₂₇	5	18	472 (13)	425 (b)	145 (13)	327 (17)	15	-	-
8-C ₂₇	6	17	-	-	159 (6)	313 (6)	6	-	-
9-C ₂₇	7	16	-	-	173 (69)	299 (90)	79	-	-
8-C ₂₉	6	19	500 (10)	453 (b)	159 (58)	341 (88)	68	-	-
9-C ₂₉	7	18	-	-	173 (17)	327 (21)	18	-	-
10-C ₂₉	8	17	-	-	187 (11)	313 (7)	8	-	-
11-C ₂₉	9	16	-	-	201 (5)	299 (7)	6	-	-
8-C ₃₁	6	21	528 (18)	481 (5)	159 (69)	369 (100)	52	45	63
9-C ₃₁	7	20	-	-	173	355	-	-	23
10-C ₃₁	8	19	-	-	187 (68)	341 (83)	47	55	14
12-C ₃₁	10	17	-	-	215 (3)	313 (b)	1	-	-
8-C ₃₃	6	23	556 (8)	509 (3)	159 (3)	397 (4)	4	-	14
10-C ₃₃	8	21	-	-	187 (80)	369 (100)	91	91	86
12-C ₃₃	10	19	-	-	215 (4)	341 (5)	5	9	-
10-C ₃₅	8	23	584 (8)	537 (b)	187 (56)	397 (100)	-	-	66
12-C ₃₅	10	21	-	-	215 (32)	369 (50)	-	-	34

^a *n*-C_m; *n* = position of double bond; *m* = chain length of alkene; for *x* and *y* see Figure 1. ^b Calculated as the average of relative abundance ratios of (A)⁺ and (B)⁺ for each positional isomer of the particular carbon chain length: - indicates less than 1%. ^c Detected in Africanized bee only.

and C₃₅, with C₃₃ as the major homologue. However, the presence of the 9-isomer in the C₃₁ alkene appears to indicate the presence of African genetic material, as the African worker bees and comb wax contained similar components by GC/MS. Also, we were interested to find that the GC peaks for alkene adducts of C₃₁, C₃₃, and C₃₅, mentioned as diagnostic for the races, appeared to be present in the diagnostic proportion when viewed as the DMDS adducts of alkenes of each race.

Alkadienes. The DMDS diadducts were formed by the addition of DMDS to the double bonds (Figure 1b). The retention indexes of the DMDS diadducts of C₃₃ alkadienes in beeswax were 1260 KI units (12.6 ECL) longer than that for a C₃₃ alkadiene. Because of the presence of the four methyl sulfide groups, diadducts of more than 37 carbons eluted after 80 min from the 12-m GC columns. Alternatively, sample introduction was performed via a solid probe. EI mass spectra of diadducts were characterized by ions (M)⁺, (M - 48)⁺, (M - 94)⁺, (M - 141)⁺, and usually (M - 188)⁺ to regenerate the original compound. More intense fragment ions were formed by cleavage of carbon-carbon bonds between the methyl sulfide substituents as well as by losses of 48 (HSCH₃) and 94 (CH₃SSCH₃) mass units from the larger fragments.

The spectrum of the diadduct of synthetic (Z,Z)-9,19-heptatriacontadiene was obtained with sample introduction (5 μg) via solid probe, that was ramped from 100 to 300 °C at 30 °C/min. The ion current signal maximized at ca. 220 °C. The pair of ions at *m/z* 173 (A)⁺ and *m/z* 299 (D)⁺ showed the presence of a double bond at 9 carbons from one end and a second at 18 carbons from the other end of the molecule (Figure 4). The fragment ions (B)⁺ (*m/z* 531) and (C)⁺ (*m/z* 405) were not detected, probably due to their instability (each would contain three SCH₃ groups). However, the fragment ions at *m/z* 483, 437, 357, and 311 result from the loss of 48 (HSCH₃, minor) and 94 (CH₃SSCH₃, major) mass units from (B)⁺ and (C)⁺. From these diagnostic ions, the unsaturated sites of the molecule were unambiguously determined as these large fragments contain unsaturated chains. Also, the characteristic diadduct molecular ion at *m/z* 704 (M)⁺ and starting material at *m/z* 516 (M - 188)⁺ were both conspicuous here. Sample introduction via solid probe gave useful spectra, as the adducts survived heating. Additional separation prior to derivatization and solid probe in-

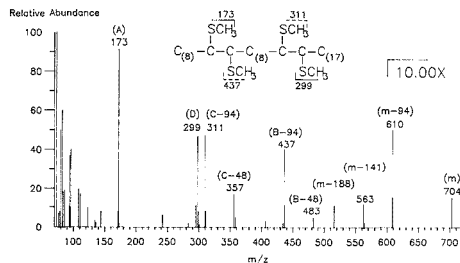


Figure 4. Mass spectrum of DMDS diadduct of (Z,Z)-9,19-heptatriacontadiene.

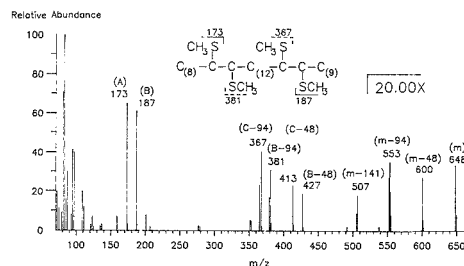


Figure 5. Mass spectrum of DMDS diadduct of (Z,Z)-9,23-tritriacontadiene from European/Florida honey bee.

roduction may be necessary for those adducts that exceed a molecular weight of 700.

A mixture of *n*-alkadienes containing only (Z,Z) configurations was separated from the hydrocarbons from European bees and derivatized and the DMDS diadducts were analyzed by capillary column GC/MS using GC parameters as above. Alkadienes having chain lengths of C₃₁, C₃₃, and C₃₅ were detected. The double bonds in most homologues were separated by 12 methylene groups, as shown in the summary (Table III). Figure 5 displays the spectrum of the major C₃₃ homologue found in the European bee sample, characterized

Table III. Mass-to-Charge Ratio of Diagnostic Ions of DMDS Derivative of Alkadienes in African, Africanized, and European/Florida Honey Bee (Major Isomer)

$n,n-C_m$ compound ^a	m/z (% relative abundance, European bee)												
	x	z	y	(A) ⁺	(D) ⁺	(B-48) ⁺	(B-94) ⁺	(C-48) ⁺	(C-94) ⁺	(M-188) ⁺	(M-141) ⁺	(M-94) ⁺	(M) ⁺
8,22-C ₃₁	6	12	7	159 (54)	173 (51)	413 (19)	367 (34)	399 (18)	353 (34)	432 (1)	479 (12)	526 (2)	620 (2)
9,22-C ₃₁ ^{b,c}	7	11	7	173 (66)	173 (66)	399 (23)	353 (33)	399 (23)	353 (33)	432 (7)	479 (10)	526 (4)	620 (2)
9,23-C ₃₃	7	12	8	173 (59)	187 (59)	427 (22)	381 (43)	413 (26)	367 (52)	459 (1)	507 (18)	553 (3)	648 (1)
				(69)	(63)	(6)	(19)	(5)	(19)	(3)	460 (3)	507 (12)	648 (2) ^c
9,23-C ₃₅	7	12	10	173 (67)	215 (43)	455 (16)	409 (32)	413 (16)	367 (32)	488 (1)	535 (8)	582 (2)	676 (1)
				(62)	(32)	(4)	(4)	(5)	(8)	488 (4)	535 (3)	582 (3)	676 (2) ^c
9,23-C ₃₇ ^c	7	12	12	173 (71)	243 (10)	484 (-)	437 (7)	414 (-)	367 (7)	-	-	-	-

^a $n,n-C_m$: n = positions of double bonds; m = total carbon length before derivatization; - indicates less than 1%. ^b African bee. ^c Africanized bee.

Table IV. Double Bond Positions in Natural Alkenes and Alkadienes by GC/MS of DMDS Adducts

sample	C27	C29	C31	C33	C35	C37
alkenes ^a						
African	8, 9 ^b	8, ^b 9, 10	8, ^b 9, 10	8, 9, 10, ^b 12	8, 10, ^b 12	10, 12, ^b 14
European	9	8, ^b 9, 10, 11	8, 10 ^b	1, 12 ^b	10, 12, ^b 14	- ^c
Africanized	9	8, 9, ^b 10	8, ^b 9, 10	8, ^b 10	10, ^b 12	-
alkadienes						
African	-	-	-	9,23-	9,23,- ^b 9,25-	9,23-
European	-	-	8,22-	9,23-	9,23-	-
Africanized	-	8,20-	9,22-, 8,23- ^b	9,23-	9,23,- ^b 9,25-	9,X-

^a Major C₂₅, C₂₅ alkenes were 9-unsaturated. ^b Major isomer. ^c -, not detected.

by the diadduct molecular ion at m/z 648 (M)⁺, in addition to fragment ions at m/z 600 (M-48)⁺, m/z 554 (M-94)⁺, and m/z 507 (M-141)⁺, which arose from loss of one, two, and three SCH₃ groups, respectively. The diagnostic ions at m/z 173, (A)⁺, and m/z 187, (D)⁺, indicated the double bond positions at carbon numbers 9 and 23. This was further supported by the presence of other diagnostic ions at m/z 427 (B-48)⁺, m/z 381 (B-94)⁺, m/z 413 (C-48)⁺, and m/z 368 (C-94)⁺. Minor fragment ions suggested that there were other minor isomers beside the 9,23 isomer, but the positions of double bonds could not be confirmed. The other alkadienes were less diverse in European honey bees, with a 12 unit methylene chain usually present between the double bonds, with 8,22-C₃₁, 9,23-C₃₃, and 9,23-C₃₅ being found in European materials. The results of GC/MS analysis of diene diadducts from African and Africanized workers (Table IV) showed more diversity than in European workers, as 9,22-C₃₁ and 9,25-C₃₅ dienes were found. Mass chromatograms of Africanized honey bee C₃₁ to C₃₅ diene diadducts (Figure 6) showed A⁺ (m/z 173) as ions common to each homologue, with (B-94)⁺ ions being characteristic for each individual homologue. The C₃₅ and C₃₇ diadducts were just separated on the short 3-m column but were separated by 14 min during GC/MS and 8 min during GC, with no evidence for thermal cleavage of the adducts during this 90 min at high temperature. However, linear DMDS diadducts may be limited to those alkadienes with 27 or fewer carbons.

The spectrum of the DMDS diadduct of the C₃₅ alkadiene extracted from *Anastrepha suspensa* males showed a molecular ion at m/z 676 (M)⁺ and m/z 486 (M-188)⁺. Only 9,25-pentatriacontadiene was detected in the peak. The positions of the double bond were interpreted as at carbons 9 and 25, determined by m/z 173 (A)⁺ and m/z 187 (D)⁺ as well as m/z 455 (B-48)⁺, m/z 409 (B-94)⁺, m/z 441 (C-48)⁺, and m/z 395 (C-94)⁺. The double bond positions in this unreported compound were separated by 14 methylene groups.

Treatment of natural (Z,Z)-7,11-penta-, hepta-, and nonacosadienes from *Drosophila melanogaster* (6) for 4 h with

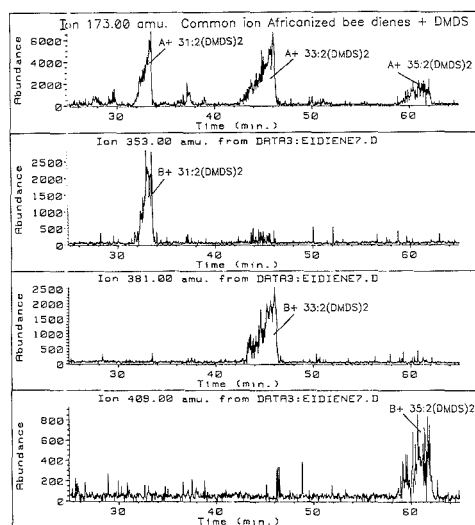


Figure 6. Mass chromatograms of DMDS diadducts of (Z,Z)-9,23-C₃₁ to C₃₅ alkadienes from Africanized honey bees.

DMDS gave both mono- and cyclic adducts of each diene. The 7,8-monoadducts and 11,12-monoadducts of each carbon number did not separate by GC, but clearly indicated both positions of unsaturation. Chromatographically cyclic adducts of all three dienes were observed that clearly fragmented next to the thiophene ring, producing alkyl fragments and fragments also containing the ring, consistent with a recent report (14). The C₂₅, C₂₇, and C₂₉ (Figure 7) diene cyclic adducts shared the common ions A⁺ (m/z 145) and (A+ring)⁺ (m/z 183/231), this last pair rising from loss of CH₃S from the larger fragment. Characteristic ions were D⁺ (m/z 243, 271, and 299)

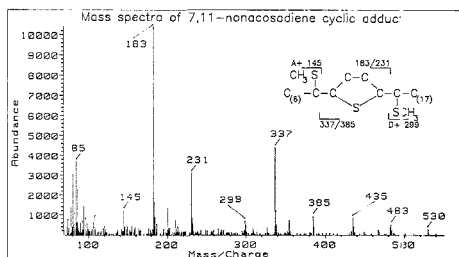


Figure 7. Mass spectrum of (Z,Z)-7,11-nonacosadiene cyclic DMDS adduct.

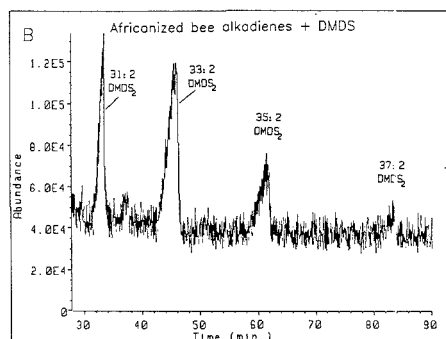
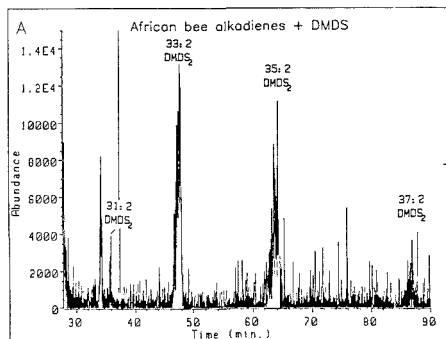


Figure 8. Reconstructed ion chromatogram of DMDS diadducts of honey bee dienes: (A) African; (B) Africanized.

and also (D + ring)⁺ (*m/z* 281/328, 309/356, and 337/384) for the C₂₉, C₂₇, and C₂₅ cyclic adducts, respectively. The M⁺, (M - 47)⁺, and (M - 94)⁺ ions were prominent for each homologue, from addition of 126, 93, and 31 amu to the respective starting materials. These cyclic adducts could not be mistaken for linear adducts because of their unusual masses. The exact criterion for successful localization remains incomplete due to lack of a range of synthetic standards. Results suggest that linear derivatives are limited to a kadienes with double bonds separated by more than four methylene groups, and cyclic thioethers are formed when three methylenes or fewer were present between the double bonds.

For rapid analysis with minimal handling the total hydrocarbon fractions of insects were derivatized with DMDS for only 4 h. Small portions of fractions from honey bees were used for GC and GC/MS analysis with excellent results. The alkanes were unaffected and eluted earliest, the alkene adducts

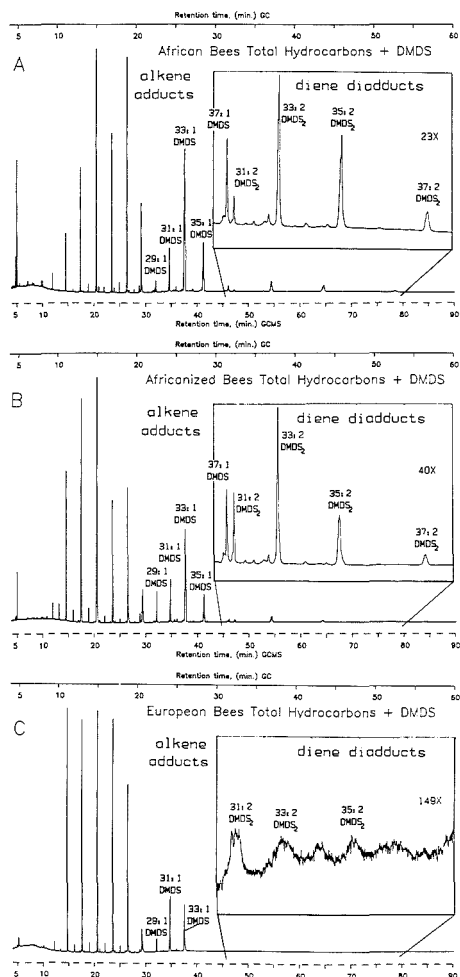


Figure 9. GC trace of total hydrocarbon fraction from honey bees after DMDS treatment, with representative GC/MS retention time under trace: (A) African; (B) Africanized; (C) European.

appeared as the next set of peaks, and the diene diadducts appeared last, with each group well separated in time for African bees (Figures 8A and 9A) and Africanized bees (Figures 8B and 9B), but the much smaller quantities of corresponding diadducts of European bee dienes (Figure 9C) were not detected under these conditions. The diene diadducts eluted after a long period of time, the C₂₇ diadduct surviving 78–90 min on a GC column. Interestingly, the same proportions of two alkenes, C_{31:1} (KI 3075) and C_{33:1} (KI 3265) mentioned as diagnostic for honey bee races (16), were also observed in the DMDS adducts, with clear differences in monoadducts in GC analyses (Figure 9) and GC/MS total ion chromatograms, just as when run previously with alkenes of different samples after TLC separation. Also, small amounts of monoadducts of dienes were seen in the 4-h reaction materials, and could be distinguished by the (B - 94)⁺ or (D - 94)⁺ ions that differed by 2 amu from large alkene adduct ion fragments.

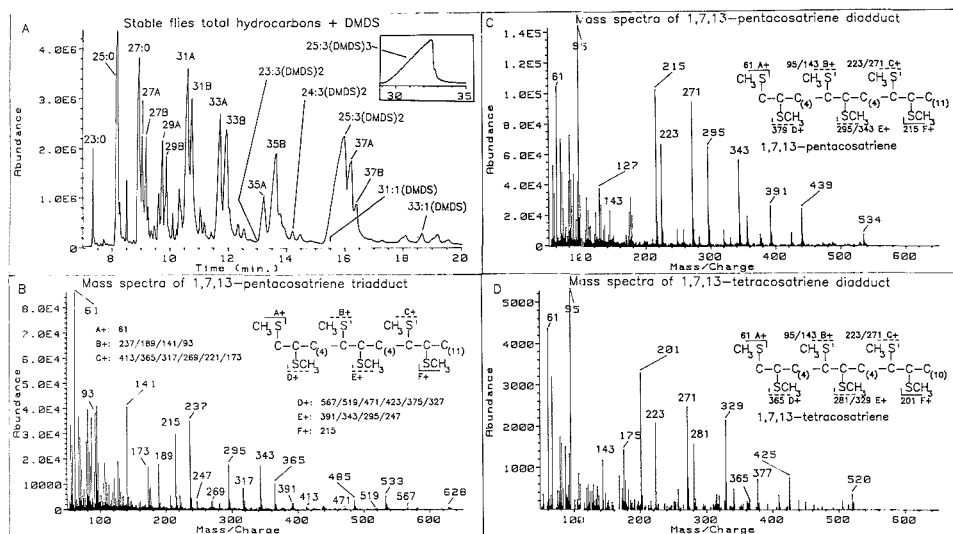


Figure 10. DMDS derivatives of total hydrocarbon fraction from stable flies: (A) total ion chromatogram after GC/MS; (B) mass spectra of 1,7,13-pentacosatriene triadduct; (C) mass spectra of 1,7,13-pentacosatriene diadduct; (D) mass spectra of 1,7,13-tetracosatriene diadduct.

Alkatrienes. The total hydrocarbon fraction of stable flies of mixed sexes was analyzed by GC and then derivatized over 4 h for GC/MS (Figure 9A). The *n*-alkane majority components C_{25} and C_{27} eluted unchanged, with the largest component, 1,7,13-pentacosatriene (original KI 2455) (17, 19) observed as a triadduct (KI 4400) eluting at 32 min using the on-column injector. Its retention index was lengthened by about 1900 units due to the presence of six CH_2S substituents. This sample was overloaded in an unsuccessful search for homologous minor $C_{23,3}$ and $C_{24,3}$ triadducts. None of the starting material was apparent. Previously reported alkanes, methylalkanes, and homologous 9-alkenes (17) were observed, with alkene adducts easy to distinguish from other materials. In the spectrum of the triadduct (Figure 10B), the one-carbon fragment A^+ (m/z 61) was seen, and the terminal fragment F^+ ($C_{12}\text{SCH}_3$, m/z 215) located the 13-position of unsaturation. Other prominent fragments, B^+ , C^+ , D^+ , and E^+ were observed with concomitant loss of CH_2S substituents. Although the M^+ ion (m/z 628) was not intense, other ions derived from the molecular ion could be followed through successive losses of 47 mass units (very small, m/z 581), 94 (m/z 533), 141 (m/z 485), 188 + 1 (m/z 439), 235 + 2 (m/z 393), and 282 + 3 (m/z 343) from the intact triadduct.

However, both homologous minor alkatrienes (19) were eluted as unresolved mixtures of diadducts, as 1,7,13-tricosatriene (original KI 2255) and 1,7,13-tetracosatriene (KI 2355) were followed by the major triene diadduct mixture. The C_{23} , C_{24} , and C_{25} diadducts were located by ion fragmentography, using fragments at m/z 187, 201, and 215, respectively, with the common m/z 271 ion confirming the elution pattern (Figure 11). Full scans were obtained for all three diadducts, with the terminal fragments F^+ and M^+ particularly obvious in each homologue. All other fragment ions were observed as pairs with concomitant loss of CH_2S substituents. For the C_{25} diadduct mixture, prominent fragments were seen for $(C - 188)^+$ (m/z 223, $C_{13,4}\text{SCH}_3$), $(E - 47)^+$ (m/z 343), and $(E - 94)^+$ (m/z 295), whereas $(B - 94)^+$ (m/z 143) and $(D - 188)^+$ (m/z 379) were less intense (Figure 9C); M^+ (m/z 534) and $(M - 1 - 94)^+$ (439) were prominent. It was not clear that one position of unsaturation was favored more than another during addition of DMDS. For the $C_{24,3}$ (Figure 9D) and $C_{23,3}$ di-

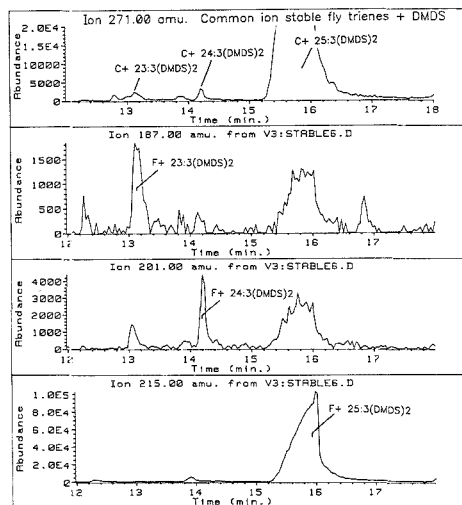


Figure 11. Ion chromatograms of DMDS diadducts of homologous 1,7,13-tricosatriene, 1,7,13-tetracosatriene, and 1,7,13-pentacosatriene.

adducts, A^+ , B^+ , and C^+ were identical with those from the $C_{25,3}$ diadduct mixture. Ions from D^+ , E^+ , F^+ , M^+ (m/z 425), and $(M - 1 - 94)^+$ (m/z 520) were one methylene smaller for $C_{24,3}$ (Figure 9D) and two methylenes smaller for $C_{23,3}$, respectively. Interpretation of diadduct spectra to determine positions of unsaturation was straightforward.

Alternatively, we attempted the derivatization of alkenes with DMDS directly in the CI source, using a mixture of DMDS and N_2 as a CI reagent gas mixture, with MS/MS to be used to determine the double bond location. The expected DMDS adducts produced by ion-molecule reaction were not observed, however, even when different source temperatures (100–190 °C) were used. Rather, the EI mass spectra were

dominated by protonated DMDS ions at m/z 95. Furthermore, the DMDS/N₂ reagent gas badly contaminated the gas lines as well as the source, and this method was abandoned.

LITERATURE CITED

- (1) Wolff, R. E.; Wolff, G.; McCloskey, J. A. *Tetrahedron* **1966**, *22*, 3093-3101.
- (2) Adams, J.; Detering, L. J.; Gross, M. L. *Spectrosc. Int.* **1987**, *5*, 199-228.
- (3) Dommès, V.; Wirtz-Peitz, F.; Kunan, W. H. J. *Chromatogr. Sci.* **1976**, *14*, 360.
- (4) McCloskey, J. A.; McClelland, M. J. J. *Am. Chem. Soc.* **1965**, *87*, 5090.
- (5) Bierl-Leonhardt, B. A.; Devilbiss, E. D.; Plimmer, J. R. J. *Chromatogr. Sci.* **1980**, *18*, 364-367.
- (6) Pechine, J. M.; Perez, F.; Antony, C.; Jallon, J. M. *Anal. Biochem.* **1985**, *145*, 177-182.
- (7) Blomquist, G. J.; Howard, R. W.; McDaniel, C. A.; Remaley, S.; Dwyer, L. A.; Nelson, D. R. *J. Chem. Ecol.* **1980**, *6*, 257-269.
- (8) Baker, R.; Bradshaw, W. S.; Speed, W. *Experientia* **1982**, *38*, 233-234.
- (9) Lankelma, J.; Ayanaglu, E.; Djerassi, C. *Lipids* **1983**, *18*, 853-858.
- (10) Nelson, D. R.; Fatland, C. L.; Baker, J. E. *Insect Biochem.* **1984**, *14*, 435-444.
- (11) Francis, G. W.; Veland, K. J. *Chromatogr.* **1981**, *219*, 379-384.
- (12) Buser, H. R.; Arn, H.; Guerin, P.; Rauscher, S. *Anal. Chem.* **1983**, *55*, 818-822.
- (13) Dunkelblum, E.; Tan, S. H.; Silk, P. J. *J. Chem. Ecol.* **1985**, *11*, 265-278.
- (14) Vincenti, M.; Gugliemetti, G.; Cassani, G.; Tonini, C. *Anal. Chem.* **1987**, *59*, 694-699.
- (15) Carlson, D. A.; Yocom, S. R. *Arch. Insect Biochem. Physiol.* **1986**, *3*, 397-412.
- (16) Carlson, D. A.; Bolten, A. B. *Bull. Entomol. Soc. Am.* **1984**, *30*, 32-35.
- (17) Sonnet, P. E.; Eubel, E. C.; Lusby, W. R.; Schwarz, M.; Miller, R. W. *J. Chem. Ecol.* **1979**, *5*, 353-361.
- (18) Bartlett, R. J.; Jones, R. L.; Kulman, H. M. *J. Chem. Ecol.* **1982**, *8*, 95-114.
- (19) Carlson, D. A.; Mackley, J. W. *J. Chem. Ecol.* **1985**, *11*, 1485-1496.

RECEIVED for review August 24, 1988. Accepted April 10, 1989. Part of this work was presented at the 189th American Chemical Society National Meeting (Miami Beach, FL, April 28-May 3, 1985) (Pest 028). Mention of a commercial or proprietary product in this paper does not constitute an endorsement of this product by the United States Department of Agriculture.

Utilization of Spectrometric Information in Linked Gas Chromatography-Fourier Transform Infrared Spectroscopy-Mass Spectrometry

John R. Cooper and Charles L. Wilkins*

Department of Chemistry, University of California, Riverside, Riverside, California 92521

Fourier transform infrared (FTIR) and mass spectral (MS) data collected with linked GC-IR-MS systems are combined in a complementary fashion to identify organic mixture components. Methodology to combine and compare infrared and mass spectral information generated by the linked system is discussed. A 30-component mixture is analyzed to demonstrate application of the system to mixture analysis. Analysis of a complex environmental soil sample further illustrates the value of the methodology. Concurrent utilization of both types of spectral information increases the reliability of library-search-based identifications. Thus, use of a 3304-member library of combined IR-MS spectral information was more efficacious than use of either type of spectral information separately.

Combined analysis methods employing gas chromatography, Fourier transform infrared spectroscopy, and mass spectrometry (GC-IR-MS) can provide complementary information related to the structures of unknown organic compounds. Advantages of concurrent use of the two spectral data types were discussed in a recent review of GC-IR-MS (1). Improvements in Fourier transform infrared (FT-IR) design and optimization of chromatographic interfaces have contributed to increased sensitivity of commercial GC-FT-IR instruments (2). As a consequence, high-resolution, high-capacity wall coated open tubular capillary gas chromatography can be used routinely with GC-IR (3). In addition, combined GC-IR-MS systems are now practical as a result of availability of low-cost FT-IR and mass spectrometers (4, 5). A number of applications of GC-IR-MS have been directed toward analysis of complex samples of environmental

concern (6-11), and analysis of polycyclic aromatic hydrocarbons (PAH) was facilitated by use of infrared spectral data in conjunction with GC-MS data (12).

Although new instrumentation is now available, the primary method still used to identify mixture components by GC-IR-MS centers upon the use of separate data bases and library search algorithms (6, 13). These data bases are quite different in size and content, with the commonly used mass spectral library being an order of magnitude larger than the infrared. Postsearch methods for combining discrete infrared and mass spectral library search results have been described (14-16). Chemical Abstracts registry numbers are used to locate common occurrences of compounds in the respective infrared and mass spectral search outputs. Comparison of these results then determines whether coincident reference compounds are present in the search lists and, by inference, in the mixture being analyzed.

In this paper, a search system employing a combined library of GC-IR-MS data for analysis of infrared and mass spectra obtained with direct-linked GC-IR-MS instrument systems is described. Where both types of spectral information are available from the measurements, both types of data (IR and MS) are used jointly; when only one type of spectrum is available experimentally, the relevant part of the spectral data base is used. Prefilter algorithms are investigated as a means of increasing search speeds and to assess the relationship between search performance and the major spectral features. The changes in identification performance resulting from using only a single type of spectral data are determined by comparison with joint IR-MS analysis. Analysis of a standard mixture of 30 components present at low levels (10-80 ng per component) and analysis of an authentic environmental soil sample concentrate of interest to the United States Envi-

ronmental Protection Agency were used to develop and test the algorithms discussed here.

EXPERIMENTAL SECTION

Instruments. Two linked gas chromatography-Fourier transform infrared-mass spectrometry systems were used in this study. One system, used in previous work (15), consisted of a Varian 3700 gas chromatograph, Nicolet 20 SXB Fourier transform infrared spectrometer, and a Hewlett-Packard 5970 mass selective detector (MSD), with a parallel split of the GC effluent between the MSD and the FT-IR instruments using a low-volume polyimide (Vespel) tee splitter. For combined data analysis and algorithm development, a Nicolet 1280 host computer system was used. A second, commercially available, combined GC-IR-MS system was used for the mixture analyses reported here. This system included a serially linked Hewlett-Packard (HP) 5890 gas chromatograph, HP 5965A Fourier transform infrared detector (IRD), and HP 5970 MSD. For application of the data analysis algorithms developed here, infrared and mass spectral data were transferred from the Hewlett-Packard GC-IRD-MSD system via an RS-232 interface by using a HP 2392A/VT100 terminal emulator software package. Nicolet software programs were written to receive the ASCII data files and to translate them into the appropriate format for use with standard Nicolet FT-IR software. Similarly, the IRD Gram-Schmidt reconstructed chromatograms and the MSD total ion current reconstructed chromatograms were translated into a format compatible with Nicolet FT-IR software. Thus, mixture separations, spectral data acquisition, and data reduction tasks were handled by the HP GC-IRD-MSD system. Algorithm development, evaluation, and applications (including library searches) were carried out, following data transfer, with the Nicolet 1280 host computer.

Chromatography. Mixture separations were performed with the Hewlett-Packard 5890 gas chromatograph. A 30-component mixture was prepared as a solution in hexane from the components listed in Table I and 1 μL of this solution injected, by heated splitless injection, onto a J&W 30 m \times 0.32 mm i.d. fused silica column coated with 5% phenylmethyl polysiloxane (DB-5, 0.5- μm film). The quantities in Table I are the amounts of each component contained in a single injection of the solution. Following injection, the temperature was programmed to increase at a rate of 4 $^{\circ}\text{C}/\text{min}$ to 100 $^{\circ}\text{C}$ and 15 $^{\circ}\text{C}/\text{min}$ from that temperature to 200 $^{\circ}\text{C}$, following a 3-min hold period at an initial temperature of 50 $^{\circ}\text{C}$. Mobile phase was high-purity helium (99.999%) with a head pressure of 10 psi.

A concentrate of a soil steam distillate was also analyzed. For this separation, a 30 m \times 0.25 mm i.d. methyl polysiloxane-coated (DB-1, 1-mm film) column was used. A 1.5- μL aliquot of a 50:1 (v/v) acetone/distillate sample mixture was injected. Temperature programming followed a 4-min hold time at 60 $^{\circ}\text{C}$. Temperature was first increased at a rate of 10 $^{\circ}\text{C}/\text{min}$ to 120 $^{\circ}\text{C}$, then at 4 $^{\circ}\text{C}/\text{min}$ to 220 $^{\circ}\text{C}$, and finally 7 $^{\circ}\text{C}/\text{min}$ to 280 $^{\circ}\text{C}$. Mobile phase was high-purity helium (99.999%) with a head pressure of 17 psi.

Spectroscopy. Infrared spectra were obtained by using the HP IRD at a spectral rate of 0.3 s/file, collecting 2048-point interferograms. Spectral resolution was 8 cm^{-1} . The IRD incorporates a 1 mm i.d. \times 12 cm internally gold-coated Pyrex lightpipe that was maintained at 300 $^{\circ}\text{C}$ during spectral measurements. A narrow-range Hg/CdTe (MCT) detector with a 750- cm^{-1} cutoff was used. Optics were purged with a Purgegas heatless regenerative dryer, which also removed carbon dioxide. Subsequently, due to reduced source lifetime resulting from this arrangement, optics were purged with dry nitrogen.

Mass spectra were obtained by using the HP 5970 MSD, interfaced serially following the IRD. To increase the quantity of eluant entering the MSD source, the restrictor/transfer line was modified. As originally installed, 1.5 m of 100 μm i.d. fused silica produces a source background pressure of (4-5) $\times 10^{-6}$ Torr. By reduction of the length of the 100- μm tubing to 0.69 m and construction of the first 0.41 m from 250 μm i.d. tubing, the source background pressure was raised to 1.2 $\times 10^{-6}$ Torr. The junction of the 250 μm to 100 μm fused silica tubing was made with Cotronics high-temperature epoxy. This arrangement maximizes MSD sensitivity while maintaining the pressure at a level acceptable for tuning. The MSD was tuned using perfluorotri-

butylamine (PFTBA) to yield 0.5 amu full width at half-height peaks. The scan range was 33-400 amu at a rate of approximately 2 scans/s.

IR-MS Spectral Library and Searches. A combined reference library of infrared and mass spectra was assembled from the Aldrich/Nicolet infrared vapor-phase library of 5010 spectra, to which was added 117 locally measured spectra (total 5127 spectra) and the NBS/EPA/MSDC mass spectral library of 44221 spectra. Comparison of Chemical Abstracts registry numbers showed that spectra of 3304 compounds appear in both libraries. These were combined to form a 3304-entry combined library with each entry containing 384 infrared spectral frequencies and up to 64 mass spectral masses packed into 256 20-bit computer words. Intensities of the 16 cm^{-1} spectral resolution infrared frequencies are normalized to 10 bits (1023 maximum value) and packed two frequencies per word. The spectral range is 625-3725 cm^{-1} . The position within the data vector represents the frequency. Within this range, 19 infrared spectral frequency windows of minimal spectral importance were eliminated to bring the total number of frequency windows to 384. This was determined by a computer survey of all spectral frequency regions represented in the library. A histogram of all library spectral features with intensities greater than 10% of the maximum was compiled; the 19 lowest entries were those eliminated from the combined library. Mass spectral ion abundances were also normalized to a maximum value of 1023, with the masses of the 64 most abundant ions in each spectrum represented. Each mass spectral computer word contains a 10-bit mass and a 10-bit abundance value. This 3304-member library was used for all searches reported here, with the exception of probability-based matching (PBM) searches, which utilized the 44261 spectrum National Bureau of Standards library, as supplied by Hewlett-Packard.

Search Algorithm. An algorithm that computes the absolute difference between experimental and reference library spectra was used for comparisons. The result was normalized in each case to yield a similarity index with a range from 1.0000 (perfect match) to 0.0000 (no match). The algorithm was constructed such that a search using only infrared spectra, only mass spectra, or both could be performed. For the combined search, the similarity index was the average of the infrared and mass spectral search indexes. Indexes are reported as integer values between 0 and 10000.

In order to reduce search times and to investigate the advantages and disadvantages of using major spectral features for presearch filtering, a separate presearch file, containing both infrared and mass spectral information, was created. This information can reside in computer memory throughout each spectral search session. The presearch file is simply a tabulation of the two most abundant mass spectral ions and the two strongest infrared absorptions for each library compound. A reverse search strategy is used. The primary presearch requires that the unknown's infrared and mass spectra each contain a spectral absorbance frequency or ion that corresponds to the frequency of strongest absorbance (IR) or the mass of the ion of greatest abundance (MS) for the library entry. However, these data points need not represent the strongest absorbances or the most abundant ions in the unknown spectra. The minimum relative intensity or abundance can be specified by the user as a percentage of the maximum normalized intensity. Thus, values between 0% (no presearch) and 100% (maximum restriction) can be selected. Library spectra for which the constraints are not met are eliminated from further comparisons.

If the first presearch criterion described above is met, then the second most abundant or second strongest absorbance value may be used to complete the presearch process. If this feature of the library spectrum is not more than 40% of the value of the strongest infrared absorbance or 25% of the most abundant mass spectral ion, in the library spectrum, then the secondary presearch is not carried out. However, if these constraints are met, then the same comparison of experimental with library data, using a user-specified threshold, is done as in the primary presearch, resulting in further screening of the library to produce a small search file. However, in this case, the user may specify only comparison thresholds between 0 and 40% (IR) and 0 and 25% (MS), rather than the 0-100% threshold range allowed for the initial presearch. The flow chart of Figure 1 outlines the search logic.

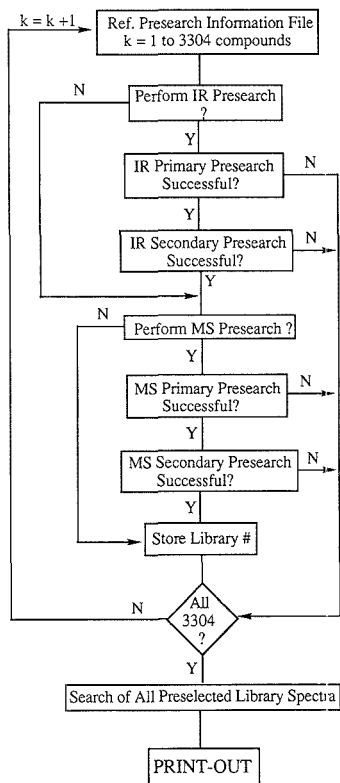


Figure 1. Presearch strategy flow chart.

Thus, a four-level filter is employed when all criteria for both infrared and mass spectral data are used. To allow maximum flexibility, the user can specify any of 12 options for the search procedure. These include use of no prefilter and IR-only, MS-only, or IR-MS for similarity index calculation or use of IR, MS, or IR-MS presearch and IR, MS, or IR-MS similarity index calculation. Software similar to that described earlier (15) correlates the two types of spectral information prior to beginning the search procedure to assure, on the basis of reconstructed chromatogram retention times, that both infrared and mass spectral information is available for each component. If only one or the other is available for a particular component, then the appropriate analysis option is employed.

For comparison of identification efficacy, the probability-based matching algorithm (PBM) (17) available with the MSD software was also investigated. The spectral data base was that supplied by Hewlett-Packard and contains 42 261 entries. For PBM the following parameters were used: $U + A = 2$; number of ions = 10; no tilt; full mass range. In the Hewlett-Packard PEM software, the value of the parameters ($U + A$) basically adjusts the level of presearch employed. Values from 1 to 3 may be chosen, with the value 3 providing the minimum filtering. Use of the parameters previously reported ($U + A = 3$; number of ions = 15, full tilt; full mass range) (9) was also investigated but gave slightly poorer results and much longer search times. For I.F.D. searches, a version of the EPA vapor-phase data base containing 3042 spectra was used with an absolute difference search algorithm.

RESULTS AND DISCUSSION

The combined infrared-mass spectral data base compiled here, although substantially smaller than either of the individual starting data bases, is essentially the same size (3304

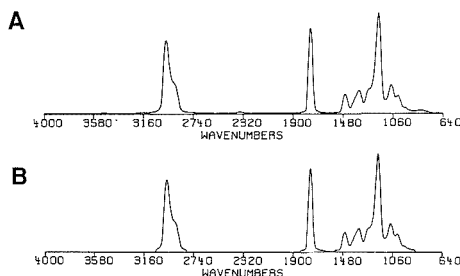


Figure 2. (a) Infrared spectrum of isopentyl propionate at 32-cm^{-1} spectral resolution. (b) Infrared spectrum of isopentyl propionate at 32-cm^{-1} resolution, truncated to the 75 highest absorbance spectral data points.

vs 3300 spectra) as one of the first and most widely used vapor-phase infrared spectral libraries, that developed by the U.S. Environmental Protection Agency. Although for many research applications the largest possible data base is desirable, for specific applications a smaller targeted data base may be preferable (18, 19). For example, because applications of GC-IR-MS are restricted to those compounds amenable to GC analysis, the full mass spectral data base contains extraneous information, including spectra of metal complexes, diatomic gases, and a number of substances unlikely to be encountered during GC separations. For environmental analysis applications, it has been suggested that the number of compounds of direct interest may be as few as 6000, which includes those volatile manufactured chemicals registered under the Toxic Substances Control Act (6, 20). Thus, the present results may have some direct relevance to the prospects of effectively using a smaller combined IR-MS data base in environmental and similarly specific applications.

Choice of format for any spectral data base is always a compromise between memory storage requirements, library search speed, and search reliability. As described in the Experimental Section, this combined library contains two complete IR-MS entries in a single 512-word data block. With the format described, it is possible to include almost all relevant infrared and mass spectral information. Although spectra are routinely measured with better resolution, the Aldrich/Nicolet library used here was available with 16-cm^{-1} resolution; the rationale behind this choice of library spectrum resolution was discussed previously (21, 22). In those studies, library search results using libraries with resolution between 8 and 64 cm^{-1} were similar. However, with 16-cm^{-1} resolution, sufficient spectral detail is retained to allow visual comparisons, while minimizing storage requirements. Others have reported use of 32-cm^{-1} reference spectra (23, 24).

An alternative to the approach described here involves concatenation of infrared and mass spectra, followed by factor analysis and eigenvector projection for data compression. Starting with a 32-cm^{-1} library of infrared spectra and unit mass resolution mass spectra over the mass range 1-256 dalton, Williams et al. found 110 of 442 eigenvectors to be significant (25). It is also possible to compress the spectral library in the spectral domain. For example, the majority of features of 32 cm^{-1} resolution infrared library spectra can be represented by 75 data points, and 27 masses can adequately represent most library mass spectra. Thus, each library entry could be reduced to 102 data points, and each 512-word block could hold five, rather than the two, IR-MS entries in the $16\text{ cm}^{-1}/64$ mass library format used to obtain the results presented here. Thus, when the 32-cm^{-1} infrared spectrum of isopentyl propionate is abbreviated to 75 data points (Figure 2), over 90% of the cumulative spectral absorbance between

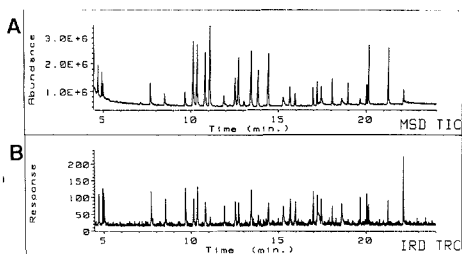


Figure 3. (a) Mass spectral total ion current reconstructed chromatogram for 30-component mixture. (b) Infrared Gram-Schmidt reconstructed chromatogram for 30-component mixture.

625 and 4000 cm^{-1} is retained. Furthermore, use of 27 masses for representing this compound's mass spectrum permits retention of all ions with relative abundances greater than 1%.

However, it is generally found that truncation of mass spectra can lead to a decrease in quality of library search results. In a previous study of GC-IR-MS, where MSD mass spectral data were used in a dot product (vector multiplication) metric comparison with a library where only the 10 most abundant ionic species for each entry were tabulated (a "10-peak" library), search performance was significantly worse for compounds such as aliphatic hydrocarbons, which show extensive mass spectral fragmentation. Attempts to use a weighted dot product metric to compensate were unsuccessful (26). When "64-peak" data were used with an absolute difference metric (i.e. the library spectrum with the smallest difference between its cumulative highest 64 ion abundances from the corresponding unknown spectrum is the closest match), significant improvement in search performance was realized. This is in accord with the results of a much earlier study which established that absolute or Euclidean distance metrics that use full mass spectra were most effective for library searches. As a consequence of these observations, although the data base could have been further compressed as described above, the less compact format was chosen for evaluation of the algorithms discussed here, so that lack of spectral detail would not be the limiting parameter.

In many literature applications, an absolute difference metric is demonstrated to work well for infrared spectral library searches. For combined IR-MS analysis, this procedure would inevitably lead to variable weighting of either the infrared or mass spectral part of the library entry. This is an obvious result of the fact that, for any particular compound, either the infrared or the mass spectrum may be more or less rich in features. Therefore, the approach adopted was to compute normalized similarity indexes for each part of the spectral information and to average the two for joint analysis (i.e. assign equal weight to the infrared and mass spectral information in combined analysis).

Thirty-Component Mixture Analysis. Figure 3 contains the reconstructed chromatograms from the infrared and mass spectral data obtained for the 30-component mixture described in Table I. It is obvious that the signal-to-noise ratio is worse for the infrared data; however, it is still well above that required for library searches. Because of somewhat better sensitivity, the MSD chromatogram also reveals a 31st component (an aromatic impurity, eluting at 13 min) that is not detected by the IRD.

As discussed earlier, a variety of search strategies are possible, once these data are in hand. The simplest is to use no presearch (threshold 0%) and use either IR, MS, or combined IR-MS library searches. Table II summarizes the results of a number of strategies. For comparison, the number of the 30 compounds whose correct library match appears in

Table I. Constituents of 30-Component Mixture

	compound	quantity injected, ng
1	1-octene	30
2	octane	impurity
3	ethyl butyrate	15
4	3-heptanone	30
5	butyl propionate	15
6	isobutyl methacrylate	20
7	2-chlorotoluene	80
8	4-chlorotoluene	80
9	1,3,5-trimethylbenzene	80
10	pentachloroethane	25
11	butyl butyrate	15
12	1,4-dichlorobenzene	40
13	α -terpinene	50
14	1,2-dichlorobenzene	80
15	indene	60
16	γ -terpinene	30
17	3-methylphenol	40
18	1-undecene	20
19	undecane	10
20	1,3,5-trichlorobenzene	20
21	1-bromooctane	20
22	2,4-dimethylphenol	40
23	1,2,4-trichlorobenzene	20
24	4-chlorophenol	40
25	α,α,α -trichlorotoluene	40
26	decyl alcohol	10
27	tridecane	10
28	2-methylnaphthalene	40
29	biphenyl	40
30	dodecyl alcohol	20

Table II. Position of 30-Component Mixture Constituents in Library Search Result Lists

position	IR only ^a	MSD only ^a	PBM	IR-MS ^a	IR-MS/IR ^b	IR-MS/MS ^b
1	20	19	19	28	23	24
2	4	7	6	1	2	3
3	2	1	2	1	1	
4			1			
5	2			1	2	
6						1
7		1				
8		1			1	2
10		1				
>10	2		1		1	
NM ^c			1			

^aUsing either 0% (no presearch) or 20% presearch threshold.

^bUsing an IR-MS presearch with 20% threshold, followed by full search using only IR or MSD data. ^cNo matches.

each position on each search list is tabulated (position 1 representing the closest library match and position 10 the worst of the 10 closest matches). Several significant facts are clear from study of this table. First, the three search procedures that used only one type of spectral information exclusively gave somewhat worse results than the combined search procedures (by the criterion that the best method is that which maximizes the number of compounds appearing in first position). Both absolute difference infrared and PBM mass spectral search placed 28 of the 30 compounds among the top 10 library matches, while absolute difference MSD mass spectral search located all 30 among the top 10.

Significantly, for the three entries where use of no prefilter was compared with use of a prefilter with a 20% threshold (IR only, MSD only, and IR-MS), identical results with respect to position in the search list were obtained in each case. This is in spite of the fact that the non-prefilter searches ranked 3304 library entries to obtain the 10 closest matches, while the 20% threshold significantly reduced the number of entries subjected to full comparison. For the combined IR-MS

Table III. Functional Groups/Isomers from Library Searches for Selected Constituents of 30-Component Mixture^a

retention time, min	compound ^b	feature ^c	no. in top 10			
			IR-MS	IR-MS ^d	IR	MSD
8.54	butyl propionate	ester	10	10	10	2
7.72	3-heptanone	ketone	9	9	10	4
10.84	1,3,5-trimethylbenzene	C ₉ H ₁₂	8	7	2	8
13.85	indene	mol wt 116-117	5	3	1	2
15.67	undecene	unbranched alkene	8	8	6	6
17.45	2,4-dimethylphenol	C ₈ H ₁₀ O	10	7	3	10
18.98	α,α,α -trichlorotoluene	isomers	5	1	1	5

^aNo presearch filter used, except as noted. ^bIdentified as closed match during IR-MS search. ^cRepresentative functional group, isomer, molecular formula, molecular weight. ^dWith 20% threshold IR presearch used.

library search, eight aromatic and chlorine-containing compounds (numbers 12, 14, 15, 20, 23, 25, 28, and 29 in Table I) returned only one library entry, following the presearch, and four other chlorine-containing compounds (numbers 7, 8, 10, and 24 in Table I) returned only two library entries, following presearch screening. For all, the closest match was the correct library entry. The maximum number of entries surviving prescreening was 341, for dodecyl alcohol. Thus, the prescreening algorithm eliminated almost 90% of the library in the worst case and significantly more most of the time. Use of a presearch decreased the search times by approximately an order of magnitude (e.g. 70 s for combined IR-MS search of the 3304 member library was reduced to between 0.2 and 8.7 s per component, when a 20% presearch threshold was used). *In no case did the presearch procedure eliminate the correct library entry.* Furthermore, the combined IR-MS search with a 20% threshold yielded clearly superior results.

To determine at what value the presearch threshold eliminated the correct library entry, a series of searches, incrementing the threshold from 20% to 75%, were carried out. For all compounds except 1,3,5-trichlorobenzene, the correct entry was not eliminated with any choice of threshold below 65%. In the trichlorobenzene case, the correct library entry was eliminated when a threshold of 31% was used. This appears to result from a serious negative base-line slope over the region from 1500 cm⁻¹ to the detector cutoff at 750 cm⁻¹. This is the only such instance of this problem encountered in the course of this study.

It also was of interest to use the combined IR-MS prefilter together with subsequent search of the screened library by either infrared or mass spectral comparisons. As might have been expected, the results are intermediate between those obtained when a single type of information is used and those when combined information is used throughout. Judging from the present data, it seems clear that use of the combined IR-MS spectral information throughout with a 20% prefilter is the best procedure.

Finally, for applications where there is a high probability that the unknown compounds being identified may not be represented in the library being searched, the desired outcome would be a search list suggesting the functionality of the unknown. For this purpose, it is probably more desirable to use the entire library with the combined information, but without a presearch. To test this premise, the 0%-threshold search results for some representative members of the 30-component test mixture were examined. Table III summarizes the relevant information. As is easily seen, although either infrared-only or mass spectral-only searches can yield information regarding functionality in selected cases, the combined IR-MS library search is consistently superior in this regard. In each of the selected seven examples, 50% or more of the 10 closest IR-MS library matches are the indicated functionality, in contrast to the results obtained with either IR or MS data alone.

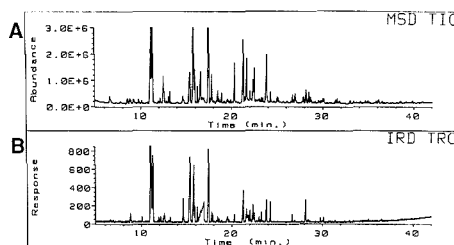


Figure 4. (a) Mass spectral total ion current reconstructed chromatogram for steam distillate sample. Maximum ordinate value was 5.4×10^6 . (b) Infrared Gram-Schmidt reconstructed chromatogram for steam distillate sample. Maximum ordinate value was 1550.

Soil Steam Distillate Analysis. A soil steam distillate sample, previously analyzed at a U.S. EPA laboratory (9), was analyzed to test the applicability of the algorithms described above to a representative real environmental mixture. In order to avoid overloading the chromatographic column, the sample was diluted 50:1 (v/v) in acetone to allow convenient analysis of the earlier-eluting polar components, which are a major part of the mixture. Figure 4 contains the infrared (Gram-Schmidt) and mass spectral (total ion current) reconstructed chromatograms for this mixture. By use of the standard GC-IRD-MSD software, 50 IRD and 82 MSD component spectra were identified. The relevant spectra were transferred to the Nicolet data system for further analysis, as described earlier.

A. Comparison of Analytical Results for Major Components. It is of interest to compare the present results with those of the previous analysis of this sample (9). Most of the soil steam distillate components are chlorinated aromatics (17 of the 25). The others, with two exceptions, are aromatics or oxygen-containing aromatics (six of the 25). Because chromatography conditions were different in the previous study, separation characteristics such as efficiency and relative retention times are different here. However, it is possible to compare the components identified with those established by Gurka and Pyle as the 25 most abundant constituents of the mixture (9). In their work with the sample, Gurka and Pyle established that components were present in quantities up to ca. 200 ng/ μ L. As mentioned above, the joint infrared-mass spectrometry analysis software uses both types of information for the combined library search, when available; otherwise, it will use only the relevant part of the library entries (IR or MS data) and report a search result based upon that procedure. With respect to the 25 components listed in Table III of ref 9, the following results are obtained in this analysis. First, tetrachloroethylene, the second-eluting material in the previous separation, is not detected in the present analysis (presumably as a result of the 50:1 dilution of the sample). The 19th and 20th components are not found because they are not represented in the combined IR-MS library (and, in

Table IV. Functional Groups/Isomers from Library Searches for Selected Constituents of Soil Steam Distillate^a

retention time, min	compound ^b	feature ^c	no. in top 10		
			IR-MS	IR	MSD
13.09	4-isopropyltoluene	C ₁₀ H ₁₄	9	4	7
15.43	4-chlorobenzaldehyde	isomers, aromatic aldehyde	3	1	3
15.94	2,6-dichlorotoluene	C ₇ H ₆ Cl ₂	9	10	3
16.61	2,3-dichlorotoluene	C ₇ H ₆ Cl ₂	8	2	8
16.94	benzoic acid	acid	8	1	9
17.92	phenylisothiocyanate	isothiocyanates	9	10	2
20.32	trichlorotoluene	C ₇ H ₆ Cl ₃		10 ^d	
21.81	<i>p</i> -toluic acid	aromatic acids	5	1	5
22.50	trichlorotoluene	C ₇ H ₆ Cl ₃		10 ^d	
			5	1	5

^aNo presearch filter used. ^bIdentified as the closest match using IR-MS search. ^cRepresentative functional group, isomer, molecular formula, molecular weight. ^dOnly infrared data available for search.

fact, the 20th entry, "2,4,6-trichlorotoluene", is probably misnamed, because it is also not represented in either the Hewlett-Packard IRD or MSD libraries). Instead, a component is identified as 2,3,6-trichlorotoluene by the present IR-MS search. If this is considered correct, then the present results are as follows: (a) Fourteen components from the previous analysis occur as the first match in the present IR-MS analysis; (b) six additional (two IR and four MS) occur as best matches when only one of the two types of spectral information is available; (c) two components are the second closest matches, using IR-MS data; (d) two components (nos. 2 and 19) are not found for reasons given above; (e) the 25th component in the previous separation (pentachlorobenzene) coeluted with another component under the present conditions and could be identified by examination of spectra other than that found at the maximum of the reconstructed chromatogram. Thus, the present algorithm provides results that are in excellent agreement with the previous analysis and is sufficiently robust for an environmental sample of this complexity.

B. Structural Feature Analysis. In addition to excellent qualitative analysis performance on the major components, it was possible to identify additional mixture constituents by using the IR-MS search algorithm without use of the prefilter procedure. As the examples in Table III suggest, examination of the closest library matches can often suggest which structural properties may be present in an unknown. Furthermore, when no *a priori* knowledge of the results is available, IR-MS is clearly preferable to the use of either type of data alone. Analysis of the entire set of data from which the examples of Table III were drawn showed IR-MS to be as good or better than IR or MS for this deducing structural features for 27 of the 30 components. Table IV lists representative examples of some other soil steam distillate constituents identified in the present study, together with information regarding the functionality of the 10 closest library matches, for combined IR-MS, IR, and MS searches. In every case, the closest match was verified to be the correct assignment by visual inspection of the experimental spectra. As the table reveals, in almost every case, use of the IR-MS search improved the functional group specificity, with the exception of those two cases where there was a large disparity in performance of the IR-alone or MS-alone searches. Thus, combined IR-MS analysis appears to be the method of choice for tentative assignment of functionality for unknowns occurring in mixtures such as that examined here.

C. Performance with MS Data. For a number of components, the infrared spectra sensitivity was insufficient to allow collection of spectra. Nevertheless, although only mass spectral information was available, the software used the appropriate part of the combined library to investigate the structural features of these compounds. In particular, nine

polychlorinated toluenes were assigned as tetrachlorotoluenes (seven) and pentachlorotoluenes (two) on the basis of finding tetrachlorotoluene isomers as the three closest matches or pentachlorotoluenes as the two closest matches in the library search. These assignments were verified by inspection of the aromatic chlorine-containing molecular ion clusters centered near *m/z* 230 and 264 and fragment ion clusters near *m/z* 195 and 229.

CONCLUSION

Use of a combined infrared-mass spectral library with the algorithms presented here can be a highly reliable means of identifying major components in complex mixtures. Further, a library structured as this one is can yield useful qualitative information about even those components for which both types of spectral information are unavailable. It appears that use of a combined IR-MS spectral library for assessment of functionality of unknowns that may not be members of the library generally should lead to more reliable conclusions than the use of either infrared or mass spectral data alone.

LITERATURE CITED

- (1) Wilkins, C. L. *Anal. Chem.* **1987**, *59*, 571A-581A.
- (2) Gurke, D. F.; Titus, R.; Griffiths, P. R.; Henry, D.; Giorgetti, A. *Anal. Chem.* **1987**, *59*, 2362-2369.
- (3) Shafer, K. H.; Cooke, M.; DeRoos, F.; Jakobsen, R. J.; Rosario, O.; Mulik, J. D. *Appl. Spectrosc.* **1981**, *35*, 469-472.
- (4) Darland, E. J.; Mesler, L. D.; Michonowicz, J. A.; Tang, C.; Hirschfeld, T. *Abstracts: 37th Pittsburgh Conference on Analytical Chemistry and Applied Spectroscopy*, Atlantic City, NJ, March 10-14, 1986; No. 494.
- (5) Strong, S. E.; Bruns, T. *Abstracts: 35th Pittsburgh Conference on Analytical Chemistry and Applied Spectroscopy*, Atlantic City, NJ, March 5-9, 1984; Nos. 297, 298.
- (6) Gurke, D. F.; Titus, R. *Anal. Chem.* **1986**, *58*, 2189-2194.
- (7) Gurke, D. F.; Hiatt, M.; Titus, R. *Anal. Chem.* **1984**, *56*, 1102-1110.
- (8) Shafer, K. H.; Hayes, T. L.; Brasch, T. W.; Jakobsen, R. J. *Anal. Chem.* **1984**, *56*, 237-240.
- (9) Gurke, D. F.; Pyle, S. M. *Environ. Sci. Technol.* **1988**, *22*, 964-967.
- (10) Gurke, D. F.; Titus, R. *Proceedings of the 28th Conference on Analytical Chemistry in Energy Technology*, Oct. 1-3, 1985. In *Anal. Chem. Instrum.*; Laing, W. R., Ed.; Lewis Publ., Inc.: New York, 1986; pp 17-22.
- (11) Gurke, D. F.; Bielowski, L. D. *Anal. Chem.* **1982**, *54*, 1819-1824.
- (12) Chiu, K. S.; Biemann, K.; Krishnan, K.; Hill, S. L. *Anal. Chem.* **1984**, *56*, 1610-1615.
- (13) Laude, D. A., Jr.; Brissett, G. M.; Ijames, C. F.; Brown, R. S.; Wilkins, C. L. *Anal. Chem.* **1984**, *56*, 1163-1168.
- (14) Laude, D. A., Jr.; Juhlman, C. L.; Cooper, J. R.; Wilkins, C. L. *Anal. Chem.* **1985**, *57*, 1044-1049.
- (15) Cooper, J. R.; Bowater, I. C.; Wilkins, C. L. *Anal. Chem.* **1986**, *58*, 2791-2796.
- (16) Cooper, J. R.; Brown, R. S.; Wilkins, C. L. *Abstracts: 38th Pittsburgh Conference on Analytical Chemistry and Applied Spectroscopy*, Atlantic City, NJ, March 9-13, 1987; No. 491.
- (17) Atwater, B. L.; Stauffer, D. B.; McLafferty, F. W.; Peterson, D. W. *Anal. Chem.* **1985**, *57*, 899-903.
- (18) Rupprecht, M.; Clerc, J. T. *J. Chem. Inf. Comput. Sci.* **1985**, *25*, 241-244.
- (19) Hippe, Z. *J. Chem. Inf. Comput. Sci.* **1985**, *25*, 344-350.
- (20) Mine, G. W. A.; Budde, W. L.; Heller, S. R.; Martinsen, D. P.; Oldham, R. R. *Org. Mass Spectrom.* **1982**, *17*, 547-552.
- (21) Lowry, S. R.; Huppler, D. A. *Anal. Chem.* **1981**, *53*, 889-893.
- (22) Lowry, S. R.; Huppler, D. A.; Anderson, C. A. *J. Chem. Inf. Comput. Sci.* **1985**, *25*, 235-241.

- (23) Harrington, P. B.; Isehour, T. L. *Appl. Spectrosc.* **1987**, *41*, 449-453.
(24) Hallowell, J. R., Jr.; Delaney, M. F. *Anal. Chem.* **1987**, *59*, 1544-1549.
(25) Williams, S. S.; Lam, R. B.; Isehour, T. L. *Anal. Chem.* **1983**, *55*, 1117-1121.
(26) Cooper, J. R.; Bowater, I. C.; Brown, R. S.; Wilkins, C. L. Presented at the 192nd National Meeting of the American Chemical Society, Anaheim, CA, Sept. 7-12, 1986, paper COMP 8.
(27) Rasmussen, G. T.; Isehour, T. L. *J. Chem. Inf. Comput. Sci.* **1979**, *19*, 179-186.

RECEIVED for review December 8, 1988. Accepted April 10,

1989. Support from the National Science Foundation under Grant CHE-85-19087 is gratefully acknowledged. Support from Cooperative Agreements CR-81-1370 and CR-81-4755 between the University of California, Riverside, and the U.S. Environmental Protection Agency, Environmental Monitoring Systems Laboratory, Las Vegas, NV, is also acknowledged. Although the research described in this paper has been funded in part by the U.S. EPA, it has not been subjected to agency review and does not necessarily reflect the views of the agency and no official endorsement should be inferred.

Optimization of a Coaxial Continuous Flow Fast Atom Bombardment Interface between Capillary Liquid Chromatography and Magnetic Sector Mass Spectrometry for the Analysis of Biomolecules

M. Arthur Moseley,¹ Leesa J. Deterding, J. S. M. de Wit,¹ and Kenneth B. Tomer*

Laboratory of Molecular Biophysics, National Institute of Environmental Health Sciences, Research Triangle Park, North Carolina 27709

Robert T. Kennedy, Nancy Bragg, and James W. Jorgenson*

Department of Chemistry, University of North Carolina at Chapel Hill, Chapel Hill, North Carolina 27514

The performance of a coaxial continuous flow fast atom bombardment (FAB) probe designed to interface both open tubular (10 μm i.d.) and packed microcapillary (50 μm i.d.) liquid chromatography with magnetic sector mass spectrometry is described. This coaxial "column within a column" interface uses two fused silica capillary columns to independently deliver the LC effluent and the FAB matrix to the FAB probe tip, and thus it allows the independent optimization of both the composition and flow rates of the two liquid streams. The goal of this work is to bring to FAB-MS the advantages of high-resolution capillary liquid chromatography, which include superior chromatographic separation efficiency, nanoliter per minute mobile phase flow rates, and the ability to analyze very small samples (typically 0.05 to 10 nL/injection). This probe has been successfully used to acquire on-the-fly (i.e. in chromatographic real time) full scan mass spectra from a variety of analyte classes, including peptides, steroids, phospholipids, and carbohydrates. By use of the tripeptide Met-Leu-Phe, detection limits have been obtained of 500 amol using the multichannel data acquisition mode and 1.8 fmol using the peak centroid data acquisition mode.

Continuous flow fast atom bombardment interfaces, first developed by Ito et al. as "frit FAB" (1), and Caprioli, Fan, and Cottrell as continuous flow FAB (2), have proven to be very useful for interfacing mass spectrometry with flowing liquid streams. The combination of liquid chromatography (LC) and continuous flow fast atom bombardment mass

spectrometry (CF-FAB-MS) has recently become the topic of active research in many laboratories (2-9) due to the suitability of both LC and CF-FAB-MS for the analysis of polar, nonvolatile, and/or thermally labile compounds such as biopolymers. In LC/CF-FAB the LC effluent flows directly through a specially designed probe onto the probe tip, where bombardment by high translational energy atoms (typically 8-kV xenon atoms) induces the desorption of the analyte molecules.

While the advantages of CF-FAB over conventional "static" FAB (lower chemical background noise, less discrimination between hydrophobic and hydrophilic analytes) are well-known (2), the advantages of packed microcapillary LC and open tubular liquid chromatography (OTLC) for use with CF-FAB have not been widely discussed. The principal advantages of packed microcapillary LC (50 μm i.d.) and OTLC (10 μm i.d.) over "conventional" LC (4.6 mm i.d.) are (1) superior chromatographic separation efficiency, (2) lower mobile phase flow rates (by 4 orders of magnitude), and (3) the ability to analyze very small samples (such as the analysis of the contents of single neurons (10)) due to the very small injection volumes used (0.05-10 nL per injection). While OTLC columns offer superior separation efficiency, packed microcapillary LC columns have a higher sample capacity. Both packed microcapillary LC columns, which are constructed from 50 μm i.d. fused silica packed with 5 or 10 μm particles, and OTLC columns are operated at flow rates of approximately 50 nL/min. Due to their high flow rates (typically 1 mL/min), the effluent from conventional LC columns must be split, with only a small fraction of the mobile phase flow (and the analytes) going into the source of the mass spectrometer. However, the flow from the packed microcapillary LC and OTLC columns is sufficiently low so that introduction of the entire LC effluent into the source of the

* Authors to whom correspondence should be addressed.

¹ Also at the Department of Chemistry, University of North Carolina at Chapel Hill, Chapel Hill, NC 27514.

mass spectrometer is possible. More importantly, it allows the introduction of the entire sample which, when coupled with the very small injection volumes used with packed microcapillary LC and OTLC, gives a definite advantage for the analysis of real world samples (i.e. biological extracts) which are limited in volume.

We have successfully interfaced OTLC with both electron impact and chemical ionization mass spectrometry (11, 12), but these approaches so far have limited utility for more polar and higher molecular weight analytes. Our interest in extending the application of OTLC/MS to the analysis of biopolymers led us to investigate methods for coupling OTLC with CF-FAB (9).

The LC/CF-FAB interfaces reported thus far have been designed to operate with larger packed LC columns (4.6–0.22 mm i.d.). In these systems the matrix (typically glycerol) needed for the FAB process either is introduced in the mobile phase and analyte solutions or is added postcolumn into the LC effluent. Introduction of the FAB matrix into the LC mobile phase can compromise the chromatography due to the resulting changes in the polarity and viscosity of the LC mobile phase. This problem is exacerbated by the low volumetric flow rates in packed capillary LC. The volumetric flow rate of the FAB matrix that is required to maintain a stable ion beam requires a correspondingly high concentration of the FAB matrix in the mobile phase (5–10%). This approach is not feasible with open tubular LC (OTLC) and packed microcapillary LC since the required flow rate of the FAB matrix is greater than the mobile phase flow rates. Also, if the FAB matrix is added to the LC mobile phase, any changes in the FAB matrix type or matrix concentration may require reevaluation of the chromatographic conditions in order to obtain the desired separation.

The postcolumn introduction of the FAB matrix into the LC effluent can circumvent the potential problems of using the FAB matrix as a component of the mobile phase. In conventional LC with effluent flow rates of 1 mL/min, postcolumn additions can be done without significant chromatographic peak broadening (8). In packed microcapillary LC columns and OTLC columns, the mobile phase flow rates are so low compared with the required flow rates of the FAB matrix that postcolumn addition of the FAB matrix can cause severe chromatographic peak broadening.

Since the customary methods of interfacing LC with CF-FAB are not suited for use with packed microcapillary LC and OTLC, we designed an interface (9) that uses a coaxial flow of the LC effluent and FAB matrix in two separate fused silica capillary columns. In this interface chromatographic band broadening is minimized since the mixing of the matrix and the LC effluent takes place only at the FAB probe tip. Since the FAB matrix flow and LC flow are independently delivered to the FAB probe tip, both the composition and flow rates of the two liquid streams can be independently optimized. We now report on the performance characteristics of this interface and its utility for CF-FAB-MS under chromatographic conditions.

EXPERIMENTAL SECTION

Capillary LC. The capillary LC system used is identical with that used in OTLC (11). To allow the identification of the optimum operational parameters of the coaxial CF-FAB interface without complications due to chromatographic effects, fused silica capillary tubing (Polymicro Technologies, Phoenix, AZ) without any stationary phase coating or packing was used in all experiments except for the separation shown in Figure 11. These "dummy columns" were operated at a flow rate of 53 nL/min, and all injections were made by using the "static split" method (11). This injection method is analogous to the "splitless/split" injection procedure used in capillary GC and allows injections of as little as 0.05 nL without the introduction of band broadening

due to the dead volumes found in loop type injectors. The time duration of the injection and the mobile phase flow rates determine the volume injected onto the column. For all experiments except for the separation shown in Figure 11, 5-s injections were made at a mobile phase flow rate of 53 nL/min, corresponding to injections of 4.4 nL. The separation was performed on a packed microcapillary column (220 cm × 50 μ m) packed with 10- μ m particles. The stationary phase was ODS 2 Spherisorb (Alltech Associates, Deerfield, IL).

MS. A VG ZAB-4F mass spectrometer (VG Analytical, Manchester, U.K.) has been used for this work and has been described previously (13). The instrument is of B₁E₁–E₂B₂ configuration and is equipped with an Ion Tech FAB gun. Xenon was used for the FAB gas. The FAB desorbed ions were accelerated to 8 keV for analysis. Ions were detected in the third field-free region using a photomultiplier-based detector system.

Three MS data acquisition modes were employed. Two used magnet scans of B₁E₁ with data acquisition in the centroid mode: (1) a narrow mass scan over 15 daltons; and (2) a full scan over 1 decade (1500 to 150 daltons). The third type of data acquisition mode used was the multichannel analysis (MCA) mode in which continuum mode scans over a 15-dalton range were summed. The data acquisition system used in all modes of operation was a VG Analytical 11-250 data system.

Capillary LC/Coaxial Continuous Flow FAB-MS Interface. The basic design of the interface has been described previously (9). In this present study, the VG CF-FAB probe was used. The fused silica capillary LC column is inserted into the sheath fused silica column through which the matrix flows. Both the LC column and the sheath column terminate at the FAB probe tip. The FAB matrix is pumped into the sheath column by a syringe pump (Isco, Inc., Lincoln, NE). All matrix flow rates refer to pump readings and have not been directly measured. The capillary LC column and sheath column are interfaced using a 1/16 in. stainless steel tee. Typical dimensions for the coaxial CF-FAB probe capillary columns are (1) an inner column (separation column) approximately 2 m long with a 10 μ m inner diameter (i.d.), 150 μ m outer diameter (o.d.), and (2) an outer column (FAB matrix column) approximately 1.8 m long, with a 200 μ m i.d., 350 μ m o.d.

Chemicals. All analytes were obtained from Sigma (St. Louis, MO). The solvents and glycerol were obtained from Fisher Scientific (Fair Lawn, NJ).

RESULTS AND DISCUSSION

Optimization of FAB Matrix Composition and Flow Rate. Seven different FAB matrix solutions have been evaluated for use with the coaxial continuous flow FAB interface: glycerol in water at glycerol concentrations (v/v) of 25, 50, and 75%; 25% glycerol/water acidified with either 0.1% trifluoroacetic acid, 0.01 M oxalic acid, or 0.1% heptafluorobutyric acid; and 25% (5/1 dithiothreitol/dithioerythritol (DT)) in water. These different FAB matrices were evaluated on the basis of stability of the ion beam (reproducibility), chromatographic effects (chromatographic peak tailing), and detection limits.

In order to maintain a stable ion beam, the probe tip face must be kept "wet" with the matrix solution (2). This requires that the FAB matrix concentration and flow rate be high enough to maintain a "wet" probe tip. However, an excessive flow rate of the FAB matrix solution will lead to the formation of a large drop on the probe tip which causes chromatographic band broadening and a loss of sensitivity. Thus, the rate of the delivery of the FAB matrix must be balanced with the rate of removal by the FAB beam and the vacuum of the mass spectrometer. The flow rates of the LC columns are less than 100 nL/min; thus the LC flow contributes very little to the formation of a "wet" FAB probe tip. Also, the FAB probe tip must be kept within a temperature range of approximately 40–60 °C in order to prevent freezing of the effluent or drying of the tip due to excessive evaporation of the FAB matrix.

Glycerol is widely used as a static FAB matrix, and it has been used in continuous flow FAB by other researchers (2).

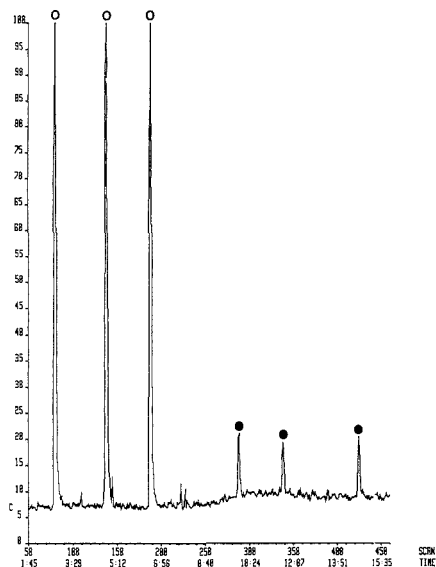


Figure 1. Selected ion mass chromatogram of the protonated molecular ion of Met-Leu-Phe ($m/z = 410$) resulting from triplicate 5-s (4.4 nL) injections of 54 fmol (open circles) and 5.4 fmol (closed circles) of the tripeptide. A 25/75 glycerol/water FAB matrix solution was used at a flow of 1.2 $\mu\text{L}/\text{min}$.

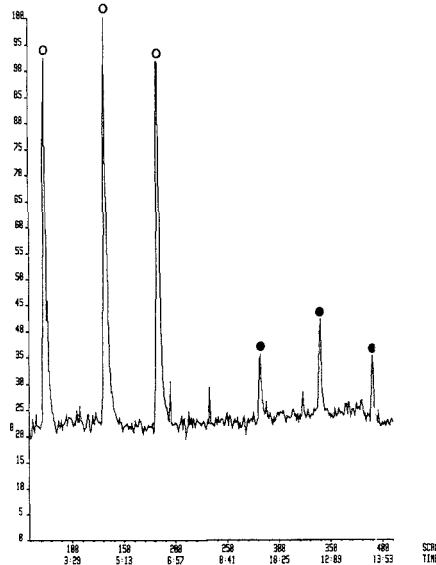


Figure 2. Selected ion mass chromatogram of the protonated molecular ion of Met-Leu-Phe ($m/z = 410$) resulting from triplicate 5-s (4.4 nL) injections of 54 fmol (open circles) and 5.4 fmol (closed circles) of the tripeptide. A 25/75 DT/water FAB matrix solution was used at a flow of 1.8 $\mu\text{L}/\text{min}$.

In our initial experiments matrix compositions of 75/25 and 50/50 glycerol/water were used. While stable ion beams were obtained at these concentrations, excessive chromatographic peak tailing was observed. Decreasing the glycerol concen-

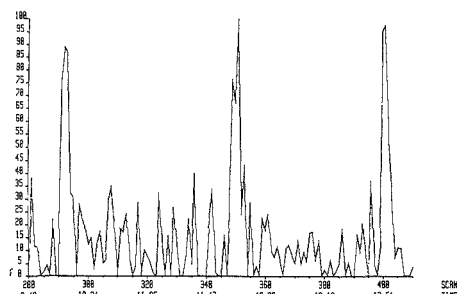


Figure 3. Selected ion mass chromatogram of the protonated molecular ion of Met-Leu-Phe ($m/z = 410$) resulting from triplicate 5-s (4.4 nL) injections of 1.8 fmol of the tripeptide. Data were acquired by scanning over a 15-dalton range at 100 s per decade using the peak centroid data acquisition mode.

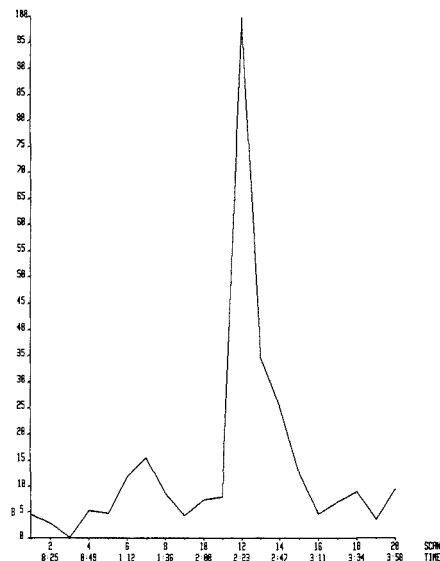


Figure 4. Selected ion mass chromatogram of the protonated molecular ion of Met-Leu-Phe ($m/z = 410$) resulting from a single 5-s (4.4 nL) injection of 54 fmol of the tripeptide. Data were acquired by scanning from 1500 to 150 daltons at a rate of 10 s per decade.

tration to 25/75 glycerol/water at a flow rate of 1.2 $\mu\text{L}/\text{min}$ significantly reduced the chromatographic peak tailing while still maintaining a stable ion beam. The MS source pressure resulting from this flow was 2×10^{-5} Torr. The selected ion trace resulting from triplicate injections of 54 fmol (22 pg in 4.4 nL) and 5.4 fmol (2.2 pg in 4.4 nL) of the tripeptide Met-Leu-Phe (MLF) is shown in Figure 1. This 25/75 glycerol/water matrix gave a signal to noise (S/N) ratio of approximately 6/1 with 5.4 fmol of MLF, good reproducibility (peak area relative standard deviation (RSD) of 1.9% with the 54 fmol injections), and little chromatographic peak tailing.

The 5/1 dithiothreitol/dithioerythritol (DT) mixture is widely used as a static FAB matrix, particularly for peptides. A 1.8 $\mu\text{L}/\text{min}$ flow of the 25/75 DT/H₂O solution was required to maintain a "wet" tip at a probe temperature of 50 $^{\circ}\text{C}$, and this gave a MS source pressure of 5×10^{-5} Torr. The chromatographic trace (Figure 2) resulting from triplicate

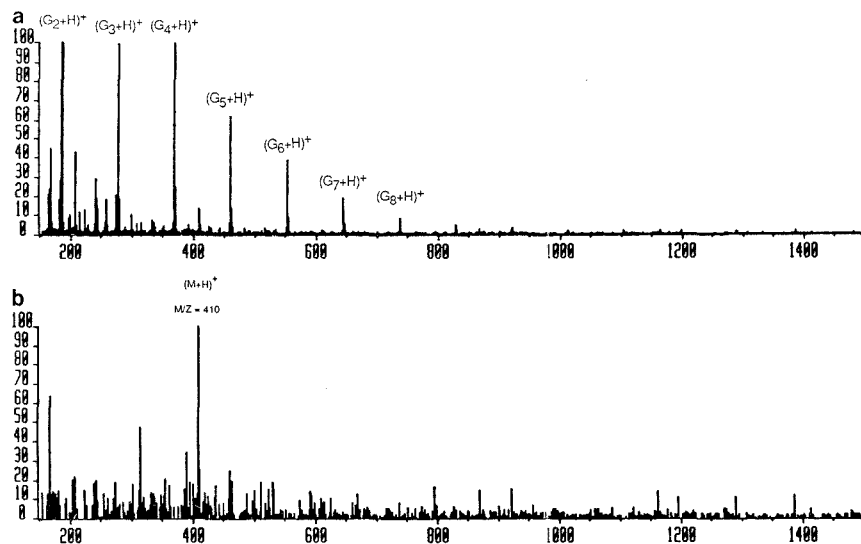


Figure 5. Mass spectrum of 54 fmol of Met-Leu-Phe acquired from scan 12 from the mass chromatogram in Figure 4: (a) raw data (G_nH^+ ions are matrix oligomers); (b) background subtracted data.

injections of 540 fmol (220 pg in 4.4 nL) and 54 fmol (22 pg in 4.4 nL) of MLF shows a S/N of approximately 6/1 with 54 fmol MLF (approximately an order of magnitude lower S/N with equivalent amounts of analyte than that obtained with 25/75 glycerol/water), moderate reproducibility (peak area RSD of 26% with the 54 fmol injections), and noticeable chromatographic peak tailing.

Acidification of the 25% glycerol/water FAB matrix was accomplished by using either 0.1% trifluoroacetic acid, 0.01 M oxalic acid, or 0.1% heptafluorobutyric acid. The goal of these experiments was to evaluate the effect of increasing the concentration of ionized analytes on the FAB probe tip. However, the acidification led to ion beam instability which resulted in an increase in base-line noise and a commensurate decrease in the S/N ratio of the spectra. Acidification of the LC mobile phase was successfully accomplished by using 0.1% trifluoroacetic acid. This was used only for the analysis of bradykinin.

Because of the higher S/N ratios, better reproducibility, and lower chromatographic peak tailing of the glycerol/water FAB matrix compared with the other matrices investigated, we have used glycerol/water at a concentration of 25/75 and at a flow rate of 1.2 μ L/min for all subsequent work.

Detection Limits. The detection limits ($S/N = 3/1$) that can be determined with this coaxial CF-FAB interface are dependent upon the MS data acquisition mode used. All data were collected from chromatographic peaks resulting from 5-s injections of aqueous solutions of MLF. Typical peak widths at half height varied from 7 to 15 s, increasing with increasing amounts injected. With the centroided data acquisition mode, scanning over a 15-dalton range (415 to 400), a detection limit of 1.8 fmol was obtained (Figure 3). The response of peak centroided data near the detection limit (54 to 1.8 fmol) was found to be linear, giving a correlation coefficient >0.999 . With full scan peak centroided data (1500 to 150 daltons), detection limits of approximately 54 fmol were obtained (Figures 4 and 5). With MCA data acquisition, a detection limit of 500 amol was obtained. To demonstrate the results of this experiment, two mass spectra are overlaid—a background spectrum containing only the FAB matrix and the mobile phase (summation of 20 scans in MCA mode) and a

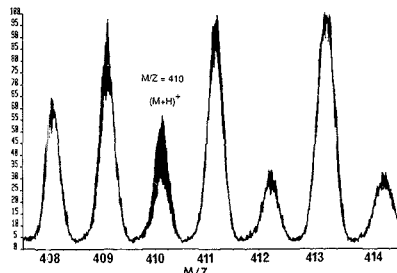


Figure 6. Overlaid mass spectra acquired by using multichannel data acquisition of glycerol background and of glycerol background + 500 amol of Met-Leu-Phe from a 5-s (4.4 nL) injection. The shaded area represents the peak area attributable to the tripeptide.

Table I. Full Scan Mass Spectral Data Obtained

compound ^a	nanograms ^b	picomoles
Met-Leu-Phe	0.022	0.054
bradykinin/H ⁺	0.90	0.85
N-acetyl argiotensin I	4.4	3.3
dipalmitoyl phosphatidyl choline	2.2	3.0
corticosterone	2.2	6.4
taurothiocholic acid 3-sulfate	4.4	7.2
glutathione	4.4	14
dihydrostreptomycin	4.4	3.0
maltotetraose	44 ^c	66

^a All data were acquired under full scan (1500 to 150 daltons) conditions from 5-s injections (4.4 nL). ^b The amounts listed do not necessarily represent detection limits. ^c Limit of detection for maltotetraose was approximately 7 pmol.

sample spectrum containing background plus 500 amol of analyte (summation of 20 scans in MCA mode) (Figure 6). In this figure the shaded area represents the peak area due to the analyte. This detection limit is approximately 2 to 3 orders of magnitude lower than the best detection limits for peptides (2) published thus far. The high mass flux of the open tubular capillary column is presumed to be responsible for a significant

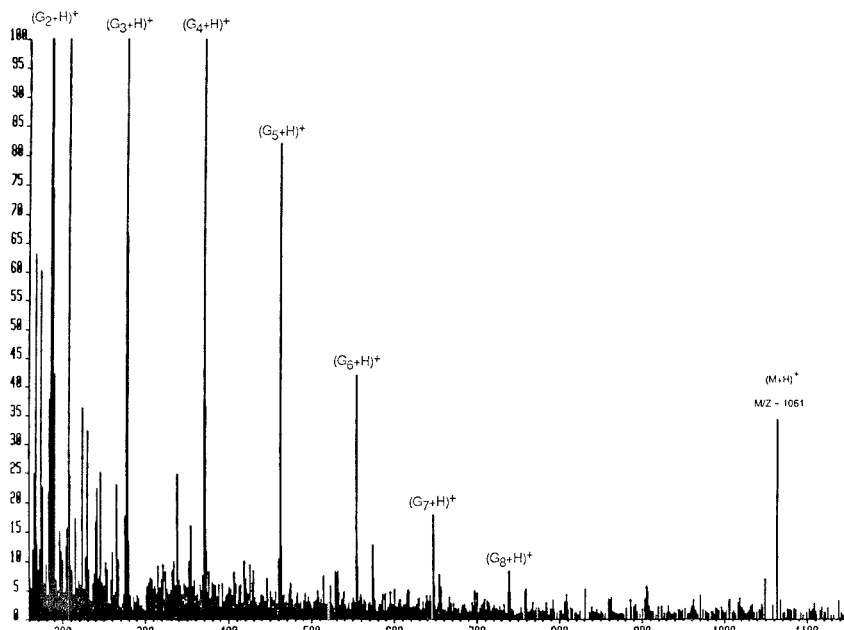


Figure 7. Mass spectrum of 0.85 pmol of bradykinin acquired from a 5-s (4.4 nL) injection. Data were acquired by scanning from 1500 to 150 daltons at a rate of 10 s per decade (G_nH^+ ions are matrix oligomers).

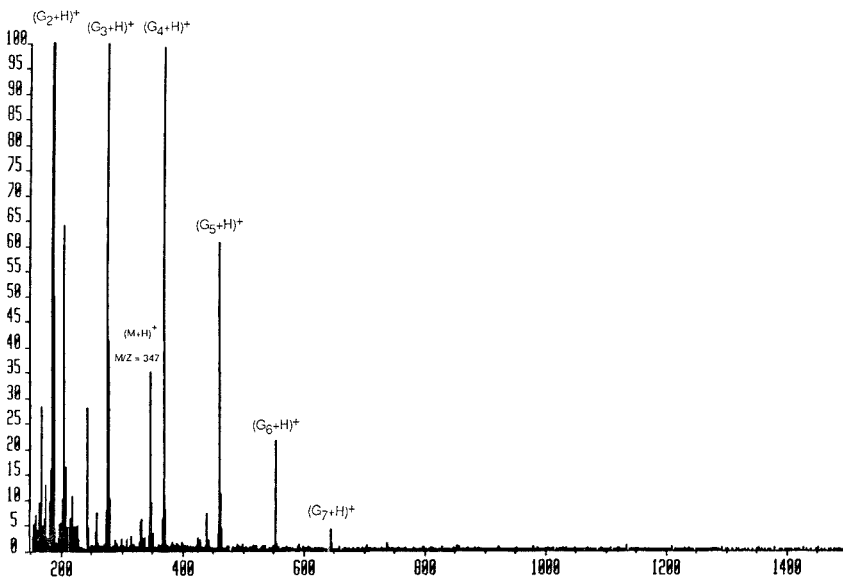


Figure 8. Mass spectrum of 6 pmol of corticosterone acquired from a 5-s (4.4 nL) injection. Data were acquired by scanning from 1500 to 150 daltons at a rate of 10 s per decade (G_nH^+ ions are matrix oligomers).

part of the improved detection limit.

Range of Applicability. This interface has been used to acquire full scan (i.e. 1500 to 150 daltons) mass spectra from 5-s injections (4.4 nL) of compounds from a variety of analyte classes, using 0.054–66 pmol of analytes (Table I). While some

spectra were acquired at or near the detection limit, the amounts used do not necessarily represent detection limits. All spectra contain the protonated molecular ion, $(M+H)^+$, with little, if any, fragmentation of the molecular ion, except for maltotetrose, where extensive fragmentation occurred. The

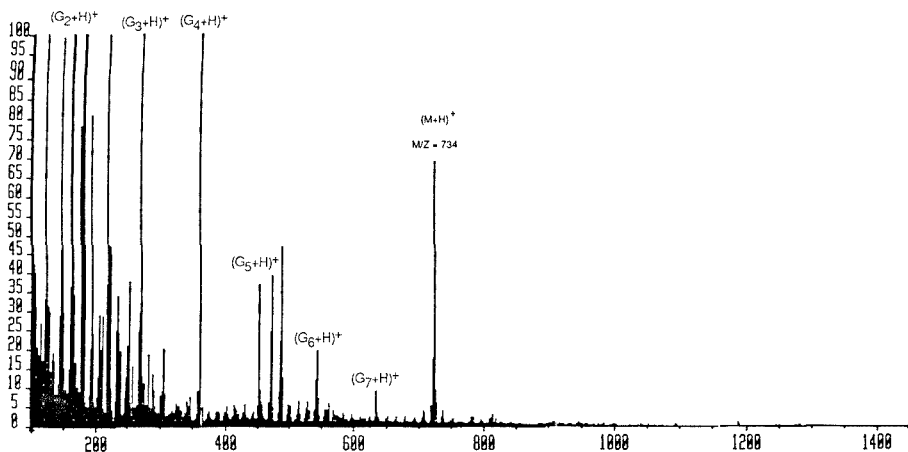


Figure 9. Mass spectrum of 6 pmol of dipalmitoyl phosphatidyl choline acquired from a 5-s (4.4 nL) injection. Data were acquired by scanning from 1500 to 100 daltons at a rate of 10 s per decade (G_nH^+ ions are matrix oligomers).

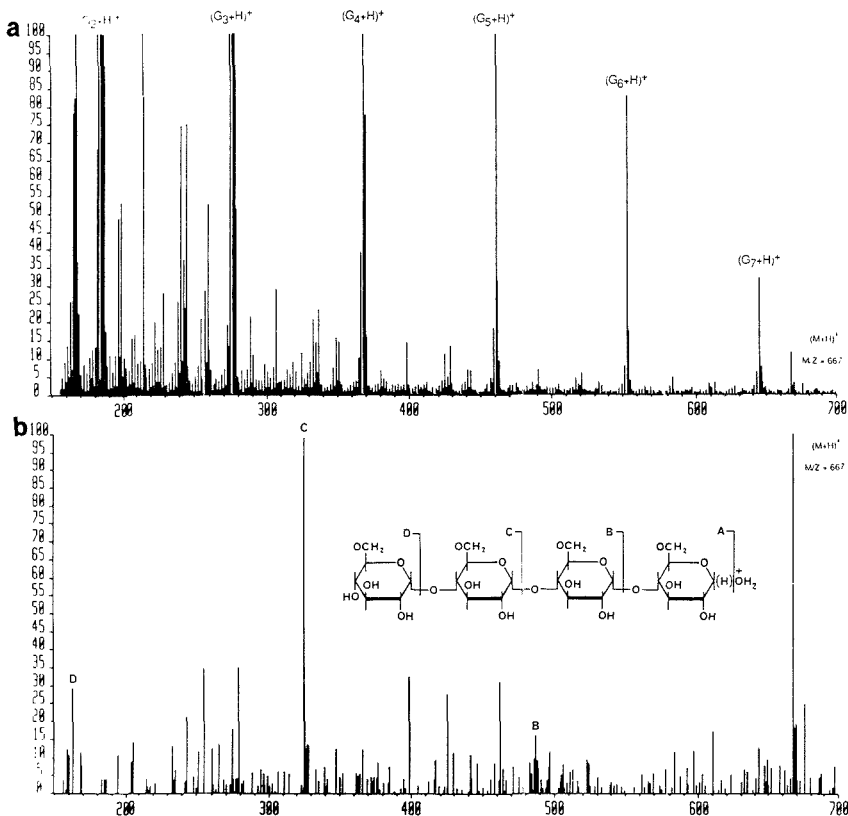


Figure 10. (a) Mass spectrum of 66 pmol of maltotetrose acquired from a 5-s (4.4 nL) injection. Data were acquired by scanning from 1500 to 150 daltons at a rate of 10 s per decade (G_nH^+ ions are matrix oligomers). (b) Background subtracted mass spectrum of 66 pmol of maltotetrose showing the fragmentation of the sugar as a result of fast atom bombardment.

analyte classes include peptides [Met-Leu-Phe (Figure 5), bradykinin (Figure 7), glutathione, and *N*-acetyl angiotensin I], steroids [corticosterone (Figure 8) and tauroolithocholic acid

3-sulfate], phospholipids [dipalmitoyl phosphatidyl choline (Figure 9)], and carbohydrates [maltotetrose (Figure 10) and dihydrostreptomycin].

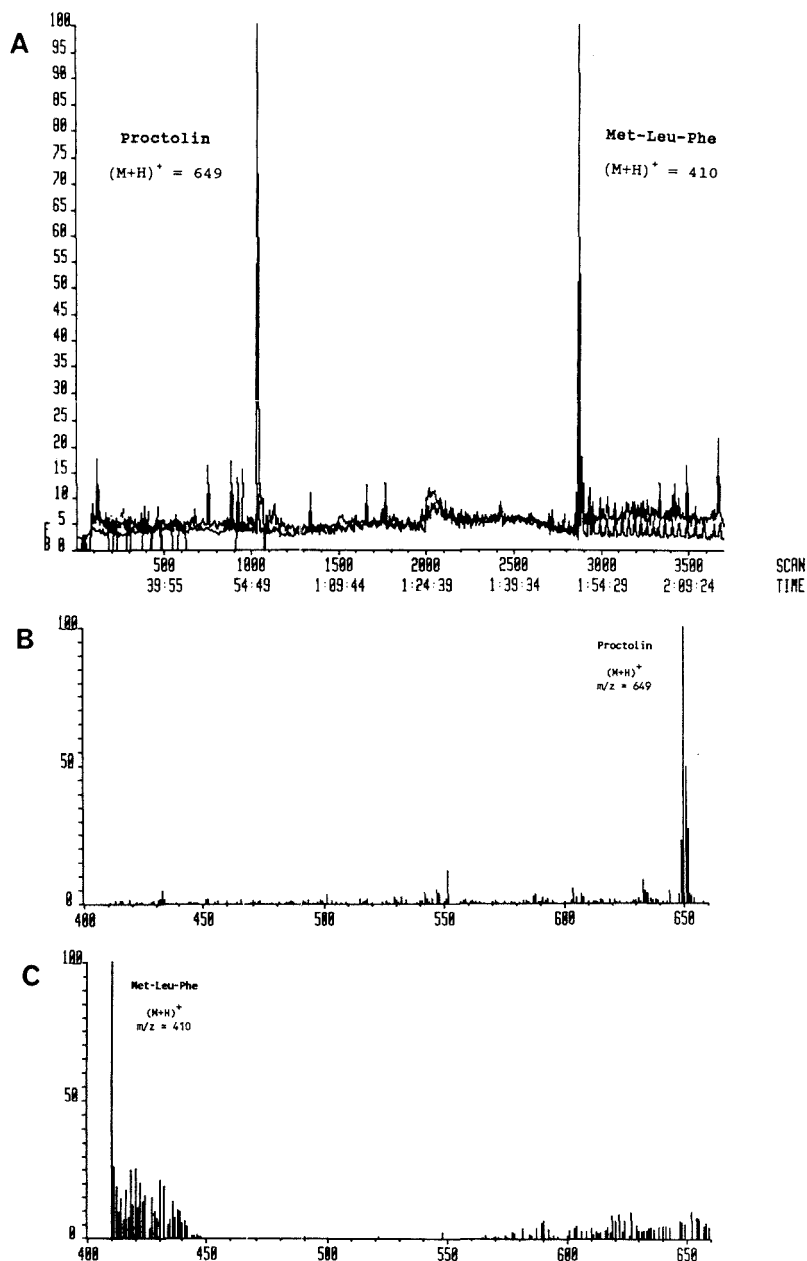


Figure 11. (A) Overlaid single ion chromatograms (protonated molecular ions) from the separation of 2 pmol of proctolin and 1 pmol of Met-Leu-Phe using a packed microcapillary column (50 μm i.d., 220 cm long packed with 10 μm C-18 coated particles). A linear acetonitrile/water mobile phase gradient was used at a flow rate of approximately 30 nL/min. (B) Background subtracted mass spectrum of proctolin obtained from separation. (C) Background subtracted mass spectrum of Met-Leu-Phe obtained from separation.

The OTLC stationary phases most suitable for the analysis of these biomolecules currently can only be utilized with borosilicate glass columns which, due to the need for a 60 cm straightened end, are not suitable for use with this coaxial

CF-FAB interface. While the development of the appropriate OTLC column technology is nearing completion, packed fused silica microcapillaries are currently used for separations with this system. The use of this interface with a packed micro-

capillary LC column (50 μm i.d., 220 cm long fused silica column packed with 10- μm C18 coated spherical particles) is demonstrated in Figure 11, where the separation of 1 pmol of MLF and 2 pmol of proctolin (Arg-Tyr-Leu-Pro-Thr) is shown. A linear acetonitrile/water gradient at a flow rate of approximately 30 nL/min was used. Each mobile phase solvent contained 0.1% trifluoroacetic acid.

CONCLUSIONS

The coaxial continuous flow fast atom bombardment interface has proven to be useful for combining capillary column LC with sector MS for the analysis of biomolecules. It yields the lowest reported limits of detection, good reproducibility, and minimal chromatographic peak broadening. The interface is uniquely well suited for the combination of high-resolution packed microcapillary LC and OTLC with FAB-MS due to its ability to independently deliver the LC eluant and the FAB matrix to the FAB probe tip.

LITERATURE CITED

- (1) Ito, Y.; Takeuchi, T.; Ishii, D.; Goto, M.; Mizuno, T. *J. Chromatogr.* **1985**, *356*, 201.

- (2) Caprioli, R. M.; Fan, T.; Cottrell, J. S. *Anal. Chem.* **1986**, *58*, 2949.
- (3) Caprioli, R. M.; Moore, W. T.; Fan, T. *Rapid Commun. Mass Spectrom.* **1987**, *1*, 15.
- (4) Ashcroft, A. E.; Chapman, J. R.; Cottrell, J. S. *J. Chromatogr.* **1987**, *394*, 15.
- (5) Ashcroft, A. E. *Org. Mass Spectrom.* **1987**, *22*, 754.
- (6) Takeuchi, T.; Watanabe, S.; Kondo, N.; Ishii, D.; Goto, M. *J. Chromatogr.* **1988**, *435*, 482.
- (7) Bouleigneur, P.; Leroy, Y.; Alonso, J. M.; Montreuil, G. R.; Colbert, C.; Duqust, D.; Dewaele, C.; Fournet, B. *Anal. Biochem.* **1988**, *166*, 164.
- (8) Games, D. E.; Pleasance, S.; Ramsey, E. D.; McDowell, M. A. *Biomed. Environ. Mass Spectrom.* **1988**, *15*, 179.
- (9) de Wit, J. S. M.; Deterding, L. J.; Moseley, M. A.; Tomer, K. B.; Jorgenson, J. W. *Rapid Commun. Mass Spectrom.* **1988**, *2*, 100.
- (10) Kennedy, R. T.; St. Clair, R. L.; White, J. G.; Jorgenson, J. W. *Microchim. Acta* **1987**, *II*, 37.
- (11) de Wit, J. S. M.; Parker, C. E.; Tomer, K. B.; Jorgenson, J. W. *Anal. Chem.* **1987**, *59*, 2400.
- (12) de Wit, J. S. M.; Parker, C. E.; Tomer, K. B.; Jorgenson, J. W. *Biomed. Environ. Mass Spectrom.* **1988**, *17*, 47.
- (13) Cole, R. B.; Guenat, C. R.; Gaskell, S. J. *Anal. Chem.* **1987**, *59*, 1139.

RECEIVED for review January 6, 1989. Accepted April 3, 1989.

Quantitation Capability of a Directly Linked Gas Chromatography/Fourier Transform Infrared/Mass Spectrometry System

Donald F. Gurka,* Irene Farnham, Billy B. Potter, and Steven Pyle

United States Environmental Protection Agency, Environmental Monitoring Systems Laboratory, Las Vegas, Nevada 89193-3478

Richard Titus

Chemistry Department, University of Nevada, Las Vegas, Nevada 89154

Wayne Duncan

Hewlett-Packard Corporation, Scientific Instruments Division, Palo Alto, California 94304

Although the identification confirmation capability of directly linked gas chromatography/Fourier transform infrared/mass spectrometry (GC/FT-IR/MS) has been reported, the capability of such a system to confirm quantitation on-line has not yet been ascertained. Accordingly, the relative quantitation abilities of the system detectors were determined by analyzing 15 typical environmental contaminants, at several concentration levels, and then subjecting the results to regression analysis. Slopes of mass spectral (MS) and Fourier transform infrared (FT-IR) area counts versus nanograms injected usually increased with increasing injection volume. MS results were acquired in the total ion chromatogram (TIC) and single ion chromatogram (SIC) modes, while FT-IR data were collected in the Gram-Schmidt (G-S), maximum absorbance (MA), and integrated absorbance (IA) modes. Correlation coefficients indicated that the degree of scatter in the regression plots increased in the order, TIC approximately equal to SIC < MA < IA which was < G-S. Omission of a single outlier result for G-S and MA made the regression scatter comparable for the five methods. The best combinations of these MS and FT-IR quantitation techniques are proposed for the environmental target list and screening approaches. The effect of sample background on selectivity and detectability was examined by analysis of a spiked crude oil sample.

INTRODUCTION

Directly linked GC/FT-IR/MS systems have been shown to be a powerful tool for environmental sample characterization (1, 2). However, very little has been reported on quantitation using these linked systems (3), and indeed little has been reported on quantitation using stand-alone gas chromatography/Fourier transform infrared (GC/FT-IR) systems (4). However, Gurka and Pyle have recently reported a mean correlation coefficient of 0.9760 for stand-alone GC/FT-IR Gram-Schmidt (G-S) quantitation on 24 standards (5). Later it was reported that the G-S quantitation slopes varied substantially from day to day, unless the gas chromatographic (GC) carrier gas, as well as the spectrometer purge gas, is rigorously dried (6). In addition to the G-S, integrated absorbance (IA) and maximum absorbance (MA) are also viable approaches to GC/FT-IR quantitation. Bowater et al. reported that a MA algorithm produces reconstructed chromatograms with superior signal to noise (S/N) to IA methods and competitive or complementary performance to the G-S technique in the universal detection mode (7).

It has been suggested that FT-IR systems have the capability for the direct usage of infrared absorbances for quantitation, but, GC/FT-IR quantitation is complicated by the uncertainties associated with estimating the percent of injected

material in the lightpipe during the spectrometric measurement process (8). Nevertheless, this percentage can be estimated from the lightpipe volume, GC peak elution volume, carrier gas flow rate, and spectrometer scan rate. Because the total error associated with environmental analysis can be quite large (being composed of a series of errors associated with field sampling, loss and degradation prior to analysis, laboratory subsampling and workup loss, and analysis and data processing errors), the estimation of the amount of analyte within the FT-IR lightpipe need not be too precise to be easily within that total error. In fact it has recently been noted that gas chromatography/mass spectrometry (GC/MS) errors associated with leachate workup and analysis are overshadowed by the errors associated with leachate field sampling (9).

Improvements in modern FT-IR spectrometers have lowered GC/FT-IR minimum identifiable quantities (MIQ) for weak infrared absorbers to the low nanogram range. This suggests that a modern lightpipe GC/FT-IR/MS system has the capability to confirm identification and quantification on-line, at the low nanogram level, for most GC-volatile analytes. However, these MIQs have been determined for pure standards in pure solvents, while the MIQs for analytes in real samples should be substantially raised by extract background materials (10). While it is known that GC/MS detection limits are substantially raised by these backgrounds (11), little has been reported about the effect of these backgrounds, on GC/FT-IR or GC/MS MIQs. If it is generally true that environmental sample extract backgrounds are dominated by hydrocarbons (12), the relatively weak infrared response to those compounds suggests that FT-IR MIQs may be affected to a lesser degree by extract background than those of the mass spectral detector.

EXPERIMENTAL SECTION

GC/FT-IR Instrumentation. The FT-IR spectrometer used in this study was a Hewlett-Packard (HP) infrared detector (IRD) Model 5965A. The IRD was interfaced to an HP Model 5890 gas chromatograph (GC). Data treatment was carried out with an HP Model 59970C Chemstation, equipped with an HP 9000 Series 300 computer with 2 megabytes of memory and an 81-megabyte Winchester disk drive.

The FT-IR system contained a narrow-band, mercury-cadmium-telluride (MCT) detector with a 750-cm^{-1} spectral cutoff and was purged with liquid nitrogen boil off. The detector D^* ($\text{cm Hz}^{1/2}/\text{W}$ at 1 kHz) was 3.5×10^{10} . The lightpipe was gold coated with dimensions of 1 mm i.d. by 12 cm. Fused silica capillary columns (FSCC) ($30\text{ m} \times 0.32\text{ mm}$), coated with $1\text{-}\mu\text{m}$ and $0.25\text{-}\mu\text{m}$ DB-5 films, were used for the quantitation studies. The $0.25\text{-}\mu\text{m}$ DB-5 column was also used for the sample background interference study. Helium carrier flow was $53\text{ cm}^3/\text{s}$ and was passed through a cartridge drier, and no makeup gas was used. The GC was ramped from 40 to 280°C at $10^\circ\text{C}/\text{min}$. One-, two-, and three-microliter injections were used with an HP Model 7673A autoinjector, equipped with a capillary on-column injection system, for quantitation and identification limit studies and for sample analysis. Quantitation was accomplished by using the integrated G-S peak areas and the MA and IA infrared methods.

GC/FT-IR data at 8-cm^{-1} resolution was collected at 3 scans/s to magnetic disk. A modified version of the U.S. EPA vapor-phase FT-IR spectral library (3054 spectra) was used for identification purposes.

GC/MS Instrumentation. The mass spectrometer was a Hewlett-Packard 5970A mass selective detector (MSD) utilizing a 40-megabyte Winchester disk drive and a Hewlett-Packard 9816 desktop computer. The MSD was scanned from 45 to 450 amu at 0.86 scans/s and at a nominal 1-amu resolution. The probability based matching (PBM) software (13) and the 42261 CIS-NIH-NBS mass spectral library were used. The PBM search strategy was $\Delta U + A = 3$, number of ions = 15, tilt option = full, and range option = scan range. Quantitation was accomplished by using the total ion chromatogram (TIC) and single ion peak areas.

IRD/MSD Interface. The GC column was inserted just into the lightpipe without blocking the optical beam. A stainless steel

Swage tee at the lightpipe exit transfer line was fitted with 0.1 mm i.d. fused silica vent and MSD transfer lines. The relative lengths of the lines were chosen to split one-fourteenth of the GC effluent to the MSD at 40°C . This split is reduced to one-eleventh at 280°C (end of GC ramp).

Preparation of Standard Solutions. Standard solutions to study the effect of injection volume on quantitation were prepared in methylene chloride to contain levels of 10, 25, 50, 100, and 250 ng in one-, two-, and three-microliter volumes, respectively. Quantitation calibration curves for each of these three volumes were prepared and each was analyzed on separate days, over a period of 3 consecutive days. Each concentration level was injected in triplicate. Standard solutions for all other quantitation studies were prepared to contain 25, 50, 100, and 250 ng in $3\text{ }\mu\text{L}$ and were injected in duplicate.

Quantitation Approach. MSD quantitation calibration curves were prepared by integrating the TIC area counts or the SIC area counts for the most abundant ion, as a function of nanograms injected.

IRD quantitation calibration curves were generated in the following ways: (1) integrating G-S chromatogram area counts as a function of nanograms injected; (2) plotting MA as a function of nanograms injected; and (3) plotting the IA across the infrared band as a function of nanograms injected.

RESULTS AND DISCUSSION

Hirschfeld has discussed in detail the quantitation errors associated with classical infrared techniques and those errors that are unique to FT-IR (14). However, it may be expected that the errors associated with the gas chromatograph are larger than those associated with the spectrometer. These errors could include poor injection technique and injector discrimination (15), irreversible column adsorption (16), and incomplete solute focusing at the column head (17).

For maximum precision, and optimum delivery of solute to the GC column, this quantitation study was carried out by automated, cold on-column injection to a FSCC. This approach should minimize the effects of injector discrimination, column adsorption, and nonreproducible injection; however, the effect of solute focusing required investigation prior to the initiation of quantitation studies. Accordingly, the effect of injection volume on quantitation results was tested. Table I shows the TIC and G-S area count results for 1-, 2-, and $3\text{-}\mu\text{L}$ injections containing 10–250 ng of 15 base-neutral standards. In general, the slope of both the G-S and TIC plots increased when the injection volume increased. Because both detectors behave similarly, a GC problem was indicated. An increase in slope indicates more material getting to the detector, which may be a result of better solute focusing with the larger solvent volumes. The mean increase in quantitation slopes upon increasing the solvent volume from 1 to $2\text{ }\mu\text{L}$ was 8.1% for G-S and 18.4% for TIC. The mean slope increase between 2 and $3\text{ }\mu\text{L}$ was 8.2% and 5.0% for G-S and TIC, respectively. The hexachloroethane results were excluded from the slope means because this compound produces highly scattered G-S plots which are very sensitive to injection volume. This scatter, which was not exhibited by the MSD plots and thus cannot result from a GC problem, was attributed to the fact that the compound exhibits a single strong IR band near the MCT detector low frequency end cut-off. Unlike hexachloroethane, 2,4-dinitrotoluene plots exhibited large slope changes with increasing injection volume for both detectors. A GC problem was indicated and was attributed to GC column focusing effects on the coelution of 2,4-dinitrotoluene with dibenzofuran.

The G-S plots invariably exhibited a large negative ordinate intercept and a positive abscissa intercept (nanograms). This was interpreted as an interference from purge and carrier gas water vapor to the total G-S response levels. Malissa has demonstrated that one effect of introducing infrared-absorbing gases to the FT-IR purge is to displace the G-S calibration

Table I. Effect of Injection Volume on Gram-Schmidt FT-IR and Total Ion Chromatogram Mass Spectral Peak Area Regression Analysis Results

retention time, min	compound	G-S (FT-IR)				MSD (TIC)			
		slope ^a counts/ng	Y intercept	r ²	rel std error ^b	slope ^a × 10 ⁴ counts/ng	Y intercept × 10 ⁴	r ²	rel std error ^b
6.86 ^b (6.88) ⁱ	1,3-dichlorobenzene	49.91 ^d	1172	0.9890		7.931 ^d	83.81	0.9920	
		53.39 ^e	1317	0.9924		9.026 ^e	74.60	0.9991	
		57.18 ^f	1206	0.9990 ^g	0.4260	9.497 ^f	64.09	0.9998 ^g	0.3747
7.00 (7.01)	1,4-dichlorobenzene	54.21	1391	0.9890		8.750	97.51	0.9922	
		58.46	1301	0.9978		9.973	93.58	0.9996	
		56.74	1829	0.9971	0.5263	10.21	57.59	0.9998	0.4699
7.40 (7.40)	1,2-dichlorobenzene	51.14	1517	0.9925		16.68	311.1	0.9866	
		53.79	1281	0.9968		18.82	278.1	0.9995	
		60.10	+658	0.9985	0.4100	19.98	296.0	0.9998	0.8356
8.01 (8.00)	hexachloroethane	34.48	1317	0.6382		6.996	32.58	0.9830	
		16.67	14	0.9329		7.475	34.35	0.9991	
		14.80	2126	0.8009	2.538	7.421	+4.75	0.9991	0.6483
8.23 (8.28)	nitrobenzene	134.3	3944	0.9813		7.728	169.3	0.9896	
		147.1	3222	0.9994		8.874	162.1	0.9989	
		164.0	4454	0.9979	1.920	9.744	193.0	0.9997	0.5353
8.82 (8.86)	isophorone	132.8	1310	0.9936		12.61	110.5	0.9928	
		141.9	2201	0.9991		13.68	116.0	0.9995	
		145.7	2051	0.9994	0.9060	14.38	142.3	0.9997	0.7323
9.70 (9.77)	1,2,4-trichlorobenzene	47.51	1330	0.9957		9.326	169.3	0.9886	
		49.76	1886	0.9805		9.985	131.0	0.9998	
		53.74	1454	0.9998	0.2190	10.49	133.5	0.9998	0.4345
10.36 (10.40)	hexachlorobutadiene	26.65 ^d	920	0.8903		9.780	79.90	0.9732	
		22.32 ^e	924	0.9811		10.03	70.14	0.9983	
		22.68 ^f	131	0.9883	0.9231	10.18	82.23	0.9992	0.8348
11.55 (11.60)	2-methylnaphthalene	25.35	977	0.9890		13.21	146.4	0.9924	
		25.40	915	0.9971		14.35	98.93	0.9920	
		28.20	1154	0.9981	0.2050	14.75	68.67	0.9990	1.359
12.15 (12.20)	hexachlorocyclopentadiene	38.93	1368	0.9945		8.800	166.4	0.9651	
		35.48	1248	0.9932		9.248	207.3	0.9991	
		40.44	2081	0.9927	1.079	9.695	268.1	0.9996	0.6003
12.74 (12.80)	2-chloronaphthalene	27.44	1621	0.9829		12.58	204.3	0.9880	
		25.08	1527	0.9829		14.16	180.7	0.9995	
		26.18	1111	0.9974	1.000	15.02	205.5	0.9995	1.000
13.89 (13.95)	2,6-dinitrotoluene	221.5	5024	0.9863		7.509	309.5	0.9942	
		233.0	4172	0.9971		9.520	369.0	0.9992	
		258.7	5463	0.9984	2.948	10.22	367.1	0.9989	1.007
14.70 (14.70)	dibenzofuran	98.48	3524	0.9824		11.17	206.0	0.9919	
		99.78	3263	0.9815		12.81	165.1	0.9999	
		109.0	2332	0.9992	1.061	13.04	136.2	0.9995	0.8146
14.85 (14.90)	2,4-dinitrotoluene	154.4	5818	0.9508		5.964	300.2	0.9559	
		191.5	5969	0.9933		9.088	398.7	0.9957	
		225.3	6561	0.9964	2.268	9.667	415.4	0.9998	0.4317
17.20 (17.20)	hexachlorobenzene	109.7	2540	0.9855		17.16	117.0	0.9699	
		106.7	3312	0.9852		17.91	83.82	0.9975	
		104.1	3195	0.9896	0.3696	17.67	45.98	0.9981	2.251

^aSlope of Gram-Schmidt area counts versus ng injected. ^bStandard error of Y on X for cited compound relative to that of 2-chloronaphthalene (selected because it exhibits a moderate response to both detectors, does not coelute, and is statistically well behaved). ^cSlope of total ion chromatogram area counts versus ng injected. ^dOne microliter injection data. ^eTwo microliter injection data. ^fThree microliter injection data. ^gMean correlation coefficient for 15 compounds using 3 μ L injections for FT-IR was 0.9835 and for the MSD was 0.9994. ^hFT-IR retention time. ⁱMSD retention time.

curves away from the origin (18). TIC intercepts were also negative but invariably were closer to the origin than those of the G-S. It should be noted that in addition to these forms of chemical noise, spectral noise may also contribute to this effect.

Comparison of Mass Spectral and FT-IR Area Count Quantitation with FT-IR Absorbance Methods. Table II shows the results of regression analyses on mass spectral and FT-IR area count and absorbance quantitation for 3- μ L injections. The SIC GC/MS approach was used because of its greater sensitivity over TIC, and because of its wide spread use in environmental monitoring. When considered in conjunction with the 3- μ L data in Table I, a comparison of TIC, SIC, G-S, IA, and MA quantitation is possible. By use of the mean regression correlation coefficients (r^2) as a measure of data scatter, it is seen that scatter increases in the order TIC approximately equal to SIC < MA < IA < G-S (0.9994, 0.9984,

0.9942, 0.9874, 0.9835, respectively). The mean G-S and IA r^2 may both be improved to 0.9966 by omitting the hexachloroethane and dibenzofuran data (because of scattered plots and coelution, respectively). This would lower the spread between the best (TIC) and worst (MA) mean r^2 to 5 parts per thousand and indicate that the regression scatter is comparable for the five approaches. However, it should be remembered that small, highly halogenated compounds like hexachloroethane are typical environmental purgeables, and also that chromatographic coelution is common, even for capillary GC columns (19, 20).

Examination of the Y-intercept data, and the quantitation plots for the five techniques, indicates that the TIC, SIC, IA, and MA intercepts are closer to the graph origin than the G-S intercept. See Figure 1 for the SIC, IA, MA, and G-S quantitation plots for 2-methylnaphthalene. The use of specific IR quantitation bands for MA and IA quantitation apparently

Table II. Comparison of Mass Spectral and Infrared Quantitation Methods by Regression Analysis^a

compound	MSD				FT-IR							
	single ion monitoring ^b				integrated absorbance ^c				maximum absorbance ^d			
	slope $\times 10^4$	Y intercept $\times 10^4$	r^2	rel std error ^e	slope	Y intercept	r^2	rel std error	slope	Y intercept	r^2	rel std error ^e
1,3-dichlorobenzene	3.457	8.646	0.9967	1.5900	0.02037	0.1119	0.9950	2.741	0.05296	0.0421	0.9985	0.8457
1,4-dichlorobenzene	3.911	+6.239	0.9960	0.9973	0.02460	0.1877	0.9994	1.187	0.06158	0.1877	0.9994	0.6023
1,2-dichlorobenzene	3.578	+1.730	0.9973	1.4710	0.01301	0.7815	0.9994	1.301	0.03034	0.2580	0.9937	1.0030
hexachloroethane	1.370	3.517	0.9972	0.5814	0.05959	0.1019	0.9992	3.278	0.14160	0.1002	0.9986	2.1730
nitrobenzene	1.932	23.03	0.9991	0.4602	0.04047	0.3433	0.9979	3.490	0.92210	0.8822	0.9997	0.6209
isophorone	9.270	9.401	0.9996	1.3080	0.03971	0.0800	0.9990	2.342	0.08679	0.1055	0.9984	1.4230
1,2,4-trichlorobenzene	3.169	1.811	0.9987	0.9189	0.02551	0.1277	0.9979	1.492	0.05258	0.4640	0.9969	1.2300
hexachlorobutadiene	2.315	0.076	0.9965	1.0850	0.01960	0.0788	0.9979	1.767	0.03580	+0.3350	0.9960	0.9690
2-methylnaphthalene	6.213	+2.247	0.9991	1.4600	0.01391	0.0615	0.9950	1.932	0.02403	+0.0217	0.9981	0.4529
hexachlorocyclopentadiene	2.905	38.61	0.9982	0.9811	0.01857	0.2917	0.9945	4.643	0.03330	0.2917	0.9862	1.6830
2-chloronaphthalene	6.448	16.81	0.9996	1.0000	0.01450	0.3450	0.9988	1.000	0.02290	0.3600	0.9997	1.0000
2,6-dinitrobenzene	1.814	31.66	0.9989	0.4863	0.06785	0.1470	0.9966	7.563	0.10770	0.5006	0.9947	3.1930
dibenzofuran	9.472	15.26	0.9996	1.4080	0.01297	0.2215	0.8579	10.01	0.03469	0.2832	0.9697	2.4880
2,4-dinitrotoluene	2.469	+48.49	0.9987	0.7126	0.06511	0.6000	0.9928	10.48	0.10230	1.3350	0.9966	2.4280
hexachlorobenzene	6.282	+2.629	0.9993	1.2710	0.04836	0.1394	0.9995	2.045	0.06835	0.3458	0.9981	1.2260
mean r^2			0.9983				0.9874				0.9942	

^aBased on duplicate 3- μ L injections of 25, 50, 100, and 250 ng. ^bBased on area counts of most abundant MSD ion. ^cIntegrated absorbance of total peak scans. ^dFT-IR scan with highest absorbance. ^eStandard error of y on x for cited compound relative to that of 2-chloronaphthalene.

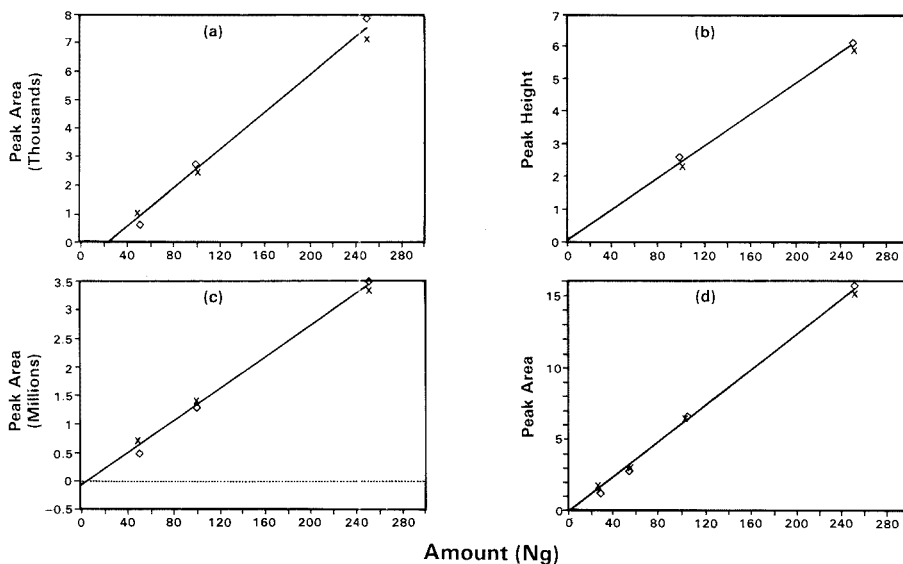


Figure 1. MS and FT-IR quantitation plots for 2-methylnaphthalene. Data collected on a directly linked GC/FT-IR/MS. Key: (a) G-S, (b) MA, (c) SIC, and (d) IA.

mimimizes the G-S graph-origin shifts, which have been attributed to residual water vapor absorption. In addition the G-S plot scatter for hexachloroethane is absent in the IA and MA quantitation plots which is difficult to rationalize on the basis of the nearness of a major spectral band to the detector frequency cutoff.

Relative Molecular Sensitivities of the Infrared and Mass Spectral Detectors. Previously, it had been shown that the relative response factors for each of these detectors exceeded an order of magnitude (21). The effect of molecular structure of five types of quantitation curve slopes is summarized in Table III. The TIC slope is least sensitive to molecular structure while the G-S approach is most sensitive. The SIC, IA, and MA approaches produce roughly comparable results. These three approaches are associated with molecular substructural information, while the TIC and G-S data provide

information about the entire molecule. If the compounds selected for this study are assumed truly representative, the suggestion is that the prediction of TIC response factors (22) will be simpler than that of those associated with the G-S. Because the selected compounds represent both strong and weak infrared absorbers, and a reasonable range of MSD response factors, it is believed that this assumption is tenable.

It should be noted that the IR quantitation methods suffer from the danger that the FT-IR scan file may not have been collected when the analytes' lightpipe concentration was at a maximum. Faster spectrometer scan rates help to ensure the synchronization of FT-IR data acquisition and the lightpipe concentration profile. If the coadded IA files vary widely in signal/noise (S/N), the resultant file S/N may be degraded leading to erroneously low absorbances. This problem may be minimized by utilizing only those scans near

Table III. Relative Molecular and Substructural Sensitivities of Infrared and Mass Spectral Detectors^a

compound	MSD		FT-IR		
	TIC	SIC	integrated absorbance	maximum absorbance	Gram-Schmidt
1,3-dichlorobenzene	0.6323	0.5361	1.435	2.314	2.184
1,4-dichlorobenzene	0.6798	0.6065	1.637	2.689	2.167
1,2-dichlorobenzene	1.330 ^b	0.5549	0.8972	1.325	2.296
hexachloroethane ^d					
nitrobenzene	0.6487	0.2997	2.791	4.027	6.264
isophorone	0.9574	1.4385	2.739	3.790	5.565
1,2,4-trichlorobenzene	0.6984	0.4915	1.759	2.296	2.053
hexachlorobutadiene	0.6778	0.3589	1.352	1.563	0.8663
2-methylnaphthalene	0.9820	0.9635	0.9593	1.049	1.077
hexachlorocyclopentadiene	0.6455	0.4505	1.231	1.455	1.545
2-chloronaphthalene	1.000	1.000	1.090	1.000	1.000
2,6-dinitrotoluene	0.6804	0.2814	4.633	4.703	9.882
dibenzofuran	0.8688	1.469	0.8945	1.515	4.163
2,4-dinitrotoluene	0.6436	0.3829	4.490	4.467	8.606
hexachlorobenzene	1.176	0.9741	3.335	2.985	3.976
high-low ratio ^c	2.103	5.220	5.235	4.703	11.41

^a For 3 μ L injection data. ^b Coeluted badly with benzyl alcohol during this run. ^c Ratio of highest to lowest relative sensitivity. ^d Data rejected because of extreme scatter in G-S plots.

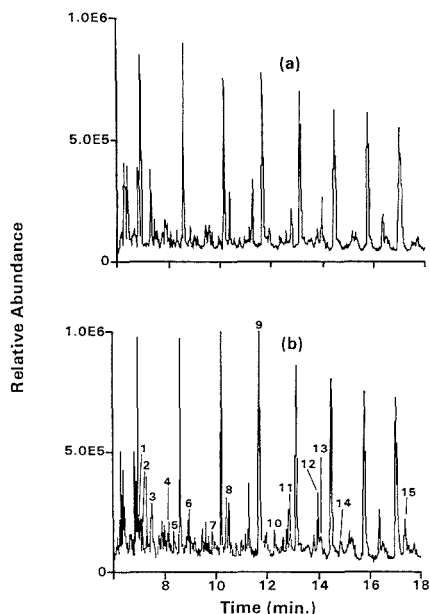


Figure 2. Total ion chromatogram of crude oil sample extract (a) and sample extract (b) spiked at 100 ng with 15 base-neutral standards (ca. 10 ng to MS detector). Numbers correlate with elution order of Table I.

to the chromatogram peak apex. It is interesting to note that the TIC approach has also been reported to suffer from the possible nonsynchronization of scan rate with analyte maximum concentration (23).

Effect of Sample Background on Infrared and Mass Spectral Selectivities and Minimum Identifiable Quantities (MIQ) in a Linked GC/FT-IR/MS System. While it is well-known that sample background raises mass spectral detection limits (11), the effect of sample background on linked GC/FT-IR/MS analysis has not been reported. (Note that while MIQ is a measure of identification capability, detection limit is a measure of the capability to distinguish

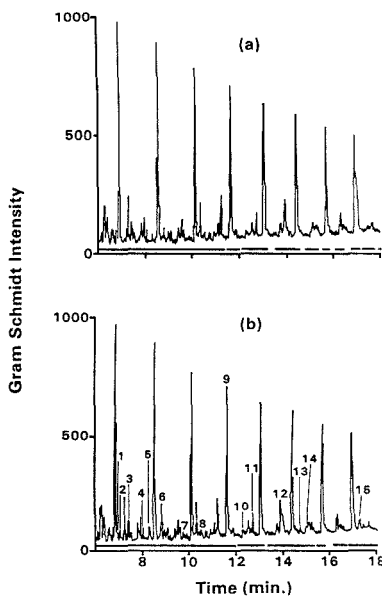


Figure 3. Gram-Schmidt reconstructed chromatogram of crude oil sample extract (a) and sample extract (b) spiked at 100 ng with 15 base-neutral standards (ca. 90 ng to FT-IR detector). Numbers correlate with elution order of Table I.

analyte response from background.) To investigate this, a crude oil sample was spiked with base-neutral compounds in the 25–250-ng range. MS and FT-IR library searches were then compared to determine the MIQ for each detector, for spikes in a pure solvent and a spiked sample, which would yield an identifiable spectrum within the first five hits. The TIC and G-S chromatograms of spiked and unspiked samples are shown in Figures 2 and 3 (remember the approximately one-tenth split to the MS). In general, the MIQs for both FT-IR and MS were elevated about a factor of 2 by sample background interferences. The split-uncorrected MS *sample* MIQs for strong FT-IR absorbers like 2,4- and 2,6-dinitrotoluene were higher than those of the FT-IR by factors of 2.5

to 5, while those of weak infrared absorbers were comparable for the two detectors. The library search fits for both detectors were often better in the spiked samples. This may be attributed to the higher spectral signal-to-noise ratio, achieved at the higher spike concentrations, which are required to achieve analyte identification in the presence of sample interferences. It should be noted that an MIQ-based comparison of relative detector performance can be influenced by the size of the search library and the search algorithm efficiency.

Implications for Target List and Screening Environmental Analyses. The target list approach (e.g. priority pollutants) implies the availability of certified standards for quantitation and for creating reference spectra. The internal standard response factors (often deuterated compounds) are used in conjunction with GC/MS analytical data for quantitation. It has been claimed that the use of multiple internal standards produces GC/MS response factors of higher precision (24). Like the effect of injection volume, postulated here to be a result of solute focusing, this multiple standard advantage may result from a more similar focusing of standard and analyte. It remains to be seen if optimization of the injection approach, or multistandard analysis, will be the most economical analytical approach to target list quantitation.

Unlike the target list approach, standards are rarely available to support the screening approach. If GC/MS response factors (22) or FT-IR absorbance coefficients are to be estimated from existing data (25), it is critical that the full amount of injected analyte reach the detector (this obviously applies to the creation of the existing data base as well).

If it is presumed that the regression fits (as measured by r^2) are comparable for the five reconstruction techniques, then a choice of the best FT-IR/MS approach to target list quantitation depends largely on the desired accuracy. The six possible MS/FT-IR combinations are TIC/G-S, TIC/MA, TIC/IA, SIC/G-S, SIC/MA, and SIC/IA. The sensitivity of G-S to water vapor problems then narrows the choices to TIC/MA, TIC/IA, SIC/MA, or SIC/IA. If maximum quantitation accuracy and the maximum number of detections are desired, then SIC/MA appears to be the method of choice.

If the nonavailability of standards is the ultimate problem for screening, then the ability to predict GC/MS response factors and GC/FT-IR absorption coefficients is of paramount importance. Because prediction would be eased by insensitivity to structure (as measured by small relative molecular and substructural sensitivities), it is proposed that the best FT-IR/MS approach to environmental screening quantitation is TIC/MA or TIC/IA because of the similar sensitivity to molecular structure of the IA and MA techniques.

CONCLUSION

Regression analysis mean correlation coefficients in the concentration range of 25–250 ng, for TIC, SIC, IA, MA, and G-S areas, were 0.9994, 0.9984, 0.9874, 0.9942, and 0.9835, respectively. Omission of one outlier each, for G-S and IA alters this ranking to 0.9994, 0.9984, 0.9966, 0.9942, and 0.9966 indicating comparable fits for the five techniques. The nonlinearity in plots of reconstructed absorbance chromatogram area ratios versus concentration, recently reported by Olson et al., were not observed in this work (26).

On-column injection volume studies indicated an increased MS and FT-IR area count response with higher injection volumes. Although Grob has indicated the feasibility of using large injection volumes ($\geq 100 \mu\text{L}$), the initial column tem-

perature must be carefully controlled during the injection and long (20–50 m) retention gaps are needed (27). It is not clear what constraints will be placed on routine environmental analysis by the Grob approach; however, quantitative analyte transfer to the GC column is required for utilization of the "standardless" FT-IR absorbance coefficient approach (i.e., one-time measurement of absorbance coefficient and direct utilization of these stored values for the subsequent quantitation of unknowns).

Consideration of possible errors from water vapor eliminate the G-S reconstruction mode from the six possible FT-IR/MS reconstruction combinations. Choice between the remaining four combinations is dictated, in part, by the desire for a maximum number of detections or for the maximum number of joint detections (choice between SIC or TIC hyphenations respectively, with FT-IR). FT-IR/MS screening quantitation (standardless) would best be carried out in the TIC/IA or TIC/MA modes, while target list quantitation would best be carried out in the SIC/MA mode.

LITERATURE CITED

- (1) Gurka, D. F.; Titus, R. *Anal. Chem.* **1986**, *58*, 2189–2194.
- (2) Olson, E. S.; Diehl, J. W. *Anal. Chem.* **1987**, *59*, 443–448.
- (3) Olson, E. S.; Diehl, J. W. Presented at the 9th Rocky Mountain ACS Regional Meeting in Las Vegas, NV, March 30, 1988; Abs 335.
- (4) Cooper, J. R.; Taylor, L. T. *Anal. Chem.* **1984**, *56*, 1989–1993.
- (5) Gurka, D. F.; Pyle, S. *Environ. Sci. Technol.* **1988**, *22*, 963–967.
- (6) Gurka, D. F.; Pyle, S. Presented at the XXV Colloquium Spectroscopicum Internationale, Toronto, Canada, June 23, 1987; Abs C3.6.
- (7) Bowater, I. C.; Brown, R. S.; Cooper, J. R.; Wilkins, C. L. *Anal. Chem.* **1986**, *58*, 2195–2199.
- (8) Griffiths, P. R. *Fourier Transform Infrared Spectroscopy*; Ferraro, J. R., Basile, L. J., Eds.; Academic Press: New York, 1978; Vol. I, Chapter 4.
- (9) Liu, S.; Chichester-Constable, D. J.; Hubbard, J.; Smith, S. R.; Stuart, J. D. *Anal. Lett.* **1987**, *20*(12), 2073–2092.
- (10) Gurka, D. F. *Appl. Spectrosc.* **1986**, *39*, 827–833.
- (11) *Fed. Regist.* **1979**, *44*(233), 69540 (Monday, December 3).
- (12) Spitzer, T.; Kuwatsuka, S. *J. Chromatogr.* **1986**, *358*, 434–437.
- (13) Pesyna, G. M.; Venkataraghavan, R.; Dayringer, H. E.; McLafferty, F. W. *Anal. Chem.* **1976**, *48*, 1362–1368.
- (14) Hirschfeld, T. *Fourier Transform Infrared Spectroscopy*; Ferraro, J. R., Basile, L. J., Eds.; Academic Press: New York, 1979; Vol. II, Chapter 6.
- (15) Grob, K.; Grob, K., Jr. *J. Chromatogr.* **1978**, *151*, 311–320.
- (16) Anthony, L. J.; Holland, R. A.; Heffner, J. A. *HRC CC, J. High Res. Chromatogr. Chromatogr. Commun.* **1988**, *11*, 167–171.
- (17) Grob, K., Jr.; Romann, A., Jr. *J. Chromatogr.* **1981**, *214*, 118–121.
- (18) Malissa, H., Jr.; Martin, K.; Winsauer, L. Proceedings of the International Conference on Fourier and Computerized Spectroscopy. *Proc. SPIE—Int. Soc. Opt. Eng.* **1986**, *533*, 340.
- (19) Rosenthal, D. *Anal. Chem.* **1982**, *54*, 63–66.
- (20) Davis, J. M.; Giddings, J. C. *Anal. Chem.* **1985**, *57*, 2178–2182.
- (21) Gurka, D. F.; Hiatt, M.; Titus, R. *Anal. Chem.* **1984**, *56*, 1102–1110.
- (22) Sauter, A. D.; Downs, J. J.; Buchner, J. D.; Ringo, N. T.; Shaw, D. L.; Dulak, J. G. *Anal. Chem.* **1986**, *58*, 1665–1670.
- (23) Eichelberger, J. W.; Kerns, E. H.; Olynk, P.; Budde, W. L. *Anal. Chem.* **1983**, *55*, 1471–1479.
- (24) Sauter, A. D.; Betowski, L. D.; Smith, T. R.; Strickler, V. A.; Beimer, R. G.; Colby, B. N.; Wilkinson, J. E. *HRC CC, J. High Resolut. Chromatogr. Chromatogr. Commun.* **1981**, *4*, 366–368.
- (25) Griffiths, P. R.; Henry, D. E. *Prog. Anal. Spectrosc.* **1986**, *9*, 455–467.
- (26) Olson, E. S.; Diehl, J. W.; Froelich, M. L. *Anal. Chem.* **1988**, *60*, 1920–1924.
- (27) Grob, K.; Schilling, B. *J. Chromatogr.* **1984**, *299*, 415–419.

RECEIVED for review September 27, 1988. Accepted April 24, 1989. Although the research described in this paper has been funded wholly or in part by the U.S. Environmental Protection Agency, it has not been subjected to Agency review and, therefore, does not necessarily reflect the views of the Agency, and no official endorsement should be inferred. Mention of trade names or commercial products does not constitute endorsement or recommendation for use.

CORRESPONDENCE

Capillary Zone Electrophoresis with Analyte Velocity Modulation. Application to Refractive Index Detection

Sir: Capillary electrophoresis (1-4) is a rapidly emerging high-resolution separation technique, with broad applications in analytical chemistry, biochemistry, and molecular biology. It provides better resolution than liquid chromatography or one-dimensional gel electrophoresis in separation of proteins (5, 6), amino acids (7), pharmaceuticals (8), and inorganic ions (9). However, the small sample size and inside diameter of the capillary remain major experimental problems in development of detection systems.

INTRODUCTION

Fluorescence, with incoherent (2) or laser (8) sources, provides adequately low detection limits but requires either prior (2) or postcolumn (6) derivatization for most analytes. Absorption detectors (10) are insensitive because of the low light throughput. Electrochemical detection (11) has low detection limits, where it is applicable.

Indirect fluorescence (7, 12) is almost universally applicable. Because of the laser intensity fluctuation and high signal background, detection limits appear to be similar to absorption detection limits. Conductance (9), which is also an indirect technique, works with many small ions, but requires delicate experimental apparatus.

Refractive index of various designs have been used in liquid chromatographic practice for many years (13). In that context they have usually been considered to be insensitive and drift-prone. However, Dovichi and co-workers (14-16) and Synovec (17, 18) have proposed laser beam deflection as a refractive index detection principle for microbore and capillary separations. In small-diameter columns and capillaries, these detectors perform much better than in large-bore systems.

Synovec (17) has shown that eq 1 adequately describes the response of a laser beam.

$$\frac{d\theta}{dn} = \frac{2D}{rn^2} \quad (1)$$

In eq 1, θ is the deflection angle of the laser beam, n is the refractive index of the mobile phase or the buffer solution, D is the offset of the laser beam from the capillary center axis, and r is the inside radius of the capillary. The sensitivity is not strongly dependent on the capillary inside diameter, because it is possible to focus laser radiation to micrometer diameters, so that a favorable $D:r$ ratio can be maintained.

Synovec (18) shows that sensitivity of about 1 mrad/0.001 refractive index (RI) unit is usually obtained in aqueous solutions. The refractive index change for aqueous solutions of most proteins is $(1-2) \times 10^{-4}$ RI unit per 1% (w/v) of protein (19). Laser beam deflection should ultimately be capable of detecting angular deviation of about 1×10^{-9} rad, about 1-2 orders of magnitude below current detection limits (14-18).

Many factors limit performance of reported laser beam deflection detectors. These include laser pointing and intensity instability along with thermal fluctuations in the capillary. Further, there is capillary movement caused by changes in the electrical double layer at the inner surface. This movement changes the efficiency of signal collection.

Pawliszyn (20-23) has demonstrated that beam deflection detectors which probe concentration gradients are stable refractive index detectors that can be used for capillary liquid chromatography or capillary electrophoresis. These devices produce a first-derivative response. A recent variant on this design by Synovec (18, 24) and a dual differential design by Pawliszyn (23) can measure refractive index differences of $(2-5) \times 10^{-8}$ RI unit. While these devices perform well, they are inherently limited to refractive index detection, or where a second laser at a suitable wavelength is available for absorbance detection via photothermal beam deflection (25).

In this paper we report a modulation system that is insensitive to thermal effects, laser beam wander, small capillary position changes, and other sources of background fluctuation. We generate an analyte velocity modulation by modulating the applied voltage across the capillary. This technique generates a response that is the first derivative of the conventional electrophoretogram. We describe application of this system to monitoring of protein free zone electrophoresis with a simple and sensitive laser beam deflection refractive index detector.

Velocity modulation has important advantages. The implementation is electrical, not optical. The technique can be used to generate a stable background derivative response with a wide variety of detector types, not just refractive index. The modulation can often be applied at a frequency where system excess noise is well below its dc level. It may prove a generally useful strategy for increasing signal to noise ratios in capillary electrophoresis systems. Unlike direct differentiation of the detector response, velocity modulation completely rejects any signals that are not within the passband of the demodulation system.

THEORY

We assume that the electrophoresis is monitored near the capillary exit by a detector with response proportional to concentration. The detector is assumed to view a length of capillary that is short compared to the length occupied by the analyte zone. With these assumptions, the expected response can be derived from considerations similar to those used in discussing mass transport in electroanalytical systems (26, 27).

In an electrophoretic separation the analyte velocity is proportional to the applied electric field in the separation capillary (eq 2).

$$v_i = \mu_i E = \mu_i \frac{V}{L} \quad (2)$$

In eq 2, v_i is the velocity of the analyte i , μ_i is its mobility, E is the electric field, V is the applied voltage, and L is the length of capillary.

The flux of analyte (26, 27) is given by eq 3, where J_i is the flux of the analyte i , D_i is its diffusion coefficient, and C_i is its concentration.

$$J_i = -D_i \frac{\partial C_i}{\partial x} - \mu_i C_i(x,t) \frac{\partial V}{\partial x} \quad (3)$$

In capillary electrophoresis, diffusion spreading is slow compared to the zone velocity (2). It is valid to consider only

the velocity of the zone center. The buffer concentration usually is much higher than the analyte concentration. In this case, at any instant in time the electric field is constant along the capillary (28). For analyte velocity modulation, an ac voltage is added to (or subtracted from) the dc driving voltage. The electric field is the instantaneous voltage, $V_{dc} + V_{ac} \cos \omega t$, divided by the length of the capillary. The flux equation becomes eq 4.

$$J_i = -\frac{\mu_i V_{dc}}{L} \left(1 + \frac{V_{ac}}{V_{dc}} \cos \omega t \right) C_i(x,t) \quad (4)$$

The equation of continuity (26, 27) connects the spatial flux gradient with the time dependence of concentration (eq 5).

$$\frac{\partial C_i}{\partial t} = -\frac{\partial J_i}{\partial x} \quad (5)$$

With one keeping in mind that eq 5 specifies *spatial* flux derivatives, differentiation of eq 4 yields eq 6.

$$\frac{\partial C_i}{\partial t} = \frac{\partial C_i(x,t)}{\partial x} \frac{V_{dc} \mu_i}{L} \left(1 + \frac{V_{ac}}{V_{dc}} \cos \omega t \right) \quad (6)$$

Conventionally, a capillary electrophoresis detector monitors the time dependence of concentration at a fixed point near the downstream end of the capillary. If the detector output is passed through a lock-in amplifier referenced to the modulation voltage, the component of its response synchronous with the modulation can be extracted. By inspection of eq 6, the output of the lock-in is seen to be eq 7.

$$V_{out} = K \mu_i \frac{V_{dc}}{L} \frac{\partial C_i}{\partial x} \frac{V_{ac}}{V_{dc}} \quad (7)$$

K is a constant that includes the detector response factor and lock-in amplifier gain. The output of the amplifier is proportional to the first derivative of concentration, $\partial C_i/\partial x$, and to V_{ac}/V_{dc} , the depth of the modulation.

If the modulation frequency is sufficiently high, thermal fluctuations of refractive index, capillary movement effects, and laser beam wander will all be rejected. As with any derivative technique, the amplitude is inversely proportional to the square of the width of a (Gaussian) band. The technique should work well for narrow bands, but may be less satisfactory for broad bands.

EXPERIMENTAL SECTION

Capillary Zone Electrophoresis. The capillary zone electrophoresis system was constructed along conventional lines (2). A 55-cm length of 75 μm i.d. capillary (Polymicro Technologies, TSP/075/375) was used as the separation capillary. The cleaning procedure of Lauer and McManigill (5) was followed. The observation region was formed by burning off a small section of the protective coating about 5 cm from the exit end of the capillary. The capillary was held in place with a locally constructed Plexiglas holder, with a through hole for observation of the laser beam. The entire capillary was placed in a safety enclosure with small openings for passage of the laser beam. Sample introduction was by electromigration (5–10 s, 3 kV).

The analyte velocity modulation system is shown in Figure 1. The dc driving voltage was provided by a high-voltage power supply (Glassman PS/LG-30R-5) operated at 10–20 kV. The dc voltage was applied between the capillary entrance and the system ground. The ac voltage was provided by an 88:1 step-up transformer (Hipotronics, RM10) connected between the capillary exit and system ground. Power was provided to the primary windings of the transformer by a pair of power operational amplifiers (Hewlett-Packard 6824A) connected to provide ± 100 V output and driven by the sinusoidal output of a signal generator (Wavetek 112). For most runs, the modulation frequency was about 390 Hz and the peak ac voltage was about 50% of the dc voltage.

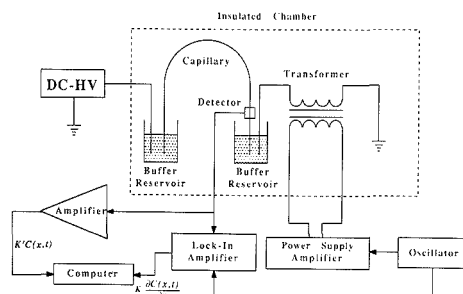


Figure 1. Instrumentation for capillary zone electrophoresis with an analyte velocity modulation system.

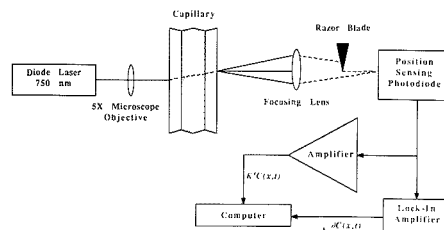


Figure 2. Laser beam deflection refractive index detector.

The derivative signal was extracted from the detector response by a lock-in amplifier (EG&G PARC 5209), which was operated with a 0.1-s time constant and 12 dB/octave rolloff. The dc (normal) signal was obtained by amplifying the entire detector response through a low-pass filter/amplifier (Ithaco 1201) operated with a 3-Hz cutoff frequency and 6 dB/octave rolloff.

Electrophoretograms were recorded on a personal computer by digitizing the lock-in amplifier output and low-pass filter/amplifier output to 12-bit resolution at 0.1-s intervals.

Detector. The laser beam deflection refractive index detector is shown in Figure 2. The detector consisted of a 3-mW 750-nm diode laser (Oriol 79401) and a position-sensing photodiode (United Detector Technology, UDT-LSC/5D). The laser was focused into the capillary with a 5X microscope objective (Rolyn 80.3045). The laser beam was focused onto the exit wall of the capillary. Proper focus was obtained when an extended diffraction pattern was observed. The diffraction pattern was centered to focus the laser in the center of the capillary. A razor blade was inserted into the beam about 1 m beyond the capillary. The blade was adjusted to block half of the beam, so that the expansion of the remaining half was observed as a deflection. The half-beam was focused on the position-sensing photodiode with a 200 mm focal length lens. The diode was positioned to give an approximately 0-V output when only the buffer was present in the capillary.

Reagents. Buffer solution, 0.02 M phosphate at pH 8.2, was prepared from dibasic sodium phosphate and adjusted to the proper pH value with 1 M HCl. Carbonic anhydrase was purchased from Sigma and used as received. Protein concentrations were 0.01% (w/v), 0.1 mg/mL, and were diluted with buffer as needed. All other reagents were of ACS reagent grade. Type I water was used to prepare all solutions.

RESULTS AND DISCUSSION

Figure 3 shows a typical electrophoretogram for 0.005% carbonic anhydrase. Both the demodulated ac (derivative) and dc (conventional) detector outputs are shown. The inset to Figure 3 shows the derivative response in greater detail. After the first 30 s, the base-line drift of the dc signal is completely absent in the demodulated ac response. The occasional noise peaks in the dc signal are attenuated or absent in the demodulated ac signal.

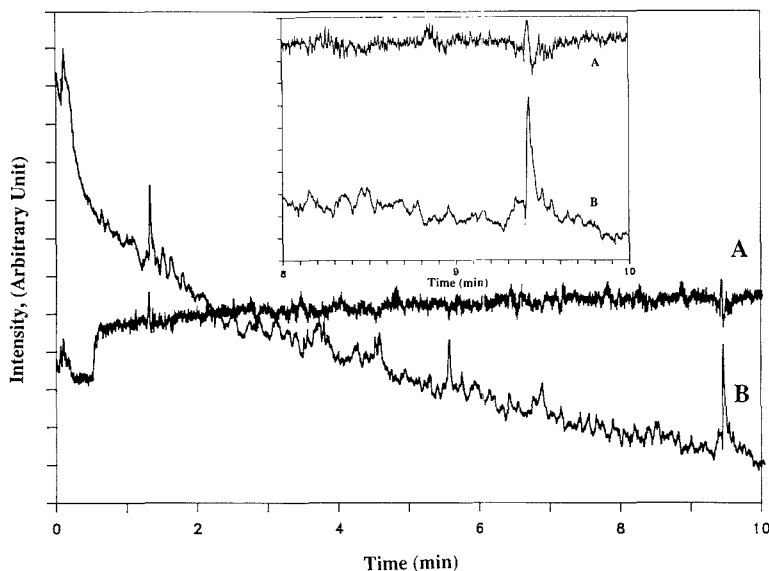


Figure 3. Electrophoretogram of 0.005% (w/v) carbonic anhydrase in 0.02 M phosphate buffer, pH = 8.2: dc, 20 kV; ac, 11 kV, 390 Hz; A, demodulated ac signal from the lock-in amplifier; B, amplified normal dc signal from photodiode. Detail electrophoretogram around the band is shown in inset.

Temperature changes in the capillary, laser beam pointing noise, and laser beam wander and amplitude drift all occur at low frequency, 0.001–10 Hz. While the data of Figure 3 does not provide information on the relative magnitude of these sources, the figure shows that analyte velocity modulation does reject low-frequency noise and drift.

We define the signal to noise ratio as the peak-peak signal intensity divided by the standard deviation of the base-line fluctuations measured over an 80-s interval in the vicinity of the signal. Although the derivative shape makes the local signal to noise ratio of the ac signal (10:1) look relatively poor, it is actually quite similar to the local signal to noise ratio of the dc signal, about 12:1. However, the bandwidth of the dc amplifier (3 Hz) is larger than the bandwidth of the ac demodulator (1.6 Hz). One would expect the ac signal to noise ratio to be about 1.3 times larger than the dc signal to noise ratio. The difference is due to the small depth of modulation, which makes the ac signal only 55% of its maximum possible value. With an instrument capable of 100% modulation, the ac and dc signal to noise ratios should be essentially the same, if the instrument bandwidths are the same.

During the first 30 s of the electrophoretogram, both the demodulated ac and the dc signals drift badly. The drift appears to be the result of capillary movement, as the double layer at the silica/buffer interface adjusts to the high voltage. This movement translates the capillary across the stationary laser beam, with a change in the intensity of the signal reaching the photodiode. The drift could be minimized, but not completely eliminated, by clamping the capillary tightly into a Plexiglas holder and reducing the diameter of the through hole for the laser beam to less than 6 mm.

The demodulated ac signals were always found to ride on a frequency-dependent constant background. The applied ac voltage caused the capillary to vibrate slightly, generating a signal that was synchronous with the driving voltage. This vibration-induced signal was large if the modulation frequency was less than about 100 Hz and decreased rapidly above that frequency. Consequently, the modulation frequency was kept

as high as possible. The upper limit, about 400 Hz, was set by the properties of the dc power supply. This unit could not maintain a constant output when higher modulation frequencies were used.

The average value of the modulation voltage is identically zero. Therefore, eq 6 predicts that there should be no effect of modulation voltage on the migration time or the dc band shape of any analyte. To test this prediction, we compared the migration times of several analytes to the values obtained with the transformer in place, but no modulation applied, and with the transformer absent and the negative end of the capillary connected to ground. We could find no difference in migration times or band shapes. To confirm refractive index data, we made similar measurements using fluorescence detection and Rhodamine 6G as an analyte. Again, the presence of the modulation voltage had no measurable effect on migration times or band shapes.

Some high-frequency base-line fluctuations remain on the ac signal. The noise appears to be primarily laser amplitude noise. This noise was observed in the absence of any ac or dc power applied to the capillary. Further confirmation comes from substitution of a 1-mW He-Ne laser for the diode laser. With the He-Ne laser, the noise was about a factor of 10 higher, with or without power applied to the system.

The specific refractivity of most proteins is about $(1-2) \times 10^{-4}$ RI unit per 1% solution (19). Using this range, we can estimate the base-line noise of our detector system as less than 5×10^{-8} RI unit. The detection limit ($S/N = 3$) for carbonic anhydrase is about 0.0015%. This performance compares favorably with the values reported for other recent designs of refractive index detectors (15, 16). The detector appears to be at least as sensitive as an absorbance detector (6) for proteins, although not as sensitive as fluorometry (6).

It is possible to approximately double the signal intensity by increasing the depth of modulation to 100%. This increase may require oil-filled transformers or other special designs to reach a secondary output voltage of 30 kV. A further decrease in noise can be achieved if a more stable laser is used.

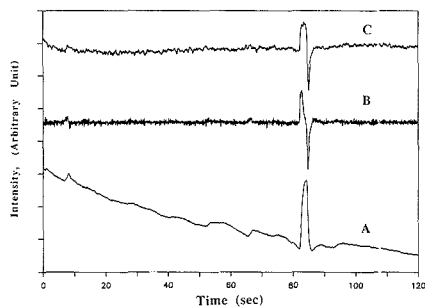


Figure 4. Electrophoretogram of 0.1 M NaCl in 0.02 M phosphate buffer, pH = 8.2: dc, 20 kV; ac, 11 kV, 390 Hz; A, amplified normal dc signal from photodiode; B, numerically differentiated dc signal; C, demodulated ac signal from the lock-in amplifier.

Although our laser is intensity-stabilized to 0.1%, even quieter systems are commercially available. With these refinements, it should be possible to measure refractive index changes as small as 1×10^{-9} RI unit.

Equations 6 and 7 are strictly valid only if buffer electrolyte is present at much higher concentration than the analyte. Figure 4 shows data taken under conditions that intentionally violated the assumption. The analyte concentration is higher than the buffer concentration. For comparison, the numerical derivative of the actual detector response is included. Even for 0.1 M NaCl in 0.02 M phosphate buffer solution, analyte velocity modulation gives an approximate derivative response, with rejection of low-frequency background fluctuations. Under the extreme conditions of this experiment, deviation from the true derivative shape is observable near the band center, where the analyte concentration is highest.

CONCLUSION

Analyte velocity modulation has been shown to be a simple and useful technique for obtaining stable backgrounds with refractive index detectors. Although other implementations are possible, a step-up transformer can be added to almost any capillary electrophoresis system with only minor modifications. If it is not needed, the transformer can be left in place with no power applied. Because the dc resistance of a transformer is small compared to the capillary resistance, an unpowered transformer causes immeasurably small decreases in the voltage drop across the capillary.

The ac performance is similar to the best results obtained for optical concentration gradient refractive index detectors (17, 18, 20–23). The dc performance of this detector is better than that of previously reported (14, 16) detectors of similar design. In part the improvements result from the relatively good temperature stability of an electrophoresis capillary and, in part, from substitution of a quieter laser source for the usual He–Ne laser. We have chosen to use a 750-nm diode laser because the beam is visible to the eye. Even shorter wave-

lengths would be preferable, both for improved visibility and because of the increased refractive index dispersion and lower water absorption.

The analyte velocity modulation system may prove useful in conjunction with other detectors that do not achieve shot-noise-limited or thermal-noise-limited performance. The benefits should be greatest for system that must measure a large background signal from the buffer/electrolyte present in the capillary. Such detectors include, but are not necessarily limited to, refractive index detectors of all kinds, absorbance detectors, conductivity detectors, and indirect fluorescence detectors. Application to other detectors will be reported in subsequent communications.

LITERATURE CITED

- (1) Mikkers, F. E. P.; Everaerts, F. M.; Verheggen, Th. P. E. M. *J. Chromatogr.* **1979**, *169*, 11–20.
- (2) Jorgenson, J. W.; Lukacs, K. D. *Anal. Chem.* **1981**, *53*, 1298–1302.
- (3) Jorgenson, J. W.; Lukacs, K. D. *Science* **1983**, *222*, 266–272.
- (4) Compton, S. W.; Brownlee, R. G. *BioTechniques* **1988**, *6*(5), 432–440.
- (5) Lauer, H. H.; McManigill, D. *Anal. Chem.* **1986**, *58*, 166–170.
- (6) Rose, D. J., Jr.; Jorgenson, J. W. *J. Chromatogr.* **1988**, *447*, 117–131.
- (7) Kuhr, W. G.; Yeung, E. S. *Anal. Chem.* **1988**, *60*, 1832–1834.
- (8) Gozel, P.; Gassmann, E.; Michelsen, H.; Zare, R. N. *Anal. Chem.* **1987**, *59*, 44–49.
- (9) Huang, X.; Pang, T. K. J.; Gordon, M. J.; Zare, R. N. *Anal. Chem.* **1987**, *59*, 2747–2749.
- (10) Walbroehl, Y.; Jorgenson, J. W. *J. Chromatogr.* **1984**, *315*, 135–143.
- (11) Wallingford, R. A.; Ewing, A. G. *Anal. Chem.* **1987**, *59*, 1762–1766.
- (12) Kuhr, W. G.; Yeung, E. S. *Anal. Chem.* **1988**, *60*, 2642–2646.
- (13) Yeung, E. S. In *Detectors for Liquid Chromatography*; Yeung, E. S., Ed.; Wiley-Interscience: New York, 1986; pp 1–28.
- (14) Bornhop, D. J.; Nolan, T. G.; Dovichi, N. J. *J. Chromatogr.* **1987**, *384*, 181–187.
- (15) Bornhop, D. J.; Dovichi, N. J. *Anal. Chem.* **1986**, *58*, 504–505.
- (16) Bornhop, D. J.; Dovichi, N. J. *Anal. Chem.* **1987**, *59*, 1632–1636.
- (17) Synovec, R. E. *Anal. Chem.* **1987**, *59*, 2877–2884.
- (18) Hancock, D. O.; Synovec, R. E. *Anal. Chem.* **1988**, *60*, 1915–1920.
- (19) Washburn, E. W. *International Critical Tables of Numerical Data, Physics, Chemistry and Technology*; McGraw-Hill: New York, 1930; Vol. VII, pp 98–99.
- (20) Pawliszyn, J. *Anal. Chem.* **1986**, *58*, 243–246.
- (21) Pawliszyn, J. *Anal. Chem.* **1986**, *58*, 3207–3215.
- (22) Pawliszyn, J. *J. Liq. Chromatogr.* **1987**, *10*(15), 3377–3392.
- (23) Pawliszyn, J. *Anal. Chem.* **1988**, *60*, 2796–2801.
- (24) Hancock, D. O.; Synovec, R. E. *Anal. Chem.* **1988**, *60*, 2812–2818.
- (25) Pawliszyn, J. *Anal. Chem.* **1988**, *60*, 766–773.
- (26) Bard, A. J.; Faulkner, L. R. *Electrochemical Methods Fundamentals and Applications*; John Wiley & Sons: New York, 1980; pp 119–121.
- (27) Rieger, P. H. *Electrochemistry*; Prentice-Hall: Englewood Cliffs, NJ, 1987; pp 152–156.
- (28) Mikkers, F. E. P.; Everaerts, F. M.; Verheggen, Th. P. E. M. *J. Chromatogr.* **1979**, *169*, 1–10.

Chang-Yuh Chen
Tshenge Demana
Shi-Duo Huang
Michael D. Morris*

Department of Chemistry
The University of Michigan
Ann Arbor, Michigan 48109

RECEIVED for review January 11, 1989. Accepted April 7, 1989. This work was supported in part by NIH Grant GM-37006 and in part by a grant from the Office of the Vice President for Research, University of Michigan.

TECHNICAL NOTES

Determination of Nuclear Magnetic Resonance Sample Temperatures through Measurement of the Probe Coil Ohmic Resistance

Rosemary Effiong and Ronald F. Evilia*

Department of Chemistry, University of New Orleans, New Orleans, Louisiana 70148

A variety of approaches to the measurement of sample temperatures in variable-temperature nuclear magnetic resonance have been reported (1-11). Most of these methods rely on some temperature-dependent chemical shift, but methods employing the clearing point of liquid crystals and a complex instrumental approach involving primary and secondary lock signals have also appeared (10, 11). In this note we report the results of an investigation of the suitability of using the temperature dependence of the sample coil ohmic resistance as a measure of the sample temperature.

Because the ohmic resistance of a typical NMR sample coil is quite low (approximately 0.2Ω in the JEOL FX90Q broad-band 5-mm probe used in this work) one cannot simply connect an ohmmeter to the probe to measure the resistance. We, therefore, constructed the circuit shown in Figure 1. The principle of operation of this circuit is quite simple: The output of a commercial audio oscillator (Interstate Electronics, Model F33 function generator, operating at 200 Hz, 0.7 V RMS in the sine wave mode) is connected to the sample coil through a high resistance (approximately 10 k Ω) thereby producing a constant current of approximately 70 μ A through the coil. The approximately 35 μ V voltage drop developed across the coil and connecting wires from this constant current is measured by a Par Model 186 lock in amplifier (LIA) and then the resistance is calculated from Ohm's law. Contact to the sample coil was made by soldering two parallel pieces of #20 stranded wire to the coil contact on switch position 6 and the common of the multinuclear observation unit of the FX90Q spectrometer. This switch position is not used for normal instrument operation but does provide a direct connection to the probe coil. When the switch is moved to one of the active channels for data acquisition, the temperature measurement circuit is disconnected from the probe. Therefore, there is no effect on the normal instrument operation caused by this method of temperature measurement, but, one must tolerate the minor inconvenience of periodic switching back and forth between the temperature measurement channel and the data acquisition channel if multiple temperatures are to be measured. To connect a similar circuit to another model of spectrometer requires that a connection be made to the probe coil in such a way that a direct current path through the coil exists. One must provide a means for disconnecting the temperature measurement circuit during data acquisition either by inserting a suitable switch or by disconnecting, for example, a connector. Whatever arrangement is used, the measurement requires a direct current path through the probe coil. This switching or disconnection between temperature and spectral measurement modes does not represent a major inconvenience, however, because no retuning of the probe is required for the temperature measurement. The approximately 1 nW of heat generated by the temperature measurement is negligible at all reasonable temperatures. Obviously, this small amount of heating could be further reduced by increasing the value of the series resistor at the expense

of a decreased signal-to-noise ratio and the signal-to-noise ratio can be improved at the expense of slight additional sample heating.

The actual sample temperature was measured by monitoring the voltage of a chromel-alumel thermocouple contained in a 5-mm NMR tube. The tube was inserted into the probe to such a depth that the thermocouple was centered in the sample coil. No anomalous temperature readings associated with the use of chromel-alumel thermocouples in high magnetic fields were noted in these studies (12). High temperatures were achieved by use of the JEOL NM-VTS variable-temperature accessory. Low temperatures were obtained by blowing dry nitrogen gas through a heat exchanger filled with liquid nitrogen. The temperature was varied by varying the flow rate of the nitrogen gas and by warming the very cold gas with the NM-VTS blast pipe heater. Each measurement was made after allowing at least 15 min for thermal equilibration which was verified by a stable reading of both the thermocouple voltage and LIA output. The LIA was operated with a 30-s time constant and 1-kHz input filter, the LIA output voltage was measured with a digital voltmeter. The output of the oscillator was measured by the LIA when the circuit function switch was set to the calibrate position. To ensure maximum stability of the measurement circuit, no measurements were recorded until after at least a 30-min warmup period.

Figure 2 shows a plot of the experimentally measured coil resistance versus temperature obtained in this work. The data shown in Figure 2 are corrected for the resistance of the connecting wires. This correction was made by extrapolating a plot of the experimentally measured total circuit resistance to zero temperature. The Y intercept of this plot had a value of 0.307 Ω and is assumed to correspond to the resistance of the connecting wires. The data plotted in Figure 2 are the experimental values minus 0.307. All the data shown in Figure 2 were obtained with the proton decoupler on its maximum value and noise modulated with a 1-kHz bandwidth. No significant differences are noted in the measurement, after the new thermal equilibrium is reached, when the decoupler is off. However, if the input low-pass filter of the measurement circuit is omitted, the decoupler signal causes the LIA to saturate. The high-temperature data set was acquired on a different day and with a different oscillator output voltage in order to test for day-to-day reproducibility. The line drawn through the data corresponds to the least-squares best fit. The slope of the line is $6.988 \times 10^{-4} \Omega \text{ deg}^{-1}$ with a correlation coefficient of 0.996. The standard deviation of the points from the least-squares line is 0.8% which results in a 90% confidence interval of $\pm 2^\circ \text{C}$ for a temperature measurement. Figure 3 shows an expanded view of a smaller temperature range of the data in Figure 2.

Examination of the data shows that the ohmic resistance is a good linear function of temperature over at least a 250 deg range and that the resistance can be measured with good

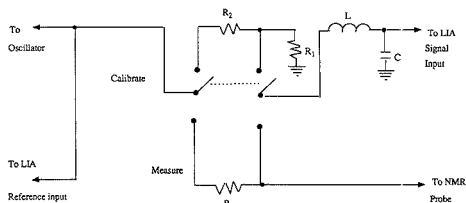


Figure 1. Schematic diagram of resistance measurement circuit. All resistors are $1/4$ W. $R_1 = 16.2 \Omega$; $R_2 = 276 \text{ k}\Omega$; $R_3 = 10 \text{ k}\Omega$; $L = 50 \mu\text{henrys}$; $C = 4.7 \text{ nF}$.

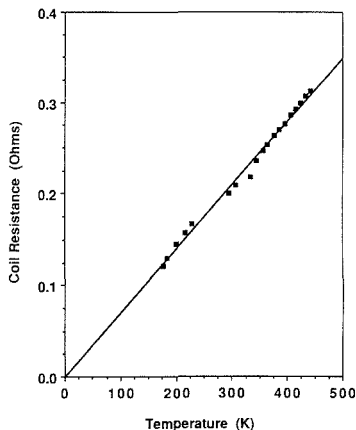


Figure 2. Corrected coil resistance versus measured sample temperature. Measurement conditions are described in text.

precision and accuracy over this range also. Although the maximum temperature measured in this work was approximately 440 K, it is clear from Figure 2 that higher temperatures than this can be measured. In fact, because the resistance increases with temperature, one can anticipate that higher temperatures can be measured more easily than lower ones. The advantage of this technique over previously reported methods lies in the large temperature range over which it is useful; the fact that the measurement is made with the actual sample in the probe rather than requiring that the sample be replaced by a thermometer of different heat capacity or the insertion of a thermocouple and the resulting difficulty of high-resolution measurements. Furthermore, these measurements are totally independent of the nucleus being observed or decoupled in the spectral acquisition.

The major limitation of this method lies in the necessity of measuring extremely small resistances quite accurately if one wishes to know the absolute temperature quite accurately. For example, to measure the temperature to an accuracy of 0.1 deg, one must measure the resistance to an accuracy of $70 \mu\Omega$. Such accuracy and precision in the measurement of the resistance are possible in principle but were not realized under the experimental conditions employed for this work. If one wishes a level of accuracy equal to 0.1 deg, considerably more care in the circuit construction would be necessary than was exercised in this work. The purpose of this work was to test the feasibility of these measurements rather than to develop an optimized circuit. The principal factors that limit the accuracy of the measurement are drift in the oscillator output, temperature variations of the current limiting resistor, and LIA drift. For 0.1° accuracy (approximately 0.03%) these variations must be controlled to a fraction of 0.03%. Elec-

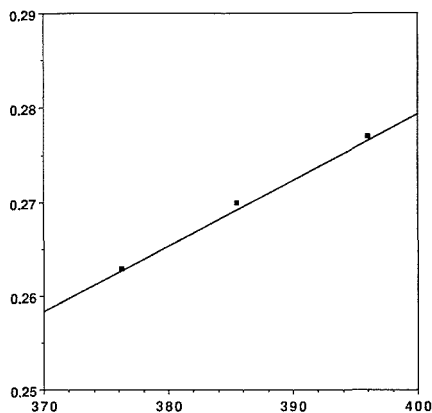


Figure 3. Expanded plot of data from Figure 2. The line is the least-squares line of the data set in Figure 2.

tronic stability of this order is clearly attainable with some difficulty but was not attempted in this work.

Because the temperature sensor employed in this scheme is not located in the sample itself, it is unlikely that the actual coil temperature is identical with the sample. This temperature difference would obviously be larger when conditions suitable for radio frequency (rf) heating of the sample exist. As in all cases where measurements are based upon calibration plots, the accuracy of the measurement is determined by the degree to which the calibration conditions are identical with those of the sample conditions. Clearly significant errors can be encountered if the resistance measurement is calibrated with a sample whose rf heating is significantly different than that of the sample.

The temperature measurement scheme reported here has several advantages over measurements made by inserting a thermocouple into the sample: there is no difficulty with sample spinning or with resolution degradation caused by an inserted device; there is no problem with reproducibility of the location of the temperature measuring device and no concern about compatibility of the thermocouple or wires with the sample (e.g. highly corrosive samples, etc.). The readability and ultimate accuracy of an accurately placed thermocouple is, however, superior to the method reported here.

Thus, we feel that receiver coil ohmic resistance measurements can provide a useful and convenient means for monitoring the true sample temperature for those cases where a large temperature range is required or for those nuclei where no suitable thermometer is available and where a temperature accuracy of 1 to 2 deg is sufficient. One can also envision circuit modifications such that the resistance measurement is gated off during spectral acquisition and, therefore, eliminates the need for manually switching off the temperature measurement circuit during data acquisition. One can also imagine circuit refinements that allow even smaller resistance changes to be measured accurately, such as the use of a four-wire resistance measurement scheme, stabilization of the oscillator, and other refinements that would result in more accurate measures of temperature than were obtained in this work.

Although the coil may actually attain a slightly different temperature than the sample tube, the linear relationship between the coil resistance and sample temperature allows one to read the sample temperature directly from the measured resistance after a suitable calibration plot has been made. The incorporation of this scheme into other spec-

trometer models that do not contain an appropriate unused switch position will require making a direct connection to the probe coil in such a way that the temperature measurement circuit can be disconnected for data acquisition as discussed above.

LITERATURE CITED

- (1) Neuman, R. C., Jr.; Roark, D. N.; Jonas, V. J. *Am. Chem. Soc.* **1967**, *89*, 3412-3416.
- (2) Van Geet, A. L. *Anal. Chem.* **1968**, *40*, 2227-2229.
- (3) Bornais, J.; Brownstein, S. J. *Magn. Reson.* **1978**, *29*, 207-211.
- (4) Yamamoto, O.; Yanagisawa, M. *Anal. Chem.* **1970**, *42*, 1463-1465.
- (5) Vidrine, D. W.; Peterson, P. E. *Anal. Chem.* **1976**, *48*, 1302-1303.
- (6) Levy, G. C.; Bailey, J. T.; Wright, D. A. *J. Magn. Reson.* **1980**, *37*, 353-356.
- (7) Gupta, R. K.; Gupta, P. J. *Magn. Reson.* **1980**, *40*, 587-589.
- (8) Schneider, H. J.; Freitary, W.; Schommer, M. J. *Magn. Reson.* **1975**, *18*, 393-395.
- (9) Combrisson, S.; Prange, T. J. *Magn. Reson.* **1975**, *19*, 108-110.
- (10) Friebohn, H.; Schilling, G.; Pohl, I. *Org. Magn. Reson.* **1979**, *12*, 569-573.
- (11) Vidrine, D. W.; Peterson, P. E. U.S. Patent 4,284,949, 1980.
- (12) Kollie, T. G.; Anderson, R. L.; Horton, J. L.; Roberts, M. J. *Rev. Sci. Instrum.* **1977**, *48*, 501-511.

RECEIVED for review January 13, 1989. Accepted March 24, 1989. Acknowledgment is made to the donors of the Petroleum Research Fund, administered by the American Chemical Society, for partial support of this research. This work was presented in part at the 16th meeting-in-miniature of the Louisiana section of the American Chemical Society, New Orleans, LA, October 21, 1988.

Capillary Gas Chromatography/Fourier Transform Infrared Spectroscopy Using an Injector/Trap and Liquid/Liquid Extraction

Allen J. Fehl and Curtis Marcott*

The Procter & Gamble Company, Miami Valley Laboratories, Cincinnati, Ohio 45239-8707

INTRODUCTION

In an earlier paper (1) we demonstrated that the sensitivity of lightpipe capillary gas chromatography/Fourier transform infrared (GC/FT-IR) spectroscopy could be improved by preconcentration and elimination of most of the solvent before placing the sample on the column. The concentration of analyte was done by simultaneous distillation-extraction of the aqueous solution of interest with Freon-11. The Freon was then removed by an automated injector/trap (2) before on-column deposition of the analyte. We have now extended this earlier work to include liquid/liquid extraction of aqueous solutions with Freon-11 at ambient temperature (23.8 °C). With this procedure, decomposition arising from steam distillation of heat-sensitive aqueous systems is avoided. This is of particular importance in the removal and identification of higher-boiling flavor/aroma components in natural systems. We describe here a continuous liquid/liquid extracting device designed to remove and concentrate analyte from large volumes of aqueous solution at room temperature. With this device we have successfully extracted fruit juices and other aqueous systems and identified their high-boiling components by lightpipe GC/FT-IR spectroscopy in conjunction with the injector/trap. Known concentrations of *p*-dioxane and benzaldehyde were also examined and sub-part-per-million sensitivities were achieved for each.

EXPERIMENTAL SECTION

The liquid/liquid extractor employed for our experiments was designed and built in-house, but in all likelihood commercially available extractors will be suitable for this purpose as well. Our motivation for using a liquid/liquid extractor stemmed from two considerations: First, attempts to collect headspace over orange juice for lightpipe infrared analysis did not collect enough mass of material for identification of any molecular species except those of low molecular weight. Second, heating of orange juice in any extraction procedure such as simultaneous distillation-extraction was precluded by the resulting foul-smelling residue that indicated decomposition. Since the aqueous systems of interest to us were available in large quantities, it seemed reasonable to devise an extraction scheme that would work with large aqueous volumes, for long periods of time, and at ambient temperatures with a highly volatile, low boiling, hydrophobic solvent. Such a solvent is

trichloromonofluoromethane (Freon-11), boiling at 23.8 °C. This fluorocarbon is nonflammable and has a density of 1.47 g/mL.

The liquid-liquid extraction apparatus we designed is shown in Figure 1. The critical dimensions of 600 and 390 mm were determined from the relative densities of Freon-11 and water. These dimensions establish the meniscus near the bottom of the column. The device is set up, in a hood, with a water-cooled cold-finger condenser inserted at A. A 100-mL round-bottom flask with boiling stones is attached loosely at B. Slowly, about 140 mL of predistilled Freon is poured into the column. Next, the aqueous solution to be extracted is similarly poured into the column, 860-920 mL being typical. During this process the Freon will run into the flask through the side arm, filling the flask about half full and establishing the meniscus as shown. At this point the flask is tightened and the Freon distilled at about 4 mL/min into the aqueous solution. The condensed stream drops, in spheres about 5 mm in diameter, through the aqueous phase, collects in the Freon phase at the meniscus, and eventually transfers to the flask to be distilled again. Simultaneously the aroma is concentrated in the Freon in the flask which remains at 23 °C. Care must be taken in adding the aqueous phase, since too rapid an addition or adding too much aqueous phase will displace the meniscus too low. This inevitably results in a siphon action that will completely fill the flask at B and render the system inoperable. Since the densities of various aqueous flavor systems may differ, the aqueous phase volume will vary from run to run.

The injector/trap/GC/FT-IR instrumentation used in the following experimental work has been described (1). All data were collected at a nominal resolution of 8 cm⁻¹ using a Digilab FTS-15E interferometer with a GC/FT-IR interface of our own design (1). About 900 mL of an aqueous sample was extracted. The extraction proceeded about 7 h each day for 3 days although there appears to be no reason why it can not be run overnight. Twenty milliliters of the Freon extract was reduced in volume by a nitrogen stream to 0.25 mL. One hundred microliters of this reduced volume was injected into the injector/trap capillary GC/FT-IR combination. A 0.32 mm, DB-1 fused silica column, 60 m long with a 1-μm film of stationary phase, was programmed at 4 °C/min to 250 °C after being held 6 min at 28 °C. Helium flow was 1.5 mL/min. These conditions were the same for the following experiments with the exception that the maximum GC temperature was not always 250 °C.

1. A 900-mL sample of commercially available pineapple juice containing no preservatives or artificial flavor was extracted for 7 h.

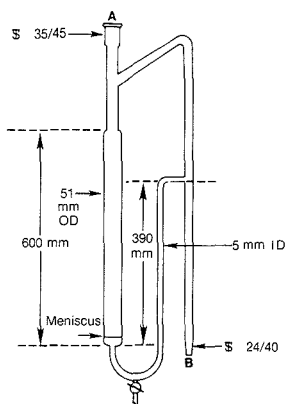


Figure 1. Liquid/liquid extraction device for use with Freon-11/water.

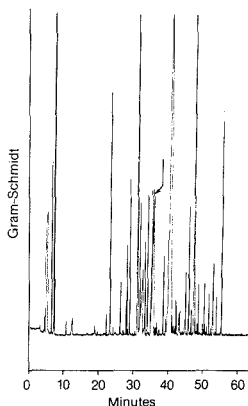


Figure 2. Infrared-detected capillary gas chromatogram of a 100- μ L injection of Freon-11 containing pineapple juice extractables. The arrow indicates the peak whose vapor-phase infrared spectrum is shown in Figure 3.

2. An 865-mL sample of thermally accelerated short-time evaporated (TASTE) (3) orange juice was Freon-extracted for 21 $\frac{1}{2}$ h.

3. A mixture of 2.0 mL of an aqueous solution containing 30 μ g of benzaldehyde and 2.3 mL of an aqueous solution containing 30.1 μ g of *p*-dioxane was diluted to 920 mL with distilled water and extracted for 21 $\frac{1}{2}$ h; 20 mL of the Freon extract was reduced to 0.5 mL.

4. A 23-mL aqueous solution containing 301 μ g of *p*-dioxane was diluted to 920 mL with distilled water and extracted for 21 $\frac{1}{2}$ h; 20 mL of the Freon extract was reduced to 0.5 mL.

RESULTS AND DISCUSSION

The extraction of pineapple juice was our first attempt at using the Freon extractor. This was of interest because pineapple juice is known to contain 2,5-dimethyl-4-hydroxy-3-(2*H*)-furanone (Furaneol) (4, 5), a potent aroma variously described as burnt pineapple or cotton candy, and we considered it an important test to be able to identify this compound. The infrared-detected Gram-Schmidt chromatogram (6) of the Freon-extracted pineapple juice is shown in Figure 2. Furaneol was identified as the peak eluting at 36 min (arrow) and its vapor-phase infrared spectrum is shown in Figure 3. The base-line slope of the spectrum was com-

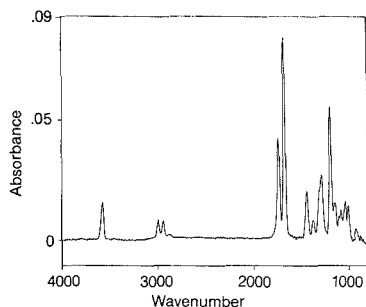


Figure 3. Furaneol, vapor-phase infrared spectrum of peak (arrow) of Figure 2.

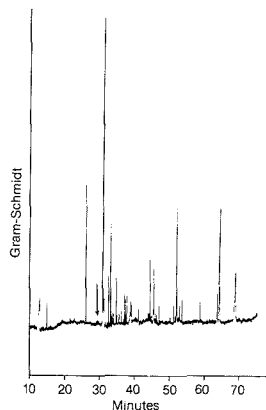


Figure 4. Infrared-detected capillary gas chromatogram of a 100- μ L injection of Freon-11 containing TASTE orange juice extractables. The peak (arrow) was tentatively identified as phenylacetaldehyde.

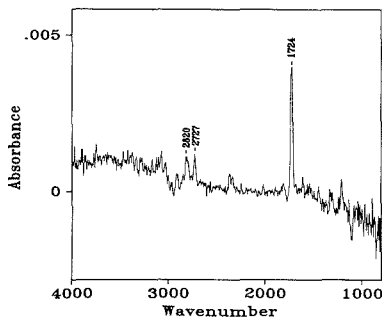


Figure 5. Vapor-phase infrared spectrum of peak (arrow) of Figure 4.

puter-corrected in the high wavenumber region. This spectrum is virtually identical with the spectrum of an authentic sample of Furaneol generated and added to our vapor-phase searching library. The identity of the authentic sample was confirmed by Kovats index and mass spectrometry. To our knowledge, this is the first report of a vapor-phase infrared spectrum of Furaneol.

TASTE is an orange juice feed-stock from which orange volatiles have been stripped. It is subsequently reconstituted in the preparation of commercial orange juice. The stripping

process can introduce unwanted off-flavor components. Once identified, steps can be taken to remove or preclude the formation of these off-flavor materials. Figure 4 shows the infrared-detected chromatogram of TASTE. The infrared spectrum of the peak at 29 min (arrow) has a signal-to-noise ratio of only 7:1 and is shown in Figure 5. The bands at 2727 and 1724 cm^{-1} strongly suggest an aldehyde. It was tentatively identified as phenylacetaldehyde by searching through a library of in-house-generated vapor-phase spectra. This unstable compound has been described as having an hyacinth-type odor and is used as an imitation flavor enhancer (7). Its presence in orange juice, however, is not desirable.

Flavor/aroma systems are known to contain compounds having olfactory impact at levels well below 1 ppm (8). It seemed important to investigate just what levels of organic materials could be detected in aqueous systems using this extractor. When 920 mL of water containing 33 ppb of both *p*-dioxane and benzaldehyde was extracted for 21 $\frac{1}{2}$ h, we easily identified benzaldehyde (whose vapor-phase infrared spectrum had a maximum absorbance of 0.007), but we did not detect dioxane. When 920 mL of water containing 328 ppb dioxane was similarly extracted, we did detect dioxane (whose vapor-phase infrared spectrum had a maximum absorbance of 0.01). Since the molar absorptivities of the strongest band in the IR spectra of benzaldehyde and *p*-dioxane are very similar, it seems likely that benzaldehyde is more efficiently partitioned into Freon-11, accounting for our

increased sensitivity to it relative to *p*-dioxane.

Thus, we are able to extract and identify, by lightpipe GC/FT-IR, typical high-boiling aroma/flavor organic compounds from aqueous solution at levels well below 1 ppm without thermal decomposition. Other aqueous systems such as urine have also been successfully extracted.

ACKNOWLEDGMENT

We thank D. E. Burton, C. L. Eddy, P. A. Rodriguez, and C. H. Tsai for helpful discussions and for supplying some of the materials in this work.

LITERATURE CITED

- (1) Fehl, A. J.; Marcott, C. *Anal. Chem.* **1986**, *58*, 2578-2581.
- (2) Rodriguez, P. A.; Eddy, C. L.; Ridder, G. M.; Culbertson, C. R. *J. Chromatogr.* **1982**, *236*, 39-49.
- (3) Carpenter, R. S.; Burgard, D. R.; Patton, D. R.; Zwerdling, S. S. In *Instrumental Analysis of Foods*; Charalambous, G., Inglett, G., Eds.; Academic: New York, 1983; Vol. 2, pp 173-186.
- (4) Rodin, J. O.; Himel, C. M.; Silverstein, R. M.; Leeper, R. W.; Gortner, W. A. *J. Food. Sci.* **1965**, *30*, 280-285.
- (5) Buchi, G.; Demole, E. *J. Org. Chem.* **1973**, *38*, 123-125.
- (6) de Fasseh, J. A.; Isenhour, T. L. *Anal. Chem.* **1977**, *49*, 1977-1981.
- (7) Arcander, S. *Perfume and Flavor Chemicals*; Steffen Arcander: Las Vegas, NV, 1969; Vol. 2, p 2470.
- (8) *Compilation of Odor and Taste Threshold Values Data*; Fazzalari, F. A., Ed.; American Society for Testing and Materials: Philadelphia, PA, 1973.

RECEIVED for review January 25, 1989. Accepted April 11, 1989.

Use of Fumed Silica To Remove Surfactant Interferences in Continuous Flow Polarographic Measurements

Wladyslaw W. Kubiak* and Zygmunt Kowalski

Institute of Materials Science, Academy of Mining and Metallurgy, 30-059 Krakow, Poland

The influence of surface-active substances on polarographic measurements makes direct analysis of samples containing organic material difficult or even impossible. Various detergents widely used in industry, homes, and laboratories are present not only in real samples, but sometimes even in standard solutions. Several approaches have been used to purify solutions and remove the effect of the surfactant presence. Use of activated charcoal (1, 2), platinumized platinum (3), and Sep-Pak extraction cartridges (4) to remove, or ultraviolet irradiation (5) to destroy, the surfactant has been proposed.

The possibility of using fumed silica in polarographic measurements was presented by Kowalski et al. (6) and in adsorptive stripping voltammetry by Kubiak and Wang (7). In contrast to other methods, fumed silica can be added directly to the polarographic cell during the deaeration step, and there is no need to remove it before measurement. Interaction of silica with the mercury electrode and adsorption of depolarizer in applied conditions was not observed. The adsorptive properties and large area per unit of weight allow fumed silica to rapidly remove organic surfactants from solution.

Flow conditions enhance adsorption on the electrode (8); thus requirements for purer samples are higher. The presence of silica suspension in the flowing solution may cause additional difficulties.

This paper describes the influence of surfactant on continuous flow polarographic measurements and the utility of fumed silica in removing the surfactant selectively and restoring measured current. Triton X-100 was used in all

measurements as a model surface-active compound (5).

EXPERIMENTAL SECTION

Apparatus. The flow system consisted of a 0.5-L solution reservoir, pump (ABU-12 autoburet Radiometer, Denmark, with 50-mL syringe), and flow detector with dropping mercury electrode, reference Ag, AgCl/saturated KCl and stainless steel tube auxiliary electrode located at the outlet of the detector. The detector, described previously (9), was operated in opposite mercury and solution flow mode. The system was connected by Tygon tubing (2.4-mm i.d.). The solution was deaerated by argon bubbling in the reservoir. Electrode drop time was controlled by the electromagnetic hammer. A pulse polarograph PP-04 (ZUT-Telpod, Poland) was used to obtain current-potential and amperometric data.

Reagents. All solutions were prepared from double-distilled water. A solution of 25 μM cadmium nitrate in 0.5 M potassium nitrate, pH = 4.5, was used in all measurements. Triton X-100 was obtained from Windsor Laboratories, Ltd. (U.K.), and silicon dioxide spectral pure was from the Silesian Institute of Technology (Poland) the closest replacement being fumed silica (Sigma No. S-5005, particle size 0.007 μm , surface area 400 m^2/g).

Procedure. A known volume of solution, usually 250 mL, was put into the solution reservoir, and after deaeration, the system was filled. The solution, after passing the detector, was returned to the reservoir. Additions of Triton and silica were made to the solution reservoir. After each addition a few pump cycles (pump/refill) were performed to obtain uniform concentration in the whole system. A silica suspension was pumped through the detector together with solution. The volume of the pump syringe (50 mL) was large enough to ensure registration of the whole polarogram at the highest utilized flow velocity. Experiments in stationary conditions were performed by stopping the

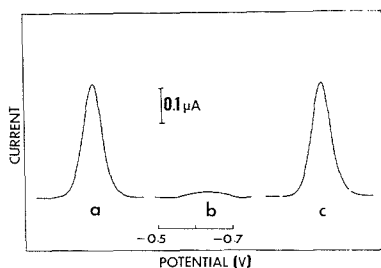


Figure 1. Differential pulse polarograms obtained in the following solutions: a, 25 μM cadmium in 0.5 M potassium nitrate pH 4.5; b, same as a with 20 ppm Triton X-100; c, same as b with 4 g/L fumed silica. Conditions: pulse amplitude, 20 mV; drop time, 3 s; flow velocity, 0.48 cm/s.

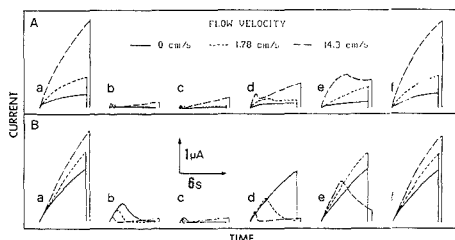


Figure 2. Chronoamperometric curves. (A) dc amperometry with current sampling; potential -0.8 V, sampling time 20 ms, waiting time 80 ms. (B) Pulse amperometry; potential switched between -0.6 and -0.8 V, sampling time 20 ms, waiting time 30 ms. Solutions: a, 25 μM cadmium in 0.5 M potassium nitrate pH 4.5; b, same as a with 27 ppm Triton; c, same as a with 53 ppm Triton; d, same as c with 3.2 g/L fumed silica; e, same as c with 7.3 g/L fumed silica; f, same as c with 12.6 g/L fumed silica.

flow. The volume of the detector was high enough to obtain a polarogram not distorted by a decrease in concentration due to depolarizer electrolysis.

RESULTS AND DISCUSSION

The use of fumed silica as a purifying agent in polarography in flowing solution is illustrated in Figure 1. In the presence of 20 ppm Triton, the differential pulse polarographic peak of cadmium in the flowing solution is almost completely depressed (b), while after the addition of silica, the peak (c) is the same as the one (a) in solution without Triton. The effects of current depression by the model surfactant as well as the recovery by fumed silica additions are investigated by various voltammetric techniques in flow conditions and compared to results for stationary conditions.

Chronoamperometry. Figure 2 shows the chronoamperometric curves obtained for a growing mercury drop at constant potential (A) and those obtained by using constant pulse amplitude with current sampling-pulse amperometry (B). At the highest flow velocity the damping effect of Triton is stronger; thus its lower concentration causes complete current suppression. With the increase of the flow velocity more silica is necessary to recover the chronoamperometric curve. In pulse amperometry, the damping/recovery effect can be seen more clearly, because current is less dependent on flow velocity. Thus a pure effect of surfactant interference can be observed. At a flow velocity of 14.3 cm/s, the backpressure from the flowing solution causes a longer drop time.

Polarography and Amperometry. Figure 3 shows the dependence of the normal pulse polarographic wave height on Triton concentration (A) and successive recovery during increasing silica additions to the solution (B). Similar de-

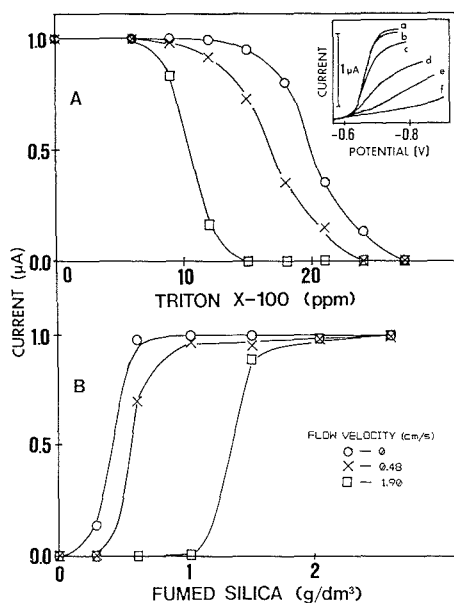


Figure 3. Suppression of normal pulse polarographic wave of 25 μM cadmium by Triton X-100 (A) and restoration by the fumed silica addition to a solution containing 25 μM cadmium and 27 ppm Triton (B) at different flow velocities. Insert shows changes of NPP wave of 25 μM cadmium (a) with Triton additions of (b) 9, (c) 15, (d) 21, (e) 27, and (f) 39 ppm at a flow velocity of 0.48 cm/s. Conditions: sampling and waiting time, 20 ms; drop time, 3 s.

pendence is observed in other polarographic and amperometric techniques. Small concentrations of Triton either do not affect the measured current (normal pulse polarography (NPP), pulse amperometry) or decrease the current slightly (differential pulse polarography (DPP), sampled direct current (dc) amperometry). Higher surfactant concentrations cause a rapid decrease of the measured current. In NPP and DPP the polarographic curve is suppressed entirely at high Triton concentration, whereas in both amperometric techniques current is not damped entirely even at very high concentration (40 ppm). An increase in the flow velocity of the solution results in a shift of the curve representing dependence on surfactant concentration toward lower surfactant concentration. Addition of fumed silica to a solution containing surfactant reverses this dependence as a result of surfactant adsorption on silica and thus its removal from solution. Because at higher flow velocities a suppression of the wave is observed at low concentrations of Triton, addition of a larger amount of fumed silica is necessary to obtain a full recovery of the wave. Normal pulse polarography and pulse amperometry are less sensitive to surfactants than other techniques, and a relatively high concentration of surfactant in solution does not affect the wave height. The insert in Figure 3 shows how the shape of the NPP wave changes with increasing Triton concentration. At low Triton concentrations only the height of the wave changes, but higher Triton concentrations affect wave slope as well.

In differential pulse polarography even small concentrations of Triton cause a significant decrease in peak current, especially at higher flow velocities; thus more silica must be added to completely recover the peak height. If a solution contains 30 ppm Triton, 2 g/L fumed silica will restore the NPP wave, but more than 4 g/L is needed to recover the DPP peak.

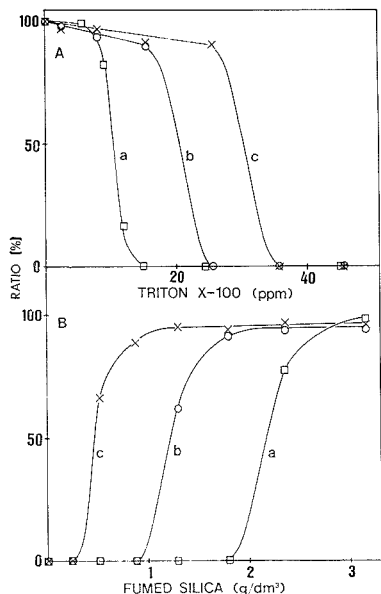


Figure 4. Effect of drop time on suppression of NPP wave of 25 μM cadmium by Triton addition (A) and restoration by the fumed silica addition to a solution containing 25 μM cadmium and 45 ppm Triton (B): drop time, (a) 1, (b) 2, and (c) 3 s. Limiting current is shown as percentage ratio of value measured in the same conditions without Triton interference. Flow velocity was 1.8 cm/s.

In all cases addition of the proper amount of fumed silica eliminates the surfactant interference.

Effect of Drop Time. Chronoamperometric curves (Figure 2) show that the effect of current suppression by surfactant is strongly dependent on drop lifetime. At the beginning of the drop lifetime, current is practically undisturbed by surfactant, due to the rapid increase of the electrode surface area and relatively low rate of the surfactant adsorption process. Duration of this phase of the drop life decreases when the surfactant concentration and flow velocity increase. As the drop is growing, the electrode area increases more slowly and thus suppression of the current is observed. Figure 4 shows the dependence of the NPP wave on surfactant concentration (A) and silica addition (B) for drop times of 1, 2, and 3 s. To suppress the NPP wave obtained for a 1-s drop, a nearly 3 times higher concentration of surfactant is required than for a 3-s drop. In contrast, nearly 3 times more silica is required to recover the NPP wave obtained for a 3-s drop than for a 1-s drop.

Effect of Flow Velocity. Surfactant adsorption and thus suppression of the polarographic current are enhanced by solution movement. Figure 5 shows the dependence of current on flow velocity when high Triton concentration is used (a) and after the addition of fumed silica to this solution in quantities partially adsorbing Triton (b) and in quantities sufficient to completely adsorb Triton (c). Curve c shows a typical low dependence of current in dc amperometry (A) and

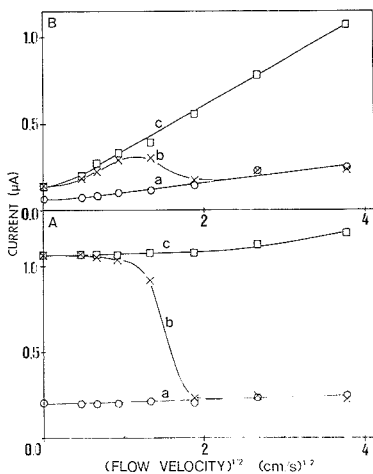


Figure 5. Effect of flow velocity on current measured in pulse amperometry at a potential of -0.6 V with a pulse amplitude of -200 mV (A) and dc amperometry at -0.8 V (B) in a solution of 25 μM cadmium in 0.5 M potassium nitrate pH 4.5 and 52 ppm Triton (a), 52 ppm Triton and 3.2 g/L fumed silica (b), and 52 ppm Triton and 12.6 g/L fumed silica (c). Drop time was 3 s.

flow independence of current in pulse amperometry (B), whereas curve b coincides with curve c at low flow velocities and with curve a at high flow velocities. This described effect has practical significance in detecting surfactant presence in solution—in this case higher flow rates cause the current to decrease instead of increase.

Conclusion. In flow conditions, interference from the surfactant is observed at lower concentrations than in stationary conditions. Surfactant interference may be decreased by use of normal pulse polarography or pulse amperometry at short drop times. The addition of the fumed silica to the solution helps restore the current value; however, more silica is required in flow conditions than in stationary conditions. The characteristic procedure parameters should be adjusted to fulfill the requirements of a particular flowing system. Because fumed silica removes surfactant from solution, it should be applicable also in the case of solid electrodes commonly used in flowing systems.

Registry No. Silica, 7631-86-9; Triton X-100, 9002-93-1; cadmium, 7440-43-9.

LITERATURE CITED

- (1) Berezina, N. P.; Nikolova-Fedorovich, N. P. *Elektrokhimiya* 1967, 3, 3.
- (2) Bednarkiewicz, E.; Kublik, Z. *J. Electroanal. Chem. Interfacial Electrochem.* 1984, 165, 195.
- (3) Hassan, M. Z.; Bruckenstein, S. *Anal. Chem.* 1974, 46, 1962.
- (4) Bond, A. M.; Reust, J. B. *Anal. Chim. Acta* 1984, 162, 389.
- (5) Van Den Berg, C. M. G. *Anal. Chem.* 1985, 57, 1532.
- (6) Kowalski, Z.; Kolder, E.; Niewiara, E. *Euroanalysis V*, Cracow, Poland, August 1984, paper I-46.
- (7) Kubiak, W. W.; Wang, J. J. *J. Electroanal. Chem. Interfacial Electrochem.* 1989, 258, 41.
- (8) De Jong, H. D.; Kok, W. Th.; Bos, P. *Anal. Chim. Acta* 1983, 155, 37.
- (9) Kowalski, Z.; Kubiak, W. W. *Anal. Chim. Acta* 1984, 159, 129.

RECEIVED for review November 28, 1988. Accepted March 27, 1989.

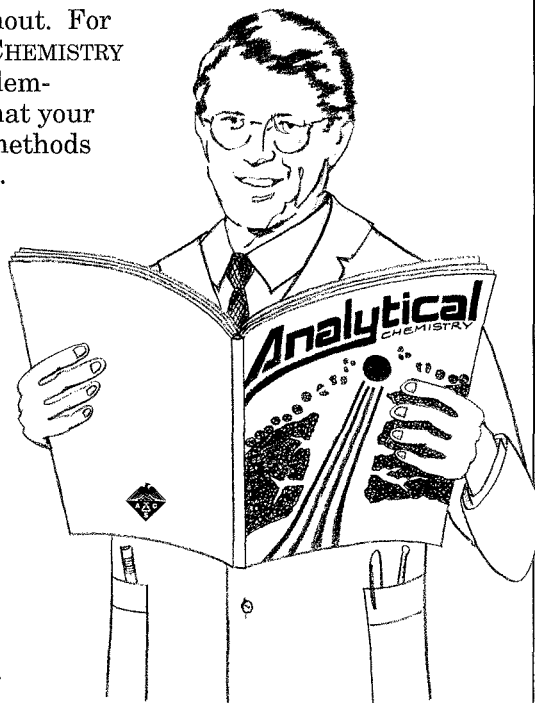
When you're confronted
with a specific "need to know"...

Analytical CHEMISTRY

Every chemist knows, having the most up to date information is essential for success. And, in the vital field of measurement science, ANALYTICAL CHEMISTRY is the one publication you cannot do without. For over sixty years, ANALYTICAL CHEMISTRY has proven to be a useful problem-solving resource, no matter what your specialty. And now, it covers methods used in the biotechnology field.

Publishing information that will help you deal more skillfully with problems such as sampling, data analysis and methodology—the papers in today's twice monthly ANALYTICAL CHEMISTRY cover real world problems involving trace analysis of air, water, soil, materials, drugs, and biopolymers.

Call now and reserve your own personal subscription.



Volume 61 (1989)	U.S.	Canada and Mexico	Europe Air-Service Included	All Other Countries Air-Service Included
ACS Member - 1 year	\$ 27	\$ 56	\$ 83	\$120
2 years	\$ 45	\$103	\$157	\$231
Nonmember	\$ 49	\$ 78	\$155	\$192

Member rates are for personal use only. Subscriptions may start any month of the year and expire one year later. Foreign payment must be made in U.S. currency by international money order, UNESCO coupons, or U.S. bank draft, or order through your subscription agency. For nonmember rates in Japan, contact Maruzen Co., Ltd. This publication is available on microfilm, microfiche, and the full text is available online on STN International.

**Call Toll-Free
1-800/227-5558
for credit card orders**

or write:

**American Chemical Society
Marketing Communication Dept.
1155 Sixteenth Street N.W.
Washington D.C. 20036**

How HP HPLC lightens your workload.

1976 HP advances HPLC with new standards in precision flow control.

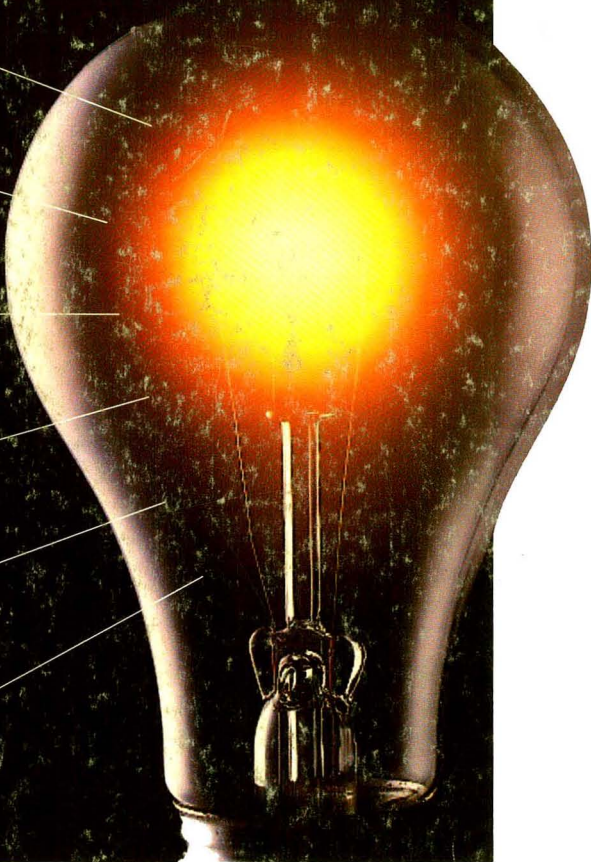
1978 HP advances HPLC with the first scanning variable wavelength detector.

1982 HP advances HPLC with the first commercial diode-array detector.

1983 HP advances HPLC with the first system optimized for low dispersion LC.

1986 HP advances HPLC with first on-line pre-column derivatization.

1988 HP advances HPLC with particle beam LC/MS.



Why are more and more chromatographers switching to HP HPLC? *Superior technology that makes your job much easier and more productive!*

Year after year, Hewlett-Packard introduces some of the brightest ideas in HPLC. Things like high precision solvent flow. Instant spectra. Push button operation. Full automation with diagnostics. All of the

advantages of low dispersion LC and particle beam LC/MS with true EI spectra. Not to mention the incredible reliability that made 99% uptime a practical reality.

Along with extraordinary power and versatility, HP offers a wide range of HPLC products. From economical modules to fully integrated systems. From a spectrum of detectors to application specific analyzers.

From integrators to lab information and control systems. All from a single vendor.

To learn more call **1 800 556-1234, EXT 10211**. In California call **1 800 441-2345, EXT 10211**.



**HEWLETT
PACKARD**